

DOCTORAL THESIS

Robust Stability Analysis of Fractional-Order Control Systems

Majid Ghorbani

TALLINN UNIVERSITY OF TECHNOLOGY
DOCTORAL THESIS
98/2025

Robust Stability Analysis of Fractional-Order Control Systems

MAJID GHORBANI



TALLINN UNIVERSITY OF TECHNOLOGY
School of Information Technologies
Department of Computer Systems

The dissertation was accepted for the defense of the degree of Doctor of Philosophy in Information and Communication Technologies on November 24, 2025.

Supervisor: Full Professor Eduard Petlenkov,
Department of Computer Systems,
Tallinn University of Technology
Tallinn, Estonia

Co-supervisor: Senior Researcher Aleksei Teplyakov,
Department of Computer Systems,
Tallinn University of Technology
Tallinn, Estonia

Opponents: Associate Professor Hassan HosseinNia,
Department of Precision and Microsystems Engineering,
Delft University of Technology (TU Delft)
Delft, Netherlands

Assistant Professor Xiaocong Li,
Assistant Professor, Eastern Institute of Technology, Ningbo,
Adjunct Assistant Professor, National University of Singapore

Defense of the thesis: December 15, 2025, Tallinn

Declaration:

Hereby I declare that this doctoral thesis, my original investigation and achievement, submitted for the doctoral degree at Tallinn University of Technology, has not been submitted for any academic degree elsewhere.

Majid Ghorbani

signature

Copyright: Majid Ghorbani, 2025
ISSN 2585-6898 (publication)
ISBN 978-9916-80-435-3 (publication)
ISSN 2585-6901 (PDF)
ISBN 978-9916-80-436-0 (PDF)
DOI <https://doi.org/10.23658/taltech.98/2025>

Ghorbani, M. (2025). *Robust Stability Analysis of Fractional-Order Control Systems* [TalTech Press]. <https://doi.org/10.23658/taltech.98/2025>

TALLINNA TEHNIKAÜLIKOOL
DOKTORITÖÖ
98/2025

Murrulistel tuletistel põhinevate juhtimissüsteemide robustse stabiilsuse analüüs

MAJID GHORBANI

Contents

List of Publications	8
Author's Contributions to the Publications	10
Abbreviations.....	11
List of Symbols.....	12
1 Introduction	13
1.1 Motivations and Problem Formulations	13
1.2 Contributions	18
1.3 Thesis Organization	18
2 Fractional-Order Interval Polynomials.....	21
2.1 Fractional Calculus	21
2.1.1 Fractional-Order Systems	21
2.1.2 Fractional-Order Controllers	22
2.2 Geometry of Value Set of Fractional-Order Interval Polynomials.....	22
2.2.1 Approach 1: Vertex Computation Method [8].....	24
2.2.2 Approach 2: Vertex Computation Method [9]	25
2.3 Robust Stability Analysis of Fractional-Order Interval Polynomials	27
2.4 Robust Stability Analysis in FOMCON Toolbox	30
3 Robust Stability Analysis of Fractional-Order Interval Systems	36
3.1 Preliminaries	36
3.2 Robust Stability Analysis	37
3.3 Numerical Examples	42
4 Robust Stability Analysis of Fractional-Order Interval Polynomials with an Interval Time Delay	52
4.1 Preliminaries and Definitions	53
4.2 Robust stability analysis.....	53
4.3 Robust stability checking function.....	59
4.4 Robust Stability Analysis in FOMCON Toolbox	61
4.5 Simulation and Experimental Results	62
5 Robust Stability Region of Fractional-Order Controllers	70
5.1 Robust stability region of Fractional-Order controllers for Fractional-Order Interval Systems without time delay	70
5.1.1 Definitions	70
5.1.2 Determination of the Robust Stability Region	71
5.1.3 Good output disturbance rejection.....	73
5.1.4 High-frequency noise rejection	74
5.2 Robust stability region of Fractional-Order controllers for Fractional-Order Interval Systems with an interval time delay.....	75
5.2.1 Definitions	75
5.2.2 Determination of the Robust Stability Region	77
5.3 High-performance Output Disturbance Rejection	79
5.4 Simulation Results.....	82

6	Robust Stability Analysis of Smith Predictors.....	88
6.1	Robust Stability Analysis of Smith Predictors for stable systems.....	88
6.1.1	Background	88
6.1.2	Definitions	89
6.1.3	Derivation of Robust Stability Conditions	91
6.2	Robust Stability Analysis of Smith Predictors for unstable systems.....	100
6.2.1	Definitions	100
6.2.2	Derivation of Robust Stability Conditions	102
6.3	Illustrative examples	106
7	Robust Stability Analysis of FOISs with Complex Uncertainties	112
7.1	Robust Stability Testing Function for A Complex Interval Family of FO Systems	112
7.2	Robust Stability Testing Function for A Complex Interval Family of FO Systems	119
7.3	Illustrative examples	123
8	Conclusions	125
	List of Figures	129
	List of Tables	130
	References	130
	Acknowledgements	139
	Abstract.....	140
	Kokkuvõte	141
	Appendix 1.....	143
	Appendix 2	153
	Appendix 3	161
	Appendix 4	183
	Appendix 5	205
	Appendix 6	213
	Appendix 7.....	227
	Appendix 8	241
	Appendix 9	249
	Appendix 10	257
	Appendix 11	265
	Appendix 12.....	279

Appendix 13.....	287
Appendix 14	303
Appendix 15.....	311
Appendix 16	335
Curriculum Vitae	351

List of Publications

This Ph.D. thesis is based on the following publications, where I served as the primary contributor.

- I. M. Ghorbani, A. Tepljakov, and E. Petlenkov. On robust stability of uncertain control systems with time delay: an approach based on the overlap of value sets. *IEEE Transactions on Automatic Control*, 69(9):6349–6356, 2024.
- II. M. Ghorbani, M. Tavakoli-Kakhki, A. Tepljakov, E. Petlenkov, A. Farnam, and G. Crevecoeur. Robust stability analysis of interval fractional-order plants with interval time delay and general form of fractional-order controllers. *IEEE Control Systems Letters*, 6:1268–1273, 2021.
- III. M. Ghorbani, H. Rezaei, A. Tepljakov, and E. Petlenkov. Robust stability testing function for a complex interval family of fractional-order polynomials. *Journal of the Franklin Institute*, 359(17):10038–10057, 2022.
- IV. M. Ghorbani, M. Tavakoli-Kakhki, A. Tepljakov, and E. Petlenkov. Robust stability analysis of Smith predictor based interval fractional-order control systems: a case study in level control process. *IEEE/CAA Journal of Automatica Sinica*, 10(3):762–780, 2022.
- V. M. Ghorbani, A. Tepljakov, and E. Petlenkov. Robust FOPID stabilization for Smith predictor structures. In *Proc. 2022 IEEE 61st Conference on Decision and Control (CDC)*, pages 1696–1701, 2022.
- VI. M. Ghorbani, A. Tepljakov, and E. Petlenkov. Stabilizing region of fractional-order proportional integral derivative controllers for interval fractional-order plants. *Transactions of the Institute of Measurement and Control*, 45(3):546–556, 2023.
- VII. M. Ghorbani, A. Tepljakov, and E. Petlenkov. Stabilizing region of fractional-order proportional integral derivative controllers for interval delayed fractional-order plants. *Asian Journal of Control*, 25(2):1145–1155, 2023.
- VIII. M. Ghorbani, A. Tepljakov, and E. Petlenkov. Fractional-order interval polynomials, stability and robust stability analysis and FOMCON implementation.¹ In *Proc. 2023 International Conference on Fractional Differentiation and Its Applications (ICFDA)*, pages 1–6, 2023.
- IX. M. Ghorbani, A. Tepljakov, and E. Petlenkov. Robust d-stability analysis of fractional-order controllers. In *Proc. 2023 American Control Conference (ACC)*, pages 3871–3876, 2023.
- X. M. Ghorbani, A. Tepljakov, and E. Petlenkov. On robust stability analysis of interval time delay systems using delayed controllers. In *Proc. 2023 European Control Conference (ECC)*, pages 1–6, 2023.
- XI. M. Ghorbani, A. Tepljakov, and E. Petlenkov. Robust stabilization of interval fractional-order plants with an interval time delay by fractional-order proportional integral derivative controllers. *IET Control Theory & Applications*, 18(5):614–625, 2024.
- XII. M. Ghorbani, K. Nosrati, A. Tepljakov, J. Belikov, and E. Petlenkov. Robust stability region of PI controllers for an interval time delayed load frequency control. In *Proc. 2024 IEEE PES Innovative Smart Grid Technologies Europe (ISGT Europe)*, pages 1–5, 2024.
- XIII. M. Ghorbani, B. Mehdizadeh Gavvani, A. Farnam, A. Tepljakov, E. Petlenkov, and G. Crevecoeur. Computing stabilising regions: FOPID controller methodology for interval fractional-order plants with time delay. *International Journal of Systems Science*, 56(8):1884–1896, 2025.

¹This paper was selected as the **Best Student Paper** at the ICFDA Conference.

XIV. M. Ghorbani, A. Farnam, A. Tepljakov, E. Petlenkov, G. Crevecoeur, and A. Eskandarian. Graphical tuning for robust stabilization: implementable stability regions for fractional-order proportional integral controllers in interval fractional-order systems. In *Proc. 2024 IEEE 63rd Conference on Decision and Control (CDC)*, pages 8902–8907, 2024.

XV. M. Ghorbani, B. B. Alagoz, A. Tepljakov, and E. Petlenkov. A graphical method to determine robust stabilizing region of FOPID controllers for stable/unstable fractional-order plants with interval uncertainties of a fractional order and model coefficients. *International Journal of General Systems*, 54(2):198–217, 2025.

XVI. M. Ghorbani, B. Mehdizadeh Gavgani, A. Farnam, A. Tepljakov, E. Petlenkov, and G. Crevecoeur. Implementable robust stability regions for fractional-order PD controllers with an application to servo system control. *Asian Journal of Control*, 2025. doi:10.1002/asjc.3881.

Author's Contributions to the Publications

Across all papers, I was the lead author and originator of the main idea: I developed the simulation code, conducted the simulations, analyzed the results, prepared the figures, and wrote the manuscript.

Abbreviations

CRB	Complex Root Boundary
FO	Fractional Order
FOPID	Fractional-Order Proportional-Integral-Derivative
FOPI	Fractional-Order Proportional-Integral
FOPD	Fractional-Order Proportional-Derivative
FOPTD	First Order Plus Time Delay
FOIP	Fractional-Order Interval Polynomial
FOIS	Fractional-Order Interval System
IRB	Infinite Root Boundary
RRB	Real Root Boundary

List of Symbols

\mathbb{R}	Set of real numbers.
\mathbb{R}^+	Set of positive real numbers.
$\mathbb{R}^{\leq 0}$	Set of non-positive real numbers.
\mathbb{R}_+^2	The set of all pairs of positive real numbers.
$\mathbb{Z}_{\geq 0}^{\leq n}$	Set of non-negative integers from 0 to n .
\mathbb{C}	Set of complex numbers.
$\sum_{i=r_1}^{r_2} u_i = 0$	Defined to be zero when $r_2 < r_1$.
$\bigcup_{i=r_1}^{r_2} U_i = \emptyset$	Defined to be the empty set when $r_2 < r_1$.
$\partial(U)$	Boundary of the value set U in the complex plane.
$e(u_1, u_2)$	Convex combination $\eta u_1 + (1 - \eta)u_2$, with $\eta \in [0, 1]$.
$e(x_1(j\omega), x_2(j\omega))$	Convex combination of x_1 and x_2 in the frequency domain.
$n(H)$	Number of distinct elements in the set H .
$\text{floor}(x)$	Greatest integer less than or equal to $x \in \mathbb{R}$.
$\text{frac}(x)$	Fractional part of $x \in \mathbb{R}$, defined as $x - \text{floor}(x)$.
$\Delta_{vs}(j\omega, \mathbf{Q})$	Value set $\{\Delta_{pb}(j\omega, \mathbf{q}) : \mathbf{q} \in \mathbf{Q}\}$ for $\omega \in \mathbb{R}$.
$\Delta_{pb}(s, \mathbf{q})$	Principal branch of $\Delta(s, \mathbf{q})$.
$\Re(z)$	Real part of the complex number $z \in \mathbb{C}$.
$\Im(z)$	Imaginary part of the complex number $z \in \mathbb{C}$.
C^*	Complex conjugate of the complex number C .

1 Introduction

With the emergence of fractional calculus, the use of noninteger-order differential operators has become increasingly prominent. Recent studies have demonstrated that fractional calculus provides powerful tools for modeling real-world systems—for example, viscoelastic materials [1] and biological processes [2]. In parallel, the application of fractional calculus in control theory has been extensively investigated due to its enhanced modeling flexibility and tuning capability. In practical applications, however, real-world systems inevitably contain uncertainties. One suitable way to incorporate such uncertainties is through *interval uncertainty structures*, where the system parameters are assumed to take values within known bounds [3, 4, 5]. Consequently, due to the unavoidable mismatch between identified models and actual processes, *robust stability analysis*—together with ensuring acceptable performance—becomes essential for the reliable operation of real-world systems [6, 7].

1.1 Motivations and Problem Formulations

In many real-world applications, the dynamics of physical systems cannot be fully captured by simple classical models due to complex behaviors such as memory effects, hereditary phenomena, or distributed-parameter characteristics. At the same time, the true parameters of these systems are rarely known with precision. Variations in operating conditions, unmodeled nonlinearities, sensor noise, and limitations in system identification inevitably introduce uncertainty into the estimated model. Consequently, the identified models obtained from experimental data often exhibit parameter variability that must be taken into account during controller design. These factors highlight the need for analytical tools that explicitly incorporate uncertainty within the modeling and control framework, with particular emphasis on ensuring robust stability under all admissible variations. To demonstrate the nature of this uncertainty, we consider the identified model of the TRAS laboratory system at TalTech University, represented as the interval plant

$$P(s) = \frac{k_1 s + k_0}{a_3 s^3 + a_2 s^2 + a_1 s - 1} e^{-\tau s}, \quad (1.1)$$

where the parameters $(k_1, k_0, a_3, a_2, a_1, \tau)$ vary from one identification experiment to another. The bounds used in (1.1) are not arbitrary; rather, they originate from repeated identification trials performed on the TRAS setup, where each iteration yields a slightly different set of parameter estimates due to sensor noise, measurement variability, nonlinear effects, and operating-condition fluctuations. Table 1.1 summarizes several such identification iterations, clearly showing how the estimated coefficients differ across experiments.

These variations highlight the inherent uncertainty in the modeling process: although the structure of the plant remains the same, its numerical parameters fluctuate within identifiable ranges. The interval representation in (1.1) provides a compact and mathematically tractable way to capture this aggregated uncertainty. By treating each parameter as lying within a bounded interval derived from the identification data, the model faithfully reflects the range of behaviors observed in the Twin Rotor Aerodynamic Systems (TRAS) and enables rigorous robustness analysis across all admissible realizations of the plant.

From the data in Table 1.1, the minimum and maximum values of each parameter can be extracted directly. These bounds are found to be

$$\begin{aligned} k_1 &\in [6.01, 7.95], & k_0 &\in [2.50, 3.68], \\ a_3 &\in [13.05, 14.82], & a_2 &\in [10.00, 10.94], \\ a_1 &\in [4.51, 5.87], & \tau &\in [0.102, 0.150]. \end{aligned}$$

Table 1.1: Identified parameters of the TRAS plant across multiple trials.

Trial	k_1	k_0	a_3	a_2	a_1	τ
1	7.95	3.68	14.82	10.94	5.87	0.149
2	6.08	2.53	13.14	10.02	4.62	0.102
3	7.42	3.29	14.11	10.47	5.35	0.138
4	6.77	2.88	13.63	10.19	4.94	0.122
5	7.88	3.61	14.73	10.91	5.71	0.150
6	6.34	2.75	13.41	10.11	4.78	0.116
7	7.21	3.12	14.02	10.39	5.19	0.131
8	6.01	2.50	13.05	10.00	4.51	0.108
9	7.69	3.49	14.58	10.76	5.48	0.142
10	6.93	3.04	13.78	10.26	5.07	0.125

Rounding these intervals to meaningful engineering bounds leads to the following interval model used throughout this chapter:

$$P(s) = \frac{[6, 8]s + [2.5, 3.7]}{[13, 15]s^3 + [10, 11]s^2 + [4.5, 6]s - 1} e^{-[0.10, 0.15]s}.$$

Such an interval plant highlights several challenges for robust control design. First, the controller must stabilize not just a single nominal plant, but *every* admissible realization within the interval family. This leads to a fundamentally more complex problem compared with nominal stability analysis. Second, the presence of a time delay—which itself is uncertain—further complicates the closed-loop stability conditions and often requires specialized techniques such as predictor-based control structures. Third, when several model coefficients vary within their respective uncertainty intervals, the resulting value set of the characteristic function in the complex plane is typically nonconvex and may exhibit irregular geometry, which makes determining its boundary analytically challenging. These issues motivate the development of rigorous problem statements and generalized robust stability criteria addressed in this thesis.

There are many papers have worked on robust stability analysis of FO closed-loop control systems. Several important studies have addressed this topic. For instance, some works have focused on the robust stability analysis of FO polynomials [8, 9], while others have investigated robust stability guarantees for time-delay FO systems with parametric uncertainties [10]–[16]. Hence, robust FO controllers achieving the specifications of H_∞ controllers for FO closed-loop control systems seems to be elusive in this literature [17, 18, 19, 20].

When industrial control problems are concerned, it is also universally acknowledged that a time delay—also referred to as transport delay and dead time in various studies—is a crucial parameter that must be thoroughly considered when modeling real-life systems [21]. Moreover, the time delay of the system may not be fixed, i.e., it can change during the operation of the real system deviating from a given nominal value. Therefore, one should consider the uncertainty in the time delay to ensure the validity of robust stability analysis of FO systems. Accordingly, the study of this problem has received considerable attention recently [3, 22]. Most of the recent studies are particularly concerned with the robust stability analysis of a closed-loop control system in terms of FO controllers and uncertain FO plants with an uncertain time delay. This problem has been treated using various approaches found in the existing literature. For instance, in [23]–[26], some numerical nonlinear optimization methods have been proposed to design FOPID controllers.



Figure 1.1: TRMS system.

However, the proposed methods cannot robustly stabilize the closed-loop control system in the face of plant uncertainties. In order to improve the robustness of FOPI controllers, a flat phase constraint has been satisfied for stable FOPTD systems in [27]. In addition, the studies [28]-[34] have proposed various methods to tune FOPD controllers and FOPID controllers for systems having time delay based on gain and phase margins. But, satisfying gain and phase margins may not be a reliable method for uncertain systems in general (see Example 2 in [35]). Also, the robust stability of uncertain FO plants with a time delay has been investigated using fractional controllers in [36, 37, 38, 39]. Also, the results reported in [36, 37, 38, 39] cannot be employed for systems having an uncertain delay term. In [41], an algorithm has been proposed to compute the stabilizing region of FOPID controllers for uncertain plants with an uncertain time delay. Furthermore, in [38], a design procedure has been presented for stable second order plus time delay systems using FOPID controllers. Theorem 3.1 in [40] and the obtained results in [41] turns out to be wrong in general for FO systems having an uncertain time delay (see the counterexample presented in [3]). Based on the above explanations, uncertainties in the numerator and denominator coefficients as well as in the time-delay term of the plant introduce significant challenges for robust stability analysis of the closed-loop control system. Consequently, the main control challenges in FO closed-loop control systems can be summarized as follows:

1. **Robust stability analysis of uncertain FO plants with uncertain time delay.** When both the coefficients of the transfer function and the time delay vary within interval bounds, the resulting uncertain characteristic function becomes highly complex. In interval time-delay systems, the uncertain parameters do not enter the characteristic equation linearly, and the delay term introduces transcendental dependencies. As a result, the value set of the characteristic function in the complex plane is generally non-convex, making its boundary extremely difficult to determine analytically.
2. **Lack of robust stability testing functions for uncertain FO delay systems.** A common strategy in robust stability analysis is to develop an appropriate stability testing function that guarantees stability for all admissible parameter variations. However,

to the best of the authors' knowledge, no such function currently exists in the literature for FO plants with simultaneous interval uncertainties and uncertain time delay.

3. **Computation of robust stabilizing regions for FO controllers.** Determining the robust stabilizing region of FOPID or other FO controllers for interval FO plants with interval time delay is a nontrivial problem. The combined effect of parameter uncertainties and delay variations leads to complicated stability boundaries, often non-convex and irregular, significantly increasing the difficulty of characterizing the admissible controller space.

In process control, the Smith predictor control structure is a well-known dead time compensator for stable processes with large time delay [42]. When the model is accurate, the closed-loop characteristic polynomial of the Smith predictor control structure will be delay free. But, in real applications, because of variation of the process parameters, the plant model cannot describe the dynamic behavior of the process accurately and this imposes robust stability analysis of the Smith predictor control structure [43]. Lately, FO controllers based on the Smith predictor structure have been applied to many engineering applications. In [44], a simple method has been presented to design internal model based FO Smith predictor control systems. In [45], a method has been proposed to tune the parameters of a filtered Smith predictor based fractional integral-fractional derivative controller by the small gain theorem. Various design methods of FO controllers such as FOPI and FOPID controllers have been given in [46]–[57]. Furthermore, to enhance the robustness of the system, various analyses have been proposed. For instance, the robustness analysis of FO controller combined with Smith predictor structure has been done in [59] in the case of the existence of time delay variations. Moreover, the flat phase property has been considered in [60] to design FOPI controllers for a large time-delay system. In [61], by benefiting from the direct synthesis, a method has been presented to design a FO controller for integer-order time delay systems in the Smith predictor structure. The methods proposed in [44]–[66] have failed to consider the effect of simultaneous uncertainties in gain, time-constants, and time delay on the robust stability of Smith predictor controllers. Accordingly, there is a need to present necessary and sufficient conditions for robust stability analysis of a FO control system in the presence of simultaneous uncertainties in the delay term, the model gain and coefficients. Hence, the open control challenges in Smith-predictor-based FO systems are as follows:

1. Finding necessary and sufficient conditions for robust stability analysis of a designed Smith predictor based FO control system having stable processes.
2. Finding necessary and sufficient conditions for robust stability analysis of a modified Smith predictor based FO control system having unstable processes.
3. The computation of the stabilizing region of FOPID controllers for the Smith predictor based control system having stable processes.
4. The computation of the stabilizing region of FOPID controllers for a modified Smith predictor based control system having unstable processes.

Most of the studies available today assume real coefficients in the description of the system with real uncertain parameters. But, in [67, 68, 69], it has been mentioned that the coefficients of LTI systems may be complex numbers, for example in aerospace applications. In [70, 71], PID controllers with complex coefficients have been designed for a

magnetically suspended rotor. Also, in [72, 73], some procedures have been presented to tune FO controllers for FO plants with complex coefficients. Moreover, in real world system, the analytical model of the plant dynamics may be influenced by uncertainties, which may be caused by modeling errors, nonlinearities, working conditions [74]. Accordingly, another challenge can be how to analyze the robust stability of FO closed-loop systems with complex uncertain parameters.

In summary, based on the above discussions, the main control problems in the literature can be formulated as follows:

1. **Robust stability analysis of uncertain FO plants with uncertain time delay.** When the numerator and denominator coefficients of the plant, together with the time-delay term, vary within interval bounds, the resulting characteristic function becomes highly complicated. In such interval time-delay systems, the uncertain parameters enter the characteristic equation nonlinearly and the delay term introduces transcendental dependencies. Consequently, the value set of the characteristic function in the complex plane becomes non-convex, making its boundary extremely difficult to determine analytically.
2. **Absence of robust stability testing functions for uncertain FO delay systems.** A standard strategy in robust stability analysis is to construct a stability testing function that guarantees stability for all admissible parameter variations. However, to the best of the authors' knowledge, no such robust stability testing function has been proposed in the literature for fractional-order plants with simultaneous interval uncertainties and uncertain time delay.
3. **Computation of robust stabilizing regions for FO controllers.** Determining the stabilizing region of FOPID or other FO controllers for interval FO plants with interval time delay is a highly nontrivial task. The combined effect of parameter uncertainties and delay variations leads to complex, frequently non-convex stability boundaries, which significantly complicates the characterization of admissible controller parameters.
4. **Robust stability of Smith-predictor-based FO control systems with stable processes.** Establishing necessary and sufficient conditions that guarantee the robust stability of Smith-predictor-based FO control schemes for stable plants under interval uncertainty and uncertain time delay remains a major problem.
5. **Robust stability of modified Smith-predictor-based FO control systems with unstable processes.** For unstable FO plants, deriving robust stability conditions for modified Smith predictor architectures under interval uncertainties and uncertain delay is even more challenging and has not been adequately addressed in existing research.
6. **Stabilizing region of FOPID controllers for Smith-predictor-based FO systems.** Computing the stabilizing region of FOPID controllers for FO plants operating under Smith predictor compensation is complicated by the interaction between model uncertainty, interval delay, and the predictor structure.
7. **Stabilizing region of FOPID controllers for modified Smith-predictor-based FO systems.** When modified Smith predictor structures are applied to unstable FO plants, the controller stabilizing region becomes significantly more complex, and no general analytical characterization exists in the literature.

8. **Robust stability of FO closed-loop systems with complex-valued uncertainties.** Fractional-order systems whose coefficients are complex-valued and uncertain introduce an additional layer of difficulty, as the characteristic equation becomes complex with multidimensional uncertainty, making robust stability verification particularly challenging.

It is also worth mentioning that the methodologies developed in this thesis are compatible with the FOMCON toolbox, a widely used MATLAB/Simulink framework for fractional-order modeling and control [76].

1.2 Contributions

This thesis addresses several significant challenges in the robust control of FO systems with uncertainties and time delays, which remain largely unsolved in the current literature. In particular, it develops novel FO controllers that achieve the H_∞ specifications, including robust stability, disturbance rejection and noise reduction. The work advances the robust stabilizability of FO plants with interval uncertainties in both system parameters and time delay, and proposes effective computational methods to determine stabilizing regions for FOPID controllers under these uncertainties. Furthermore, the thesis provides necessary and sufficient conditions for robust stability analysis of Smith predictor-based FO control systems, considering stable and unstable processes subject to simultaneous uncertainties in gains, time constants, and delay terms. In addition, it extends robust stability analysis techniques to FO systems with complex uncertain parameters, enhancing their applicability to advanced engineering domains. Finally, all developed methods are integrated into the widely used FOMCON MATLAB toolbox to facilitate practical implementation and validation. The key contributions of this thesis are summarized as follows:

1. A design methodology for robust FO controllers that satisfy key H_∞ control specifications for FO closed-loop systems.
2. A general framework for the robust stabilization of uncertain FO plants with interval uncertainties in coefficients and time delay, using arbitrary linear FO controllers.
3. A graphical and computational approach to determine stabilizing regions of FOPID controllers for interval FO plants with interval time delays.
4. Derivation of necessary and sufficient conditions for the robust stability of Smith predictor-based FO control systems with stable processes.
5. Derivation of necessary and sufficient conditions for the robust stability of modified Smith predictor-based FO control systems with unstable processes.
6. A novel method for the robust stability analysis of FO closed-loop systems with complex parametric uncertainties.
7. Practical implementation and integration of the proposed methods into the FOMCON MATLAB toolbox to support controller design and analysis.

1.3 Thesis Organization

The work of this thesis is presented in seven chapters, Chapters 1-7, and is finalized with some conclusions and final suggestions for future research, Chapter 7. In Chapter 2 we introduce the notation and some mathematical concepts that are at the basis of the results achieved in this thesis. Chapters 2-7 are the core of this thesis, whose contents can

be summarized as follows:

Chapter 2

In this chapter, an introduction to FO systems is first provided. Then, inspired by the work in [9], the robust stability analysis of FOIPs is discussed. A method is presented to compute the vertex polynomials of the value set associated with FOIPs. Furthermore, novel necessary and sufficient conditions are derived for the robust stability analysis of FOIPs. The chapter also demonstrates how the FOMCON toolbox can be employed to verify the robust stability of such systems. **The publications related to this chapter are VIII and IX.**

Chapter 3

This chapter investigates the robust stability of FO plants with interval uncertainties using FO controllers. Based on the zero-exclusion principle, novel necessary and sufficient conditions are first proposed for analyzing the robust stability of the associated characteristic polynomial. Subsequently, an auxiliary function is introduced to facilitate the verification of these stability criteria. An important advantage of the proposed method is the significant reduction in computational effort, as the vertex polynomials employed in the auxiliary function remain fixed for all positive frequencies. Finally, the effectiveness of the proposed approach is demonstrated through some numerical examples. **The publication related to this chapter is XVI.**

Chapter 4

This chapter investigates the robust stability of interval FO plants with interval time delays, controlled by a general class of FO controllers. Utilizing a straightforward graphical approach, novel necessary and sufficient criteria are developed for the robust stability analysis of such systems. Furthermore, the concept of the *robust stability testing function* is extended to facilitate robust stability assessment for the considered class of systems. Lower and upper frequency bounds are also established to support simulations and significantly reduce computational complexity. The effectiveness and applicability of the proposed methods are demonstrated through several illustrative examples. **The publications related to this chapter are I, II and X.**

Chapter 5

In recent studies, certain methods have inaccurately presented the computation of robust stability regions for FOPID controllers applied to interval FO plants with interval time delays. Motivated by the need for both accuracy and reliability—as well as the increasing significance and widespread adoption of FO controllers in control systems, owing to their enhanced flexibility in controller design—this chapter introduces a dependable and systematic procedure for determining the stabilizing region of FOPID controllers for such systems. An interval FO plant is defined by a FO transfer function whose numerator and denominator coefficients are uncertain but bounded within predefined intervals. Additionally, an interval time delay refers to a delay term whose value varies within a specified range. To facilitate a comprehensive robust stability analysis, two lemmas and two theorems are introduced in this chapter, forming the theoretical foundation of the proposed approach. Subsequently, a robust stabilization method is proposed for interval FO plants with interval time delays using FOPID controllers. To further enhance system performance, an auxiliary function is also introduced. The practicality and effectiveness of the proposed method are demonstrated through numerical simulations and experimental validation. **The publications related to this chapter are VI, VII, XI, XII, XIII and XV.**

Chapter 6

This chapter presents a novel methodology for analyzing the robust stability of FO control systems incorporating a Smith predictor structure. The study specifically addresses the presence of interval uncertainties in plant parameters, including the system gain, time constants, and time delay—common issues in practical modeling scenarios. The employed control architecture includes a FOPID controller, known for its superior tuning flexibility and enhanced performance characteristics in FO systems. The proposed approach leverages the value set concept and a graphical analysis framework to derive explicit necessary and sufficient conditions for robust stability. The key contributions of this chapter are twofold:

- Finding necessary and sufficient conditions for robust stability analysis of Smith predictor-based FO system in the presence of simultaneous parametric uncertainties.
- It introduces an auxiliary function—referred to as the robust stability testing function—which significantly simplifies the computational burden associated with stability verification.

To further enhance the controller's practical performance, an auxiliary function is proposed to support robust disturbance rejection. The validity and efficiency of the developed methodology are demonstrated through some numerical examples. **The publications related to this chapter are IV and V.**

Chapter 7

This chapter investigates the robust stability analysis of interval FO plants with complex uncertain parameters, using FO controllers. In these systems, the coefficients of both the numerator and the denominator are uncertain complex numbers that lie within specified intervals. A graphical approach is first developed to derive necessary and sufficient conditions for the robust stability of such systems. This method offers an intuitive and visual framework for assessing stability in the presence of complex uncertainties. Additionally, a robust stability testing function is proposed, based on simple geometric properties of convex polygons, to formally verify the graphical criteria. To further reduce the computational burden, an upper bound is introduced that simplifies the verification process without compromising accuracy. The proposed methods are illustrated through a numerical example, demonstrating their effectiveness in analyzing the robust stability of FO systems with interval uncertainties. **The publication related to this chapter is III.**

Chapter 8

In this chapter, several potential future research directions were proposed to further develop and extend the robust analysis and design methods for FO control systems.

2 Fractional-Order Interval Polynomials

FOIPs represent a critical area of study in control systems, combining the principles of fractional calculus with the challenges of interval uncertainty. This chapter begins by introducing the foundational concepts of fractional calculus, including FO systems and controllers, which are essential for understanding the behavior of FOIPs. It then explores the geometry of the value set of FOIPs, presenting two vertex computation methods to analyze their properties. The chapter culminates with a discussion on robust stability analysis, detailing theoretical conditions and practical tools, such as the FOMCON toolbox, for ensuring stability in the presence of uncertainties.

2.1 Fractional Calculus

Fractional calculus generalizes integration and differentiation to non-integer order operators. The fundamental operator is denoted as ${}_a\mathcal{D}_t^\alpha$, where:

- a and t denote the lower and upper limits of the operation,
- $\alpha \in \mathbb{R}$ represents the fractional order.

The operator is defined piecewise as:

$${}_a\mathcal{D}_t^\alpha = \begin{cases} \frac{d^\alpha}{dt^\alpha} & \Re(\alpha) > 0, \quad (\text{Differentiation}) \\ 1 & \Re(\alpha) = 0, \quad (\text{Identity}) \\ \int_a^t (d\tau)^{-\alpha} & \Re(\alpha) < 0, \quad (\text{Integration}) \end{cases} \quad (2.1)$$

where $\Re(\alpha)$ denotes the real part of α .

2.1.1 Fractional-Order Systems

A continuous-time dynamic system can be expressed as:

$$\sum_{k=0}^n a_k \mathcal{D}^{\alpha_k} y(t) = \sum_{k=0}^m b_k \mathcal{D}^{\beta_k} u(t), \quad (2.1)$$

where $(a_i, b_j) \in \mathbb{R}^2$, $(\alpha_i, \beta_j) \in \mathbb{R}_+^2$. For commensurate-order systems:

$$\sum_{k=0}^n a_k \mathcal{D}^{kq} y(t) = \sum_{k=0}^m b_k \mathcal{D}^{kq} u(t). \quad (2.2)$$

The Laplace transform yields:

$$G(s) = \frac{Y(s)}{U(s)} = \frac{\sum_{k=0}^m b_k s^{\beta_k}}{\sum_{k=0}^n a_k s^{\alpha_k}}. \quad (2.11)$$

A FO system is:

- *Commensurate-order* if all derivation orders α_k, β_k are integer multiples of a base order $q \in \mathbb{R}^+$:

$$\alpha_k = kq, \quad \beta_k = kq \quad \text{for } k \in \mathbb{Z}_{\geq 0}^{\leq n}$$

This leads to simplified representations like (2.2).

- *Non-commensurate-order* if no such q exists, requiring independent handling of each $\alpha_k, \beta_k \in \mathbb{R}^+$.

2.1.2 Fractional-Order Controllers

The FOPID controller, also known as the $PI^\lambda D^\mu$ controller, generalizes the classical PID controller by introducing fractional orders λ (integration) and μ (differentiation). Its transfer function is given by:

$$C(s) = K_p + \frac{K_i}{s^\lambda} + K_d s^\mu, \quad \lambda, \mu \in \mathbb{R}^+. \quad (2.12)$$

Key Features [78, 79]:

- **Enhanced Flexibility:** With two additional tuning parameters (λ and μ), FOPID controllers provide finer control over system dynamics compared to classical PID controllers.
- **Memory Effects:** The fractional operators enable modeling of system memory and hereditary properties, making them ideal for viscoelastic materials, thermal systems, and electrochemical processes.
- **Robustness:** Improved performance under parameter variations and external disturbances.

Controller Variants:

- FOPI: Obtained by setting $\mu = 0$:

$$C(s) = K_p + \frac{K_i}{s^\lambda}, \quad (2.3)$$

- FOPD: Obtained by setting $\lambda = 0$:

$$C(s) = K_p + K_d s^\mu. \quad (2.4)$$

FO controllers find widespread application across diverse engineering domains due to their enhanced control capabilities. In industrial control systems, they demonstrate superior performance in regulating temperature for chemical reactors [80], while in robotics, they enable precise trajectory tracking for manipulators [81]. The renewable energy sector benefits from their implementation in maximum power point tracking for solar arrays [82], and in biomedical engineering, they contribute to improved models for blood-glucose regulation systems [83].

Compared to classical PID controllers, FOPID controllers offer several distinct advantages: they more effectively handle systems with inherent FO dynamics, provide additional degrees of freedom through their tuning parameters (λ, μ) for meeting precise design specifications, exhibit enhanced robustness against system uncertainties, and demonstrate superior noise attenuation capabilities particularly in FOPI configurations. These characteristics make FOPID controllers particularly effective for complex processes exhibiting non-exponential relaxation or frequency-dependent behavior, as the additional tuning parameters allow for customized control solutions tailored to specific system requirements [84, 85, 86].

2.2 Geometry of Value Set of Fractional-Order Interval Polynomials

Consider the following FOIPs:

$$\Delta(s, \mathbf{q}) = \sum_{i=0}^n \mathbf{q}_i s^{\alpha_i} = \mathbf{q}_0 s^{\alpha_0} + \mathbf{q}_1 s^{\alpha_1} + \cdots + \mathbf{q}_n s^{\alpha_n}, \quad (2.5)$$

where $\alpha_i \in \mathbb{R}^+$ and the orders satisfy $0 = \alpha_0 < \alpha_1 < \alpha_2 < \dots < \alpha_n$. Assume that the coefficients \mathbf{q}_i for $i = 0, 1, \dots, n$ are interval coefficients, i.e., $\mathbf{q}_i \in [\mathbf{q}_i^-, \mathbf{q}_i^+]$, with the condition that $\mathbf{q}_n \neq 0$. Furthermore, the principal branch of the FO interval polynomials $\Delta(s)$ in (4.2) is defined as a single-valued function $\Delta_{pb}(s, \mathbf{q}) : \mathbb{C} \rightarrow \mathbb{C}$ such that

$$\Delta_{pb}(s, \mathbf{q}) = \begin{cases} \mathbf{q}_0 + \sum_{i=1}^n \mathbf{q}_i |s|^{\alpha_i} e^{j\alpha_i \arg(s)}, & \text{for } s \neq 0, \\ \mathbf{q}_0, & \text{for } s = 0. \end{cases} \quad (2.6)$$

In the following lemma, we present the core principles and key findings for determining the boundary of the value set of $\Delta_{pb}(s, \mathbf{q})$, namely $\Delta_{vs}(s, \mathbf{q})$.

Lemma 2.1. [9] Consider the set $M = M_0 + \sum_{r=1}^m q_r e^{j\pi\gamma_r}$ where M_0 can be a complex/real number, $q_r \in [q_r^-, q_r^+]$, $0 \leq \gamma_0 < \gamma_1 < \gamma_2 < \dots < \gamma_m < 1$. Then, the value set of M is a convex parpolygon in the complex plane with the following $2m$ consecutive vertices:

$$\begin{aligned} v_k &= \sum_{r=1}^{k-1} q_r^+ e^{j\pi\gamma_r} + \sum_{r=k}^m q_r^- e^{j\pi\gamma_r} + M_0, \\ v_{k+m} &= \sum_{r=1}^{k-1} q_r^- e^{j\pi\gamma_r} + \sum_{r=k}^m q_r^+ e^{j\pi\gamma_r} + M_0, \quad k = 1, \dots, m. \end{aligned} \quad (2.7)$$

This lemma establishes that the value set of $\Delta_{pb}(s, \mathbf{q})$ in (4.2) forms a convex polygon in the complex plane. To verify this, consider the interval FO polynomial given in (4.3).

$$\Delta(s, \mathbf{q}) = [6, 8] + [1, 1.5]s^{0.8} + [3, 4]s^{1.2} + [1, 2]s^{2.2}. \quad (2.8)$$

Figure 2.1 shows the value set of $\Delta_{pb}(j\omega, \mathbf{q})$ plotted at $\omega = 1$ rad/sec. As observed, the boundary of the value set forms a convex shape in the complex plane. The methods pro-

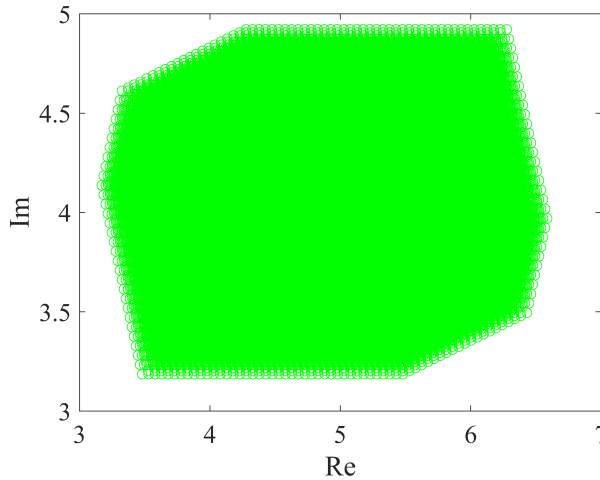


Figure 2.1: $\Delta_{vs}(j\omega, \mathbf{q})$ in (4.3) at $\omega = 1$ rad/sec.

posed in [8, 9] are now presented for computing the vertices and boundary of the value set of $\Delta_{pb}(j\omega, \mathbf{q})$ at a specified frequency.

2.2.1 Approach 1: Vertex Computation Method [8]

In [8], it is proposed that the value set of $\Delta_{pb}(s, \mathbf{q})$ consists of 2^{n+1} vertices and $(n+1)2^n$ exposed edges, corresponding to the $n+1$ uncertain parameters. By leveraging the upper and lower bounds of these parameters, all 2^{n+1} vertex polynomials of $\Delta(s, q)$ can be expressed as:

$$\begin{cases} V_{pb}^1(s) = \underline{\mathbf{q}}_0 + \underline{\mathbf{q}}_1 s^{\alpha_1} + \underline{\mathbf{q}}_2 s^{\alpha_2} + \cdots + \underline{\mathbf{q}}_n s^{\alpha_n}, \\ V_{pb}^2(s) = \bar{\mathbf{q}}_0 + \underline{\mathbf{q}}_1 s^{\alpha_1} + \underline{\mathbf{q}}_2 s^{\alpha_2} + \cdots + \underline{\mathbf{q}}_n s^{\alpha_n}, \\ V_{pb}^3(s) = \underline{\mathbf{q}}_0 + \bar{\mathbf{q}}_1 s^{\alpha_1} + \underline{\mathbf{q}}_2 s^{\alpha_2} + \cdots + \underline{\mathbf{q}}_n s^{\alpha_n}, \\ \vdots \\ V_{pb}^{2^{n+1}}(s) = \bar{\mathbf{q}}_0 + \bar{\mathbf{q}}_1 s^{\alpha_1} + \bar{\mathbf{q}}_2 s^{\alpha_2} + \cdots + \bar{\mathbf{q}}_n s^{\alpha_n}. \end{cases} \quad (2.9)$$

For simplicity, we assume that $V_i(s) = V_{pb}^i(s)$. The exposed edges can then be derived from these vertex polynomials in (6.47). For instance, the vertex polynomials $V_1(s)$ and $V_2(s)$ share the same structure, except that the parameter $\underline{\mathbf{q}}_0$ takes its lower bound in $V_1(s)$ and its upper bound in $V_2(s)$. Similarly, the remaining exposed edges can be constructed. Define the set containing all the exposed edges of (4.3) as follows:

$$P_E(s) = \{e(V_1(s), V_2(s)), e(V_1(s), V_3(s)), \dots, e(V_{2^{n+1}-1}(s), V_{2^{n+1}}(s))\}. \quad (2.10)$$

For example, consider the interval fractional order polynomial $\Delta(s, \mathbf{q})$ in (4.3). Based on the above discussion, the vertices and exposed edges of $\Delta(s, \mathbf{q})$ in (4.3) are as follows:

$$\begin{cases} V_1(s) = 6 + s^{0.8} + 3s^{1.2} + s^{2.2}, \\ V_2(s) = 8 + s^{0.8} + 3s^{1.2} + s^{2.2}, \\ V_3(s) = 6 + 1.5s^{0.8} + 3s^{1.2} + s^{2.2}, \\ V_4(s) = 8 + 1.5s^{0.8} + 3s^{1.2} + s^{2.2}, \\ V_5(s) = 6 + s^{0.8} + 4s^{1.2} + s^{2.2}, \\ V_6(s) = 8 + s^{0.8} + 4s^{1.2} + s^{2.2}, \\ V_7(s) = 6 + 1.5s^{0.8} + 4s^{1.2} + s^{2.2}, \\ V_8(s) = 8 + 1.5s^{0.8} + 4s^{1.2} + s^{2.2}, \\ V_9(s) = 6 + s^{0.8} + 3s^{1.2} + 2s^{2.2}, \\ V_{10}(s) = 8 + s^{0.8} + 3s^{1.2} + 2s^{2.2}, \\ V_{11}(s) = 6 + 1.5s^{0.8} + 3s^{1.2} + 2s^{2.2}, \\ V_{12}(s) = 8 + 1.5s^{0.8} + 3s^{1.2} + 2s^{2.2}, \\ V_{13}(s) = 6 + s^{0.8} + 4s^{1.2} + 2s^{2.2}, \\ V_{14}(s) = 8 + s^{0.8} + 4s^{1.2} + 2s^{2.2}, \\ V_{15}(s) = 6 + 1.5s^{0.8} + 4s^{1.2} + 2s^{2.2}, \\ V_{16}(s) = 8 + 1.5s^{0.8} + 4s^{1.2} + 2s^{2.2}, \end{cases} \quad (2.11)$$

$$\begin{aligned} P_E(s) = & \{e(V_1(s), V_2(s)), e(V_1(s), V_3(s)), e(V_1(s), V_5(s)), e(V_1(s), V_9(s)), \\ & e(V_2(s), V_4(s)), e(V_2(s), V_6(s)), e(V_2(s), V_{10}(s)), e(V_3(s), V_4(s)), e(V_3(s), V_7(s)), \\ & e(V_3(s), V_{11}(s)), e(V_4(s), V_8(s)), e(V_4(s), V_{12}(s)), e(V_5(s), V_6(s)), e(V_5(s), V_7(s)), \\ & e(V_5(s), V_{13}(s)), e(V_6(s), V_8(s)), e(V_6(s), V_{14}(s)), e(V_7(s), V_8(s)), e(V_7(s), V_{15}(s)), \\ & e(V_8(s), V_{16}(s)), e(V_9(s), V_{10}(s)), e(V_9(s), V_{11}(s)), e(V_9(s), V_{13}(s)), \\ & e(V_{10}(s), V_{12}(s)), e(V_{10}(s), V_{14}(s)), e(V_{11}(s), V_{12}(s)), e(V_{11}(s), V_{15}(s)), \\ & e(V_{12}(s), V_{16}(s)), e(V_{13}(s), V_{14}(s)), e(V_{13}(s), V_{15}(s)), e(V_{14}(s), V_{16}(s)), \\ & e(V_{15}(s), V_{16}(s))\}. \end{aligned} \quad (2.12)$$

Figure 2.2 illustrates the vertices $V_i(s)$, $i = 1, 2, \dots, 16$ in (6.9) along with the exposed edges $P_E(s)$ in (6.10). As observed in the figure, $\partial(\Delta_{vs}(j\omega, q)) \subseteq P_E(s)$. This implies that the boundary of the value set of $\Delta(s, q)$ in (4.3) can be effectively determined by $P_E(s)$ in (6.10).

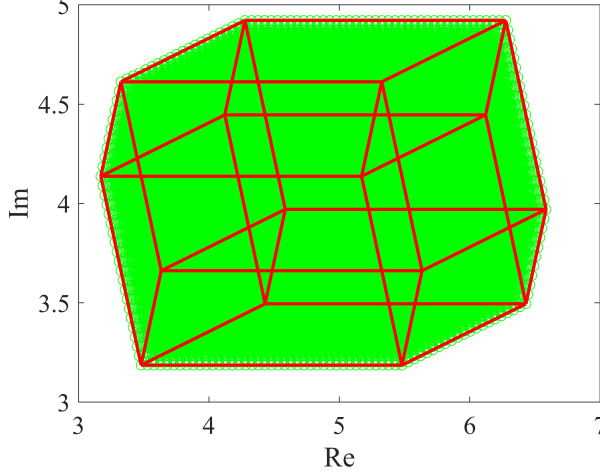


Figure 2.2: Value set of $\Delta(j\omega, \mathbf{q})$ in (4.3) (green) and its boundary (red) at $\omega = 1$ rad/sec.

2.2.2 Approach 2: Vertex Computation Method [9]

Let $\Delta(s, \mathbf{q})$ represent a family of interval FO polynomials as defined in (4.2), where $0 = \alpha_0 < \alpha_1 < \alpha_2 < \dots < \alpha_n$ and $\mathbf{q}_i \leq \bar{\mathbf{q}}_i$. Assume that $H_0 = \{i : \mathbf{q}_i < \bar{\mathbf{q}}_i\}$ and $H_0 \neq \emptyset$. For $\omega = 0$, $\Delta_{vs}(j0, \mathbf{q})$ is equal to $[\mathbf{q}_0, \bar{\mathbf{q}}_0]$. For $\omega > 0$, define $\beta_0 = \{\text{frac}(0.5\alpha_i) : i \in H_0\}$. Also, assume that the distinct numbers of the set β_0 is m and sorted as $0 \leq \beta_1 < \beta_2 < \dots < \beta_m$. Now, define the following sets:

$$H_b = \{i \in H_0 : \text{floor}(0.5\alpha_i) \text{ is an even number and } \text{frac}(0.5\alpha_i) = \beta_b\},$$

$$H'_b = \{i \in H_0 : \text{floor}(0.5\alpha_i) \text{ is an odd number and } \text{frac}(0.5\alpha_i) = \beta_b\},$$

$$b = 1, 2, 3, \dots, m.$$

and the following vectors for $k = 1, 2, \dots, m$ and $i = 0, 1, \dots, n$:

$$\mathbf{q}^k = [\mathbf{q}_0^k \mathbf{q}_1^k \dots \mathbf{q}_n^k], \bar{\mathbf{q}} = [\bar{\mathbf{q}}_0 \bar{\mathbf{q}}_1 \dots \bar{\mathbf{q}}_n], \underline{\mathbf{q}} = [\mathbf{q}_0 \mathbf{q}_1 \dots \mathbf{q}_n]$$

$$\mathbf{q}^{m+k} = [\mathbf{q}_0^{m+k} \mathbf{q}_1^{m+k} \dots \mathbf{q}_n^{m+k}] = \bar{\mathbf{q}} + \underline{\mathbf{q}} - \mathbf{q}^k,$$

$$\mathbf{q}_i^k = \begin{cases} \bar{\mathbf{q}}_i, & \text{if } i \in \left(\bigcup_{b=1}^{k-1} H_b\right) \cup \left(\bigcup_{b=k}^m H'_b\right), \\ \underline{\mathbf{q}}_i, & \text{if otherwise.} \end{cases}$$

$$\mathbf{q}_i^{m+k} = \bar{\mathbf{q}} + \underline{\mathbf{q}} - \mathbf{q}_i^k.$$

The consecutive vertices $V_k(j\omega)$, $k = 1, 2, \dots, 2m$, are defined as follows:

$$V_k(j\omega) = \Delta_{pb}(j\omega, \mathbf{q}^k). \quad (2.13)$$

$$V_{m+k}(j\omega) = \Delta_{pb}(j\omega, \mathbf{q}^{m+k}). \quad (2.14)$$

According to the vertices $V_r(s), r = 1, \dots, 2m$, the boundary of $\Delta_{vs}(s, \mathbf{q})$ can be determined by $P_E(s)$ in (6.11).

$$P_E(s) = \left\{ e(V_1(s), V_2(s)), e(V_2(s), V_3(s)), \dots, e(V_{2m-1}(s), V_{2m}(s)), e(V_{2m}(s), V_1(s)) \right\}. \quad (2.15)$$

Next, we calculate the vertices and exposed edges of $\Delta(s, \mathbf{q})$ in (4.3) using the proposed approach. The results can be easily obtained as follows:

$$\begin{aligned} H_0 &= \{0, 1, 2, 3\}, \quad \beta_0 = \{0, 0.1, 0.4, 0.6\}, \quad m = 4, \quad \beta_0 = 0, \beta_1 = 0.1, \\ \beta_2 &= 0.4, \beta_3 = 0.6, H_1 = \{0\}, H'_2 = \{3\}, \\ H_3 &= \{1\}, H_4 = \{2\}, H'_1 = H_2 = H'_3 = H'_4 = \emptyset, \\ \mathbf{q}^1 &= [6 \ 1 \ 3 \ 2]^T, \mathbf{q}^2 = [8 \ 1 \ 3 \ 2]^T, \mathbf{q}^3 = [8 \ 1 \ 3 \ 1]^T, \mathbf{q}^4 = [8 \ 1.5 \ 3 \ 1]^T, \\ \mathbf{q}^5 &= [8 \ 1.5 \ 4 \ 1]^T, \mathbf{q}^6 = [6 \ 1.5 \ 4 \ 1]^T, \mathbf{q}^7 = [6 \ 1.5 \ 4 \ 2]^T, \mathbf{q}^8 = [6 \ 1 \ 4 \ 2]^T. \end{aligned} \quad (2.16)$$

$$\left\{ \begin{array}{l} V_1(s) = 6 + s^{0.8} + 3s^{1.2} + 2s^{2.2}, \\ V_2(s) = 8 + s^{0.8} + 3s^{1.2} + 2s^{2.2}, \\ V_3(s) = 8 + s^{0.8} + 3s^{1.2} + s^{2.2}, \\ V_4(s) = 8 + 1.5s^{0.8} + 3s^{1.2} + s^{2.2}, \\ V_5(s) = 8 + 1.5s^{0.8} + 4s^{1.2} + s^{2.2}, \\ V_6(s) = 6 + 1.5s^{0.8} + 4s^{1.2} + s^{2.2}, \\ V_7(s) = 6 + s^{0.8} + 4s^{1.2} + 2s^{2.2}, \\ V_8(s) = 6 + s^{0.8} + 4s^{1.2} + 2s^{2.2}. \end{array} \right. \quad (2.17)$$

$$P_E(s) = \left\{ e(V_1(s), V_2(s)), e(V_2(s), V_3(s)), e(V_3(s), V_4(s)), e(V_4(s), V_5(s)), e(V_5(s), V_6(s)), e(V_6(s), V_7(s)), e(V_7(s), V_8(s)), e(V_8(s), V_1(s)) \right\}. \quad (2.18)$$

Figure 2.3 depicts the exact outer vertices and the outer boundary of the value set.

Remark 2.1. From the example of $\Delta_{pb}(s, \mathbf{q})$ in (4.3), it is shown that using **Approach 1** requires 2^4 vertices and 4×2^3 edges to describe the boundary of the value set $\Delta_{pb}(s, \mathbf{q})$ at each frequency. In contrast to Approach 1, which involves redundant computations, **Approach 2** focuses only on the critical elements of the value set boundary, requiring just 2×4 vertices and edges to determine $\partial(\Delta_{vs}(j\omega, \mathbf{q}))$. This significantly reduces computational complexity while still providing an accurate and explicit representation of the boundary. Such efficiency is particularly advantageous for robust stability analysis, where precisely characterizing the value set boundary is crucial for verifying the zero-exclusion condition. By directly addressing the geometric structure of the value set and offering an exact description of its vertices and edges, Approach 2 provides a practical and scalable framework for analyzing systems with large uncertainty regions. Therefore, in the remainder of this thesis, **Approach 2** is employed to compute the vertices and exposed edges of $\partial(\Delta_{vs}(j\omega, \mathbf{q}))$ for robust stability analysis, ensuring both computational efficiency and accuracy.

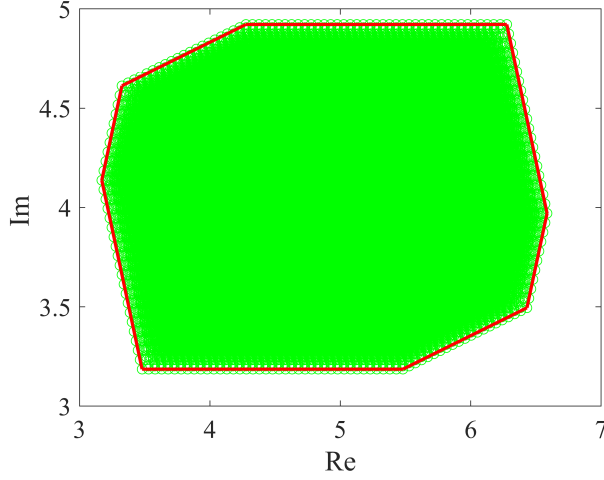


Figure 2.3: Value set of $\Delta(j\omega, \mathbf{q})$ in (4.3) (green) and its boundary (red) at $\omega = 1$ rad/sec.

2.3 Robust Stability Analysis of Fractional-Order Interval Polynomials

This subsection focuses on the robust stability analysis of FOIPs, a critical component for ensuring robust stability under parametric uncertainty. Subsection 2.3 introduces the theoretical foundations, outlining necessary and sufficient conditions for robust stability, including mathematical criteria and boundary constraints that FOIPs must satisfy. Subsection 2.4 transitions to practical aspects, demonstrating how the FOMCON toolbox can be used to conduct robust stability analysis through computational techniques and graphical visualization. Together, these subsubsections form a cohesive framework that connects theory with practice, offering a comprehensive methodology for analyzing and validating the robust stability of FOIPs in real-world applications. In this subsection, we will discuss the robust stability of a FO interval system whose characteristic polynomials are as follows.

$$\Delta(s, \mathbf{q}) = \mathbf{q}_0 s^{\alpha_0} + \mathbf{q}_1 s^{\alpha_1} + \cdots + \mathbf{q}_n s^{\alpha_n}. \quad (2.19)$$

where $\alpha_i \in \mathbb{R}^+$ and $\alpha_0 = 0 < \alpha_1 < \alpha_2 < \cdots < \alpha_n$. Supposing that $\mathbf{q}_i, i = 0, 1, \dots, n$ are the interval coefficients as $\mathbf{q}_i \in [\underline{\mathbf{q}}_i, \bar{\mathbf{q}}_i]$ and $\mathbf{q}_n \neq 0$.

Now, the following definitions are introduced for the rest of the chapter.

Definition 2.1. The principal branch of FO interval polynomials $\Delta(s)$ in (4.2) is defined as a single-valued function $\Delta_{pb}(s, \mathbf{q}) : \mathbb{C} \rightarrow \mathbb{C}$ such that

$$\Delta_{pb}(s, \mathbf{q}) = \begin{cases} \mathbf{q}_0 + \sum_{r=1}^n \mathbf{q}_r |s|^{\alpha_r} e^{j\alpha_r \arg(s)}, & \text{for } s \neq 0, \\ \mathbf{q}_0, & \text{for } s = 0. \end{cases} \quad (2.20)$$

Definition 2.2. Based on [87], a FO system is stable if and only if the principal branch of the characteristic function of the system has no zero in the closed right-half plane. Therefore, a FO system with the FO interval polynomials $\Delta(s, \mathbf{q})$ in (4.2) is robust stable if and only if all members of $\Delta(s)$ have no zero in the closed right-half plane.

Zero Exclusion Condition Theorem [10]: $\Delta(s, \mathbf{q})$ in (4.2) is robust stable if and only if $\Delta(s, \mathbf{q})$ contains at least one stable polynomial and $0 \notin \Delta(s, \mathbf{q})$ for $\omega \in [0, +\infty)$. According to this theorem, stability of one member of the family $\Delta(s, \mathbf{q})$ in (4.2) as $\delta(s)$ must be checked. So, the following lemma should be used for stability analysis.

Lemma 2.2. [88] (**Mikhailov stability criterion**) The FO polynomial $\delta(s) = \hat{\mathbf{q}}_0 + \hat{\mathbf{q}}_1 s^{\alpha_1} + \dots + \hat{\mathbf{q}}_n s^{\alpha_n}$ (of commensurate or non-commensurate type) is stable if and only if

$$\Delta \arg \psi(j\omega) = \frac{\delta(j\omega)}{\hat{\mathbf{q}}_n(j\omega + c)^{\alpha_n}} = 0, -\infty < \omega < \infty, c \in \mathbb{R}^+. \quad (2.21)$$

Lemma 2.2 implies that $\delta(s)$ is stable if and only if $\psi(j\omega)$ does not encircle the origin of the complex plane as ω traverses from $-\infty$ to $+\infty$.

Now, to derive the necessary and sufficient robust conditions of the FO interval system, the value set of $\Delta(s, \mathbf{q})$ in (4.2) must be checked. Just we need to investigate the zero exclusion condition $0 \notin \Delta(j\omega, \mathbf{q})$ and $\omega \geq 0$. Now, we should also use the following lemma which is valuable for simulation purposes.

Lemma 2.3. [9] All zeros of $\Delta(s, \mathbf{q})$ in (4.2) lie in the set $\{s \in \mathbb{C} : |s| \leq S_{\max}\}$ where S_{\max} is defined as follows.

$$S_{\max} = \max\left\{1, \left(\frac{\sum_{i=0}^{n-1} \max\{|\underline{q}_i|, |\bar{q}_i|\}}{\min\{|\underline{q}_n|, |\bar{q}_n|\}}\right)^{\frac{1}{\alpha_n - \alpha_{n-1}}}\right\}.$$

So, based on this lemma, the condition $0 \in \Delta(s, \mathbf{q})$ is only checked for the frequencies lying in the interval $[0, S_{\max}]$. According to the zero-exclusion principle and Lemma 2.3, it is necessary to examine the relationship between the origin and the value set. To this end, the following theorem—referred to as the **Value Sets Overlap Theorem**—explicitly addresses the condition $0 \in \Delta^{vs}(j\omega)$.

Value Sets Overlap Theorem: Assume that $\Delta(s, \mathbf{q})$ can be written as $\Delta(s, \mathbf{q}) = \Delta^1(s, \mathbf{q}^1) + \Delta^2(s, \mathbf{q}^2)$. Then, at a given frequency $\omega = \omega_0$, $0 \in \Delta(j\omega_0, \mathbf{q})$ if and only if the value sets of $\Delta^1(j\omega_0, \mathbf{q}^1)$ and $-\Delta^2(j\omega_0, \mathbf{q}^2)$ have an overlap.

$0 \in \Delta^{vs}(j\omega) \iff -\Delta_1^{vs}(s = j\omega_0)$ and $\Delta_2^{vs}(s = j\omega_0)$ have an overlap in the complex plane.

Proof. *Proof of necessity:* If $0 \in \Delta^{vs}(j\omega_0)$, we can express this as $\{z_0 - z_0\} \in \Delta^{vs}(j\omega_0)$. Consequently, there exists $z_0 \in \mathbb{C}$ such that:

$$z_0 \in -\Delta_1^{vs}(j\omega_0) \quad \text{and} \quad z_0 \in \Delta_2^{vs}(j\omega_0)$$

This establishes that $-\Delta_1^{vs}(j\omega_0)$ and $\Delta_2^{vs}(j\omega_0)$ must overlap.

Proof of sufficiency: Given the overlap between $-\Delta_1^{vs}(j\omega_0)$ and $\Delta_2^{vs}(j\omega_0)$, there exists $z_0 \in \mathbb{C}$ satisfying:

$$z_0 \in -\Delta_1^{vs}(j\omega_0) \quad \text{and} \quad z_0 \in \Delta_2^{vs}(j\omega_0)$$

Thus, we can identify:

$$z_0 = -\tilde{\Delta}_1(j\omega_0) \quad \text{and} \quad z_0 = \tilde{\Delta}_2(j\omega_0)$$

for some $\tilde{\Delta}_1(j\omega_0) \in \Delta_1^{vs}(j\omega_0)$ and $\tilde{\Delta}_2(j\omega_0) \in \Delta_2^{vs}(j\omega_0)$.

Consider $\tilde{\Delta}(j\omega) = \tilde{\Delta}_1(j\omega) + \tilde{\Delta}_2(j\omega) \in \Delta(j\omega)$. At $\omega = \omega_0$, we have:

$$\tilde{\Delta}(j\omega_0) = \tilde{\Delta}_1(j\omega_0) + \tilde{\Delta}_2(j\omega_0) = -z_0 + z_0 = 0$$

which proves $0 \in \Delta^{vs}(j\omega)$. □

Now, we derive necessary and sufficient conditions for robust stability analysis of the FO

interval polynomial $\Delta(s, \mathbf{q})$ in (4.2). Due to the programming purposes, a robust stability testing function should be constructed to check the zero exclusion condition easier. Indeed, by this auxiliary function, it can be derived if the boundary of the value set of $\Delta(j\omega, \mathbf{q})$ touches the origin in the complex. The auxiliary function introduced in the next lemma, is constructed by a few members of the uncertainty space of $\Delta(s, \mathbf{q})$ i.e., vertex polynomials for the robust stability assessment of both FO interval polynomials of commensurate and non-commensurate.

Lemma 2.4. *The FO polynomial $\Delta(s, \mathbf{q})$ in (4.2) is robustly stable if and only if:*

- *one member of the FO interval polynomial is stable.*
- *the inequality $\Lambda_1(\omega) > 0$ holds for $\omega \in [0, S_{\max}]$.*

$$\begin{aligned}\Lambda_1(\omega) &= \min\{\lambda_r(\omega) : r = 1, 2, \dots, 2m, V_{2m+1}(j\omega) = V_1(j\omega)\}, \\ \lambda_r(\omega) &= |V_r(j\omega)| + |V_{r+1}(j\omega)| - |V_r(j\omega) - V_{r+1}(j\omega)|.\end{aligned}\quad (2.22)$$

Proof. According to the zero exclusion condition theorem and Lemma 2.3, we show that if $\Lambda_1(\omega) > 0$ holds then the origin does not intersect the boundary of $\Delta(s, \mathbf{q})$ for all frequencies lying in $[0, S_{\max}]$. Indeed, the sufficient conditions can be simply proved by the triangle inequality. So, the necessary condition is only discussed in the following. As a contradiction argument, it is supposed that $\Lambda_1(\omega) > 0$ does not hold at a given frequency $\omega = \omega_0$ i.e., $\Lambda_1(\omega) = 0$. This means that there are at least one $\lambda_x(\omega_0)$, $x \in \{1, \dots, 2m\}$ such that

$$\begin{aligned}|V_x(j\omega)| + |V_{x+1}(j\omega)| - |V_x(j\omega) - V_{x+1}(j\omega)| &= 0, \implies \\ |V_x(j\omega)| |V_{x+1}(j\omega)| + \Re(V_x(j\omega)V_{x+1}^*(j\omega)) &= 0\end{aligned}\quad (2.23)$$

From (6.10), it is visible that $V_x(j\omega_0)V_{x+1}^*(j\omega_0) \in \mathbb{R}^{\leq 0}$. Therefore, we only need to show that $V_x(j\omega_0)V_{x+1}^*(j\omega_0) \in \mathbb{R}^{\leq 0}$ leads to $0 \in \lambda V_x(j\omega_0) + (1 - \lambda)V_{x+1}(j\omega_0)$ and consequently $0 \in \partial(\Delta(j\omega, \mathbf{q}))$ ($\partial(\cdot)$ shows the boundary of a value set.). Therefore, we have

$$\begin{aligned}\lambda V_x(j\omega_0) + (1 - \lambda)V_{x+1}(j\omega_0) &= 0 \implies \\ \lambda V_x(j\omega_0)V_{x+1}^*(j\omega_0) + (1 - \lambda)|V_{x+1}(j\omega_0)|^2 &= 0\end{aligned}\quad (2.24)$$

From (6.12), one can simply deduce $V_x(j\omega_0)V_{x+1}^*(j\omega_0) \in \mathbb{R}^{\leq 0}$. This implies $0 \in \partial(\Delta(j\omega, \mathbf{q}))$ and consequently $0 \in \Delta(j\omega_0, \mathbf{q})$. This contradicts the zero exclusion condition and the proof is completed. \square

Now, we take another approach to derive robust stability analysis. Indeed, $\Delta(s, \mathbf{q})$ in (4.2) can be rewritten as $\Delta(s, \mathbf{q}) = \Delta^1(s, \mathbf{q}^1) + \Delta^2(s, \mathbf{q}^2)$. For example, $\Delta(s, \mathbf{q}) = [1, 2]s^{1+\sqrt{5}} + [-1, 1]s^{\sqrt{5}} + [2, 4]s + [0.3, 1]$ can be written as $\Delta(s, \mathbf{q}) = \Delta^1(s, \mathbf{q}^1) + \Delta^2(s, \mathbf{q}^2)$ where $\Delta^1(s, \mathbf{q}^1) = [1, 2]s^{1+\sqrt{5}} + [-1, 1]s^{\sqrt{5}}$ and $\Delta^2(s, \mathbf{q}^2) = [2, 4]s + [0.3, 1]$ or $\Delta^1(s, \mathbf{q}^1) = [1, 2]s^{1+\sqrt{5}}$ and $\Delta^2(s, \mathbf{q}^2) = [-1, 1]s^{\sqrt{5}} + [2, 4]s + [0.3, 1]$ and so on. Now, the next lemma presents necessary and sufficient conditions for robust stability assessment of $\Delta(s, \mathbf{q})$ in (4.2).

Lemma 2.5. *The FO polynomial $\Delta(s, \mathbf{q})$ in (4.2) is robust stable if and only if:*

- *one member of the FO interval polynomial is stable.*
- *the value sets of $\Delta^1(s, \mathbf{q}^1)$ and $-\Delta^2(s, \mathbf{q}^2)$ do not have any overlap for $s = j\omega$ and $\omega \in [0, S_{\max}]$.*

Proof. The proof is directly from the value sets overlap theorem and the zero exclusion condition theorem. \square

Lemma 2.5 gives us a way to present another robust stability testing function in the following lemma.

Lemma 2.6. *The FO polynomial $\Delta(s, \mathbf{q})$ in (4.2) is robustly stable if and only if:*

- *one member of the FO interval polynomial is stable.*
- *the inequality $\Lambda_2(\omega) > 0$ holds for $\omega \in [0, S_{\max}]$.*

$$\begin{aligned}
\Lambda_2(\omega) &= \min\{\lambda_r^2(\omega) : r = 1, 2\}, \\
\lambda_1^2(\omega) &= \min\{\hat{\lambda}_{r_1, r_2}^2(\omega) : r_1 = 1, \dots, 2m_1, r_2 = 1, \dots, 2m_2\}, \\
\hat{\lambda}_{r_1, r_2}^2(\omega) &= |V_{r_1}^1(j\omega) + V_{r_2}^2(j\omega)| + \\
&\quad |V_{r_1+1}^1(j\omega) + V_{r_2}^2(j\omega)| - |V_{r_1}^1(j\omega) - V_{r_1+1}^1(j\omega)|, \\
\lambda_2^2(\omega) &= \min\{\hat{\lambda}_{r_1, r_2}^2(\omega) : r_1 = 1, \dots, 2m_1, r_2 = 1, \dots, 2m_2\}, \\
\hat{\lambda}_{r_1, r_2}^2(\omega) &= |V_{r_1}^1(j\omega) + V_{r_2}^2(j\omega)| + \\
&\quad |V_{r_1}^1(j\omega) + V_{r_2+1}^2(j\omega)| - |V_{r_2}^2(j\omega) - V_{r_2+1}^2(j\omega)|,
\end{aligned} \tag{2.25}$$

where $V_{i_1}^1(j\omega), i_1 = 1, \dots, 2m_1$ and $V_{i_2}^2(j\omega), i_2 = 1, \dots, 2m_2$ show the vertices of the value set of $\Delta^1(s, \mathbf{q}^1)$ and $-\Delta^2(s, \mathbf{q}^2)$ calculated by Procedure 1. Moreover, $V_{2m_1+1}^1(j\omega) = V_1^1(j\omega)$ and $V_{2m_2+1}^2(j\omega) = V_1^2(j\omega)$.

Proof. We show that if $\Lambda_2(\omega) > 0$ holds then the statements of Lemma 2.5 are satisfied. According to Lemma 2.4, $\hat{\lambda}_{r_1, r_2}^2(\omega) > 0$ implies that the vertices $-V_{i_2}^2(j\omega), i_2 = 1, \dots, 2m_2$ do not intersect the value set of $\Delta^1(s, \mathbf{q}^1)$. In the same way, $\hat{\lambda}_{r_1, r_2}^2(\omega) > 0$ assures that the vertices $V_{i_1}^1(j\omega), i_1 = 1, \dots, 2m_1$ do not intersect $-\Delta^2(s, \mathbf{q}^2)$. This means that convex polygons $\Delta^1(s, \mathbf{q}^1)$ and $-\Delta^2(s, \mathbf{q}^2)$ have no overlap for $\omega \in [0, S_{\max}]$ and based on Lemma 2.5, the robust stability is guaranteed. \square

Remark 2.2. *In Lemmas 2.4-2.6, various necessary and sufficient conditions have been presented to inspect the robust stability of FO interval polynomials $\Delta(s, \mathbf{q})$. All the results of the aforementioned lemmas are applicable to both FO interval polynomials of commensurate and non-commensurate. Moreover, in Lemma 2.5, a graphical method has been proposed which may be arduous. So, we should use the auxiliary functions obtained in Lemma 2.4 and Lemma 2.6. Also, one can check the stability of a chosen member of $\Delta(s, \mathbf{q})$ by Lemma 2.2 as a suggestion.*

2.4 Robust Stability Analysis in FOMCON Toolbox

In the following section, a possible software implementation of the above items is presented. The implementation is a new development for the popular FOMCON toolbox for MATLAB. The toolbox is currently one of the most popular toolboxes for FO modeling and control, and the present contribution serves as the foundation for further development of a framework for studying systems with interval uncertainties, including integer-order and FO models.

Concerning the placement of the current contribution into the toolbox architecture, the best fit for it is a new module dedicated to implementing Robust Control with FO systems. The updated structure of the toolbox is depicted in Figure 2.4.

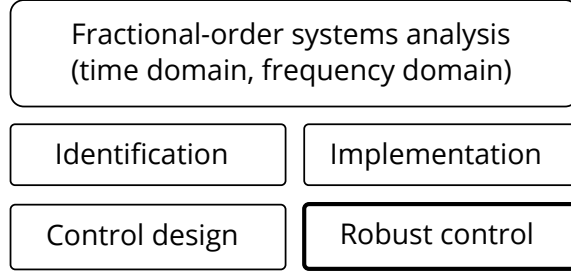


Figure 2.4: The modules of FOMCON toolbox for MATLAB. The newly developed module for Robust Control is highlighted.

In fact, the present contribution does not yet provide the ability to create, e.g., FO transfer functions with interval uncertainties, but what it does provide is a fundamental part of the implementation of a `ufotf` object, namely, a FO polynomial with interval uncertainties.

Remark 2.3. *The following examples should not be considered as an ultimate reference implementation. This FOMCON toolbox module is still under active development, and has not been released yet, available only for testing purposes. Consequently, some items, such as function calling sequences or class names may eventually change. However, the presented results may be useful to early adopters of these new features.*

Remark 2.4. *The original `fotf` object in FOMCON toolbox was implemented without introducing the concept of a FO polynomial `fpoly` first, but with this development, in the upcoming major version of the toolbox the architecture may change to be consistent with the present development.*

Formulation of the Fractional-Order polynomial with uncertainty intervals and related functionality In the present contribution, the fundamental mathematical object is a FO polynomial with uncertainties having the following form:

$$p(s) = [\underline{a}_0, \bar{a}_0]s^{[\alpha_0, \bar{\alpha}_0]} + [\underline{a}_1, \bar{a}_1]s^{[\alpha_1, \bar{\alpha}_1]} + \dots + [\underline{a}_n, \bar{a}_n]s^{[\alpha_n, \bar{\alpha}_n]}, \quad (2.26)$$

where $[\underline{a}_i, \bar{a}_i]$ denotes an uncertainty interval for the coefficient a_i , and $[\alpha_i, \bar{\alpha}_i]$ denotes the same for the exponent α_i . Furthermore, for generality, if in a given uncertain k th interval the limits are equal, i.e., $\underline{a}_k = \bar{a}_k$, then the interval collapses to a fixed scalar value a_k . Finally, we assume that

$$\underline{a}_i, \bar{a}_i, \alpha_i, \bar{\alpha}_i \in \mathbb{R}, \quad \forall i.$$

With these considerations, a class called `ufpoly` is designed in MATLAB, meaning “a fractional polynomial with uncertainty intervals”. The calling sequence to create the corresponding object can be

$$p = \text{ufpoly}(a, na)$$

where a is an $n \times 2$ matrix containing the lower and upper bounds for the n th coefficient, and na is a matrix having the exactly same dimensions as a and containing the lower and upper bounds for the n th exponent. Or, the polynomial can also be created in a more convenient way by passing a string:

$$p = \text{ufpoly}(\text{str})$$

In the latter case, the string may be, e.g.,

```
str='s^[1.5,1.7]+[1.2,1.9]s^0.2+10';
```

which corresponds to the polynomial

$$s^{[1.5,1.7]} + [1.2,1.9]s^{0.2} + 10. \quad (2.27)$$

By default, the variable symbol is s , but it can be changed by providing the optional final argument to the call to `ufpoly`.

The following basic methods have been implemented for the class:

- `display` — the method by which the object is printed in the MATLAB Command Window.
- `eq(p1, p2)` — compare two `ufpoly` polynomials $p1$ and $p2$; they are considered equal only if corresponding matrices $a1$ and $a2$ have the same dimensions, all parameters in the matrices $a1$ and $a2$ and also in $na1$ and $na2$ are equal and `symb` is the same in both polynomials.
- `polyval(p, x)` — evaluate a sampled `ufpoly` object p (a fractional polynomial with fixed coefficients and exponents) at points specified in vector x and return a vector y . Running this on a fractional polynomial that has interval uncertainties results in an error.
- `sample(p)` — returns a *sample* (a member) of a set of FO polynomials with interval uncertainties specified by p . By default, for each interval uncertainty, a value is sampled assuming a uniform distribution. Choosing other types of distributions are going to be eventually supported as well.
- `ufpoly2str(p)` — a convenience function that returns a string corresponding to the object p . This can be used, for example, to copy the string into word processing software such as \LaTeX for rendering the corresponding equation in a document.

Besides that, two additional utilities have been implemented to support the functionality related to parsing and generating strings representing the `ufpoly` object:

- `[a, na]=str2ufpoly(str)` — convert a string to two matrices a (matrix which holds the coefficient intervals), and na (matrix which holds the exponent intervals). The rules for formatting the string are described below.
- `ufpoly2str(a,na,symb,muls)` — convert a set of matrices a and na to a string. Optional arguments `symb` and `muls` represent the desired variable symbol, and the kind of multiplication sign to use (by default, the symbol is s , and the multiplication sign is omitted, i.e., `muls=''`).

The string parsers assumes the same format of the string as in (2.26) with the following additional conditions:

- Exponentiation signs \wedge are required.
- Multiplication signs $*$ are optional, the parser automatically detects multiplications.
- The intervals must be specified in square brackets $[]$.

- The lower and upper bounds in the uncertainty intervals may be separated by either a comma , (default and preferred method) or a semicolon ; .
- The minus sign appearing before an uncertainty interval is treated as a factor by which both lower and upper bounds are multiplied. So, for example, when the parser encounters an expression $-[2, 3]$, the expression is interpreted as $[-3, -2]$ which also emits a warning.
- Each term must have a unique exponent or a unique exponent interval. For example, using a string 's+s+[1,2]' to create a `ufpoly` will fail.
- Only one variable is allowed, and is automatically inferred from the string.

These utilities may be used independently from the `ufpoly` object and hence may be generally useful to the user.

The current development version of the toolbox which has the above described features can be found in the `devel-ufotf` branch on the official GitHub repository.

Basic usage example In this section, a basic usage example is provided based on the discussion above. The procedure for checking stability is described in a separate section. Suppose, that the object of study is a FO polynomial with interval uncertainties defined as

$$[6, 21.5]s^{[1.5, 1.8]} + 5s^{[0.5, 0.7]} + [11, 19]. \quad (2.28)$$

Let us first define this fractional polynomial with uncertainty intervals in two different ways which are absolutely equivalent. The first way is to use a string:

```
pstr = [ '[6,21.5]s^[1.5,1.8]' ...
          '+5s^[0.5,0.7]+[11,19]' ];
p1 = ufpoly(pstr);
```

And the second way is to provide matrix definitions for the same:

```
a = [6, 21.5; 5 5; 11, 19];
na = [1.5, 1.8; 0.5, 0.7; 0 0];
p2 = ufpoly(a, na);
```

One can check whether the two objects are equivalent by simply doing

```
p1 == p2
```

which should result in a logical 1. To sample 100 members from the FO polynomial with interval uncertainties one can run

```
m = {};
numSamples = 100;
for k=1:100, m{k} = sample(p1); end
```

Finally, to plot 1000 points of the magnitude response of all the sampled members in the frequency range between $[10^{-2}, 10^2]$ rad/s, one can do

```
figure; w = logspace(-2, 2, 1000);
for k=1:numSamples
    r = polyval(m{k}, sqrt(-1)*w);
    semilogx(w, 20*log10(abs(r)), 'b');
    hold on;
end
grid; xlabel('w [rad/s]');
```



```

ylabel('Magnitude [dB]');
t = sprintf(['Magnitude response of %d'...
            ' members'], numSamples);
title(t);

```

The resulting plot is shown in Fig. 2.5.

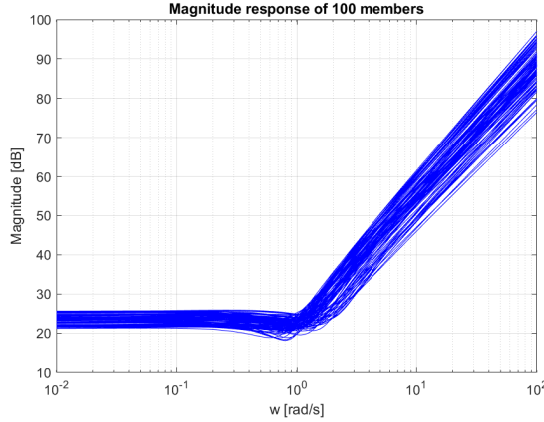


Figure 2.5: The magnitude response of a randomly sampled member subset of 100 of the FO polynomial with interval uncertainties in (2.28).

Robust stability assessment by FOMCON Toolbox In order to check the robust stability of a FO interval polynomial as $\Delta(s, \mathbf{q})$ in (4.2) some steps should be performed. Therefore, we demonstrate these steps by an example. In [8], it has been shown that $\Delta(s, \mathbf{q}) = [6, 14] + [9, 12]s^{0.5} + [0.4, 1.6]s + [0.8, 1.2]s^{1.5} + s^2$ is robust stable (see Example 1 in [8]).

Step 1: Check the stability of one chosen member in the uncertainty space of $\Delta(s, \mathbf{q})$. We use Lemma 2.2 to check the stability of the following chosen member.

$$P = 6 + 9s^{0.5} + 0.4s + 0.8s^{1.5} + s^2. \quad (2.29)$$

Hence, at first, the polynomial P in (2.29) can be defined by `ufpoly` tool as follows.

```
P = ufpoly('6+9s^0.5+0.4s+0.8s^1.5 + s^2')
```

A method `mikhailovfo` has been provided to check the **Mikhailov stability criterion** (see Lemma 2.2). So, by typing `mikhailovfo(P)`, the Mikhailov's resulting plot is depicted as Fig. 2.6. Therefore, the stability of the polynomial P can be inferred from this figure and **Mikhailov stability criterion** in Lemma 2.2. Surely, if the chosen member P is unstable then there is no need to perform next step. Since, the interval polynomial cannot be robustly stable.

Step 2: Lemma 2.4 and Lemma 2.6 have presented two different robust stability checking functions. Hence, the user can select one of the methods as stated in the following. For those who want to check the robust stability by Lemma 2.4, `robstabfo1` tool has been provided. As discussed earlier, the FO interval polynomial $\Delta(s, \mathbf{q})$ can be made by `ufpoly` tool as follows.

```
Delta=ufpoly(' [6, 14]+[9,12] s^0.5+
[0.4,1.6] s + [0.8,1.2] s^1.5 + s^2')
```

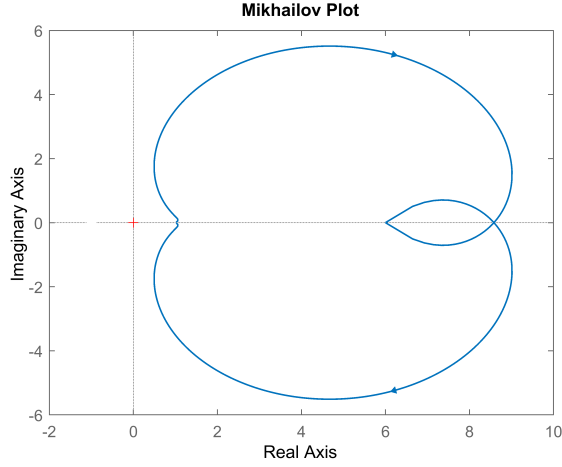


Figure 2.6: Mikhailov'plot for the FO polynomial P in (2.29).

```
s^{2}+[0.8, 1.2]s^{1.5}+[0.4, 1.6]s+
[9, 12]s^{0.5}+[6, 14]
Fractional polynomial with uncertainty
intervals.
```

Now, by typing `robstabfo1(Delta)` in command window we have:

```
robstabfo1(Delta)
"robustly stable"
```

This shows that all members of the interval polynomial $\Delta(s, \mathbf{q})$ are robust stable.

For those who want to check the robust stability by Lemma 2.6, `robstabfo2` tool has been provided. At first the interval polynomials $\Delta^1(s, \mathbf{q}^1)$ and $\Delta^2(s, \mathbf{q}^2)$ should be selected. For this example, we consider $\Delta^1(s, \mathbf{q}^1) = [6, 14] + [9, 12]s^{0.5}$ and $\Delta^2(s, \mathbf{q}^2) = [0.4, 1.6]s + [0.8, 1.2]s^{1.5} + s^2$. Then by `ufpoly` tool, the both interval polynomials can be defined as follows.

```
Delta1=ufpoly('[6, 14]+[9,12]s^{0.5}')
[9, 12]s^{0.5}+[6, 14]
Fractional polynomial with uncertainty
intervals.
Delta2=ufpoly('[0.4,1.6]s + [0.8,1.2]s^{1.5}
+ s^2')
s^{2}+[0.8, 1.2]s^{1.5}+[0.4, 1.6]s
Fractional polynomial with uncertainty
intervals.
```

`robstabfo2` tool can be used to check the robust stability of $\Delta(s, \mathbf{q})$ as follows.

```
robstabfo2(Delta1,Delta2)
"robustly stable"
```

So, the robust stability is also verified by this method.

3 Robust Stability Analysis of Fractional-Order Interval Systems

Recently, many efforts have been done to develop the fractional order calculus in different fields of research [89]. Analogously, the application of the fractional order calculus in control systems has been extensively studied. In this regard, the stability analysis of fractional order systems has been investigated in several studies [8, 9]. Furthermore, various design methods for fractional order controllers have been proposed in the literature [90, 91]. Also, in [92], a procedure has been proposed to design a fractional order PID controller for time delay systems.

In this chapter, first, efficient necessary and sufficient criteria are proposed for analyzing the robust stability of the corresponding characteristic polynomial. In fact, by using the criteria mentioned, it is shown that the robust stability analysis of a FOIS can be done without needing to specify the outer vertices of the value set of the corresponding characteristic polynomial. Therefore, the additional computations, which are calculated in literature for finding the outer vertices, are omitted based on the chapter results. Then, an auxiliary function is offered to check the robust stability criteria. This auxiliary function is formed by some fixed vertices. In fact, the results of the chapter lead to reduce the computational cost noticeably in comparison with the existing methods proposed in the literature.

3.1 Preliminaries

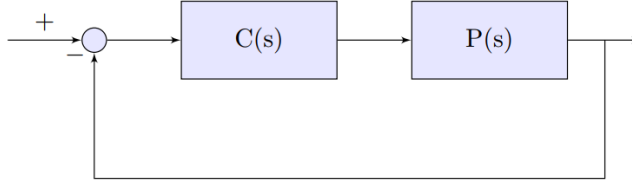


Figure 3.1: The closed-loop system.

In this chapter, an interval fractional order plant $P(s)$ and a fractional order controller $C(s)$ are described by

$$P(s) = \frac{N_p(s)}{D_p(s)} = \frac{\sum_{r_p=0}^{m_p} b_{r_p}^p s^{\beta_{r_p}^p}}{\sum_{i_p=0}^{n_p} a_{i_p}^p s^{\alpha_{i_p}^p}}, \quad (3.1)$$

$$C(s) = \frac{N_c(s)}{D_c(s)} = \frac{\sum_{r_c=0}^{m_c} b_{r_c}^c s^{\beta_{r_c}^c}}{\sum_{i_c=0}^{n_c} a_{i_c}^c s^{\alpha_{i_c}^c}}, \quad (3.2)$$

where $0 = \alpha_0^p < \alpha_1^p < \dots < \alpha_{n_p-1}^p < \alpha_{n_p}^p$, $0 = \beta_0^p < \beta_1^p < \dots < \beta_{m_p-1}^p < \beta_{m_p}^p$, $0 = \alpha_0^c < \alpha_1^c < \dots < \alpha_{n_c-1}^c < \alpha_{n_c}^c$ and $0 = \beta_0^c < \beta_1^c < \dots < \beta_{m_c-1}^c < \beta_{m_c}^c$ are positive real numbers. The real uncertain coefficients of the plant (3.1) contain the interval uncertainties $a_{i_p}^p \in [\underline{a}_{i_p}^p, \overline{a}_{i_p}^p]$ ($i_p = 0, 1, \dots, n_p$) and $b_{r_p}^p \in [\underline{b}_{r_p}^p, \overline{b}_{r_p}^p]$ ($r_p = 0, 1, \dots, m_p$). In addition, the coefficients of the controller (3.2) i.e. $a_{i_c}^c$ ($i_c = 0, 1, \dots, n_c$) and $b_{r_c}^c$ ($r_c = 0, 1, \dots, m_c$) are real numbers and $a_{n_c}^c \neq 0$. Furthermore, $a_{i_p}^p$ ($i_p = 0, 1, \dots, n_p$) and $b_{r_p}^p$ ($r_p = 0, 1, \dots, m_p$) are independent uncertain parameters and $a_{n_p}^p \neq 0$, $\alpha_{n_p}^p > \beta_{m_p}^p$ and $\alpha_{n_p}^c + \alpha_{n_c}^c > \beta_{m_p}^p + \beta_{m_c}^c$.

From Figure 3.1, the corresponding characteristic polynomial for the plant $P(s)$ in (3.1) and the controller $C(s)$ in (3.2) is obtained as $F(s)$ in (3.3).

$$F(s) = D_c(s) D_p(s) + N_c(s) N_p(s). \quad (3.3)$$

Assumption 3.1. Assume that the vertices of $N_p(j\omega)$ and $D_p(j\omega)$ in (3.1) are respectively $v_i^N(j\omega)$ ($i = 1, \dots, m_N$) and $v_r^D(j\omega)$ ($r = 1, \dots, m_D$), which are determined according to Approach 2 in Subsection 2.2.2.

Assumption 3.2. Assume that $F(s)$ in (3.3) has at least one Hurwitz-stable member by applying the controller $C(s)$ in (3.2). Therefore, based on the zero exclusion principle, it is sufficient to show that whether the origin belongs to the value set of $F(j\omega)$ in (3.3) or not.

3.2 Robust Stability Analysis

In this section, unlike the procedures in [93, 94, 95], by presenting the following theorems it is shown that without specifying the outer vertices of the value set of $F(j\omega)$ in (3.3), it is possible to find out whether the origin belongs to the value set of $F(j\omega)$ in (3.3) or not. This procedure omits the difficulty of obtaining the outer vertices of the parpolygon $F(j\omega)$.

Theorem 3.1. The characteristic polynomial in (3.3) is robust stable if and only if the exposed edges $F_N(j\omega)$ in (3.4) and $F_D(j\omega)$ in (3.5) do not have the overlap in the complex plane for $\omega \geq 0$.

$$F_N(j\omega) \triangleq \left\{ e\left(N_c(j\omega)v_1^N(j\omega), N_c(j\omega)v_2^N(j\omega)\right), \right. \\ \left. e\left(N_c(j\omega)v_2^N(j\omega), N_c(j\omega)v_3^N(j\omega)\right), \dots, e\left(N_c(j\omega)v_{m_N}^N(j\omega), N_c(j\omega)v_1^N(j\omega)\right) \right\}. \quad (3.4)$$

$$F_D(j\omega) \triangleq \left\{ e\left(-D_c(j\omega)v_1^D(j\omega), -D_c(j\omega)v_2^D(j\omega)\right), \right. \\ \left. e\left(-D_c(j\omega)v_2^D(j\omega), -D_c(j\omega)v_3^D(j\omega)\right), \dots, e\left(-D_c(j\omega)v_{m_D}^D(j\omega), -D_c(j\omega)v_1^D(j\omega)\right) \right\}. \quad (3.5)$$

Proof. According to previous sections the value sets of $\partial(N_p(j\omega))$ and $\partial(D_p(j\omega))$ would be two parpolygons at a fixed frequency. It can be also shown that the corresponding vertices of the value sets of $\partial(N_c(j\omega)N_p(j\omega))$ and $\partial(D_c(j\omega)D_p(j\omega))$ are $N_c(j\omega)v_i^N(j\omega)$ ($i = 1, \dots, m_N$) and $D_c(j\omega)v_r^D(j\omega)$ ($r = 1, \dots, m_D$), respectively (see Figure 3.2). Assume that Z_0 represents a complex number of the complex plane and $Z_0 \in N_c(j\omega)N_p(j\omega)$. If the origin is included in the value set of $F(j\omega)$ in (3.3), then $Z_0 \in -D_c(j\omega)D_p(j\omega)$ and this implies that two value sets of $F_N(j\omega)$ in (3.4) and $F_D(j\omega)$ in (3.5) have the overlap in the complex plane. Accordingly, the zero exclusion principle completes the proof. \square

Based on Theorem 3.1, investigating the overlap between the value sets of $F_N(j\omega)$ in (3.4) and $F_D(j\omega)$ in (3.5) has to be done. Accordingly, the necessary and sufficient conditions of the overlap between two parpolygons $F_N(j\omega)$ in (3.4) and $F_D(j\omega)$ in (3.5) are given by the following theorem.

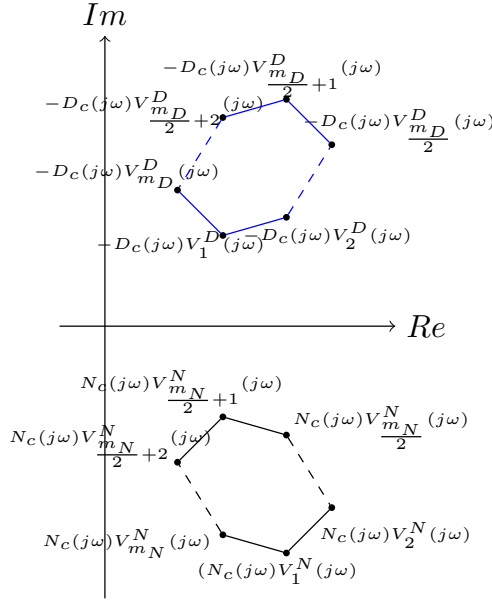


Figure 3.2: The boundaries $\partial(N_c(j\omega) N_p(j\omega))$ and $\partial(-D_c(j\omega) D_p(j\omega))$ for $\omega > 0$, $m_D, m_N > 1$.

Theorem 3.2. Two parpolygons $F_N(j\omega)$ in (3.4) and $F_D(j\omega)$ in (3.5) don't have the overlap in the complex plane for $\omega > 0$ if and only if:

1. The vertices $N_c(j\omega) v_i^N(j\omega)$ ($i = 1, \dots, m_N$) are not included in the value set $-D_c(j\omega) D_p(j\omega)$;
2. The vertices $-D_c(j\omega) v_r^D(j\omega)$ ($r = 1, \dots, m_D$) are not included in the value set $N_c(j\omega) N_p(j\omega)$.

Proof. There are two probabilities to have the overlap between two parpolygons $F_N(j\omega)$ in (3.4) and $F_D(j\omega)$ in (3.5) which are as follows:

(i) The vertices of $\partial(N_c(j\omega) N_p(j\omega))$ (i.e. $N_c(j\omega) v_i^N(j\omega)$ $i = 1, \dots, m_N$) intersect with the value set of $\partial(-D_c(j\omega) D_p(j\omega))$ in the complex plane.

(ii) The vertices of $\partial(-D_c(j\omega) D_p(j\omega))$ (i.e. $-D_c(j\omega) v_r^D(j\omega)$ $r = 1, \dots, m_D$) intersect with the value set of $\partial(N_c(j\omega) N_p(j\omega))$ in the complex plane.

Therefore, if no vertices of the value sets of $\partial(N_c(j\omega) N_p(j\omega))$ and $\partial(-D_c(j\omega) D_p(j\omega))$ respectively intersect with $\partial(-D_c(j\omega) D_p(j\omega))$ and $\partial(N_c(j\omega) N_p(j\omega))$, then two parpolygons $F_N(j\omega)$ in (3.4) and $F_D(j\omega)$ in (3.5) don't have the overlap in the complex plane. \square

For facilitating the robust stability analysis, an auxiliary function is presented to investigate the conditions in the statement of Theorem 3.2.

Theorem 3.3. The system depicted in Figure 3.1 with the characteristic polynomial $F(s)$ in (3.3) is robustly stable if and only if the inequality $\Lambda(\omega) = \chi_1(\omega) \chi_2(\omega) > 0$ holds, where

$\chi_1(\omega)$ and $\chi_2(\omega)$ are defined as follows.

$$\chi_1(\omega) \triangleq \min \left\{ \kappa_{h,g}(\omega) \mid h \in \{1, \dots, m_D\}, g \in \{1, \dots, m_N\} \right\}, \quad (3.6)$$

$$\kappa_{h,g}(\omega) \triangleq \left| D_c(j\omega) v_h^D(j\omega) + N_c(j\omega) v_g^N(j\omega) \right| + \left| D_c(j\omega) v_h^D(j\omega) + N_c(j\omega) v_{g+1}^N(j\omega) \right| - \left| N_c(j\omega) (v_{g+1}^N(j\omega) - v_g^N(j\omega)) \right|.$$

and

$$\chi_2(\omega) \triangleq \min \left\{ \tilde{\kappa}_{h,g}(\omega) \mid h \in \{1, \dots, m_N\}, g \in \{1, \dots, m_D\} \right\},$$

$$\tilde{\kappa}_{h,g}(\omega) \triangleq \left| N_c(j\omega) v_h^N(j\omega) + D_c(j\omega) v_g^D(j\omega) \right| + \left| N_c(j\omega) v_h^N(j\omega) + D_c(j\omega) v_{g+1}^D(j\omega) \right| - \left| D_c(j\omega) (v_{g+1}^D(j\omega) - v_g^D(j\omega)) \right|, \quad (3.7)$$

where, $v_{m_D+1}^D(j\omega) = v_1^D(j\omega)$ and $v_{m_N+1}^N(j\omega) = v_1^N(j\omega)$.

Proof. Regarding Theorem 3.1 and Theorem 3.2, if the conditions in the statement of Theorem 3.2 are satisfied, then the closed loop fractional order system is robust stable. According to Figure 1 and Theorem 3.2, if the triangle inequality is satisfied for any vertex of the parpolygon $\partial(N_c(j\omega) N_p(j\omega))$ (i.e. $N_c(j\omega) v_i^N(j\omega)$ $i = 1, \dots, m_N$) and any two consecutive vertices of the parpolygon $\partial(-D_c(j\omega) D_p(j\omega))$, then no vertices of the value set of $\partial(N_c(j\omega) N_p(j\omega))$ intersect with $\partial(-D_c(j\omega) D_p(j\omega))$. This implies that the first condition in the statement of Theorem 3.2 is satisfied. Likewise, satisfying the triangle inequality for any vertex of the parpolygon $\partial(-D_c(j\omega) D_p(j\omega))$ (i.e. $-D_c(j\omega) v_r^D(j\omega)$ $r = 1, \dots, m_D$) and any two consecutive vertices of the parpolygon $\partial(N_c(j\omega) N_p(j\omega))$ implies that the second condition in the statement of Theorem 3.2 is satisfied. Therefore, satisfying the inequality $\Lambda(\omega) = \chi_1(\omega) \chi_2(\omega) > 0$ guarantees that the conditions in the statement of Theorem 3.2 are met. Hence, this completes the proof. \square

In fact, it is unrealistic to check whether the origin belongs to the value set of $F(j\omega)$ in (4.3) for $\omega \in [0, \infty)$ or not, since the length of the frequency range $[0, \infty)$ is infinite. In the following lemma, a finite frequency range is presented instead of the frequency range $[0, \infty)$.

Lemma 3.1. *The origin would not be included in the value set of $F(j\omega)$ in (3), if $\omega \in [0, \infty) \setminus [\omega_{\min}, \omega_{\max}]$, where*

$$\omega_{\max} = \max \left\{ 1, \sigma_1^{\frac{1}{\alpha_{n_c} + \alpha_{n_p} - \varepsilon_1}} \right\}, \quad (3.8)$$

$$\varepsilon_1 = \max \left\{ \alpha_{n_c}^c + \alpha_{n_{p-1}}^p, \alpha_{n_c-1}^c + \alpha_{n_p}^p, \beta_{m_c}^c + \beta_{m_p}^p \right\},$$

$$\sigma_1 = \left(\left(\sum_{i^1=0}^{n_c-1} |a_{i^1}^c| \right) \left(\sum_{i^2=0}^{n_p-1} \max\{|a_{i^2}^p|, |\bar{a}_{i^2}^p|\} \right) + |a_{n_c}^c| \left(\sum_{i^2=0}^{n_p-1} \max\{|a_{i^2}^p|, |\bar{a}_{i^2}^p|\} \right) + \right. \\ \left. \max\{|a_{n_p}^p|, |\bar{a}_{n_p}^p|\} \left(\sum_{i^1=0}^{n_c-1} |a_{i^1}^c| \right) + \left(\sum_{j^1=0}^{m_c} |b_{j^1}^c| \right) \left(\sum_{j^2=0}^{m_p} \max\{|b_{j^2}^p|, |\bar{b}_{j^2}^p|\} \right) \right) \\ \left. / \left(|a_{n_c}^c| \min\{|a_{n_p}^p|, |\bar{a}_{n_p}^p|\} \right), \right.$$

$$\omega_{\min} = \min\{1, \sigma_2^{\frac{1}{\varepsilon_2}}\}, \\ \sigma_2 = E / \left(\left(\sum_{i^1=1}^{n_c} |a_{i^1}^c| \right) \sum_{i^2=1}^{n_p} \max\{|a_{i^2}^p|, |\bar{a}_{i^2}^p|\} + \max\{|a_0^p|, |\bar{a}_0^p|\} \left(\sum_{i^1=1}^{n_c} |a_{i^1}^c| \right) + \right. \\ \left. |a_0^c| \left(\sum_{i^2=1}^{n_p} \max\{|a_{i^2}^p|, |\bar{a}_{i^2}^p|\} \right) + \left(\sum_{j^1=1}^{m_c} |b_{j^1}^c| \right) \left(\sum_{j^2=1}^{m_p} \max\{|b_{j^2}^p|, |\bar{b}_{j^2}^p|\} \right) + \right. \\ \left. |b_0^c| \left(\sum_{j^2=1}^{m_p} \max\{|b_{j^2}^p|, |\bar{b}_{j^2}^p|\} \right) + \max\{|b_0^p|, |\bar{b}_0^p|\} \left(\sum_{j^1=1}^{m_c} |b_{j^1}^c| \right) \right), \quad (3.9)$$

$$\varepsilon_2 \triangleq \min\{\alpha_1^c, \alpha_1^p, \beta_1^c, \beta_1^p\},$$

$$E = \begin{cases} E_1, & \text{for } 0 \notin [\underline{a}_0^p, \bar{a}_0^p] \text{ and } E_1 > 0, \\ E_2, & \text{for } 0 \notin [\underline{b}_0^p, \bar{b}_0^p] \text{ and } E_2 > 0, \\ 0, & \text{otherwise,} \end{cases}$$

$$E_1 = \min\{|\underline{a}_0^p|, |\bar{a}_0^p|\} |a_0^c| - \max\{|\underline{b}_0^p|, |\bar{b}_0^p|\} |b_0^c|,$$

$$E_2 = \min\{|\underline{b}_0^p|, |\bar{b}_0^p|\} |b_0^c| - \max\{|\underline{a}_0^p|, |\bar{a}_0^p|\} |a_0^c|.$$

Proof. It is a straightforward result based on Theorem 3 in [94]. □

Note that if $n_c = 0$, then $\alpha_{n_c-1}^c + \alpha_{n_p}^p$ and α_1^c are respectively considered as \emptyset in ε_1 and ε_2 presented in Lemma 3.1. Likewise, in ε_2 , β_1^c and β_1^p are considered as \emptyset for $m_c = 0$ and $m_p = 0$, respectively.

Remark 3.1. Based on the zero exclusion principle, at first, the stability of one member of $F(s)$ in (3.3) has to be checked. To do this, some methods were presented by [87, 88]. Obviously, if the chosen characteristic polynomial is not stable, then the characteristic polynomial $F(s)$ in (3.3) is not robust stable. Otherwise, the values of the function $\Lambda(\omega)$ in Theorem 3.3 should be checked within $\omega \in [\omega_{\min}, \omega_{\max}]$. Therefore, the robust stability of the characteristic polynomial $F(s)$ in (3.3) can be analyzed by the following steps:

1. Check the stability of one member of the characteristic polynomial $F(s)$ in (3.3). If the chosen characteristic polynomial is stable, continue. Otherwise, the system is not robust stable. (In this thesis, Theorem 3 in [88] is used to analyze the stability of the chosen characteristic polynomial.)

2. Obtain the vertices $v_i^N(j\omega)$ ($i = 1, \dots, m_N$) and $v_r^D(j\omega)$ ($r = 1, \dots, m_D$) based on Approach 2 in Subsection 2.2.2.
3. Obtain the bounds ω_{\min} and ω_{\max} by Lemma 3.1.
4. Check the sign of the auxiliary function $\Lambda(\omega)$ presented in Theorem 3.3 for $\omega \in [\omega_{\min}, \omega_{\max}]$. Based on Theorem 3.3, the system is robust stable when the values of the function $\Lambda(\omega)$ are positive for $\omega \in [\omega_{\min}, \omega_{\max}]$.

Remark 3.2. Based on Theorem 3.1 and Theorem 3.2, if the polynomials

$$P_r^N(s) \triangleq D_c(s) v_r^D(s) + N_c(s) N_p(s), \quad r = 1, \dots, m_D,$$

and

$$P_i^D(s) \triangleq D_c(s) D_p(s) + N_c(s) v_i^N(s), \quad i = 1, \dots, m_N,$$

are robustly stable, then the characteristic polynomial (4.3) is also robustly stable.

The sensitivity function characterizes important properties of a feedback system such as disturbance rejection, robust performance, and other performance specifications. Accordingly, the robust FO controller $C(s)$ should satisfy the following inequalities.

$$\left| \frac{1}{1 + \frac{N_c(j\omega) N_p(j\omega)}{D_c(j\omega) v_r^D(j\omega)}} \right| < |M_s(j\omega)|, \quad r = 1, \dots, m_D, \quad (3.10)$$

$$\left| \frac{1}{1 + \frac{N_c(j\omega) v_i^N(j\omega)}{D_c(j\omega) D_p(j\omega)}} \right| < |M_s(j\omega)|, \quad i = 1, \dots, m_N, \quad (3.11)$$

where, $M_s(j\omega) = N_s(j\omega)/D_s(j\omega)$ denotes the weighting function, which describes the frequency characteristic of the performance specifications and the size of the disturbance [96]. Based on the inequalities (3.10), (3.11), the maximum modulus theorem [97], the following inequality can be simply derived.

$$\Xi(\omega) \triangleq \min_{i=1,2} \Xi_i(\omega) > 0, \quad (3.12)$$

where,

$$\Xi_1(\omega) \triangleq \min_{r=1, \dots, m_D} \Delta_r(\omega),$$

$$\Delta_r(\omega) \triangleq |N_s(j\omega)| \left(\min_{e_l \in P_E} |e_l| \right) - |D_s(j\omega)| |D_c(j\omega) v_r^D(j\omega)|,$$

$$P_E \triangleq \{e_1, e_2, \dots, e_{m_N}\},$$

$$\begin{cases} e_1 \triangleq e(D_c(j\omega) v_r^D(j\omega) + N_c(j\omega) v_1^N(j\omega), D_c(j\omega) v_r^D(j\omega) + N_c(j\omega) v_2^N(j\omega)), \\ e_2 \triangleq e(D_c(j\omega) v_r^D(j\omega) + N_c(j\omega) v_2^N(j\omega), D_c(j\omega) v_r^D(j\omega) + N_c(j\omega) v_3^N(j\omega)), \\ \dots \\ e_{m_N} \triangleq e(D_c(j\omega) v_r^D(j\omega) + N_c(j\omega) v_{m_N}^N(j\omega), D_c(j\omega) v_r^D(j\omega) + N_c(j\omega) v_1^N(j\omega)). \end{cases} \quad (3.13)$$

$$\Xi_2(\omega) \triangleq \min_{i=1, \dots, m_N} \tilde{\Delta}_i(\omega),$$

$$\tilde{\Delta}_i(\omega) \triangleq |N_s(j\omega)| - |D_s(j\omega)| \left(\max_{\tilde{e}_l \in \tilde{P}_E} |\tilde{e}_l| \right), \quad (3.14)$$

$$\tilde{P}_E \triangleq \{\tilde{e}_1, \tilde{e}_2, \dots, \tilde{e}_{m_D}\},$$

$$\left\{ \begin{array}{l} \tilde{e}_1 \triangleq \frac{1}{1 + \frac{N_c(j\omega) v_l^N(j\omega)}{D_c(j\omega) e(v_1^D(j\omega), v_2^D(j\omega))}}, \\ \tilde{e}_2 \triangleq \frac{1}{1 + \frac{N_c(j\omega) v_l^N(j\omega)}{D_c(j\omega) e(v_2^D(j\omega), v_3^D(j\omega))}}, \\ \dots \\ \tilde{e}_{m_D} \triangleq \frac{1}{1 + \frac{N_c(j\omega) v_l^N(j\omega)}{D_c(j\omega) e(v_{m_D}^D(j\omega), v_1^D(j\omega))}}, \end{array} \right.$$

where $l = 1, \dots, m_N$ and $\tilde{l} = 1, \dots, m_D$. As mentioned before, $M_s(j\omega) = N_s(j\omega)/D_s(j\omega)$ is a weighting function selected by the designer. Hence, the sign of the function $\Xi(\omega)$ in (3.12) helps the designer to evaluate the output disturbance rejection of the control system and many other performance specifications.

3.3 Numerical Examples

This subsection is devoted to the numerical evaluation of the robust stability criteria presented in this chapter.

Example 3.1. Consider the following fractional order plant $P(s)$ (see Example 3 in [93]):

$$P(s) = \frac{[9, 11]}{[4, 6]s^{2.1} + [1.5, 2.5]}, \quad (3.15)$$

and the FOPID controller

$$C(s) = 5 + \frac{1}{s^{0.3}} + s^{0.9}. \quad (3.16)$$

According to Remark 3.1, Theorem 3 in [3] is used to check the stability of a member of the corresponding characteristic polynomial. Figure 3.3 shows the values of the function $\psi(j\omega)$ in (3.17). Hence, the numerator of the function $\psi(j\omega)$ in (3.17) is stable (see Theorem 3 in [88]).

$$\psi(s) = \frac{s^{0.3}(4s^{2.1} + 1.5) + 9(5s^{0.3} + 1 + s^{1.2})}{4(s+1)^{2.4}}, s = j\omega, \omega \in [-1000, 1000]. \quad (3.17)$$

Based on Approach 1, the vertices $v_i^N(s)$ ($i = 1, 2$) and $v_r^D(s)$ ($r = 1, \dots, 4$) are presented as follows.

$$\left\{ \begin{array}{l} v_1^N(s) = 9, \\ v_2^N(s) = 11, \end{array} \right. \quad (3.18)$$

$$\left\{ \begin{array}{l} v_1^D(s) = 6s^{2.1} + 1.5, \\ v_2^D(s) = 6s^{2.1} + 2.5, \\ v_3^D(s) = 4s^{2.1} + 2.5, \\ v_4^D(s) = 4s^{2.1} + 1.5, \end{array} \right. \quad (3.19)$$

where

$$s = \omega e^{j\frac{\pi}{2}}.$$

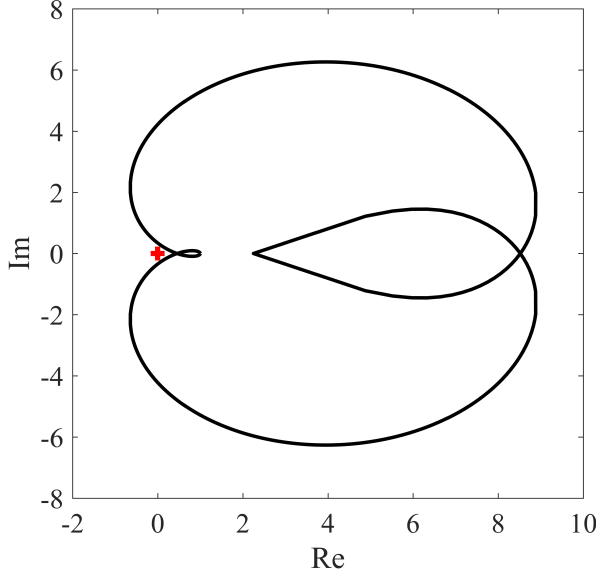


Figure 3.3: The function $\psi(j\omega)$ in (3.17) for $\omega \in [-1000, 1000]$ rad/sec.

According to Lemma 3.1, the frequency bounds are obtained as

$$\omega_{\min} = 8.7154 \times 10^{-4} \text{ rad/sec}, \quad \omega_{\max} = 12.076 \text{ rad/sec}.$$

Hence, the curve of $\Lambda(\omega)$ is checked for

$$\omega \in [8.7154 \times 10^{-4}, 12.076] \text{ rad/sec}.$$

The values of $\Lambda(\omega)$ are shown in Figure 3.4 for this frequency range. It is seen from Figure 3.4 that the inequality $\Lambda(\omega) > 0$ holds. Therefore, the corresponding closed-loop system is robust stable based on Theorem 3.3.

Example 3.2. Consider the plant $P(s)$ and the controller $C(s)$ as follows (see Example 1 in [23]).

$$P(s) = \frac{[1, 19]}{[1, 5]s^{1.2} + [-4, 6]s^{0.8} + [-5, 15]s^{0.4} + [4, 10]}, \quad (3.20)$$

$$C(s) = 5 + 1.5 \frac{s^{0.8}}{1 + 0.05s^{0.8}}. \quad (3.21)$$

Based on Remark 3.1, the stability of one member of the corresponding characteristic polynomial has to be checked. The values of the function $\psi(j\omega)$ in (3.22) have been presented in Figure 3.5. Hence, the numerator of the function $\psi(j\omega)$ in (3.22) is stable.

$$\psi(s) = \frac{(1 + 0.05 s^{0.8}) (s^{1.2} + 6s^{0.8} + 15s^{0.4} + 4) + 5 + 1.75s^{0.8}}{0.05(s+1)^2} \quad (3.22)$$

$s = j\omega, \omega \in [-10000, 10000].$

Based on Approach 1, the vertices $v_i^N(s)$ ($i = 1, 2$) and $v_r^D(s)$ ($r = 1, \dots, 8$) are presented

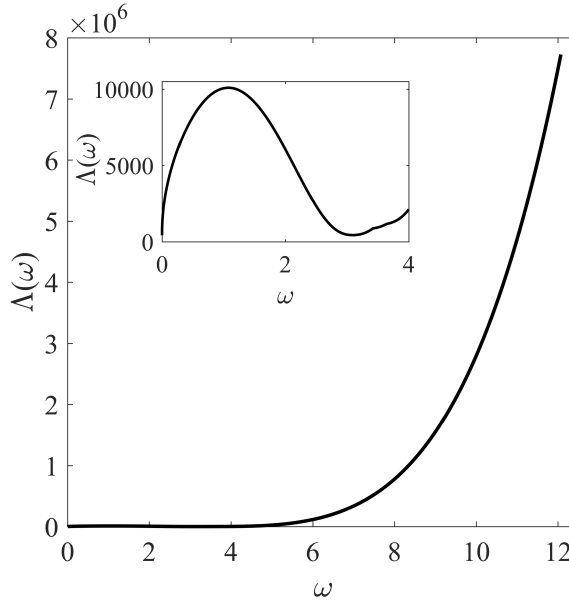


Figure 3.4: The values of the function $\Lambda(\omega)$ for $\omega \in [8.7154 \times 10^{-4}, 12.076]$ rad/sec.

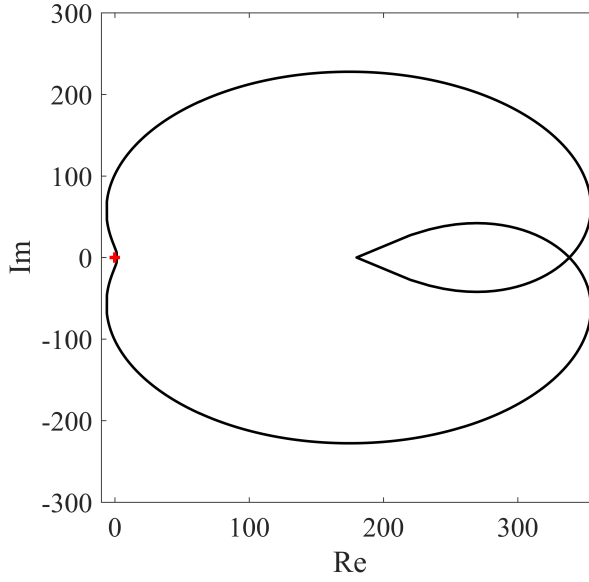


Figure 3.5: The function $\psi(j\omega)$ in (3.22) for $\omega \in [-10000, 10000]$ rad/sec.

as follows.

$$\begin{cases} v_1^N(s) = 1, \\ v_2^N(s) = 19. \end{cases} \quad (3.23)$$

$$\begin{cases} v_1^D(s) = s^{1.2} - 4s^{0.8} - 5s^{0.4} + 4, \\ v_2^D(s) = s^{1.2} - 4s^{0.8} - 5s^{0.4} + 10, \\ v_3^D(s) = s^{1.2} - 4s^{0.8} + 15s^{0.4} + 10, \\ v_4^D(s) = s^{1.2} + 6s^{0.8} + 15s^{0.4} + 10, \\ v_5^D(s) = 5s^{1.2} + 6s^{0.8} + 15s^{0.4} + 10, \\ v_6^D(s) = 5s^{1.2} + 6s^{0.8} + 15s^{0.4} + 4, \\ v_7^D(s) = 5s^{1.2} + 6s^{0.8} - 5s^{0.4} + 4, \\ v_8^D(s) = 5s^{1.2} - 4s^{0.8} - 5s^{0.4} + 4. \end{cases} \quad (3.24)$$

where $s = \omega e^{j\frac{\pi}{2}}$. Based on Lemma 3.1, the frequencies ω_{\min} and ω_{\max} are obtained as 0 rad/sec and 6.3319×10^8 rad/sec, respectively. Hence, the function $\Lambda(\omega)$ is drawn for $\omega \in [0, 6.3319 \times 10^8]$ rad/sec in Figure 3.6. From this figure, $\Lambda(\omega) = 0$ emerges within $\omega \in [0, 6.3319 \times 10^8]$ rad/sec. Therefore, based on Theorem 3.3, this controller cannot stabilize the closed loop system. For more clarification, the overlap between $F_N(\omega)$ in (3.4) and $F_D(j\omega)$ in (3.5) has been shown in Figure 3.7 at $\omega = 5$ rad/sec. Consequently, the proposed controller $C(s)$ in (3.20) cannot stabilize the plant $P(s)$ in (3.21).

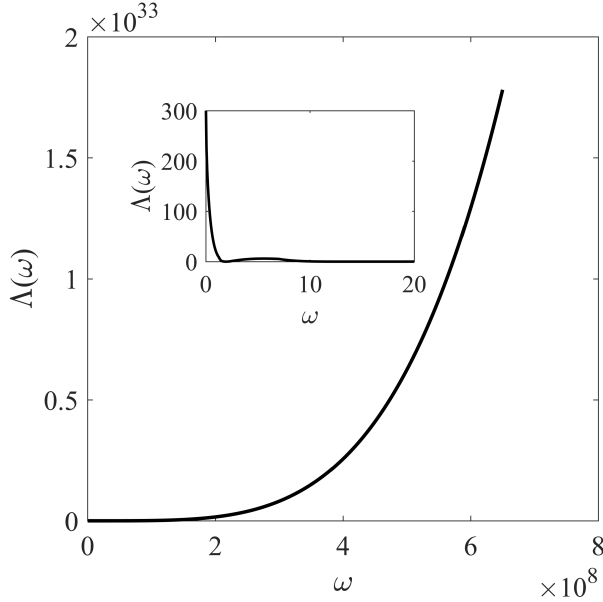


Figure 3.6: The auxiliary function $\Lambda(\omega)$ within $\omega \in [0, 6.3319 \times 10^8]$ rad/sec.

Example 3.3. Consider the fractional order plant in (3.25) and the controllers $C_1(s)$ in (3.26) and $C_2(s)$ in (3.27).

$$P(s) = \frac{[0.5, 1]s^{0.4} + [1, 2]}{[0.5, 1.5]s^{0.8} + [0.1, 1]s^{0.4} + [0.5, 1]}. \quad (3.25)$$

$$C_1(s) = 25 \left(1 + \frac{1}{s^{0.8}}\right). \quad (3.26)$$

$$C_2(s) = 5 \left(1 + \frac{1}{s^{0.8}}\right). \quad (3.27)$$

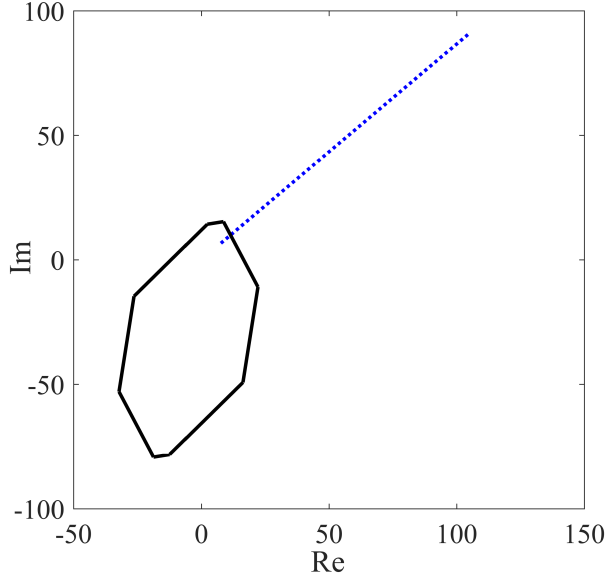


Figure 3.7: The overlap between $F_N(\omega)$ in (3.4) (dotted line) and $F_D(j\omega)$ in (3.5) (solid line) at $\omega = 5$ rad/sec.

In the following, based on Remark 3.1, by applying the controllers $C_1(s)$ in (3.26) and $C_2(s)$ in (3.27), the robust stability of the closed loop system is analyzed. In fact, at first, it is shown that the controllers $C_1(s)$ in (3.26) and $C_2(s)$ in (3.27) can stabilize the closed loop system. Then, based on Remark 3.2, the output disturbance rejection of the control system is analyzed by using these controllers.

The values of the functions $\psi_1(j\omega)$ in (3.28) and $\psi_2(j\omega)$ in (3.29) have been presented in Figure 3.8. Therefore, the numerators of the functions $\psi_i(j\omega)$ ($i=1,2$) are stable.

$$\psi_1(s) = \frac{s^{0.8} (s^{0.8} + s^{0.4} + 1) + 25 (1 + s^{0.8}) (s^{0.4} + 1)}{(s + 1)^{1.6}}, s = j\omega, \omega \in [-10000, 10000]. \quad (3.28)$$

$$\psi_2(s) = \frac{s^{0.8} (s^{0.8} + s^{0.4} + 1) + 10 (1 + s^{0.8}) (s^{0.4} + 1)}{(s + 1)^{1.6}}, s = j\omega, \omega \in [-10000, 10000]. \quad (3.29)$$

Based on Approach 1, the vertices $v_i^N(s)$ ($i = 1, 2, 3, 4$) and $v_r^D(s)$ ($r = 1, \dots, 6$) are given as follows.

$$\begin{cases} v_1^N(s) = 0.5s^{0.4} + 1, \\ v_2^N(s) = 0.5s^{0.4} + 2, \\ v_3^N(s) = s^{0.4} + 2, \\ v_4^N(s) = s^{0.4} + 1. \end{cases} \quad (3.30)$$

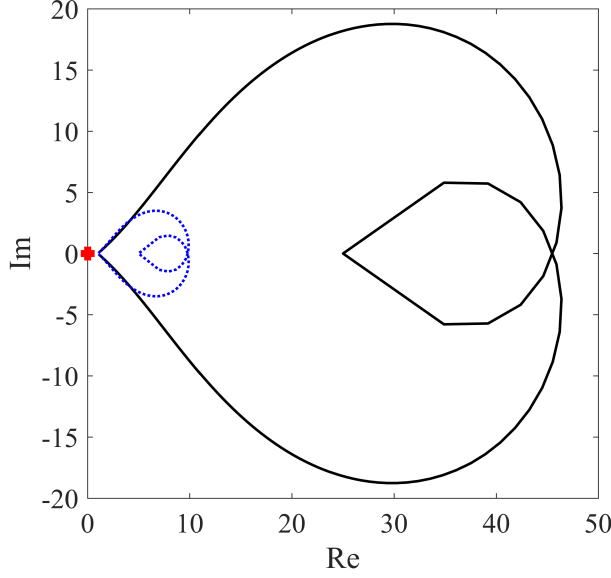


Figure 3.8: The values of the functions $\psi_1(j\omega)$ in (3.28) (solid line) and $\psi_2(j\omega)$ in (3.29) (dotted line).

$$\begin{cases} v_1^D(s) = 0.5s^{0.8} + 0.1s^{0.4} + 0.5, \\ v_2^D(s) = 0.5s^{0.8} + 0.1s^{0.4} + 1, \\ v_3^D(s) = 0.5s^{0.8} + s^{0.4} + 1, \\ v_4^D(s) = 1.5s^{0.8} + s^{0.4} + 1, \\ v_5^D(s) = 1.5s^{0.8} + s^{0.4} + 0.5, \\ v_6^D(s) = 1.5s^{0.8} + 0.1s^{0.4} + 0.5. \end{cases} \quad (3.31)$$

Based on Remark 3.1 and Lemma 3.1, the frequency ranges corresponding to the controllers $C_1(s)$ in (3.26) and $C_2(s)$ in (3.27) are given by:

$$\omega \in [0.0287, 1.6113 \times 10^6] \text{ rad/sec} \quad \text{and} \quad \omega \in [0.0209, 32768] \text{ rad/sec},$$

respectively. The values of the auxiliary function $\Lambda(\omega)$ for these controllers are shown in Figure 3.9 and Figure 3.10. As illustrated in these figures, the condition $\Lambda(\omega) > 0$ is satisfied over the entire respective frequency ranges. Therefore, the closed-loop system is robustly stable when either controller $C_1(s)$ or $C_2(s)$ is employed.

In the following, the output disturbance rejection and the closed loop performance are evaluated for the weighting function $M_s(j\omega)$, which is presented in (3.32).

$$M_s(s) = \frac{N_s(s)}{D_s(s)} = \frac{(s + 0.01)(s + 10)(0.001s + 1)}{s^2 + 10s + 100}, \quad s = j\omega. \quad (3.32)$$

Figure 3.11 and Figure 3.12 show the values of the function $\Xi(\omega)$ in (3.12) corresponding to the controller $C_1(s)$ in (3.26) and the controller $C_2(s)$ in (3.27), respectively. As the figures depict, the controller $C_1(s)$ in (3.26) can satisfy the inequality $\Xi(\omega) > 0$ in (3.12). Based on Remark 3.2, the designer should choose the controller $C_1(s)$ in (3.26). The controllers $C_1(s)$ in (3.26) and $C_2(s)$ in (3.27) are implemented based on the approximation method proposed in [98]. Therefore, the order and the frequency range of the approximation filter

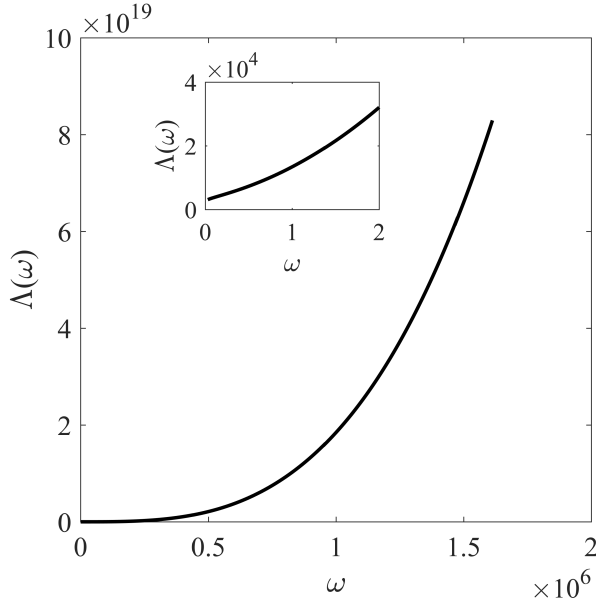


Figure 3.9: The auxiliary function $\Lambda(\omega)$ corresponding to the controller $C_1(s)$ within $\omega \in [0.0013, 6.3319 \times 10^8]$ rad/sec.

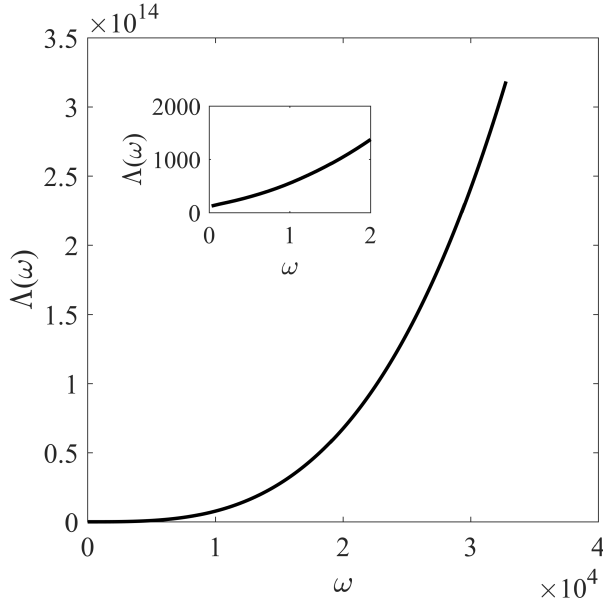


Figure 3.10: The auxiliary function $\Lambda(\omega)$ corresponding to the controller $C_2(s)$ within $\omega \in [0.0209, 32768]$ rad/sec.

are considered as $N = 3$ and $[\omega_l, \omega_h] = [0.001, 100]$ rad/sec. Also, the applied disturbance is considered as an additive step disturbance at time instant $t = 50$ sec. The closed loop step responses, which are given by applying the controllers $C_1(s)$ in (3.26) and $C_2(s)$ in

(3.27), are shown in Figure 3.13 and Figure 3.14, respectively. From Figures 3.13-3.16, it can be simply concluded that by applying the controller $C_1(s)$ in (3.26) the output disturbance rejection of the closed loop control system is better than what is achieved by applying the controller $C_2(s)$ in (3.27).

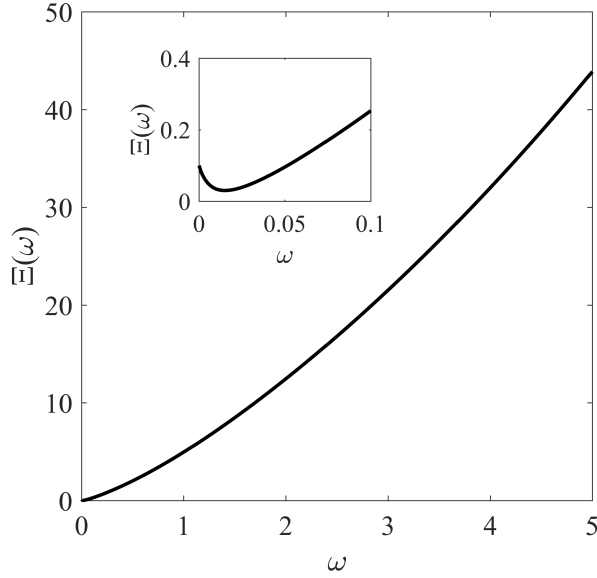


Figure 3.11: The values of the function $\Xi(\omega)$ in (3.12) corresponding to the controller $C_1(s)$ in (3.26).

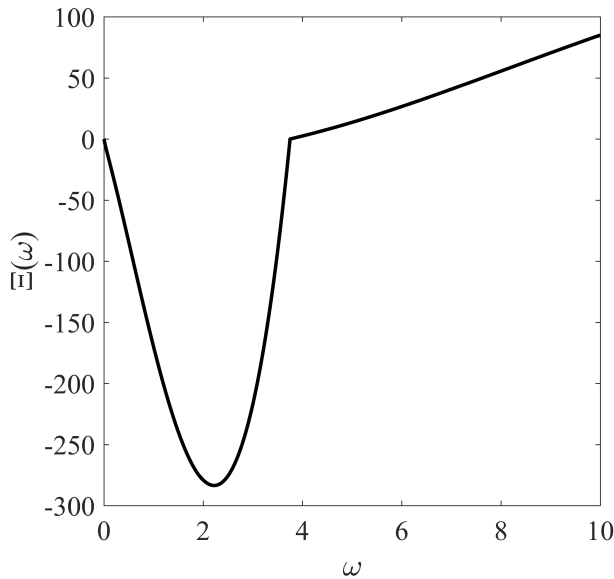


Figure 3.12: The values of the function $\Xi(\omega)$ in (3.12) corresponding to the controller $C_2(s)$ in (3.27).

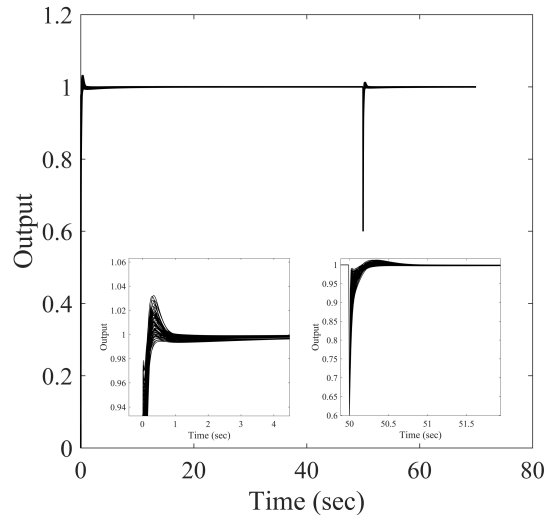


Figure 3.13: The closed loop step responses corresponding to the controller $C_1(s)$ in (3.26).

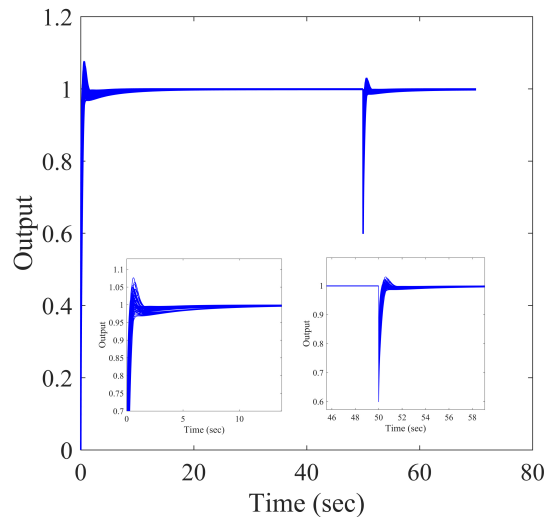


Figure 3.14: The closed loop step responses corresponding to the controller $C_2(s)$ in (3.27).

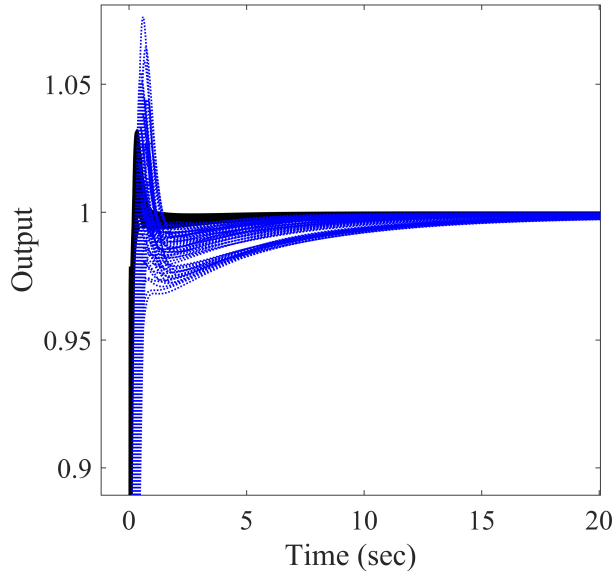


Figure 3.15: Closed loop performance of the controllers $C_1(s)$ in (3.26) (solid line) and $C_2(s)$ in (3.27) (dotted line).

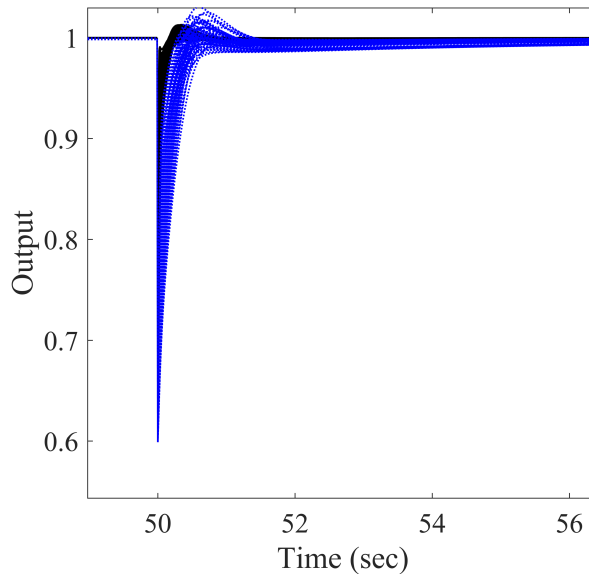


Figure 3.16: Output disturbance rejection by applying the controllers $C_1(s)$ in (3.26) (solid line) and $C_2(s)$ in (3.27) (dotted line).

4 Robust Stability Analysis of Fractional-Order Interval Polynomials with an Interval Time Delay

In the work [100], the authors have discussed several items which block the at-scale deployment of FOPID controllers in the industry. One of those issues is related to the trust in this new technology which must be addressed from several viewpoints, one of which being a thorough analysis of the control loop to ensure robust stability thereof. Furthermore, when industrial control problems are concerned, it is also universally acknowledged that a time delay—also referred to as *transport delay* and *dead time* in various studies—is a crucial parameter that must be thoroughly considered when modeling real-life systems [10, 23, 35]. Moreover, the time delay of the system may not be fixed, i.e., it can change during the operation of the real system deviating from a given nominal value. Therefore, one should consider the uncertainty in the time delay to ensure the validity of robust stability analysis of FO systems. Accordingly, the study of this problem has received considerable attention recently.

In this chapter, we are particularly concerned with the robust stability analysis of a closed-loop control system in terms of FO controllers and uncertain FO plants with an uncertain time delay. The uncertainties are represented with numerical intervals which also contain the nominal values of the model parameters. This problem has been treated using various approaches found in the existing literature. For instance, in previous works [101, 102, 103], some numerical nonlinear optimization methods have been proposed to design FOPID controllers. However, the proposed methods cannot robustly stabilize the closed-loop control system in the face of plant uncertainties. In order to improve the robustness of FOPI controllers, a flat phase constraint has been satisfied for stable FOPTD systems [104]. In addition, previous works [105, 106, 107] have proposed various methods to tune FOPD controllers and FOPID controllers for systems having time delay based on gain and phase margins. But, satisfying gain and phase margins may not be a reliable method for uncertain systems in general (see Example 4.2). In addition, some robust stability conditions of FO delay systems was proposed in the work of Yu and Wang [109]. Also, the robust stability of uncertain FO plants with a time delay has been investigated using fractional controllers in previous works [110, 111]. The results reported in the works [109, 110, 111] cannot be employed for systems having an uncertain delay term.

In the work of Liang et al., [40], an algorithm has been proposed to compute the stabilizing Theorem 3.1 [40] and the obtained results [41] turns out to be wrong in general for FO systems having an uncertain time delay (See Remark 4.1 and Example 4.3). More precisely, in previous works [8, 9], the authors have proven that the value set of FO polynomials with uncertain coefficients is a convex polygon and it does not mean that the value set of a characteristic function having uncertain time delay would also have a polygon shape in the complex plane. In the present work, it is shown that robust stability analysis of systems having uncertain time delay turns out to be more complicated than uncertain FO polynomials and the unreliable extensions in works [40, 41]. Based on the above explanations, uncertainties in the numerator and denominator coefficients and the time delay term of the plant brings challenges to robust stability analysis for the closed-loop control system. Consequently, this issue motivates us to investigate the closed-loop control systems having an uncertain time delay. Motivated by the previous works, in this chapter, some methods are developed to investigate the robust stability of plants having uncertainties in the numerator and denominator coefficients and the time delay term using FO controllers. Since the numerator and denominator coefficients and the time delay term are assumed to be unknown lying in specified intervals and consequently typical methods in robust stability analysis such as Kharitanov's theorem are no longer applicable.

4.1 Preliminaries and Definitions

Consider the transfer function of a controller denoted by $C(s)$ that has the form

$$C(s) = \frac{N_C(s)}{D_C(s)} = \frac{\sum_{i_1=0}^{m_C} b_{i_1}^C s^{\beta_{i_1}^C}}{\sum_{i_2=0}^{n_C} a_{i_2}^C s^{\alpha_{i_2}^C}}, \quad (4.1)$$

where $\beta_{m_C}^C > \beta_{m_C-1}^C > \dots > \beta_1^C > \beta_0^C = 0$ and $\alpha_{n_C}^C > \alpha_{n_C-1}^C > \dots > \alpha_1^C > \alpha_0^C = 0$ and the coefficients $b_{i_1}^C$ and $a_{i_2}^C$ are real numbers. Furthermore, consider a plant described by an uncertain FO transfer function with an uncertain time delay that has the following form:

$$P(s) = \frac{N_P(s)}{D_P(s)} e^{-Ls} = \frac{\sum_{i_1=0}^{m_P} b_{i_1}^P s^{\beta_{i_1}^P}}{\sum_{i_2=0}^{n_P} a_{i_2}^P s^{\alpha_{i_2}^P}} e^{-Ls}, \quad (4.2)$$

in which the numerator and denominator coefficients of the plant are subjected to $b_{i_1}^P \in [\underline{b}_{i_1}^P, \bar{b}_{i_1}^P] (b_{m_P}^P \neq 0)$ and $a_{i_2}^P \in [\underline{a}_{i_2}^P, \bar{a}_{i_2}^P] (a_{n_P}^P \neq 0)$ and the time delay L lies in $L \in [\underline{L}, \bar{L}]$ and also $\beta_{m_P}^P > \beta_{m_P-1}^P > \dots > \beta_1^P > \beta_0^P = 0$ and $\alpha_{n_P}^P > \alpha_{n_P-1}^P > \dots > \alpha_1^P > \alpha_0^P = 0$, $\alpha_n^P > \beta_m^P$ and $\alpha_{n_P}^P + \alpha_{n_C}^C > \beta_{m_P}^P + \beta_{m_C}^C$ are arbitrary real numbers. Moreover, in this chapter, it is considered that the FO polynomial (4.3) represents the characteristic function of the negative unity feedback control system and is of the following form

$$\Delta(s) = D_C(s) D_P(s) + N_C(s) N_P(s) e^{-Ls}. \quad (4.3)$$

Study of robust stability of the closed-loop control system with the function $\Delta(s)$ in the presence of uncertainties in the numerator and denominator coefficients and the time delay term of the plant is the main object in this chapter. Towards setting up the discussion that follows, consider also Definition 4.1.

Definition 4.1. Based on Approach 2 in Subsection 2.2.2, the value sets of $N_P(s)$ and $D_P(s)$ are two convex polygons in the complex plane for $s = j\omega$ & $\omega > 0$. In this chapter, the vertex polynomials corresponding to $N_P(s)$ and $D_P(s)$ are respectively considered as $V_{i_1}^N(s) (i_1 = 1, 2, \dots, L_N)$ and $V_{i_2}^D(s) (i_2 = 1, 2, \dots, L_D)$.

Before concluding this section, consider also an important property of the value sets that is introduced by the following lemma (Lemma 4.1).

Lemma 4.1. [112] Let Q_1 and $Q_2 \neq 0$ be two complex plane polygons, then $\partial(\frac{Q_1}{Q_2}) \subset (\frac{V_{Q_1}}{E_{Q_2}}) \cup (\frac{E_{Q_1}}{V_{Q_2}})$ where ∂ shows the boundary and V_{Q_i} and E_{Q_i} are, respectively, the vertex sets and the edge sets of Q_i .

4.2 Robust stability analysis

Based on the zero exclusion principle, the condition $0 \notin \Delta(j\omega)$ has to be checked for $\omega \geq 0$. Hence, in the following theorem a test frequency interval instead of the infinite frequency range is obtained to check the condition $0 \notin \Delta(j\omega)$.

Theorem 4.1. *The zero exclusion condition $0 \notin \Delta(j\omega)$ in (4.3) is held for the frequency range $\omega \in [0, S_{\min}) \cup (S_{\max}, \infty)$ in which*

$$\begin{aligned}
S_{\max} &= \min\{S_{\max_1}, S_{\max_2}\}, \\
S_{\max_1} &= \max\{\sigma_1^{\frac{1}{\alpha_{n_C}^C + \alpha_{n_P}^P - \varepsilon_1}}, 1\}, \\
\varepsilon_1 &= \max\{\alpha_{n_C}^C + \alpha_{n_P-1}^P, \alpha_{n_C-1}^C + \alpha_{n_P}^P, \beta_{m_C}^C + \beta_{m_P}^P\}, \\
\sigma_1 &= \frac{\sigma_1^1 + \sigma_1^2 + \sigma_1^3 + \sigma_1^4}{\sigma_1^5}, \\
\sigma_1^1 &= \left(\sum_{i^2=0}^{n_C-1} |a_{i^2}^C|\right) \left(\sum_{i^2=0}^{n_P-1} \max\{|\underline{a}_{i^2}^P|, |\bar{a}_{i^2}^P|\}\right), \\
\sigma_1^2 &= |a_{n_C}^C| \left(\sum_{i^2=0}^{n_P-1} \max\{|\underline{a}_{i^2}^P|, |\bar{a}_{i^2}^P|\}\right), \\
\sigma_1^3 &= \max\{|\underline{a}_{n_P}^P|, |\bar{a}_{n_P}^P|\} \left(\sum_{i^2=0}^{n_C-1} |a_{i^2}^C|\right), \\
\sigma_1^4 &= \left(\sum_{i_1=0}^{m_C} |b_{i_1}^C|\right) \left(\sum_{i_1=0}^{m_P} \max\{|\underline{b}_{i_1}^P|, |\bar{b}_{i_1}^P|\}\right), \\
\sigma_1^5 &= |a_{n_C}^C| \min\{|\underline{a}_{n_P}^P|, |\bar{a}_{n_P}^P|\}.
\end{aligned} \tag{4.4}$$

$$S_{\max_2} = (1 + \sigma_2)^{\frac{1}{\varepsilon_2}}, \quad \sigma_2 = \frac{M R}{|a_{n_C}^C| \min\{|\underline{a}_{n_P}^P|, |\bar{a}_{n_P}^P|\}}, \tag{4.5}$$

$$M = \max\{\bigcup_{k=1}^4 M_k\},$$

$$M_1 = \begin{cases} \emptyset, & \text{for } n_C = 0, \\ \left(\max\left\{\bigcup_{i^1=0}^{n_C-1} |a_{i^1}^C|\right\}\right) \times \\ \left(\max\left\{\bigcup_{i^2=0}^{n_P-1} \max\{|\underline{a}_{i^2}^P|, |\bar{a}_{i^2}^P|\}\right\}\right), & \text{for } n_C > 0, \end{cases}$$

$$\begin{aligned}
M_2 &= |a_{n_C}^C| \left(\max\left\{\bigcup_{i^2=0}^{n_P-1} \max\{|\underline{a}_{i^2}^P|, |\bar{a}_{i^2}^P|\}\right\}\right), \\
M_3 &= \begin{cases} \emptyset, & \text{if } n_C = 0, \\ \max\{|\underline{a}_{n_P}^P|, |\bar{a}_{n_P}^P|\} \times \\ \left(\max\left\{\bigcup_{i^1=0}^{n_C-1} |a_{i^1}^C|\right\}\right), & \text{if } n_C > 0, \end{cases} \\
M_4 &= \left(\max\left\{\bigcup_{j^1=0}^{m_C} |b_{j^1}^C|\right\}\right) \left(\max\left\{\bigcup_{j^2=0}^{m_P} \max\{|\underline{b}_{j^2}^P|, |\bar{b}_{j^2}^P|\}\right\}\right),
\end{aligned}$$

and $\varepsilon_2 = \min\{\mathfrak{K}_1, \frac{\mathfrak{K}_2}{2}, \dots, \frac{\mathfrak{K}_{\hat{n}}}{\hat{n}}\}$, $0 < \mathfrak{K}_1 < \mathfrak{K}_2 < \dots < \mathfrak{K}_{\hat{n}}$ and \mathfrak{K}_i are the distinct members of the set H defined as follows.

$$\begin{aligned}
 H = & \left(\bigcup_{i^1=0}^{n_C-1} \bigcup_{i^2=0}^{n_P-1} \{ \alpha_{n_C}^C + \alpha_{n_P}^P - (\alpha_{i_1}^C + \alpha_{i_2}^P) \} \right) \cup \\
 & \left(\bigcup_{i^2=0}^{n_P-1} \{ \alpha_{n_P}^P - \alpha_{i_2}^P \} \right) \cup \left(\bigcup_{i^1=0}^{n_C-1} \{ \alpha_{n_C}^C - \alpha_{i_1}^C \} \right) \cup \\
 & \left(\bigcup_{j^1=0}^{m_C} \bigcup_{j^2=0}^{m_P} \{ \alpha_{n_C}^C + \alpha_{n_P}^P - (\beta_{j_1}^C + \beta_{j_2}^P) \} \right).
 \end{aligned} \tag{4.6}$$

Also, S_{\min} is defined as follows.

$$\begin{aligned}
 S_{\min} &= \min\{\sigma_3^{\frac{1}{\varepsilon_3}}, 1\}, \varepsilon_3 = \min\{\alpha_1^C, \alpha_1^P, \beta_1^C, \beta_1^P\}, \\
 \sigma_3 &= \frac{\kappa}{\sigma_3^1 + \sigma_3^2 + \sigma_3^3 + \sigma_3^4 + \sigma_3^5 + \sigma_3^6}, \\
 \sigma_3^1 &= \left(\sum_{i^1=1}^{n_C} |a_{i^1}^C| \right) \left(\sum_{i^2=1}^{n_P} \max\{|\underline{a}_{i^2}^P|, |\bar{a}_{i^2}^P|\} \right), \\
 \sigma_3^2 &= \max\{|\underline{a}_0^P|, |\bar{a}_0^P|\} \left(\sum_{i^1=1}^{n_C} |a_{i^1}^C| \right), \\
 \sigma_3^3 &= |a_0^C| \left(\sum_{i^2=1}^{n_P} \max\{|\underline{a}_{i^2}^P|, |\bar{a}_{i^2}^P|\} \right), \\
 \sigma_3^4 &= \left(\sum_{j^1=1}^{m_C} |b_{j^1}^C| \right) \left(\sum_{j^2=1}^{m_P} \max\{|\underline{b}_{j^2}^P|, |\bar{b}_{j^2}^P|\} \right), \\
 \sigma_3^5 &= |b_0^C| \left(\sum_{j^2=1}^{m_P} \max\{|\underline{b}_{j^2}^P|, |\bar{b}_{j^2}^P|\} \right), \\
 \sigma_3^6 &= \max\{|\underline{b}_0^P|, |\bar{b}_0^P|\} \left(\sum_{j^1=1}^{m_C} |b_{j^1}^C| \right), \\
 \kappa &= \begin{cases} \kappa_1, & \text{for } 0 \notin [\underline{a}_0^P, \bar{a}_0^P] \text{ and } \kappa_1 > 0, \\ \kappa_2, & \text{for } 0 \notin [\underline{b}_0^P, \bar{b}_0^P] \text{ and } \kappa_2 > 0, \\ 0, & \text{otherwise,} \end{cases} \\
 \kappa_1 &= \min\{|\underline{a}_0^P|, |\bar{a}_0^P|\} |a_0^C| - \max\{|\underline{b}_0^P|, |\bar{b}_0^P|\} |b_0^C|, \\
 \kappa_2 &= \min\{|\underline{b}_0^P|, |\bar{b}_0^P|\} |b_0^C| - \max\{|\underline{a}_0^P|, |\bar{a}_0^P|\} |a_0^C|.
 \end{aligned} \tag{4.7}$$

Proof. By using the triangle inequality and assuming $\omega > 1$, we have

$$\begin{aligned}
|\Delta(j\omega)| &\geq |a_{n_C}^C| \min\{|\underline{a}_{n_P}^P|, |\bar{a}_{n_P}^P|\} \omega^{\alpha_{n_C}^C + \alpha_{n_P}^P} - \\
&\left(\left(\sum_{i^1=0}^{n_C-1} |a_{i^1}^C| \omega^{\alpha_{i^1}^C} \right) \left(\sum_{i^2=0}^{n_P-1} \max\{|\underline{a}_{i^2}^P|, |\bar{a}_{i^2}^P|\} \omega^{\alpha_{i^2}^P} \right) + \right. \\
&|a_{n_C}^C| \omega^{\alpha_{n_C}^C} \left(\sum_{i^2=0}^{n_P-1} \max\{|\underline{a}_{i^2}^P|, |\bar{a}_{i^2}^P|\} \omega^{\alpha_{i^2}^P} \right) + \\
&\max\{|\underline{a}_{n_P}^P|, |\bar{a}_{n_P}^P|\} \omega^{\alpha_{n_P}^P} \left(\sum_{i^1=0}^{n_C-1} |a_{i^1}^C| \omega^{\alpha_{i^1}^C} \right) + |e^{-\omega L j}| \\
&\left. \left(\sum_{r^1=0}^{m_C} |b_{r^1}^C| \omega^{\beta_{r^1}^C} \right) \left(\sum_{r^2=0}^{m_P} \max\{|\underline{b}_{r^2}^P|, |\bar{b}_{r^2}^P|\} \omega^{\beta_{r^2}^P} \right) \right) \\
&\geq |a_{n_C}^C| \min\{|\underline{a}_{n_P}^P|, |\bar{a}_{n_P}^P|\} \omega^{\varepsilon_1} \left(\omega^{\alpha_{n_C}^C + \alpha_{n_P}^P - \varepsilon_1} - \sigma_1 \right).
\end{aligned} \tag{4.8}$$

From (4.8), if $\omega > S_{\max_1}$, then $|\Delta(j\omega)| > 0$ and this implies $0 \notin \Delta(j\omega)$. For S_{\max_2} , we have

$$\begin{aligned}
|\Delta(j\omega)| &\geq |a_{n_C}^C| \min\{|\underline{a}_{n_P}^P|, |\bar{a}_{n_P}^P|\} \omega^{\alpha_{n_C}^C + \alpha_{n_P}^P} - \\
&\left(\left(\sum_{i^1=0}^{n_C-1} |a_{i^1}^C| \omega^{\alpha_{i^1}^C} \right) \left(\sum_{i^2=0}^{n_P-1} \max\{|\underline{a}_{i^2}^P|, |\bar{a}_{i^2}^P|\} \omega^{\alpha_{i^2}^P} \right) + \right. \\
&|a_{n_C}^C| \omega^{\alpha_{n_C}^C} \left(\sum_{i^2=0}^{n_P-1} \max\{|\underline{a}_{i^2}^P|, |\bar{a}_{i^2}^P|\} \omega^{\alpha_{i^2}^P} \right) + \\
&\max\{|\underline{a}_{n_P}^P|, |\bar{a}_{n_P}^P|\} \omega^{\alpha_{n_P}^P} \left(\sum_{i^1=0}^{n_C-1} |a_{i^1}^C| \omega^{\alpha_{i^1}^C} \right) + |e^{-\omega L j}| \\
&\left. \left(\sum_{r^1=0}^{m_C} |b_{r^1}^C| \omega^{\beta_{r^1}^C} \right) \left(\sum_{r^2=0}^{m_P} \max\{|\underline{b}_{r^2}^P|, |\bar{b}_{r^2}^P|\} \omega^{\beta_{r^2}^P} \right) \right) \geq
\end{aligned} \tag{4.9}$$

$$\begin{aligned}
&|a_{n_C}^C| \min\{|\underline{a}_{n_P}^P|, |\bar{a}_{n_P}^P|\} \omega^{\alpha_{n_C}^C + \alpha_{n_P}^P} \left(1 - \right. \\
&\left. MR \left((\omega^{-1})^{\aleph_1} + (\omega^{-1})^{\aleph_2} + \dots + (\omega^{-1})^{\aleph_{\hat{n}}} \right) \right) \geq \\
&\frac{|a_{n_C}^C| \min\{|\underline{a}_{n_P}^P|, |\bar{a}_{n_P}^P|\}}{|a_{n_C}^C| \min\{|\underline{a}_{n_P}^P|, |\bar{a}_{n_P}^P|\}} \left(1 - \right. \\
&\left. \frac{\sigma_2 (\omega^{-1})^{\varepsilon_2} (1 - (\omega^{-1})^{\hat{n}\varepsilon_2})}{(1 - (\omega^{-1})^{\varepsilon_2})} \right) \geq |a_{n_C}^C| \min\{|\underline{a}_{n_P}^P|, |\bar{a}_{n_P}^P|\} \\
&\omega^{\alpha_{n_C}^C + \alpha_{n_P}^P} \left(1 - \frac{\sigma_2 (\omega^{-1})^{\varepsilon_2}}{(1 - (\omega^{-1})^{\varepsilon_2})} \right).
\end{aligned}$$

According to (4.9), if $\omega > S_{\max_2}$, then $|\Delta(j\omega)| > 0$ and consequently $0 \notin \Delta(j\omega)$. Also, the proof of S_{\min} is similar to S_{\max_1} .

□

Now, in the following, it is checked that whether or not the value set of $\Delta(s)$ encircles the origin for $\omega \in [S_{\min}, S_{\max}]$.

Theorem 4.2. Assume the value set of the characteristic function $\Delta(j\omega)$ is defined as $\Delta^{vs}(j\omega)$ at each frequency. Also, consider $\Delta(j\omega) = \Delta_1(j\omega) + \Delta_2(j\omega)$. Then, at a fixed frequency $\omega = \omega_0 \in [S_{\min}, S_{\max}]$, $0 \in \Delta^{vs}(j\omega)$, if and only if the value sets of $-\Delta_1^{vs}(s = j\omega_0)$ and $\Delta_2^{vs}(s = j\omega_0)$ have an overlap in the complex plane.

Proof. *Proof of the necessity:* $0 \in \Delta^{vs}(j\omega_0)$ can be written as $\{z_0 - z_0\} \in \Delta^{vs}(j\omega_0)$. Hence, one can simply deduce that $z_0 \in -\Delta_1^{vs}(j\omega_0)$ and $z_0 \in \Delta_2^{vs}(j\omega_0)$. This means that in the complex plane, $-\Delta_1^{vs}(j\omega_0)$ and $\Delta_2^{vs}(j\omega_0)$ have an overlap.

Proof of the sufficiency: Because of the overlap between $-\Delta_1^{vs}(j\omega_0)$ and $\Delta_2^{vs}(j\omega_0)$, there is an arbitrary complex number as z_0 such that $z_0 \in -\Delta_1^{vs}(j\omega_0)$ and $z_0 \in \Delta_2^{vs}(j\omega_0)$. This implies that there is a member of the family $-\Delta_1^{vs}(j\omega_0)$ as $-\tilde{\Delta}_1(j\omega_0)$ which is equal to z_0 i.e. $z_0 = -\tilde{\Delta}_1(j\omega_0)$. Likewise, one can show that $z_0 = \tilde{\Delta}_2(j\omega_0)$. Assume that $\{\tilde{\Delta}(j\omega) = \tilde{\Delta}_1(j\omega) + \tilde{\Delta}_2(j\omega)\} \in \Delta(j\omega)$. Hence, at the fixed frequency $\omega = \omega_0$, it is obvious that $0 \in \Delta^{vs}(j\omega)$. \square

Lemma 4.2. Assume $D_C(s) \mathbf{D}_P(s) \neq 0$ for $s = j\omega_0$ and $\omega_0 \in [S_{\min}, S_{\max}]$. Then, $0 \notin \Delta^{vs}(j\omega_0)$ if and only if, $\Theta_1(j\omega_0)$ and $\Theta_2(j\omega_0)$ in (4.10) have no overlap in the complex plane.

$$\Theta_1(j\omega) = -e^{Lj\omega}, \Theta_2(j\omega) = \left(\frac{N_v^{r_1}}{D_E^{r_2}} \right) \cup \left(\frac{N_E^{r_1}}{D_v^{r_2}} \right), \quad (4.10)$$

in which

$$\begin{cases} N_v^{r_1} = N_c(j\omega) V_{r_1}^N(j\omega), r_1 = 1, 2, \dots, L_N, \\ D_v^{r_2} = D_c(j\omega) V_{r_2}^D(j\omega), r_2 = 1, 2, \dots, L_D, \\ V_1^N(j\omega) = V_{L_N+1}^N(j\omega), V_1^D(j\omega) = V_{L_D+1}^D(j\omega), \end{cases} \quad (4.11)$$

$$\begin{cases} N_E^{r_1} = e(N_c(j\omega) V_{r_1}^N(j\omega), N_c(j\omega) V_{r_1+1}^N(j\omega)), \\ D_E^{r_2} = e(D_c(j\omega) V_{r_2}^D(j\omega), D_c(j\omega) V_{r_2+1}^D(j\omega)). \end{cases}$$

where for two arbitrary polynomials X and Y , we have $e(X, Y) = \eta X + (1 - \eta)Y$, $\eta \in [0, 1]$.

Proof. According to the work [9], the value sets of $D_C(s) \mathbf{D}_P(s)$ and $N_C(s) \mathbf{N}_P(s)$ would be two parpolygons in the complex plane for $s = j\omega$. On the other hand, the following holds for $s = j\omega_0$.

$$0 \in \Delta(s) \iff 0 \in e^{Ls} + \frac{N_C(s) \mathbf{N}_P(s)}{D_C(s) \mathbf{D}_P(s)}. \quad (4.12)$$

Moreover, based on **Lemma 4.1**, it can be inferred that

$$\partial \left(\frac{N_C(s) \mathbf{N}_P(s)}{D_C(s) \mathbf{D}_P(s)} \right) \subset \Theta_2(s), s = j\omega_0. \quad (4.13)$$

From (4.13), **Theorem 4.1** and **Theorem 4.2**, the proof is simply completed. \square

Lemma 4.3. Assume $N_C(s) \mathbf{N}_P(s) \neq 0$ for $s = j\omega_0$ and $\omega_0 \in [S_{\min}, S_{\max}]$. Then, $0 \notin \Delta^{vs}(j\omega_0)$ if and only if, $(\Theta_1(j\omega_0))^{-1}$ and $\Theta_3(j\omega_0)$ have no overlap, where $\Theta_1(j\omega_0)$ and $\Theta_3(j\omega_0)$ are respectively defined in (4.10) and (4.14).

$$\Theta_3(j\omega) = \left(\frac{D_E^{r_2}}{N_v^{r_1}} \right) \cup \left(\frac{D_v^{r_2}}{N_E^{r_1}} \right). \quad (4.14)$$

All elements defined in (4.14) are given by (4.11).

Proof. The proof follows from Lemma 4.1. \square

Theorem 4.3. Assume that $S_{\min} < \frac{2\pi}{L-L} \leq S_{\max}$. Then, the controller $C(s)$ robustly stabilizes the closed-loop control system, if and only if:

1. The controller $C(s)$ can stabilize one member of the closed-loop control system with the characteristic function $\Delta_0(s)$.
2. For $\omega \in [S_{\min}, \frac{2\pi}{L-L})$, the value sets of $D_E^{i_2}(j\omega)$ and $N_V^{i_1}(j\omega)(\Theta_1(j\omega))^{-1}$ do not have any overlap.
3. For $\omega \in [S_{\min}, \frac{2\pi}{L-L})$, the value sets of $D_V^{i_2}(j\omega)\Theta_1(j\omega)$ and $N_E^{i_1}(j\omega)$ do not have any overlap.
4. For $\omega \in [\frac{2\pi}{L-L}, S_{\max}]$, $\bar{\Lambda}(\omega) > 0$ is satisfied where

$$\begin{aligned} \bar{\Lambda}(\omega) &= \min_{D_E^{i_2} \in P_D} |D_E^{i_2}| - \max\{N_V^1(j\omega), \dots, N_V^{L_N}(j\omega)\}, \\ P_D &= \{D_E^1, \dots, D_E^{L_D}\}, \end{aligned} \quad (4.15)$$

in which $D_E^{i_2}, N_V^{i_1}(j\omega), i_1 = 1, \dots, L_D$ and $\Theta_1(j\omega)$ can be found in **Lemma 4.2**.

Proof. For the case $\omega \in [S_{\min}, \frac{2\pi}{L-L})$, the proof can be simply concluded from **Lemma 4.2** and **Lemma 4.2**. Hence, in the following, the necessary and sufficient conditions are discussed for $\omega \in [\frac{2\pi}{L-L}, S_{\max}]$.

Proof of the sufficiency: It can be simply proven that the maximum magnitude of a parpolygon occurs at vertex and the minimum magnitude of a parpolygon also occurs on its boundary. Since, $\bar{\Lambda}(\omega) > 0$ is held, then it can be inferred from equation (4.3), $\min |D_C(s) \mathbf{D}_P(s)| > \max |N_C(s) \mathbf{N}_P(s)|$ for $s = j\omega$ and $\omega \in [\frac{2\pi}{L-L}, S_{\max}]$ and consequently $0 \notin \Delta(j\omega)$.

Proof of the Necessity: Since the characteristic function (4.3) is robust stable, based on the zero exclusion principle $0 \notin \Delta(j\omega)$. Also, it is apparent that for $s = j\omega$ and $\omega \rightarrow \infty$, $|D_C(s) \mathbf{D}_P(s)| / |N_C(s) \mathbf{N}_P(s)| \rightarrow \infty$. Assume that the inequality $\bar{\Lambda}(\omega) > 0$ is not met. Because of the continuity $|D_C(s) \mathbf{D}_P(s)| / |N_C(s) \mathbf{N}_P(s)|$, there exists $\omega^* \in [\frac{2\pi}{L-L}, \infty]$ such that $|D_C(s) \mathbf{D}_P(s)| / |N_C(s) \mathbf{N}_P(s)| = 1$ and this means that $-D_C(s) \mathbf{D}_P(s)$ and $N_C(s) \mathbf{N}_P(s) e^{-Ls}$ have an overlap and based on **Theorem 4.1**, it can be concluded that $0 \in \Delta(j\omega^*)$. It contradicts stability of the system. \square

Remark 4.1. Based on **Theorem 4.3**, because of the uncertain delay term $e^{-Lj\omega}$ (or $e^{Lj\omega}$), the value set of $\Delta(j\omega)$ is non-convex shape. Therefore, Theorem 3.1 in [40] and the extensions of the value set in the work [41] may lead to unreliable results because the authors of the aforementioned papers assumed that $\Delta^{vs}(j\omega)$ is a convex shape.

Corollary 4.1. Assume that $S_{\max} < \frac{2\pi}{L-L}$. Then, the controller $C(s)$ robustly stabilizes the closed-loop control system, if and only if:

1. The controller $C(s)$ can stabilize one member of the closed-loop control system with the characteristic function $\Delta_0(s)$.
2. For $\omega \in [S_{\min}, S_{\max}]$, the value sets of $D_E^{i_2}(j\omega)$ and $N_V^{i_1}(j\omega)(\Theta_1(j\omega))^{-1}$ do not have any overlap.

3. For $\omega \in [S_{\min}, S_{\max}]$, the value sets of $D_V^{i2}(j\omega)\Theta_1(j\omega)$ and $N_E^{i1}(j\omega)$ do not have any overlap.

Proof. The proof follows immediately from **Theorem 4.3**.

Corollary 4.2. Assume that $S_{\min} \geq \frac{2\pi}{L-L}$. Then, the controller $C(s)$ robustly stabilizes the closed-loop control system, if and only if:

1. The controller $C(s)$ can stabilize one member of the closed-loop control system with the characteristic function $\Delta_0(s)$.
2. For $\omega \in [S_{\min}, S_{\max}]$, $\Lambda(\omega) > 0$ is satisfied where $\Lambda(\omega)$ is defined in equation (4.15)

Proof. The proof is directly from **Theorem 4.3**. □

4.3 Robust stability checking function

Combining the previous results and some geometric features allows us to provide a robust stability checking function represented by the following theorem (Theorem 4.4).

Theorem 4.4. Assume that $S_{\min} < \frac{2\pi}{L-L} \leq S_{\max}$. Then, the controller $C(s)$ robustly stabilizes the closed-loop system, if:

1. The controller $C(s)$ can stabilize one member of the closed-loop control system with the characteristic function $\Delta_0(s)$.
2. For $\omega \in [S_{\min}, S_{\max}]$, $\Lambda(\omega) > 0$ is satisfied in which

$$\Lambda(\omega) = \begin{cases} \min\{\underline{\Lambda}_i(\omega) | i = 1, 2, 3, 4\}, & \text{for } \omega \in [S_{\min}, \frac{2\pi}{L-L}], \\ \overline{\Lambda}(\omega) & \text{for } \omega \in [\frac{2\pi}{L-L}, S_{\max}], \end{cases} \quad (4.16)$$

in which

$$\begin{aligned} \underline{\Lambda}_1(\omega) &= \min\{\kappa_{h,g,i}^1(j\omega) | h \in \{1, \dots, L_N\}, i \in \{1, \dots, L_D\}, g \in \{1, 2, \dots, 4N_1 + 2\}\}, \\ \kappa_{h,g,i}^1(j\omega) &= \left| D_c(j\omega)V_i^D(j\omega) + N_c(j\omega)V_h^N(j\omega)P_g^1(j\omega) \right| + \\ &\quad \left| D_c(j\omega)V_{i+1}^D(j\omega) + N_c(j\omega)V_h^N(j\omega)P_g^1(j\omega) \right| - \left| D_c(j\omega)(V_i^D(j\omega) - V_{i+1}^D(j\omega)) \right|, \end{aligned} \quad (4.17)$$

$$\begin{aligned} \underline{\Lambda}_2(\omega) &= \min\{\kappa_{h,g,i}^2(j\omega) | h \in \{1, \dots, L_N\}, i \in \{1, \dots, L_D\}, g \in \{1, 2, \dots, 4N_1 + 2\}\}, \\ \kappa_{h,g,i}^2(j\omega) &= \left| D_c(j\omega)V_i^D(j\omega) + N_c(j\omega)V_h^N(j\omega)P_g^1(j\omega) \right| + \\ &\quad \left| D_c(j\omega)V_i^D(j\omega) + N_c(j\omega)V_h^N(j\omega)P_{g+1}^1(j\omega) \right| - \left| N_c(j\omega)V_h^N(j\omega)(P_{g+1}^1(j\omega) - P_g^1(j\omega)) \right|, \end{aligned} \quad (4.18)$$

$$\begin{aligned} \underline{\Lambda}_3(\omega) &= \min\{\kappa_{h,g,i}^3(j\omega) | h \in \{1, \dots, L_N\}, i \in \{1, \dots, L_D\}, g \in \{1, 2, \dots, 4N_2 + 2\}\}, \\ \kappa_{h,g,i}^3(j\omega) &= \left| D_c(j\omega)V_i^D(j\omega)P_g^2(j\omega) + N_c(j\omega)V_h^N(j\omega) \right| + \\ &\quad \left| D_c(j\omega)V_i^D(j\omega)P_g^2(j\omega) + N_c(j\omega)V_{h+1}^N(j\omega) \right| - \left| N_c(j\omega)(V_{h+1}^N(j\omega) - V_h^N(j\omega)) \right|, \end{aligned} \quad (4.19)$$

$$\begin{aligned}\underline{\Delta}_4(\omega) &= \min\{\kappa_{h,g,i}^4(j\omega) \mid h \in \{1, \dots, L_N\}, i \in \{1, \dots, L_D\}, g \in \{1, 2, \dots, 4N_2 + 2\}\}, \\ \kappa_{h,g,i}^4(j\omega) &= \left| D_c(j\omega) V_i^D(j\omega) P_g^2(j\omega) + N_c(j\omega) V_h^N(j\omega) \right| + \\ &\quad \left| D_c(j\omega) V_i^D(j\omega) P_{g+1}^2(j\omega) + N_c(j\omega) V_h^N(j\omega) \right| - \left| D_c(j\omega) V_i^D(j\omega) (P_{g+1}^2(j\omega) - P_g^2(j\omega)) \right|,\end{aligned}\quad (4.20)$$

where $P_g^1(j\omega)$, $P_g^2(j\omega)$ are defined as follows:

$$P_g^1(j\omega) = \begin{cases} \bar{P}_{g-1}^1(j\omega), & \text{for } 1 \leq g \leq 2N_1 + 1, \\ \underline{P}_{(2N_1)}^1(j\omega), & \text{for } g = 2N_1 + 2, \\ \underline{P}_{(2N_1-1)}^1(j\omega), & \text{for } g = 2N_1 + 3, \\ \dots & \\ \underline{P}_0^1(j\omega), & \text{for } g = 4N_1 + 2, \\ \bar{P}_0^1(j\omega), & \text{for } g = 4N_1 + 3, \end{cases} \quad (4.21)$$

$$\bar{P}_g^1(j\omega) = \begin{cases} e^{-j\omega \left(\tau + g \frac{\bar{\tau} - \tau}{2N_1} \right)}, & \text{for } g = 0, 2, \dots, 2N_1, \\ \frac{e^{-j\omega \left(\tau + g \frac{\bar{\tau} - \tau}{2N_1} \right)}}{\cos \left(\omega \frac{\bar{\tau} - \tau}{2N_1} \right)}, & \text{for } g = 1, 3, \dots, 2N_1 - 1, \end{cases}$$

$$\underline{P}_g^1(j\omega) = e^{-j\omega \left(\tau + g \frac{\bar{\tau} - \tau}{2N_1} \right)}, \quad g = 0, 1, 2, \dots, 2N_1.$$

$$P_g^2(j\omega) = \begin{cases} \bar{P}_{g-1}^2(j\omega), & \text{for } 1 \leq g \leq 2N_2 + 1, \\ \underline{P}_{(2N_2)}^2(j\omega), & \text{for } g = 2N_2 + 2, \\ \underline{P}_{(2N_2-1)}^2(j\omega), & \text{for } g = 2N_2 + 3, \\ \dots & \\ \underline{P}_0^2(j\omega), & \text{for } g = 4N_2 + 2, \\ \bar{P}_0^2(j\omega), & \text{for } g = 4N_2 + 3, \end{cases} \quad (4.22)$$

$$\bar{P}_g^2(j\omega) = \begin{cases} e^{j\omega \left(\tau + g \frac{\bar{\tau} - \tau}{2N_2} \right)}, & \text{for } g = 0, 2, \dots, 2N_2, \\ \frac{e^{j\omega \left(\tau + g \frac{\bar{\tau} - \tau}{2N_2} \right)}}{\cos \left(\omega \frac{\bar{\tau} - \tau}{2N_2} \right)}, & \text{for } g = 1, 3, \dots, 2N_2 - 1, \end{cases}$$

$$\underline{P}_g^2(j\omega) = e^{j\omega \left(\tau + g \frac{\bar{\tau} - \tau}{2N_2} \right)}, \quad g = 0, 1, 2, \dots, 2N_2.$$

where $N_1 \& N_2 \geq 3$.

Proof. It is proven that satisfying the inequality $\Lambda(\omega) > 0$ ensures that the second and third statements in Theorem 4.3 are held. In the following, at first, the overlap is investigated between the value sets of $D_E^{i_2}(j\omega)$ and $N_v^{i_1}(j\omega)(\Theta_1(j\omega))^{-1}$. On the other hand, based on Figure 4.1, the following geometric feature $\bar{P}_{r+1}^1(j\omega) = \bar{P}_r^1(j\omega)e^{-j\theta}/\cos(\theta)$ can

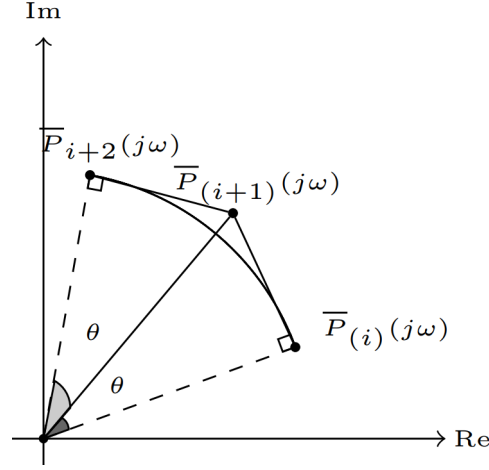


Figure 4.1: Value set of $e^{-j\omega}$ and $\bar{P}_r^1(j\omega)$.

be simply derived. From Figure 4.1, one can simply deduce that $e^{-Lj\omega}$ is located inside the exposed edges $P_g^1(j\omega)$ in (6.37). Also, satisfying the triangle inequality for any vertex of the value set $D_E^{i_2}(j\omega)$ and any two consecutive vertices of $N_v^{i_1}(j\omega)P_g^1(j\omega)$ implies that no vertex of $D_E^{i_2}(j\omega)$ intersects $N_v^{i_1}(j\omega)P_g^1(j\omega)$. Furthermore, satisfying the triangle inequality for any vertex of $N_v^{i_1}(j\omega)P_g^1(j\omega)$ and any two consecutive vertices of $D_E^{i_2}(j\omega)$ implies that no vertex of $N_v^{i_1}(j\omega)P_g^1(j\omega)$ intersects $D_E^{i_2}(j\omega)$. This means that the value sets $N_v^{i_1}(j\omega)P_g^1(j\omega)$ and $D_E^{i_2}(j\omega)$ do not have any overlap for $\omega \in (0, \frac{2\pi}{L-L}]$. Hence, if the inequalities $\underline{\Delta}_1(\omega) > 0$ and $\underline{\Delta}_2(\omega) > 0$ are held, then the second statement in Theorem 4.3 is met. Likewise, the inequalities $\underline{\Delta}_3(\omega) > 0$ and $\underline{\Delta}_4(\omega) > 0$ ensure that the third statement in Theorem 4.3 is also met. \square

Corollary 4.3. Assume that $S_{\max} < \frac{2\pi}{L-L}$. Then, the controller $C(s)$ robustly stabilizes the closed-loop control system if:

1. The controller $C(s)$ can stabilize one member of the closed-loop control system with the characteristic function $\Delta_0(s)$.
2. $\Lambda(\omega) = \min\{\underline{\Delta}_i(\omega) | i = 1, 2, 3, 4\} > 0$ is met for $\omega \in [S_{\min}, S_{\max}]$.

Proof. The proof follows immediately from **Theorem 4.4**. \square

Remark 4.2. The stability of the arbitrary characteristic function $\Delta_0(s)$ can be checked by Busłowicz [88] (as a suggestion). Moreover, based on the values of S_{\min} , S_{\max} and $\frac{2\pi}{L-L}$, one can choose **Theorem 4.3**, **Theorem 4.4** and **Corollaries 4.1-4.3**.

4.4 Robust Stability Analysis in FOMCON Toolbox

Analyzing the robust stability of interval FO systems is essential in control design when accounting for parameter uncertainties and modeling errors. The FOMCON toolbox in MATLAB provides a convenient and powerful set of tools to facilitate such analysis. The process generally involves two main steps:

Step 1: Define the Interval FO Transfer Function

To define an interval FO transfer function in MATLAB, we use the `ufotf` command provided by the FOMCON toolbox. This command allows users to construct transfer functions with fractional orders and interval uncertainties in the coefficients.

Step 2: Perform Robust Stability Analysis

Robust stability of the defined system can be checked using the following sub-steps:

1. **Check the Stability of a Nominal Member:** First, select one specific member from within the uncertainty set and evaluate its stability. This can be done using the `mikhailovfoc1cs` function, which checks the stability of the closed-loop control system via the Mikhailov criterion tailored for FO systems.
2. **Evaluate Robust Stability:** Next, use the `robstabfoc1cs` tool to assess the robust stability of the entire interval system. This function performs a comprehensive analysis over the uncertainty space and determines whether all admissible systems remain stable.

These tools help automate the tedious task of verifying stability across uncertain systems, making them particularly useful in the context of safety-critical applications. They can be applied to both interval FO systems with or without time delays, thereby extending their usefulness to a wide range of practical systems. The FOMCON toolbox also supports additional analysis tools and visualization features, which can further aid in controller design and validation.

4.5 Simulation and Experimental Results

In what follows, several examples as a comparison with the previous works [107, 110, 40, 41] are provided that show the magnificence of the approach for robust stability analysis of uncertain FO control systems proposed in this chapter.

Example 4.1. *In the work of Gao[110], it has been shown that the system in the term of the plant in (4.23) and the FOPI controller in (4.24) is robust stable.*

$$P(s) = \frac{[1.3, 1.7]s^{0.3} + [1.4, 1.6]}{[1.5, 2.5]s^{0.6} + [2.5, 3.5]s^{0.3} + [1.5, 2.5]}e^{-0.1s}, \quad (4.23)$$

$$C(s) = \frac{0.5 + 2s^{0.3}}{s^{0.3}}, \quad (4.24)$$

Now, let us consider uncertainty in the time delay term as $e^{-[0.01, 0.15]s}$ and the robust stability is again investigated by **Theorem 4.1**. Curve of the function $\Lambda(\omega)$ has been reported in Figure 4.2 for $N_1 = N_2 = 3$ and $\omega \in [2.9817 \times 10^{-5}, 1024]$ rad/sec. It is visible that the values of $\Lambda(\omega)$ are positive. Hence, the FOPI controller $C(s)$ in (4.24) can robustly stabilize the closed-loop control system in the presence of the uncertainties in numerator and denominator coefficients and the time delay term of the plant.

Example 4.2. *In the work of Senol et al.,[107], the FOPD controller $C(s)$ in (4.25) was designed for the plant $P(s)$ in (4.26).*

$$C(s) = 190.643 + 49.0765s^{1.14686}. \quad (4.25)$$

$$P(s) = \frac{0.3}{2s^2 + 3s + 1}e^{-0.01s}. \quad (4.26)$$

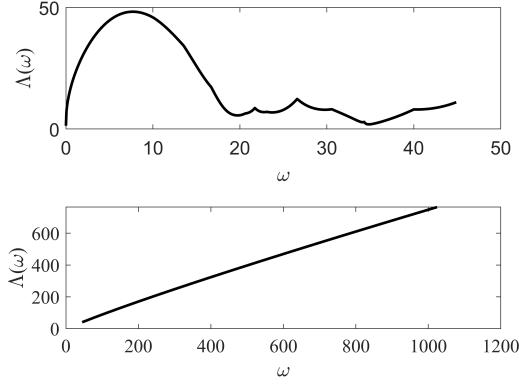


Figure 4.2: Curve of the function $\Lambda(\omega)$ in (6.30).

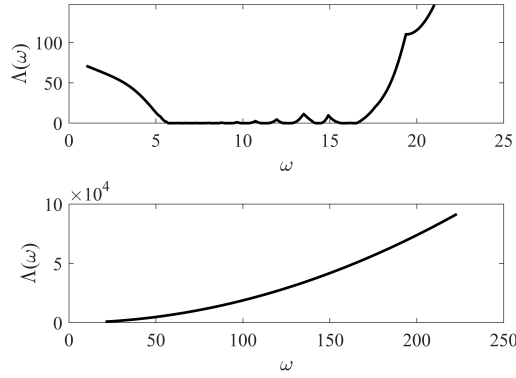


Figure 4.3: Curve of the function $\Lambda(\omega)$ in (6.30).

Now, let us consider uncertainties in the plant as

$$P(s) = \frac{[0.2, 0.4]}{[1.8, 2.2]s^2 + [2.8, 3.2]s + [0.9, 1.1]} e^{-[0.001, 0.3]s}. \quad (4.27)$$

It may be questionable that the FOPD controller $C(s)$ in (4.25) can robustly stabilize the interval plant $P(s)$ in (4.27). By benefiting from **Theorem 4.4**, the values of the function $\Lambda(\omega)$ are checked for $\omega \in [1, 222.1435]$ rad/sec. $\Lambda(\omega)$ is plotted for $N_1 = N_2 = 3$ in Figure 4.3. From this figure, $\Lambda(\omega) > 0$ is not satisfied. There may exist $0 \in \Delta(j\omega)$ for $\omega \in [1, 111.1785]$ rad/sec. Figure 4.4 shows that there is an overlap between the value sets $D_E^{i_2}(j\omega)$ and $N_v^{i_1}(j\omega)(\Theta_1(j\omega))^{-1}$ at $\omega = 6$ rad/sec. Based on **Theorem 4.3**, this system cannot be robust stable. This example shows that satisfying gain and phase margins may not be a reliable method for systems having uncertainties.

Example 4.3. Consider an uncertain plant with an uncertain time delay as (4.28).

$$P(s) = \frac{[0.66, 0.68]}{[0.5, 0.6]s^{1.6} + 1} e^{-[1, 2.5]s}. \quad (4.28)$$

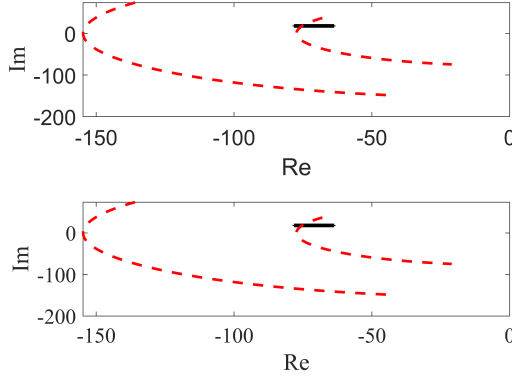


Figure 4.4: The overlap between $D_E^{i_2}(j\omega)$ (solid line) and $N_v^{i_1}(j\omega)(\Theta_1(j\omega))^{-1}$ (dotted line) at $\omega = 6$ rad/sec.

Also, the FOPID controllers is as follows:

$$C(s) = 0.51 + \frac{0.4}{s^{0.2}} + 0.001s^{0.2}. \quad (4.29)$$

At first, Theorem 3.1 in the work [40] is employed for robust stability analysis. The stability of the vertices mentioned in Theorem 3.1 [40] is checked based on the graphical method presented in [105]. From Figure 4.5 and Theorem 3.1 [40], the closed-loop control system is robust stable. But, Figure 4.6 shows that there is an overlap between $D_E^{i_2}(j\omega)$ and $N_v^{i_1}(j\omega)(\Theta_1(j\omega))^{-1}$ at $\omega = 1.2$ rad/sec. Therefore, the system is not robust stable based on Theorem 4.3. The stability of $\hat{\Delta}(s)$ in (4.30) has been analyzed based on the work of Busłowicz [88]. This implies that Theorem 3.1 in the work [40] and the results obtained in the work [41] are not reliable. Because, the value set of characteristics functions having uncertain time delay would be non-convex shape in the complex plane.

$$\hat{\Delta}(s) = s^{0.2}(0.5s^{1.6} + 1) + 0.67(0.51s^{0.2} + 0.4 + 0.001s^{0.4})e^{-1.8s}. \quad (4.30)$$

Example 4.4. In this example, the primary objective is to control the pitch of the TRAS, as illustrated in Figure 1.1. The open-loop system has been identified as (4.31).

$$P(s) = \frac{[6, 8]s + [2.5, 3.7]}{[13, 15]s^3 + [10, 11]s^2 + [4.5, 6]s - 1} e^{-[0.1, 0.15]s}. \quad (4.31)$$

Our aim is to check the robust stability of the closed-loop control system using FOMCON toolbox by applying the FOPID controller in (4.32).

$$C(s) = 1.9 + \frac{0.65}{s} + 0.9s^{1.3}. \quad (4.32)$$

Step 1: Check the stability of one chosen member in the uncertainty space of the plant. We use Lemma 2.2 to check the stability of the following chosen member.

$$P_0(s) = \frac{6s + 2.5}{13s^3 + 10s^2 + 4.5s - 1} e^{-0.1s}. \quad (4.33)$$

Hence, at first, $P_0(s)$ in (4.33) and the FOPID controller (4.32) can be defined by ufof tool as follows.

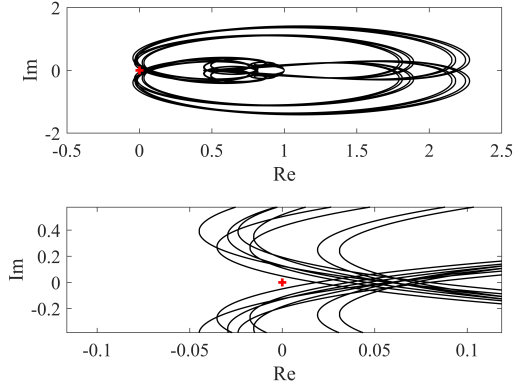


Figure 4.5: The robust stability analysis of the system described in Example 4.3 by Theorem 3. 1 in [40].

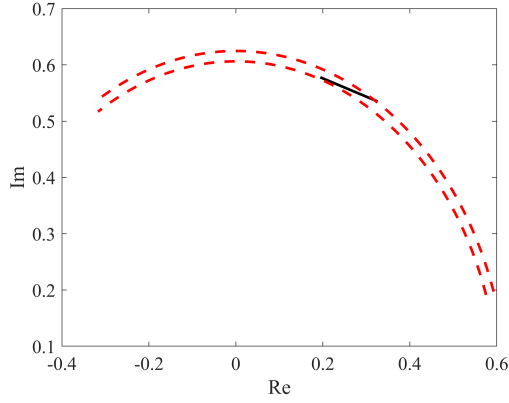


Figure 4.6: The overlap between $D_E^{i_2}(j\omega)$ (solid line) and $N_v^{i_1}(j\omega)(\Theta_1(j\omega))^{-1}$ (dotted line) at $\omega = 1.2$ rad/sec for Example 4.3.

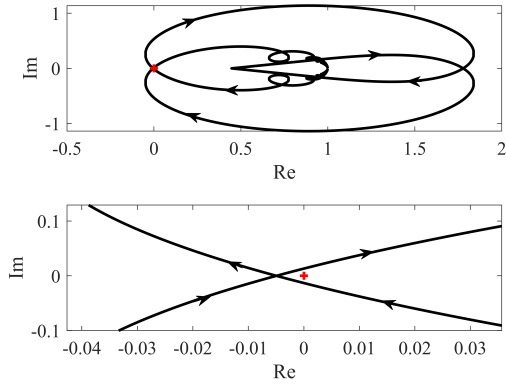


Figure 4.7: Stability analysis of $\hat{\Delta}(s)$ in (4.30) by the method presented in [88].


```
P_0 = ufotf('6s+2.5', '13s^3+10s^2+4.5s-1',.1);
C = ufotf('.9s^2.3+ 1.9s+ .65','s');
```

A method called `mikhailovfoclbs` is provided to verify the **Mikhailov stability criterion** (see Lemma 2.2). By executing `mikhailovfoclbs(P_0)`, the resulting Mikhailov plot is generated, as shown in Figure 4.8. The stability of the nominal closed-loop control system can then be assessed using this figure in conjunction with the **Mikhailov stability criterion** described in Lemma 2.2. If the selected nominal system is found to be unstable, there is no need to proceed to the next step, since the corresponding interval polynomial cannot exhibit robust stability.

Step 2: As discussed earlier, the FO interval transfer functions $P(s)$ can be made by `ufotf` tool as follows.

```
P = ufotf('[6,8]s+[2.5,3.7]', '[13,15]s^3+[10,11]s^2
+[4.5,6]s-1',[.1 .15])
```

$$\frac{[6, 8]s + [2.5, 3.7]}{[13, 15]s^3 + [10, 11]s^2 + [4.5, 6]s - 1} \exp(-[0.1, 0.15]s)$$

FO transfer function with uncertainty intervals.

Now, by typing `robstabfoclbs(C, P)` in command window we have:

```
robstabfoclbs(C, P)
"the system is robustly stable"
```

Figures 4.9 and 4.10 present the pitch angle response and the control signal of the TRAS system, respectively. This example demonstrates the applicability of the proposed method for real-world systems.

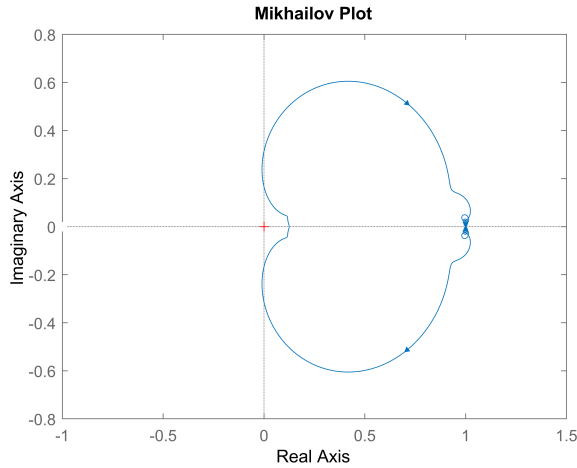


Figure 4.8: Mikhailov plot for the nominal case.

Example 4.5. In this example we utilize FMINCON toolbox to robustly stabilize a modular servo system of the Centre for Intelligent Systems of TalTech University, as depicted in Figure 4.11.

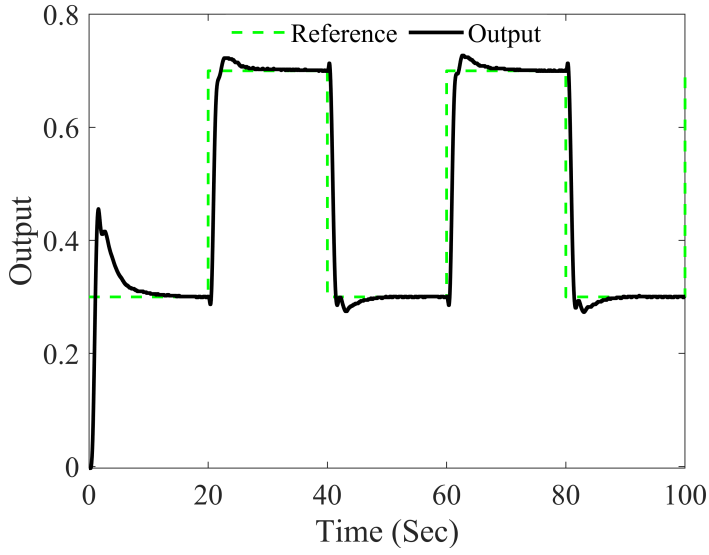


Figure 4.9: Output (the pitch angle).

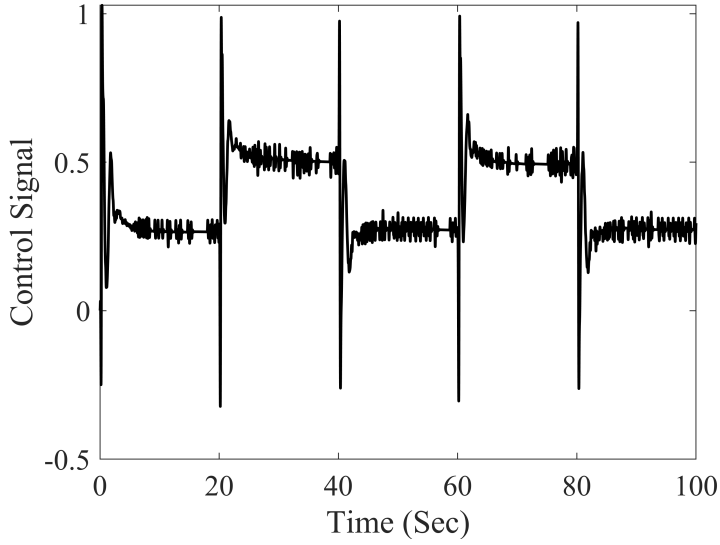


Figure 4.10: Control signal.

The velocity transfer function is identified using the MATLAB system identification toolbox [113] as follows:

$$P_v(s) = \frac{[558, 565.5]s^2 + [9.2, 10.3]s + [0.02, 0.04]}{s^3 + [3, 4]s^2 + [0.06, 0.07]s + [0.0002, 0.0003]}. \quad (4.34)$$

and the angle transfer function is derived by incorporating an integrator

$$P(s) = \frac{[558, 565.5]s^2 + [9.2, 10.3]s + [0.02, 0.04]}{s(s^3 + [3, 4]s^2 + [0.06, 0.07]s + [0.0002, 0.0003])}. \quad (4.35)$$

It is shown that the following FOPD controller can robustly stabilize the closed-loop control



Figure 4.11: Servo system of the Centre for Intelligent Systems of TalTech University.

system.

$$C_{FOPD}(s) = 0.052 + 0.018 s^{0.8}.$$

At first, $P_0(s)$ and the FOPD controller are defined by `ufotf` tool as follows.

```
P_0=ufotf('558s^2 + 9.2s + .02', 's^4 + 3s^3
+ .06s^2 + .0002s', 0);
C = ufotf(' .052+ .018s^ .8', '1');
```

From Figure 4.12, it is seen that the chosen member is stable.

The FO interval transfer functions $P(s)$ can be made by `ufotf` tool as follows.

```
P=ufotf('[558,565.5]s^2 + [9.2,10.3]s + [.02,.04]',
's^4 + [3,4]s^3 +
[.06,.07]s^2 + [.0002,.0003]s', 0)

[558, 565.5]s^{2}+[9.2, 10.3]s+[0.02, 0.04]
----- exp(-[0, 0]s)
s^{4}+[3, 4]s^{3}+[0.06, 0.07]s^{2}+[0.0002, 0.0003]s
```

FO transfer function with uncertainty intervals.

Now, by typing `robstabfoc1cs(C, P)` in the command window, the message “the system is robustly stable” appears, indicating that the system is indeed robustly stable. Output and Control signal have been shown in Figure 4.13 and Figure 4.14, respectively.

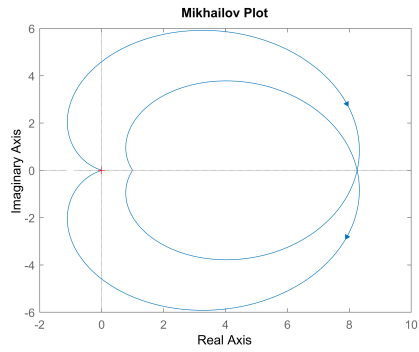


Figure 4.12: Mikhailov'plot for the nominal case.

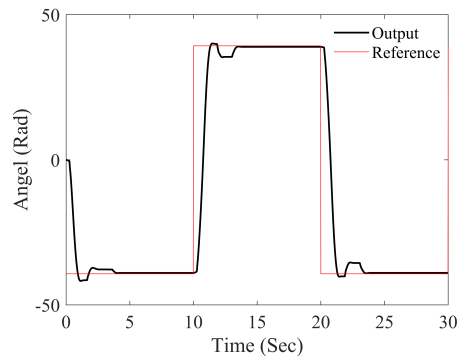


Figure 4.13: Output (blue) and reference (red).

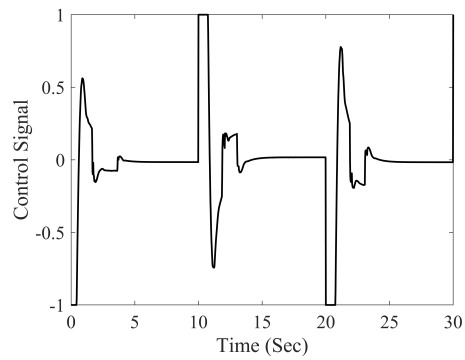


Figure 4.14: Control signal.

5 Robust Stability Region of Fractional-Order Controllers

This chapter focuses on computing the stabilizing region of FOPID controllers for interval FO plants, both with and without interval time delays. First, several theorems are presented to analyze the robust stability of the closed-loop system. Then, algorithms are proposed to address the problem of robustly stabilizing the interval FO plant using FOPID controllers. Additionally, two auxiliary functions are introduced to fulfill control requirements related to disturbance rejection and noise attenuation. Finally, some numerical examples are provided to validate the proposed methods and confirm the effectiveness of the obtained results.

5.1 Robust stability region of Fractional-Order controllers for Fractional-Order Interval Systems without time delay

5.1.1 Definitions

Consider the transfer function of an interval FO plant given as the following expression:

$$P(s, \mathbf{b}, \mathbf{a}) = \frac{N(s, \mathbf{b})}{D(s, \mathbf{a})} = \frac{\sum_{i_1=0}^m b_{i_1} s^{\beta_{i_1}}}{\sum_{i_2=0}^n a_{i_2} s^{\alpha_{i_2}}}, \quad (5.1)$$

where s is the Laplace operator, $m \in \mathbb{Z}^{\geq 0}$, $n \in \mathbb{Z}^{\geq 1}$, $\beta_m > \beta_{m-1} > \dots > \beta_1 > \beta_0 = 0$ and $\alpha_n > \alpha_{n-1} > \dots > \alpha_1 > \alpha_0 = 0$ are arbitrary real numbers. Also, $\mathbf{b} = [b_0, b_1, \dots, b_m]^T$ and $\mathbf{a} = [a_0, a_1, \dots, a_n]^T$ are the coefficients vectors and they belong to the uncertainty bounding sets:

$$\begin{aligned} \mathbf{b} \in \mathbf{B} &= \{\mathbf{b} \in \mathbb{R}^{m+1} | b_{i_1} \in [b_{i_1}^-, b_{i_1}^+], b_m, b_0 \neq 0, i_1 \in \mathbb{Z}_{\geq 0}^{\leq m}\}, \\ \mathbf{a} \in \mathbf{A} &= \{\mathbf{a} \in \mathbb{R}^{n+1} | a_{i_2} \in [a_{i_2}^-, a_{i_2}^+], a_n \neq 0, i_2 \in \mathbb{Z}_{\geq 1}^{\leq n}\}, \end{aligned} \quad (5.2)$$

where, $[b_{i_1}^-, b_{i_1}^+]$ and $[a_{i_2}^-, a_{i_2}^+]$ are specified intervals. In this chapter, we consider the parallel form of the FOPID controller expressed by the transfer function

$$C(s) = \frac{k_p s^\lambda + k_i + k_d s^{\mu+\lambda}}{s^\lambda}, 0 < \lambda, \mu < 2, \alpha_n > \mu + \beta_m. \quad (5.3)$$

Furthermore, in this chapter it is considered that the FO polynomial (5.4) represents the characteristic function of the negative unity feedback control system.

$$\Delta(s) = s^\lambda D(s, \mathbf{a}) + (k_p s^\lambda + k_i + k_d s^{\mu+\lambda}) N(s, \mathbf{b}). \quad (5.4)$$

Assumption 5.1. According to Approach 2 in Subsection 2.2.2, the vertex polynomials corresponding to $N(j\omega, \mathbf{b})$ and $D(j\omega, \mathbf{a})$ are denoted by $V_{r_1}^+(\omega)$ and $V_{r_2}^-(\omega)$, respectively, for $r_1 = 1, 2, \dots, 2m_N$ and $r_2 = 1, 2, \dots, 2m_D$.

Remark 5.1. Consider a certain polynomial of $\Delta(s)$ in (5.4) as $\hat{\Delta}(s)$ in (5.5).

$$\hat{\Delta}(s) = s^\lambda \sum_{i_2=0}^n \hat{a}_{i_2} s^{\alpha_{i_2}} + (k_p s^\lambda + k_i + k_d s^{\mu+\lambda}) \sum_{i_1=0}^m \hat{b}_{i_1} s^{\beta_{i_1}}. \quad (5.5)$$

Then, the boundaries of the stabilizing region $\hat{\Delta}(s)$ in (5.5) are specified by IRB, RRB and CRB which can be determined by using the algorithm in [105]. In summary, the mentioned boundaries are stated based on the procedure proposed in [105] as follows.

- **RRB:** $\hat{\Delta}(0) = k_i \hat{b}_0$. If $k_i \hat{b}_0 \neq 0$, then $k_i = 0$. Otherwise, the boundary does not exist.
- **IRB:** $\hat{\Delta}(\infty) = 0$.

$$\begin{cases} k_d = 0 & \text{for } \alpha_n = \beta_m \text{ or } (\alpha_n > \beta_m \text{ and } \mu > \alpha_n - \beta_\mu), \\ k_d = \frac{-\hat{a}_0}{\hat{b}_0} & \text{for } (\alpha_n > \beta_m \text{ and } \mu = \alpha_n - \beta_\mu), \\ \text{none} & \text{for } (\alpha_n > \beta_m \text{ and } \mu < \alpha_n - \beta_\mu), \end{cases} \quad (5.6)$$

- **CRB:** By partitioning $\hat{\Delta}(j\omega) = 0$ into its real and imaginary parts and equating them to zero, we obtain

$$\begin{cases} \Re(\hat{\Delta}(j\omega) = 0 \implies B_1 k_p + B_3 k_i = -(A_1 + k_d B_5), \\ \Im(\hat{\Delta}(j\omega) = 0 \implies B_2 k_p + B_4 k_i = -(A_2 + k_d B_6). \end{cases} \quad (5.7)$$

Finally, by solving the equation (5.7), the k_p and k_i parameters in terms of k_d , λ and μ are obtained as Follows.

$$\begin{aligned} k_p &= \left(A_2(\omega)B_1(\omega) - A_1(\omega)B_2(\omega) + k_d(B_1(\omega)B_6(\omega) - B_2(\omega)B_5(\omega)) \right) / \\ &\quad \left(B_2(\omega)B_3(\omega) - B_1(\omega)B_4(\omega) \right), \\ k_i &= \left(A_1(\omega)B_4(\omega) - A_2(\omega)B_3(\omega) + k_d(B_4(\omega)B_5(\omega) - B_3(\omega)B_6(\omega)) \right) / \\ &\quad \left(B_2(\omega)B_3(\omega) - B_1(\omega)B_4(\omega) \right), \end{aligned} \quad (5.8)$$

in which

$$\begin{cases} A_1(\omega) = \sum_{i_2=0}^n \hat{a}_{i_2} \omega^{\lambda+\alpha_{i_2}} \cos\left(\frac{\pi(\alpha_{i_2}+\lambda)}{2}\right), \\ A_2(\omega) = \sum_{i_2=0}^n \hat{a}_{i_2} \omega^{\lambda+\alpha_{i_2}} \sin\left(\frac{\pi(\alpha_{i_2}+\lambda)}{2}\right), \\ B_1(\omega) = \sum_{i_1=0}^m \hat{b}_{i_1} \omega^{\beta_{i_1}} \cos\left(\frac{\pi\beta_{i_1}}{2}\right), \\ B_2(\omega) = \sum_{i_1=0}^m \hat{b}_{i_1} \omega^{\beta_{i_1}} \sin\left(\frac{\pi\beta_{i_1}}{2}\right), \\ B_3(\omega) = \sum_{i_1=0}^m \hat{b}_{i_1} \omega^{\beta_{i_1}+\lambda} \cos\left(\frac{\pi(\beta_{i_1}+\lambda)}{2}\right), \\ B_4(\omega) = \sum_{i_1=0}^m \hat{b}_{i_1} \omega^{\beta_{i_1}+\lambda} \sin\left(\frac{\pi(\beta_{i_1}+\lambda)}{2}\right), \\ B_5(\omega) = \sum_{i_1=0}^m \hat{b}_{i_1} \omega^{\beta_{i_1}+\lambda+\mu} \cos\left(\frac{\pi(\beta_{i_1}+\lambda+\mu)}{2}\right), \\ B_6(\omega) = \sum_{i_1=0}^m \hat{b}_{i_1} \omega^{\beta_{i_1}+\lambda+\mu} \sin\left(\frac{\pi(\beta_{i_1}+\lambda+\mu)}{2}\right). \end{cases} \quad (5.9)$$

Accordingly, the stabilizing region can be determined by checking one arbitrary test point inside each region [105].

Regarding the above analysis, the problem is to compute a set of FOPID controllers stabilizing the interval FO plant of $P(s, \mathbf{b}, \mathbf{a})$ in (5.1).

5.1.2 Determination of the Robust Stability Region

Theorem 5.1. *The characteristic function (5.4) is robust stable if and only if, the characteristic functions $\Delta_{r_1}^D(s)$ ($r_1 = 1, 2, \dots, 2m_N$) in (5.10) and $\Delta_{r_2}^N(s)$ ($r_2 = 1, 2, \dots, 2m_D$) in (5.11) are also robust stable.*

$$\Delta_{r_1}^D(s) = s^\lambda D(s, \mathbf{a}) + (k_p s^\lambda + k_i + k_d s^{\mu+\lambda}) V_{r_1}^+(\omega), (r_1 = 1, \dots, 2m_N). \quad (5.10)$$

$$\Delta_{r_2}^N(s) = s^\lambda V_{r_2}^-(\omega) + (k_p s^\lambda + k_i + k_d s^{\mu+\lambda}) N(s, \mathbf{b}), (r_2 = 1, \dots, 2m_D). \quad (5.11)$$

Proof. Proof of the sufficiency: The value sets of $s^\lambda D(s, \mathbf{a})$ and $(k_p s^\lambda + k_i + k_d s^{\mu+\lambda}) N(s, \mathbf{b})$ are two parpolygons in the complex plane for $s = j\omega$. If the characteristic functions $\Delta_{r_1}^D(s) (r_1 = 1, 2, \dots, 2m_N)$ in (5.10) are robust stable, then one can simply deduce that

$$-(k_p s^\lambda + k_i + k_d s^{\mu+\lambda}) V_{r_1}^+(\omega) \notin s^\lambda D(s, \mathbf{a}), (r_1 = 1, 2, \dots, 2m_N) \text{ and } s = j\omega. \quad (5.12)$$

Likewise, from (5.11), one can infer that

$$-s^\lambda V_{r_2}^-(\omega) \notin (k_p s^\lambda + k_i + k_d s^{\mu+\lambda}) N(s, \mathbf{b}), (r_2 = 1, 2, \dots, 2m_D) \text{ and } s = j\omega. \quad (5.13)$$

From (5.12) and (5.13), it is apparent that two parpolygons $s^\lambda D(j\omega, \mathbf{a})$ and $(k_p (j\omega)^\lambda + k_i + k_d (j\omega)^{\mu+\lambda}) N(j\omega, \mathbf{b})$ do not have any overlap in the complex plane and this implies that $0 \notin \Delta(j\omega)$.

Proof of the Necessity: Since the characteristic function (5.4) is robust stable, based on the zero exclusion principle $0 \notin \Delta(j\omega)$. By using the zero exclusion principle, the origin is located outside the value set of $\Delta(j\omega)$. Therefore, from (5.12)-(5.13), the robust stability of $\Delta_{r_1}^D(s) (r_1 = 1, 2, \dots, 2m_N)$ in (5.10) and $\Delta_{r_2}^N(s) (r_2 = 1, 2, \dots, 2m_D)$ in (5.11) are concluded. \square

Remark 5.2. Theorem 1 reveals that the robust stability analysis of the characteristic function $\Delta(s)$ in (5.4) is equivalent to the robust stability analysis of the characteristic functions $\Delta_{r_1}^D(s) (r_1 = 1, 2, \dots, 2m_N)$ in (5.10) and $\Delta_{r_2}^N(s) (r_2 = 1, 2, \dots, 2m_D)$ in (5.11). Hence, the only issue lies in the determination of the boundaries (i.e. RRB, IRB and CRB) of the characteristic functions $\Delta_{r_1}^D(s) (r_1 = 1, 2, \dots, 2m_N)$ in (5.10) and $\Delta_{r_2}^N(s) (r_2 = 1, 2, \dots, 2m_D)$ in (5.11). To do this, the calculation of the stabilizing region is presented in Algorithm 5.1.

Algorithm 5.1:

Step 1: Obtain the vertices $V_{r_1}^+(\omega) (r_1 = 1, 2, \dots, 2m_N)$ and $V_{r_2}^-(\omega) (r_2 = 1, 2, \dots, 2m_D)$ using Approach 2 in Subsection 2.2.2.

Step 2: Obtain RRB, IRB and CRB and the stability regions by sweeping over $\eta \in [0, 1]$ for $\Delta_{r_1}^D(s)$ in (5.14):

$$\begin{aligned} \Delta_{r_1}^D(s) &= s^\lambda (e(V_{r_2}^-(\omega), V_{r_2+1}^-(\omega))) + V_{r_1}^+(\omega) \\ &(k_p s^\lambda + k_i + k_d s^{\mu+\lambda}), r_1 = 1, 2, \dots, 2m_N, \\ r_2 &= 1, 2, \dots, 2m_D, V_{2m_D+1}^-(\omega) = V_1^-(\omega). \end{aligned} \quad (5.14)$$

Step 3: Obtain RRB, IRB and CRB and the stability regions by sweeping over $\eta \in [0, 1]$ for $\Delta_{r_2}^N(s)$ in (5.15):

$$\begin{aligned} \Delta_{r_2}^N(s) &= s^\lambda V_{r_2}^-(\omega) + (k_p s^\lambda + k_i + k_d s^{\mu+\lambda}) \\ &(e(V_{r_1}^+(\omega), V_{r_1+1}^+(\omega))), r_1 = 1, 2, \dots, 2m_N, \\ r_2 &= 1, 2, \dots, 2m_D, V_{2m_N+1}^+(\omega) = V_1^+(\omega). \end{aligned} \quad (5.15)$$

Step 4: The final stabilizing region for the interval FO plant is the intersection of all the computed stable regions in Step 2 and Step 3.

Now, in the next theorem, an auxiliary function is presented to determine whether or not a designed controller can robustly stabilize the closed-loop system.

Theorem 5.2. Assume that a certain characteristic function of $\Delta(s)$ in (5.4) as $\Delta_0(s)$ is stable. Then, the closed-loop system is robust stable if and only if the inequality $\Lambda(\omega) < 0$ holds for $\omega \geq 0$, where

$$\Lambda(\omega) \triangleq \max\{\Lambda_1(\omega), \Lambda_2(\omega)\}, \quad (5.16)$$

in which

$$\begin{aligned} \Lambda_1(\omega) &\triangleq \max \left\{ \Lambda_{r_1, r_2}^D(\omega) \mid r_1 \in \{1, \dots, 2m_N\}, r_2 \in \{1, \dots, 2m_D\} \right\}, \\ \Lambda_{r_1, r_2}^D(\omega) &\triangleq \left| (j\omega)^\lambda (V_{r_2}^-(\omega) - V_{r_2+1}^-(\omega)) \right| - \\ &\quad \left| (j\omega)^\lambda V_{r_2}^-(\omega) + (k_p(j\omega)^\lambda + k_i + k_d(j\omega)^{\mu+\lambda}) V_{r_1}^+(\omega) \right| - \\ &\quad \left| (j\omega)^\lambda V_{r_2+1}^-(\omega) + (k_p(j\omega)^\lambda + k_i + k_d(j\omega)^{\mu+\lambda}) V_{r_1}^+(\omega) \right|. \end{aligned} \quad (5.17)$$

$$\begin{aligned} \Lambda_2(\omega) &\triangleq \max \left\{ \Lambda_{r_1, r_2}^N(\omega) \mid r_1 \in \{1, \dots, 2m_N\}, r_2 \in \{1, \dots, 2m_D\} \right\}, \\ \Lambda_{r_1, r_2}^N(\omega) &\triangleq \left| (k_p(j\omega)^\lambda + k_i + k_d(j\omega)^{\mu+\lambda}) (V_{r_1}^+(\omega) - V_{r_1+1}^+(\omega)) \right| - \\ &\quad \left| (j\omega)^\lambda V_{r_2}^-(\omega) + (k_p(j\omega)^\lambda + k_i + k_d(j\omega)^{\mu+\lambda}) V_{r_1}^+(\omega) \right| - \\ &\quad \left| (j\omega)^\lambda V_{r_2}^-(\omega) + (k_p(j\omega)^\lambda + k_i + k_d(j\omega)^{\mu+\lambda}) V_{r_1+1}^+(\omega) \right|. \end{aligned} \quad (5.18)$$

Proof. We know that the value set of $\Delta_{r_1}^D(s)$ in (5.10) and $\Delta_{r_2}^N(s)$ in (5.11) are two parpolygons in the complex plane. Also, if the triangle inequality is satisfied for each two consecutive vertices of $\Delta_{r_1}^D(s)$ in (5.10), then one can conclude that $0 \notin \Delta_{r_1}^D(j\omega)$ and this implies that the inequality $\Lambda_1(\omega) < 0$ is satisfied. Likewise, satisfying the inequality $\Lambda_2(\omega) < 0$ leads to $0 \notin \Delta_{r_2}^N(j\omega)$ in (5.11). Hence, if the inequality $\Lambda(\omega) < 0$ in (5.16) is satisfied, then based on **Theorem 1** and the zero exclusion principle, the proof is completed. \square

5.1.3 Good output disturbance rejection

In order to improve the output disturbance rejection, the following constraint on the sensitivity function $S(j\omega)$ should be satisfied.

$$|S(j\omega)| = \left| \frac{1}{1 + C(j\omega)P(j\omega)} \right| < |M_s(j\omega)|, \quad (5.19)$$

where $M_s(j\omega) = N_s(j\omega)/D_s(j\omega)$ denotes the weighting function, which describes the frequency characteristic of the performance specifications.

Based on **Theorem 5.1** and (5.19), a robust FOPID controller should satisfy the following inequalities:

$$\left| \frac{1}{1 + \frac{(k_p s^\lambda + k_i + k_d s^{\mu+\lambda}) V_{r_1}^+(\omega)}{s^\lambda D(s, \mathbf{a})}} \right| < |M_s(s)|, \quad (r_1 = 1, 2, \dots, 2m_N), s = j\omega. \quad (5.20)$$

$$\left| \frac{1}{1 + \frac{(k_p s^\lambda + k_i + k_d s^{\mu+\lambda}) N(s, \mathbf{b})}{s^\lambda V_{r_2}^-(\omega)}} \right| < |M_s(s)|, (r_2 = 1, 2, \dots, 2m_D), s = j\omega. \quad (5.21)$$

From (5.20), (5.21) and the maximum modulus theorem [97], the following inequality should be satisfied.

$$\Lambda_S(\omega) \triangleq \max_{r=1,2} \Lambda_r^S(\omega) < 0, \quad (5.22)$$

where

$$\left\{ \begin{array}{l} \Lambda_1^S(\omega) \triangleq \max_{i=1, \dots, 2m_N} \Lambda_i^D(\omega), \\ \Lambda_i^D(\omega) \triangleq \max_{e_{l^D}^D \in P_E^D} |e_{l^D}^D| - |M_s(j\omega)|, \\ l^D = 1, 2, \dots, 2m_D, \\ P_E^D \triangleq \{e_1^D, e_2^D, \dots, e_{2m_D}^D\}, \\ e_1^D \triangleq \frac{1}{1 + \frac{(k_p s^\lambda + k_i + k_d s^{\mu+\lambda}) V_i^+(\omega)}{s^\lambda (e(V_1^-(\omega), V_2^-(\omega)))}}, \\ e_2^D \triangleq \frac{1}{1 + \frac{(k_p s^\lambda + k_i + k_d s^{\mu+\lambda}) V_i^+(\omega)}{s^\lambda (e(V_2^-(\omega), V_3^-(\omega)))}}, \\ \vdots \\ e_{2m_D}^D \triangleq \frac{1}{1 + \frac{(k_p s^\lambda + k_i + k_d s^{\mu+\lambda}) V_i^+(\omega)}{s^\lambda (e(V_{2m_D}^-(\omega), V_1^-(\omega)))}}, \\ s = j\omega. \end{array} \right. \quad (5.23)$$

$$\left\{ \begin{array}{l} \Lambda_2^S(\omega) \triangleq \max_{i=1, \dots, 2m_D} \Lambda_i^N(\omega), \\ \Lambda_i^N(\omega) \triangleq \max_{e_{l^N}^N \in P_E^N} |e_{l^N}^N| - |M_s(j\omega)|, \\ l^N = 1, 2, \dots, 2m_N, \\ P_E^N \triangleq \{e_1^N, e_2^N, \dots, e_{2m_N}^N\}, \\ e_1^N \triangleq \frac{1}{1 + \frac{(k_p s^\lambda + k_i + k_d s^{\mu+\lambda}) e(V_1^+(\omega), V_2^+(\omega))}{s^\lambda V_i^-(\omega)}}, \\ e_2^N \triangleq \frac{1}{1 + \frac{(k_p s^\lambda + k_i + k_d s^{\mu+\lambda}) e(V_2^+(\omega), V_3^+(\omega))}{s^\lambda V_i^-(\omega)}}, \\ \vdots \\ e_{2m_N}^N \triangleq \frac{1}{1 + \frac{(k_p s^\lambda + k_i + k_d s^{\mu+\lambda}) e(V_1^+(\omega), V_{2m_N}^+(\omega))}{s^\lambda V_i^-(\omega)}}, \\ s = j\omega. \end{array} \right. \quad (5.24)$$

Remark 5.3. Assume that a robust FOPID controller is designed by **Algorithm 5.1**. Then, the designed controller should satisfy the inequality $\Lambda_S(\omega) < 0$ in (5.22) to improve the output disturbance rejection. Note that some useful guidelines can be given by [96] for the selection of the weighting function $M_s(j\omega)$.

5.1.4 High-frequency noise rejection

To satisfy high-frequency noise rejection, the following constraint on the complementary sensitivity function $T(j\omega)$ should be fulfilled.

$$|T(j\omega)| = \left| \frac{C(j\omega)P(j\omega)}{1 + C(j\omega)P(j\omega)} \right| < |M_T(j\omega)|, \quad (5.25)$$

where $M_T(j\omega) = N_T(j\omega)/D_T(j\omega)$ denotes the frequency characteristics of the noise signal [96].

By using **Theorem 5.1** and (5.25), a robust FOPID controller should also satisfy the inequality $\Lambda_T(\omega) < 0$ in (5.26).

$$\Lambda_T(\omega) \triangleq \max_{r=1,2} \Lambda_r^T(\omega) < 0, \quad (5.26)$$

where

$$\left\{ \begin{array}{l} \Lambda_1^T(\omega) \triangleq \max_{i=1,\dots,2m_N} \hat{\Lambda}_i^D(\omega), \\ \hat{\Lambda}_i^D(\omega) \triangleq \max_{\hat{e}_i^D \in \hat{P}_E^D} |\hat{e}_i^D| - |M_T(j\omega)|, \\ l^D = 1, 2, \dots, 2m_D, \\ \hat{P}_E^D \triangleq \{\hat{e}_1^D, \hat{e}_2^D, \dots, \hat{e}_{2m_D}^D\}, \\ \hat{e}_1^D \triangleq \frac{(k_p s^\lambda + k_i + k_d s^{\mu+\lambda}) V_i^+(\omega)}{s^\lambda (e(V_1^-(\omega), V_2^-(\omega))) + (k_p s^\lambda + k_i + k_d s^{\mu+\lambda}) V_i^+(\omega)}, \\ \hat{e}_2^D \triangleq \frac{(k_p s^\lambda + k_i + k_d s^{\mu+\lambda}) V_i^+(\omega)}{s^\lambda (e(V_2^-(\omega), V_3^-(\omega))) + (k_p s^\lambda + k_i + k_d s^{\mu+\lambda}) V_i^+(\omega)}, \\ \vdots \\ \hat{e}_{2m_D}^D \triangleq \frac{(k_p s^\lambda + k_i + k_d s^{\mu+\lambda}) V_i^+(\omega)}{s^\lambda (e(V_1^-(\omega), V_{2m_D}^-(\omega))) + (k_p s^\lambda + k_i + k_d s^{\mu+\lambda}) V_i^+(\omega)}, \\ s = j\omega. \end{array} \right. \quad (5.27)$$

$$\left\{ \begin{array}{l} \Lambda_2^T(\omega) \triangleq \max_{i=1,\dots,2m_D} \hat{\Lambda}_i^N(\omega), \\ \hat{\Lambda}_i^N(\omega) \triangleq \max_{\hat{e}_i^N \in \hat{P}_E^N} |\hat{e}_i^N| - |M_T(j\omega)|, \\ l^N = 1, 2, \dots, 2m_N, \\ \hat{P}_E^N \triangleq \{\hat{e}_1^N, \hat{e}_2^N, \dots, \hat{e}_{2m_N}^N\}, \\ \hat{e}_1^N \triangleq \frac{(k_p s^\lambda + k_i + k_d s^{\mu+\lambda}) e(V_1^+(\omega), V_2^+(\omega))}{s^\lambda V_i^-(\omega) + (k_p s^\lambda + k_i + k_d s^{\mu+\lambda}) e(V_1^+(\omega), V_2^+(\omega))}, \\ \hat{e}_2^N \triangleq \frac{(k_p s^\lambda + k_i + k_d s^{\mu+\lambda}) e(V_2^+(\omega), V_3^+(\omega))}{s^\lambda V_i^-(\omega) + (k_p s^\lambda + k_i + k_d s^{\mu+\lambda}) e(V_2^+(\omega), V_3^+(\omega))}, \\ \vdots \\ \hat{e}_{2m_N}^N \triangleq \frac{(k_p s^\lambda + k_i + k_d s^{\mu+\lambda}) e(V_{2m_N}^+(\omega), V_1^+(\omega))}{s^\lambda V_i^-(\omega) + (k_p s^\lambda + k_i + k_d s^{\mu+\lambda}) e(V_{2m_N}^+(\omega), V_1^+(\omega))}, \\ s = j\omega. \end{array} \right. \quad (5.28)$$

Remark 5.4. The designer can design a robust FO controller by using **Algorithm 5.1**. Besides, the designed controller should satisfy the inequalities $\Lambda_S(\omega) < 0$ in (5.22) and $\Lambda_T(\omega) < 0$ in (5.26) to improve the control requirements on the disturbance rejection and the noise reduction.

Remark 5.5. It is apparent that **Theorem 5.1**, **Algorithm 5.1**, the inequalities $\Lambda_S(\omega) < 0$ in (5.22) and $\Lambda_T(\omega) < 0$ in (5.26) can be employed for FOPI controllers.

5.2 Robust stability region of Fractional-Order controllers for Fractional-Order Interval Systems with an interval time delay

5.2.1 Definitions

Consider a FO plant with uncertainties as

$$P(s, \mathbf{b}, \mathbf{a}, l) = \frac{N(s, \mathbf{b})}{D(s, \mathbf{a})} e^{-ls} = \frac{\sum_{i_1=0}^m b_{i_1} s^{\beta_{i_1}}}{\sum_{i_2=0}^n a_{i_2} s^{\alpha_{i_2}}} e^{-ls}, \quad (5.29)$$

where $\beta_m > \beta_{m-1} > \dots > \beta_1 > \beta_0 = 0$ and $\alpha_n > \alpha_{n-1} > \dots > \alpha_1 > \alpha_0 = 0$ are arbitrary real values. Additionally, l represents the positive time delay $l \in [l^-, l^+]$, and $\mathbf{a} = [a_0, a_1, \dots, a_n]^T$ and $\mathbf{b} = [b_0, b_1, \dots, b_m]^T$ belong to the following sets:

$$\begin{aligned} \mathbf{a} \in \mathbf{A} &= \{\mathbf{a} \in \mathbb{R}^{n+1} | a_{i_2} \in [a_{i_2}^-, a_{i_2}^+], a_n \neq 0, i_2 \in \mathbb{Z}_{\geq 1}^{\leq n}\}, \\ \mathbf{b} \in \mathbf{B} &= \{\mathbf{b} \in \mathbb{R}^{m+1} | b_{i_1} \in [b_{i_1}^-, b_{i_1}^+], b_m, b_0 \neq 0, i_1 \in \mathbb{Z}_{\geq 0}^{\leq m}\}, \end{aligned} \quad (5.30)$$

where, $[b_{i_1}^-, b_{i_1}^+]$ and $[a_{i_2}^-, a_{i_2}^+]$ are specified intervals. The transfer function of the parallel form of a FOPID controller is given as (5.31).

$$C(s) = \frac{N_c(s)}{s^\lambda} = \frac{K_p s^\lambda + K_i + K_d s^{\mu+\lambda}}{s^\lambda}, \quad 0 < \lambda, \quad \mu < 2, \quad \alpha_n > \beta_m + \mu. \quad (5.31)$$

In this investigation, we posit that $\Delta(s)$ in (5.32) delineates the characteristic function of the negative unity control system:

$$\Delta(s) = s^\lambda D(s, \mathbf{a}) + N_c(s) N(s, \mathbf{b}) e^{-ls}. \quad (5.32)$$

Thus, the vertex polynomials corresponding to $N(j\omega, \mathbf{b})$ and $D(j\omega, \mathbf{a})$ are denoted as $V_{r_1}^+(\omega)$ ($r_1 = 1, 2, \dots, 2m_N$) and $V_{r_2}^-(\omega)$ ($r_2 = 1, 2, \dots, 2m_D$), respectively, and can be computed using **Approach 2**.

Remark 5.6. Let us regard a specific quasi-polynomial $\Delta(s)$ in (5.32) as $\hat{\Delta}(s)$ in (5.33).

$$\hat{\Delta}(s) = s^\lambda \sum_{i_2=0}^n \hat{a}_{i_2} s^{\alpha_{i_2}} + N_c(s) \left(\sum_{i_1=0}^m \hat{b}_{i_1} s^{\beta_{i_1}} \right) e^{-ls}. \quad (5.33)$$

Subsequently, the boundaries of the stability region defined by $\hat{\Delta}(s)$ in (5.33) are delineated by IRB, CRB, and RRB, which can be ascertained through the procedure outlined in [105]. To summarize, these boundaries are established based on the method proposed in [105] as follows.

RRB and IRB can be simply obtained by substituting $\omega = 0$ and $\omega = \infty$ in $\hat{\Delta}(j\omega)$. The CRB can be determined by solving $\hat{\Delta}(j\omega) = 0$, yielding the parameters K_p and K_i as follows:

$$\begin{aligned} K_p &= \left(E_2(\omega)F_1(\omega) - E_1(\omega)F_2(\omega) + K_d(F_1(\omega)F_6(\omega) - F_2(\omega)F_5(\omega)) \right) / \\ &\quad \left(F_2(\omega)F_3(\omega) - F_1(\omega)F_4(\omega) \right), \\ K_i &= \left(E_1(\omega)F_4(\omega) - E_2(\omega)F_3(\omega) + K_d(F_4(\omega)F_5(\omega) - F_3(\omega)F_6(\omega)) \right) / \\ &\quad \left(F_2(\omega)F_3(\omega) - F_1(\omega)F_4(\omega) \right), \end{aligned} \quad (5.34)$$

where

$$\begin{cases} E_1(\omega) = \sum_{i_2=0}^n \hat{a}_{i_2} \omega^{\lambda+\alpha_{i_2}} \cos\left(\frac{\pi(\alpha_{i_2}+\lambda)}{2} + l\omega\right), \\ E_2(\omega) = \sum_{i_2=0}^n \hat{a}_{i_2} \omega^{\lambda+\alpha_{i_2}} \sin\left(\frac{\pi(\alpha_{i_2}+\lambda)}{2} + l\omega\right), \\ F_1(\omega) = \sum_{i_1=0}^m \hat{b}_{i_1} \omega^{\beta_{i_1}} \cos\left(\frac{\pi\beta_{i_1}}{2}\right), \\ F_2(\omega) = \sum_{i_1=0}^m \hat{b}_{i_1} \omega^{\beta_{i_1}} \sin\left(\frac{\pi\beta_{i_1}}{2}\right), \\ F_3(\omega) = \sum_{i_1=0}^m \hat{b}_{i_1} \omega^{\beta_{i_1}+\lambda} \cos\left(\frac{\pi(\beta_{i_1}+\lambda)}{2}\right), \\ F_4(\omega) = \sum_{i_1=0}^m \hat{b}_{i_1} \omega^{\beta_{i_1}+\lambda} \sin\left(\frac{\pi(\beta_{i_1}+\lambda)}{2}\right), \\ F_5(\omega) = \sum_{i_1=0}^m \hat{b}_{i_1} \omega^{\beta_{i_1}+\lambda+\mu} \cos\left(\frac{\pi(\beta_{i_1}+\lambda+\mu)}{2}\right), \\ F_6(\omega) = \sum_{i_1=0}^m \hat{b}_{i_1} \omega^{\beta_{i_1}+\lambda+\mu} \sin\left(\frac{\pi(\beta_{i_1}+\lambda+\mu)}{2}\right). \end{cases} \quad (5.35)$$

Hence, the stabilizing region can be established by examining one arbitrary test point within each region.

Lemma 5.1. Denote by $e(x, y)$ a line segment connecting the points x and y . At a particular frequency $\omega \in (0, \frac{2\pi}{l^+-l^-})$, the set of values of $b_1 e^{-ls}$ is situated within $G_E(j\omega)$ as expressed in (6.8).

$$G_E(j\omega) \triangleq \{e(G_1(j\omega), G_2(j\omega)), e(G_2(j\omega), G_3(j\omega)), \dots, e(G_{4N+1}(j\omega), G_{4N+2}(j\omega)), e(G_{4N+2}(j\omega), G_1(j\omega))\}, \quad (5.36)$$

$$G_k(j\omega) \triangleq \begin{cases} \bar{G}_{(k-1)}(j\omega), & \text{if } 1 \leq k \leq 2M+1, \\ \underline{G}_{(2M)}(j\omega), & \text{if } k = 2M+2, \\ \underline{G}_{(2M-1)}(j\omega), & \text{if } k = 2M+3, \\ \vdots & \\ \underline{G}_0(j\omega), & \text{if } k = 4M+2, \end{cases}$$

$$\bar{G}_k(j\omega) \triangleq \begin{cases} b_1 e^{-j\omega \left(l^- + k \frac{l^+ - l^-}{2M}\right)}, & \text{if } k = 0, 2, \dots, 2M, \\ \frac{b_1 e^{-j\omega \left(l^- + k \frac{l^+ - l^-}{2M}\right)}}{\cos\left(\omega \frac{l^+ - l^-}{2M}\right)}, & \text{if } k = 1, 3, \dots, 2M-1, \end{cases}$$

$$\underline{G}_k(j\omega) \triangleq b_1 e^{-j\omega \left(l^- + k \frac{l^+ - l^-}{2M}\right)}, \quad k = 0, 1, 2, \dots, 2M.$$

Here, M is a member of the set of natural numbers greater than or equal to 3.

Remark 5.7. Assume that the value sets of $X_1(j\omega)$ and $X_2(j\omega)$ are both bounded and closed in the complex plane. If at a particular frequency, the boundaries $\partial(X_1(j\omega))$ and $\partial(X_2(j\omega))$ have no overlap in the complex plane, it implies that no common real or complex number exists in their respective value sets.

5.2.2 Determination of the Robust Stability Region

Based on *Value Sets Overlap Theorem*, we introduce the following result that can be utilized to examine whether the origin is part of the value set of $\Delta(j\omega)$. Now, considering *Theorem 4.2*, *Lemma 4.2*, *Lemma 4.3*, and the principle of excluding zeros, the following theorem presents the analysis of robust stability for $\Delta(j\omega)$.

Theorem 5.3. Assume that a certain polynomial of $\Delta(s)$ in (5.32) as $\hat{\Delta}(s)$ in (5.33) is stable. Then, $\Delta(s)$ is robust stable if and only if, the characteristic functions $\Delta_{h_1}^D(s)$ ($h_1 = 1, \dots, 2m_N$) in (5.37) and $\Delta_{h_2}^N(s)$ ($h_2 = 1, \dots, 2m_D$) in (5.38) are also robust stable.

$$\Delta_{h_1}^D(s) = s^\lambda D(s, \mathbf{a}) + N_c(s) e^{-ls} V_{h_1}^+(\omega), \quad (h_1 = 1, \dots, 2m_N). \quad (5.37)$$

$$\Delta_{h_2}^N(s) = s^\lambda V_{h_2}^-(\omega) + N_c(s) e^{-ls} N(s, \mathbf{b}), \quad (h_2 = 1, \dots, 2m_D). \quad (5.38)$$

Proof. Sufficiency: If the characteristic functions $\Delta_{h_1}^D(s)$ (for $h_1 = 1, \dots, 2m_N$) in (5.37) exhibit robust stability, then according to Theorem 4.2, it follows that

$$-N_c(s) V_{h_1}^+(\omega) e^{-ls} \notin s^\lambda D(s, \mathbf{a}), \quad (h_1 = 1, 2, \dots, m_N) \text{ and } s = j\omega. \quad (5.39)$$

Likewise, from (5.38) and Theorem 4.2, one can infer that

$$-s^\lambda V_{h_2}^-(\omega) \notin N_c(s) N(s, \mathbf{b}) e^{-ls}, \quad (h_2 = 1, 2, \dots, m_D) \text{ and } s = j\omega. \quad (5.40)$$

From (5.39) and (5.40), together with Theorem 1, it is evident that the sets $\Theta_1(\omega_0)$ in (5.41) and $\Theta_2(\omega_0)$ in (5.42) do not overlap in the complex plane for $s^\lambda D(s, \mathbf{a}) \neq 0$ and $s = j\omega_0$. Similarly, the sets

$$(\Theta_1(\omega_0))^{-1} \quad \text{and} \quad (\Theta_2(\omega_0))^{-1}$$

do not overlap for

$$\left(K_p s^\lambda + K_i + K_d s^{u+\lambda} \right) N(j\omega_0, \mathbf{b}) \neq 0 \quad \text{and} \quad s = j\omega_0.$$

Therefore, we conclude that $0 \notin \Delta(j\omega)$.

$$\Theta_1(j\omega) = -e^{lj\omega}. \quad (5.41)$$

$$\Theta_2(j\omega) = \left(\frac{N_v^{r_1}}{D_E^{r_2}} \right) \cup \left(\frac{N_E^{r_1}}{D_v^{r_2}} \right), \quad (5.42)$$

in which

$$\begin{cases} N_v^{r_1} = N_c(j\omega) V_{r_1}^+(\omega), r_1 = 1, 2, \dots, 2m_N, \\ D_v^{r_2} = s^\lambda V_{r_2}^-(j\omega), r_2 = 1, 2, \dots, 2m_D, \\ N_E^{r_1} = e(N_c(j\omega) V_{r_1}^+(\omega), N_c(j\omega) V_{r_1+1}^+(\omega)), \\ D_E^{r_2} = e((j\omega)^\lambda V_{r_2}^-(j\omega), (j\omega)^\lambda V_{r_2+1}^-(j\omega)), \\ V_1^+(\omega) = V_{2m_N+1}^+(\omega), V_1^-(j\omega) = V_{2m_D+1}^-(j\omega). \end{cases} \quad (5.43)$$

Necessity: Given that the characteristic function (5.32) is robustly stable, as per the zero exclusion principle, 0 does not belong to $\Delta(j\omega)$. This implies that the origin lies outside the value set of $\Delta(j\omega)$. Suppose $s^\lambda D(s, \mathbf{a}) \neq 0$ for $s = j\omega_0$. Then, from Lemma 1, it can be inferred that $\Theta_1(\omega_0)$ in (5.41) and $\Theta_2(\omega_0)$ in (5.42) do not overlap in the complex plane for $s^\lambda D(s, \mathbf{a}) \neq 0$ and $s = j\omega_0$. Consequently, the robust stability of $\Delta_{h_1}^D(s)$ (for $h_1 = 1, 2, \dots, 2m_N$) in (5.41) and $\Delta_{h_2}^N(s)$ (for $h_2 = 1, 2, \dots, 2m_D$) in (5.42) is inferred based on the zero exclusion principle. \square

Remark 5.8. Theorem 5.3 illustrates that examining the robust stability properties of the characteristic function $\Delta(s)$ in (5.32) is tantamount to evaluating the robust stability of $\Delta_{h_1}^D(s)$ (for $h_1 = 1, \dots, 2m_N$) in (5.37) and $\Delta_{h_2}^N(s)$ (for $h_2 = 1, \dots, 2m_D$) in (5.38). As a result, the primary hurdles involve delineating RRB, IRB, and CRB of $\Delta_{h_1}^D(s)$ (for $h_1 = 1, \dots, 2m_N$)

in (5.37) and $\Delta_{h_1}^N(s)$ (for $h_2 = 1, \dots, 2m_D$) in (5.38). To accomplish this task, **Algorithm 5.2** outlines the procedure for computing the stability region while maintaining fixed values of λ , μ , and k_d .

Algorithm 5.2:

Step 1: Derive the vertices $V_{h_1}^+(\omega)$ (for $h_1 = 1, \dots, 2m_N$) and $V_{h_2}^-(\omega)$ (for $h_2 = 1, \dots, 2m_D$) using **Approach 2**.

Step 2: Determine RRB, IRB and CRB by sweeping over $\eta \in [0, 1]$ for

$$\Delta_{r_1}^D(j\omega) = \begin{cases} \Delta_{r_1}^{D_1}(j\omega), & 0 < \omega < \frac{2\pi}{l^+ - l^-}, \\ \Delta_{r_1}^{D_2}(j\omega), & \omega \geq \frac{2\pi}{l^+ - l^-}, \end{cases} \quad (5.44)$$

in which,

$$\begin{cases} \Delta_{h_1}^{D_1}(j\omega) = s^\lambda e(V_{h_2}^-(\omega), V_{h_2+1}^-(\omega)) + V_{h_1}^+(\omega) N_c(s) e^{-ls}, \\ \Delta_{h_1}^{D_2}(j\omega) = s^\lambda e(V_{h_2}^-(\omega), V_{h_2+1}^-(\omega)) + V_{h_1}^+(\omega) N_c(s) e^{j[0, 2\pi]}, \\ h_1 = 1, 2, \dots, 2m_N, h_2 = 1, 2, \dots, 2m_D. \end{cases} \quad (5.45)$$

Step 3: Obtain RRB, IRB and CRB by sweeping over $\eta \in [0, 1]$ for

$$\Delta_{h_2}^N(s) = \begin{cases} \Delta_{h_2}^{N_1}(j\omega), & 0 < \omega < \frac{2\pi}{l^+ - l^-}, \\ \Delta_{h_2}^{N_2}(j\omega), & \omega \geq \frac{2\pi}{l^+ - l^-}, \end{cases} \quad (5.46)$$

$$\begin{cases} \Delta_{h_2}^{N_1}(s) = s^\lambda V_{h_2}^-(\omega) + N_c(s) e^{-ls} (e(V_{h_1}^-(\omega), V_{h_1+1}^-(\omega))), \\ \Delta_{h_2}^{N_2}(s) = s^\lambda V_{h_2}^-(\omega) + N_c(s) e^{j[0, 2\pi]} e(V_{h_1}^-(\omega), V_{h_1+1}^-(\omega)), \\ h_1 = 1, \dots, 2m_N, h_2 = 1, \dots, 2m_D. \end{cases} \quad (5.47)$$

Step 4: The final robust stability region for $\Delta(s)$ is the intersection of all the computed stable regions in **Step 2** and **Step 3**.

5.3 High-performance Output Disturbance Rejection

We need the following lemma for the rest of this subsection.

Lemma 5.2. Denote by $e(x, y)$ a line segment connecting the points x and y . At a particular frequency $\omega \in (0, \frac{2\pi}{l^+ - l^-})$, the set of values of $b_1 e^{-ls}$ is situated within $G_E(j\omega)$ as expressed in (6.8).

$$G_E(j\omega) \triangleq \{e(G_1(j\omega), G_2(j\omega)), e(G_2(j\omega), G_3(j\omega)), \dots, e(G_{4N+1}(j\omega), G_{4N+2}(j\omega)), e(G_{4N+2}(j\omega), G_1(j\omega))\}, \quad (5.48)$$

$$G_k(j\omega) \triangleq \begin{cases} \overline{G}_{(k-1)}(j\omega), & \text{if } 1 \leq k \leq 2M+1, \\ \underline{G}_{(2M)}(j\omega), & \text{if } k = 2M+2, \\ \underline{G}_{(2M-1)}(j\omega), & \text{if } k = 2M+3, \\ \vdots & \\ \underline{G}_0(j\omega), & \text{if } k = 4M+2, \end{cases}$$

$$\bar{G}_k(j\omega) \triangleq \begin{cases} b_1 e^{-j\omega \left(l^- + k \frac{l^+ - l^-}{2N} \right)}, & \text{if } k = 0, 2, \dots, 2M, \\ \frac{b_1 e^{-j\omega \left(l^- + k \frac{l^+ - l^-}{2M} \right)}}{\cos \left(\omega \frac{l^+ - l^-}{2M} \right)}, & \text{if } k = 1, 3, \dots, 2M-1, \end{cases}$$

$$\underline{G}_k(j\omega) \triangleq b_1 e^{-j\omega \left(l^- + k \frac{l^+ - l^-}{2M} \right)}, \quad k = 0, 1, 2, \dots, 2M.$$

Here, M is a member of the set of natural numbers greater than or equal to 3.

Proof. The proof follows from Theorem 4.4. □

As noted by [96], the sensitivity function encompasses crucial aspects of a feedback system, including its capability to track references and reject disturbances. A low sensitivity function at lower frequencies plays a pivotal role in attaining the desired performance of the closed-loop system. Hence, we formulate a robust FO controller to fulfill the inequality constraint (5.49).

$$|S(j\omega)| = \left| \frac{1}{1 + C(j\omega)P(j\omega, \mathbf{b}, \mathbf{a}, \mathbf{l})} \right| < |M_s(j\omega)| \rightarrow \left| \frac{1}{1 + \frac{N_c(s)N(s, \mathbf{b})}{s^\lambda D(s, \mathbf{a})} e^{-l_s}} \right| < |M_s(s)|,$$

$$M_s(s) = \frac{N_m(s)}{D_m(s)}, s = j\omega. \quad (5.49)$$

In (5.49), $M_s(s)$ represents the weighting function, elucidating the frequency characteristics of performance specifications and the frequency bandwidth of disturbances. As per (5.49), the maximum modulus theorem [97], Lemma 5.2 and Theorem 4.4, the robustly designed FOPID controller should adhere to the inequality $\chi_s(\omega) < 0$.

$$\chi_s(\omega) \triangleq \begin{cases} \max\{\chi_s^i | i = 1, 2, 3, 4\}, & \text{for } \omega \in [0, \frac{2\pi}{l^+ - l^-}), \\ \frac{1}{\left| \frac{\max\{\bar{V}_1^N, \bar{V}_2^N, \bar{V}_3^N, \bar{V}_4^N\}}{\min_{e_P^D \in P_E^D} |e_P^D|} - 1 \right|} - |M_s(j\omega)|, & \text{for } \omega \in [\frac{2\pi}{l^+ - l^-}, \infty), \end{cases} \quad (5.50)$$

where

$$\begin{aligned} \chi_s^1(\omega) &\triangleq \max_{r=1, \dots, 4N+1} \tilde{\chi}_{S_1}^r(\omega) - |M_s(j\omega)|, \\ \tilde{\chi}_{S_1}^r(\omega) &\triangleq \max_{e_{S_1 r_1, r_2} \in P_{S_1}} |e_{S_1 r_1, r_2}|, \\ r_1 &\in \{1, \dots, 2m_N\}, r_2 \in \{1, \dots, 2m_D\}, \\ P_{S_1} &\triangleq \{e_{S_1 1, 1}, \dots, e_{S_1 r_1, r_2}, \dots, e_{S_1 2m_n, 2m_D}\}, \\ e_{S_1 r_1, r_2} &\triangleq \frac{1}{1 + \frac{N_c(s)V_{r_1}^+(\omega)G_r(s)}{s^\lambda e(V_{r_2}^-(\omega), V_{r_2+1}^-(\omega))}}. \end{aligned} \quad (5.51)$$

$$\begin{aligned}\chi_S^2(\omega) &\triangleq \max_{r_1=1,\dots,2m_N} \tilde{\chi}_{S_2}^{r_1}(\omega) - |M_s(j\omega)|, \\ \tilde{\chi}_{S_2}^{r_1}(\omega) &\triangleq \max_{e_{S_2r,r_2} \in P_{S_2}} \in |e_{S_2r,r_2}|, \\ r &\in \{1, \dots, 4N+1\}, r_2 \in \{1, \dots, 2m_D\},\end{aligned}\tag{5.52}$$

$$P_{S_2} \triangleq \{e_{S_21,1}, \dots, e_{S_2r,r_2}, \dots, e_{S_24N+1,2m_D}\},$$

$$e_{S_2r,r_2} \triangleq \frac{1}{1 + \frac{N_c(s)V_{r_1}^+(\omega)e(G_r(s), G_{r+1}(s))}{s^\lambda V_{r_2}^-(\omega)}}.$$

$$\begin{aligned}\chi_S^3(\omega) &\triangleq \max_{r=1,\dots,4N+1} \tilde{\chi}_{S_3}^r(\omega) - |M_s(j\omega)|, \\ \tilde{\chi}_{S_3}^r(\omega) &\triangleq \max_{e_{S_3r_1,r_2} \in P_{S_3}} \in |e_{S_3r_1,r_2}|, \\ r_1 &\in \{1, \dots, 2m_N\}, r_2 \in \{1, \dots, 2m_D\},\end{aligned}\tag{5.53}$$

$$P_{S_3} \triangleq \{e_{S_31,1}, \dots, e_{S_3r_1,r_2}, \dots, e_{S_32m_N,2m_D}\},$$

$$e_{S_3r_1,r_2} \triangleq \frac{s^\lambda V_{r_2}^-(\omega)}{s^\lambda V_{r_2}^-(\omega)G_r'(s) + N_c(s)e(V_{r_1}^+(\omega), V_{r_1+1}^+(\omega))}.$$

$$\begin{aligned}\chi_S^4(\omega) &\triangleq \max_{r_2=1,\dots,2m_D} \tilde{\chi}_{S_4}^{r_2}(\omega) - |M_s(j\omega)|, \\ \tilde{\chi}_{S_4}^{r_2}(\omega) &\triangleq \max_{e_{S_4r_1,r} \in P_{S_4}} \in |e_{S_4r_1,r}|, \\ r_1 &\in \{1, \dots, 2m_N\}, r \in \{1, \dots, 4N+1\},\end{aligned}\tag{5.54}$$

$$P_{S_4} \triangleq \{e_{S_41,1}, \dots, e_{S_4r_1,r}, \dots, e_{S_42m_N,4N+1}\},$$

$$e_{S_4r_1,r_2} \triangleq \frac{s^\lambda V_{r_2}^-(\omega)}{s^\lambda V_{r_2}^-(\omega)e(G_r'(s), G_{r+1}'(s)) + N_c(s)V_{r_1}^+(\omega)},$$

where $G_r'(j\omega)$ is given by

$$\begin{aligned}G_i'(j\omega) &\triangleq \begin{cases} \overline{G}_{(i-1)}'(j\omega), & \text{if } 1 \leq i \leq 2M+1, \\ \underline{G}_{(2M)}'(j\omega), & \text{if } i = 2M+2, \\ \underline{G}_{(2M-1)}'(j\omega), & \text{if } i = 2M+3, \\ \vdots \\ \underline{G}_0'(j\omega), & \text{if } i = 4M+2, \end{cases} \\ \overline{G}_i'(j\omega) &\triangleq \begin{cases} e^{j\omega \left(l^- + i \frac{l^+ - l^-}{2M} \right)}, & \text{if } i = 0, 2, \dots, 2M, \\ \frac{e^{j\omega \left(l^- + i \frac{l^+ - l^-}{2M} \right)}}{\cos \left(\omega \frac{l^+ - l^-}{2M} \right)}, & \text{if } i = 1, 3, \dots, 2M-1, \end{cases} \\ \underline{G}_i'(j\omega) &\triangleq e^{j\omega \left(l^- + i \frac{l^+ - l^-}{2N} \right)}, \quad i = 0, 1, 2, \dots, 2M. \end{aligned}$$

Remark 5.9. Using the graphical tuning method proposed in **Algorithm 5.2**, a robust FOPID controller for the interval system can be designed. To enhance the system's performance, the designed robust controller should satisfy $\chi_S(\omega) \leq 0$ in (6.37). The subsequent section will complement the results presented in this chapter with illustrative examples demonstrating the application of the contributed methods.

5.4 Simulation Results

Example 5.1. Consider a plant with interval uncertainties as follows:

$$\begin{aligned} P(s) &= \frac{N_P(s)}{D_P(s)} e^{-[0.5, 0.9]s}, \\ N_P(s) &= [-0.6, -0.3]s + [0.9, 1.1], \\ D_P(s) &= s^3 + [1.8, 2.2]s^2 + [2.8, 3.2]s + [0.8, 1]. \end{aligned} \quad (5.55)$$

Suppose our initial objective is to determine the stability region of PI controllers by setting $k_d = 0$ and $\lambda = 1$ in the FOPID controller introduced in (5.31). In this scenario, we utilize **Algorithm 5.2** to identify the robust stability region of PI controllers, as illustrated in Figure 5.1 (green region). From this figure, it becomes apparent that the PI controller $C(s) = 1 + \frac{0.2}{s}$ is located in the green region and using Lemma 2.2, the stability of the characteristic function has been checked for some randomly generated values in the uncertainty space. From Figure 5.2, all chosen characteristic functions are stable. From the given figure, it is evident that the PI controller, denoted as $C(s) = 1 + \frac{0.2}{s}$, is positioned within the green region. By applying Lemma 2.2, the stability of the characteristic function has been verified using randomly generated values within the uncertainty space. As illustrated in Figure 5.2, all selected characteristic functions are observed to be stable.

The robust stability region (depicted in green) of FOPI controllers has been illustrated in Figure 5.3 for $\lambda = 0.5$. To validate this region, the robust stability of the closed-loop system has been examined in Figure 5.4 using one of the controllers situated within the green region, such as the controller $C(s) = \frac{0.5}{s^{0.5}}$, as demonstrated in Lemma 2.2.

Similarly, the robust stability region (also in green) of FOPID controllers has been delineated in Figure 5.5 for $\lambda = 0.5$, $\mu = 1$, and $K_d = 0.01$. To confirm the obtained region, Figure 5.6 verifies the robust stability of the system using a controller located within the green region, for instance, the controller $C(s) = 0.1 + \frac{0.1}{s^{0.5}} + 0.01s$, as per Lemma 2.2. This underscores the sophistication and novelty of the method introduced in this chapter.

Example 5.2. Consider a plant with interval uncertainties as follows:

$$P(s) = \frac{[2, 4]}{[70, 80]s + 1} e^{-[0.5, 1]s}. \quad (5.56)$$

Our objective is to ascertain the robust stability region of FOPID controllers with $\mu = 0.65$, $\lambda = 1$, and $k_d = 1$. Utilizing **Algorithm 1**, we have delineated the robust stability region of the controller in the green area, as depicted in Figure 5.7. According to this figure, the controllers identified fall within the confines of the green region.

$$C_1(s) = 2 + \frac{2}{s} + s^{0.65}. \quad (5.57)$$

$$C_2(s) = 18 + \frac{1.3}{s} + s^{0.65}. \quad (5.58)$$

Additionally, the plot of $\chi(\omega)$ is presented in Figure 5.8 for

$$M_s(s) = 0.021 \frac{(s + 1000)(s + 30.67)(s + 0.001)}{s^2 + 30.67s + 247.3}$$

corresponding to both controllers $C_1(s)$ and $C_2(s)$. Observing this figure, it is evident that controller $C_2(s)$ satisfies the inequality $\chi(\omega) < 0$. Consequently, the designer should opt for controller $C_2(s)$. Figure 5.9 and Figure 5.10 depict the step responses of the closed-loop system. Notably, these figures highlight that controller $C_2(s)$ exhibits superior performance, characterized by fewer oscillations.

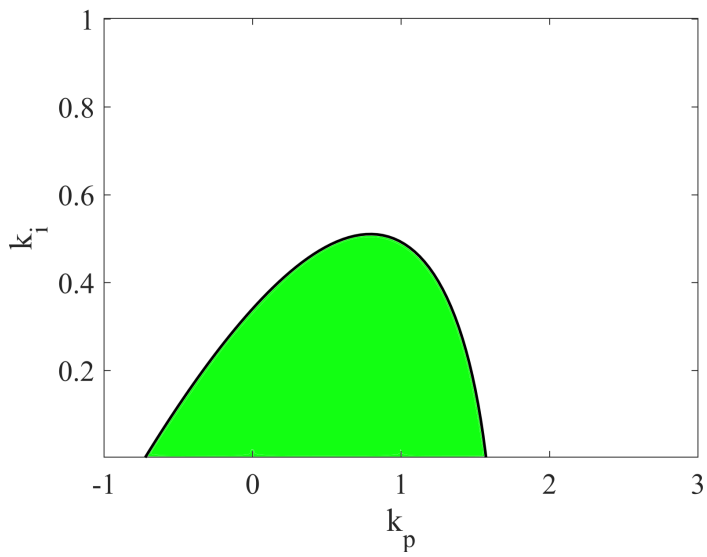


Figure 5.1: Robust stability region of PI controllers.

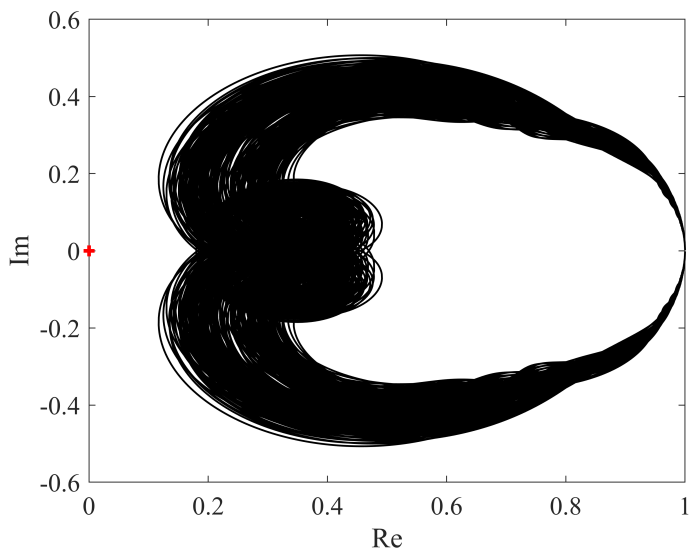


Figure 5.2: Verification of the robust PI stabilization $C(s) = 1 + \frac{0.2}{s}$ using Lemma 2.2.

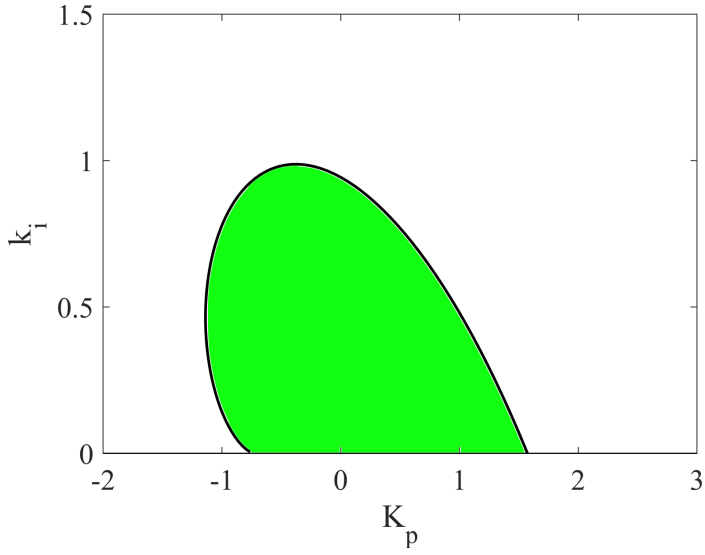


Figure 5.3: Robust stability region of FOPI controllers with $\lambda = 0.5$.

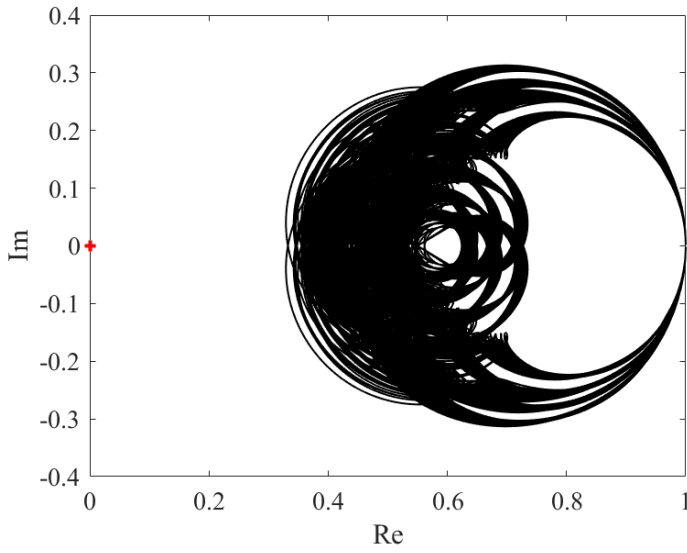


Figure 5.4: Verification of the robust FOPI stabilization $C(s) = \frac{0.5}{s^{0.5}}$ using Lemma 2.2 .

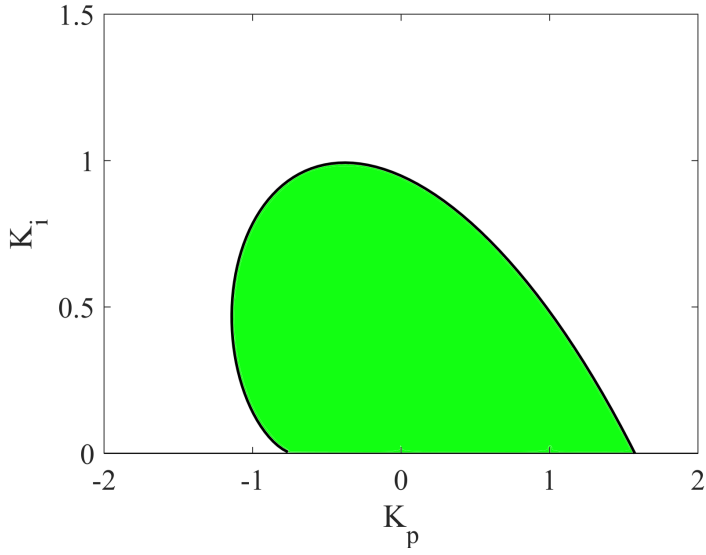


Figure 5.5: Robust stability region of FOPID controllers with $\lambda = 0.5, \mu = 1$ and $K_d = 0.01$.

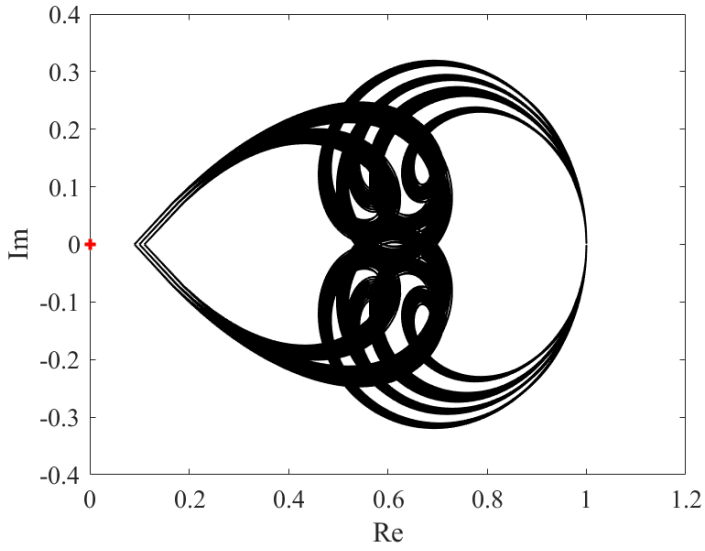


Figure 5.6: Verification of the robust FOPID stabilization $C(s) = 0.1 + \frac{0.1}{s^{0.5}} + 0.01s$ using Lemma 2.2.

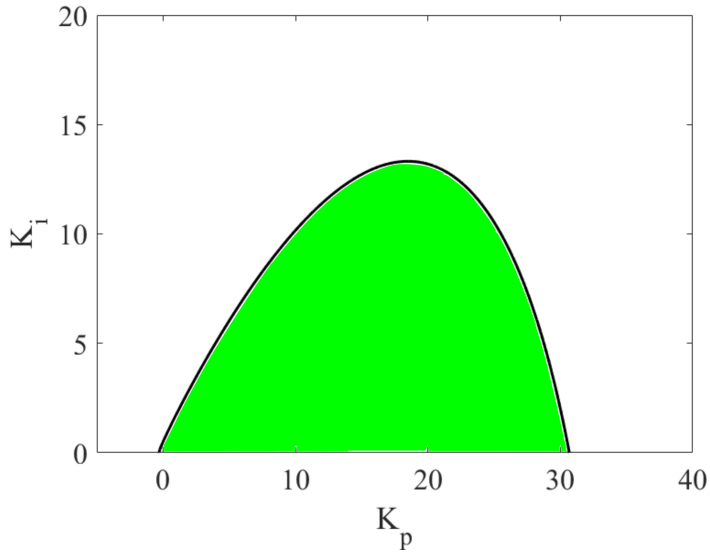


Figure 5.7: Robust stability region of FOPID controllers with $\mu = 0.65$, $\lambda = 1$ and $k_d = 1$.

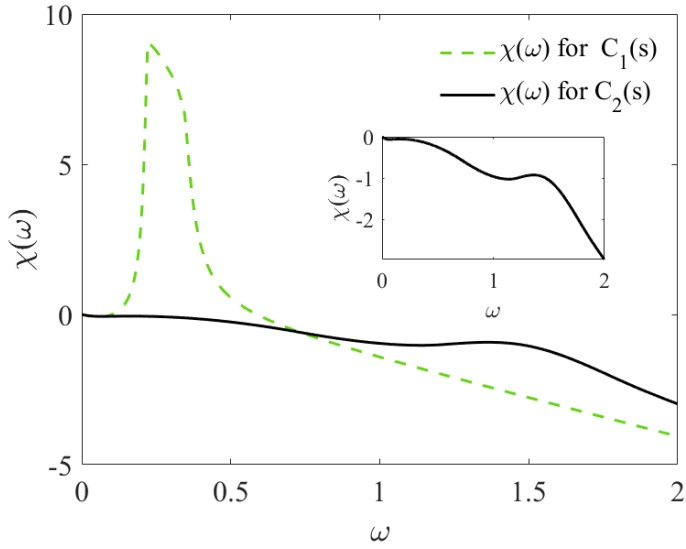


Figure 5.8: Curves of $\chi(\omega)$ corresponding to the controllers $C_1(s)$ (dashed line) and $C_2(s)$ (solid line).

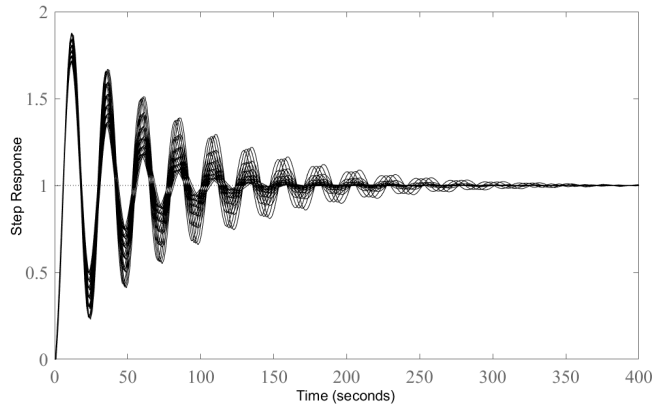


Figure 5.9: Step responses corresponding to $C_1(s)$.

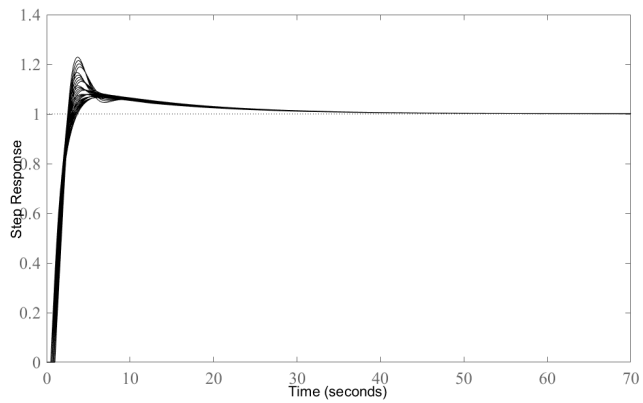


Figure 5.10: Step responses corresponding to $C_2(s)$.

6 Robust Stability Analysis of Smith Predictors

This chapter presents a new approach to analyze the robust stability of a FO control system using a Smith predictor, considering interval uncertainties in gain, time constants, and time delay. The method proposed utilizes the value set concept and graphical techniques to obtain explicit necessary and sufficient conditions for the stability analysis. This work contributes in two ways: firstly, it establishes a set of conditions to determine if the FO controller can stabilize the control system robustly. Secondly, it introduces an auxiliary function to simplify the computational complexity of the analysis. Some examples are provided to demonstrate the effectiveness of the proposed approach.

6.1 Robust Stability Analysis of Smith Predictors for stable systems

6.1.1 Background

Dead time is an inherent feature of many physical systems, such as chemical processes, transportation systems, and communication networks [114, 115]. When designing a control system for such processes, the presence of time delays can have a significant impact on the system's stability and performance. Time delays can lead to instability, oscillations, and poor transient response, which can cause the system to be unable to meet the desired performance specifications. Hence, it is crucial to consider time delay effects when designing and analyzing control systems, especially in the case of systems with long or uncertain delays [42].

In recent years, several control strategies, such as the Smith predictor [116], have been proposed to deal with time delay in control systems. The Smith Predictor compensates for the time delay by estimating the future output of the system and using this estimate to improve the control action [117]. When the accuracy of the model is ensured, the closed-loop characteristic polynomial of the Smith predictor control structure attains a delay-free nature. Nonetheless, in practical applications, the dynamic behavior of the process cannot be adequately captured by the plant model, primarily due to fluctuations in the process parameters, mandating the need for a robust stability analysis of the Smith predictor control system [42]. Thus, the aforementioned requirements necessitate an in-depth investigation of the existing literature. Various strategies have been proposed to address these requirements, each offering unique benefits. For instance, in [118], the performance of Smith predictor-based control systems has been significantly enhanced by leveraging convex optimization techniques.

FOPID controllers are an extension of the classical PID controllers that are widely used in control engineering. In a FOPID controller, the derivative and/or integral actions are realized through FO differentiation and integration, respectively, instead of the traditional integer-order differentiation and integration. This approach allows for more flexibility in the design of control systems and can improve their performance, particularly in systems with complex dynamics or non-linearities.

As a consequence of the performance benefits conferred by the Smith predictor and FO controllers, a growing number of researchers have taken to integrating FO controllers within the framework of Smith predictors. The work [59] presented a novel approach to tuning FO integral controllers that have been integrated into the Smith predictor architecture. Additionally, in [44, 51], a pair of distinct techniques have been introduced for the purpose of designing FOPID controllers and fractional integral-fractional derivative controllers specifically targeted at interval first order time-delayed processes, utilizing Smith predictor control structures as the foundational framework. It is worth noting that a plethora of additional scholarly contributions [44]-[61] are available within the lit-

erature, which aim to establish the design of FO controllers for employment in Smith predictor structures. In contrast to the previous investigations, the present study adopts an assumption whereby the coefficients of both the denominator and numerator, in addition to the time delay term, of the Smith predictor process contain interval uncertainties. To address this scenario, the necessary and sufficient conditions for robust stability analysis are then derived. Moreover, two auxiliary functions are introduced, with the objective of elevating the robust stability and the performance of the Smith predictor.

6.1.2 Definitions

The control scheme under investigation in this chapter is a Smith predictor control configuration, which is visually depicted in Figure 6.1. Within this particular control framework,

- The transfer function $P(s)$, denoting the underlying dynamics of the process at hand, is regarded as a comprehensive representation of interval plants in the equation (6.42).

$$P(s) = \frac{N_p(s)}{D_p(s)} = \frac{\sum_{r_1=0}^m q_{r_1}^N s^{r_1}}{\sum_{r_2=0}^n q_{r_2}^D s^{r_2}} e^{-\tau s}, n > m \geq 0, \quad (6.1)$$

where,

$$\begin{cases} q_{r_1}^N \in [\underline{q}_{r_1}^N, \bar{q}_{r_1}^N], q_m^N \neq 0, \\ q_{r_2}^D \in [\underline{q}_{r_2}^D, \bar{q}_{r_2}^D], q_n^D \neq 0, \\ \tau \in [\underline{\tau}, \bar{\tau}]. \end{cases} \quad (6.2)$$

- The process's idealized model $P_0(s)$, which disregards any time delay in its dynamics, is precisely explicated in equation (6.44).

$$P_0(s) = \frac{N_0(s)}{D_0(s)} = \frac{\sum_{r_1=0}^m q_{r_1}^{N_0} s^{r_1}}{\sum_{r_2=0}^n q_{r_2}^{D_0} s^{r_2}}, \quad (6.3)$$

in which,

$$\begin{cases} q_{r_1}^{N_0} = \frac{q_{r_1}^N + \bar{q}_{r_1}^N}{2}, \\ q_{r_2}^{D_0} = \frac{q_{r_2}^D + \bar{q}_{r_2}^D}{2}. \end{cases} \quad (6.4)$$

- The controller $C(s)$ is a FOPID controller defined in (6.46).

$$C(s) = \frac{N_c(s)}{s^\lambda} = \frac{K_p s^\lambda + K_i + K_d s^{\mu+\lambda}}{s^\lambda}, \quad (6.5)$$

$\lambda \in (0, 2), \mu \in [0, n-m), K_i \neq 0, K_p, K_d \in \mathbb{R}.$

- The value assigned to the dead time parameter $\hat{\tau}$ of the process, as determined through estimation procedures, is postulated as expressed in equation (6.47).

$$\hat{\tau} = \frac{\underline{\tau} + \bar{\tau}}{2}. \quad (6.6)$$

Ascertained from the information presented in Figure 6.1, the FO characteristic quasi-polynomial governing the closed-loop characteristic equation is delineated as follows:

$$F(s) = s^\lambda D_0(s) D_p(s) + N_c(s) \left(N_0(s) D_p(s) (1 - e^{-\hat{\tau}s}) + N_p(s) D_0(s) e^{-\tau s} \right). \quad (6.7)$$

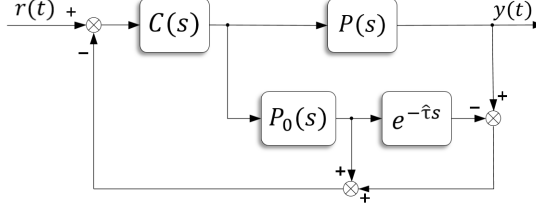


Figure 6.1: Smith predictor control configuration [42].

The methodologies previously introduced do not ensure the robust stability of the FO characteristic quasi-polynomial (6.50) in the presence of concurrent uncertainties in all model parameters. In light of this, the present chapter centers on scrutinizing the robust stability of the FO characteristic quasi-polynomial of the Smith predictor control configuration, specifically $F(s)$ as portrayed in equation (6.50). To explore the robust stability criteria, this investigation employs the value set approach. Subsequently, several beneficial frequency domain properties of the value sets of systems featuring parametric uncertainties are introduced herein (See [120]).

- At $s = j\omega$,

$$\partial(\mathbf{N}_p(s)) \subset \mathbf{N}_E := \{e(V_1^N, V_2^N) \cup e(V_2^N, V_3^N) \cup e(V_3^N, V_4^N) \cup e(V_4^N, V_1^N)\}, \quad (6.8)$$

where,

$$\begin{cases} V_1^N = \underline{q}_0^N + \underline{q}_0^N s + \bar{q}_0^N s^2 + \bar{q}_0^N s^3 + \dots, \\ V_2^N = \bar{q}_0^N + \underline{q}_0^N s + \underline{q}_0^N s^2 + \bar{q}_0^N s^3 + \dots, \\ V_3^N = \bar{q}_0^N + \bar{q}_0^N s + \underline{q}_0^N s^2 + \underline{q}_0^N s^3 + \dots, \\ V_4^N = \underline{q}_0^N + \bar{q}_0^N s + \bar{q}_0^N s^2 + \underline{q}_0^N s^3 + \dots \end{cases} \quad (6.9)$$

- At $s = j\omega$,

$$\partial(\mathbf{D}_p(s)) \subset \mathbf{D}_E := \{(V_1^D, V_2^D) \cup e(V_2^D, V_3^D) \cup e(V_3^D, V_4^D) \cup e(V_4^D, V_1^D)\}, \quad (6.10)$$

where

$$\begin{cases} V_1^D = \underline{q}_0^D + \underline{q}_0^D s + \bar{q}_0^D s^2 + \bar{q}_0^D s^3 + \dots, \\ V_2^D = \bar{q}_0^D + \underline{q}_0^D s + \underline{q}_0^D s^2 + \bar{q}_0^D s^3 + \dots, \\ V_3^D = \bar{q}_0^D + \bar{q}_0^D s + \underline{q}_0^D s^2 + \underline{q}_0^D s^3 + \dots, \\ V_4^D = \underline{q}_0^D + \bar{q}_0^D s + \bar{q}_0^D s^2 + \underline{q}_0^D s^3 + \dots \end{cases} \quad (6.11)$$

- At $s = j\omega$,

$$\partial\left(\frac{N_p(s)}{D_p(s)}\right) \subset \mathbf{G}_E := \frac{\mathbf{N}_V}{\mathbf{D}_E} \cup \frac{\mathbf{N}_E}{\mathbf{D}_V}, \quad (6.12)$$

where, \mathbf{N}_E and \mathbf{D}_E are respectively defined in (6.8) and (6.10). Also, \mathbf{N}_V and \mathbf{D}_V are as follows:

$$\begin{cases} \mathbf{N}_V = \{V_1^N, V_2^N, V_3^N, V_4^N\}, \\ \mathbf{D}_V = \{V_1^D, V_2^D, V_3^D, V_4^D\}. \end{cases} \quad (6.13)$$

Assumption 6.1. This current investigation operates under the presumption that both $F(j0) \neq 0$ and $D_p(s)$ does not possess unstable poles.

Definition 6.1. The characteristic equation $F(s)$ in (6.50) is said to be robustly Hurwitz-stable if and only if the characteristic quasi-polynomial remains Hurwitz-stable for all possible values within the uncertainty space.

6.1.3 Derivation of Robust Stability Conditions

In this section, we commence by presenting Theorem 6.1, which delineates the necessary and sufficient conditions for the robust stability of the Smith predictor control configuration $F(s)$ as illustrated in equation (6.50).

Theorem 6.1. Assume that the nominal characteristic polynomial $F_0(s)$ in (6.14) is stabilized by the FOPID controller (6.46).

$$F_0(s) = s^\lambda D_0(s) + N_c(s) N_0(s). \quad (6.14)$$

Then, the Smith predictor control configuration attains robust stability if and only if:

- The value sets $F_1(j\omega)$ in (6.15) and $F_2(j\omega)$ in (6.16) do not have any overlap for $\omega \in [0, \frac{2\pi}{\bar{\tau}-\underline{\tau}})$,

$$F_1(j\omega) = -e^{\tau j\omega} \left((j\omega)^\lambda + N_c(j\omega) \left(P_0(j\omega) (1 - e^{-\hat{\tau} j\omega}) \right) \right). \quad (6.15)$$

$$F_2(j\omega) = \frac{N_c(j\omega) N_p(j\omega)}{D_p(j\omega)}. \quad (6.16)$$

- The inequality $\chi(\omega) > 0$ is met for $\omega \in [\frac{2\pi}{\bar{\tau}-\underline{\tau}}, \infty)$, where

$$\begin{aligned} \chi(\omega) &= \min_{e_l^D \in P_E^D} |e_l^D| - \max_i \bar{V}_i^N, \\ P_E^D &= \{e_1^D, e_2^D, e_3^D, e_4^D\}, \\ e_i^D &= e(V_i^D(s^\lambda D_0(s) + N_c(s) N_0(s)(1 - e^{-\hat{\tau}s})), \\ V_{i+1}^D &= (s^\lambda D_0(s) + N_c(s) N_0(s)(1 - e^{-\hat{\tau}s})), \\ \bar{V}_i^N &= |V_i^N N_c(s) D_0(s)|, \end{aligned} \quad (6.17)$$

In (6.17), $i \in \{1, 2, 3, 4\}$, $V_1^D = V_5^D$ and 's' is equal to ' $j\omega$ '.

Proof. The proof of this claim can be demonstrated using the zero exclusion principle, which is illustrated in [10]. Thus, it can be established that the origin of the complex plane is not part of the value set of $F(j\omega)$, as presented in (6.50), by the conditions articulated in Theorem 6.1.

Sufficiency: Here, we can deduce that $\Theta_1(j\omega)$, as represented in equation (6.18), denotes the boundary of $F_1(j\omega)$ over the range of $\omega \in (0, \frac{2\pi}{\bar{\tau}-\underline{\tau}})$.

$$\begin{aligned} \Theta_1(j\omega) &= -e^{e(\underline{\tau}, \bar{\tau})j\omega} H(j\omega), \\ H(j\omega) &= \left((j\omega)^\lambda + N_c(j\omega) P_0(j\omega) (1 - e^{-\hat{\tau} j\omega}) \right). \end{aligned} \quad (6.18)$$

Furthermore, by utilizing (6.12), we can assert that $\Theta_2(j\omega)$, as given in (6.19), represents the boundary of $F_2(j\omega)$.

$$\Theta_2(j\omega) = N_c(j\omega) \mathbf{G}_E, \quad (6.19)$$

where \mathbf{G}_E is defined in (6.12). We can derive equation (6.20) based on (6.50).

$$\frac{F(j\omega)e^{\tau j\omega}}{D_p(j\omega)} = -F_1(j\omega) + F_2(j\omega). \quad (6.20)$$

Assuming a fixed frequency $\omega = \omega_0 \in (0, \frac{2\pi}{\tau-\underline{\tau}})$, if the value sets of $F_1(j\omega)$ in (6.15) and $F_2(j\omega)$ in (6.16) have overlap in the complex plane, it implies the existence of a complex number, denoted as Z_0 , such that Z_0 belongs to $F_1(j\omega_0)$ (or $-Z_0$ belongs to $-F_1(j\omega_0)$) and Z_0 belongs to $F_2(j\omega_0)$. Consequently, we can express this situation as follows:

$$\begin{cases} Z_0 \in F_1(j\omega_0), \\ Z_0 \in F_2(j\omega_0), \end{cases} \Rightarrow 0 \in F(j\omega_0). \quad (6.21)$$

Thus, if there is no overlap between the value sets of $F_1(j\omega)$ in (6.15) and $F_2(j\omega)$ in (6.16) for $\omega \in (0, \frac{2\pi}{\tau-\underline{\tau}})$, then it follows that 0 does not belong to $F(j\omega)$. Moreover, for $\omega \in [\frac{2\pi}{\tau-\underline{\tau}}, \infty)$, the value set of $F_1(j\omega)$ in (6.15) can be expressed as (6.22).

$$F_1(j\omega) = \left| (j\omega)^\lambda + N_c(j\omega) \left(P_0(j\omega)(1 - e^{-\hat{\tau}j\omega}) \right) \right| e^{j[0, 2\pi]}. \quad (6.22)$$

Furthermore, it should be noted that the maximum absolute magnitude exhibited by $F_2(j\omega)$, denoted as $|F_2^{\max}(\omega)|$ and specified in (6.23), represents the upper bound of its value set.

$$|F_2^{\max}(\omega)| = \frac{|N_c(j\omega)| \max\{|V_1^N|, |V_2^N|, |V_3^N|, |V_4^N|\}}{\min_{e_l \in D_E} |e_l|}. \quad (6.23)$$

From equations (6.9) and (6.10), where $l = 1, 2, 3, 4$, V_l^N and D_E are defined, it follows that if the inequality $|F_1(j\omega)| > |F_2^{\max}(\omega)|$ is satisfied for $\omega \in [\frac{2\pi}{\tau-\underline{\tau}}, \infty)$, then $0 \notin F(j\omega)$ can be concluded from equation (6.20). Conversely, we can express this as follows:

$$\begin{aligned} |F_1(j\omega)| > |F_2^{\max}(\omega)| &\Rightarrow \\ \left| 1 + C(j\omega) \left(P_0(j\omega)(1 - e^{-\hat{\tau}j\omega}) \right) \right| &> \\ \frac{|C(j\omega)| \max\{|V_1^N|, |V_2^N|, |V_3^N|, |V_4^N|\}}{\min_{e_l \in D_E} |e_l|} &\Rightarrow \chi(\omega) > 0. \end{aligned} \quad (6.24)$$

Thus, by virtue of the zero exclusion principle, it can be concluded that the Smith predictor control structure exhibits robust stability.

Necessity: If the Smith predictor control structure exhibits robust stability, it follows that the frequency response of the system, denoted by $F(j\omega)$, does not contain the complex plane origin, due to the zero exclusion principle. Consequently, the value sets of $F_1(j\omega)$ and $F_2(j\omega)$ in equations (6.15) and (6.16), respectively, do not overlap in the complex plane for frequencies ω in the interval $(0, \frac{2\pi}{\tau-\underline{\tau}})$. For frequencies ω in the range $[\frac{2\pi}{\tau-\underline{\tau}}, \infty)$, it is assumed that the inequality $\chi(\omega) > 0$ does not hold, i.e., $\chi(\omega) \leq 0$. This is due to the fact that the limit of the magnitude of $F_1(j\omega)$ as ω approaches infinity is greater than the

limit of the magnitude of $F_2^{\max}(\omega)$, which ensures that the inequality $\chi(\omega) > 0$ holds as ω approaches infinity. As a result, there must exist a frequency $\omega_{\text{overlap}} \in [\frac{2\pi}{\tau-\underline{\tau}}, \infty)$ at which the value sets of $F_1(j\omega_{\text{overlap}})$ and $F_2(j\omega_{\text{overlap}})$ have an overlap in the complex plane, i.e., $0 \in F(j\omega_{\text{overlap}})$. This contradicts the assumption of robust stability, thus completing the proof. \square

The subsequent objective is to narrow down the test frequency range to facilitate a more manageable investigation of the conditions described in Theorem 6.1. In practical terms, evaluating the value set of the fractional-order characteristic quasi-polynomial over the entire positive frequency axis is both computationally expensive and analytically unnecessary. Therefore, it is useful to determine an upper bound on the frequency beyond which the value set cannot include the origin. This enables the reduction of the semi-infinite frequency domain $(0, \infty)$ to a finite interval $(0, \omega_{\text{max}}]$, within which the robust stability verification can be fully conducted. The derivation of this upper bound relies on bounding arguments for the magnitude of the fractional-order terms and establishing conservative estimates that guarantee exclusion of the origin outside this interval. Theorem 6.2 formalizes this idea and provides the corresponding analytical expression for ω_{max} .

Theorem 6.2. *The frequency range $\omega \in (\omega_{\text{max}}, \infty)$ must be devoid of the origin in the value set of the FO characteristic quasi-polynomial $F(s)$ i.e., $0 \notin F(j\omega)$ as expressed in (6.50). Furthermore, ω_{max} is defined in the following manner.*

$$\begin{aligned}
\omega_{\text{max}} &= \max\{1, R^{\frac{1}{\Upsilon}}\}, \Upsilon = 2n - \max\{2n-1, n+m+\mu\}, \\
R &= \frac{\sum_{r=1}^4 R_r}{|q_n^{D_0}| \min\{|q_n^D|, |\bar{q}_n^D|\}}, \\
R_1 &= \left(\sum_{h_1=0}^{n-1} \max\{|q_{h_1}^D|, |\bar{q}_{h_1}^D|\} \right) \left(\sum_{h_2=0}^{n-1} |q_{h_2}^{D_0}| \right), \\
R_2 &= |q_n^{D_0}| \left(\sum_{h_1=0}^{n-1} \max\{|q_{h_1}^D|, |\bar{q}_{h_1}^D|\} \right), \\
R_3 &= \left(\max\{|q_n^D|, |\bar{q}_n^D|\} \right) \left(\sum_{h_2=0}^{n-1} |q_{h_2}^{D_0}| \right), \\
R_4 &= (|K_p| + |K_i| + |K_d|) \left(2 \left(\sum_{h_1=0}^n \max\{|q_{h_1}^D|, |\bar{q}_{h_1}^D|\} \right) \right. \\
&\quad \left. \left(\sum_{h_3=0}^m |q_{h_3}^{N_0}| \right) + \left(\sum_{h_4=0}^m \max\{|q_{h_4}^N|, |\bar{q}_{h_4}^N|\} \right) \left(\sum_{h_2=0}^n |q_{h_2}^{D_0}| \right) \right).
\end{aligned} \tag{6.25}$$

Proof. The inequality $|F(j\omega)| > 0$ establishes with certainty that the origin lies beyond the set of values taken by the function $F(j\omega)$. This conclusion is drawn from the application of the triangle inequality, under the assumption that $\omega > 1$, leading to the derivation of inequality (6.26).

$$\begin{aligned}
|F(j\omega)| &\geq |q_n^{D_0}| \max\{|\underline{q}_n^D|, |\bar{q}_n^D|\} |\omega|^{2n+\lambda} - \\
&\left(|\omega|^\lambda \left(\sum_{h_1=0}^{n-1} \max\{|\underline{q}_{h_1}^D|, |\bar{q}_{h_1}^D|\} |\omega|^{h_1} \right) \left(\sum_{h_2=0}^{n-1} |q_{h_2}^{D_0}| |\omega|^{h_2} \right) \right. \\
&+ |q_n^{D_0}| \left(\sum_{h_1=0}^{n-1} \max\{|\underline{q}_{h_1}^D|, |\bar{q}_{h_1}^D|\} |\omega|^{h_1+n+\lambda} \right) \\
&+ \left(\max\{|\underline{q}_n^D|, |\bar{q}_n^D|\} \right) \left(\sum_{h_2=0}^{n-1} |q_{h_2}^{D_0}| |\omega|^{h_2+n+\lambda} \right) + \\
&\left. (|K_p| |\omega|^\lambda + |K_i| + |K_d| |\omega|^{\lambda+\mu}) \left(\left(\sum_{h_1=0}^n \max\{|\underline{q}_{h_1}^D|, |\bar{q}_{h_1}^D|\} |\omega|^{h_1} \right) \right. \right. \\
&\left. \left(\sum_{h_3=0}^m |q_{h_3}^{N_0}| |\omega|^{h_3} \right) (|1| + |e^{-\tau_0 j \omega}|) + \right. \\
&\left. \left. \left(\sum_{h_4=0}^m \max\{|\underline{q}_{h_4}^N|, |\bar{q}_{h_4}^N|\} |\omega|^{h_4} \right) \left(\sum_{h_2=0}^n |q_{h_2}^{D_0}| |\omega|^{h_2} \right) \right) \right). \tag{6.26}
\end{aligned}$$

The set of inequalities (6.27) is valid for values of the frequency parameter ω that satisfy the condition $\omega > 1$.

$$|\omega|^{2n+\lambda} > |\omega|^{\max\{2n-1, n+m+\mu\}+\lambda} \geq \dots > 1 \tag{6.27}$$

Consequently, by combining equations (6.26) and (6.27), the inequality expressed in equation (6.28) can be deduced.

$$\begin{aligned}
|F(j\omega)| &\geq |q_n^{D_0}| \max\{|\underline{q}_n^D|, |\bar{q}_n^D|\} |\omega|^{2n+\lambda} - \\
&\left(|\omega|^\lambda \left(\sum_{h_1=0}^{n-1} \max\{|\underline{q}_{h_1}^D|, |\bar{q}_{h_1}^D|\} |\omega|^{h_1} \right) \left(\sum_{h_2=0}^{n-1} |q_{h_2}^{D_0}| |\omega|^{h_2} \right) \right. \\
&+ |q_n^{D_0}| \left(\sum_{h_1=0}^{n-1} \max\{|\underline{q}_{h_1}^D|, |\bar{q}_{h_1}^D|\} |\omega|^{h_1+n+\lambda} \right) \\
&+ \left(\max\{|\underline{q}_n^D|, |\bar{q}_n^D|\} \right) \left(\sum_{h_2=0}^{n-1} |q_{h_2}^{D_0}| |\omega|^{h_2+n+\lambda} \right) + \\
&\left. (|K_p| |\omega|^\lambda + |K_i| + |K_d| |\omega|^{\lambda+\mu}) \left(\left(\sum_{h_1=0}^n \max\{|\underline{q}_{h_1}^D|, |\bar{q}_{h_1}^D|\} \right. \right. \right. \\
&|\omega|^{h_1} \left. \left(\sum_{h_3=0}^m |q_{h_3}^{N_0}| |\omega|^{h_3} \right) (|1| + |e^{-\tau_0 j \omega}|) + \right. \\
&\left. \left. \left(\sum_{h_4=0}^m \max\{|\underline{q}_{h_4}^N|, |\bar{q}_{h_4}^N|\} |\omega|^{h_4} \right) \left(\sum_{h_2=0}^n |q_{h_2}^{D_0}| |\omega|^{h_2} \right) \right) \right) \geq \tag{6.28}
\end{aligned}$$

$$\begin{aligned}
& |q_n^{D_0}| \max\{|q_n^D|, |\bar{q}_n^D|\} |\omega|^{2n+\lambda} - \left(\left(\sum_{h_1=0}^{n-1} \max\{|q_{h_1}^D|, |\bar{q}_{h_1}^D|\} \right) \right. \\
& \left(\sum_{h_2=0}^{n-1} |q_{h_2}^{D_0}| \right) + |q_n^{D_0}| \left(\sum_{h_1=0}^{n-1} \max\{|q_{h_1}^D|, |\bar{q}_{h_1}^D|\} \right) + \\
& \left(\max\{|q_n^D|, |\bar{q}_n^D|\} \right) \left(\sum_{h_2=0}^{n-1} |q_{h_2}^{D_0}| \right) + \\
& (|K_p| + |K_i| + |K_d|) \left(2 \left(\sum_{h_1=0}^n \max\{|q_{h_1}^D|, |\bar{q}_{h_1}^D|\} \right) \right. \\
& \left. \left(\sum_{h_3=0}^m |q_{h_3}^{N_0}| |\omega|^{h_3} \right) + \left(\sum_{h_4=0}^m \max\{|q_{h_4}^N|, |\bar{q}_{h_4}^N|\} \right) \left(\sum_{h_2=0}^n |q_{h_2}^{D_0}| \right) \right) \\
& \left. |\omega|^{\lambda + \max\{2n-1, n+m+\mu\}} \right).
\end{aligned}$$

Moreover, it is possible to express the right-hand side of inequality (6.28) in the form of expression (6.29).

$$\begin{aligned}
& |q_n^{D_0}| \max\{|q_n^D|, |\bar{q}_n^D|\} |\omega|^{\lambda + \max\{2n-1, n+m+\mu\}} \\
& \left(|\omega|^{2n - \max\{2n-1, n+m+\mu\}} - R \right). \tag{6.29}
\end{aligned}$$

Should the condition $|\omega| > \omega_{\max}$ holds true, it follows that the inequality $|F(j\omega)| > 0$ is simultaneously fulfilled. \square

The application of Theorem 6.2 leads to the conclusion that the robust stability of the system can be verified solely in the frequency range $\omega \in [0, \omega_{\max}]$ as opposed to the entire frequency domain $\omega \in [0, \infty)$. To streamline the robust stability analysis of the Smith predictor control structure, the ensuing corollaries have been proposed based on Theorem 6.1 and Theorem 6.2.

Corollary 6.1. Assume that the nominal characteristic polynomial $F_0(s)$ in (6.14) is stable and $\omega_{\max} \geq \frac{2\pi}{\tau - \underline{\tau}}$. Then, the Smith predictor control structure is robustly stable if and only if:

- The value sets $F_1(j\omega)$ in (6.15) and $F_2(j\omega)$ in (6.16) do not have overlap for $\omega \in (0, \frac{2\pi}{\tau - \underline{\tau}})$,
- the inequality $\chi(\omega) > 0$ is met for $\omega \in [\frac{2\pi}{\tau - \underline{\tau}}, \omega_{\max}]$.

Corollary 6.2. Assume that the nominal characteristic polynomial $F_0(s)$ in (6.14) is stable and $\omega_{\max} < \frac{2\pi}{\tau - \underline{\tau}}$. Then, the Smith predictor control structure is robustly stable if and only if the value sets $F_1(j\omega)$ in (6.15) and $F_2(j\omega)$ in (6.16) do not have overlap for $\omega \in (0, \omega_{\max})$.

In general, when ω lies within the range $(0, \frac{2\pi}{\tau - \underline{\tau}})$, the examination of the value sets of $F_1(j\omega)$ in (6.15) and $F_2(j\omega)$ in (6.16) can prove to be a challenging task. Consequently, it becomes imperative to introduce an auxiliary function to explore the overlap between the aforementioned value sets. As a result, an additional objective is to propose a robust stability testing function that can enhance the computational efficiency of analyzing the robust stability. In the forthcoming theorem, we leverage some elementary geometric properties to derive a novel robust stability testing function.

Theorem 6.3. Under the assumption that the nominal characteristic polynomial $F_0(s)$ in (6.14) is stable and ω_{\max} satisfies $\omega_{\max} \geq \frac{2\pi}{\bar{\tau}-\underline{\tau}}$, the robust stability of the Smith predictor control structure is guaranteed if the inequality $\Xi(\omega) > 0$ holds for all ω within the interval $[0, \omega_{\max}]$.

$$\Xi(\omega) = \begin{cases} \min\{\chi_i(\omega) | i = 1, 2, 3, 4\}, & \text{for } \omega \in (0, \frac{2\pi}{\bar{\tau}-\underline{\tau}}), \\ \chi(\omega), & \text{for } \omega \in [\frac{2\pi}{\bar{\tau}-\underline{\tau}}, \infty), \end{cases} \quad (6.30)$$

where,

$$\begin{aligned} \chi_1(\omega) &= \min \left\{ \kappa_{h,g,i}^{(1)}(j\omega) \mid h, i \in \{1, 2, 3, 4\}, g \in \{1, 2, \dots, 4N_1 + 2\} \right\}, \\ \kappa_{h,g,i}^{(1)}(j\omega) &= \left| \frac{N_c(j\omega)V_h^N(j\omega)}{V_i^D} + P_g^{(1)}(j\omega) \right| + \\ &\quad \left| \frac{N_c(j\omega)V_{h+1}^N(j\omega)}{V_i^D} + P_g^{(1)}(j\omega) \right| - \left| \frac{N_c(j\omega)V_h^N(j\omega)}{V_i^D} - \frac{N_c(j\omega)V_{h+1}^N(j\omega)}{V_i^D} \right|, \end{aligned} \quad (6.31)$$

$$\begin{aligned} \chi_2(\omega) &= \min \left\{ \kappa_{h,g,i}^{(2)}(j\omega) \mid h, i \in \{1, 2, 3, 4\}, g \in \{1, 2, \dots, 4N_1 + 2\} \right\}, \\ \kappa_{h,g,i}^{(2)}(j\omega) &= \left| \frac{N_c(j\omega)V_h^N(j\omega)}{V_i^D} + P_g^{(1)}(j\omega) \right| + \\ &\quad \left| \frac{N_c(j\omega)V_h^N(j\omega)}{V_i^D} + P_{g+1}^{(1)}(j\omega) \right| - \left| P_{g+1}^{(1)}(j\omega) - P_g^{(1)}(j\omega) \right|, \end{aligned}$$

$$\begin{aligned} \chi_3(\omega) &= \min \left\{ \kappa_{h,g,i}^{(3)}(j\omega) \mid h, i \in \{1, 2, 3, 4\}, g \in \{1, \dots, 4N_2 + 2\} \right\}, \\ \kappa_{h,g,i}^{(3)}(j\omega) &= \left| H(\omega)V_i^D + P_{g,h}^{(2)}(j\omega) \right| + \\ &\quad \left| H(\omega)V_{i+1}^D + P_{g,h}^{(2)}(j\omega) \right| - \left| H(\omega)V_i^D - H(\omega)V_{i+1}^D \right|, \end{aligned}$$

$$\begin{aligned} \chi_4(\omega) &= \min \left\{ \kappa_{h,g,i}^{(4)}(j\omega) \mid h, i \in \{1, 2, 3, 4\}, g \in \{1, \dots, 4N_2 + 2\} \right\}, \\ \kappa_{h,g,i}^{(4)}(j\omega) &= \left| H(\omega)V_i^D + P_{g,h}^{(2)}(j\omega) \right| + \\ &\quad \left| H(\omega)V_i^D + P_{g+1,h}^{(2)}(j\omega) \right| - \left| P_{g,h}^{(2)}(j\omega) - P_{g+1,h}^{(2)}(j\omega) \right|. \end{aligned}$$

In (6.31), $P_g^{(1)}(j\omega)$, $P_{g,h}^{(2)}(j\omega)$ and $H(j\omega)$ are defined in (6.67).

$$P_g^{(1)}(j\omega) = \begin{cases} \bar{P}_{g-1}^{(1)}(j\omega), & \text{for } 1 \leq g \leq 2N_1 + 1, \\ \underline{P}_{(2N_1)}^{(1)}(j\omega), & \text{for } g = 2N_1 + 2, \\ \underline{P}_{(2N_1-1)}^{(1)}(j\omega), & \text{for } g = 2N_1 + 3, \\ \vdots \\ \underline{P}_0^{(1)}(j\omega), & \text{for } g = 4N_1 + 2, \end{cases} \quad (6.32)$$

$$\bar{P}_g^{(1)}(j\omega) = \begin{cases} H(j\omega)e^{j\omega\left(\tau+g\frac{\bar{\tau}-\tau}{2N_1}\right)}, & \text{for } g = 0, 2, \dots, 2N_1, \\ \frac{H(j\omega)e^{j\omega\left(\tau+g\frac{\bar{\tau}-\tau}{2N_1}\right)}}{\cos\left(\omega\frac{\bar{\tau}-\tau}{2N_1}\right)}, & \text{for } g = 1, 3, \dots, 2N_1 - 1, \end{cases}$$

$$\underline{P}_g^{(1)}(j\omega) = H(j\omega)e^{j\omega\left(\tau+g\frac{\bar{\tau}-\tau}{2N_1}\right)}, \quad g = 0, 1, 2, \dots, 2N_1.$$

$$P_{g,h}^{(2)}(j\omega) = \begin{cases} \bar{P}_{g-1,h}^{(2)}(j\omega), & \text{for } 1 \leq g \leq 2N_2 + 1, \\ \underline{P}_{(2N_2,h)}^{(2)}(j\omega), & \text{for } g = 2N_2 + 2, \\ \underline{P}_{(2N_2-1,h)}^{(2)}(j\omega), & \text{for } g = 2N_2 + 3, \\ \vdots \\ \underline{P}_{0,h}^{(2)}(j\omega), & \text{for } g = 4N_2 + 2, \end{cases} \quad (6.33)$$

$$\bar{P}_{i,h}^{(2)}(j\omega) = \begin{cases} N_c(j\omega)V_h^N(j\omega)e^{-j\omega\left(\tau+i\frac{\bar{\tau}-\tau}{2N_2}\right)}, & \text{for } i = 0, 2, \dots, 2N_2, \\ \frac{N_c(j\omega)V_h^N(j\omega)e^{-j\omega\left(\tau+i\frac{\bar{\tau}-\tau}{2N_2}\right)}}{\cos\left(\omega\frac{\bar{\tau}-\tau}{2N_2}\right)}, & \text{for } i = 1, 3, \dots, 2N_2 - 1, \end{cases}$$

$$\bar{P}_{i,h}^{(2)}(j\omega) = N_c(j\omega)V_h^N(j\omega)e^{-j\omega\left(\tau+i\frac{\bar{\tau}-\tau}{2N_2}\right)}, \quad i = 0, 1, 2, \dots, 2N_2,$$

where, N_1 and N_2 are arbitrary integer numbers and $N_1, N_2 \geq 3$ and also, $V_5^N(j\omega) = V_1^N(j\omega)$, $V_5^D(j\omega) = V_1^D(j\omega)$, $P_{4N_1+3}^{(1)}(j\omega) = P_1^{(1)}(j\omega)$, $P_{4N_2+3,h}^{(2)}(j\omega) = P_{1,h}^{(2)}(j\omega)$ and $H(j\omega)$ is defined in (6.15).

Proof. It has been established that the satisfaction of the inequality $\Xi(\omega) > 0$ guarantees the absence of overlap between the value sets $F_1(j\omega)$ in (6.15) and $F_2(j\omega)$ in (6.16) in the complex plane, for ω within the range of $(0, \frac{2\pi}{\bar{\tau}-\tau})$.

Based on the expressions given in (6.12) and (6.19), it can be concluded that $\Theta_2(j\omega)$ can be expressed as the union of $\underline{\Theta}_2(j\omega)$ and $\bar{\Theta}_2(j\omega)$, i.e., $\Theta_2(j\omega) = \underline{\Theta}_2(j\omega) \cup \bar{\Theta}_2(j\omega)$, where:

$$\begin{aligned} \underline{\Theta}_2(j\omega) &= \frac{N_c(s)N_V}{D_E}, \\ \bar{\Theta}_2(j\omega) &= \frac{N_c(s)N_E}{D_V}. \end{aligned} \quad (6.34)$$

Furthermore, by analyzing Figure 6.2, it is possible to easily derive the following geometric feature.

$$\bar{P}_{i+1}(j\omega) = \frac{\bar{P}_i(j\omega)e^{j\theta}}{\cos(\theta)}. \quad (6.35)$$

By examining (6.35) in conjunction with Figure 6.2, it is apparent that the location of $\partial(H(j\omega)e^{\tau j\omega})$ lies within the exposed edges denoted by $P_g^{(1)}(j\omega)$ in (6.67). Notably, ensuring the satisfaction of the triangle inequality for any vertex within the value set $\bar{\Theta}_2(j\omega)$,

in conjunction with any two consecutive vertices of $P_g^{(1)}(j\omega)$ implies that there exists no overlap between any vertex of $\bar{\Theta}_2(j\omega)$ and $P_g^{(1)}(j\omega)$. Correspondingly, ensuring the satisfaction of the triangle inequality for any vertex of $P_g^{(1)}(j\omega)$ and any two consecutive vertices of $\bar{\Theta}_2(j\omega)$ implies that no vertex of $P_g^{(1)}(j\omega)$ intersects $\bar{\Theta}_2(j\omega)$. Consequentially, there exists no overlap between the value sets $P_g^{(1)}(j\omega)$ and $\bar{\Theta}_2(j\omega)$ for $\omega \in (0, \frac{2\pi}{\tau-\underline{\tau}})$, and as such, the absence of overlap between the value sets $\Theta_1(j\omega)$ in (6.15) and $\bar{\Theta}_2(j\omega)$ in (6.34) is ensured if the inequalities $\chi_1(\omega) > 0$ and $\chi_2(\omega) > 0$ are met. Similarly, if the inequalities $\chi_3(\omega) > 0$ and $\chi_4(\omega) > 0$ are satisfied, then the value sets $\Theta_1(j\omega)$ in (6.15) and $\bar{\Theta}_2(j\omega)$ in (6.34) do not have any overlap in the complex plane. Hence, one can effortlessly complete the proof of Theorem 6.1 and Theorem 6.2. \square

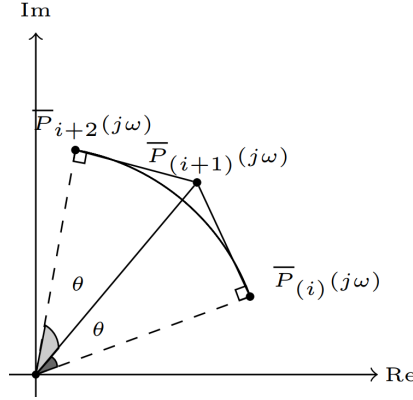


Figure 6.2: A depiction of the consecutive vertices $\bar{P}_i(j\omega)$, $\bar{P}_{i+1}(j\omega)$ and $\bar{P}_{i+2}(j\omega)$.

Given Theorem 6.2 and Theorem 6.3, it is possible to readily establish the subsequent corollary.

Corollary 6.3. Assume that the nominal characteristic polynomial $F_0(s)$ in (6.14) is stable and $\omega_{\max} < \frac{2\pi}{\tau-\underline{\tau}}$. Then, the Smith predictor control structure is robustly stable if the inequality $\Xi(\omega) = \min\{\chi_i(\omega) \mid i = 1, 2, 3, 4\} > 0$ is met for $\omega \in [0, \omega_{\max}]$, where $\chi_i(\omega)$, ($i = 1, 2, 3, 4$) are presented in (6.30).

Remark 6.1. Drawing upon the aforementioned material, one can assess the robust stability of the Smith predictor control structure depicted in Figure 1 via the following methodology.

1. Verify whether the stability of $F_0(s)$ in (6.14) is ensured. If $F_0(s)$ is stable, proceed to the next step. Otherwise, the Smith predictor control structure is not robustly stable.
2. Utilize Theorem 6.2 to obtain the frequency range $[0, \omega_{\max}]$.
3. If $\omega_{\max} < \frac{2\pi}{\tau-\underline{\tau}}$, employ either Corollary 6.2 or Corollary 6.3 to evaluate the robust stability. On the other hand, if $\omega_{\max} \geq \frac{2\pi}{\tau-\underline{\tau}}$, employ either Corollary 6.1 or Theorem 6.3 to verify the robust stability of the Smith predictor control structure.

Remark 6.2. The sensitivity function is critical in determining the performance of feedback control systems as it affects reference tracking and disturbance rejection. Achieving

desired performance in these two areas relies on having a small sensitivity function at low frequencies. Thus, sensitivity function plays a pivotal role in the closed-loop system performance. Therefore, in order to enhance the efficacy of output disturbance rejection, it is imperative to satisfy the ensuing constraint.

$$|S(j\omega)| = \left| \frac{1 + C(j\omega)P_0(j\omega)(1 - e^{-j\omega\hat{\tau}})}{1 + C(j\omega)P_0(j\omega)(1 - e^{-j\omega\hat{\tau}}) + C(j\omega)P(j\omega)} \right| < |F_s(j\omega)|. \quad (6.36)$$

In (6.36), $F_s(j\omega)$ serves as the weighting function, which is carefully selected by the designer to ensure fulfillment of the control objectives pertaining to reference tracking and disturbance rejection. With respect to the inequality presented in (6.36), the designer is advised to meet the condition $\chi_S(\omega) < 0$, as per Theorem 6.3 and the maximum modulus theorem, where $\chi_S(\omega)$ is computed as follows.

$$\chi_S(\omega) = \begin{cases} \max\{\chi_S^i | i = 1, 2, 3, 4\}, & \text{for } \omega \in [0, \frac{2\pi}{\tau - \underline{\tau}}), \\ \frac{1}{|\frac{\max\{\bar{V}_1^N, \bar{V}_2^N, \bar{V}_3^N, \bar{V}_4^N\}}{\min_{e_l^D \in P_E^D} |e_l^D|} - 1|} - |F_s(j\omega)|, & \text{for } \omega \in [\frac{2\pi}{\tau - \underline{\tau}}, \infty), \end{cases} \quad (6.37)$$

where,

$$\begin{aligned} \chi_S^1(\omega) &= \max_{r=1, \dots, 4N_1+2} \tilde{\chi}_{S_1}^r(\omega) - |F_s(j\omega)|, \\ \tilde{\chi}_{S_1}^r(\omega) &= \max_{e_{S_1 r_1, r_2} \in P_{S_1}} |e_{S_1 r_1, r_2}|, r_1, r_2 \in \{1, 2, 3, 4\}, \\ P_{S_1} &= \{e_{S_1 1, 1}, e_{S_1 1, 2}, \dots, e_{S_1 4, 4}\}, \\ e_{S_1 r_1, r_2} &= \frac{H(j\omega)}{e(P_r^{(1)}(j\omega), P_{r+1}^{(1)}(j\omega)) + \frac{N_c(j\omega)V_{r_1}^N(j\omega)}{V_{r_2}^D}}. \end{aligned} \quad (6.38)$$

$$\begin{aligned} \chi_S^2(\omega) &= \max_{r=1, \dots, 4} \tilde{\chi}_{S_2}^r(\omega) - |F_s(j\omega)|, \\ \tilde{\chi}_{S_2}^r(\omega) &= \max_{e_{S_2 r_1, r_2} \in P_{S_2}} |e_{S_2 r_1, r_2}|, \\ r_1 &\in \{1, \dots, 4N_1 + 2\}, r_2 \in \{1, 2, 3, 4\}, \\ P_{S_2} &= \{e_{S_2 1, 1}, e_{S_2 1, 2}, \dots, e_{S_2 4N_1+2, 4}\}, \\ e_{S_2 r_1, r_2} &= \frac{H(j\omega)}{P_{r_1}^{(1)}(j\omega) + \frac{N_c(j\omega)e(V_r^N(j\omega), V_{r+1}^N(j\omega))}{V_{r_2}^D}}. \end{aligned} \quad (6.39)$$

$$\begin{aligned} \chi_S^3(\omega) &= \max_{r=1, 2, 3, 4} \tilde{\chi}_{S_3}^r(\omega) - |F_s(j\omega)|, \\ \tilde{\chi}_{S_3}^r(\omega) &= \max_{e_{S_3 r_1, r_2} \in P_{S_3}} |e_{S_3 r_1, r_2}|, \\ r_1 &\in \{1, \dots, 4N_2 + 2\}, r_2 \in \{1, 2, 3, 4\}, \\ P_{S_3} &= \{e_{S_3 1, 1}, e_{S_3 1, 2}, \dots, e_{S_3 4N_2+2, 4}\}, \\ e_{S_3 r_1, r_2} &= \frac{H(j\omega)}{H(j\omega) + \frac{P_{r_1, r_2}^{(2)}(j\omega)}{e(V_r^D, V_{r+1}^D)}}. \end{aligned} \quad (6.40)$$

$$\begin{aligned}
\chi_S^4(\omega) &= \max_{r=1, \dots, 4N_2+2} \tilde{\chi}_{S_4}^r(\omega) - |F_s(j\omega)|, \\
\tilde{\chi}_{S_4}^r(\omega) &= \max_{e_{S_4 r_1, r_2} \in P_{S_4}} |e_{S_4 r_1, r_2}|, r_1, r_2 \in \{1, 2, 3, 4\}, \\
P_{S_4} &= \{e_{S_4 1, 1}, e_{S_4 1, 2}, \dots, e_{S_4 4, 4}\}, \\
e_{S_4 r_1, r_2} &= \frac{H(j\omega)}{H(j\omega) + \frac{e^{(P_{r, r_1}^{(2)}(j\omega), P_{r+1, r_1}^{(2)}(j\omega))}}{V_{r_2}^D}}}.
\end{aligned} \tag{6.41}$$

6.2 Robust Stability Analysis of Smith Predictors for unstable systems

6.2.1 Definitions

Figure 6.3 illustrates the modified SP discussed in this subsection. In this figure, $G_p(s)$ represents the actual process to be controlled. $G_m(s)$ and $e^{-\theta_m s}$ represent the delay-free component and the time delay of the process model. $G_{cs}(s)$ and $G_{cd}(s)$ are the set-point tracking controller and the load disturbance rejection controller, respectively, responsible for stabilization and effective disturbance rejection. An additional controller, G_{pd} , is introduced into the predicted disturbance path to mitigate periodic disturbances and increase robustness.

Based on Figure 6.3, the closed-loop transfer functions can be given by

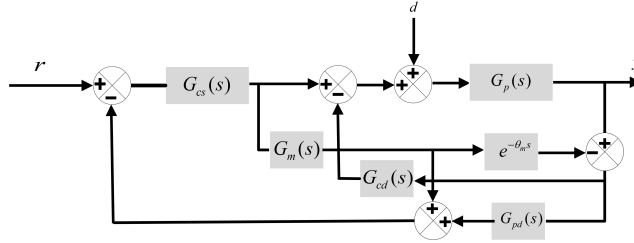


Figure 6.3: The modified Smith predictor [0, 122].

$$\begin{aligned}
\frac{y}{r} &= \frac{A_r(s)}{B_r(s)}, \\
A_r(s) &= (1 + G_{cd}(s)G_m(s)e^{-\theta_m s})(G_{cs}(s)G_p(s), \\
B_r(s) &= 1 + G_p(s)G_{cd}(s) + G_p(s)G_{cs}(s)G_{pd}(s) - \\
&G_{pd}(s)G_{cs}(s)G_m(s)e^{-\theta_m s} + G_m(s)G_{cs}(s) \\
&+ G_p(s)G_{cd}(s)G_m(s)G_{cs}(s).
\end{aligned} \tag{6.42}$$

$$\begin{aligned}
\frac{y}{d} &= \frac{A_d(s)}{B_d(s)}, \\
A_d(s) &= (1 + G_m(s)G_{cs}(s)(1 - G_{pd}(s)e^{-\theta_m s}))G_p(s), \\
B_d(s) &= B_r(s).
\end{aligned} \tag{6.43}$$

The transfer functions for $\frac{y}{r}$ and $\frac{y}{d}$ are derived under the assumption of perfect model conditions, where the model transfer function and the plant transfer function are identical

(i.e., $G_p(s) = G_m(s)e^{-\theta_m s}$), resulting in no model mismatch, as follows:

$$\frac{y}{r} = \frac{G_m(s)G_{cs}(s)e^{-\theta_m s}}{1 + G_m(s)G_{cs}(s)}. \quad (6.44)$$

$$\frac{y}{d} = \frac{(1 + G_m(s)G_{cs}(s) - G_{cs}(s)G_{pd}(s)G_m(s)e^{-\theta_m s})}{(1 + G_m(s)G_{cs}(s))(1 + G_{cd}(s)G_m(s)e^{-\theta_m s})} \times G_m(s)e^{-\theta_m s}, \quad (6.45)$$

In this subsection, the uncertain transfer function of the actual system is described as:

$$G_p(s) = \frac{K}{\tau s - 1} e^{-\theta s}, \quad (6.46)$$

where, the positive coefficients K , τ and θ lie within the specified intervals $K \in [\underline{K}, \overline{K}]$, $\tau \in [\underline{\tau}, \overline{\tau}]$ and $\theta \in [\underline{\theta}, \overline{\theta}]$, respectively. Moreover, the nominal model $G_m(s)$ is defined as (6.47).

$$G_m(s) = \frac{K_m}{\tau_m s - 1}, K_m = \frac{\underline{K} + \overline{K}}{2}, \tau_m = \frac{\underline{\tau} + \overline{\tau}}{2}. \quad (6.47)$$

In line with references [0]-[125], the controllers considered in this subsection are as follows:

$$\begin{cases} G_{cs}(s) = k_{ps} + \frac{k_{is}}{s}, \\ G_{cd}(s) = k_{pd} + \frac{k_{id}}{s}, \\ G_{pd}(s) = \frac{1 + G_{cs}G_m}{(G_{cs}G_m)(\lambda_p s + 1)}. \end{cases} \quad (6.48)$$

In Figure 6.3, θ_m is also defined as $\frac{\underline{\theta} + \overline{\theta}}{2}$. Based on (6.42), the characteristic function of the system can be derived as follows:

$$\Delta(s) = (\tau s - 1)A_\Delta(s) + KB_\Delta(s)e^{-\theta s}, \quad (6.49)$$

in which

$$\begin{aligned} A_\Delta(s) &= A_\Delta^1(s) + A_\Delta^2(s) + A_\Delta^3(s), \\ A_\Delta^1(s) &= K_m s^2 (\tau_m s - 1)(k_{ps}s + k_{is})(\lambda_p s + 1), \\ A_\Delta^2(s) &= K_m^2 (k_{ps}s + k_{is})^2 s (\lambda_p s + 1), \\ A_\Delta^3(s) &= -K_m (k_{ps}s + k_{is})s \times \\ &\quad (s(\tau_m s - 1) + K_m (k_{ps}s + k_{is}))e^{-\theta_m s}. \\ B_\Delta(s) &= B_\Delta^1(s) + B_\Delta^2(s) + B_\Delta^3(s), \\ B_\Delta^1(s) &= K_m s (k_{pd}s + k_{id})(\tau_m s - 1) \times \\ &\quad (k_{ps}s + k_{is})(\lambda_p s + 1), \\ B_\Delta^2(s) &= K_m^2 (k_{pd}s + k_{id})(k_{ps}s + k_{is})^2 (\lambda_p s + 1), \\ B_\Delta^3(s) &= s(k_{ps}s + k_{is})(\tau_m s - 1) \times \\ &\quad (s(\tau_m s - 1) + K_m (k_{ps}s + k_{is})). \end{aligned} \quad (6.51)$$

In references [0]-[125], several methods have been proposed to stabilize the modified Smith predictors depicted in Figure 6.3. These controller designs assume perfect model conditions i.e., $G_p(s) = G_m(s)e^{-\theta_m s}$. However, in practical scenarios, systems often encounter uncertainties, which can make the assumption $G_p(s) = G_m(s)e^{-\theta_m s}$ unrealistic. Therefore, $\Delta(s)$ in (6.46) incorporates multiple time-delay systems and interval uncertainties.

6.2.2 Derivation of Robust Stability Conditions

According to the zero exclusion principle for $\omega \geq 0$, it is essential to confirm that $0 \notin \Delta(s)$. Therefore, the following theorem defines a finite frequency range within which the condition $0 \notin \Delta(s)$ is satisfied.

Theorem 6.4. *The condition $0 \notin \Delta(j\omega)$ is satisfied for $\omega > \omega_u$ where*

$$\begin{aligned}
 \omega_u &= \frac{\omega_u^n}{\omega_u^d}, \\
 \omega_u^n &= \omega_u^{n1} + \omega_u^{n2} + \omega_u^{n3}, \\
 \omega_u^{n1} &= K_m \max\{\underline{\tau}, \bar{\tau}\} \left(\tau_m (|k_{is}| |\lambda_p| + |k_{ps}|) + |k_{ps}| |\lambda_p| + \right. \\
 &\quad \tau_m |k_{is}| + |k_{is}| |\lambda_p| + |k_{ps}| + |k_{is}| + K_m (|k_{ps}| + |k_{is}|)^2 \times \\
 &\quad (|\lambda_p| + 1) + (|k_{ps}| + |k_{is}|) (|\tau_m| + 1 + \\
 &\quad \left. K_m (|k_{ps}| + |k_{is}|)) \right), \\
 \omega_u^{n2} &= K_m (|\tau_m| + 1) (|k_{ps}| + |k_{is}|) (|\lambda_p| + 1) + \\
 &\quad K_m^2 (|k_{ps}| + |k_{is}|)^2 \times (|\lambda_p| + 1) + K_m (|k_{ps}| + |k_{is}|) \times \\
 &\quad (|\tau_m| + 1) + K_m (|k_{ps}| + |k_{is}|), \\
 \omega_u^{n3} &= \bar{K} \left(K_m (|k_{pd}| + |k_{id}|) (|\tau_m| + 1) (|k_{ps}| + |k_{is}|) \times \right. \\
 &\quad (|\lambda_p| + 1) + K_m^2 (|k_{pd}| + |k_{id}|) (|k_{ps}| + |k_{is}|)^2 (|\lambda_p| + 1) + \\
 &\quad \left. (|k_{ps}| + |k_{is}|) (|\tau_m| + 1) (|\tau_m| + 1 + K_m (|k_{ps}| + |k_{is}|)) \right). \\
 \omega_u^d &= |K_m \tau_m k_{ps} \lambda_p| \min\{\underline{\tau}, \bar{\tau}\}.
 \end{aligned} \tag{6.52}$$

Proof. Demonstrating that the inequality $|\Delta(s)| > 0$ holds confirms that $0 \notin \Delta(j\omega)$. Therefore, applying the triangle inequality for $\omega > 1$ gives:

$$\begin{aligned}
 |\Delta(j\omega)| &> |K_m \tau_m k_{ps} \lambda_p| \min\{\underline{\tau}, \bar{\tau}\} |\omega|^6 - \\
 &\quad |K_m| \max\{\underline{\tau}, \bar{\tau}\} \left((\tau_m (|k_{is}| |\lambda_p| + |k_{ps}|) + |k_{ps}| |\lambda_p|) |\omega|^5 + \right. \\
 &\quad (\tau_m |k_{is}| + |k_{is}| |\lambda_p| + |k_{ps}|) |\omega|^4 + |k_{is}| |\omega|^3 + \\
 &\quad K_m^2 |\omega|^2 (|k_{ps}| |\omega| + |k_{is}|)^2 (|\lambda_p| |\omega| + 1) + \\
 &\quad |K_m| |\omega|^2 (|k_{ps}| |\omega| + |k_{is}|) (|\tau_m| |\omega| + 1) + \\
 &\quad \left. |K_m| |\omega| (|k_{ps}| |\omega| + |k_{is}|) \right) \\
 &\quad - |K_m| |\omega|^2 (|\tau_m| |\omega| + 1) (|k_{ps}| |\omega| + |k_{is}|) (|\lambda_p| |\omega| + 1) + \\
 &\quad K_m^2 (|k_{ps}| |\omega| + |k_{is}|)^2 |\omega| (|\lambda_p| |\omega| + 1) + \\
 &\quad |K_m| |\omega| (|k_{ps}| |\omega| + |k_{is}|) (|\tau_m| |\omega| + 1) \\
 &\quad + |K_m| (|k_{ps}| |\omega| + |k_{is}|) - \\
 &\quad \bar{K} \left(|K_m| |\omega| (|k_{pd}| |\omega| + |k_{id}|) (|\tau_m| |\omega| + 1) (|k_{ps}| |\omega| + |k_{is}|) \right. \\
 &\quad (|\lambda_p| |\omega| + 1) + K_m^2 (|k_{pd}| |\omega| + |k_{id}|) (|k_{ps}| |\omega| + |k_{is}|)^2 \\
 &\quad (|\lambda_p| |\omega| + 1) + |\omega| (|k_{ps}| |\omega| + |k_{is}|) (|\tau_m| + 1) \\
 &\quad \left. (|\omega| (|\tau_m| |\omega| + 1) + |K_m| (|k_{ps}| |\omega| + |k_{is}|)) \right).
 \end{aligned} \tag{6.53}$$

Due to $\omega > 1$, inequality (6.53) can be rewritten as follows:

$$|\Delta(j\omega)| \geq \omega_u^d |\omega|^6 - \omega_u^n |\omega|^5 = |\omega|^5 \omega_u^d \left(\omega - \frac{\omega_u^n}{\omega_u^d} \right) \quad (6.54)$$

Therefore, if $\omega > \frac{\omega_u^n}{\omega_u^d}$ then $|\Delta(j\omega)| > 0$. \square

According to Theorem 6.4, we only need to verify the condition $0 \notin \Delta(j\omega)$ for $\omega \in [0, \omega_u]$. However, due to the interval time delay in $\Delta(j\omega)$, the value set of $\Delta(j\omega)$ forms a nonconvex shape. This makes it challenging to determine the boundary of the value set at each frequency within $[0, \omega_u]$. Therefore, in the following theorem, the condition $0 \notin \Delta(j\omega)$ is checked by analyzing the overlap of two value sets that form the value set of the characteristic function $\Delta(j\omega)$. Nevertheless, the necessary and sufficient conditions for robust stability are derived in the following theorem.

Theorem 6.5. Consider $\bar{\omega} = \frac{2\pi}{\bar{\tau} - \underline{\tau}}$ and $\Delta_1(s) = (\tau s - 1)A_\Delta(s)$ and $\Delta_2(s) = KB_\Delta(s)e^{-\theta s}$ and also the sets $\chi_1(j\omega)$ and $\chi_2(j\omega)$ are respectively defined in (6.55) and (6.56).

$$\chi_1(j\omega) = -A_\Delta(s)e(\underline{\tau}s - 1, \bar{\tau}s - 1). \quad (6.55)$$

$$\begin{aligned} \chi_2(j\omega) = & \left\{ e(\underline{KB}_\Delta(s)e^{-\underline{\theta}j\omega}, \bar{KB}_\Delta(s)e^{-\bar{\theta}j\omega}), \right. \\ & e(\underline{KB}_\Delta(s)e^{-\bar{\theta}j\omega}, \bar{KB}_\Delta(s)e^{-\underline{\theta}j\omega}), \\ & \left. \underline{KB}_\Delta(s)e^{-e(\underline{\theta}, \bar{\theta})j\omega}, \bar{KB}_\Delta(s)e^{-e(\underline{\theta}, \bar{\theta})j\omega} \right\}. \end{aligned} \quad (6.56)$$

Case I: Let the inequality $\omega_u \geq \bar{\omega}$ hold. Under this condition, the modified SP system illustrated in Figure 6.3 remains robustly stable if and only if

1. the controllers $G_{cs}(s)$ and $G_{cd}(s)$ can respectively stabilize the nominal systems $1 + G_m(s)G_{cs}(s)$ and $1 + G_{cd}(s)G_m(s)e^{-\theta_m s}$.
2. The sets $\chi_1(j\omega)$ from (6.14) and $\chi_2(j\omega)$ from (6.56) do not overlap for the interval $(0, \bar{\omega})$.
3. $\bar{H}(\omega) > 0$ holds over the interval $[\bar{\omega}, \omega_u]$, where

$$\begin{aligned} \bar{H}(\omega) = & \min_{e_1 \in P_E} |e_1| - |\bar{KB}_\Delta(s)|, \\ P_E \triangleq & \left\{ \underbrace{e(A_\Delta(s)(\underline{\tau}s - 1), A_\Delta(s)(\bar{\tau}s - 1))}_{e_1} \right\}, \end{aligned} \quad (6.57)$$

Case II: Let the inequality $0 < \omega_u < \bar{\omega}$ hold. Under this condition, the modified SP system illustrated in Figure 6.3 remains robustly stable if and only if the sets $\chi_1(j\omega)$ from (6.55) and $\chi_2(j\omega)$ from (6.56) do not overlap for the interval $(0, \bar{\omega})$.

Proof. By applying the zero exclusion principle and Theorem 6.4, it is necessary to evaluate the set of values $\Delta(j\omega)$ needs to be checked for $\omega \in [0, \omega_u]$. The resulting equality from (6.58) occurs due to $\Delta(j\omega) = 0$.

$$-\Delta_1(s) = \Delta_2(s). \quad (6.58)$$

Proof of Case I: Assume that $\omega_u \geq \bar{\omega}$.

Sufficiency: In this scenario, the frequency interval $(0, \omega_u]$ can be split into two segments: $\omega \in (0, \bar{\omega})$ and $\omega \in [\bar{\omega}, \omega_u]$. Consider Z_n as an arbitrary complex number in the complex

plane, and assume that $Z_n \in \Delta_2(j\omega)$ for $\omega = \omega_n$. If $0 \in \Delta(j\omega_n)$, it follows from (6.58) that $-Z_n \in \Delta_1(j\omega)$. Conversely, if $-Z_n \in \Delta_1(j\omega)$, then $Z_n \in -\Delta_1(j\omega)$. This suggests that the sets of values $\Delta_2(j\omega)$ and $-\Delta_1(j\omega)$ overlap in the complex plane.

The minimum magnitude of $\Delta_2(j\omega)$ is given by $\min_{e_1 \in P_E} |e_1|$. Additionally, it is clear that the maximum absolute magnitude of $\Delta_2(j\omega)$ is $|\overline{KB}_\Delta(s)|$. Also for $\omega \in [\overline{\omega}, \omega_u]$, it follows that $0 \notin \Delta(j\omega)$ if $\overline{H}(\omega) > 0$. This is due to the fact that for $\omega = \infty$ the inequality

$$\lim_{\omega \rightarrow \infty} \min_{e_1 \in P_E} |e_1| > \lim_{\omega \rightarrow \infty} |\overline{KB}_\Delta(s)|$$

holds. Thus, fulfilling $\overline{H}(\omega) > 0$ guarantees that the sets of values $\Delta_2(j\omega)$ and $-\Delta_1(j\omega)$ do not overlap in the complex plane for $\omega \in [\overline{\omega}, \omega_u]$, which implies that $0 \notin \Delta(j\omega)$.

Necessity: Given that $\Delta(j\omega)$ is robustly stable, Theorem 6.4 indicates that $0 \notin \Delta(j\omega)$ for $\omega \in (\omega_u, \infty)$. Therefore, $\Delta(0) \neq 0$ and two sets $\chi_1(j\omega)$ in (6.55) and $\chi_2(j\omega)$ in (6.15) do not overlap for $\omega \in (0, \overline{\omega})$. For $\omega \in [\overline{\omega}, \omega_u]$, we use a proof by contradiction, assuming that $\overline{H}(\omega) > 0$ is not met. Because of

$$\lim_{\omega \rightarrow \infty} \min_{e_1 \in P_E} |e_1| > \lim_{\omega \rightarrow \infty} |\overline{KB}_\Delta(s)|$$

and Theorem 6.4, $\overline{H}(\omega) > 0$ is true for $\omega \in (\omega_u, \infty)$. Since, $\overline{H}(\omega)$ is a continuous function and $\Lambda(\omega) \leq 0$, there must exist $\omega_0 \in [\frac{2\pi}{\tau - \underline{\tau}}, \omega_{\max}]$ such that $\overline{H}(\omega) = 0$. Consequently, at $\omega = \omega_0 \in [\frac{2\pi}{\tau - \underline{\tau}}, \omega_{\max}]$, $\Delta_2(j\omega)$ and $-\Delta_1(j\omega)$ overlap in the complex plane. Thus, at $\omega = \omega_0 \in [\overline{\omega}, \omega_u]$, there are elements in $\Delta_1(j\omega, \mathbf{q})$ represented as $\hat{\Delta}_1(j\omega, \mathbf{q})$ and elements in $\Delta_2(j\omega)$ represented as $\hat{\Delta}_2(j\omega)$, which correspond to $-Z_0$ and Z_0 , respectively. Consequently, at $\omega = \omega_0$, a member of $\Delta(j\omega_0)$ can be expressed as $\hat{\Delta}(j\omega_0) = \hat{\Delta}_a(j\omega) + \hat{\Delta}_p(j\omega)$, equating to $Z_0 - Z_0 = 0$. This creates a contradiction with $0 \notin \Delta(j\omega)$.

Proof of Case II: Assume that $0 < \omega_u < \overline{\omega}$. The necessary and sufficient conditions for this scenario can be demonstrated in a manner analogous to the proof presented in **Case I**, by applying the zero exclusion principle along with Theorem 6.4. \square

Although Theorem 6.5 presents the necessary and sufficient conditions for the robust stability evaluation of the modified Smith Predictor, assessing the overlap between $\chi_1(j\omega)$ in (6.55) and $\chi_2(j\omega)$ in (6.56) is not straightforward. Therefore, the following theorem simplifies this challenge by introducing a robust stability testing function.

Theorem 6.6. Suppose that the controllers $G_{cs}(s)$ and $G_{cd}(s)$ can respectively stabilize the nominal systems $1 + G_m(s)G_{cs}(s)$ and $1 + G_{cd}(s)G_m(s)e^{-\theta_{ms}}$.

Case I: If $\omega_u \geq \overline{\omega}$, the modified Smith predictor system illustrated in Figure 6.3 remains robustly stable if $H(\omega) > 0$ holds for $\omega \in [0, \omega_u]$ where

$$H(\omega) = \begin{cases} \min\{\underline{H}_r(\omega) | r = 1, 2\}, & \text{for } \omega \in [0, \overline{\omega}), \\ \overline{H}(\omega), & \text{for } \omega \in [\overline{\omega}, \omega_u], \end{cases} \quad (6.59)$$

at which

$$\begin{aligned} \underline{H}_1(\omega) &= \min\{\hat{\underline{H}}_{m,t}(\omega) | m \in \{1\}, t \in \{1, \dots, 4M + 2\}\}, \\ \hat{\underline{H}}_{m,t}(\omega) &= |\underline{\Delta}_m(s) + \Upsilon_t(s)| + |\underline{\Delta}_{m+1}(s) + \Upsilon_t(s)| \\ &\quad - |\underline{\Delta}_m(s) - \underline{\Delta}_{m+1}(s)|, \end{aligned} \quad (6.60)$$

$$\begin{aligned} \underline{H}_2(\omega) &= \min\{\hat{\underline{H}}_{m,t}(\omega) | m \in \{1, 2\}, t \in \{1, \dots, 4M + 2\}\}, \\ \hat{\underline{H}}_{m,t}(\omega) &= |\underline{\Delta}_m(s) + \Upsilon_t(s)| + |\underline{\Delta}_m(s) + \Upsilon_{t+1}(s)| \\ &\quad - |\Upsilon_t(s) - \Upsilon_{t+1}(s)|, \end{aligned} \quad (6.61)$$

$$\Upsilon_t(s = j\omega) = \begin{cases} \bar{\Upsilon}_{(t-1)}(s), & \text{for } 1 \leq t \leq 2M+1, \\ \underline{\Upsilon}_{(2M)}(s), & \text{for } t = 2M+2, \\ \underline{\Upsilon}_{(2M-1)}(s), & \text{for } t = 2M+3, \\ \vdots & \\ \underline{\Upsilon}_0(s), & \text{for } t = 4M+2, \end{cases}$$

$$\bar{\Upsilon}_i(s = j\omega) = \begin{cases} \bar{K}B_\Delta(s)e^{-s\left(\frac{\theta+i\bar{\theta}-\theta}{2M}\right)}, & \text{for } i = 0, 2, \dots, 2M, \\ \frac{\bar{K}B_\Delta(s)e^{-s\left(\frac{\theta+i\bar{\theta}-\theta}{2M}\right)}}{\cos\left(\frac{\bar{\theta}-\theta}{2M}\right)}, & \text{for } i = 1, 3, \dots, 2M-1, \end{cases}$$

$$\underline{\Upsilon}_i(s = j\omega) = \underline{K}B_\Delta(s)e^{-s\left(\frac{\theta+i\bar{\theta}-\theta}{2M}\right)}, \quad i = 0, 1, 2, \dots, 2M,$$

where $\underline{\Delta}_1(s) = (\underline{\tau}s - 1)A_\Delta(s)$, $\underline{\Delta}_2(s) = (\bar{\tau}s - 1)A_\Delta(s)$ and $M \in \mathbb{N}^{\geq 3}$.

Case II: If $\omega_u \geq \bar{\omega}$, the modified Smith Predictor system illustrated in Figure 6.3 remains robustly stable if $H(\omega) = \min\{\underline{H}_r(\omega) | r = 1, 2\} > 0$ holds for $\omega \in [0, \omega_u]$

Proof. From (6.59) and Figure 6.5a, it is straightforward to deduce that the set of values $\Delta_2(j\omega)$ lies within the convex hull of $\Upsilon_i(j\omega)$. This implies that we only need to verify that the value set of $\chi_1(j\omega)$ in (6.55) and the convex hull of $\Upsilon_i(j\omega)$ do not overlap, as described below.

If the inequality $\underline{H}_1(\omega) > 0$ is true, then by the triangle inequality, it follows that the vertices $\Upsilon_i(j\omega)$ do not lie on the line segment $\Delta_1(j\omega)$. Furthermore, if $\underline{H}_2(\omega) > 0$ is true, the vertices $\underline{\Delta}_i(s)$ do not intersect $\Delta_2(j\omega)$, implying that the sets $-\Delta_1(s)$ and $\Delta_2(s)$ do not overlap in the interval $\omega \in [0, \omega_u]$. \square

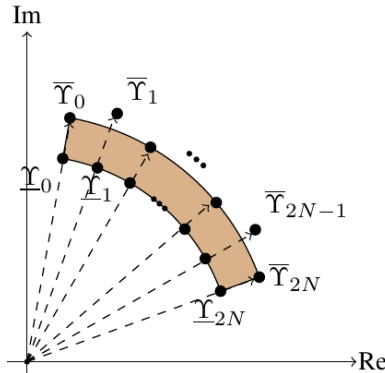


Figure 6.4: Set of values $\Delta_2(j\omega)$ (brown area) and the vertices $\Upsilon_i(j\omega)$.

Remark 6.3. Based on Theorems 6.5 and 6.6, the controllers $G_{cs}(s)$ and $G_{cd}(s)$ must respectively stabilize the nominal systems $1 + G_m(s)G_{cs}(s)$ and $1 + G_{cd}(s)G_m(s)e^{-\theta_m s}$. Here, the D-decomposition method [105] is employed to design the controllers. First, we explain this method for $1 + G_{cd}(s)G_m(s)e^{-\theta_m s}$, and it can be applied similarly to $1 + G_m(s)G_{cs}(s)$.

The boundaries of the stability region of $F(s) = 1 + G_{cd}(s)G_m(s)e^{-\theta_m s}$ are determined by CRB, RRB, and IRB. IRB and RRB can be easily determined by substituting $\omega = 0$ and $\omega \rightarrow \infty$ into $F(\omega)$, respectively. For the CRB, by setting $F(j\omega) = 0$, we obtain:

$$\begin{cases} k_{pd} = \frac{-Im(s(\tau_m s - 1)e^{\theta_m s})}{k_m \omega}, \\ k_{id} = \frac{-Re(s(\tau_m s - 1)e^{\theta_m s})}{k_m}. \end{cases} \quad (6.62)$$

Consequently, the stabilizing region can be identified by evaluating one arbitrary test point within each region. Furthermore, the CRB for G_{cs} can be calculated by setting $\theta_m = 0$, $k_{pd} = k_{ps}$, and $k_{is} = k_{is}$ in (5.34) as shown in (6.63).

$$\begin{cases} k_{ps} = \frac{-Im(s(\tau_m s - 1))}{k_m \omega}, \\ k_{is} = \frac{-Re(s(\tau_m s - 1))}{k_m}. \end{cases} \quad (6.63)$$

The control coefficients of G_{cs} and $G_{cd}(s)$ are selected from the stability regions to obtain the parameters of the controllers.

6.3 Illustrative examples

Example 6.1. Initially, let us direct our attention towards the subsequent process transfer function denoted by $P(s)$ in the Laplace transform domain

$$P(s) = \frac{[0.5, 1.5]s + [0.4, 1.6]}{[0.4, 1.6]s^2 + [0.5, 1.5]s + [0.3, 1.7]} e^{-[1, 3]s} \quad (6.64)$$

The statement suggests that the Smith predictor control structure illustrated in Figure ?? can be effectively stabilized through the utilization of the FOPID controller (6.65), as demonstrated by the available evidence.

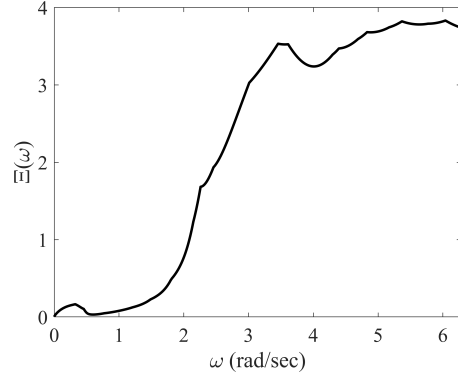
$$C(s) = 0.1 + \frac{0.01}{s^{0.8}} + 0.02 s^{0.9}. \quad (6.65)$$

Verification of the stability of the nominal characteristic polynomial $F_0(s)$ in (6.55) is a straightforward matter. Drawing on the insights of Theorem 2, the frequency ω_{\max} can be readily computed as 93.7658 rad/sec. Furthermore, the function $\chi(\omega)$ has been mapped out for the entire frequency range of interest, $\omega \in [0, 93.7658]$ rad/sec, as depicted in Figures 6.5a-6.5b. An inspection of these figures reveals that the inequality $\Xi(\omega) > 0$ holds true for all frequencies within this test range. Hence, we can confidently assert, in accordance with the provisions of Theorem 3, the robust stability of the Smith predictor control structure. Methods in [44, 45, 46, 47, 48, 49, 50, 51, 59, 60, 61] for verifying the robust stability of closed-loop control systems have proven to be elusive. In contrast, our study has unveiled a set of compelling findings that enable us to effortlessly confirm the robust stability of the considered control system. Furthermore, the step responses are illustrated in Figure 6.6.

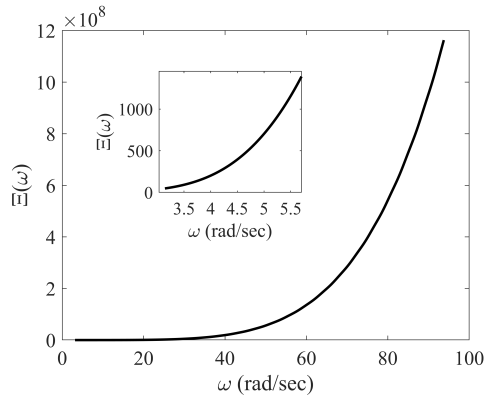
Example 6.2. Consider the interval plant as (6.66).

$$P(s) = \frac{[0.9, 1.1]}{[3.9, 4.1]s + 1} e^{-[8, 10]s}. \quad (6.66)$$

The present task at hand involves assessing the stability of a system through the application of a controller characterized by the transfer function $C(s) = 1.2 + \frac{0.2}{s}$. Following



(a)



(b)

Figure 6.5: (a) $\Xi(j\omega)$ for $\omega \in (0, \pi)$ rad/sec. (b) $\Xi(j\omega)$ for $\omega \in [\pi, 93.7658]$ rad/sec.

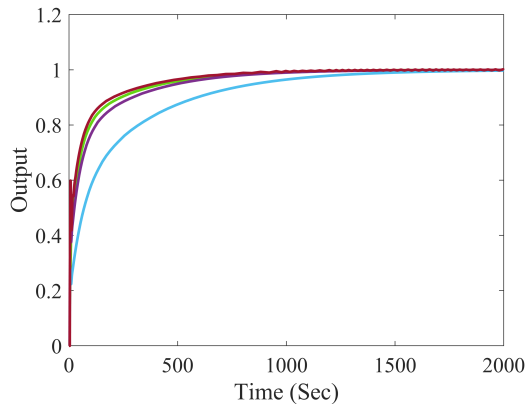


Figure 6.6: Step responses.

the guidelines laid out in Theorem 6.2, the critical frequency, denoted as ω_{\max} , has been determined to be 9.8923 rad/sec. The stability of $F_0(s) = 4s^2 + 2.2s + 0.2$ can be readily

inferred. Hence, it is necessary to verify the inequality $\Xi(\omega) > 0$ for the range of frequencies $[0, 9.8923]$ rad/sec. The robust stability can be easily inferred from Figures 6.7a-6.7b in conjunction with Theorem 6.3. Furthermore, it has been reported in Figure 6.8 that the values of $\chi_s(\omega)$ for $F_s(s) = \frac{1.2(1.9s+0.03)}{(s+0.5)}$ adhere to the condition $\chi_s(\omega) < 0$. Additionally, Figure 6.9 presents the step responses of the closed-loop control system, including the nominal system, exhibiting a commendable and robust performance. Moreover, as demonstrated by this example, the results of this chapter are applicable to integer-order systems.

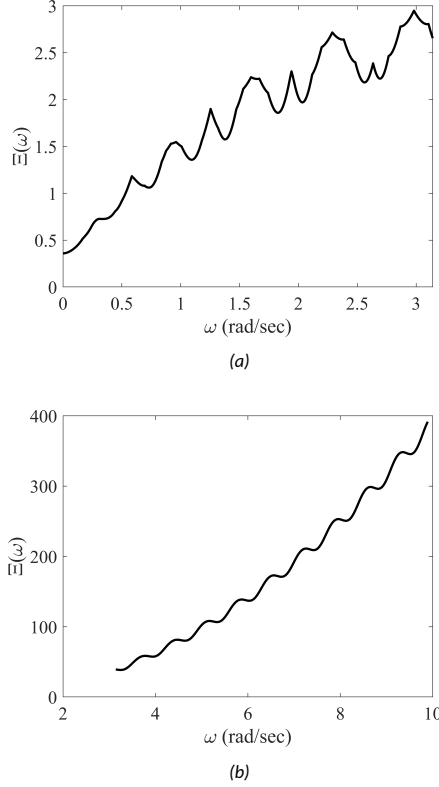


Figure 6.7: (a) $\Xi(j\omega)$ for $\omega \in (0, \pi)$ rad/sec. (b) $\Xi(j\omega)$ for $\omega \in [\pi, 9.8923]$ rad/sec.

Example 6.3. Consider the actual plant given by $G_p(s) = \frac{4}{4s-1}e^{-2s}$ [122]. We assume that the actual plant is within the following interval:

$$G_p(s) = \frac{[3.8, 4.2]}{[3.8, 4.2]s - 1}e^{-[1.8, 2.2]s}. \quad (6.67)$$

Based on the D-decomposition discussed in Remark 6.3, the stability regions for the controllers $G_{cs}(s)$ and $G_{cd}(s)$ are highlighted in green in Figure 6.10 and Figure 6.11, respectively. Thus, we select the controllers $G_{cs}(s) = 1.25 + \frac{0.25}{s}$ and $G_{cd}(s) = 0.4262 + \frac{0.0146}{s}$ from the identified regions. Additionally, $\lambda_p = 3.5$ is chosen to tune $G_{pd}(s)$. Furthermore, according to Theorem 6.4, $\omega_u = 17.6119$ can be obtained. Moreover, the curve $H(\omega)$ is shown in Figure 6.12 and Figure 6.13. As can be seen from these figures, $H(\omega) > 0$ holds

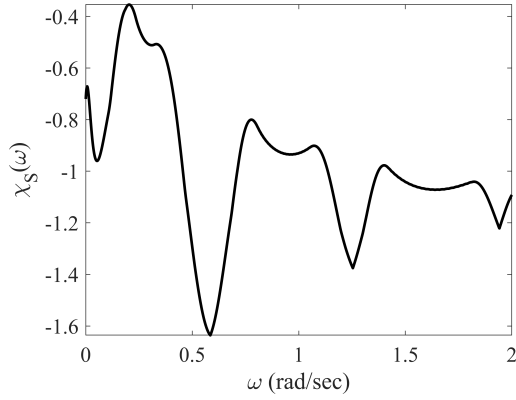


Figure 6.8: Curve of $\chi_s(\omega)$.

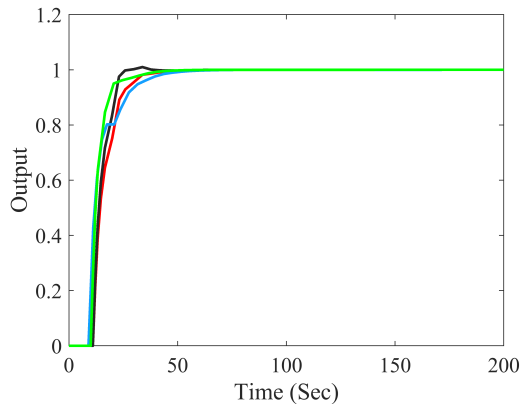


Figure 6.9: Step responses.

for $\omega \in [0, 17.6119]$, indicating that the system is robustly stable. Several step responses are shown in Figure 6.14 to confirm the system's robust stability. It is noteworthy that none of the existing works [0]-[125] can verify the robust stability of the systems. However, this chapter proposes a simple and reliable method for verifying the system's robust stability.

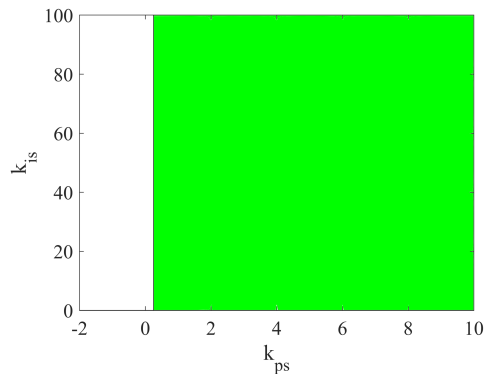


Figure 6.10: The stability region of G_{CS} (green region).

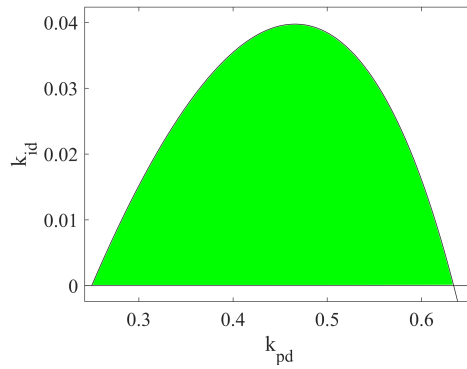


Figure 6.11: The stability region of G_{cd} (green region).

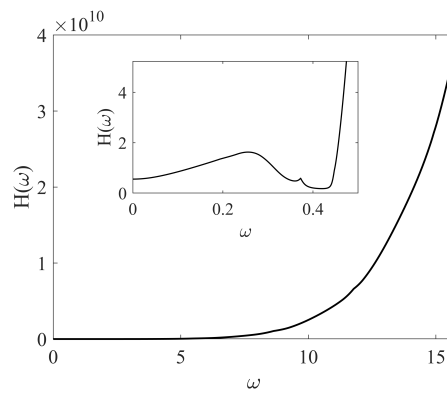


Figure 6.12: Curve $H(\omega)$ for $\omega \in [0, \bar{\omega})$.

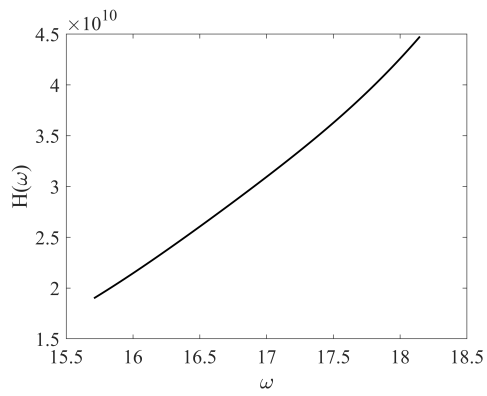


Figure 6.13: Curve $H(\omega)$ for $\omega \in [\bar{\omega}, \omega_u]$.

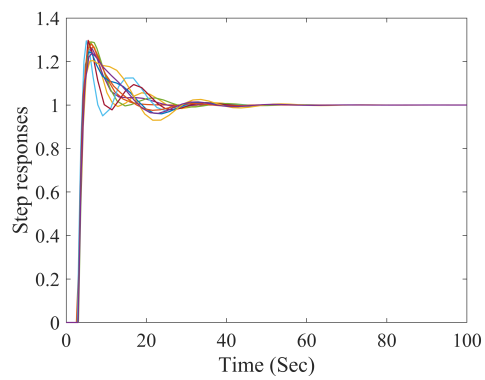


Figure 6.14: Step responses of several randomly selected members.

7 Robust Stability Analysis of FOISs with Complex Uncertainties

The robust stability of a family of interval FO polynomials with complex coefficients will be addressed further in this research. There are at least two factors that the earlier works may have overlooked. The first factor concerns the FO system's interval complex structure. Existing techniques all presume that interval uncertainties only exist in the FO system's real coefficients. However, the coefficient of any system may also have complex numbers. This phenomenon has been mentioned in [127, 128]. The second aspect concerns the uncertainties in real-world system. It is more likely to have uncertainties in modelling real-world systems. Accordingly, in this chapter, the robust stability of a family of interval FO systems with complex coefficients is investigated. The term "a family of interval FO systems with complex coefficients" refers to systems whose closed-loop characteristic equations may involve both commensurate and non-commensurate fractional orders, uncertain parameters within specified intervals, and complex-valued coefficients. The chapter begins by introducing a simple graphical method for verifying the necessary and sufficient conditions for robust stability. Building on this foundation, the concept of a robust stability testing function is extended to more systematically assess the stability of the system under uncertainty. An auxiliary function is proposed for analyzing the robust stability of this class of systems. Furthermore, explicit lower and upper frequency bounds are derived to enhance the computational efficiency of the stability verification process. Finally, several analytical examples and numerical simulations are presented to demonstrate the effectiveness and validity of the proposed methods.

7.1 Robust Stability Testing Function for A Complex Interval Family of FO Systems

Consider a complex interval family of polynomials as

$$\delta(s) = (q_0^R + jq_0^I) + (q_1^R + jq_1^I)s + \cdots + (q_n^R + jq_n^I)s^n, \quad (7.1)$$

with

$$q_t^R \in [\underline{q}_t^R, \overline{q}_t^R], \quad t = 0, 1, \dots, n, \quad (7.2)$$

and

$$q_t^I \in [\underline{q}_t^I, \overline{q}_t^I], \quad t = 0, 1, \dots, n, \quad (7.3)$$

in which the uncertain parameters q_t^R and q_t^I are the real and imaginary parts of the uncertainties. Also, \underline{q}_t^R and \underline{q}_t^I respectively denote the lower bounds of the uncertainties q_t^R and q_t^I . Moreover, \overline{q}_t^R and \overline{q}_t^I respectively represent the upper bounds of the uncertainties q_t^R and q_t^I . In (7.1), it is also assumed that $0 \notin (q_n^R + jq_n^I)$. In [120], it has been proven that $\delta(s)$ is robust stable if and only if the eight polynomials in (7.10) are all stable.

$$\left\{ \begin{array}{l}
P_1(s) = (\underline{q}_0^R + j\underline{q}_0^I) + (\underline{q}_1^R + j\underline{q}_1^I)s + (\underline{q}_2^R + j\underline{q}_2^I)s^2 + (\underline{q}_3^R + j\underline{q}_3^I)s^3 + (\underline{q}_4^R + j\underline{q}_4^I)s^4 \\
+ (\underline{q}_5^R + j\underline{q}_5^I)s^5 + \dots, \\
P_2(s) = (\underline{q}_0^R + j\underline{q}_0^I) + (\underline{q}_1^R + j\underline{q}_1^I)s + (\underline{q}_2^R + j\underline{q}_2^I)s^2 + (\underline{q}_3^R + j\underline{q}_3^I)s^3 + (\underline{q}_4^R + j\underline{q}_4^I)s^4 \\
+ (\underline{q}_5^R + j\underline{q}_5^I)s^5 + \dots, \\
P_3(s) = (\underline{q}_0^R + j\underline{q}_0^I) + (\underline{q}_1^R + j\underline{q}_1^I)s + (\underline{q}_2^R + j\underline{q}_2^I)s^2 + (\underline{q}_3^R + j\underline{q}_3^I)s^3 + (\underline{q}_4^R + j\underline{q}_4^I)s^4 \\
+ (\underline{q}_5^R + j\underline{q}_5^I)s^5 + \dots, \\
P_4(s) = (\underline{q}_0^R + j\underline{q}_0^I) + (\underline{q}_1^R + j\underline{q}_1^I)s + (\underline{q}_2^R + j\underline{q}_2^I)s^2 + (\underline{q}_3^R + j\underline{q}_3^I)s^3 + (\underline{q}_4^R + j\underline{q}_4^I)s^4 \\
+ (\underline{q}_5^R + j\underline{q}_5^I)s^5 + \dots, \\
P_5(s) = (\underline{q}_0^R + j\underline{q}_0^I) + (\underline{q}_1^R + j\underline{q}_1^I)s + (\underline{q}_2^R + j\underline{q}_2^I)s^2 + (\underline{q}_3^R + j\underline{q}_3^I)s^3 + (\underline{q}_4^R + j\underline{q}_4^I)s^4 \\
+ (\underline{q}_5^R + j\underline{q}_5^I)s^5 + \dots, \\
P_6(s) = (\underline{q}_0^R + j\underline{q}_0^I) + (\underline{q}_1^R + j\underline{q}_1^I)s + (\underline{q}_2^R + j\underline{q}_2^I)s^2 + (\underline{q}_3^R + j\underline{q}_3^I)s^3 + (\underline{q}_4^R + j\underline{q}_4^I)s^4 \\
+ (\underline{q}_5^R + j\underline{q}_5^I)s^5 + \dots, \\
P_7(s) = (\underline{q}_0^R + j\underline{q}_0^I) + (\underline{q}_1^R + j\underline{q}_1^I)s + (\underline{q}_2^R + j\underline{q}_2^I)s^2 + (\underline{q}_3^R + j\underline{q}_3^I)s^3 + (\underline{q}_4^R + j\underline{q}_4^I)s^4 \\
+ (\underline{q}_5^R + j\underline{q}_5^I)s^5 + \dots, \\
P_8(s) = (\underline{q}_0^R + j\underline{q}_0^I) + (\underline{q}_1^R + j\underline{q}_1^I)s + (\underline{q}_2^R + j\underline{q}_2^I)s^2 + (\underline{q}_3^R + j\underline{q}_3^I)s^3 + (\underline{q}_4^R + j\underline{q}_4^I)s^4 \\
+ (\underline{q}_5^R + j\underline{q}_5^I)s^5 + \dots.
\end{array} \right. \quad (7.4)$$

Now, let us consider a complex interval family of FO polynomials as

$$\begin{aligned}
\Delta(s) &= \Delta^R(s) + j\Delta^I(s) = \underline{q}_0^R + \sum_{h=1}^n \underline{q}_h^R s^{\alpha_h} + j(\underline{q}_0^I + \sum_{h=1}^n \underline{q}_h^I s^{\alpha_h}) = \\
&(\underline{q}_0^R + j\underline{q}_0^I) + \sum_{h=1}^n (\underline{q}_h^R + j\underline{q}_h^I) s^{\alpha_h},
\end{aligned} \quad (7.5)$$

in which $\Delta^R(s)$ and $\Delta^I(s)$ are respectively the real and imaginary polynomials parts of $\Delta(s)$ and also the intervals \underline{q}_i^R and \underline{q}_i^I are respectively defined in (7.2) and (7.3). Moreover, the orders α_i , ($i = 1, \dots, n$) satisfy $0 < \alpha_1 < \alpha_2 < \dots < \alpha_n$. It is apparent that $\delta(s)$ in (7.1) is only a special case of the complex interval family considered in this chapter i.e. $\Delta(s)$ in (7.11).

Remark 7.1. Based on discussion in Section 2, the value set of $\Delta^R(s)$ is a parpolygon whose vertices can be obtained by the following pattern:

$$\left\{ \begin{array}{l}
V_1^R(s) = \underline{q}_0^R + \underline{q}_1^R s^{\alpha_1} + \dots + \underline{q}_n^R s^{\alpha_n}, \\
V_2^R(s) = \underline{q}_0^R + \underline{q}_1^R s^{\alpha_1} + \dots + \underline{q}_n^R s^{\alpha_n}, \\
V_3^R(s) = \underline{q}_0^R + \underline{q}_1^R s^{\alpha_1} + \dots + \underline{q}_n^R s^{\alpha_n}, \\
\vdots \\
V_{2^{n+1}}^R(s) = \underline{q}_0^R + \underline{q}_1^R s^{\alpha_1} + \dots + \underline{q}_n^R s^{\alpha_n}.
\end{array} \right. \quad (7.6)$$

The exposed edges can be determined by (7.6). For instance, $V_1^R(s)$ and $V_2^R(s)$ have the same structure except \underline{q}_0^R . Accordingly, one of the edges can be considered as $e(V_1^R(s), V_2^R(s))$. The remaining edges can be built in a similar way. Create a set that includes all of the vertices $V_{i_1}^R(s)$ ($i_1 = 1, \dots, 2^{n+1}$) as

$$P_E^R(s) = \left\{ e(V_1^R(s), V_2^R(s)), e(V_1^R(s), V_3^R(s)), \dots, e(V_{2^{n+1}-1}^R(s), V_{2^{n+1}}^R(s)) \right\}. \quad (7.7)$$

Likewise, the vertex polynomials $V_{i_1}^I(s)$ ($i_1 = 1, \dots, 2^{n+1}$) and the set of exposed edges

$P_E^I(s)$ corresponding to $\Delta^I(s)$ are respectively defined in (7.8) and (6.10).

$$\begin{cases} V_1^I(s) = \underline{q}_0^I + \underline{q}_1^I s^{\alpha_1} + \dots + \underline{q}_n^I s^{\alpha_n}, \\ V_2^I(s) = \bar{q}_0^I + \bar{q}_1^I s^{\alpha_1} + \dots + \bar{q}_n^I s^{\alpha_n}, \\ V_3^I(s) = \underline{q}_0^I + \bar{q}_1^I s^{\alpha_1} + \dots + \underline{q}_n^I s^{\alpha_n}, \\ \dots \\ V_{2n+1}^I(s) = \bar{q}_0^I + \bar{q}_1^I s^{\alpha_1} + \dots + \bar{q}_n^I s^{\alpha_n}. \end{cases} \quad (7.8)$$

$$P_E^I(s) = \left\{ e(V_1^I(s), V_2^I(s)), e(V_1^I(s), V_3^I(s)), \dots, e(V_{2n+1}^I(s), V_{2n+1}^I(s)) \right\}. \quad (7.9)$$

Definition 7.1. In this chapter, for the sake of simplicity, we define

$$\begin{aligned} T_{-\hat{v}(s)}\{P_E^R(s)\} &= T_{-\hat{v}(s)}^R \triangleq \left\{ \underbrace{|V_1^R(s) + \hat{v}(s)| + |V_2^R(s) + \hat{v}(s)| - |V_1^R(s) - V_2^R(s)|}_{I_1^R}, \right. \\ &\quad \underbrace{|V_1^R(s) + \hat{v}(s)| + |V_3^R(s) + \hat{v}(s)| - |V_1^R(s) - V_3^R(s)|}_{I_2^R}, \dots, \\ &\quad \left. \underbrace{|V_{2n+1}^R(s) + \hat{v}(s)| + |V_{2n+1}^R(s) + \hat{v}(s)| - |V_{2n+1}^R(s) - V_{2n+1}^R(s)|}_{I_{(n+1)2n}^R} \right\}. \end{aligned} \quad (7.10)$$

In (7.10), $\hat{v}(s)$ is a FO polynomial. Likewise, we define

$$\begin{aligned} T_{-\hat{v}(s)}\{jP_E^I(s)\} &= T_{-\hat{v}(s)}^I \triangleq \left\{ \underbrace{|jV_1^I(s) + \hat{v}(s)| + |jV_2^I(s) + \hat{v}(s)| - |jV_1^I(s) - jV_2^I(s)|}_{I_1^I}, \right. \\ &\quad \underbrace{|jV_1^I(s) + \hat{v}(s)| + |jV_3^I(s) + \hat{v}(s)| - |jV_1^I(s) - jV_3^I(s)|}_{I_2^I}, \dots, \\ &\quad \left. \underbrace{|jV_{2n+1}^I(s) + \hat{v}(s)| + |jV_{2n+1}^I(s) + \hat{v}(s)| - |jV_{2n+1}^I(s) - jV_{2n+1}^I(s)|}_{I_{(n+1)2n}^I} \right\}. \end{aligned} \quad (7.11)$$

In **Theorem 7.1**, the zero exclusion condition is checked using an exact graphical method. As a result, necessary and sufficient conditions of the complex interval family $\Delta(s)$ are derived for robust stability analysis.

Theorem 7.1. $\Delta(s)$ in (7.11) is robustly stable if and only if:

1. $\Delta(s)$ contains one stable polynomial as $\Delta_0(s)$.
2. The exposed edges $-P_E^R(j\omega)$ and $jP_E^I(j\omega)$ do not have any overlap for $\omega \in (-\infty, \infty)$ in the complex plane.

Proof. The 'if' portion: Based on Section 2, at a given frequency $\omega = \omega_0$, it has be shown that

$$\begin{cases} \partial(\Delta^R(j\omega)) \subseteq P_E^R(j\omega), \\ \partial(\Delta^I(j\omega)) \subseteq P_E^I(j\omega). \end{cases} \quad (7.12)$$

As a contradiction argument it is supposed that at $\omega = \omega_0$, the value sets of $-P_E^R(j\omega)$ and $jP_E^I(j\omega)$ have an overlap. As a result, a complex number as Z_0 exists such that

$Z_0 \in -P_E^R(j\omega)$ (or $-Z_0 \in P_E^R(j\omega)$) and $Z_0 \in jP_E^I(j\omega)$. Therefore, from (7.11), it can be concluded that

$$\begin{cases} -Z_0 \in P_E^R(j\omega), \\ Z_0 \in jP_E^I(j\omega), \end{cases} \Rightarrow 0 \in \Delta(j\omega_0). \quad (7.13)$$

Then, by the zero exclusion principle, because of $0 \in \Delta(j\omega_0)$, the system is not robustly stable. It contracts the robust stability condition of the closed-loop control system.

The ‘only if’ portion: Since, the system is robustly stable, then $0 \notin \Delta(j\omega)$ by the zero exclusion principle. Assume the value sets of $-P_E^R(j\omega)$ and $jP_E^I(j\omega)$ are respectively defined as $-\Delta_{vs}^R(j\omega)$ and $\Delta_{vs}^I(j\omega)$. Now, assume that there are two arbitrary complex numbers as $Z_1, Z_2 \in \mathbb{C}$ such that $Z_1 \in -\Delta_{vs}^R(j\omega)$ (or $-Z_1 \in \Delta_{vs}^R(j\omega)$) and $Z_2 \in \Delta_{vs}^I(j\omega)$.

$$\begin{cases} -Z_1 \in \Delta_{vs}^R(j\omega), \\ Z_2 \in \Delta_{vs}^I(j\omega), \end{cases} \Rightarrow Z_2 - Z_1 \in \Delta_{vs}(j\omega_0). \quad (7.14)$$

Because of $0 \notin \Delta(j\omega)$, it can be simply concluded that $Z_2 - Z_1 \neq 0$ or $Z_1 \neq Z_2$. This implies that the arbitrary complex number Z_1 is not equal to Z_2 and consequently the exposed edges of $-P_E^R(j\omega)$ and $jP_E^I(j\omega)$ do not have any overlap. Hence, using the zero exclusion principle, the proof is ended. \square

For robust stability analysis by using **Theorem 7.1**, the overlap between the exposed edges $-P_E^R(j\omega)$ and $jP_E^I(j\omega)$ has to be checked at each frequency. In other words, it is needed to depict two-dimensional graphs of the exposed edges $-P_E^R(j\omega)$ and $jP_E^I(j\omega)$ in the complex plane at each frequency and it may be too difficult to examine the overlap between the exposed edges. Accordingly, in the following theorem, the overlap between the exposed edges $-P_E^R(j\omega)$ and $jP_E^I(j\omega)$ is developed using the geometric properties of parpolygons.

Theorem 7.2. *The exposed edges $-P_E^R(j\omega)$ and $jP_E^I(j\omega)$ have no overlap for $\omega \in (-\infty, \infty)$, if and only if:*

1. $-V_{i_1}^R(j\omega)(i_1 = 1, \dots, 2^{n+1}) \notin jP_E^I(j\omega)$,
2. $jV_{i_1}^I(j\omega)(i_1 = 1, \dots, 2^{n+1}) \notin -P_E^R(j\omega)$.

Proof. *The ‘if’ portion:* In the complex plane, consider two parpolygons having the vertices $V_i^D(j\omega)(i = 1, \dots, m_D)$ and $V_r^N(j\omega_0)(r = 1, \dots, m_N)$ as shown in Figure 7.1. As seen from this figure, the conditions 1 and 2 in this theorem are met. Figure 7.1 shows the geometric structure of parpolygons, and it is easy to see that these parpolygons have no overlap.

The ‘only if’ portion: It is assumed that as a contradiction argument, this theorem’s initial condition is not fulfilled. This indicates that at least one vertex as $V_x^R(j\omega_0)$ exists which is included in the value set of $jP_E^I(j\omega_0)$ i.e. $V_x^R(j\omega_0) \in -jP_E^I(j\omega_0)$ or $-V_x^R(j\omega_0) \in jP_E^I(j\omega_0)$. As a result, it may be deduced from **Theorem 7.1** that $0 \in \Delta(j\omega_0)$ and this signifies that the exposed edges $-P_E^R(j\omega)$ and $jP_E^I(j\omega)$ have the overlap at $\omega = \omega_0$. This is in contrast to the requirement of no overlap between the exposed edges $-P_E^R(j\omega)$ and $jP_E^I(j\omega)$. \square

Combining the results of **Theorem 7.1** and **Theorem 7.2** allows us to handle Problem 2. An auxiliary function is introduced as a robust stability testing function in the following theorem to analyze the conditions (1) and (2) in **Theorem 7.2**.

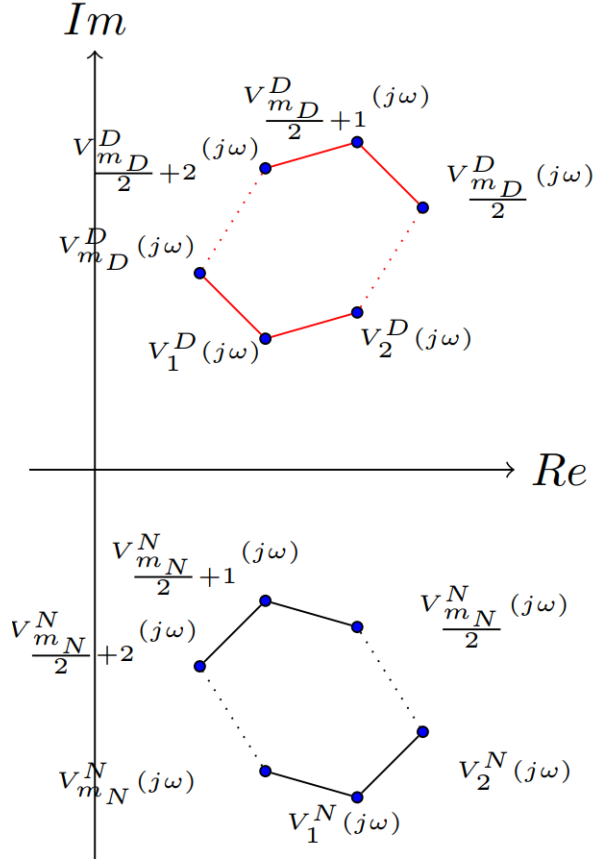


Figure 7.1: An illustration of two parpolygons with the vertices $V_i^D(j\omega)$ ($i = 1, \dots, m_D$) and $V_r^N(j\omega)$ ($r = 1, \dots, m_N$).

Theorem 7.3. $\Delta(s)$ in (7.11) is robust stable if and only if:

1. $\Delta(s)$ contains a stable polynomial as $\Delta_0(s)$.
2. For $\omega \in (-\infty, \infty)$, the inequality $\Xi(\omega) > 0$ is met in which $\Xi(\omega)$ is introduced in (7.15).

$$\Xi(\omega) \triangleq \min \left\{ \bar{\Xi}_1(j\omega), \bar{\Xi}_2(j\omega), \dots, \bar{\Xi}_{2^{n+1}}(j\omega), \underline{\Xi}_1(j\omega), \underline{\Xi}_2(j\omega), \dots, \underline{\Xi}_{2^{n+1}}(j\omega) \right\}, \quad (7.15)$$

$$\bar{\Xi}_{i_1}(j\omega) \triangleq \min_{l_i^R \in T_{-jV_{i_1}^I}^R(j\omega)} l_i^R, \quad i \in \{1, 2, \dots, (n+1)2^n\}, i_1 \in \{1, 2, \dots, 2^{n+1}\},$$

$$\underline{\Xi}_{i_2}(j\omega) \triangleq \min_{l_i^I \in T_{-V_{i_2}^R}^I(j\omega)} l_i^I, \quad i \in \{1, 2, \dots, (n+1)2^n\}, i_2 \in \{1, 2, \dots, 2^{n+1}\},$$

where, $T_{-jV_{i_1}^I}^R$ and $T_{V_{i_2}^R}^I$ are given by **Definition 7.1**.

Proof. This theorem is proven using the triangle inequality. The vertices $jV_{i_2}^I(j\omega)$ and $e(-V_{i_1}^R(j\omega), -V_{i_1+1}^R(j\omega))$ are schematically shown in Figure 7.2. Based on Figure 7.2 and the triangle inequality, the statements below can be deduced.

- If the values of $\bar{\Xi}_{i_2}(j\omega)$ in (7.15) are positive, then the vertices $jV_{i_2}^I(j\omega)$ do not intersect the edges $e(-V_{i_1}^R(j\omega), -V_{i_1+1}^R(j\omega))$.
- If the function $\bar{\Xi}_{i_2}(j\omega)$ in (6.14) is equal to zero at $\omega = \omega_0$, then the vertices $jV_{i_2}^I(j\omega)$ intersect the edges $e(-V_{i_1}^R(j\omega), -V_{i_1+1}^R(j\omega))$.

On the other hand we know that $\partial(\Delta^R(j\omega)) \subseteq P_E^R(j\omega)$. Hence, satisfying the inequalities $\bar{\Xi}_{i_2}(j\omega) > 0$ assure that the vertices $jV_{i_2}^I(j\omega)$ do not intersect $\partial(\Delta^R(j\omega))$. Therefore, the condition (1) is satisfied in **Theorem 7.2**. Similarly, if the inequalities $\bar{\Xi}_{i_2}(j\omega) > 0$ are satisfied then the condition (2) in **Theorem 7.2** is also met as well. Accordingly, based on **Definition 7.1**, **Theorem 7.1** and **Theorem 7.2**, the theorem is easily completed. \square

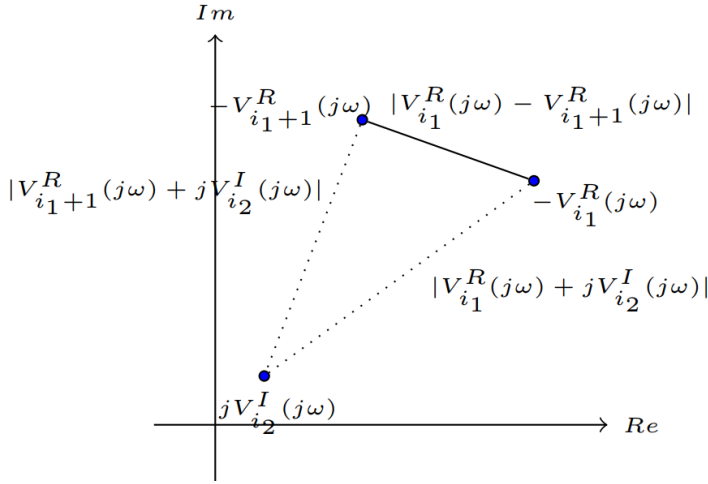


Figure 7.2: the edges $e(-V_{i_1}^R(j\omega), -V_{i_1+1}^R(j\omega))$ (bold line), distance between the vertices $jV_{i_2}^I(j\omega)$ and the vertices $-V_{i_1}^R(j\omega)$ and $-V_{i_1+1}^R(j\omega)$ (dotted lines).

It would be impossible to take into account the frequency range $\omega \in (-\infty, +\infty)$ in the simulation. We define non-zero and finite bounds on ω using the following theorem in order to achieve the correct scenario for using **Theorem 7.1** and **Theorem 7.3** in simulations.

Theorem 7.4. The roots of $\Delta(s)$ in (7.11) lie in $\{s \in \mathbb{C} | S_{\min} \leq |s| \leq S_{\max}\}$ in which

$$\begin{aligned}
 S_{\max} &\triangleq \max\{1, R_{\max}^{\frac{1}{\alpha_n - \alpha_{n-1}}}\}, \\
 R_{\max} &\triangleq \frac{\sum_{h=0}^{n-1} \left(\max\{|\underline{q}_h^R|, |\bar{q}_h^R|\} + \max\{|\underline{q}_h^I|, |\bar{q}_h^I|\} \right)}{F}, \\
 F &\triangleq \sqrt{F_1^2 + F_2^2}, \\
 F_1 &\triangleq \begin{cases} 0, & 0 \in q_n^R, \\ \min\{|\underline{q}_n^R|, |\bar{q}_n^R|\}, & 0 \notin q_n^R, \end{cases} \\
 F_2 &\triangleq \begin{cases} 0, & 0 \in q_n^I, \\ \min\{|\underline{q}_n^I|, |\bar{q}_n^I|\}, & 0 \notin q_n^I. \end{cases}
 \end{aligned} \tag{7.16}$$

$$\begin{aligned}
S_{\min} &\triangleq \min\{1, R_{\min}^{\frac{1}{\alpha_1}}\}, \\
R_{\min} &\triangleq \frac{E}{\sum_{h=1}^n \left(\max\{|\underline{q}_h^R|, |\bar{q}_h^R|\} + \max\{|\underline{q}_h^I|, |\bar{q}_h^I|\} \right)}, \\
E &\triangleq \sqrt{E_1^2 + E_2^2}, \\
E_1 &\triangleq \begin{cases} 0, & 0 \in q_0^R, \\ \min\{|\underline{q}_0^R|, |\bar{q}_0^R|\}, & 0 \notin q_0^R, \end{cases} \\
E_2 &\triangleq \begin{cases} 0, & 0 \in q_0^I, \\ \min\{|\underline{q}_0^I|, |\bar{q}_0^I|\}, & 0 \notin q_0^I. \end{cases}
\end{aligned} \tag{7.17}$$

Proof. The inequality $|\Delta(s)| > 0$ guarantees the condition $0 \notin \Delta(s)$. Therefore, we need to show that for $\{s \in \mathbb{C} | S_{\min} > |s| \text{ \& } |s| > S_{\max}\}$, $|\Delta(s)| > 0$ is met. From (7.11), the triangle inequality $|A| - |B + C| > |A| - |B| - |C|$ and the assumption $|s| > 1$, we have

$$\begin{aligned}
|\Delta(s)| &\geq F |s|^{\alpha_n} - \sum_{h=0}^n \left(\max\{|\underline{q}_h^R|, |\bar{q}_h^R|\} + \max\{|\underline{q}_h^I|, |\bar{q}_h^I|\} \right) |s|^{\alpha_h} \geq \\
&F |s|^{\alpha_{n-1}} \left(|s|^{\alpha_n - \alpha_{n-1}} - R_{\max} \right).
\end{aligned} \tag{7.18}$$

From (7.18) it can be inferred that $|\Delta(s)| > 0$ is satisfied for $\{s \in \mathbb{C} | |s| > S_{\max}\}$. Also, we can write for $|s| < 1$,

$$\begin{aligned}
|\Delta(s)| &\geq E - \sum_{h=1}^n \left(\max\{|\underline{q}_h^R|, |\bar{q}_h^R|\} + \max\{|\underline{q}_h^I|, |\bar{q}_h^I|\} \right) |s|^{\alpha_h} \geq \\
&\sum_{h=1}^n \left(\max\{|\underline{q}_h^R|, |\bar{q}_h^R|\} + \max\{|\underline{q}_h^I|, |\bar{q}_h^I|\} \right) \left(R_{\min} - |s|^{\alpha_1} \right).
\end{aligned} \tag{7.19}$$

From (7.19), it can be seen that $|\Delta(s)| > 0$ is also satisfied for $\{s \in \mathbb{C} | |s| < S_{\min}\}$. \square

The following corollaries are offered to assess the robust stability of $\Delta(s)$ in (6.46) as a simple consequence of **Theorem 7.4**.

Corollary 7.1. *The characteristic function $\Delta(s)$ in (7.11) is robust stable if and only if:*

1. $\Delta(s)$ contains one stable polynomial as $\Delta_0(s)$.
2. The inequality $\Xi(\omega) > 0$ is met for $\omega \in [-S_{\max}, -S_{\min}] \cup [S_{\min}, S_{\max}]$ in which $\Xi(\omega)$ is introduced in (6.14).

Proof. The proof can be completed quickly by applying **Theorems 7.1-7.4**. \square

Corollary 7.2. *Assume that $\Delta^I(s) = 0$ in (7.11). Then, the characteristic function $\Delta(s)$ in (6.46) is robust stable if and only if:*

1. $\Delta(s)$ contains one stable polynomial as $\Delta_0(s)$.
2. The inequality $\Xi(\omega) = \bar{\Xi}_{i_1}(j\omega) > 0$ is met for $\omega \in [S_{\min}, S_{\max}]$ where $\Xi(\omega)$ is defined in (7.15).

Proof. Because of $\Delta^I(s) = 0$, $\Delta(s)$ in (6.46) is a real-valued function. Hence, with respect to the real axis, the roots of $\Delta(s)$ are mirror symmetric. As a result of **Corollary 7.1**, the proof can be easily completed.

Remark 7.2. The following are the steps for examining the robust stability of $\Delta(s)$:

1. Examine the stability of a member of $\Delta(s)$ as $\Delta_0(s)$. In this chapter, the Principle of Argument theorem [126] is used to check the stability of $\Delta_0(s)$. If $\Delta_0(s)$ is stable, carry on the next steps. Otherwise, $\Delta(s)$ is not robustly stable.
2. Obtain the exposed edges $P_E^R(j\omega)$ and $P_E^I(j\omega)$ by using **Remark 7.1**.
3. Examine the robust stability by benefiting from **Corollary 7.1** and **Corollary 7.2**.

Remark 7.3. It is notable that all Theorems 7.1-7.4 are applicable to integer-order polynomials as $\delta(s)$ in (6.42). It is because that based on Remark 7.1, $\partial(\delta(j\omega)) \subseteq P_E(j\omega)$ and $\partial(\Delta(j\omega)) \subseteq P_E(j\omega)$. On the other hand, Theorem 7.1 and Theorem 7.3 exactly determine whether or not $0 \in P_E(j\omega)$. Because of $\partial(\delta(j\omega)) \subseteq P_E(j\omega)$ and $\partial(\Delta(j\omega)) \subseteq P_E(j\omega)$, it can be inferred that the robust stability analysis presented in Remark 7.3 can be employed for $\delta(j\omega)$.

7.2 Robust Stability Testing Function for A Complex Interval Family of FO Systems

In this subsection, we study the closed-loop system shown in Figure 7.4. Consider $P(s)$ and $C(s)$ as

$$P(s) = \frac{N_p(s)}{D_p(s)} = \frac{N_p^R(s) + jN_p^I(s)}{D_p^R(s) + jD_p^I(s)} = \frac{\sum_{r_p=0}^{m_p} (b_{r_p}^{PR} + jb_{r_p}^{PI})s^{\beta_{r_p}^p}}{\sum_{i_p=0}^{n_p} (a_{i_p}^{PR} + ja_{i_p}^{PI})s^{\alpha_{i_p}^p}}, \quad (7.20)$$

$$C(s) = \frac{N_c(s)}{D_c(s)} = \frac{N_c^R(s) + jN_c^I(s)}{D_c^R(s) + jD_c^I(s)} = \frac{\sum_{r_c=0}^{m_c} b_{r_c}^c s^{\beta_{r_c}^c}}{\sum_{i_c=0}^{n_c} a_{i_c}^c s^{\alpha_{i_c}^c}}, \quad (7.21)$$

in which, the intervals $b_{r_p}^{PR}$, $b_{r_p}^{PI}$, $a_{i_p}^{PR}$ and $a_{i_p}^{PI}$ are defined in (7.22) and also, the orders $0 = \beta_0^p < \beta_1^p < \dots < \beta_{m_p-1}^p < \beta_{m_p}^p$, $0 = \alpha_0^p < \alpha_1^p < \dots < \alpha_{n_p-1}^p < \alpha_{n_p}^p$, $0 = \alpha_0^c < \alpha_1^c < \dots < \alpha_{n_c-1}^c < \alpha_{n_c}^c$ and $0 = \beta_0^c < \beta_1^c < \dots < \beta_{m_c-1}^c < \beta_{m_c}^c$ are positive real numbers. Furthermore, the coefficients $b_{r_c}^c$ and $a_{i_c}^c$ may be complex/real numbers. Moreover, it is assumed that $a_{n_p}^{PR} \neq 0$, $\alpha_{n_p}^p > \beta_{m_p}^p$ and $\alpha_{n_p}^p + \alpha_{n_c}^c > \beta_{m_p}^p + \beta_{m_c}^c$, $a_{n_c}^c \neq 0$ and $0 \notin a_{n_p}^{PR} + ja_{n_p}^{PI}$.

$$\begin{cases} b_{r_p}^{PR} \in [\underline{b}_{r_p}^{PR}, \bar{b}_{r_p}^{PR}], & r_p = 0, 1, \dots, m_p, \\ b_{r_p}^{PI} \in [\underline{b}_{r_p}^{PI}, \bar{b}_{r_p}^{PI}], & r_p = 0, 1, \dots, m_p, \\ a_{i_p}^{PR} \in [\underline{a}_{i_p}^{PR}, \bar{a}_{i_p}^{PR}], & i_p = 0, 1, \dots, n_p, \\ a_{i_p}^{PI} \in [\underline{a}_{i_p}^{PI}, \bar{a}_{i_p}^{PI}], & i_p = 0, 1, \dots, n_p. \end{cases} \quad (7.22)$$

The characteristic polynomial of the closed-loop control system shown in Figure 7.4 can be obtained as

$$\Delta(s) = N_p(s)N_c(s) + D_p(s)D_c(s). \quad (7.23)$$

In this study, the goal is to analyze the robust stability of $\Delta(s)$ in (7.23). To do this, Remark 7.4 is presented in the following.

Remark 7.4. Based on Section 2, the value set of $N_c(s)N_p(s)$ is a polygon in the complex plane. Also, the vertex polynomials of $N_c(s)N_p(s)$ in (7.20) can be obtained by the following

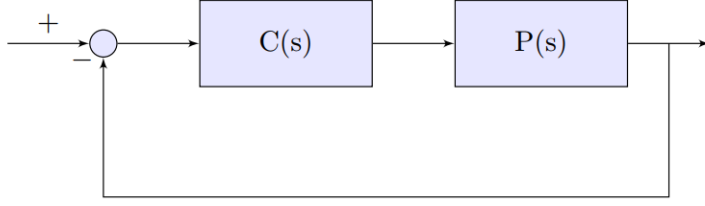


Figure 7.3: The closed-loop system.

pattern:

$$\begin{cases} V_1^N(s) = N_c(s) \left(\underline{b}_0^{PR} + \underline{b}_1^{PR} s^{\beta_1^p} + \dots + \underline{b}_{m_p}^{PR} s^{\beta_{m_p}^p} + j\underline{b}_0^{PI} + \dots + j\underline{b}_{m_p}^{PI} s^{\beta_{m_p}^p} \right), \\ V_2^N(s) = N_c(s) \left(\bar{b}_0^{PR} + \bar{b}_1^{PR} s^{\beta_1^p} + \dots + \bar{b}_{m_p}^{PR} s^{\beta_{m_p}^p} + j\underline{b}_0^{PI} + \dots + j\underline{b}_{m_p}^{PI} s^{\beta_{m_p}^p} \right), \\ V_3^N(s) = N_c(s) \left(\underline{b}_0^{PR} + \bar{b}_1^{PR} s^{\beta_1^p} + \dots + \underline{b}_{m_p}^{PR} s^{\beta_{m_p}^p} + j\underline{b}_0^{PI} + \dots + j\underline{b}_{m_p}^{PI} s^{\beta_{m_p}^p} \right), \\ \dots \\ V_{2^{2m_p+2}}^N(s) = N_c(s) \left(\bar{b}_0^{PR} + \bar{b}_1^{PR} s^{\beta_1^p} + \dots + \bar{b}_{m_p}^{PR} s^{\beta_{m_p}^p} + j\underline{b}_0^{PI} + \dots + j\underline{b}_{m_p}^{PI} s^{\beta_{m_p}^p} \right). \end{cases} \quad (7.24)$$

The exposed edges can be specified by (7.24). For example, the vertices $V_1^N(s)$ and $V_2^N(s)$ have the same structure except the parameter \underline{b}_0^P . Therefore, one of the exposed edges can be expressed as $e(V_1^N(s), V_2^N(s))$. The remaining exposed edges can be similarly constructed. Define a set which contains all of the vertices $V_{i_1}^N(s) (i_1 = 1, \dots, 2^{2m_p+2})$ as

$$P_E^N(s) = \left\{ e(V_1^N(s), V_2^N(s)), e(V_1^N(s), V_3^N(s)), \dots, e(V_{2^{2m_p+2}-1}^N(s), V_{2^{2m_p+2}}^N(s)) \right\}. \quad (7.25)$$

Likewise, regarding Remark 7.4, it is assumed that the vertices and the exposed edges of $D_c(s) D_p(s)$ are respectively considered as $V_{i_2}^D(s) (i_2 = 1, \dots, 2^{2n_p+2})$ and $P_E^D(s)$.

To derive sufficient and necessary conditions for robust stability, we need to check the relationship between the origin and the value set of $\Delta(j\omega)$ in (7.23). In the following theorem, a graphical method is presented to determine the zero exclusion condition. The result subsequently provides necessary and sufficient conditions for robust stability analysis of the closed-loop control system.

Theorem 7.5. $\Delta(s)$ in (7.23) can be robustly stabilized by the FO controller $C(s)$, if and only if:

1. $\Delta(s)$ in (7.23) contains one Hurwitz-stable polynomial.
2. The exposed edges $-P_E^D(s)$ and $P_E^N(s)$ do not have any overlap for $\omega \in (-\infty, \infty)$ in the complex plane.

Proof. Based on Remark 7.4, it is apparent that

$$\partial(N_c(j\omega)N_p(j\omega)) \subset P_E^N(s) \quad \text{and} \quad \partial(D_c(j\omega)D_p(j\omega)) \subset P_E^D(s).$$

Assume that at a fixed frequency $\omega = \omega_0$, the value sets of $-P_E^D(s)$ and $P_E^N(s)$ overlap in the complex plane.

Therefore, one can deduce that there exists a complex number Z_0 such that

$$Z_0 \in -P_E^D(s) \quad \text{and} \quad Z_0 \in P_E^N(s).$$

Thus, from (7.23), it can be concluded that

$$\begin{cases} -Z_0 \in P_E^D(j\omega_0), \\ Z_0 \in P_E^N(j\omega_0), \end{cases} \Rightarrow 0 \in \Delta(j\omega_0). \quad (7.26)$$

This implies that if the exposed edges of $-P_E^D(s)$ and $P_E^N(s)$ have no overlap in the complex plane, then the origin is not included in the value set of $\Delta(j\omega)$. Hence, based on the zero exclusion principle we can complete the proof. \square

Theorem 7.6. *The exposed edges $-P_E^D(j\omega)$ and $P_E^N(j\omega)$ do not have any overlap at a fixed frequency $-\infty < \omega < \infty$, if and only if:*

1. $-V_{i_1}^D(j\omega)(i_1 = 1, \dots, 2^{2n_p+2}) \notin P_E^N(j\omega),$
2. $V_{i_2}^N(j\omega)(i_2 = 1, \dots, 2^{2m_p+2}) \notin -P_E^D(j\omega).$

Proof. The proof follows from Theorem 7.2. \square

Now, the next goal is to introduce an auxiliary function to check the conditions (1) and (2) presented in the statements of Theorem 7.6. For the sake of simplicity, Definition 7.2 is presented as follows.

Definition 7.2. *Assume that $E_1 = e(v_1(s), v_2(s))$ is an edge of the exposed edges of a value set. Then, we define*

$$Tr^{\hat{v}(s)}(E_1) \triangleq |v_1(s) + \hat{v}(s)| + |v_2(s) + \hat{v}(s)| - |v_1(s) - v_2(s)|, \quad (7.27)$$

where, $\hat{v}(s)$ is a FO polynomial.

Theorem 7.7. *Let $E_1^N, E_2^N, \dots, E_{i_N}^N$ and $E_1^D, E_2^D, \dots, E_{i_D}^D$ be all edges of the exposed edges $P_E^N(s)$ and $P_E^D(s)$, respectively. Then, $\Delta(s)$ can be robustly stabilized by the FO controller $C(s)$, if and only if:*

1. $\Delta(s)$ in (7.23) contains one Hurwitz-stable member.
2. The inequality $\Xi(\omega) > 0$ is satisfied for $\omega \in (-\infty, \infty)$ where $\Xi(\omega)$ is defined in (7.28).

$$\begin{aligned} \Xi(\omega) &\triangleq \\ \min &\left\{ \bar{\Xi}_1(j\omega), \bar{\Xi}_2(j\omega), \dots, \bar{\Xi}_{t_N}(j\omega), \underline{\Xi}_1(j\omega), \underline{\Xi}_2(j\omega), \dots, \underline{\Xi}_{t_D}(j\omega) \right\}, \end{aligned} \quad (7.28)$$

$$\bar{\Xi}_{i_1}(j\omega) \triangleq \min_{i=1,2,\dots,2^{2n_p+2}} Tr^{V_i^D(s)}(E_{i_1}^N), \quad i_1 \in \{1, 2, \dots, t_N\},$$

$$\underline{\Xi}_{i_2}(j\omega) \triangleq \min_{i=1,2,\dots,2^{2m_p+2}} Tr^{V_i^N(s)}(E_{i_2}^D), \quad i_2 \in \{1, 2, \dots, t_D\}.$$

Proof. The proof follows from Theorem 7.3. \square

Clearly, it is not optimal to check whether or not the origin is included in the value set of $\Delta(j\omega)$ in (7.23) for $\omega \in (-\infty, \infty)$, because the length of $(-\infty, \infty)$ is infinite. The next theorem provides an area for the roots of $\Delta(s)$ in (7.23). This area reduces the computational burden for robust stability analysis.

Theorem 7.8. All roots of $\Delta(s)$ in (7.23) lie in $\{s \in \mathbb{C} \mid |s| \leq S_{\max}\}$ where

$$S_{\max} = \max\{1, \sigma_1^{\frac{1}{\alpha_{n_c}^p + \alpha_{n_p}^p - \varepsilon_1}}\}, \quad (7.29)$$

$$\varepsilon_1 = \max\left\{\alpha_{n_c}^c + \alpha_{n_{p-1}}^p, \alpha_{n_c-1}^c + \alpha_{n_p}^p, \beta_{m_c}^c + \beta_{m_p}^p\right\},$$

$$\begin{aligned} \sigma_1 = & \left(\left(\sum_{i^1=0}^{n_c} |a_{i^1}^c| \right) \left(\sum_{i^2=0}^{n_p-1} \left(\max\{|\underline{a}_{i_2}^{PR}|, |\bar{a}_{i_2}^{PR}|\} + \max\{|\underline{a}_{i_2}^{PI}|, |\bar{a}_{i_2}^{PI}|\} \right) \right) + \right. \\ & \left(\max\{|\underline{a}_{n_p}^{PR}|, |\bar{a}_{n_p}^{PR}|\} + \max\{|\underline{a}_{n_p}^{PI}|, |\bar{a}_{n_p}^{PI}|\} \right) \left(\sum_{i^1=0}^{n_c-1} |a_{i^1}^c| \right) + \left(\sum_{j^1=0}^{m_c} |b_{j^1}^c| \right) \\ & \left. \left(\sum_{j^2=0}^{m_p} \left(\max\{|\underline{b}_{j^2}^{PR}|, |\bar{b}_{j^2}^{PR}|\} + \max\{|\underline{b}_{j^2}^{PI}|, |\bar{b}_{j^2}^{PI}|\} \right) \right) \right) / F, \end{aligned}$$

$$F \triangleq F_1 + F_2,$$

$$F_1 \triangleq \begin{cases} 0, & 0 \in a_{n_p}^{PR}, \\ |a_{n_c}^c| \min\{|\underline{a}_{n_p}^{PR}|, |\bar{a}_{n_p}^{PR}|\}, & 0 \notin a_{n_p}^{PR}, \end{cases}$$

$$F_2 \triangleq \begin{cases} 0, & 0 \in a_{n_p}^{PI}, \\ |a_{n_c}^c| \min\{|\underline{a}_{n_p}^{PI}|, |\bar{a}_{n_p}^{PI}|\}, & 0 \notin a_{n_p}^{PI}. \end{cases}$$

Proof. The inequality $|\Delta(s)| > 0$ ensures that $0 \notin \Delta(s)$. Therefore, it is sufficient to prove that for $\{s \in \mathbb{C} \mid |s| > S_{\max}\}$, the inequality $|\Delta(s)| > 0$ is met. From (7.23) and assuming $|s| > 1$, we have

$$\begin{aligned} |\Delta(s)| & \geq F|s|^{\alpha_{n_p}^p + \alpha_{n_c}^c} - \\ & \left(\left(\sum_{i^1=0}^{n_c} |a_{i^1}^c| |s|^{\alpha_{i^1}^c} \right) \left(\sum_{i^2=0}^{n_p-1} \left(\max\{|\underline{a}_{i_2}^{PR}|, |\bar{a}_{i_2}^{PR}|\} + \max\{|\underline{a}_{i_2}^{PI}|, |\bar{a}_{i_2}^{PI}|\} \right) |s|^{\alpha_{i_2}^p} \right) + \right. \\ & \left(\max\{|\underline{a}_{n_p}^{PR}|, |\bar{a}_{n_p}^{PR}|\} + \max\{|\underline{a}_{n_p}^{PI}|, |\bar{a}_{n_p}^{PI}|\} \right) \left(\sum_{i^1=0}^{n_c-1} |a_{i^1}^c| |s|^{\alpha_{i^1}^c + \alpha_{n_p}^p} \right) + \\ & \left. \left(\sum_{j^1=0}^{m_c} |b_{j^1}^c| |s|^{\beta_{j^1}^c} \right) \left(\sum_{j^2=0}^{m_p} \left(\max\{|\underline{b}_{j^2}^{PR}|, |\bar{b}_{j^2}^{PR}|\} + \max\{|\underline{b}_{j^2}^{PI}|, |\bar{b}_{j^2}^{PI}|\} \right) |s|^{\beta_{j^2}^p} \right) \right) \geq \\ & F|s|^{\alpha_{n_p}^p + \alpha_{n_c}^c} - \\ & \left(\left(\sum_{i^1=0}^{n_c} |a_{i^1}^c| |s|^{\alpha_{i^1}^c} \right) \left(\sum_{i^2=0}^{n_p-1} \left(\max\{|\underline{a}_{i_2}^{PR}|, |\bar{a}_{i_2}^{PR}|\} + \max\{|\underline{a}_{i_2}^{PI}|, |\bar{a}_{i_2}^{PI}|\} \right) |s|^{\alpha_{i_2}^p} \right) + \right. \\ & \left(\max\{|\underline{a}_{n_p}^{PR}|, |\bar{a}_{n_p}^{PR}|\} + \max\{|\underline{a}_{n_p}^{PI}|, |\bar{a}_{n_p}^{PI}|\} \right) \left(\sum_{i^1=0}^{n_c-1} |a_{i^1}^c| |s|^{\alpha_{i^1}^c + \alpha_{n_p}^p} \right) + \\ & \left. \left(\sum_{j^1=0}^{m_c} |b_{j^1}^c| |s|^{\beta_{j^1}^c} \right) \left(\sum_{j^2=0}^{m_p} \left(\max\{|\underline{b}_{j^2}^{PR}|, |\bar{b}_{j^2}^{PR}|\} + \max\{|\underline{b}_{j^2}^{PI}|, |\bar{b}_{j^2}^{PI}|\} \right) |s|^{\beta_{j^2}^p} \right) \right) \\ & \geq F|s|^{\varepsilon_1} \left(|s|^{\alpha_{n_p}^p + \alpha_{n_c}^c - \varepsilon_1} - \sigma_1 \right). \end{aligned} \quad (7.30)$$

From (6.33), it is seen that the inequality $|\Delta(s)| > 0$ is met for $\{s \in \mathbb{C} \mid |s| > S_{\max}\}$. \square

As an easy consequence of *Theorem 7.8*, the following corollaries are presented to check the robust stability of $\Delta(s)$ in (7.23).

Corollary 7.3. $\Delta(s)$ in (7.23) can be robustly stabilized by the FO controller $C(s)$, if and only if:

1. $\Delta(s)$ in (7.23) contains one Hurwitz-stable polynomial.
2. The inequality $\Xi(\omega) > 0$ is satisfied for $\omega \in [-S_{\max}, S_{\max}]$ where $\Xi(\omega)$ is defined in (7.28).

Proof. By using *Theorems 7.5-7.8*, the proof can be simply done. \square

Corollary 7.4. Assume that $N_p^I(s) = D_p^I = N_c^I(s) = D_c^I = 0$ in (7.20) and (7.21). $\Delta(s)$ in (7.23) can be robustly stabilized by the FO controller $C(s)$, if and only if:

1. $\Delta(s)$ in (7.23) contains one Hurwitz-stable polynomial.
2. The inequality $\Xi(\omega) > 0$ is satisfied for $\omega \in [0, S_{\max}]$, where $\Xi(\omega)$ is defined in (7.28).

Proof. Because of $N_p^I(s) = D_p^I = N_c^I(s) = D_c^I = 0$, the characteristic function $\Delta(s)$ in (6.45) is a real-valued function. Hence, the roots of $\Delta(s)$ are mirror symmetric with respect to the real axis. Therefore, based on *Corollary 1*, the proof can be simply deduced. \square

7.3 Illustrative examples

Example 7.1. Consider the following FO plant $P(s)$.

$$P(s) = \frac{[1, 2] + j[0.01, 0.1]}{[1, 2]s^{0.8} + [2, 3] + j[0.1, 0.2]}. \quad (7.31)$$

It is shown that the FO controller (7.32) can robustly stabilize the closed-loop system.

$$C(s) = \frac{1}{s^{0.5}}. \quad (7.32)$$

$\Delta_0(s)$ is considered as (7.33).

$$\Delta_0(s) = s^{0.5}(s^{0.8} + 2 + j0.1) + (1 + j0.01). \quad (7.33)$$

Consider the Jordan curve as $\{s = j\omega \mid \omega \in [-S_{\max}, S_{\max}]\} \cup \{s = S_{\max}e^{j\theta} \mid \theta \in [\frac{-\pi}{2}, \frac{\pi}{2}]\}$, where S_{\max} can be given by *Theorem 7.8*. Hence, one can simply obtain $S_{\max} = 28.09$ rad/sec. The path obtained by $\Delta_0(s)$ in (7.33) when s traverses the Jordan curve is depicted in Figure 7.4. From this figure, it is apparent that the total number of encirclements of the origin by the path is equal to zero. Therefore, based on *Principle of Argument*, $\Delta_0(s)$ is stable. Moreover, the curve of the auxiliary function $\Xi(\omega)$ in (7.28) for $\omega \in [-28.09, 28.09]$ rad/sec has been shown in Figure 7.5. Hence, based on Figure 7.5 and *Corollary 7.3*, the closed-loop system is robust stable.

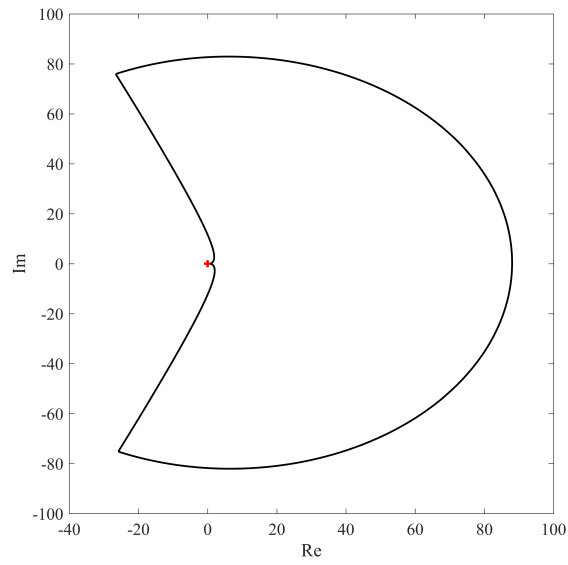


Figure 7.4: The path obtained by $\Delta_0(s)$ in (6.31) when s traverses the Jordan curve.

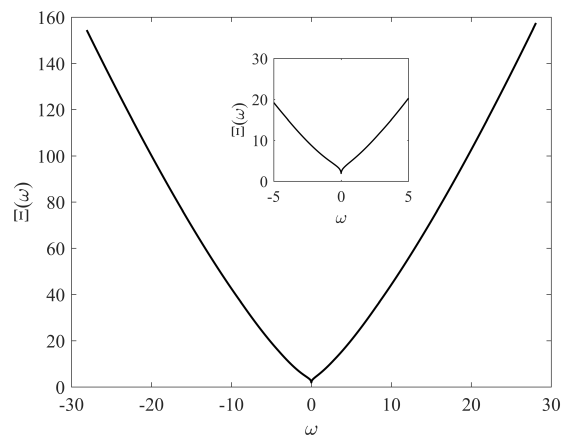


Figure 7.5: Curve of $\Xi(\omega)$ in (7.28) for $\omega \in [-28.09, 28.09]$ rad/sec.

8 Conclusions

This thesis has developed a comprehensive framework for the **robust stability analysis of fractional-order control systems** subject to various structural uncertainties. These include *interval coefficients*, *time delays*, and *complex-valued parameter variations*, which frequently arise in practical modeling and controller design. Motivated by the increasing use of fractional-order controllers in engineering applications, the thesis proposed several novel, low-complexity methods to assess and ensure the robust stability of such systems.

The contributions span **seven chapters**, each focusing on a distinct class of uncertain systems. The core findings and their interconnections are summarized as follows:

- **Chapter 2** laid the mathematical foundations by analyzing *fractional-order interval polynomials (FOIPs)* using value set theory. A method was proposed to compute vertex polynomials, and new necessary and sufficient conditions were introduced for robust stability analysis. It also demonstrated how tools like FOMCON can assist in verification.
- **Chapter 3** presented a novel graphical approach based on the zero-exclusion principle and introduced an *auxiliary function* that fixes the vertex polynomials across all frequencies. This method reduces computational burden while maintaining rigorous stability guarantees.
- **Chapter 4** extended the analysis to fractional-order interval systems with time delays, offering a simple yet effective graphical test. A *robust stability testing function* was introduced alongside upper and lower frequency bounds, yielding a practical method for verifying stability with reduced complexity.
- **Chapter 5** addressed gaps in recent literature regarding the stability region of FOPID-controlled systems with delay. The chapter proposed a corrected methodology for accurately determining these regions and demonstrated its effectiveness through case studies.
- **Chapter 6** focused on *Smith predictor-based control systems* affected by parametric uncertainties. A key contribution was the derivation of exact necessary and sufficient conditions for robust stability. An extended auxiliary function was also introduced to support robust disturbance rejection, enhancing controller reliability.
- **Chapter 7** tackled robust stability of systems with *complex interval uncertainties* in both numerator and denominator coefficients. A graphical method based on convex polygons was proposed, along with a new upper-bound simplification to reduce computational complexity.

Taken together, the chapters of this thesis form a cohesive contribution to the theory and practice of robust fractional-order control. The unified features of the proposed methods are:

- **Exactness:** All proposed criteria are necessary and sufficient for robust stability, ensuring no conservatism in conclusions.
- **Graphical interpretability:** Most methods yield intuitive visual tools that aid in controller design and verification.

- **Computational efficiency:** By fixing vertex polynomials and introducing frequency bounds and auxiliary functions, the methods dramatically reduce the number of evaluations required.

These attributes make the developed techniques suitable not only for academic analysis but also for engineering applications, including controller tuning, robust design, and performance verification.

Future Research Directions

While this thesis has laid strong theoretical and practical foundations, several promising directions remain open for future work:

- **Toolchain integration:** Embedding the proposed methods into controller design environments like FOMCON could enable a fully automated design and verification process.
- **Uncertainty in fractional orders:** Extending the stability analysis to systems where the fractional orders themselves are uncertain or time-varying is a key open challenge.
- **Systems with multiple interval time delays:** Extending the proposed robust stability analysis framework to fractional-order systems that contain multiple, possibly interacting, interval time delays would be a valuable future direction. Developing graphical or analytical conditions that explicitly account for simultaneous delay uncertainties could significantly enhance the applicability of the method to complex delayed processes.
- **Distributed and networked control:** Investigating how robust fractional-order control can be applied in consensus or formation problems in multi-agent systems is a natural next step.
- **Robust performance regions:** Identifying and characterizing the robust-performance regions in the fractional-order controller parameter space—rather than only the robust-stability regions—can provide deeper insight into how parameter choices affect both stability and closed-loop performance under uncertainty. This direction enables a unified framework where robust stability and robust performance are jointly analyzed for FO controllers.
- **Iterative learning-based fractional-order controllers:** Designing iterative learning control schemes that incorporate fractional-order structures represents a promising research direction. Integrating the robust stability results with learning-based or repetition-based FO controllers may provide improved transient behavior, enhanced tracking accuracy, and guaranteed stability across iterations.
- **Experimental validation:** Testing the proposed methods on real hardware platforms or in hardware-in-the-loop setups would provide further evidence of practical value.

Final Remarks

In conclusion, this thesis has contributed a set of robust, theoretically grounded, and computationally efficient tools for the analysis of fractional-order systems under uncertainty.

By bridging theoretical rigor with visual intuition and reduced computational effort, these contributions provide a solid platform for both researchers and practitioners working on robust control of complex dynamic systems.

List of Figures

1.1	TRMS system.....	15
2.1	$\Delta_{vs}(j\omega, \mathbf{q})$ in (4.3) at $\omega = 1$ rad/sec.	23
2.2	Value set of $\Delta(j\omega, \mathbf{q})$ in (4.3) (green) and its boundary (red) at $\omega = 1$ rad/sec.	25
2.3	Value set of $\Delta(j\omega, \mathbf{q})$ in (4.3) (green) and its boundary (red) at $\omega = 1$ rad/sec.	27
2.4	The modules of FOMCON toolbox for MATLAB. The newly developed module for Robust Control is highlighted.	31
2.5	The magnitude response of a randomly sampled member subset of 100 of the FO polynomial with interval uncertainties in (2.28).	34
2.6	Mikhailov'plot for the FO polynomial P in (2.29).	35
3.1	The closed-loop system.	36
3.2	The boundaries $\partial(N_c(j\omega) N_p(j\omega))$ and $\partial(-D_c(j\omega) D_p(j\omega))$ for $\omega > 0$, $m_D, m_N > 1$	38
3.3	The function $\psi(j\omega)$ in (3.17) for $\omega \in [-1000, 1000]$ rad/sec.	43
3.4	The values of the function $\Lambda(\omega)$ for $\omega \in [8.7154 \times 10^{-4}, 12.076]$ rad/sec.	44
3.5	The function $\psi(j\omega)$ in (3.22) for $\omega \in [-10000, 10000]$ rad/sec.	44
3.6	The auxiliary function $\Lambda(\omega)$ within $\omega \in [0, 6.3319 \times 10^8]$ rad/sec.	45
3.7	The overlap between $F_N(\omega)$ in (3.4) (dotted line) and $F_D(j\omega)$ in (3.5) (solid line) at $\omega = 5$ rad/sec.	46
3.8	The values of the functions $\psi_1(j\omega)$ in (3.28) (solid line) and $\psi_2(j\omega)$ in (3.29) (dotted line).	47
3.9	The auxiliary function $\Lambda(\omega)$ corresponding to the controller $C_1(s)$ within $\omega \in [0.0013, 6.3319 \times 10^8]$ rad/sec.	48
3.10	The auxiliary function $\Lambda(\omega)$ corresponding to the controller $C_2(s)$ within $\omega \in [0.0209, 32768]$ rad/sec.	48
3.11	The values of the function $\Xi(\omega)$ in (3.12) corresponding to the controller $C_1(s)$ in (3.26).	49
3.12	The values of the function $\Xi(\omega)$ in (3.12) corresponding to the controller $C_2(s)$ in (3.27).	49
3.13	The closed loop step responses corresponding to the controller $C_1(s)$ in (3.26).	50
3.14	The closed loop step responses corresponding to the controller $C_2(s)$ in (3.27).	50
3.15	Closed loop performance of the controllers $C_1(s)$ in (3.26) (solid line) and $C_2(s)$ in (3.27) (dotted line).	51
3.16	Output disturbance rejection by applying the controllers $C_1(s)$ in (3.26) (solid line) and $C_2(s)$ in (3.27) (dotted line).	51
4.1	Value set of $e^{-j\omega}$ and $\bar{P}_r^1(j\omega)$	61
4.2	Curve of the function $\Lambda(\omega)$ in (6.30).	63
4.3	Curve of the function $\Lambda(\omega)$ in (6.30).	63
4.4	The overlap between $D_E^{i_2}(j\omega)$ (solid line) and $N_v^{i_1}(j\omega)(\Theta_1(j\omega))^{-1}$ (dotted line) at $\omega = 6$ rad/sec.	64
4.5	The robust stability analysis of the system described in Example 4.3 by Theorem 3. 1 in [40].	65
4.6	The overlap between $D_E^{i_2}(j\omega)$ (solid line) and $N_v^{i_1}(j\omega)(\Theta_1(j\omega))^{-1}$ (dotted line) at $\omega = 1.2$ rad/sec for Example 4.3.	65
4.7	Stability analysis of $\Delta(\hat{s})$ in (4.30) by the method presented in [88].	65
4.8	Mikhailov'plot for the nominal case.	66

4.9	Output (the pitch angle).	67
4.10	Control signal.	67
4.11	Servo system of the Centre for Intelligent Systems of TalTech University. . . .	68
4.12	Mikhailov'plot for the nominal case.	69
4.13	Output (blue) and reference (red).	69
4.14	Control signal.	69
5.1	Robust stability region of PI controllers.	83
5.2	Verification of the robust PI stabilization $C(s) = 1 + \frac{0.2}{s}$ using Lemma 2.2. . .	83
5.3	Robust stability region of FOPI controllers with $\lambda = 0.5$	84
5.4	Verification of the robust FOPI stabilization $C(s) = \frac{0.5}{s^{0.5}}$ using Lemma 2.2 . .	84
5.5	Robust stability region of FOPID controllers with $\lambda = 0.5, \mu = 1$ and $K_d = 0.01$	85
5.6	Verification of the robust FOPID stabilization $C(s) = 0.1 + \frac{0.1}{s^{0.5}} + 0.01s$ using Lemma 2.2.	85
5.7	Robust stability region of FOPID controllers with $\mu = 0.65, \lambda = 1$ and $k_d = 1$. .	86
5.8	Curves of $\chi(\omega)$ corresponding to the controllers $C_1(s)$ (dashed line) and $C_2(s)$ (solid line).	86
5.9	Step responses corresponding to $C_1(s)$	87
5.10	Step responses corresponding to $C_2(s)$	87
6.1	Smith predictor control configuration [42].	90
6.2	A depiction of the consecutives vertices $\bar{P}_i(j\omega), \bar{P}_{i+1}(j\omega)$ and $\bar{P}_{i+2}(j\omega)$. . .	98
6.3	The modified Smith predictor [0, 122].	100
6.4	Set of values $\Delta_2(j\omega)$ (brown area) and the vertices $\Upsilon_i(j\omega)$	105
6.5	Two numerical solutions	107
6.6	Step responses.	107
6.7	Two numerical solutions	108
6.8	Curve of $\chi_s(\omega)$	109
6.9	Step responses.	109
6.10	The stability region of G_{cs} (green region).	110
6.11	The stability region of G_{cd} (green region).	110
6.12	Curve $H(\omega)$ for $\omega \in [0, \bar{\omega})$	110
6.13	Curve $H(\omega)$ for $\omega \in [\bar{\omega}, \omega_u]$	111
6.14	Step responses of several randomly selected members.	111
7.1	An illustration of two parpolygons with the vertices $V_i^D(j\omega)(i = 1, \dots, m_D)$ and $V_r^N(j\omega_0)(r = 1, \dots, m_N)$	116
7.2	the edges $e(-V_{i_1}^R(j\omega), -V_{i_1+1}^R(j\omega))$ (bold line), distance between the vertices $jV_{i_2}^I(j\omega)$ and the vertices $-V_{i_1}^R(j\omega)$ and $-V_{i_1+1}^R(j\omega)$ (dotted lines). . .	117
7.3	The closed-loop system.	120
7.4	The path obtained by $\Delta_0(s)$ in (6.31) when s traverses the Jordan curve. . . .	124
7.5	Curve of $\Xi(\omega)$ in (7.28) for $\omega \in [-28.09, 28.09]$ rad/sec.	124

References

- [1] M. Ezzat, A. El-Karamany, and A. El-Bary. Thermo-viscoelastic materials with fractional relaxation operators. *Applied Mathematical Modelling*, 39(23-24):7499–7512, 2015.
- [2] T. J. Freeborn, A. S. Elwakil, and B. Maundy. Compact wide frequency range fractional-order models of human body impedance against contact currents. *Mathematical Problems in Engineering*, 2016(1):4967937, 2016.
- [3] M. Ghorbani, M. Tavakoli-Kakhki, and A. A. Estarami. Robust fopid stabilization of retarded type fractional order plants with interval uncertainties and interval time delay. *Journal of the Franklin Institute*, 356(16):9302–9329, 2019.
- [4] M. Ghorbani and M. Tavakoli-Kakhki. Robust stabilizability of fractional order proportional integral controllers for fractional order plants with uncertain parameters: A new value set based approach. *Journal of Vibration and Control*, 26(11-12):965–975, 2020.
- [5] R. Mohsenipour and M. Fathi Jegarkandi. Robust-stability analysis of fractional order interval systems of commensurate and incommensurate orders. *IET Control Theory & Applications*, 13(8):1039–1050, 2019.
- [6] N. Sayyaf and M. S. Tavazoei. Robust fractional-order compensation in the presence of uncertainty in a pole/zero of the plant. *IEEE Transactions on Control Systems Technology*, 26(3):797–812, 2017.
- [7] R. Mohsenipour and M. F. Jegarkandi. Robust d-stabilization analysis of fractional-order control systems with complex and linearly dependent coefficients. *IEEE Transactions on Systems, Man, and Cybernetics: Systems*, 52(3):1823–1837, 2020.
- [8] N. Tan, Ö. F. Özgüven, and M. M. Özyetkin. Robust stability analysis of fractional order interval polynomials. *ISA transactions*, 48(2):166–172, 2009.
- [9] K. Akbari Moornani and M. Haeri. Robust stability testing function and kharitonov-like theorem for fractional order interval systems. *IET control theory & applications*, 4(10):2097–2108, 2010.
- [10] K. A. Moornani and M. Haeri. On robust stability of lti fractional-order delay systems of retarded and neutral type. *Automatica*, 46(2):362–368, 2010.
- [11] Z. Gao and X. Liao. Robust stability criterion of fractional-order functions for interval fractional-order systems. *IET Control Theory & Applications*, 7(1):60–67, 2013.
- [12] Z. Gao. Robust stabilization criterion of fractional-order controllers for interval fractional-order plants. *Automatica*, 61:9–17, 2015.
- [13] Z. Gao. An analytical method on the stabilization of fractional-order plants with one fractional-order term and interval uncertainties using fractional-order $PI^\lambda D^\mu$ controllers. *Transactions of the Institute of Measurement and Control*, 40(15):4133–4142, 2018.
- [14] R. Mohsenipour and M. Fathi Jegarkandi. Robust stability analysis of fractional-order interval systems with multiple time delays. *International Journal of Robust and Non-linear Control*, 29(6):1823–1839, 2019.

- [15] Z. Gao. Analytical method on stabilisation of fractional-order plants with interval uncertainties using fractional-order $pi^\lambda d^\mu$ controllers. *International Journal of Systems Science*, 50(5):935–953, 2019.
- [16] Z. Gao. Analytical criterion on stabilization of fractional-order plants with interval uncertainties using fractional-order pd^μ controllers with a filter. *ISA transactions*, 83:25–34, 2018.
- [17] S. Zheng, X. Tang, and B. Song. A graphical tuning method of fractional order proportional integral derivative controllers for interval fractional order plant. *Journal of Process Control*, 24(11):1691–1709, 2014.
- [18] M. Ghorbani. Robust stability analysis of interval fractional-order plants by fractional-order controllers: an approach to reduce additional calculation. *International Journal of General Systems*, 50(1):1–25, 2021.
- [19] F. Xie, Y. Chai, X. Chen, K. Zhang, and Q. Liu. Robust fractional-order PID controller design for fixed-wing UAVs through proximal-policy-optimization for disturbance rejection. *International Journal of Machine Learning and Cybernetics*, 2025:1–16, 2025.
- [20] D. Pullaguram, S. Mishra, N. Senroy, and M. Mukherjee. Design and tuning of robust fractional order controller for autonomous microgrid VSC system. *IEEE Transactions on Industry Applications*, 54(1):91–101, 2017.
- [21] B. B. Alagoz, A. Tepljakov, A. Ates, E. Petlenkov, and C. Yeroglu. Time-domain identification of one noninteger order plus time delay models from step response measurements. *International Journal of Modeling, Simulation, and Scientific Computing*, 10(1):1941011, 2019.
- [22] S. Zheng and W. Li. Stabilizing region of PD controller for fractional order system with general interval uncertainties and an interval delay. *Journal of the Franklin Institute*, 355(3):1107–1138, 2018.
- [23] C. A. Monje, Y. Chen, B. M. Vinagre, D. Xue, and V. Feliu. Tuning and auto-tuning of fractional order controllers for industry applications. *Control Engineering Practice*, 16(7):798–812, 2008.
- [24] C. Yeroglu and N. Tan. Note on fractional-order proportional–integral–differential controller design. *IET Control Theory & Applications*, 5(17):1978–1989, 2011.
- [25] A. Tepljakov, E. Petlenkov, and J. Belikov. FOPID controller tuning for fractional FOPDT plants subject to design specifications in the frequency domain. In *Proc. European Control Conference (ECC)*, pages 1502–1507, Linz, Austria, 2015.
- [26] X. Li and L. Gao. Robust Fractional-order PID Tuning Method for a Plant with an Uncertain Parameter. *International Journal of Control, Automation and Systems*, 19(3):1302–1310, 2021.
- [27] Y. Luo and Y. Q. Chen. Stabilizing and robust fractional order PI controller synthesis for first order plus time delay systems. *Automatica*, 48(9):2159–2167, 2012.
- [28] S. E. Hamamci. An algorithm for stabilization of fractional-order time delay systems using fractional-order PID controllers. *IEEE Transactions on Automatic Control*, 52(10):1964–1969, 2007.

- [29] B. Verma and P. K. Padhy. Optimal PID controller design with adjustable maximum sensitivity. *IET Control Theory & Applications*, 12(8):1156–1165, 2018.
- [30] S. Y. Chen and H. X. Huang. Design of fractional order proportional integral controller using stability and robustness criteria in time delay system. *Measurement and Control*, 52(9-10):1552–1566, 2019.
- [31] B. Şenol, U. Demiroğlu, and R. Matušů. Fractional order proportional derivative control for time delay plant of the second order: The frequency frame. *Journal of the Franklin Institute*, 357(12):7944–7961, 2020.
- [32] B. Şenol and U. Demiroğlu. Fractional order proportional derivative control for first order plus time delay plants: achieving phase and gain specifications simultaneously. *Transactions of the Institute of Measurement and Control*, 41(15):4358–4369, 2019.
- [33] S. Zhang, X. Liu, Y. Wang, Z. Liu, and D. Li. Synthesised fractional-order PD controller design for fractional-order time-delay systems based on improved robust stability surface analysis. *IET Control Theory & Applications*, 14(20):3723–3730, 2020.
- [34] R. Trivedi, B. Verma, and P. K. Padhy. Indirect optimal tuning rules for fractional order proportional integral derivative controller. *International Journal of Numerical Modelling: Electronic Networks, Devices and Fields*, 34(2):e2838, 2021.
- [35] M. Ghorbani, M. Tavakoli-Kakhki, E. Petlenkov, and J. Belikov. Robust Stability Analysis of Interval Fractional-Order Plants with Interval Time delay and General Form of Fractional-Order Controllers. *IEEE Control Systems Letters*, 2021.
- [36] Y. J. Yu and Z. H. Wang. A graphical test for the interval stability of fractional-delay systems. *Computers & Mathematics with Applications*, 62(3):1501–1509, 2011.
- [37] Z. Gao. Robust stabilization of interval fractional-order plants with one time-delay by fractional-order controllers. *Journal of the Franklin Institute*, 354(2):767–786, 2017.
- [38] M. Ghorbani and M. Tavakoli-Kakhki. Robust stability analysis of a general class of interval delayed fractional order plants by a general form of fractional order controllers. *Mathematical Methods in the Applied Sciences*, 44(13):10172–10189, 2021.
- [39] E. Yumuk. Design and performance evaluation of a novel fractional order filtered PI controller for fractional order time delay systems. *International Journal of Systems Science*, 2025:1–12, 2025.
- [40] T. Liang, J. Chen, and C. Lei. Algorithm of robust stability region for interval plant with time delay using fractional order PID controller. *Communications in Nonlinear Science and Numerical Simulation*, 17(2):979–991, 2012.
- [41] H. Hamamidian and M. T. H. Beheshti. A robust fractional-order PID controller design based on active queue management for TCP network. *International Journal of Systems Science*, 49(1):211–216, 2018.
- [42] J. E. Normey-Rico and E. F. Camacho. Dead-time compensators: A survey. *Control Engineering Practice*, 16(4):407–428, 2008.
- [43] T. H. Lee, Q. G. Wang, and K. K. Tan. Robust Smith-predictor controller for uncertain delay systems. *AIChE Journal*, 42(4):1033–1040, 1996.

- [44] R. Azarmi, A. Razminia, M. Afshari, and M. G. Sadeghi. Robustness improvement using the filtered Smith predictor based fractional integral-fractional derivative controllers: Application to a pressure plant. In *Proc. 7th International Conference on Systems and Control (ICSC)*, pages 325–330, 2018.
- [45] C. I. Pop, M. Necula, M. Radulescu, and A. Iosif. Robustness evaluation of fractional order control for varying time delay processes. *Signal, Image and Video Processing*, 6(3):453–461, 2012.
- [46] V. Feliu-Batlle and R. Rivas-Perez. Smith predictor based fractional-order integral controller for robust temperature control in a steel slab reheating furnace. *Transactions of the Institute of Measurement and Control*, 41(16):4521–4534, 2019.
- [47] M. Bettayeb, T. Ahmed, I. Draou, and K. Djamel. Smith predictor based fractional-order-filter PID controllers design for long time delay systems. *Asian Journal of Control*, 19(2):587–598, 2017.
- [48] P. R. Hemavathy, Y. Mohamed Shuaib, and S. K. Lakshmanaprabu. Design of Smith predictor based fractional controller for higher order time delay process. *Computer Modeling in Engineering Sciences*, 119(3):481–498, 2019.
- [49] N. S. Ozbek and İ. Eker. An experimental comparative study of modified Smith Predictor based fractional order controller design strategies for a time delay process. In *Proc. 4th International Conference on Electrical and Electronic Engineering (ICEEE)*, pages 340–345, 2017.
- [50] P. K. Bhamre and C. B. Kadu. Design of a Smith predictor based fractional order PID controller for a coupled tank system. In *Proc. 2016 International Conference on Automatic Control and Dynamic Optimization Techniques (ICACDOT)*, pages 1062–1067. IEEE, 2016.
- [51] R. Azarmi, A. Razminia, M. Afshari, and A. Tabesh. Design and implementation of Smith predictor based fractional order PID controller on MIMO flow-level plant. In *Proc. 23rd Iranian Conference on Electrical Engineering (ICEE)*, pages 1096–1101. IEEE, 2015.
- [52] P. Singha, S. Chakraborty, and U. Mehta. Fractional-Order Tilt and Smith Predictor Scheme for Non-Minimum Phase Processes. *Optimal Control Applications and Methods*, <https://doi.org/10.1002/oca.3303>, 2025.
- [53] P. Singha, R. Meena, and S. Chakraborty. 2-DOF fractional-order control for delay-dominant industrial processes with experimental validation. *International Journal of Dynamics and Control*, 13(2):72, 2025.
- [54] S. Singh, V. K. Tayal, H. P. Singh, and V. K. Yadav. Design of PSO-tuned FOPI & Smith predictor controller for nonlinear polymer electrolyte membrane fuel cell. *Energy Sources, Part A: Recovery, Utilization, and Environmental Effects*, 47(2):2025954, 2025.
- [55] A. Yonezawa, H. Yonezawa, S. Yahagi, I. Kajiwara, and S. Kijimoto. Fractional-order controller tuning via minimization of integral of time-weighted absolute error without multiple closed-loop tests. *Asian Journal of Control*, <https://doi.org/10.1002/asjc.3788>, 2025.

- [56] C. I. Muresan, M. D. Mihai, E. Hegedus, N. Badau, T. Popescu, and I. R. Birs. Robust fractional order control of a multivariable hemodynamic system. In *Proc. 33rd Mediterranean Conference on Control and Automation (MED)*, pages 678–683. IEEE, 2025.
- [57] E. Khatoonabadi, V. Bohlouri, and A. R. Kosari. Using a fractional-order controller to improve the performance of a spacecraft attitude control in the presence of uncertainties and disturbances. *Proc. Inst. Mech. Eng., Part G: J. Aerospace Eng.*, page 09544100251342544. SAGE, 2025.
- [58] S. Wang, P. Huang, Y. Luo, X. Wang, and X. Luo. A fractional-order ADRC with improved robustness to plant gain variations. *IEEE Trans. Ind. Electron.*, 2025, DOI: 10.1109/TIE.2025.3552274.
- [59] V. Feliu-Batlle, J. M. Maestre, R. Rivas-Pérez, and J. M. Montes. Smith predictor based robust fractional order control: Application to water distribution in a main irrigation canal pool. *Journal of Process Control*, 19(3):506–519, 2009.
- [60] R. Xin, J. Xu, H. Cai, and Y. Yang. The design of FOPI and FO[PI] controllers for large time-delay system based on Smith Predictor. In *Proc. 2016 IEEE Chinese Guidance, Navigation and Control Conference (CGNCC)*, pages 2357–2361. IEEE, 2016.
- [61] M. Safaei and S. Tavakoli. Smith predictor based fractional-order control design for time-delay integer-order systems. *International Journal of Dynamics and Control*, 6(1):179–187, 2018.
- [62] C. Hu, J. Bai, and H. Zou. A new design of predictive plus PID control for second order plus time delay systems. *The Canadian Journal of Chemical Engineering*, 103(7):3230–3246, 2025.
- [63] Y. Zeng, Q. Yang, Y. Lin, Y. Chen, X. Chen, and J. Wen. Fractional-order virtual inertia control and parameter tuning for energy-storage system in low-inertia power grid. *Prot. Control Mod. Power Syst.*, 9(5):70–83. PSPC, 2024.
- [64] S. Chakraborty, D. Das, A. K. Naskar, and S. Ghosh. Frequency loop-shaping and IMC-based integer-order robust PID controller design for fractional-order processes with time-delay. *IETE J. Res.*, 70(10):7820–7830. Taylor & Francis, 2024.
- [65] K. Gnaneshwar, V. Kumar, S. Sharma, and P. K. Padhy. Non-parametric fractional-order controller design for stable process based on modified relay. *J. Control Decis.*, 11(4):590–602. Taylor & Francis, 2024.
- [66] D. K. Gupta, G. Dei, A. K. Soni, A. V. Jha, B. Appasani, N. Bizon, A. Srinivasulu, and P. Nsengiyumva. Fractional order PID controller for load frequency control in a deregulated hybrid power system using Aquila Optimization. *Results Eng.*, 23:102442. Elsevier, 2024.
- [67] R. J. Minnichelli, J. J. Anagnost, and C. A. Desoer. An elementary proof of Kharitonov's stability theorem with extensions. *IEEE Transactions on Automatic Control*, 34(9):995–998, 1989.
- [68] F. L. Janssens and J. C. van der Ha. Stability of spinning satellite under axial thrust, internal mass motion, and damping. *Journal of Guidance, Control, and Dynamics*, 38(4):761–771, 2015.

- [69] F. L. Janssens and J. C. van der Ha. Stability of spinning satellite under axial thrust and internal mass motion. *Acta Astronautica*, 94(1):502–514, 2014.
- [70] Y. Ren and J. Fang. Complex-coefficient frequency domain stability analysis method for a class of cross-coupled antisymmetrical systems and its extension in MSR systems. *Mathematical Problems in Engineering*, 2014: Article ID 737915, 2014.
- [71] J. Wei, K. Liu, and G. Radice. Study on stability and rotating speed stable region of magnetically suspended rigid rotors using extended Nyquist criterion and gain-stable region theory. *ISA Transactions*, 66:154–163, 2017.
- [72] P. Sathishkumar and N. Selvaganesan. Fractional controller tuning expressions for a universal plant structure. *IEEE Control Systems Letters*, 2(3):345–350, 2018.
- [73] P. Sathishkumar and N. Selvaganesan. Tuning of complex coefficient PI/PD/PID controllers for a universal plant structure. *International Journal of Control*, 94(11):3190–3212, 2021.
- [74] S. Zheng, X. Tang, and B. Song. Graphical tuning method of FOPID controllers for fractional order uncertain system achieving robust-stability. *International Journal of Robust and Nonlinear Control*, 26(5):1112–1142, 2016.
- [75] R. Mohsenipour and M. F. Jegarkandi. A comment on “Algorithm of robust stability region for interval plant with time delay using fractional order PID controller” [Commun Nonlinear Sci Numer Simulat 17 (2012) 979–991]. *Communications in Nonlinear Science and Numerical Simulation*, 63:202–204, 2018.
- [76] A. Tepljakov, E. Petlenkov, and J. Belikov. FOMCON toolbox for modeling, design and implementation of fractional-order control systems. In *Volume 6 Applications in Control*, pages 211–236. De Gruyter, 2019.
- [77] D. Baleanu, K. Diethelm, E. Scalas, and J. J. Trujillo. Fractional calculus: models and numerical methods. In *World Scientific*, 2012.
- [78] C. Ionescu, A. Lopes, D. Copot, J. T. Machado, and J. H. Bates. The role of fractional calculus in modeling biological phenomena: A review. *Communications in Nonlinear Science and Numerical Simulation*, 51:141–159, 2017.
- [79] C. A. Monje, Y. Chen, B. M. Vinagre, D. Xue, and V. Feliu-Batlle. Fractional-order systems and controls: fundamentals and applications. *Springer Science & Business Media*, 2010.
- [80] H. Abdelfattah, A. O. Aseeri, and M. Abd Elaziz. Optimized FOPID controller for nuclear research reactor using enhanced planet optimization algorithm. *Alexandria Engineering Journal*, 97:267–282, 2024.
- [81] Z. Jiang, X. Zhang, and G. Liu. Trajectory tracking control of a 6-DOF robotic arm based on improved FOPID. *International Journal of Dynamics and Control*, 13(4):137, 2025.
- [82] P. Jeba and A. Immanuel Selvakumar. FOPID based MPPT for photovoltaic system. *Energy Sources, Part A: Recovery, Utilization, and Environmental Effects*, 40(13):1591–1603, 2018.

- [83] H. M. Paiva, W. S. Keller, and L. G. da Cunha. Blood-glucose regulation using fractional-order PID control. *Journal of Control, Automation and Electrical Systems*, 31(1):1–9, 2020.
- [84] M. J. Mohamed and A. Khashan. Comparison between PID and FOPID controllers based on particle swarm optimization. In *Proceedings of the Second Engineering Conference of Control, Computers and Mechatronics Engineering (ECCCM2)*, 2014.
- [85] Z. Bingul and O. Karahan. Comparison of PID and FOPID controllers tuned by PSO and ABC algorithms for unstable and integrating systems with time delay. *Optimal Control Applications and Methods*, 39(4):1431–1450, 2018.
- [86] O. F. Nami, A. Widaryanto, M. P. Rasuanta, T. Pramudya, M. Y. Firdaus, P. L. Widadati, S. P. Anggraeni, H. Dwiyantri, M. Rahmadiansyah, M. A. Purwoadi, and S. Rahardjo. Performance comparison of PID, FOPID, and NN-PID controller for AUV steering problem. *Jurnal Elektronika dan Telekomunikasi*, 24(1):72–79, 2024.
- [87] C. Bonnet and J. R. Partington. Coprime factorizations and stability of fractional differential systems. *Systems & Control Letters*, 41(3):167–174, 2000.
- [88] M. Busłowicz. Stability of linear continuous-time fractional order systems with delays of the retarded type. *Bulletin of the Polish Academy of Sciences: Technical Sciences*, 56(4), 2008.
- [89] D. Bouagada, S. Melchior, and P. Van Dooren. Calculating the H^∞ norm of a fractional system given in state-space form. *Applied Mathematics Letters*, 79:51–57, 2018.
- [90] P. Badri and M. Sojoodi. Robust stabilisation of fractional-order interval systems via dynamic output feedback: an LMI approach. *International Journal of Systems Science*, 50(9):1718–1730, 2019.
- [91] M. Tavakoli-Kakhki and M. Haeri. Temperature control of a cutting process using fractional order proportional-integral-derivative controller. *Journal of Dynamic Systems, Measurement, and Control*, 133(5):051014, 2011.
- [92] R. Sumathi and P. Umasankar. Optimal design of fractional order PID controller for time-delay systems: an IWLQR technique. *International Journal of General Systems*, 47(7):714–730, 2018.
- [93] Z. Gao. An analytical method on the stabilization of fractional-order plants with one fractional-order term and interval uncertainties using fractional-order $PI^\lambda D^\mu$ controllers. *Transactions of the Institute of Measurement and Control*, 40(15):4133–4142, 2018.
- [94] Z. Gao. Robust stabilization criterion of fractional-order controllers for interval fractional-order plants. *Automatica*, 61:9–17, 2015.
- [95] Z. Gao. Analytical criterion on stabilization of fractional-order plants with interval uncertainties using fractional-order PD^μ controllers with a filter. *ISA Transactions*, 83:25–34, 2018b.
- [96] W. S. Levine. The Control Handbook (three volume set). *CRC Press*, 2018.
- [97] J. W. Brown, R. V. Churchill, et al. Complex Variables and Applications. *McGraw-Hill Higher Education*, Boston, 2009.

- [98] A. Oustaloup, F. Levron, B. Mathieu, and F. M. Nanot. Frequency-band complex non-integer differentiator: Characterization and synthesis. *IEEE Transactions on Circuits and Systems I: Fundamental Theory and Applications*, 47(1):25–39, 2000.
- [99] A. Oustaloup, F. Levron, B. Mathieu, and F. M. Nanot. Frequency-band complex non-integer differentiator: Characterization and synthesis. *IEEE Transactions on Circuits and Systems I: Fundamental Theory and Applications*, 47(1):25–39, 2000.
- [100] A. Tepljakov, B. B. Alagoz, C. Yeroglu, E. A. Gonzalez, S. H. Hosseinnia, E. Petlenkov, A. Ates, and M. Cech. Towards industrialization of FOPID controllers: A survey on milestones of fractional-order control and pathways for future developments. *IEEE Access*, 9:21016–21042, 2021.
- [101] C. A. Monje, B. M. Vinagre, V. Feliu, and Y. Chen. Tuning and auto-tuning of fractional order controllers for industry applications. *Control Engineering Practice*, 16(7):798–812, 2008.
- [102] C. Yeroglu and N. Tan. Note on fractional-order proportional-integral-differential controller design. *IET Control Theory & Applications*, 5(17):1978–1989, 2011.
- [103] C. Yeroglu and N. Tan. Note on fractional-order proportional-integral-differential controller design. *IET Control Theory & Applications*, 5(17):1978–1989, 2011.
- [104] Y. Luo and Y. Chen. Stabilizing and robust fractional order PI controller synthesis for first-order plus time delay systems. *Automatica*, 48(9):2159–2167, 2012.
- [105] S. E. Hamamci. An algorithm for stabilization of fractional-order time delay systems using fractional-order PID controllers. *IEEE Transactions on Automatic Control*, 52(10):1964–1969, 2007.
- [106] B. Verma and P. K. Padhy. Optimal PID controller design with adjustable maximum sensitivity. *IET Control Theory & Applications*, 12(8):1156–1165, 2018.
- [107] B. Şenol, U. Demiroğlu, and R. Matušů. Fractional order proportional derivative control for time delay plant of the second order: The frequency frame. *Journal of the Franklin Institute*, 357(12):7944–7961, 2020.
- [108] R. Trivedi and P. K. Padhy. Fractional order automatic tuning of PI λ D controller for stable processes. *ISA Transactions*, 99:351–360, 2020.
- [109] Y. Yu and Z. Wang. A graphical test for the interval stability of fractional-delay systems. *Computers & Mathematics with Applications*, 62(3):1501–1509, 2011.
- [110] Z. Gao. Robust stabilization of interval fractional-order plants with one time-delay by fractional-order controllers. *Journal of the Franklin Institute*, 354(2):767–786, 2017.
- [111] M. Ghorbani and M. Tavakoli-Kakhki. Robust stability analysis of a general class of interval delayed fractional order plants by a general form of fractional order controllers. *Mathematical Methods in the Applied Sciences*, 44(13):10172–10189, 2021.
- [112] N. Tan. Computation of the frequency response of multilinear affine systems. *IEEE Transactions on Automatic Control*, 47(10):1691–1696, 2002.
- [113] L. Ljung. *System Identification Toolbox: User's Guide*. Citeseer, 1995.

- [114] J. E. Normey-Rico and E. F. Camacho. Dead-time compensators: A survey. *Control Engineering Practice*, 16(4):407–428, 2008.
- [115] J. Lam, H. Gao, and C. Wang. Stability analysis for continuous systems with two additive time-varying delay components. *Systems & Control Letters*, 56(1):16–24, 2007.
- [116] O. J. Smith. Closer control of loops with dead time. *Chemical Engineering Progress*, 53:217–219, 1957.
- [117] Z. Palmor and M. Blau. An auto-tuner for Smith dead time compensator. *International Journal of Control*, 60(1):117–135, 1994.
- [118] V. De Oliveira, A. Nicoletti, and A. Karimi. Robust Smith predictor design for time-delay systems with H_∞ performance. In *Recent Results on Time-Delay Systems: Analysis and Control*, pages 287–307. Springer, 2016.
- [119] F. N. Deniz, N. Tan, S. E. Hamamci, and I. Kaya. Stability region analysis in Smith predictor configurations using a PI controller. *Transactions of the Institute of Measurement and Control*, 37(5):606–614, 2015.
- [120] S. P. Bhattacharyya and L. H. Keel. Robust control: the parametric approach. In *Advances in Control Education 1994*, pages 49–52. Pergamon, 1995.
- [121] K. C. Karanam, S. Selvanathan, and S. R. Ambati. Modified Smith predictor design for unstable processes with step and periodic disturbances. *Proceedings of the Institution of Mechanical Engineers, Part I: Journal of Systems and Control Engineering*, 227(2):146–160, 2013.
- [122] S. Uma and A. S. Rao. Enhanced modified Smith predictor for second-order non-minimum phase unstable processes. *International Journal of Systems Science*, 47(4):966–981, 2016.
- [123] S. Uma and A. Seshagiri Rao. Enhanced modified Smith predictor for second-order non-minimum phase unstable processes. *International Journal of Systems Science*, 47(4):966–981, 2016.
- [124] M. Ajmeri and A. Ali. Analytical design of modified Smith predictor for unstable second-order processes with time delay. *International Journal of Systems Science*, 48(8):1671–1681, 2017.
- [125] S. Karan and C. Dey. IMC based modified Smith predictor for second order delay dominated processes with RHP. *ISA Transactions*, 142:254–269, 2023.
- [126] M. Marden. *Geometry of Polynomials*. No. 3, American Mathematical Society, 1949.
- [127] J. Wei, K. Liu, and G. Radice. Study on stability and rotating speed stable region of magnetically suspended rigid rotors using extended Nyquist criterion and gain-stable region theory. *ISA Transactions*, 66:154–163, 2017.
- [128] Y. Ren and J. Fang. Complex-coefficient frequency domain stability analysis method for a class of cross-coupled antisymmetrical systems and its extension in MSR systems. *Mathematical Problems in Engineering*, 2014. <https://doi.org/10.1155/2014/765858>.

Acknowledgements

With the completion of this thesis, I am drawing to a close one of the most significant chapters of my life. This journey, though marked by many highs and lows, has been deeply transformative. I am profoundly grateful—not only for the scientific growth it has fostered, but even more so for the personal evolution it has inspired. These past four years have been anything but ordinary for a PhD student; In light of this, I wish to take a moment to honor and thank all those who stood by me, whose support, encouragement, and presence made this work—and this journey—possible.

My sincere gratitude goes first and foremost to my supervisors, Prof. Eduard Petlenkov and Dr. Aleksei Teplyakov. Their unwavering guidance, insightful feedback, and constant encouragement have been instrumental throughout this journey. Their mentorship not only shaped the direction of this research but also helped me grow as an independent thinker and researcher. I am truly fortunate to have had the opportunity to learn from their expertise and to walk this path under their thoughtful supervision.

I would like to extend my heartfelt thanks to Prof. Guillaume Crevecoeur, Dr. Arash Farnam, Prof. Patrick Gruber, and Dr. Umberto Montanaro for giving me the invaluable opportunity to join their research groups as a visiting PhD student at Ghent University and the University of Surrey. Working with them on diverse topics in control engineering broadened my academic perspective and allowed me to gain a wealth of knowledge and experience for which I am truly grateful.

Last but certainly not least, I am deeply grateful to my family—my parents, my brothers, and my sisters. My heartfelt thanks go to them for standing by my side since childhood, for their boundless love and unwavering support, and for enduring the many days of my absence from home with patience and understanding. Their presence, even from afar, has been a constant source of strength throughout this journey.

I also wish to express my sincere appreciation to my homeland, Iran—a country whose rich cultural and scientific heritage has always inspired me to pursue knowledge with passion and purpose. It is from this soil that my curiosity took root and my academic journey began. As the timeless adage goes, "Seek knowledge from the cradle to the grave"—a philosophy deeply embedded in Iranian culture and one that continues to guide my path.

Finally, I wish happiness and success to all my esteemed professors who have supported me throughout my studies by enhancing my knowledge and insight.

"Twenty years from now you will be more disappointed by the things you didn't do than by the ones you did. So throw off the bowlines. Sail away from the safe harbor. Catch the trade winds in your sails. Explore. Dream. Discover."

— Mark Twain

Abstract

Robust Stability Analysis of Fractional-Order Control Systems

The objective of this thesis is the research and development of advanced methods for the robust stability analysis of fractional-order control systems, which are increasingly employed in modern control applications due to their superior modeling capabilities and design flexibility. The study focuses on addressing the challenges posed by system uncertainties, time delays, and the non-integer nature of system dynamics, which complicate traditional stability analysis techniques. To this end, novel analytical and graphical approaches are proposed to assess and guarantee the stability of closed-loop fractional-order systems under structured uncertainties. Special attention is given to implementable and computationally efficient techniques that allow for the construction of stability regions in the controller parameter space, facilitating the robust tuning of fractional-order controllers such as FOPID. The developed methods are capable of handling interval uncertainties and delay variations that commonly arise in practical systems. Several case studies and simulation results are provided to validate the effectiveness of the proposed approaches, demonstrating their potential for real-world implementation in uncertain and complex control scenarios. By extending classical stability concepts to the fractional-order domain and providing systematic tools for robust controller design, this thesis contributes to the theoretical foundation and practical advancement of robust control strategies for next-generation dynamical systems.

Kokkuvõte

Murrulistel tuletistel põhinevate juhtimissüsteemide robustse stabiilsuse analüüs

Selle doktoritöö eesmärgiks on arendada uusi meetodeid murrulistel tuletistel põhinevate juhtimissüsteemide robustse stabiilsuse analüüsiks. Murrulistel tuletistel põhinevaid mudeleid kasutatakse tänapäevastes juhtimissüsteemides üha enam tänu nende paremale modelleerimisvõimele ja paindlikkusele juhtimissüsteemide projekteerimisel. Töö keskendub probleemidele, mis on seotud süsteemide määramatuse, hilineamise ja murruliste tuletistega modelleeritava dünaamika eripäradega, mis raskendavad traditsiooniliste meetodite rakendamist stabiilsuse analüüsis. Töö raames on välja pakutud uued analüütilised ja graafilised lähenemised, mis võimaldavad hinnata ja tagada murrulistel tuletistel põhinevate suletud ahelaga süsteemide stabiilsust struktuurse määramatuse tingimustes. Eri tähelepanu pööratakse rakendatavatele ja arvutuslikult tõhusatele meetoditele, mis võimaldavad määrata juhtimissüsteemi parameetrite stabiilsuspiirkonnad ning hõlbustavad robustset FOPID-tüüpi regulaatorite häälestamist. Väljatöötatud meetodid suudavad käsitleda intervall- määramatust ja hilineamise varieeruvust, mis esinevad sageli reaalses maailmas. Töö sisaldab mitmeid juhtumiuuringuid ja simulatsioone, mis kinnitavad pakutud lähenemiste tõhusust ning nende rakendatavust ebakindlates ja keerukates juhtimissituatsioonides. Laiendades klassikalisi stabiilsuskontseptsioone murrulistel tuletistel põhinevate süsteemidele ja pakkudes süsteemseid tööriistu robustse regulaatorite projekteerimise jaoks, annab see doktoritöö olulise panuse nii teoreetilisse kui ka praktilisse arengusse kaasaegsete juhtimissüsteemide valdkonnas.

Appendix 1

I

M. Ghorbani, A. Tepljakov, and E. Petlenkov. On robust stability of uncertain control systems with time delay: an approach based on the overlap of value sets. *IEEE Transactions on Automatic Control*, 69(9):6349–6356, 2024.

On Robust Stability of Uncertain Control Systems With Time Delay: An Approach Based on the Overlap of Value Sets

Majid Ghorbani¹, Graduate Student Member, IEEE, Aleksei Teplyakov², Senior Member, IEEE, and Eduard Petlenkov³, Member, IEEE

Abstract—This study provides some methods to analyze robust stabilizability of uncertain plants with an uncertain time delay using arbitrary linear controllers. In this work, an uncertain plant with an uncertain time delay means that the numerator and denominator coefficients and the time delay term of the transfer function of the plant have interval uncertainties. Towards solving the above-mentioned problem, first, robust stability is investigated for the closed-loop system in terms of a general class of linear controllers and uncertain plants with an uncertain time delay. Then, by using some interesting geometric features, a robust stability checking function and frequency bounds are provided to improve the computational efficiency of robust stability analysis. Furthermore, due to the widespread industrial use of the well-known proportional–integral–derivative (PID) controller structure, the robust stability region of PID controllers has been determined for an uncertain plant with an uncertain time delay. Finally, two numerical examples are given to verify the obtained results.

Index Terms—Delay systems, interval time delay, real parametric uncertainties, robust controllers.

I. INTRODUCTION

When industrial control problems are concerned, it is universally acknowledged that a time delay—also referred to as *transport delay* and *dead time* in various studies—is a crucial parameter that fundamentally affects the operation of the control system and thus, must be thoroughly considered when modeling real-life systems [1], [2]. Moreover, the time delay of the system may not be fixed, i.e., it can change during the operation of the real system deviating from a given nominal value [3]. Therefore, one should consider the uncertainty in the time delay to ensure the validity of robust stability analysis. Accordingly, the study of this problem has received considerable attention recently.

In this study, we are particularly concerned with the robust stability analysis of a closed-loop control system in terms of linear controllers and uncertain plants with an uncertain time delay. The uncertainties are represented with numerical intervals which also contain the nominal values of the model parameters.

Manuscript received 19 October 2023; accepted 15 March 2024. Date of publication 26 March 2024; date of current version 29 August 2024. This work was supported in part by the European Union's Horizon Europe research and innovation programme under Grant 101120657, in part by project ENFIELD (European Lighthouse to Manifest Trustworthy and Green AI), in part by the Estonian Research Council through under Grant PRG658, and in part by the Estonian Centre of Excellence in Energy Efficiency, ENER under Grant TK230 funded by the Estonian Ministry of Education and Research. Recommended by Associate Editor A. Chaillet. (Corresponding author: Majid Ghorbani.)

The authors are with the Department of Computer Systems, Tallinn University of Technology, 19086 Tallinn, Estonia (e-mail: majid.ghorbani@taltech.ee; aleksei.teplyakov@taltech.ee; eduard.petlenkov@taltech.ee).

Digital Object Identifier 10.1109/TAC.2024.3381912

Many different approaches for improving the robustness of control systems have been proposed to date in scientific literature. For instance, in [4], [5], [6], [7], and [8], based on gain and phase margins, various methods have been proposed to tune proportional–integral–derivative (PID) controllers for unstable and stable systems having time delay. However, satisfying the gain and phase margins may not be a reliable method for uncertain systems.

Some numerical nonlinear optimization methods have been proposed to design PID controllers in [9] and [10]. In order to improve the robustness of PID and PI controllers, a flat phase constraint has been satisfied in [11] and [12]. In [13], [14], and [15], the D-composition method was employed to find a set of PID controllers stabilizing the delayed systems. However, the proposed methods cannot robustly stabilize the closed-loop control system in the face of plant uncertainties.

For systems having fixed delays, the continuous pole placement has been presented in [16], [17], [18], and [19]. However, it is worth once again emphasizing that the methods proposed in the aforementioned papers cannot be applied to time delays with an interval uncertainty. Consequently, the problem of tuning a robust controller for systems in the presence of uncertain time delay in the system has attracted many researchers. Varied procedures have been proposed to design robust controllers using pole placement strategy and finding the delay margin by which the system robustly remains stable. For instance, in [20] and [21], two different methods were proposed to calculate the delay margin of unstable systems. Also, in the works [22] and [23], robust PID controllers have been designed for systems having interval time delays; however, there is a shortcoming such that the cited methods cannot be employed for systems that simultaneously have uncertainties in the time delay and numerators and denominator coefficients.

Motivated by the previous works, in this study, some methods are developed to investigate the robust stability of plants having uncertainties in the numerator and denominator coefficients and the time delay term using linear controllers. Since the numerator and denominator coefficients and the time delay term are assumed to be unknown and lying in specified intervals, typical methods in robust stability analysis such as Kharitonov's theorem are not applicable, and the present work aims to close this research gap. The contributions and novelties of this study are as follows.

- 1) An approach to finding a test frequency interval instead of the infinite frequency range is proposed.
- 2) The necessary and sufficient conditions of robustness for control systems involving uncertain delayed plants with controllers are derived. The controllers are assumed to have a general transfer function form.
- 3) A robust stability checking function for robust stability analysis of the closed-loop control system is presented.

The rest of this article is organized as follows. Section II covers control system preliminaries and background on the value set concept. Section III introduces two new methods for checking robust stability in systems with uncertain time delays. Moreover, in Section IV, the

robust stability region of PID controllers has been calculated. Next, in Section V, simulation results are presented to demonstrate the validity of the proposed approaches. A comprehensive comparison with existing works has been conducted in Section VI. Finally, Section VII concludes this article.

II. BACKGROUND AND PRELIMINARIES

Notations: Define $A \setminus B \triangleq \{x \mid x \in A, x \notin B\}$ for any two sets A and B. Assume $\sum_{i=k_1}^{k_2} f_i = 0$ for $k_2 < k_1$ where f_i , ($i = k_1, \dots, k_2$) are scalar functions. We use $\partial(X)$ to denote the boundary of the value set of X . For two arbitrary polynomials X and Y , we have $e(X, Y) = \eta X + (1 - \eta)Y$, $\eta \in [0, 1]$.

Consider the transfer function of a controller denoted by $C(s)$ that has the form

$$C(s) = \frac{N_C(s)}{D_C(s)} = \frac{\sum_{i_1=0}^{m_C} b_{i_1}^C s^{i_1}}{\sum_{i_2=0}^{n_C} a_{i_2}^C s^{i_2}} \quad (1)$$

where the coefficients $b_{i_1}^C$ and $a_{i_2}^C$ are real numbers. Furthermore, consider a plant described by an uncertain transfer function with an uncertain time delay that has the following form:

$$\mathbf{P}(s) = \frac{\mathbf{N}_P(s)}{\mathbf{D}_P(s)} e^{-Ls} = \frac{\sum_{i_1=0}^{m_P} b_{i_1}^P s^{i_1}}{\sum_{i_2=0}^{n_P} a_{i_2}^P s^{i_2}} e^{-Ls} \quad (2)$$

in which the numerator and denominator coefficients of the plant are subjected to $b_{i_1}^P \in [\underline{b}_{i_1}^P, \bar{b}_{i_1}^P]$ ($b_{m_P}^P \neq 0$) and $a_{i_2}^P \in [\underline{a}_{i_2}^P, \bar{a}_{i_2}^P]$ ($a_{n_P}^P \neq 0$) and the time delay L lies in $L \in [\underline{L}, \bar{L}]$ and $n_P + n_C > m_P + m_C$. Moreover, in this study, it is assumed that the quasi-polynomial (3) indicates the characteristic function of the negative unity feedback control system and is of the following form:

$$\Delta(s) = D_C(s) \mathbf{D}_P(s) + N_C(s) \mathbf{N}_P(s) e^{-Ls}. \quad (3)$$

Definition 1: Based on [24] and Kharitonov's theorem, in the complex plane, the value sets of $\mathbf{N}_P(s)$ and $\mathbf{D}_P(s)$ are two rectangles for $s = j\omega$ and $\omega > 0$. In this article, the vertex polynomials corresponding to $\mathbf{N}_P(s)$ and $\mathbf{D}_P(s)$ are respectively, considered as $V_{i_1}^N(s)$ ($i_1 = 1, 2, 3, 4$) and $V_{i_2}^D(s)$ ($i_2 = 1, 2, 3, 4$) as follows:

$$\begin{cases} V_1^N(s) = \underline{b}_0^P + \underline{b}_0^P s + \bar{b}_0^P s^2 + \bar{b}_0^P s^3 + \dots, \\ V_2^N(s) = \bar{b}_0^P + \underline{b}_0^P s + \underline{b}_0^P s^2 + \bar{b}_0^P s^3 + \dots, \\ V_3^N(s) = \bar{b}_0^P + \bar{b}_0^P s + \underline{b}_0^P s^2 + \underline{b}_0^P s^3 + \dots, \\ V_4^N(s) = \underline{b}_0^P + \bar{b}_0^P s + \bar{b}_0^P s^2 + \underline{b}_0^P s^3 + \dots. \end{cases} \quad (4)$$

$$\begin{cases} V_1^D(s) = \underline{a}_0^P + \underline{a}_0^P s + \bar{a}_0^P s^2 + \bar{a}_0^P s^3 + \dots, \\ V_2^D(s) = \bar{a}_0^P + \underline{a}_0^P s + \underline{a}_0^P s^2 + \bar{a}_0^P s^3 + \dots, \\ V_3^D(s) = \bar{a}_0^P + \bar{a}_0^P s + \underline{a}_0^P s^2 + \underline{a}_0^P s^3 + \dots, \\ V_4^D(s) = \underline{a}_0^P + \bar{a}_0^P s + \bar{a}_0^P s^2 + \underline{a}_0^P s^3 + \dots. \end{cases} \quad (5)$$

Before concluding this section, consider also an important property of the value sets that is introduced by Lemma 1.

Lemma 1: Let Q_1 and $Q_2 \neq 0$ be two complex plane polygons, then, $\partial(\frac{Q_1}{Q_2}) \subset (\frac{V_{Q_1}}{E_{Q_2}}) \cup (\frac{E_{Q_1}}{V_{Q_2}})$ where ∂ shows the boundary and V_{Q_i} and E_{Q_i} are, respectively, the vertex sets and the edge sets of Q_i [25].

Definition 2: Assume that the value sets of $\Xi_i(j\omega)$, $i = 1, 2$ are closed and bounded in the complex plane. If $\partial(\Xi_1(j\omega))$ and $\partial(\Xi_2(j\omega))$ have no overlap at a given frequency in the complex plane, then, it means that there is no common complex/real numbers in their value sets.

III. MAIN RESULTS

A. Robust Stability Analysis

Based on the zero exclusion principle, for $\omega \geq 0$, the condition $0 \notin \Delta(j\omega)$ must be checked. Hence, in the following theorem a finite frequency range is obtained to check the condition $0 \notin \Delta(j\omega)$.

Theorem 1: The zero exclusion condition $0 \notin \Delta(j\omega)$ is held for the frequency range $\omega \in [0, \infty) \setminus [S_{\min}, S_{\max}]$ in which

$$\begin{aligned} S_{\max} &= \max\{\sigma_{\max}, 1\}, \\ \sigma_{\max} &= \frac{\sigma_{\max}^1 + \sigma_{\max}^2 + \sigma_{\max}^3 + \sigma_{\max}^4}{\sigma_{\max}^5}, \\ \sigma_{\max}^1 &= \left(\sum_{i^2=0}^{n_C-1} |a_{i^2}^C| \right) \left(\sum_{i^2=0}^{n_P-1} \max\{|\underline{a}_{i^2}^P|, |\bar{a}_{i^2}^P|\} \right), \\ \sigma_{\max}^2 &= |a_{n_C}^C| \left(\sum_{i^2=0}^{n_P-1} \max\{|\underline{a}_{i^2}^P|, |\bar{a}_{i^2}^P|\} \right), \\ \sigma_{\max}^3 &= \max\{|\underline{a}_{n_P}^P|, |\bar{a}_{n_P}^P|\} \left(\sum_{i^2=0}^{n_C-1} |a_{i^2}^C| \right), \\ \sigma_{\max}^4 &= \left(\sum_{i_1=0}^{m_C} |b_{i_1}^C| \right) \left(\sum_{i_1=0}^{m_P} \max\{|\underline{b}_{i_1}^P|, |\bar{b}_{i_1}^P|\} \right), \\ \sigma_{\max}^5 &= |a_{n_C}^C| \min\{|\underline{a}_{n_P}^P|, |\bar{a}_{n_P}^P|\}. \end{aligned} \quad (6)$$

$$\begin{aligned} S_{\min} &= \min\{\sigma_{\min}, 1\}, \\ \sigma_{\min} &= \frac{\kappa}{\sigma_{\min}^1 + \sigma_{\min}^2 + \sigma_{\min}^3 + \sigma_{\min}^4 + \sigma_{\min}^5 + \sigma_{\min}^6}, \\ \sigma_{\min}^1 &= \left(\sum_{i^1=1}^{n_C} |a_{i^1}^C| \right) \left(\sum_{i^2=1}^{n_P} \max\{|\underline{a}_{i^2}^P|, |\bar{a}_{i^2}^P|\} \right), \\ \sigma_{\min}^2 &= \max\{|\underline{a}_0^P|, |\bar{a}_0^P|\} \left(\sum_{i^1=1}^{n_C} |a_{i^1}^C| \right), \\ \sigma_{\min}^3 &= |a_0^C| \left(\sum_{i^2=1}^{n_P} \max\{|\underline{a}_{i^2}^P|, |\bar{a}_{i^2}^P|\} \right), \\ \sigma_{\min}^4 &= \left(\sum_{j^1=1}^{m_C} |b_{j^1}^C| \right) \left(\sum_{j^2=1}^{m_P} \max\{|\underline{b}_{j^2}^P|, |\bar{b}_{j^2}^P|\} \right), \\ \sigma_{\min}^5 &= |b_0^C| \left(\sum_{j^2=1}^{m_P} \max\{|\underline{b}_{j^2}^P|, |\bar{b}_{j^2}^P|\} \right), \end{aligned} \quad (7)$$

$$\sigma_{\min}^6 = \max\{|\underline{b}_0^P|, |\bar{b}_0^P|\} \left(\sum_{j^1=1}^{m_C} |b_{j^1}^C| \right),$$

$$\kappa = \begin{cases} \kappa_1, & \text{for } 0 \notin [\underline{a}_0^P, \bar{a}_0^P] \text{ and } \kappa_1 > 0, \\ \kappa_2, & \text{for } 0 \notin [\underline{b}_0^P, \bar{b}_0^P] \text{ and } \kappa_2 > 0, \\ 0, & \text{otherwise,} \end{cases}$$

$$\kappa_1 = \min\{|\underline{a}_0^P|, |\bar{a}_0^P|\} |a_0^C| - \max\{|\underline{b}_0^P|, |\bar{b}_0^P|\} |b_0^C|,$$

$$\kappa_2 = \min\{|\underline{b}_0^P|, |\bar{b}_0^P|\} |b_0^C| - \max\{|\underline{a}_0^P|, |\bar{a}_0^P|\} |a_0^C|.$$

Proof: By using the triangle inequality and assuming $\omega > 1$, we have

$$\begin{aligned} |\Delta(j\omega)| &\geq |a_{n_C}^C| \min\{|\underline{a}_{n_P}^P|, |\bar{a}_{n_P}^P|\} \omega^{n_C+n_P} - \\ &\left(\left(\sum_{i=1}^{n_C-1} |a_{i1}^C| \omega^{i1} \right) \left(\sum_{i=2}^{n_P-1} \max\{|\underline{a}_{i2}^P|, |\bar{a}_{i2}^P|\} \omega^{i2} \right) \right. \\ &+ |a_{n_C}^C| \omega^{n_C} \left(\sum_{i=2}^{n_P-1} \max\{|\underline{a}_{i2}^P|, |\bar{a}_{i2}^P|\} \omega^{i2} \right) \\ &+ \max\{|\underline{a}_{n_P}^P|, |\bar{a}_{n_P}^P|\} \omega^{n_P} \left(\sum_{i=1}^{n_C-1} |a_{i1}^C| \omega^{i1} \right) + |e^{-\omega L}| \\ &\left. \left(\sum_{r=1}^{m_C} |b_{r1}^C| \omega^{r1} \right) \left(\sum_{r=2}^{m_P} \max\{|\underline{b}_{r2}^P|, |\bar{b}_{r2}^P|\} \omega^{r2} \right) \right) \\ &\geq |a_{n_C}^C| \min\{|\underline{a}_{n_P}^P|, |\bar{a}_{n_P}^P|\} \omega^{n_C+n_P-1} (\omega - \sigma_{\max}). \quad (8) \end{aligned}$$

From (8), if $\omega > S_{\max,1}$, then, $|\Delta(j\omega)| > 0$ and this implies $0 \notin \Delta(j\omega)$. Proof for S_{\min} is analogous. ■

Now, in the following, it is checked that whether or not the value set of $\Delta(s)$ encircles the origin for $\omega \in [S_{\min}, S_{\max}]$.

Theorem 2: Assume $\Delta^{vs}(j\omega)$ denotes the value set of the characteristic function $\Delta(j\omega)$ at each frequency and $\Delta(j\omega) = \Delta_1(j\omega) + \Delta_2(j\omega)$ where $\Delta_1(j\omega)$ and $\Delta_2(j\omega)$ are two independent, closed and bounded value sets. Then, at $\omega = \omega_0 \in [S_{\min}, S_{\max}]$, $0 \in \Delta^{vs}(j\omega)$, iff $-\Delta_1^{vs}(s = j\omega_0)$ and $\Delta_2^{vs}(s = j\omega_0)$ have an overlap in the complex plane.

Proof: Proof of the necessity: We can write $0 \in \Delta^{vs}(j\omega_0)$ as $\{z_0 - z_0\} \in \Delta^{vs}(j\omega_0)$. Hence, one can simply deduce that $z_0 \in -\Delta_1^{vs}(j\omega_0)$ and $z_0 \in \Delta_2^{vs}(j\omega_0)$. This means that $-\Delta_1^{vs}(j\omega_0)$ and $\Delta_2(j\omega_0)$ have an overlap.

Proof of the sufficiency: Because of the overlap between $-\Delta_1^{vs}(j\omega_0)$ and $\Delta_2^{vs}(j\omega_0)$, there is $z_0 \in \mathbb{C}$ so that $z_0 \in -\Delta_1^{vs}(j\omega_0)$ and $z_0 \in \Delta_2^{vs}(j\omega_0)$. Therefore, there exists a member of $-\Delta_1^{vs}(j\omega_0)$ as $-\Delta_1(j\omega_0)$ which is equivalent to z_0 i.e., $z_0 = -\Delta_1(j\omega_0)$. Likewise, one can show that $z_0 = \Delta_2(j\omega_0)$. Assume that $\{\tilde{\Delta}(j\omega) = \tilde{\Delta}_1(j\omega) + \tilde{\Delta}_2(j\omega)\} \in \Delta(j\omega)$. Hence, at $\omega = \omega_0$, $0 \in \Delta^{vs}(j\omega)$. ■

Lemma 2: Assume $D_C(s) \mathbf{D}_P(s) \neq 0$ for $s = j\omega_0$ and $\omega_0 \in [S_{\min}, S_{\max}]$. Then, $0 \notin \Delta^{vs}(j\omega_0)$ iff, $\Theta_1(j\omega_0)$ and $\Theta_2(j\omega_0)$ in (9) have no overlap

$$\Theta_1(j\omega) = -e^{Lj\omega}, \Theta_2(j\omega) = \left(\frac{N_v^{r_1}}{D_E^{r_2}} \right) \cup \left(\frac{N_E^{r_1}}{D_v^{r_2}} \right) \quad (9)$$

in which

$$\begin{cases} N_v^{r_1} = N_C(j\omega) V_{r_1}^N(j\omega), r_1 = 1, 2, 3, 4, \\ D_v^{r_2} = D_C(j\omega) V_{r_2}^D(j\omega), r_2 = 1, 2, 3, 4, \\ V_1^N(j\omega) = V_5^N(j\omega), V_1^D(j\omega) = V_5^D(j\omega), \end{cases} \quad (10)$$

$$\begin{cases} N_E^{r_1} = e(N_C(j\omega) V_{r_1}^N(j\omega), N_C(j\omega) V_{r_1+1}^N(j\omega)), \\ D_E^{r_2} = e(D_C(j\omega) V_{r_2}^D(j\omega), D_C(j\omega) V_{r_2+1}^D(j\omega)). \end{cases}$$

Proof: According to the Kharitonov theorem, the value sets of $D_C(s) \mathbf{D}_P(s)$ and $N_C(s) \mathbf{N}_P(s)$ would be two parpolygons for $s = j\omega$. Moreover, the following holds true:

$$0 \in \Delta(s) \iff 0 \in e^{Ls} + \frac{N_C(s) \mathbf{N}_P(s)}{D_C(s) \mathbf{D}_P(s)}, s = j\omega_0. \quad (11)$$

Moreover, based on Lemma 1, it can be inferred that

$$\partial \left(\frac{N_C(s) \mathbf{N}_P(s)}{D_C(s) \mathbf{D}_P(s)} \right) \subset \Theta_2(s), s = j\omega_0. \quad (12)$$

From (12), Theorems 1 and 2, the proof is simply completed. ■

Lemma 3: Assume $N_C(s) \mathbf{N}_P(s) \neq 0$ for $s = j\omega_0$ and $\omega_0 \in [S_{\min}, S_{\max}]$. Then, $0 \notin \Delta^{vs}(j\omega_0)$ iff, $(\Theta_1(j\omega_0))^{-1}$ and $\Theta_3(j\omega_0)$ have no overlap, where $\Theta_1(j\omega_0)$ and $\Theta_3(j\omega_0)$ are respectively defined in (9) and (13).

$$\Theta_3(j\omega) = \left(\frac{D_E^{r_2}}{N_v^{r_1}} \right) \cup \left(\frac{D_v^{r_2}}{N_E^{r_1}} \right). \quad (13)$$

All elements defined in (13) are given by (10).

Proof: The proof follows from Lemma 2. ■

Theorem 3: Assume that $S_{\min} < \frac{2\pi}{L-L} \leq S_{\max}$. Then, $C(s)$ robustly stabilizes the system, iff

- 1) $C(s)$ can stabilize one member of the system with the characteristic function $\Delta_0(s)$.
- 2) For $\omega \in [S_{\min}, \frac{2\pi}{L-L})$, the value sets of $D_E^{i_2}(j\omega)$ and $N_v^{i_1}(j\omega)(\Theta_1(j\omega))^{-1}$ do not have any overlap.
- 3) For $\omega \in [\frac{2\pi}{L-L}, S_{\max})$, the value sets of $D_v^{i_2}(j\omega)\Theta_1(j\omega)$ and $N_E^{i_1}(j\omega)$ do not have any overlap.
- 4) For $\omega \in [\frac{2\pi}{L-L}, S_{\max}]$, $\bar{\Lambda}(\omega) > 0$ is satisfied where

$$\begin{aligned} \bar{\Lambda}(\omega) &= \min_{D_E^{i_2} \in P_D} |D_E^{i_2}| - \max_{N_E^{i_1} \in P_N} |N_E^{i_1}|, \\ P_D &= \{D_E^1, \dots, D_E^4\}, P_N = \{N_E^1, \dots, N_E^4\} \end{aligned} \quad (14)$$

in which $D_E^{i_2}, N_v^{i_1}(j\omega), i_1 = 1, 2, 3, 4$ and $\Theta_1(j\omega)$ can be found in Lemma 2.

Proof: For the case $\omega \in [S_{\min}, \frac{2\pi}{L-L})$, the proof can be simply concluded from Lemmas 2 and 3. Hence, in the following, the necessary and sufficient conditions are discussed for $\omega \in [\frac{2\pi}{L-L}, S_{\max}]$.

Proof of the sufficiency: It can be simply proven that the maximum magnitude of a parpolygon occurs at vertex and the minimum magnitude of a parpolygon also occurs on its boundary. Since, $\bar{\Lambda}(\omega) > 0$ is held, then it can be inferred from (3), $\min |D_C(s) \mathbf{D}_P(s)| > \max |N_C(s) \mathbf{N}_P(s)|$ for $s = j\omega$ and $\omega \in [\frac{2\pi}{L-L}, S_{\max}]$ and consequently $0 \notin \Delta(j\omega)$.

Proof of the Necessity: Since the characteristic function (3) is robust stable, based on the zero exclusion principle $0 \notin \Delta(j\omega)$. Also, it is apparent that for $s = j\omega$ and $\omega \rightarrow \infty$, $|D_C(s) \mathbf{D}_P(s)|/|N_C(s) \mathbf{N}_P(s)| \rightarrow \infty$. Assume that the inequality $\bar{\Lambda}(\omega) > 0$ is not met. Because of the continuity $|D_C(s) \mathbf{D}_P(s)|/|N_C(s) \mathbf{N}_P(s)|$, there exists $\omega^* \in [\frac{2\pi}{L-L}, \infty]$ such that $|D_C(s) \mathbf{D}_P(s)|/|N_C(s) \mathbf{N}_P(s)| = 1$ and this means that $-D_C(s) \mathbf{D}_P(s)$ and $N_C(s) \mathbf{N}_P(s)e^{-Ls}$ have an overlap and according to Theorem 1, it is deduced that $0 \in \Delta(j\omega^*)$. It contradicts stability of the system. ■

Corollary 1: Assume that $S_{\max} < \frac{2\pi}{L-L}$. Then, the controller $C(s)$ robustly stabilizes the closed-loop control system, iff the statements (1), (2), and (3) in Theorem 3 are held for $\omega \in [S_{\min}, S_{\max}]$.

Proof: The proof follows immediately from Theorem 3.

Corollary 2: Assume that $S_{\min} \geq \frac{2\pi}{L-L}$. Then, the controller $C(s)$ robustly stabilizes the system, iff

- 1) $C(s)$ can stabilize one member of the system with the function $\Delta_0(s)$.
- 2) For $\omega \in [S_{\min}, S_{\max}]$, $\bar{\Lambda}(\omega) > 0$ is satisfied where $\bar{\Lambda}(\omega)$ is defined in (14).

Proof: The proof is directly from Theorem 3. \blacksquare

B. Robust Stability Checking Function

Combining the previous results and some geometric features allows us to provide a robust stability checking function represented by the following theorem (Theorem 4).

Theorem 4: Assume that $S_{\min} < \frac{2\pi}{L-L} \leq S_{\max}$. Then, the controller $C(s)$ robustly stabilizes the closed-loop system, if

- 1) $C(s)$ can stabilize one member of the system with the function $\Delta_0(s)$.
- 2) For $\omega \in [S_{\min}, S_{\max}]$, $\Lambda(\omega) > 0$ is satisfied in which

$$\Lambda(\omega) = \begin{cases} \min\{\underline{\Lambda}_i(\omega) | i = 1, 2, 3, 4\}, & \text{for } \omega \in [S_{\min}, \frac{2\pi}{L-L}), \\ \bar{\Lambda}(\omega), & \text{for } \omega \in [\frac{2\pi}{L-L}, S_{\max}] \end{cases} \quad (15)$$

in which

$$\begin{aligned} \underline{\Lambda}_1(\omega) &= \min\{\kappa_{h,g,i}^1(j\omega) | h \in \{1, \dots, 4\}, i \in \{1, \dots, 4\}, \\ g &\in \{1, 2, \dots, 4N_1 + 2\}\}, \\ \kappa_{h,g,i}^1(s = j\omega) &= \left| D_c(s)V_i^D(s) + N_c(s)V_h^N(s)P_g^1(s) \right| \\ &\quad + \left| D_c(s)V_{i+1}^D(s) + N_c(s)V_h^N(s)P_g^1(s) \right| \\ &\quad - \left| D_c(s)(V_i^D(s) - V_{i+1}^D(s)) \right|, \end{aligned} \quad (16)$$

$$\begin{aligned} \underline{\Lambda}_2(\omega) &= \min\{\kappa_{h,g,i}^2(j\omega) | h \in \{1, \dots, 4\}, i \in \{1, \dots, 4\}, \\ g &\in \{1, 2, \dots, 4N_1 + 2\}\}, \\ \kappa_{h,g,i}^2(s = j\omega) &= \left| D_c(s)V_i^D(j\omega) + N_c(s)V_h^N(s)P_g^1(s) \right| \\ &\quad + \left| D_c(s)V_i^D(s) + N_c(s)V_h^N(s)P_{g+1}^1(s) \right| \\ &\quad - \left| N_c(s)V_h^N(s)(P_{g+1}^1(s) - P_g^1(s)) \right|, \end{aligned} \quad (17)$$

$$\begin{aligned} \underline{\Lambda}_3(\omega) &= \min\{\kappa_{h,g,i}^3(j\omega) | h \in \{1, \dots, 4\}, i \in \{1, \dots, 4\}, \\ g &\in \{1, 2, \dots, 4N_2 + 2\}\}, \\ \kappa_{h,g,i}^3(s = j\omega) &= \left| D_c(s)V_i^D(s)P_g^2(s) + N_c(s)V_h^N(s) \right| \\ &\quad + \left| D_c(s)V_i^D(j\omega)P_g^2(s) + N_c(s)V_{h+1}^N(s) \right| \\ &\quad - \left| N_c(s)(V_{h+1}^N(s) - V_h^N(s)) \right|, \end{aligned} \quad (18)$$

$$\begin{aligned} \underline{\Lambda}_4(\omega) &= \min\{\kappa_{h,g,i}^4(j\omega) | h \in \{1, \dots, 4\}, i \in \{1, \dots, 4\}, \\ g &\in \{1, 2, \dots, 4N_2 + 2\}\}, \\ \kappa_{h,g,i}^4(s = j\omega) &= \left| D_c(s)V_i^D(s)P_g^2(s) + N_c(s)V_h^N(s) \right| \\ &\quad + \left| D_c(s)V_i^D(s)P_{g+1}^2(s) + N_c(s)V_h^N(s) \right| \\ &\quad - \left| D_c(s)V_i^D(s)(P_{g+1}^2(s) - P_g^2(s)) \right| \end{aligned} \quad (19)$$

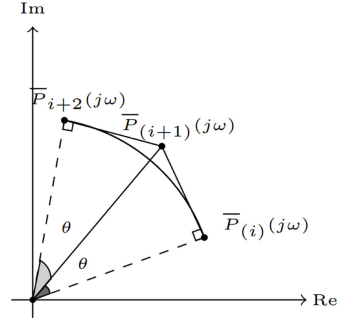


Fig. 1. Value set of $e^{-j\omega}$ and $\bar{P}_r^1(j\omega)$.

where $P_g^1(j\omega)$, $P_g^2(j\omega)$ are defined as follows:

$$P_g^1(s = j\omega) = \begin{cases} \bar{P}_{g-1}^1(s), & \text{if } 1 \leq g \leq 2N_1 + 1, \\ \bar{P}_{(2N_1)}^1(s), & \text{if } g = 2N_1 + 2, \\ \bar{P}_{(2N_1-1)}^1(s), & \text{if } g = 2N_1 + 3, \\ \dots & \\ \bar{P}_0^1(s), & \text{if } g = 4N_1 + 2, \\ \bar{P}_0^1(s), & \text{if } g = 4N_1 + 3, \end{cases} \quad (20)$$

$$\begin{aligned} \bar{P}_g^1(j\omega) &= \begin{cases} e^{-j\omega \left(\frac{L}{2} + g \frac{\bar{L}-L}{2N_1} \right)}, & \text{for } g = 0, 2, \dots, 2N_1, \\ \frac{e^{-j\omega \left(\frac{L}{2} + g \frac{\bar{L}-L}{2N_1} \right)}}{\cos \left(\omega \frac{\bar{L}-L}{2N_1} \right)}, & \text{for } g = 1, 3, \dots, 2N_1 - 1, \end{cases} \\ \underline{P}_g^1(j\omega) &= e^{-j\omega \left(\frac{L}{2} + g \frac{\bar{L}-L}{2N_1} \right)}, \quad g = 0, 1, 2, \dots, 2N_1. \end{aligned}$$

$$P_g^2(s = j\omega) = \begin{cases} \bar{P}_{g-1}^2(s), & \text{if } 1 \leq g \leq 2N_2 + 1, \\ \bar{P}_{(2N_2)}^2(s), & \text{if } g = 2N_2 + 2, \\ \bar{P}_{(2N_2-1)}^2(s), & \text{if } g = 2N_2 + 3, \\ \dots & \\ \bar{P}_0^2(s), & \text{if } g = 4N_2 + 2, \\ \bar{P}_0^2(s), & \text{if } g = 4N_2 + 3, \end{cases} \quad (21)$$

$$\begin{aligned} \bar{P}_g^2(s = j\omega) &= \begin{cases} e^{s \left(\frac{L}{2} + g \frac{\bar{L}-L}{2N_2} \right)}, & \text{if } g = 0, 2, \dots, 2N_2, \\ \frac{e^{s \left(\frac{L}{2} + g \frac{\bar{L}-L}{2N_2} \right)}}{\cos \left(\omega \frac{\bar{L}-L}{2N_2} \right)}, & \text{if } g = 1, 3, \dots, 2N_2 - 1, \end{cases} \\ \underline{P}_g^2(s = j\omega) &= e^{s \left(\frac{L}{2} + g \frac{\bar{L}-L}{2N_2} \right)}, \quad g = 0, 1, 2, \dots, 2N_2 \end{aligned}$$

where $N_1 \geq 3$ and $N_2 \geq 3$.

Proof: It is proven that satisfying the inequality $\Lambda(\omega) > 0$ ensures that the second and third statements in Theorem 3 are held. In the following, at first, the overlap is investigated between the value sets of $D_E^{i2}(j\omega)$ and $N_v^{i1}(j\omega)(\Theta_1(j\omega))^{-1}$. On the other hand, based on Fig. 1,

the following geometric feature can be simply derived:

$$|\bar{P}_{r+1}^1(j\omega)| = \frac{|\bar{P}_r^1(j\omega)|}{\cos(\theta)}. \quad (22)$$

From (22) and Fig. 1, one can simply deduce that $e^{-Lj\omega}$ is located inside the exposed edges $P_g^1(j\omega)$ in (20). Also, satisfying the triangle inequality for any vertex of the value set $D_E^{i2}(j\omega)$ and any two consecutive vertices of $N_v^{i1}(j\omega)P_g^1(j\omega)$ implies that no vertex of $D_E^{i2}(j\omega)$ intersects $N_v^{i1}(j\omega)P_g^1(j\omega)$. Furthermore, satisfying the triangle inequality for any vertex of $N_v^{i1}(j\omega)P_g^1(j\omega)$ and any two consecutive vertices of $D_E^{i2}(j\omega)$ implies that no vertex of $N_v^{i1}(j\omega)P_g^1(j\omega)$ intersects $D_E^{i2}(j\omega)$. This means that the value sets $N_v^{i1}(j\omega)P_g^1(j\omega)$ and $D_E^{i2}(j\omega)$ do not have any overlap for $\omega \in (0, \frac{2\pi}{L-L}]$. Hence, if the inequalities $\underline{\Lambda}_1(\omega) > 0$ and $\underline{\Lambda}_2(\omega) > 0$ are held, then the second statement in Theorem 3 is met. Likewise, the inequalities $\underline{\Lambda}_3(\omega) > 0$ and $\underline{\Lambda}_4(\omega) > 0$ ensure that the third statement in Theorem 3 is also met. ■

Corollary 3: Assume that $S_{\max} < \frac{2\pi}{L-L}$. Then, the controller $C(s)$ robustly stabilizes the system if

- 1) $C(s)$ can stabilize one member of the system with the function $\Delta_0(s)$.
- 2) $\Lambda(\omega) = \min\{\underline{\Lambda}_i(\omega) | i = 1, 2, 3, 4\} > 0$ is met for $\omega \in [S_{\min}, S_{\max}]$.

Proof: The proof follows from Theorem 4. ■

Remark 1: The stability of the arbitrary characteristic function $\Delta_0(s)$ can be checked by plotting the polar plot of $\psi(s) = \frac{\Delta_0(s)}{a(s+c)^{n_p+n_c}}$ for $s = j\omega$ where $-\infty < \omega < \infty$ and a and c are positive real numbers (as a suggestion). Then, according to the principle of argument theorem, $\Delta_0(s)$ is stable iff $\psi(s)$ does not encircle the origin in the complex plane. This approach allows us to effectively address the challenge of establishing the number of encirclements of the origin by manipulating the values of a and c . This means that by manipulating the values of a and c we can overcome the difficulty to establish how many times the origin is encircled in the complex plane. Moreover, based on the values of S_{\min} , S_{\max} , and $\frac{2\pi}{L-L}$, one can choose Theorem 3, Theorem 4 and Corollaries 1–3.

Remark 2: $\Lambda(\omega)$ may exhibit a discontinuity at the frequency $\omega = \frac{2\pi}{L-L}$. This discontinuity arises because $\Lambda(\omega)$ has been derived based on the triangle inequalities for $\omega \in [S_{\min}, \frac{2\pi}{L-L}]$. In addition, $\Lambda(\omega)$ has been determined using the distance between the convex shape $D_C(s)\mathbf{D}_P(s)$ and the nonconvex shape $N_C(s)\mathbf{N}_P(s)e^{-Ls}$ for $\omega \in [\frac{2\pi}{L-L}, S_{\max}]$. Consequently, in simulations, $\Lambda(\omega)$ is plotted within the intervals $\omega \in [S_{\min}, \frac{2\pi}{L-L}]$ and $\omega \in [\frac{2\pi}{L-L}, S_{\max}]$. However, this discontinuity does not impact the final result of robust stability analysis, as only the sign of the auxiliary function $\Lambda(\omega)$ is essential for the analysis of robust stability.

IV. DETERMINATION OF ROBUST STABILIZING REGION OF PID CONTROLLERS

In this section, we will discuss on calculating the stabilizing region of PID controllers for the uncertain transfer function $\mathbf{P}(s)$ in (2). The transfer function for the parallel form of the PID controller is provided in

$$C(s) = \frac{N_{\text{PID}}}{s} = \frac{k_p s + k_i + k_d s^2}{s}. \quad (23)$$

Hence, the characteristic function can be derived as follows:

$$\Delta_{\text{PID}}(s) = s \mathbf{D}_P(s) + N_{\text{PID}} \mathbf{N}_P(s) e^{-Ls}. \quad (24)$$

The goal is to calculate the robust stability region of PID controllers in the parameter space (k_p, k_i) . To accomplish this, we begin by defining a nominal case for the transfer function $\mathbf{P}(s)$ in (2) as $\hat{P}(s) = \frac{\hat{N}_P(s)}{\hat{D}_P(s)} e^{-\hat{L}s}$. From this, we derive its characteristic function $\hat{\Delta}_{\text{PID}}(s)$ as follows:

$$\hat{\Delta}_{\text{PID}}(s) = s \hat{D}_P(s) + (k_p s + k_i + k_d s^2) \hat{N}_P(s) e^{-\hat{L}s}. \quad (25)$$

Next, by setting the real and imaginary parts of $\hat{\Delta}_{\text{PID}}(j\omega)$ equal to zero, we can obtain a curve in the (k_p, k_i) plane, representing the complex root boundary (CRB), with k_d fixed and ω ranging from 0 to infinity. In addition, substituting $\omega = 0$ and $\omega = \infty$, we can also derive the boundaries for the real root boundary (RRB) and the infinite root boundary (IRB), respectively [14]. The stabilizing boundaries, namely RRB, IRB, and CRB, partition the parameter space (k_p, k_i) into stable and unstable regions. The stabilizing region can be identified by examining an arbitrary test point within each of these regions. Through this approach, we can determine the stabilizing region of PID controllers for the nominal case. Nevertheless, our primary goal is to assess the robust stabilizing region of PID controllers for the transfer function $\mathbf{P}(s)$ as defined in (2), accounting for uncertainties in both the numerator and denominator coefficients, as well as the time delay term. Hence, it is essential to establish the robust stability conditions for $\Delta_{\text{PID}}(j\omega)$ in (25). To this end, initially, we provide the following definition.

Definition 3: For terms e^{-Ls} , $\mathbf{N}_P(s)$, and $\mathbf{D}_P(s)$, define

$$\begin{aligned} \mathbf{V}^L &= \{\underline{L}, \bar{L}\}, \mathbf{I}^L = [\underline{L}, \bar{L}] = e(\underline{L}, \bar{L}), \\ \mathbf{V}^N &= \{V_1^N(j\omega), V_2^N(j\omega), V_3^N(j\omega), V_4^N(j\omega)\}, \\ \mathbf{I}^N &= \{\mathbf{I}_1^N, \mathbf{I}_2^N, \mathbf{I}_3^N, \mathbf{I}_4^N\}, \\ \mathbf{I}_h^N &= e(V_h^N(j\omega), V_{h+1}^N(j\omega)), V_5^N(j\omega) = V_1^N(j\omega), \\ \mathbf{V}^D &= \{V_1^D(j\omega), V_2^D(j\omega), V_3^D(j\omega), V_4^D(j\omega)\}, \\ \mathbf{I}^D &= \{\mathbf{I}_1^D, \mathbf{I}_2^D, \mathbf{I}_3^D, \mathbf{I}_4^D\}, \\ \mathbf{I}_r^D &= e(V_r^D(j\omega), V_{r+1}^D(j\omega)), V_5^D(j\omega) = V_1^D(j\omega). \end{aligned} \quad (26)$$

Theorem 5: Assume that a certain polynomial of $\Delta_{\text{PID}}(s)$ in (24) as $\hat{\Delta}(s)$ is stable. Then, the characteristic function $\Delta_{\text{PID}}(s)$ is robust stable iff, the characteristic functions $\Delta_{r_1}^{\text{PID}}(s)$ ($r_1 = 1, 2, 3, 4$) in (27) and $\Delta_{r_2}^{\text{PID}}(s)$ ($r_2 = 1, 2, 3, 4$) in (28) are also robust stable.

$$\Delta_{r_1}^{\text{PID}}(s) = s \mathbf{D}_P(s) + N_{\text{PID}} V_{r_1}^N(s) e^{-Ls}. \quad (27)$$

$$\Delta_{r_2}^{\text{PID}}(s) = s V_{r_2}^D(s) + N_{\text{PID}} \mathbf{N}_P(s) e^{-Ls}. \quad (28)$$

Proof. *Proof of the sufficiency:* If the characteristic functions $\Delta_{r_1}^{\text{PID}}(s)$ in (27) are robust stable, then, in accordance with Theorem 2 and (27), it can be inferred that

$$-N_{\text{PID}} V_{r_1}^N(s) e^{-Ls} \notin s \mathbf{D}_P(s), s = j\omega. \quad (29)$$

By referring to (28) and Theorem 2, it can be deduced that

$$-s V_{r_2}^D(s) e^{Ls} \notin N_{\text{PID}} \mathbf{N}_P(s), s = j\omega. \quad (30)$$

From (29) and (30) and Theorem 1, it is apparent that $\Theta_1(\omega_0)$ and $\Theta_2(\omega_0)$ in (9) do not have any overlap in the complex plane for $s \mathbf{D}_P(s) \neq 0$ and $s = j\omega_0$. Likewise, $(\Theta_1(\omega_0))^{-1}$ and $\Theta_3(\omega_0)$ in (13) do not have any overlap in the complex plane for $N_{\text{PID}} \mathbf{N}_P(s) \neq 0$ and $s = j\omega_0$. This implies that $0 \notin \Delta^{\text{PID}}(j\omega)$.

Algorithm 1:

Step 1: Obtain the sets \mathbf{V}^N and \mathbf{V}^D as defined in (4) and (5).

Step 2: Calculate the boundaries RRB, IRB and CRB for the characteristic functions $\Delta^D(j\omega)$ defined in (31).

$$\Delta^D(j\omega) = \begin{cases} s\mathbf{I}^D + \mathbf{V}^N N_{PID} e^{-Ls}, & 0 < \omega < \frac{2\pi}{L-L_-}, \\ s\mathbf{I}^D + \mathbf{V}^N N_{PID} e^{j[0,2\pi]}, & \omega \geq \frac{2\pi}{L-L_-}. \end{cases} \quad (31)$$

Step 3: Calculate the boundaries RRB, IRB and CRB for the characteristic functions $\Delta^N(j\omega)$ defined in (32).

$$\Delta^N(j\omega) = \begin{cases} s\mathbf{V}^D + \mathbf{I}^N N_{PID} e^{-Ls}, & 0 < \omega < \frac{2\pi}{L-L_-}, \\ s\mathbf{V}^D + \mathbf{I}^N N_{PID} e^{j[0,2\pi]}, & \omega \geq \frac{2\pi}{L-L_-}. \end{cases} \quad (32)$$

Step 4: The final stabilizing region of PID controllers for the interval plant with an interval time delay $\mathbf{P}(s)$ is the intersection of all the computed stable regions in Steps 2-3.

Proof of the Necessity: Because the characteristic function $\Delta^{\text{PID}}(s)$ in (24) demonstrates robust stability, it follows from the zero exclusion principle that $0 \notin \Delta^{\text{PID}}(j\omega)$. This implies that the origin is located outside the value set of $\Delta^{\text{PID}}(j\omega)$. Assume that $s\mathbf{D}_P(s) \neq 0$ for $s = j\omega_0$. Then, from Lemma 2, it is concluded that $\Theta_1(\omega_0)$ and $\Theta_2(\omega_0)$ do not have any overlap in the complex plane. Therefore, the robust stability of $\Delta_{r_1}^{\text{PID}}(s)$ in (27) and $\Delta_{r_2}^{\text{PID}}(s)$ in (28) are concluded based on the zero exclusion principle. ■

Remark 3: Theorem 5 reveals that the robust stability analysis of the characteristic function $\Delta_{\text{PID}}(s)$ in (24) is equivalent to the robust stability analysis of the characteristic functions $\Delta_{r_1}^{\text{PID}}(s)$ ($r_1 = 1, 2, 3, 4$) in (27) and $\Delta_{r_2}^{\text{PID}}(s)$ ($r_2 = 1, 2, 3, 4$) in (28). Hence, the difficulties of determining the robust stabilizing region of PID controllers are only related to the determination of RRB, IRB, and CRB boundaries of the characteristic functions $\Delta_{r_1}^{\text{PID}}(s)$ ($r_1 = 1, 2, 3, 4$) in (27) and $\Delta_{r_2}^{\text{PID}}(s)$ ($r_2 = 1, 2, 3, 4$) in (28). In order to achieve this, we present the computation of the stabilizing region for PID controllers in Algorithm 1, within the parameter space (k_p, k_i) .

V. ILLUSTRATIVE EXAMPLES

Example 1: Let us consider an interval plant with an interval time delay as $\mathbf{P}(s)$ in (33).

$$\mathbf{P}(s) = \frac{[0.2, 0.4]}{[1.8, 2.2]s^2 + [2.8, 3.2]s + [0.9, 1.1]} e^{-[0.1, 1]s}. \quad (33)$$

Also, the PID controller is as follows:

$$C(s) = 0.4 + \frac{0.1}{s} + 0.001 s. \quad (34)$$

Based on Remark 1, the stability of $\Delta_0(s)$ in (35) can be verified by plotting $\psi(s) = \frac{\Delta_0(s)}{1.8(s+0.6)^3}$ as depicted in Fig. 2.

$$\Delta_0(s) = s(1.8s^2 + 2.8s + 0.9) + 0.2(0.4s + 0.1) + 0.001s^2 e^{-0.2s}. \quad (35)$$

Moreover, the values of the function $\Lambda(\omega)$ are checked for $\omega \in [0.003, 2.5002]$ rad/s as shown in Fig. 3. Therefore, the robust stability of the system is guaranteed by Theorem 4. Furthermore, Fig. 4 illustrates the determined robust stability region of PID controllers, as derived using Algorithm 1 with a selected value of $k_d = 0.001$. This finding serves to validate the robust stabilization capabilities of the PID controller in (34) in effectively stabilizing the interval plant (33).

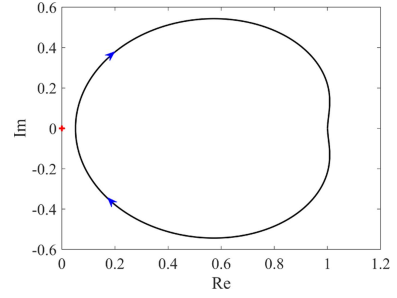


Fig. 2. Curve of $\psi(s) = \frac{\Delta_0(s)}{1.8(s+0.6)^3}$ for $s = j\omega$.

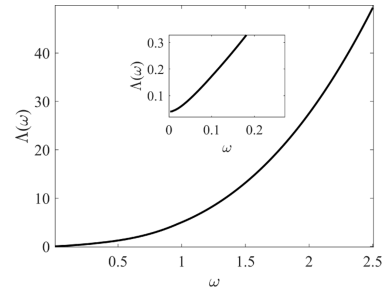


Fig. 3. Curve of $\Lambda(\omega)$ for $\omega \in [0.003, 2.5002]$ rad/sec in Example 1.

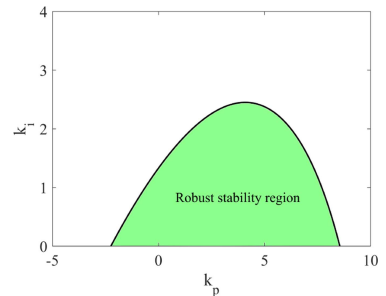


Fig. 4. Robust stability region (green color) of PID controllers in Example 1 for $k_d = 0.001$.

It is worth noting that in [26], a methodology has been proposed for designing various types of PID controllers for standard second-order plus time-delay systems without uncertainties. This implies that the method described in [26] cannot be applied to interval time delay systems. The works [21], [22], and [29] do not tackle the robust stability analysis of time-delay systems affected by simultaneous uncertainties in both numerator and denominator coefficients, as seen in (33), along with variations in time delays. However, as demonstrated in this example, utilizing the robust stability testing function outlined in Theorem 4, the robust stability of the interval plant (33) can be easily verified by employing the PID controller.

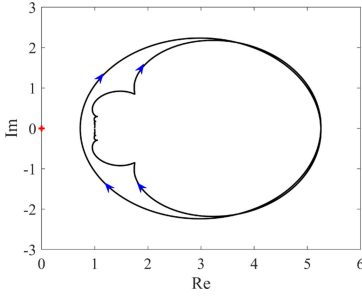


Fig. 5. Plot of $\psi(s) = \frac{\Delta_0(s)}{(s+1)^4}$ in example 2.

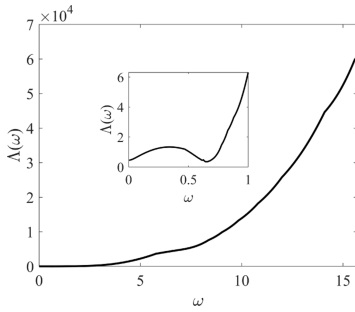


Fig. 6. Curve of $\Lambda(\omega)$ for $\omega \in [0.0041, 5\pi]$ rad/s in example 2.

Example 2: Consider an unstable plant with interval uncertainties as follows:

$$\begin{aligned} \mathbf{P}(s) &= \frac{\mathbf{N}_P(s)}{\mathbf{D}_P(s)} e^{-[0.5, 0.9]s}, \\ \mathbf{N}_P(s) &= [1, 1.1]s + [0.8, 0.9], \\ \mathbf{D}_P(s) &= s^4 + [9.5, 10]s^3 + [23.1, 23.5]s^2 \\ &\quad + [-11.6, -11]s + [-22.5, -22]. \end{aligned} \quad (36)$$

In the following, the robust stability analysis of the control system is checked by applying the PD controller:

$$C(s) = 12.5s + 28.41. \quad (37)$$

We first assess stability for $\Delta_0(s)$ (38) following Remark 1:

$$\begin{aligned} \Delta_0(s) &= s^4 + 9.5s^3 + 23.1s^2 - 11.6s - 22.5 \\ &\quad + (12.5s + 28.41)(s + 0.8)e^{-0.5s}. \end{aligned} \quad (38)$$

We make the assumption that $a = 1$ and $c = 1$ in the expression $\psi(s) = \frac{\Delta_0(s)}{a(s+c)^4}$. The graph of $\psi(s) = \frac{\Delta_0(s)}{(s+1)^4}$ is depicted in Fig. 5 for $s = j\omega$. As evident from the plot, the origin is not encompassed by the curve of $\psi(s)$. Consequently, the system described by $\Delta_0(s)$ in (38) is stable.

Utilizing Theorem 4, we examine the values of the function $\Lambda(\omega)$ over the range of $\omega \in [0.0041, 149.92]$ rad/s. In Figs. 6 and 7, we present the plot of $\Lambda(\omega)$ for the case where $N_1 = N_2 = 3$. As depicted in Figs. 6 and 7, the condition $\Lambda(\omega) > 0$ is met. Consequently, the PD controller robustly stabilizes the system despite uncertainties in coefficients and plant time delay.

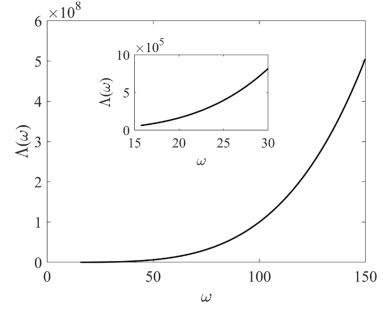


Fig. 7. Curve of $\Lambda(\omega)$ for $\omega \in [5\pi, 149.92]$ rad/s in example 2.

VI. DISCUSSION

Let us now compare our findings with those of related prior studies. Given that the problem at hand involves an unknown time delay term within specified intervals, conventional robust analysis methods like Kharitonov's theorem or Generalized Kharitonov's Theorem [28] cannot be employed. This is primarily due to the nonconvex nature of the value set of the characteristic function having an interval time delay, making it exceedingly challenging to establish a relationship between the origin and this value set.

By selecting an appropriate nominal model and weighting function, it is possible to replace the model with interval uncertainties, denoted as $\mathbf{P}(s)$, with a model featuring unstructured uncertainties, as discussed in [30] and [31]. Consequently, this enables the design of an H_∞ controller. However, it is important to note that the conservatism of the H_∞ controller depends on the choice of the nominal model and weighting function. In contrast, Theorem 3, Corollary 1, and Corollary 2 present necessary and sufficient conditions for the robust stability analysis of interval time delay systems. Furthermore, Theorem 4 offers a sufficient condition for the robust stability analysis of interval time delay systems, utilizing a finite and critical members of the characteristic function of the interval system. This implies that the results derived in this article exhibit less conservatism compared to the H_∞ controller.

In prior studies [4], [5], [6], [7], [8], [13], [14], [15], [26], [27], researchers calculated the robust stability region of PI and PID controllers for time delay systems (excluding uncertainties). However, as detailed in Section IV and exemplified in example 1, the present article provides a straightforward method to determine the robust stability region of PI and PID controllers.

The works [21], [22], and [29] focused on conducting robust stability analysis for a time delay system with the interval plant $L \in [0, \bar{L}]$ using PID controllers. However, it is worth noting that the aforementioned papers do not address the robust stability analysis of time delay systems affected by simultaneous uncertainties in numerator and denominator coefficients, as well as variations in time delays, as demonstrated in Examples 1 through 2.

VII. CONCLUSION

Robust stability analysis of the control systems in terms of controllers and uncertain plants with an uncertain time delay was studied in the present article. It is remarkable that general controllers represented by transfer functions have been considered in the present analysis. We also considered the problem in which the numerator and denominator coefficients and the time delay term of the transfer function of the plant are all unknown, but fall into known intervals. Robust stability analysis of such systems was presented. Then, to focus on the simplicity of the

criteria, a robust stability checking function was provided. A graphical tuning method for interval delayed plants was developed, involving PID controller robust stability analysis. The proposed results were finally validated through numerical examples.

REFERENCES

- [1] G. L. Guzmán, P. Garcia, T. Häggglund, S. Dormido, P. Albertos, and M. Berenguel, "Interactive tool for analysis of time-delay systems with dead-time compensators," *Control Eng. Pract.*, vol. 16, no. 7, pp. 824–835, 2008.
- [2] M. Ghorbani, M. Tavakoli-Kakhki, and A. A. Estarami, "Robust FOPID stabilization of retarded type fractional order plants with interval uncertainties and interval time delay," *J. Franklin Inst.*, vol. 356, no. 16, pp. 9302–9329, 2019.
- [3] M. Ghorbani, M. Tavakoli-Kakhki, A. Tepljakov, and E. Petlenkov, "Robust stability analysis of smith predictor based interval fractional-order control systems: A case study in level control process," *IEEE/CAA J. Automatica Sinica*, vol. 10, no. 3, pp. 762–780, 2022.
- [4] Q. B. Jin, Q. Liu, and B. Huang, "New results on the robust stability of PID controllers with gain and phase margins for UFOPTD processes," *ISA Trans.*, vol. 61, pp. 240–250, 2016.
- [5] S. Srivastava and V. S. Pandit, "A PI/PID controller for time delay systems with desired closed loop time response and guaranteed gain and phase margins," *J. Process Control*, vol. 37, pp. 70–77, 2016.
- [6] C. Onat, "A new design method for PI–PD control of unstable processes with dead time," *ISA Trans.*, vol. 84, pp. 69–81, 2019.
- [7] M. I. Kalim and A. Ali, "A graphical approach for controller design with desired stability margins for a DC–DC boost converter," *IET Power Electron.*, vol. 14, no. 7, pp. 1323–1335, 2021.
- [8] E. E. Amini and M. Rahmani, "Stabilising PID controller for time-delay systems with guaranteed gain and phase margins," *Int. J. Syst. Sci.*, vol. 53, no. 5, pp. 1004–1016, 2022.
- [9] X. Liang, S. C. Li, and A. B. Hassan, "A novel PID controller tuning method based on optimization technique," *J. Central South Univ. Technol.*, vol. 17, no. 5, pp. 1036–1042, 2010.
- [10] O. Toscano, "A simple robust PI/PID controller design via numerical optimization approach," *J. Process Control*, vol. 15, no. 1, pp. 81–88, 2005.
- [11] Y. Q. Chen, C. H. Hu, and K. L. Moore, "Relay feedback tuning of robust PID controllers with iso-damping property," in *Proc. IEEE 42nd Int. Conf. Decis. Control*, 2003, vol. 3, pp. 2180–2185.
- [12] N. Yadaiah and S. Malladi, "An optimized relation between T_i and T_d in Modified Ziegler Nichols PID controller tuning," in *Proc. IEEE Int. Conf. Control Appl.*, 2013, pp. 1275–1280.
- [13] G. J. Silva, A. Datta, and S. P. Bhattacharyya, "New results on the synthesis of PID controllers," *IEEE Trans. Autom. Control*, vol. 47, no. 2, pp. 241–252, Feb. 2002.
- [14] N. Tan and D. P. Atherton, "Design of stabilizing PI and PID controllers," *Int. J. Syst. Sci.*, vol. 37, no. 8, pp. 543–554, 2006.
- [15] N. Hohenbichler, "All stabilizing PID controllers for time delay systems," *Automatica*, vol. 45, no. 11, pp. 2678–2684, 2009.
- [16] W. Michiels, K. Engelborghs, P. Vansevenant, and D. Roose, "Continuous pole placement for delay equations," *Automatica*, vol. 38, no. 5, pp. 747–761, 2002.
- [17] W. Michiels, T. Vyhldal, and P. Zitek, "Continuous pole placement for delay equations," *J. Process Control*, vol. 20, no. 3, pp. 337–343, 2010.
- [18] J. Fišer and P. Zitek, "PID controller tuning via dominant pole placement in comparison with Ziegler-Nichols tuning," *IFAC-PapersOnLine*, vol. 52, no. 18, pp. 43–48, 2019.
- [19] H. Özbay and A. N. Gündes, "PID and low-order controller design for guaranteed delay margin and pole placement," *Int. J. Robust Nonlinear Control*, vol. 32, no. 18, pp. 9438–9451, 2022.
- [20] R. H. Middleton and D. E. Miller, "On the achievable delay margin using LTI control for unstable plants," *IEEE Trans. Autom. Control*, vol. 52, no. 7, pp. 1194–1207, Jul. 2007.
- [21] D. Ma, J. Chen, A. Liu, J. Chen, and S. I. Niculescu, "Explicit bounds for guaranteed stabilization by PID control of second-order unstable delay systems," *Automatica*, vol. 100, pp. 407–411, 2019.
- [22] X. G. Li, S. I. Niculescu, J. X. Chen, and T. Chai, "Characterizing PID controllers for linear time-delay systems: A parameter-space approach," *IEEE Trans. Autom. Control*, vol. 66, no. 10, pp. 4499–4513, Oct. 2021.
- [23] D. Ma, I. Boussaada, J. Chen, C. Bonnet, S. I. Niculescu, and J. Chen, "PID control design for first-order delay systems via MID pole placement: Performance vs robustness," *Automatica*, vol. 137, 2022, Art. no. 110102.
- [24] S. P. Bhattacharyya, H. Chapellat, and L. H. Keel, *ROBUST CONTROL: The Parametric Approach*. Englewood Cliffs, NJ, USA: Prentice Hall PTR, 1995.
- [25] N. Tan, "Computation of the frequency response of multilinear affine systems," *IEEE Trans. Autom. Control*, vol. 4, no. 10, pp. 1691–1696, Oct. 2002.
- [26] S. Srivastava, A. Misra, S. K. Thakur, and V. S. Pandit, "An optimal PID controller via LQR for standard second order plus time delay systems," *ISA Trans.*, vol. 60, pp. 244–253, 2016.
- [27] N. Tan, "Computation of stabilizing PI and PID controllers for processes with time delay," *ISA Trans.-Instrum. Soc. Amer.*, vol. 44, no. 2, pp. 213–224, 2005.
- [28] H. Chapellat and S. P. Bhattacharyya, "A generalization of Kharitonov's theorem; Robust stability of interval plants," *IEEE Trans. Autom. Control*, vol. 34, no. 3, pp. 306–311, Mar. 1989.
- [29] D. Ma and J. Chen, "Delay margin of low-order systems achievable by PID controllers," *IEEE Trans. Autom. Control*, vol. 64, no. 5, pp. 1958–1973, May 2019.
- [30] M. Radek, S. Bilal, and P. Libor, "Regions of robust relative stability for PI controllers and LTI plants with unstructured multiplicative uncertainty: A second-order-based example," *Heliyon*, vol. 9, no. 8, 2023, Art. no. e18924.
- [31] M. Morari and E. Zafriou, *Robust Process Control*, New Jersey, USA: Prentice-Hall Publications, 1989.

Appendix 2

II

M. Ghorbani, M. Tavakoli-Kakhki, A. Tepljakov, E. Petlenkov, A. Farnam, and G. Crevecoeur. Robust stability analysis of interval fractional-order plants with interval time delay and general form of fractional-order controllers. *IEEE Control Systems Letters*, 6:1268–1273, 2021.

Robust Stability Analysis of Interval Fractional-Order Plants With Interval Time Delay and General Form of Fractional-Order Controllers

Majid Ghorbani^{1b}, Mahsan Tavakoli-Kakhki^{1b}, Aleksei Tepljakov^{1b}, *Senior Member, IEEE*,
Eduard Petlenkov^{1b}, Arash Farnam^{1b}, and Guillaume Crevecoeur^{1b}

Abstract—This letter aims to investigate the robust stability of an interval fractional-order plant with an interval time delay by a general form of fractional-order controllers. Based on a simple graphical procedure, necessary and sufficient criteria are proposed to analyze the robust stability of an interval fractional-order plant. Then, the idea of “robust stability testing function” is extended to analyze the robust stability of the considered type of systems. Besides, an upper frequency bound is provided which is useful for the simulation purposes and it helps to reduce the computational cost. Finally, two examples are presented to verify the usefulness of the obtained results.

Index Terms—Interval time delay, fractional-order system, robust stability analysis, fractional-order controllers.

I. INTRODUCTION

RECENTLY, many studies have been reported on fractional-order differential equations for modeling real-world phenomena [1], [2]. In this regard, some results on designing the fractional-order controllers have been studied in [3]–[9].

The necessary and sufficient conditions for the stability of the fractional-order systems have been provided in [10]. Also,

in [11], an effective graphical method has been proposed to check the stability of fractional-order systems.

Literature review discloses that there are two main classes of procedures to investigate whether a controller can stabilize an interval fractional-order system or not, i.e., Linear Matrix Inequalities (LMIs) method [12] and the value set method [13]. LMI method may present the sufficient condition for the stability test [14], whereas the value set method provides the necessary and sufficient conditions for checking the robust stability of interval fractional-order systems [15].

The value set method is mainly based on the zero exclusion principle. In [16], it has been shown that the value set of an interval fractional-order polynomial is a parpolygon shape (Procedure 1 in [16]). Using the results presented in [16] and fractional-order controllers the robust stability of a fractional-order plant subjected to the parameters uncertainties has been addressed in [17]. The value set of a fractional-order characteristic function possessing an interval time delay is a nonconvex shape in the complex plane [18]. In [19], some intuitive extensions of the zero exclusion principle for these systems were presented without providing any rigorous proof. These extensions however incorrectly assume that an interval time delay systems leads to a polygon shape [20]. Hence, for such systems the issue of checking the relationship between the origin and the value set of the characteristic function remains challenging. To tackle this problem, in this letter, Theorem 1 named as “Value Sets Overlap Theorem” is presented in such a way that one can check whether a nonconvex or convex shaped value set includes the origin or not. In summary, the main novelties and contributions of this letter can be summarized as follows.

- 1) Presenting a procedure to exactly investigate whether or not the origin is included in the value set of characteristic functions having an interval time delay (see Theorem 1).
- 2) Presenting necessary and sufficient conditions of analyzing robust stability of fractional-order characteristic functions having an interval time delay (see Theorem 2).
- 3) Constructing a set of the exposed edges for the value set of the nonconvex term of characteristic functions possessing an interval time delay (see Lemma 1).

Manuscript received March 19, 2021; revised May 24, 2021; accepted June 9, 2021. Date of publication June 22, 2021; date of current version July 1, 2021. This work was supported by the Estonian Research Council under Grant PRG658. Recommended by Senior Editor V. Ugrinovskii. (Corresponding author: Majid Ghorbani.)

This work did not involve human subjects or animals in its research. Majid Ghorbani and Mahsan Tavakoli-Kakhki are with the Faculty of Electrical Engineering, K. N. Toosi University of Technology, Tehran 1631714191, Iran (e-mail: m.ghorbani@alumni.kntu.ac.ir; matavakoli@kntu.ac.ir).

Aleksei Tepljakov and Eduard Petlenkov are with the Department of Computer Systems, Tallinn University of Technology, 12618 Tallinn, Estonia (e-mail: aleksei.tepljakov@taltech.ee; eduard.petlenkov@taltech.ee).

Arash Farnam and Guillaume Crevecoeur are with the Department of Electrical Energy, Metals, Mechanical Constructions and Systems, Ghent University, 9000 Ghent, Belgium (e-mail: arash.farnam@ugent.be; guillaume.crevecoeur@ugent.be).

Digital Object Identifier 10.1109/LCSYS.2021.3091525

2475-1456 © 2021 IEEE. Personal use is permitted, but republication/redistribution requires IEEE permission.
See <https://www.ieee.org/publications/rights/index.html> for more information.

4) Introducing a robust stability testing function to considerably improve the computational efficiency (see Theorem 3). To the best of the authors' knowledge, no robust stability testing function has been presented up to now to analyze the robust stability of a closed-loop system containing an interval fractional-order plant with an interval time delay and a general form of fractional-order controller.

This letter is structured as follows. Notations and some necessary definitions are given in Section II. Section III provides the main results. In Section IV, the validity of the obtained results and their usefulness are verified by two examples. Finally, this letter is concluded in Section V.

II. PRELIMINARIES

Notations: Let u_i denote scalar functions and U_i denote numerical sets. Suppose $\sum_{i=r_1}^{r_2} u_i = 0$ for $r_2 < r_1$ and $\bigcup_{i=r_1}^{r_2} U_i = \emptyset$ for $r_2 < r_1$. Also, $A_1 \cup A_2 \triangleq \{x | x \in A_1 \text{ or } x \in A_2\}$ for any two sets A_1 and A_2 . $\partial(F)$ shows the boundary of the value set F in the complex plane. $e(u_1, u_2) \triangleq \eta u_1 + (1 - \eta)u_2$, $\eta \in [0, 1]$ for any two complex numbers u_1 and u_2 . Define $\mathbb{R}^{\geq 0} \triangleq \{x \in \mathbb{R} : x \geq 0\}$ and $\mathbb{N}^{\leq n} \triangleq \{x \in \mathbb{N} : x \leq n\}$. $n(B)$ denotes the number of the distinct members of the set B . $\text{floor}(x)$ is the largest integer less than or equal to $x \in \mathbb{R}$. $\text{frac}(x) \triangleq x - \text{floor}(x)$ for all $x \in \mathbb{R}$.

In this letter, the closed-loop system shown in Fig. 1 is studied.

Definition 1: An interval fractional-order plant is defined as a fractional-order transfer function whose denominator and numerator coefficients are all uncertain and lie in specified intervals. Also, an interval time delay points to a delay term whose value varies in a specific interval.

Consider an interval fractional-order plant with an interval time delay $P(s)$ as

$$P(s) = \frac{N_p(s)}{D_p(s)} = \frac{k e^{-\tau s}}{\sum_{i=0}^n q_i s^{\alpha_i}}, \quad (1)$$

and general form of fractional-order controllers as

$$C(s) = \frac{N_c(s)}{D_c(s)} = \frac{\sum_{i=1}^{m_1} b_i s^{\beta_i}}{\sum_{i=2}^{m_2} a_i s^{\mu_i}}, \quad (2)$$

where

- $k \in [\underline{k}, \bar{k}]$, $\tau \in [\underline{\tau}, \bar{\tau}]$, $\underline{k}, \bar{k}, \underline{\tau}, \bar{\tau} \in \mathbb{R}^{>0}$, $\underline{k} < \bar{k}$ and $\underline{\tau} < \bar{\tau}$.
- $q_i \in [\underline{q}_i, \bar{q}_i]$ and $q_n \neq 0$. b_{i_1} ($i_1 = 0, \dots, m_1$), a_{i_2} ($i_2 = 0, \dots, m_2$) $\in \mathbb{R}$ and $a_{m_2}, b_{m_1} \neq 0$.
- $\alpha_0 = 0 < \alpha_1 < \dots < \alpha_n$, $\gamma_0 = 0 < \gamma_1 < \dots < \gamma_{m_1}$, $\mu_0 = 0 < \mu_1 < \dots < \mu_{m_2}$ and $\gamma_{m_1} < \alpha_n + \mu_{m_2}$.
- k, τ and q_i are the independent real uncertain parameters.

From Fig. 1 and (1), the characteristic function of such systems is given by

$$F(s) = \underbrace{N_p(s) N_c(s)}_{F_1(s)} + \underbrace{D_p(s) D_c(s)}_{F_2(s)}. \quad (3)$$

Remark 1: According to the wide spread use of transfer function $P(s)$ in (1) for modeling real word phenomena, the problem of designing robust controller for such a system is of great importance. Some examples of physical systems identified as transfer function $P(s)$ in (1) are Titanium billet heating

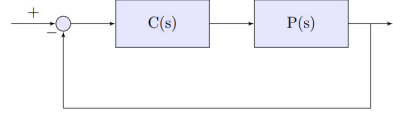


Fig. 1. The closed loop system.

process [5], DC motor speed control system [3], [8] and liquid level system [7].

Remark 2: From the zero exclusion principle, the relationship between the origin and the value set of $F(s)$ in (3) for $s = j\omega$ needs to be investigated. Hence, the focus of this letter is to check whether or not $0 \in F(j\omega)$ for any positive frequency. Note that the value set of $D_p(s) = \sum_{i=0}^n q_i s^{\alpha_i}$ for $s = j\omega$ ($\omega > 0$) is as a convex parpolygon with $2m$ vertices calculated by Procedure 1. In this letter, the vertices of $D_p(j\omega)$ are considered as $V_i(j\omega)$ ($i = 1, 2, \dots, 2m$).

Procedure 1 in [16]: Let D be a family of interval fractional-order functions as follows:

$$D \triangleq \{D(s, q) : q \in Q\}, D(s, q) = \sum_{i_2=0}^n q_{i_2} s^{\alpha_{i_2}} + q_0,$$

$$Q \triangleq \{[q_0, \dots, q_n]^T : q_{i_2} \in [\underline{q}_{i_2}, \bar{q}_{i_2}], i_2 = 0, 1, \dots, n\}. \quad (4)$$

Define $M_0 \triangleq \{i_2 \in \mathbb{Z}_{\geq 0}^n : \underline{q}_{i_2} < \bar{q}_{i_2}\}$. The value set $D(j\omega, q)$ is determined for $\omega \in \mathbb{R}^{\geq 0}$ as follows.

1. For $M_0 = \emptyset$ and $\omega \geq 0$, $D(j\omega, q) = D_0(j\omega, q)$ where

$$D_0(j\omega, q) \triangleq \sum_{i_2=0}^n \underline{q}_{i_2} s^{\alpha_{i_2}}. \quad (5)$$

2. For $M_0 \neq \emptyset$,

- If $\omega = 0$, then $D(j\omega, q) = D(j0, q) = [q_0, \bar{q}_0]$.
- If $\omega > 0$, then define $T_0 \triangleq \{\text{frac}(0.5\alpha_{i_2}) : i_2 \in M_0\}$ and $m \triangleq n(T_0)$. Consider $\gamma_1, \dots, \gamma_{m-1}, \gamma_m$ as all the distinct members of T_0 sorted as $0 \leq \gamma_1 < \dots < \gamma_{m-1} < \gamma_m < 1$. Then, define the following sets:

$$M'_r \triangleq \{i_2 \in M_0 : \text{floor}(0.5\alpha_{i_2}) \text{ is an odd number and } \text{frac}(0.5\alpha_{i_2}) = \gamma_r\},$$

$$M_r \triangleq \{i_2 \in M_0 : \text{floor}(0.5\alpha_{i_2}) \text{ is an even number and } \text{frac}(0.5\alpha_{i_2}) = \gamma_r\}, \quad r = 1, 2, \dots, m. \quad (6)$$

The vectors q^1, q^2, \dots, q^{2m} are defined as follows:

$$q^k \triangleq [q_0^k \ q_1^k \ \dots \ q_n^k]^T, q^{m+k} \triangleq [q_0^{m+k} \ q_1^{m+k} \ \dots \ q_n^{m+k}]^T$$

$$= \bar{q} + \underline{q} - q^k, \quad k = 1, \dots, m,$$

$$\underline{q} \triangleq [\underline{q}_0 \ \underline{q}_1 \ \dots \ \underline{q}_n]^T, \bar{q} \triangleq [\bar{q}_0 \ \bar{q}_1 \ \dots \ \bar{q}_n]^T, \quad (7)$$

$$q_{i_2}^k \triangleq \begin{cases} \bar{q}_{i_2}, & \text{for } i_2 \in \left(\bigcup_{i=1}^{k-1} M_i\right) \cup \left(\bigcup_{i=k}^m M_i\right), \\ \underline{q}_{i_2} & \text{for otherwise.} \end{cases} \quad (8)$$

$$q_{i_2}^{m+k} \triangleq \bar{q}_{i_2} + \underline{q}_{i_2} - q_{i_2}^k \quad (9)$$

where $i_2 = 0, 1, \dots, n$ and $k = 1, \dots, m$. Hence, the consecutive vertices $V_i(j\omega)$ ($i = 1, \dots, 2m$) are calculated by

$$\begin{aligned} V_k(j\omega) &\triangleq D(j\omega, q^k), \\ V_{m+k}(j\omega) &\triangleq D(j\omega, q^{m+k}) \quad (k = 1, 2, \dots, m). \end{aligned} \quad (10)$$

Assumption 1: Based on the zero exclusion principle, the closed-loop system is robust stable, if and only if $F(s)$ has one Hurwitz-stable member and the origin is not included in the value set of $F(j\omega)$ in (3) for $\omega \geq 0$. Therefore, it is assumed that the controller $C(s)$ in (1) stabilizes one member of the characteristic function $F(s)$ in (3) as $F_0(s)$.

Regarding the above analysis, the following design problems are formulated.

Problem 1: The value set of $F(j\omega)$ in (3) is a nonconvex shape in the complex plane. On the other hand, to the best of the authors' knowledge, no method has been presented to construct the boundary of the value set of a characteristic function having an interval time delay. Note that in [19], an exposed edge has been obtained to construct the boundary of the value set of a characteristic function possessing an interval time delay. But, as it was proven in [20], the exposed edge presented in [19] is incorrect for the general case of non-convex shaped value sets. Hence, the difficulty lies in the issue of how to specify whether the origin is included in the value set of $F(j\omega)$ in (3) or not.

Problem 2: Presenting a robust stability testing function is a common way to efficiently assess and perform the robust stability analysis. Existing robust stability testing functions are only valid for the characteristic functions whose value sets have convex shapes (see [16, Th. 1]). Due to the nonconvexity of the value set of $F(j\omega)$ in (3), another difficulty is to extend the idea of "robust stability testing function" for characteristic functions possessing nonconvex shapes as $F(j\omega)$ in (3).

These two underlying problems as the main motivations have prompted the authors to investigate the robust stability of $F(j\omega)$ in (3).

III. MAIN RESULT

A. Robust Stability Analysis

To tackle the first problem mentioned in the previous section, Theorem 1 is presented by which it is possible to check whether or not the origin is included in the value set of a nonconvex or convex shaped value sets.

Theorem 1 (Value Sets Overlap Theorem): Assume the value set of $F(j\omega)$ is defined as $F^{vs}(j\omega)$. Then, at a fixed frequency $\omega = \omega_0$, $0 \in F^{vs}(j\omega)$, if and only if the value sets of $F_1^{vs}(j\omega_0)$ and $-F_2^{vs}(j\omega_0)$ have an overlap in the complex plane.

Proof (Proof of the Sufficiency): Since $F_1^{vs}(j\omega_0)$ and $-F_2^{vs}(j\omega_0)$ have an overlap in the complex plane, then there is an arbitrary complex number as $z_0 \in \mathbb{C}$ such that $z_0 \in F_1^{vs}(j\omega_0)$ and $z_0 \in -F_2^{vs}(j\omega_0)$. This implies that there is a member of the family $F_1^{vs}(j\omega_0)$ as $\bar{F}_1(j\omega_0)$ which is equal to z_0 , i.e., $z_0 = \bar{F}_1(j\omega_0)$. Likewise, one can show that $z_0 = -\bar{F}_2(j\omega_0)$ or $-z_0 = \bar{F}_2(j\omega_0)$. Consider $\{\bar{F}(j\omega) = \bar{F}_1(j\omega) + \bar{F}_2(j\omega)\} \in F(j\omega)$. Hence, at the fixed frequency $\omega = \omega_0$, it is apparent that $0 \in F^{vs}(j\omega)$.

Proof of the Necessity: $0 \in F^{vs}(j\omega_0)$ can be written as $\{z_0 - z_0\} \in F^{vs}(j\omega_0)$. Hence, one can simply deduce that

$z_0 \in F_1^{vs}(j\omega_0)$ and $z_0 \in -F_2^{vs}(j\omega_0)$. This implies that the value sets of $F_1^{vs}(j\omega_0)$ and $-F_2^{vs}(j\omega_0)$ have an overlap in the complex plane. ■

Regarding Value Sets Overlap Theorem and Zero Exclusion Principle, the robust stability analysis of $F(j\omega)$ in (3) is presented by the following theorem.

Theorem 2: The closed-loop system (1) depicted in Fig. 1 is robust stable under Assumption 1, if and only if

- the sets $F_1(j\omega)$ and $F_2(j\omega)$ do not have an overlap for $\omega \in [0, \frac{2\pi}{\tau-\underline{\tau}}]$, where

$$\begin{aligned} F_1(j\omega) &\triangleq \left\{ e(kN_c(j\omega)e^{-\underline{\tau}j\omega}, \bar{k}N_c(j\omega)e^{-\underline{\tau}j\omega}), \right. \\ &\quad e(kN_c(j\omega)e^{-\bar{\tau}j\omega}, \bar{k}N_c(j\omega)e^{-\bar{\tau}j\omega}), \\ &\quad \left. kN_c(j\omega)e^{-e(\underline{\tau}, \bar{\tau})j\omega}, \bar{k}N_c(j\omega)e^{-e(\underline{\tau}, \bar{\tau})j\omega} \right\}, \end{aligned} \quad (11)$$

$$\begin{aligned} F_2(j\omega) &\triangleq \{e(-D_c(j\omega)V_1(j\omega), -D_c(j\omega)V_2(j\omega)), \\ &\quad e(-D_c(j\omega)V_2(j\omega), -D_c(j\omega)V_3(j\omega)), \\ &\quad \dots, e(-D_c(j\omega)V_{2m}(j\omega), -D_c(j\omega)V_1(j\omega))\}. \end{aligned} \quad (12)$$

- the inequality $H(\omega) > 0$ is held for $\omega \in [\frac{2\pi}{\tau-\underline{\tau}}, \infty)$, where

$$\begin{aligned} H(\omega) &\triangleq \min_{e_l \in P_E} |e_l| - |\bar{k}N_c(j\omega)|, P_E \triangleq \{e_1, \dots, e_{2m}\}, \\ e_l &\triangleq e(D_c(j\omega)V_l(j\omega), D_c(j\omega)V_{l+1}(j\omega)), \\ V_{2m+1}(j\omega) &= V_1(j\omega), l = 1, \dots, 2m. \end{aligned} \quad (13)$$

Proof: $F_1(j\omega)$ in (12) and $F_2(j\omega)$ in (13) depict $\partial(N_p(j\omega) N_c(j\omega))$ and $\partial(-D_p(j\omega) D_c(j\omega))$, respectively. Hence, one can easily prove the first statement of the theorem for $\omega \in [0, \frac{2\pi}{\tau-\underline{\tau}}]$ by Value Sets Overlap Theorem and Zero Exclusion Principle. In the following, the proof of the necessity and sufficiency is only proven for $\omega \in [\frac{2\pi}{\tau-\underline{\tau}}, \infty)$.

Proof of the Sufficiency: The following holds for $\omega \in [\frac{2\pi}{\tau-\underline{\tau}}, \infty)$.

$$N_p(j\omega) N_c(j\omega) = [|kN_c(j\omega)|, |\bar{k}N_c(j\omega)|]e^{j[0, 2\pi]}. \quad (14)$$

Also, $\min_{e_l \in P_E} |e_l|$ in (13) indicates the minimum distance of $\partial(-D_p(j\omega) D_c(j\omega))$. From (14), it can be inferred that $\max |N_p(j\omega) N_c(j\omega)| = |\bar{k}N_c(j\omega)|$. Hence, satisfying the inequality $H(\omega) > 0$ guarantees $0 \notin F(j\omega)$.

Proof of the Necessity: As a contradiction argument it is supposed that the inequality $H(\omega) > 0$ is not satisfied. Because of $\lim_{\omega \rightarrow \infty} \min_{e_l \in P_E} |e_l| > \lim_{\omega \rightarrow \infty} |\bar{k}N_c(j\omega)|$ and Value Sets Overlap Theorem, the inequality $H(\omega) > 0$ holds for $\omega \in [\frac{2\pi}{\tau-\underline{\tau}}, \infty)$. Since, $H(\omega)$ is a continuous function and $H(\omega) \leq 0$, there must exist at least a frequency as $\omega_0 \in [\frac{2\pi}{\tau-\underline{\tau}}, \infty)$ for which $H(\omega) = 0$. This shows that at $\omega_0 \in [\frac{2\pi}{\tau-\underline{\tau}}, \infty)$, $F_1^{vs}(j\omega_0)$ and $-F_2^{vs}(j\omega_0)$ have an overlap in the complex plane, i.e., $0 \in F^{vs}(j\omega_0)$ and it contradicts the condition $0 \notin F(j\omega_0)$. This completes the proof. ■

B. Robust Stability Testing Function

In this subsection, a robust stability testing function is proposed to facilitate the robust stability analysis. As it has been mentioned in Theorem 2, investigating the sign of the function $H(j\omega)$ in (13) shows the overlap between the value sets $F_1(j\omega)$ and $-F_2(j\omega)$ in (11) for $\omega \in [\frac{2\pi}{\tau-\underline{\tau}}, \infty)$. Therefore,

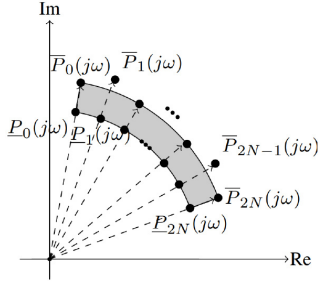


Fig. 2. The relationship between the value set of $N_p(j\omega)N_c(j\omega)$, the vertices $\bar{P}_i(j\omega)$ and $\underline{P}_i(j\omega)$.

in order to present a robust stability testing function it is useful to introduce another auxiliary function to check the overlap between $F_1(j\omega)$ and $F_2(j\omega)$ for $\omega \in [0, \frac{2\pi}{\bar{\tau}-\underline{\tau}})$. In Lemma 1, an exposed edge is constructed to contain all the value sets of $F_1(j\omega)$ in (12) for $\omega \in [0, \frac{2\pi}{\bar{\tau}-\underline{\tau}})$. This lemma helps to introduce the robust stability testing function later.

Lemma 1: At a fixed frequency $\omega = \omega_0 \in (0, \frac{2\pi}{\bar{\tau}-\underline{\tau}})$, the value set of $N_p(j\omega)N_c(j\omega)$ is located inside the exposed edges of $P_E(j\omega)$ defined in (15).

$$P_E(j\omega) \triangleq \{e(A_1(j\omega), A_2(j\omega)), e(A_2(j\omega), A_3(j\omega)), \dots, e(A_{4N+1}(j\omega), A_{4N+2}(j\omega)), e(A_{4N+2}(j\omega), A_1(j\omega))\},$$

$$A_r(j\omega) \triangleq \begin{cases} \bar{P}_{(r-1)}(j\omega), & \text{for } 1 \leq r \leq 2N+1, \\ \underline{P}_{(2N)}(j\omega), & \text{for } r = 2N+2, \\ \underline{P}_{(2N-1)}(j\omega), & \text{for } r = 2N+3, \\ \vdots & \\ \underline{P}_0(j\omega), & \text{for } r = 4N+2, \end{cases}$$

$$\bar{P}_r(j\omega) \triangleq \begin{cases} \bar{k}N_c(j\omega)e^{-j\omega(\underline{\tau}+r\frac{\bar{\tau}-\underline{\tau}}{2N})}, & \text{for } r = 0, 2, \dots, 2N, \\ \frac{\bar{k}N_c(j\omega)e^{-j\omega(\underline{\tau}+r\frac{\bar{\tau}-\underline{\tau}}{2N})}}{\cos(\omega\frac{\bar{\tau}-\underline{\tau}}{2N})}, & \text{for } r = 1, 3, \dots, 2N-1, \end{cases}$$

$$\underline{P}_r(j\omega) \triangleq \underline{k}N_c(j\omega)e^{-j\omega(\underline{\tau}+r\frac{\bar{\tau}-\underline{\tau}}{2N})}, \quad r = 0, 1, 2, \dots, 2N \quad (15)$$

where N is an arbitrary number and $N \in \mathbb{N}^{\geq 3}$.

Proof: Fig. 2 shows the value set of $N_p(j\omega)N_c(j\omega)$ and the vertices $\bar{P}_i(j\omega)$ and $\underline{P}_i(j\omega)$ for $i = 1, \dots, 2N$. Also, the edges of the three consecutive vertices $\bar{P}_i(j\omega)$, $\bar{P}_{i+1}(j\omega)$ and $\bar{P}_{i+2}(j\omega)$ are depicted in Fig. 3. It is worth mentioning that $\theta = \omega(\bar{\tau}-\underline{\tau})$ in Fig. 3. Regarding Fig. 3, the three consecutive vertices for $i = 0$ are given by (16) - (18).

$$\bar{P}_0(j\omega) = \bar{k}N_c(j\omega)e^{-\underline{\tau}j\omega}. \quad (16)$$

$$\bar{P}_1(j\omega) = \frac{\bar{k}N_c(j\omega)e^{-j\omega(\underline{\tau}+\frac{\bar{\tau}-\underline{\tau}}{2N})}}{\cos(\omega\frac{\bar{\tau}-\underline{\tau}}{2N})}. \quad (17)$$

$$\bar{P}_2(j\omega) = \bar{k}N_c(j\omega)e^{-j\omega(\underline{\tau}+2\frac{\bar{\tau}-\underline{\tau}}{2N})}. \quad (18)$$

The vertices $\underline{P}_i(j\omega)$ for $i = 1, \dots, 2N$ are located on the small-est arc of $N_p(j\omega)N_c(j\omega)$, i.e., $\underline{k}N_c(j\omega)e^{-\underline{\tau}j\omega}$. Also, $\omega\frac{\bar{\tau}-\underline{\tau}}{2N} \in (0, \frac{\pi}{N})$ and $\lim_{N \rightarrow \infty} \cos(\frac{\pi}{N}) \approx 0$ for $N = 2$. Therefore, (17)

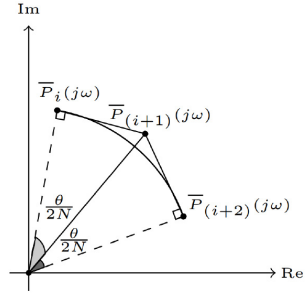


Fig. 3. The edges of the three consecutive vertices $\bar{P}_i(j\omega)$, $\bar{P}_{i+1}(j\omega)$ and $\bar{P}_{i+2}(j\omega)$.

is bounded for $N \in \mathbb{N}^{\geq 3}$. Hence, $N_p(j\omega)N_c(j\omega) \subseteq P_E(j\omega)$ for $\omega \in (0, \frac{2\pi}{\bar{\tau}-\underline{\tau}})$ and $N \in \mathbb{N}^{\geq 3}$. ■

Now, the next goal is to find the solution of *Problem 2*. Although the value set of $F(j\omega)$ in (3) is nonconvex shape in the complex plane, in the following theorem a robust stability testing function is presented to tackle the second problem.

Theorem 3: The closed-loop system is robust stable if the inequality $\chi(\omega) > 0$ is held, where

$$\chi(\omega) \triangleq \begin{cases} \min\{\chi_b(\omega)|b = 1, 2\}, & \text{for } \omega \in [0, \frac{2\pi}{\bar{\tau}-\underline{\tau}}), \\ H(\omega), & \text{for } \omega \in [\frac{2\pi}{\bar{\tau}-\underline{\tau}}, \infty), \end{cases} \quad (19)$$

in which $H(\omega)$ is defined in Theorem 2 and $\chi_b(\omega)$ for $b = 1, 2$ are presented as follows.

$$\chi_1(\omega) \triangleq \min\{\kappa_{h,g}(j\omega)|h \in \{1, \dots, 2m\}, g \in \{1, \dots, 4N+2\}\},$$

$$\kappa_{h,g}(j\omega) \triangleq |D_c(j\omega)V_{h+1}(j\omega) + A_g(j\omega)| + |D_c(j\omega)V_h(j\omega) + A_g(j\omega)| - |D_c(j\omega)(V_h(j\omega) - V_{h+1}(j\omega))|, \quad (20)$$

$$\chi_2(\omega) \triangleq \min\{\bar{\kappa}_{h,g}(j\omega)|h \in \{1, \dots, 2m\}, g \in \{1, \dots, 4N+2\}\},$$

$$\bar{\kappa}_{h,g}(j\omega) \triangleq |D_c(j\omega)V_h(j\omega) + A_g(j\omega)| + |D_c(j\omega)V_{h+1}(j\omega) + A_{g+1}(j\omega)| - |A_{g+1}(j\omega) - A_g(j\omega)|, \quad (21)$$

where $V_{2m+1}(j\omega) = V_1(j\omega)$ and $A_{4N+3}(j\omega) = A_1(j\omega)$.

Proof: If it is proven that $F_2(j\omega)$ in (12) and $P_E(j\omega)$ in (15) do not have any overlap in the complex plane, then from Lemma 1 and Theorem 2, the robust stability of the closed-loop system is deduced. It is apparent that if the triangle inequality holds for two vertices $-D_c(j\omega)V_i(j\omega)$ and $-D_c(j\omega)V_{i+1}(j\omega)$ and any vertices of $A_h(j\omega)$ ($h = 1, \dots, 4N+2$), then no vertices of $P_E(j\omega)$ intersect $F_2(j\omega)$. On the other hand, satisfying the inequality $\chi_2(\omega) > 0$ means that no vertices of $F_2(j\omega)$ lie in $P_E(j\omega)$ and this implies that $F_2(j\omega)$ in (12) and $P_E(j\omega)$ in (15) do not have any overlap in the complex plane for $\omega \in [0, \frac{2\pi}{\bar{\tau}-\underline{\tau}})$. Hence, based on the above explanations, if the inequalities $\chi_1(\omega) > 0$ and $\chi_2(\omega) > 0$ hold, then $F_2(j\omega)$ in (12) and $P_E(j\omega)$ in (15) have no overlap in the complex plane for $\omega \in [0, \frac{2\pi}{\bar{\tau}-\underline{\tau}})$. Therefore based on Theorem 2, one can easily complete the proof. ■

C. Upper Frequency Bound for Simulation Purposes

Clearly, it is not optimal to check whether or not the origin is included in the value set of the characteristic function

$F(j\omega)$ in (3) for $\omega \in [0, \infty)$, because the length of $[0, \infty)$ is infinite. The following theorem shows that $0 \notin F(j\omega)$ for $\omega \in (\omega_{\max}, \infty)$ where ω_{\max} is introduced in (22).

Theorem 4: The origin is not included in the value set of $F(j\omega)$ for $\omega \in (\omega_{\max}, \infty)$, where

$$\begin{aligned} \omega_{\max} &\triangleq \max\{1, \eta^{\frac{1}{\alpha_n + \mu_{m_2} - \epsilon}}\}, \\ \epsilon &\triangleq \begin{cases} \max\{\mu_{m_2} + \alpha_{n-1}, \gamma_{m_1}\}, & \text{for } m_2 = 0, \\ \max\{\alpha_n + \mu_{m_2-1}, \mu_{m_2} + \alpha_{n-1}, \gamma_{m_1}\}, & \text{for } m_2 > 0. \end{cases} \\ \eta &\triangleq \left(|a_{m_2}| \sum_{i=0}^{n-1} \max\{|\bar{q}_i|, |\underline{q}_i|\} + \max\{|\bar{q}_n|, |\underline{q}_n|\} \left(\sum_{i_2=0}^{m_2-1} |a_{i_2}| \right) \right. \\ &\quad \left. + \left(\sum_{i_2=0}^{m_2-1} |a_{i_2}| \right) \left(\sum_{i=0}^{n-1} \max\{|\bar{q}_i|, |\underline{q}_i|\} + |\bar{k}| \sum_{i_1=0}^{m_1} |b_{i_1}| \right) / \right. \\ &\quad \left. \left(\min\{|\bar{q}_n|, |\underline{q}_n|\} |a_{m_2}| \right) \right). \end{aligned} \quad (23)$$

Proof: Satisfying the inequality $|F(j\omega)| > 0$ means that $0 \notin F(j\omega)$. Therefore, it is proven that $|F(j\omega)| > 0$ is held for $\omega \in (\omega_{\max}, \infty)$. The inequalities $\omega^{\alpha_n + \mu_{m_2}} > \omega^\epsilon > \dots > \omega^0$ hold for $\omega > 1$. From (22) and using the triangle inequality, it can be deduced that

$$\begin{aligned} |F(j\omega)| &\geq \min\{|\bar{q}_n|, |\underline{q}_n|\} |a_{m_2}| |\omega|^{\alpha_n + \mu_{m_2}} - \left(|a_{m_2}| \sum_{i=0}^{n-1} \max\{|\bar{q}_i|, |\underline{q}_i|\} |\omega|^{\alpha_i + \mu_{m_2}} + \max\{|\bar{q}_n|, |\underline{q}_n|\} \left(\sum_{i_2=0}^{m_2-1} |a_{i_2}| \right) \right. \\ &\quad \left. |\omega|^{\mu_{i_2} + \alpha_n} \right) + \left(\sum_{i_2=0}^{m_2-1} |a_{i_2}| |\omega|^{\mu_{i_2}} \right) \left(\sum_{i=0}^{n-1} \max\{|\bar{q}_i|, |\underline{q}_i|\} |\omega|^{\alpha_i} \right) \\ &\quad + |\bar{k}| \sum_{i_1=0}^{m_1} |b_{i_1}| |\omega|^{\gamma_{i_1}} \geq \min\{|\bar{q}_n|, |\underline{q}_n|\} |a_{m_2}| |\omega|^{\alpha_n + \mu_{m_2}} \\ &\quad - \left(|a_{m_2}| \sum_{i=0}^{n-1} \max\{|\bar{q}_i|, |\underline{q}_i|\} + \max\{|\bar{q}_n|, |\underline{q}_n|\} \left(\sum_{i_2=0}^{m_2-1} |a_{i_2}| \right) + \left(\sum_{i_2=0}^{m_2-1} |a_{i_2}| \right) \left(\sum_{i=0}^{n-1} \max\{|\bar{q}_i|, |\underline{q}_i|\} \right) \right. \\ &\quad \left. + |\bar{k}| \sum_{i_1=0}^{m_1} |b_{i_1}| \right) \omega^{\max\{\alpha_n + \mu_{m_2-1}, \mu_{m_2} + \alpha_{n-1}, \gamma_{m_1}\}}. \end{aligned} \quad (24)$$

The right hand side of (24) is equal to

$$\min\{|\bar{q}_n|, |\underline{q}_n|\} |a_{m_2}| |\omega|^\epsilon (|\omega|^{\alpha_n + \mu_{m_2} - \epsilon} - \eta). \quad (25)$$

Due to $\min\{|\bar{q}_n|, |\underline{q}_n|\} |a_{m_2}| |\omega|^\epsilon > 0$, if $\omega > \omega_{\max}$ then $|F(j\omega)| > 0$ is achieved. ■

Remark 3: According to Theorem 4, it is concluded that $0 \notin F^{vs}(j\omega)$ in (3) for $\omega \in (\omega_{\max}, \infty)$. Therefore, for applying Theorem 3 it suffices to depict $\chi(\omega)$ in (19) for $\omega \in [0, \omega_{\max}]$. Therefore, Theorem 2 can be also employed by checking the value set of $F(j\omega)$ in the finite frequency range $[0, \omega_{\max}]$ rad/sec. In summary, based on the proposed Theorems 2–4, the robust stability of the closed-loop system can be investigated according to following steps.

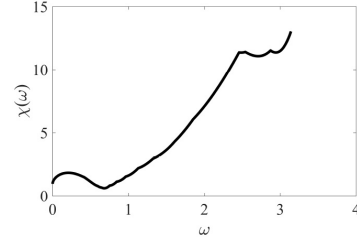


Fig. 4. The values of $\chi(\omega)$ for $\omega \in [0, \pi)$ rad/sec.

- 1) Check the stability of an arbitrary characteristic function of $F(s)$ as $F_0(s)$. If $F_0(s)$ is stable, continue steps. Otherwise, $F(s)$ is not robust stable.
- 2) Obtain all the vertices $V_i(s)$, $i = 1, \dots, 2m$ by using *Procedure 1* and calculate ω_{\max} via Theorem 4.
- 3) Check the conditions presented in Theorem 2 or Theorem 3 only for $\omega \in [0, \omega_{\max}]$ as stated below.
 - a) When employing Theorem 2, if all the conditions presented in the statement of Theorem 2 are held for $\omega \in [0, \omega_{\max}]$, then the system is robust stable. Otherwise, this system would not be robust stable.
 - b) When employing Theorem 3, if there exists $N \in \mathbb{N}^{\geq 3}$ by which the inequality $\chi(\omega) > 0$ in (19) holds for $\omega \in [0, \omega_{\max}]$, then this system is robust stable. Also, if the inequality $\chi(\omega) > 0$ does not hold for $\omega \in [\frac{2\pi}{T-L}, \omega_{\max}]$, this system is not robust stable (see the second statement of Theorem 2).

IV. ILLUSTRATIVE EXAMPLES

Example 1: By using the steps presented in Remark 3, it is shown that the closed-loop system corresponding to the plant (26) and the controller $C(s)$ in (27) is robust stable.

$$P(s) = \frac{[1.2, 1.5]e^{-[1,3]s}}{[1.3, 1.5]s^{1.2} + [1, 2]s^{0.5} + [1, 2]}, \quad (26)$$

$$C(s) = 0.5 + \frac{0.4}{s^{0.5}} + 0.1s^{0.5}, \quad (27)$$

The stability of the arbitrary characteristic function $F_0(s) = s^{0.5} (1.5s^{1.2} + 2s^{0.5} + 2) + 1.5 e^{-s} (0.5s^{0.5} + 0.4 + 0.1s)$ can be shown by the method presented in [11]. Regarding Procedure 1, the vertices $V_h(s)$ ($h = 1, 2, \dots, 6$, $s = j\omega$) are obtained as $V_1(s) = 1.3s^{1.2} + s^{0.5} + 1$, $V_2(s) = 1.3s^{1.2} + s^{0.5} + 2$, $V_3(s) = 1.3s^{1.2} + 2s^{0.5} + 2$, $V_4(s) = 1.5s^{1.2} + 2s^{0.5} + 2$, $V_5(s) = 1.5s^{1.2} + 2s^{0.5} + 1$, $V_6(s) = 1.5s^{1.2} + 1s^{0.5} + 1$. Also, from (22), ω_{\max} is obtained as 11.4199 rad/sec. To analyze robust stability of the closed-loop system, Theorem 3 is employed. The values of $\chi(\omega)$ in (19) have been reported in Fig. 4 and Fig. 5 for $N = 3$. Based on Theorem 3, this system is robust stable because the inequality $\chi(\omega) > 0$ holds for $\omega \in [0, 11.4199]$.

Example 2: In [5], the FOPI controller $C(s) = 2.56796 + 28.3814/s^{0.963957}$ has been designed for the nominal plant $P(s) = e^{-0.01s}/(0.4s + 1)$. Let us consider the nominal plant as the interval plant $P(s) = [0.9, 1.1]e^{-[0.001, 0.5]s}/([0.3, 0.5]s + [0.9, 1.1])$.

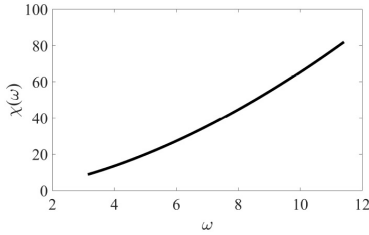


Fig. 5. The values of $\chi(\omega)$ for $\omega \in [\pi, 11.4199]$ rad/sec.

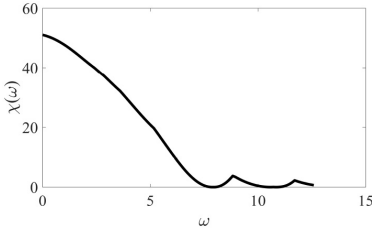


Fig. 6. The values of $\chi(\omega)$ for $\omega \in [0, 12.5916]$ rad/sec.

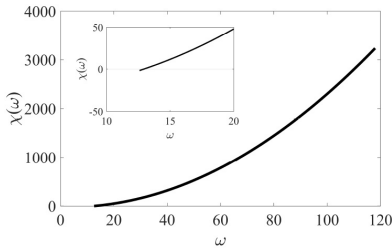


Fig. 7. $\chi(\omega)$ for $\omega \in [12.5916, 117.1477]$ rad/sec.

Regarding Procedure 1, the vertices are obtained as $V_1(s) = 0.3s + 0.9$, $V_2(s) = 0.3s + 1.1$, $V_3(s) = 0.5s + 1.1$, $V_4(s) = 0.5s + 0.9$. Based on Theorem 4, ω_{\max} is obtained as 117.1477 rad/sec. The values of $\chi(\omega)$ have been reported in Fig. 6 and Fig. 7 for $N = 3$. It seems that the inequality $\chi(\omega) > 0$ does not hold for $\omega \in [\frac{2\pi}{T}, 117.1477]$ rad/sec. Therefore, regarding Remark 3 and Theorem 2, this system would not be robust stable.

V. CONCLUSION

The robust stability of an interval fractional-order plant with an interval time delay by fractional-order controllers was studied in this letter. Theorem 1 was proposed as an easy graphical method for checking whether the origin is included in the value set of a nonconvex (or convex) shaped value set or not. Then, the necessary and sufficient criteria for robust stability of an interval fractional-order plant with an interval time delay were presented in Theorem 2. Moreover, by using some simple geometric features, an explicit robust stability testing function was

introduced to improve the efficiency of the proposed approach. Finally, two examples were provided to verify the usefulness of the achievements of this letter.

REFERENCES

- [1] A. A. Kilbas, H. M. Srivastava, and J. J. Trujillo, *Theory and Applications of Fractional Differential Equations*, vol. 204. Boston, MA, USA: Elsevier, 2006.
- [2] R. Hilfer *et al.*, *Applications of Fractional Calculus in Physics*, vol. 35. River Edge, NJ, USA: World Sci., 2000.
- [3] P. P. Arya and S. Chakrabarty, "A robust internal model-based fractional order controller for fractional order plus time delay processes," *IEEE Control Syst. Lett.*, vol. 4, no. 4, pp. 862–867, Oct. 2020.
- [4] Z. Nie, Q. Wang, R. Liu, and Y. Lan, "Identification and PID control for a class of delay fractional-order systems," *IEEE/CAA J. Automatica Sinica*, vol. 3, no. 4, pp. 463–476, Oct. 2016.
- [5] B. Şenol and U. Demiroğlu, "Frequency frame approach on loop shaping of first order plus time delay systems using fractional order PI controller," *ISA Trans.*, vol. 86, pp. 192–200, Mar. 2019.
- [6] A. Tepljakov, E. Petlenkov, and J. Belikov, "Robust FOPI and FOPID controller design for FFOPDT plants in embedded control applications using frequency-domain analysis," in *Proc. Amer. Control Conf. (ACC)*, 2015, pp. 3868–3873.
- [7] C. A. Monje, B. M. Vinagre, V. Feliu, and Y. Q. Chen, "Tuning and autotuning of fractional order controllers for industry applications," *Control Eng. Pract.*, vol. 16, no. 7, pp. 798–812, 2008.
- [8] K. Kothari, U. Mehta, and J. Vanuallailai, "Fractional-order models of time delay systems using Walsh operational matrices," in *Proc. 15th Int. Conf. Control Autom. Robot. Vis. (ICARCV)*, 2018, pp. 1555–1560.
- [9] P. Sathishkumar and N. Selvaganesan, "Fractional controller tuning expressions for a universal plant structure," *IEEE Control Syst. Lett.*, vol. 2, no. 3, pp. 345–350, Jul. 2018.
- [10] C. Bonnet and J. R. Partington, "Analysis of fractional delay systems of retarded and neutral type," *Automatica*, vol. 38, no. 7, pp. 1133–1138, Jul. 2000.
- [11] M. Bustołowicz, "Stability of linear continuous-time fractional order systems with delays of the retarded type," *Bull. Polish Acad. Sci. Tech. Sci.*, vol. 56, no. 4, pp. 825–831, 2008.
- [12] L. Chen, R. Wu, Y. He, and L. Yin, "Robust stability and stabilization of fractional-order linear systems with polytopic uncertainties," *Appl. Math. Comput.*, vol. 257, pp. 274–284, Apr. 2015.
- [13] K. A. Moornani and M. Haeri, "On robust stability of linear time invariant fractional-order systems with real parametric uncertainties," *ISA Trans.*, vol. 48, no. 4, pp. 484–490, 2009.
- [14] B. Aguiar, T. González, and M. Bernal, "Comments on 'Robust stability and stabilization of fractional-order interval systems with the fractional order α : The $0 < \alpha < 1$ case,'" *IEEE Trans. Autom. Control*, vol. 60, no. 2, pp. 582–583, Feb. 2015.
- [15] K. A. Moornani and M. Haeri, "On robust stability of LTI Sfractional-order delay systems of retarded and neutral type," *Automatica*, vol. 46, no. 2, pp. 362–368, 2010.
- [16] K. A. Moornani and M. Haeri, "Robust stability testing function and Kharitonov-like theorem for fractional order interval systems," *IET Control Theory Appl.*, vol. 4, no. 10, pp. 2097–2108, 2010.
- [17] M. Ghorbani, "Robust stability analysis of interval fractional-order plants by fractional-order controllers: An approach to reduce additional calculation," *Int. J. Gen. Syst.*, vol. 50, no. 1, pp. 1–25, 2020, doi: 10.1080/03081079.2020.1832485.
- [18] M. Ghorbani, M. Tavakoli-Kakhki, and A. A. Estarami, "Robust FOPID stabilization of retarded type fractional order plants with interval uncertainties and interval time delay," *J. Franklin Inst.*, vol. 356, no. 16, pp. 9302–9329, 2019.
- [19] T. Liang, J. Chen, and C. Lei, "Algorithm of robust stability region for interval plant with time delay using fractional order $PI^\lambda D^\mu$ controller," *Commun. Nonlinear Sci. Numer. Simulat.*, vol. 17, no. 2, pp. 979–991, 2012.
- [20] R. Mohsenipour and M. F. Jegarkandi, "A comment on 'Algorithm of robust stability region for interval plant with time delay using fractional order $PI^\lambda D^\mu$ controller' [Commun Nonlinear Sci Numer Simulat 17 (2012) 979–991]," *Commun. Nonlinear Sci. Numer. Simulat.*, vol. 63, pp. 202–204, Oct. 2018.

Appendix 3

III

M. Ghorbani, H. Rezaei, A. Tepljakov, and E. Petlenkov. Robust stability testing function for a complex interval family of fractional-order polynomials. *Journal of the Franklin Institute*, 359(17):10038–10057, 2022.



Robust stability testing function for a complex interval family of fractional-order polynomials

Majid Ghorbani^a, Hossein Rezaei^{b,*}, Aleksei Tepljakov^a,
Eduard Petlenkov^a

^aTallinn University of Technology, Department of Computer Systems, Estonia

^bDepartment of Electrical Engineering, Sahand University of Technology, Tabriz, Iran

Received 3 January 2021; received in revised form 26 April 2022; accepted 25 September 2022

Available online 11 October 2022

Abstract

The robust stability of a family of interval fractional-order systems with complex coefficients is investigated in this study. The concept of “a family of interval fractional-order systems with complex coefficients” means that the characteristic function of a control system can be of both commensurate and non-commensurate orders, the coefficients of the characteristic function can be uncertain parameters, and may be complex numbers. At first, a simple graphical procedure is presented for robust stability analysis. The “robust stability testing function” is then extended to look at the robust conditions. To the best of the authors’ knowledge, no auxiliary function for analyzing the robust stability of the systems under investigation has been introduced until now. Moreover, lower and upper frequency bounds are provided which are useful to improve the computational efficiency of testing the robust stability conditions. Eventually, to verify the results, analytical examples and numerical simulations are provided.

© 2022 The Franklin Institute. Published by Elsevier Ltd. All rights reserved.

* Corresponding author.

E-mail address: h_rezaei@sut.ac.ir (H. Rezaei).

1. Introduction

1.1. Background

Recently, many studies are conducted on Fractional-Order (FO) calculus, since the behavior of real-world physical phenomena may tend to FO differential equation representation such as chaotic systems [1], human operator behaviors [2], heat diffusion [3], flexible beam vibration [4] and biology [5].

In practical applications, It is critical to conduct a robust stability study of the intended control system. It is because that uncertainties may exist in the model of systems. Hence, many researchers have focused on the design of different robust FO controllers, for instance FO sliding mode controls [6,7], FO phase lead and lag compensator [8], FOPD controllers [9], FOPID controllers [10,11] and internal model based FO controller [12].

Many researchers have expressed some interest in robust stability analysis of FO systems. In [13–16], several approaches for testing the stability of uncertain FO systems have been developed. On the other hand, the value set tools are useful for checking the robustness of FO control systems. One of these tools is the zero exclusion condition. To do this, the value set of the characteristic function is plotted at each frequency. After then, the connection between the value set and the origin is examined. In [17,18], the zero exclusion condition has been developed to investigate the robust stability of FO control systems. As shown in Moornani and Haeri [19], the value set of an interval FO polynomial is a parpolygon form and an auxiliary function was then proposed to inspect the robust stability of the control system. In addition, the robust stability of FO plants having an uncertain time delay has been investigated in Ghorbani et al. [20]. Also, the robust stabilization of FO plants with interval uncertainties by FO controllers has been studied in Ghorbani and Tavakoli-Kakhki [21], Ghorbani [22]. Furthermore, the robust stability of FO polynomials with uncertainties in both the orders and the coefficients has been discussed in Ghorbani and Tavakoli-Kakhki [23].

1.2. Motivations and contributions

The robust stability of a family of interval FO polynomials with complex coefficients will be addressed further in this research. There are at least two factors that the earlier works may have overlooked. The first factor concerns the FO system's interval complex structure. Existing techniques all presume that interval uncertainties only exist in the FO system's real coefficients. However, the coefficient of any system may also have complex numbers. This phenomenon has been mentioned in Wei et al. [24], Ren and Fang [25]. The second aspect concerns the uncertainties in real-world system. It is more likely to have uncertainties in modeling real-world systems. One of the most popular ways among the latest published papers to involve the uncertainties in the model of integer/fractional systems is to use the interval uncertainty structure [26].

Most of the current works have assumed real uncertain coefficients in the control system model. Nevertheless, we investigate uncertainty structures in coefficients of a complex family of FO polynomials in this study. In [27], some helpful results have been proven for stability analysis of uncertain integer-order systems having complex coefficients. This paper is a natural attempt to extend some of these results for complex FO polynomial families. Although, the papers [28–30] have stated that the coefficients of control systems can possess complex numbers, for instance, applications in aerospace. Hence, the importance of FO systems as

well as the integer- order counterparts motivates us to investigate necessary and sufficient robust conditions of FO systems with uncertain complex coefficients.

In [31,32], for the boundary of the value sets, several exposed edges have been made. [Theorem 1](#) presents necessary and sufficient robust assessment for interval FO systems with complex coefficients inspired by the results reported in Tan et al. [31], Tan [32] and simple geometric properties of polygons. [Theorem 2](#) then reveals some properties of convex polygons. Also, in [Theorem 3](#), an explicit robust stability testing function is presented to perform the robust stability assessment. For simulation purposes, [Theorem 4](#) offers a frequency range. The following are the most important contributions of this paper:

- Finding simple robust stability assessments of FO systems suffering from complex coefficients.
- Presenting an auxiliary function to make the process of analyzing robust stability easier.
- Presenting a frequency range to lessen the computation complexity.

1.3. Organization

The remainder of the present paper is arranged as follows: In [Section 2](#), a preliminary review is recalled. [Section 3](#) presents the key findings. In [Section 4](#), four numerical examples show the accuracy of the presented methods. Eventually, [Section 5](#) concludes the paper.

2. Preliminaries

In [Section 2.1](#), the rest of the paper requires some background resources, which are provided. Also in [Section 2.2](#), the problems in this literature are stated in more detail.

2.1. Definitions and background materials

Notations Assume $\sum_{i=k_1}^{k_2} f_i = 0$ for $k_2 < k_1$ and $\bigcup_{i=k_1}^{k_2} F_i = \emptyset$ for $k_2 < k_1$. Also, $\partial(\Delta(j\omega))$ symbolizes the boundary of the value set $\Delta(j\omega)$ in the complex plane. $e(x_1, x_2) \triangleq \eta x_1 + (1 - \eta)x_2$, $\eta \in [0, 1]$ for any two complex numbers x_1 and x_2 .

As mentioned before, most of real systems are suffering from the uncertainties [33]. On the other hand, obtaining an accurate model of a system is impossible. A recent trend in the literature of system identification is to model the system uncertainties [27]. The interval uncertainty structure is one of the most popular methods among engineers to consider the uncertainty in the model of systems. For some examples in this regard, see [34–37]. Therefore, consider a complex interval family of polynomials as

$$\delta(s) = (q_0^R + jq_0^I) + (q_1^R + jq_1^I)s + \dots + (q_n^R + jq_n^I)s^n, \quad (1)$$

with

$$q_t^R \in [\underline{q}_t^R, \bar{q}_t^R], \quad t = 0, 1, \dots, n, \quad (2)$$

and

$$q_t^I \in [\underline{q}_t^I, \bar{q}_t^I], \quad t = 0, 1, \dots, n, \quad (3)$$

in which the uncertain parameters q_t^R and q_t^I are the real and imaginary parts of the uncertainties. Also, \underline{q}_t^R and \underline{q}_t^I respectively denote the lower bounds of the uncertainties q_t^R and q_t^I .

Moreover, \bar{q}_i^R and \bar{q}_i^I respectively represent the upper bounds of the uncertainties q_i^R and q_i^I . In Eq. (1), it is also assumed that $0 \notin (q_n^R + jq_n^I)$. In [27], it has been proven that $\delta(s)$ is robust stable if and only if the eight polynomials in Eq. (4) are all stable.

$$\begin{cases} P_1(s) = (q_0^R + jq_0^I) + (q_1^R + j\bar{q}_1^I)s + (\bar{q}_2^R + jq_2^I)s^2 + (\bar{q}_3^R + j\bar{q}_3^I)s^3 + (q_4^R + jq_4^I)s^4 + (q_5^R + j\bar{q}_5^I)s^5 + \dots, \\ P_2(s) = (q_0^R + j\bar{q}_0^I) + (\bar{q}_1^R + j\bar{q}_1^I)s + (\bar{q}_2^R + jq_2^I)s^2 + (q_3^R + jq_3^I)s^3 + (q_4^R + j\bar{q}_4^I)s^4 + (\bar{q}_5^R + j\bar{q}_5^I)s^5 + \dots, \\ P_3(s) = (q_0^R + j\bar{q}_0^I) + (\bar{q}_1^R + j\bar{q}_1^I)s + (\bar{q}_2^R + jq_2^I)s^2 + (q_3^R + jq_3^I)s^3 + (q_4^R + j\bar{q}_4^I)s^4 + (\bar{q}_5^R + j\bar{q}_5^I)s^5 + \dots, \\ P_4(s) = (\bar{q}_0^R + j\bar{q}_0^I) + (\bar{q}_1^R + j\bar{q}_1^I)s + (q_2^R + jq_2^I)s^2 + (q_3^R + j\bar{q}_3^I)s^3 + (\bar{q}_4^R + j\bar{q}_4^I)s^4 + (\bar{q}_5^R + j\bar{q}_5^I)s^5 + \dots, \\ P_5(s) = (q_0^R + jq_0^I) + (q_1^R + jq_1^I)s + (\bar{q}_2^R + j\bar{q}_2^I)s^2 + (q_3^R + j\bar{q}_3^I)s^3 + (q_4^R + jq_4^I)s^4 + (\bar{q}_5^R + jq_5^I)s^5 + \dots, \\ P_6(s) = (q_0^R + j\bar{q}_0^I) + (q_1^R + jq_1^I)s + (\bar{q}_2^R + jq_2^I)s^2 + (\bar{q}_3^R + j\bar{q}_3^I)s^3 + (q_4^R + j\bar{q}_4^I)s^4 + (q_5^R + jq_5^I)s^5 + \dots, \\ P_7(s) = (\bar{q}_0^R + jq_0^I) + (\bar{q}_1^R + j\bar{q}_1^I)s + (q_2^R + j\bar{q}_2^I)s^2 + (q_3^R + jq_3^I)s^3 + (\bar{q}_4^R + jq_4^I)s^4 + (\bar{q}_5^R + j\bar{q}_5^I)s^5 + \dots, \\ P_8(s) = (\bar{q}_0^R + j\bar{q}_0^I) + (q_1^R + j\bar{q}_1^I)s + (q_2^R + jq_2^I)s^2 + (\bar{q}_3^R + jq_3^I)s^3 + (\bar{q}_4^R + j\bar{q}_4^I)s^4 + (q_5^R + j\bar{q}_5^I)s^5 + \dots \end{cases} \quad (4)$$

Now, let us consider a complex interval family of FO polynomials as

$$\begin{aligned} \Delta(s) &= \Delta^R(s) + j\Delta^I(s) = q_0^R + \sum_{h=1}^n q_h^R s^{\alpha_h} + j \left(q_0^I + \sum_{h=1}^n q_h^I s^{\alpha_h} \right) \\ &= (q_0^R + jq_0^I) + \sum_{h=1}^n (q_h^R + jq_h^I) s^{\alpha_h}, \end{aligned} \quad (5)$$

in which $\Delta^R(s)$ and $\Delta^I(s)$ are respectively the real and imaginary polynomial parts of $\Delta(s)$ and also the intervals q_i^R and q_i^I are respectively defined in Eqs. (2) and (3). Moreover, the orders α_i , ($i = 1, \dots, n$) satisfy $0 < \alpha_1 < \alpha_2 < \dots < \alpha_n$. It is apparent that $\delta(s)$ in Eq. (1) is only a special case of the complex interval family considered in this paper i.e. $\Delta(s)$ in Eq. (5).

Definition 1. $\Delta(s)$ is a FO system of commensurate order α if there exists a $\alpha \in \mathbb{R}^{\geq 0}$ such that $\alpha_i/\alpha \in \mathbb{N}$. Otherwise, $\Delta(s)$ is a FO systems of non-commensurate order.

Remark 1. Based on [31], the value set of $\Delta^R(s)$ is a parpolygon whose vertices can be obtained by the following pattern:

$$\begin{cases} V_1^R(s) = q_0^R + q_1^R s^{\alpha_1} + \dots + q_n^R s^{\alpha_n}, \\ V_2^R(s) = \bar{q}_0^R + q_1^R s^{\alpha_1} + \dots + q_n^R s^{\alpha_n}, \\ V_3^R(s) = q_0^R + \bar{q}_1^R s^{\alpha_1} + \dots + q_n^R s^{\alpha_n}, \\ \dots \\ V_{2^{n+1}}^R(s) = \bar{q}_0^R + \bar{q}_1^R s^{\alpha_1} + \dots + \bar{q}_n^R s^{\alpha_n}. \end{cases} \quad (6)$$

The exposed edges can be determined by Eq. (6). For instance, $V_1^R(s)$ and $V_2^R(s)$ have the same structure except q_0^R . Accordingly, one of the edges can be considered as $e(V_1^R(s), V_2^R(s))$. The remaining edges can be built in a similar way. Create a set that includes all of the vertices $V_{i_1}^R(s)$ ($i_1 = 1, \dots, 2^{n+1}$) as

$$P_E^R(s) = \{e(V_1^R(s), V_2^R(s)), e(V_1^R(s), V_3^R(s)), \dots, e(V_{2^{n+1}-1}^R(s), V_{2^{n+1}}^R(s))\}. \quad (7)$$

Likewise, the vertex polynomials $V_i^I(s) (i_1 = 1, \dots, 2^{n+1})$ and the set of exposed edges $P_E^I(s)$ corresponding to $\Delta^I(s)$ are respectively defined in Eqs. (8) and (9).

$$\begin{cases} V_1^I(s) = \underline{q}_0^I + \underline{q}_1^I s^{\alpha_1} + \dots + \underline{q}_n^I s^{\alpha_n}, \\ V_2^I(s) = \overline{q}_0^I + \underline{q}_1^I s^{\alpha_1} + \dots + \underline{q}_n^I s^{\alpha_n}, \\ V_3^I(s) = \underline{q}_0^I + \overline{q}_1^I s^{\alpha_1} + \dots + \underline{q}_n^I s^{\alpha_n}, \\ \dots \\ V_{2^{n+1}}^I(s) = \overline{q}_0^I + \overline{q}_1^I s^{\alpha_1} + \dots + \overline{q}_n^I s^{\alpha_n}. \end{cases} \quad (8)$$

$$P_E^I(s) = \{e(V_1^I(s), V_2^I(s)), e(V_1^I(s), V_3^I(s)), \dots, e(V_{2^{n+1}-1}^I(s), V_{2^{n+1}}^I(s))\}. \quad (9)$$

Consider the FO polynomial below as an example.

$$\Delta^R(s) = [0.6, 1]s^{2.2} + 3.73s^{1.15} + [0.3, 0.7]s^{0.9} + [21.3, 21.7]. \quad (10)$$

Based on the points mentioned the above, the vertex polynomials and the exposed edges of $\Delta^R(s)$ are as follows:

$$\begin{cases} V_1^R(s) = 0.6s^{2.2} + 3.73s^{1.15} + 0.3s^{0.9} + 21.3, \\ V_2^R(s) = 0.6s^{2.2} + 3.73s^{1.15} + 0.3s^{0.9} + 21.7, \\ V_3^R(s) = 0.6s^{2.2} + 3.73s^{1.15} + 0.7s^{0.9} + 21.3, \\ V_4^R(s) = 0.6s^{2.2} + 3.73s^{1.15} + 0.7s^{0.9} + 21.7, \\ V_5^R(s) = s^{2.2} + 3.73s^{1.15} + 0.3s^{0.9} + 21.3, \\ V_6^R(s) = s^{2.2} + 3.73s^{1.15} + 0.3s^{0.9} + 21.7, \\ V_7^R(s) = s^{2.2} + 3.73s^{1.15} + 0.7s^{0.9} + 21.3, \\ V_8^R(s) = s^{2.2} + 3.73s^{1.15} + 0.7s^{0.9} + 21.7. \end{cases} \quad (11)$$

$$P_E(s) = \left\{ e(V_1^R(s), V_2^R(s)), e(V_1^R(s), V_3^R(s)), e(V_1^R(s), V_5^R(s)), e(V_2^R(s), V_4^R(s)), \right. \\ e(V_2^R(s), V_6^R(s)), e(V_3^R(s), V_4^R(s)), e(V_3^R(s), V_7^R(s)), e(V_4^R(s), V_8^R(s)), \\ \left. e(V_5^R(s), V_6^R(s)), e(V_5^R(s), V_7^R(s)), e(V_6^R(s), V_8^R(s)), e(V_7^R(s), V_8^R(s)) \right\}. \quad (12)$$

Definition 2. In this paper, for the sake of simplicity, we define

$$T_{-\hat{v}(s)}\{P_E^R(s)\} = T_{-\hat{v}(s)}^R \triangleq \left\{ \underbrace{|V_1^R(s) + \hat{v}(s)| + |V_2^R(s) + \hat{v}(s)| - |V_1^R(s) - V_2^R(s)|}_{I_1^R}, \right. \\ \underbrace{|V_1^R(s) + \hat{v}(s)| + |V_3^R(s) + \hat{v}(s)| - |V_1^R(s) - V_3^R(s)|, \dots,}_{I_2^R} \\ \left. \underbrace{|V_{2^{n+1}-1}^R(s) + \hat{v}(s)| + |V_{2^{n+1}}^R(s) + \hat{v}(s)| - |V_{2^{n+1}-1}^R(s) - V_{2^{n+1}}^R(s)|}_{I_{(n+1)2^n}^R} \right\}. \quad (13)$$

In Eq. (13), $\hat{v}(s)$ is a FO polynomial. Likewise, we define

$$T_{-\hat{v}(s)}\{jP_E^I(s)\} = T_{-\hat{v}(s)}^I \triangleq \left\{ \underbrace{|jV_1^I(s) + \hat{v}(s)| + |jV_2^I(s) + \hat{v}(s)| - |jV_1^I(s) - jV_2^I(s)|}_{l_1^I}, \right. \\ \left. \underbrace{|jV_1^I(s) + \hat{v}(s)| + |jV_3^I(s) + \hat{v}(s)| - |jV_1^I(s) - jV_3^I(s)|}_{l_2^I}, \dots, \right. \\ \left. \underbrace{|jV_{2^{n+1}-1}^I(s) + \hat{v}(s)| + |jV_{2^{n+1}}^I(s) + \hat{v}(s)| - |jV_{2^{n+1}-1}^I(s) - jV_{2^{n+1}}^I(s)|}_{l_{(n+1)2^n}^I} \right\}. \quad (14)$$

2.2. Problem definition

These two problems are addressed in this paper:

1. To present a graphical method for testing the robust stability of $\Delta(s)$ in Eq. (5).
2. To verify the robust stability of $\Delta(s)$ using finite numbers of its members (i.e. some FO polynomials of the whole family $\Delta(s)$).

Concerning the first problem, the zero exclusion principle and the value set are employed. Based on the methods presented in Moornani and Haeri [17,18], Mohsenipour and Liu [30], the approximated shape of the value set is obtained by plotting too many randomly produced points in the uncertainty space. But, these methods are clearly numerical and computationally cumbersome. However, since Theorems 1 and 2 of this paper provide some exposed edges of the value set explicitly, from a computational aspect, this may be appealing.

Concerning the paper's second problem, in Moornani and Haeri [17,18], Mohsenipour and Liu [30], it is needed to depict two-dimensional graphs of the value sets at each frequency by numerous polynomials and it may be too difficult to investigate the value sets. Also, a frequent technique to examine and perform the process of robust stability analysis is to present an auxiliary function. Accordingly, Theorem 3 presents a robust stability assessment function based on geometric characteristics and explicit descriptions of the value sets instead of two-dimensional graphs of the value sets. Therefore, the computational complexity of the robust stability conditions can be decreased significantly by the auxiliary function $\Xi(\omega)$ presented in Theorem 3.

3. Main result

3.1. Robust stability analysis

To address the first problem raised in Section 2.2, Theorem 1 is presented by which it is possible to determine whether or not a system with $\Delta(j\omega)$ in Eq. (5) is robust stable. In Theorem 1, the zero exclusion condition is checked using an exact graphical method. As a result, necessary and sufficient conditions of the complex interval family $\Delta(s)$ are derived for robust stability analysis.

Theorem 1. $\Delta(s)$ in Eq. (5) is robustly stable if and only if:

1. $\Delta(s)$ contains one stable polynomial as $\Delta_0(s)$.
2. The exposed edges $-P_E^R(j\omega)$ and $jP_E^I(j\omega)$ do not have any overlap for $\omega \in (-\infty, \infty)$ in the complex plane.

Proof. The ‘if’ portion: Based on [32] and Remark 1, at a given frequency $\omega = \omega_0$, it has been shown that

$$\begin{cases} \partial(\Delta^R(j\omega)) \subseteq P_E^R(j\omega), \\ \partial(\Delta^I(j\omega)) \subseteq P_E^I(j\omega). \end{cases} \quad (15)$$

As a contradiction argument it is supposed that at $\omega = \omega_0$, the value sets of $-P_E^R(j\omega)$ and $jP_E^I(j\omega)$ have an overlap. As a result, a complex number as Z_0 exists such that $Z_0 \in -P_E^R(j\omega)$ (or $-Z_0 \in P_E^R(j\omega)$) and $Z_0 \in jP_E^I(j\omega)$. Therefore, from Eq. (5), it can be concluded that

$$\begin{cases} -Z_0 \in P_E^R(j\omega), \\ Z_0 \in jP_E^I(j\omega), \end{cases} \Rightarrow 0 \in \Delta(j\omega_0). \quad (16)$$

Then, by the zero exclusion principle, because of $0 \in \Delta(j\omega_0)$, the system is not robustly stable. It contradicts the robust stability condition of the closed-loop control system.

The ‘only if’ portion: Since, the system is robustly stable, then $0 \notin \Delta(j\omega)$ by the zero exclusion principle. Assume the value sets of $-\Delta^R(j\omega)$ and $j\Delta^I(j\omega)$ are respectively defined as $-\Delta_{vs}^R(j\omega)$ and $\Delta_{vs}^I(j\omega)$. Now, assume that there are two arbitrary complex numbers as $Z_1, Z_2 \in \mathbb{C}$ such that $Z_1 \in -\Delta_{vs}^R(j\omega)$ (or $-Z_1 \in \Delta_{vs}^R(j\omega)$) and $Z_2 \in \Delta_{vs}^I(j\omega)$.

$$\begin{cases} -Z_1 \in \Delta_{vs}^R(j\omega), \\ Z_2 \in \Delta_{vs}^I(j\omega), \end{cases} \Rightarrow Z_2 - Z_1 \in \Delta_{vs}(j\omega). \quad (17)$$

Because of $0 \notin \Delta(j\omega)$, it can be simply concluded that $Z_2 - Z_1 \neq 0$ or $Z_1 \neq Z_2$. This implies that the arbitrary complex number Z_1 is not equal to Z_2 and consequently the exposed edges of $-P_E^R(j\omega)$ and $jP_E^I(j\omega)$ do not have any overlap. Hence, using the zero exclusion principle, the proof is ended. \square

Remark 2. In Theorem 1, one can check the overlap between the exposed edges $P_E^R(j\omega)$ and $-jP_E^I(j\omega)$ instead of the exposed edges $-P_E^R(j\omega)$ and $jP_E^I(j\omega)$ at each frequency.

3.2. Robust stability testing function

For robust stability analysis by using Theorem 1, the overlap between the exposed edges $-P_E^R(j\omega)$ and $jP_E^I(j\omega)$ has to be checked at each frequency. In other words, it is needed to depict two-dimensional graphs of the exposed edges $-P_E^R(j\omega)$ and $jP_E^I(j\omega)$ in the complex plane at each frequency and it may be too difficult to examine the overlap between the exposed edges. Accordingly, in the following theorem, the overlap between the exposed edges $-P_E^R(j\omega)$ and $jP_E^I(j\omega)$ is developed using the geometric properties of parpolygons.

Theorem 2. The exposed edges $-P_E^R(j\omega)$ and $jP_E^I(j\omega)$ have no overlap for $\omega \in (-\infty, \infty)$, if and only if:

1. $-V_{i_1}^R(j\omega)(i_1 = 1, \dots, 2^{n+1}) \notin jP_E^I(j\omega)$, which means that $-V_{i_1}^R(j\omega)$ are not located inside (or on) the value set with the exposed edges $jP_E^I(j\omega)$.
2. $jV_{i_1}^I(j\omega)(i_1 = 1, \dots, 2^{n+1}) \notin -P_E^R(j\omega)$.

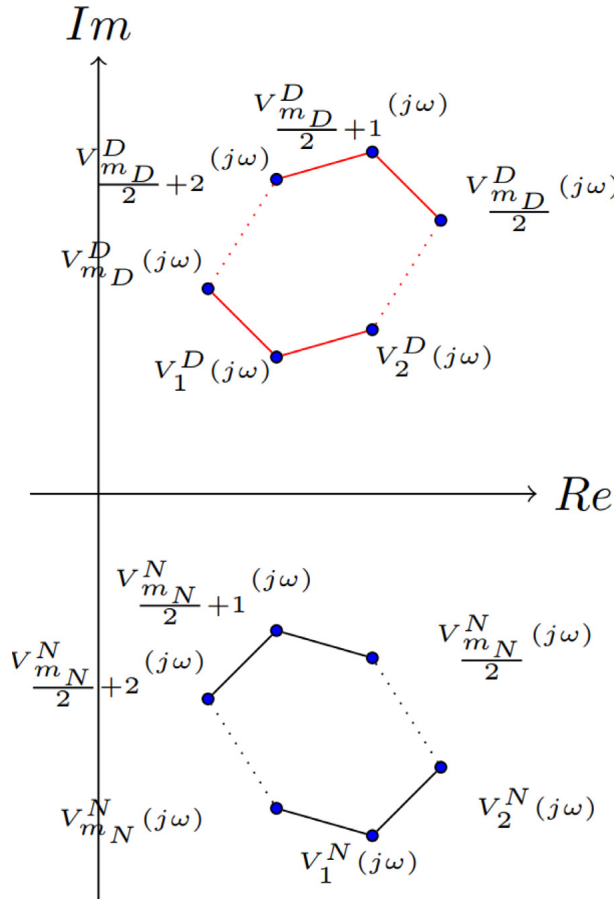


Fig. 1. An illustration of two parpolygons with the vertices $V_i^D(j\omega)$ ($i = 1, \dots, m_D$) and $V_r^N(j\omega)$ ($r = 1, \dots, m_N$).

Proof. *The ‘if’ portion:* In the complex plane, consider two parpolygons having the vertices $V_i^D(j\omega)$ ($i = 1, \dots, m_D$) and $V_r^N(j\omega)$ ($r = 1, \dots, m_N$) as shown in Fig. 1. As seen from Fig. 1, the conditions 1 and 2 in this theorem are met. Fig. 1 shows the geometric structure of parpolygons, and it is easy to see that these parpolygons have no overlap.

The ‘only if’ portion: It is assumed that as a contradiction argument, this theorem’s initial condition is not fulfilled. This indicates that at least one vertex as $V_x^R(j\omega_0)$ exists which is included in the value set with the boundary $jP_E^I(j\omega_0)$ i.e. $V_x^R(j\omega_0) \in -jP_E^I(j\omega_0)$ or $-V_x^R(j\omega_0) \in jP_E^I(j\omega_0)$. As a result, it may be deduced from Theorem 1 that $0 \in \Delta(j\omega_0)$ and this signifies that the exposed edges $-P_E^R(j\omega)$ and $jP_E^I(j\omega)$ have the overlap at $\omega = \omega_0$. This is in contrast to the requirement of no overlap between the exposed edges $-P_E^R(j\omega)$ and $jP_E^I(j\omega)$. \square

The next goal is to figure out how to solve Problem 2. Combining the results of Theorems 1 and 2 allows us to handle Problem 2. An auxiliary function is introduced as a robust stability testing function in the following theorem to analyze the conditions (1) and (2) in Theorem 2.

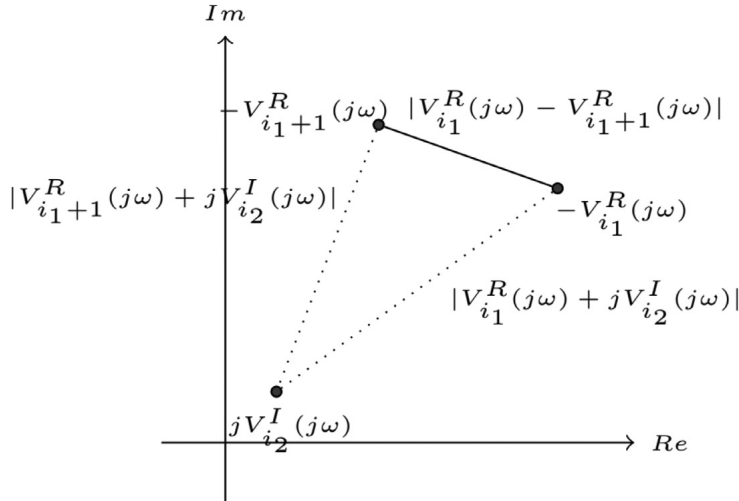


Fig. 2. the edges $e(-V_{i_1}^R(j\omega), -V_{i_1+1}^R(j\omega))$ (bold line), distance between the vertices $jV_{i_2}^I(j\omega)$ and the vertices $-V_{i_1}^R(j\omega)$ and $-V_{i_1+1}^R(j\omega)$ (dotted lines).

Theorem 3. $\Delta(s)$ in Eq. (5) is robust stable if and only if:

1. $\Delta(s)$ contains a stable polynomial as $\Delta_0(s)$.
2. For $\omega \in (-\infty, \infty)$, the inequality $\Xi(\omega) > 0$ is met in which $\Xi(\omega)$ is introduced in Eq. (18).

$$\Xi(\omega) \triangleq \min \{ \overline{\Xi}_1(j\omega), \overline{\Xi}_2(j\omega), \dots, \overline{\Xi}_{2^{n+1}}(j\omega), \underline{\Xi}_1(j\omega), \underline{\Xi}_2(j\omega), \dots, \underline{\Xi}_{2^{n+1}}(j\omega) \}, \quad (18)$$

$$\overline{\Xi}_{i_1}(j\omega) \triangleq \min_{l_i^R \in T_{-jV_{i_1}^I(j\omega)}^R} l_i^R, \quad i \in \{1, 2, \dots, (n+1)2^n\}, i_1 \in \{1, 2, \dots, 2^{n+1}\},$$

$$\underline{\Xi}_{i_2}(j\omega) \triangleq \min_{l_i^I \in T_{-V_{i_2}^R(j\omega)}^I} l_i^I, \quad i \in \{1, 2, \dots, (n+1)2^n\}, i_2 \in \{1, 2, \dots, 2^{n+1}\},$$

where, $T_{-jV_{i_1}^I(j\omega)}^R$ and $T_{V_{i_2}^R(j\omega)}^I$ are given by Definition 2.

Proof. This theorem is proven using the triangle inequality. The vertices $jV_{i_2}^I(j\omega)$ and $e(-V_{i_1}^R(j\omega), -V_{i_1+1}^R(j\omega))$ are schematically shown in Fig. 2. Based on Fig. 2 and the triangle inequality, the statements below can be deduced.

- If the values of $\overline{\Xi}_{i_2}(j\omega)$ in Eq. (18) are positive, then the vertices $jV_{i_2}^I(j\omega)$ do not intersect the edges $e(-V_{i_1}^R(j\omega), -V_{i_1+1}^R(j\omega))$.
- If the function $\overline{\Xi}_{i_2}(j\omega)$ in Eq. (18) is equal to zero at $\omega = \omega_0$, then the vertices $jV_{i_2}^I(j\omega)$ intersect the edges $e(-V_{i_1}^R(j\omega), -V_{i_1+1}^R(j\omega))$.

On the other hand we know that $\partial(\Delta^R(j\omega)) \subseteq P_E^R(j\omega)$. Hence, satisfying the inequalities $\overline{\Xi}_{i_2}(j\omega) > 0$ assure that the vertices $jV_{i_2}^I(j\omega)$ do not intersect $\partial(\Delta^R(j\omega))$. Therefore, the

condition (1) is satisfied in [Theorem 2](#). Similarly, if the inequalities $\underline{\Xi}_{i_2}(j\omega) > 0$ are satisfied then the condition (2) in [Theorem 2](#) is also met as well. Accordingly, based on [Definition 2](#), [Theorems 1](#) and [2](#), the theorem is easily completed. \square

3.3. Frequency bounds for simulation purposes

It would be impossible to take into account the frequency range $\omega \in (-\infty, +\infty)$ in the simulation. We define non-zero and finite bounds on ω using the following theorem in order to achieve the correct scenario for using [Theorems 1](#) and [3](#) in simulations.

Theorem 4. *The roots of $\Delta(s)$ in [Eq. \(5\)](#) lie in $\{s \in \mathbb{C} | S_{\min} \leq |s| \leq S_{\max}\}$ in which*

$$\begin{aligned}
 S_{\max} &\triangleq \max \left\{ 1, R_{\max}^{\frac{1}{\alpha_n - \alpha_{n-1}}} \right\}, R_{\max} \triangleq \frac{\sum_{h=0}^{n-1} \left(\max\{|q_h^R|, |\bar{q}_h^R|\} + \max\{|q_h^I|, |\bar{q}_h^I|\} \right)}{F}, \\
 F &\triangleq \sqrt{F_1^2 + F_2^2}, \\
 F_1 &\triangleq \begin{cases} 0, 0 \in q_n^R, \\ \min\{|q_n^R|, |\bar{q}_n^R|\}, 0 \notin q_n^R, \end{cases} \\
 F_2 &\triangleq \begin{cases} 0, 0 \in q_n^I, \\ \min\{|q_n^I|, |\bar{q}_n^I|\}, 0 \notin q_n^I. \end{cases} \tag{19}
 \end{aligned}$$

$$\begin{aligned}
 S_{\min} &\triangleq \min \left\{ 1, R_{\min}^{\frac{1}{\alpha_1}} \right\}, R_{\min} \triangleq \frac{E}{\sum_{h=1}^n \left(\max\{|q_h^R|, |\bar{q}_h^R|\} + \max\{|q_h^I|, |\bar{q}_h^I|\} \right)}, \\
 E &\triangleq \sqrt{E_1^2 + E_2^2}, \\
 E_1 &\triangleq \begin{cases} 0, 0 \in q_0^R, \\ \min\{|q_0^R|, |\bar{q}_0^R|\}, 0 \notin q_0^R, \end{cases} \\
 E_2 &\triangleq \begin{cases} 0, 0 \in q_0^I, \\ \min\{|q_0^I|, |\bar{q}_0^I|\}, 0 \notin q_0^I. \end{cases} \tag{20}
 \end{aligned}$$

Proof. The inequality $|\Delta(s)| > 0$ guarantees the condition $0 \notin \Delta(s)$. Therefore, we need to show that for $\{s \in \mathbb{C} | S_{\min} > |s| \text{ \& } |s| > S_{\max}\}$, $|\Delta(s)| > 0$ is met. From [Eq. \(5\)](#), the triangle inequality $|A| - |B + C| > |A| - |B| - |C|$ and the assumption $|s| > 1$, we have

$$\begin{aligned}
 |\Delta(s)| &\geq F |s|^{\alpha_n} - \sum_{h=0}^n \left(\max\{|q_h^R|, |\bar{q}_h^R|\} + \max\{|q_h^I|, |\bar{q}_h^I|\} \right) |s|^{\alpha_h} \\
 &\geq F |s|^{\alpha_{n-1}} \left(|s|^{\alpha_n - \alpha_{n-1}} - R_{\max} \right). \tag{21}
 \end{aligned}$$

From [Eq. \(21\)](#) it can be inferred that $|\Delta(s)| > 0$ is satisfied for $\{s \in \mathbb{C} | |s| > S_{\max}\}$. Also, we can write for $|s| < 1$,

$$|\Delta(s)| \geq E - \sum_{h=1}^n \left(\max\{|q_h^R|, |\bar{q}_h^R|\} + \max\{|q_h^I|, |\bar{q}_h^I|\} \right) |s|^{\alpha_h}$$

$$\geq \sum_{h=1}^n \left(\max \left\{ |\underline{q}_h^R|, |\overline{q}_h^R| \right\} + \max \left\{ |\underline{q}_h^I|, |\overline{q}_h^I| \right\} \right) (R_{\min} - |s|^{\alpha_1}). \quad (22)$$

From Eq. (22), it can be seen that $|\Delta(s)| > 0$ is also satisfied for $\{s \in \mathbb{C} \mid |s| < S_{\min}\}$. \square

The following corollaries are offered to assess the robust stability of $\Delta(s)$ in Eq. (5) as a simple consequence of Theorem 4.

Corollary 1. *The characteristic function $\Delta(s)$ in Eq. (5) is robust stable if and only if:*

1. $\Delta(s)$ contains one stable polynomial as $\Delta_0(s)$.
2. The inequality $\Xi(\omega) > 0$ is met for $\omega \in [-S_{\max}, -S_{\min}] \cup [S_{\min}, S_{\max}]$ in which $\Xi(\omega)$ is introduced in Eq. (18).

Proof. The proof can be completed quickly by applying Theorems 1–4. \square

Corollary 2. *Assume that $\Delta^I(s) = 0$ in Eq. (5). Then, the characteristic function $\Delta(s)$ in Eq. (5) is robust stable if and only if:*

1. $\Delta(s)$ contains one stable polynomial as $\Delta_0(s)$.
2. The inequality $\Xi(\omega) = \overline{\Xi}_{i_1}(j\omega) > 0$ is met for $\omega \in [S_{\min}, S_{\max}]$ where $\Xi(\omega)$ is defined in Eq. (18).

Proof. Because of $\Delta^I(s) = 0$, $\Delta(s)$ in Eq. (5) is a real-valued function. Hence, with respect to the real axis, the roots of $\Delta(s)$ are mirror symmetric. As a result of Corollary 1, the proof can be easily completed. \square

Remark 3. The following are the steps for examining the robust stability of $\Delta(s)$:

1. Examine the stability of a member of $\Delta(s)$ as $\Delta_0(s)$. In this paper, the Principle of Argument theorem [38] is used to check the stability of $\Delta_0(s)$ (See Examples 2 and 4). If $\Delta_0(s)$ is stable, carry on the next steps. Otherwise, $\Delta(s)$ is not robustly stable.
2. Obtain the exposed edges $P_E^R(j\omega)$ and $P_E^I(j\omega)$ by using Remark 1.
3. Examine the robust stability by benefiting from Corollaries 1 and 2.

Remark 4. It is notable that all Theorems 1–4 are applicable to integer-order polynomials as $\delta(s)$ in Eq. (1). It is because that based on Remark 1, $\partial(\delta(j\omega)) \subseteq P_E(j\omega)$ and $\partial(\Delta(j\omega)) \subseteq P_E(j\omega)$. On the other hand, Theorems 1 and 3 exactly determine whether or not $0 \in P_E(j\omega)$. Because of $\partial(\delta(j\omega)) \subseteq P_E(j\omega)$ and $\partial(\Delta(j\omega)) \subseteq P_E(j\omega)$, it can be inferred that the robust stability analysis presented in Remark 3 can be employed for $\delta(j\omega)$.

Remark 5. Note that all theorems presented in this section are applicable to systems of non-commensurate order and accordingly of commensurate order.

4. Illustrative examples

Four numerical examples are provided in this section to verify and exemplify the acquired results. Based on the methodologies described in the prior literature, it is shown that studying the robust stability of FO polynomials with complex uncertainties is difficult, but this difficulty is alleviated by the robust stability testing function $\Xi(\omega)$ in Eq. (18).

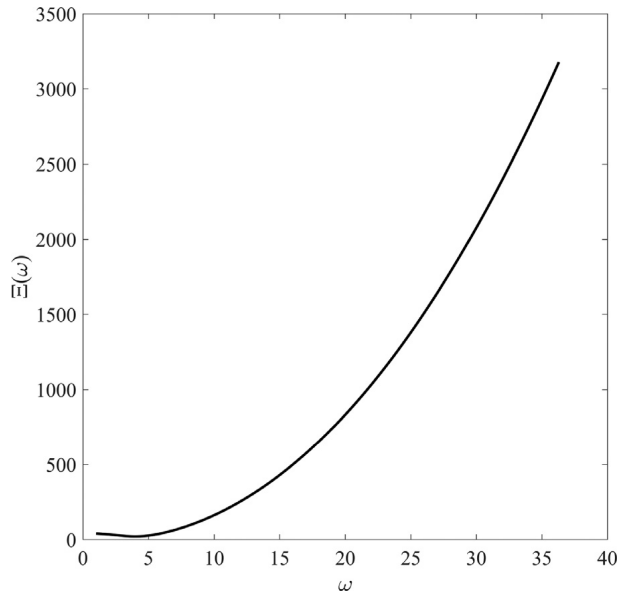


Fig. 3. $\Xi(\omega)$ within the frequency range $[1, 36.3866]$ rad/s.

Example 1. Firstly, let us consider an interval FO polynomial with the characteristic function presented in Eq. (10).

In [31], it has been shown that $\Delta(s)$ in Eq. (10) is robust stable. We check these results by benefiting from Corollary 2. Based on Remark 1, the vertices and the exposed edges of $\Delta(s)$ in Eq. (10) are respectively presented in Eqs. (11) and (12). According to Theorem 4, S_{\min} and S_{\max} are respectively obtained as 1 rad/s and 36.3866 rad/s. Moreover, the function $\Xi(\omega)$ is plotted in Fig. 3. As seen from Fig. 3, $\Xi(\omega) > 0$ is held. From Corollary 2, the robust stability can be simply concluded.

In [31], the value sets of the exposed edges of $\Delta^R(j\omega)$ must be plotted for $\omega \in [0, \infty)$. Whereas, based on the method described in this paper, the sign of the robust stability testing function $\Xi(\omega)$ within the finite frequency range $\omega \in [1, 36.3866]$ rad/s verifies the robust stability. Hence, instead of depicting the value sets $\Delta^R(j\omega)$ as two-dimensional graphs for $\omega \in [0, \infty)$, the sign of $\Xi(\omega)$ in Eq. (18) is only checked for $\omega \in [1, 36.3866]$ rad/s. It is visible that the robust stability testing function $\Xi(\omega)$ considerably reduces the computational cost.

Example 2. Let us study the robust stability of the characteristic function Eq. (23).

$$\Delta(s) = (1 + 0.01j)s^{1.3} + ([2, 3] + [0.01, 0.2]j)s^{1.1} + (1 + j)s^{0.6} + [0.2, 0.4] + [0.5, 6]j. \quad (23)$$

Based on Theorem 4, one obtains $S_{\min} = 0.1561$ and $S_{\max} = 2.0998 \times 10^5$. Also, $\Delta_0(s)$ is considered as Eq. (24).

$$\Delta_0(s) = (1 + 0.01j)s^{1.3} + (2 + 0.1j)s^{1.1} + (1 + j)s^{0.6} + 0.2 + 0.5j. \quad (24)$$

As mentioned in Remark 2, the Principle of Argument theorem is employed to check the stability of $\Delta_0(s)$. Consider the Jordan curve as $\{s = j\omega | \omega \in [S_{\min}, S_{\max}], \omega \in [-S_{\max}, -S_{\min}]\} \cup$

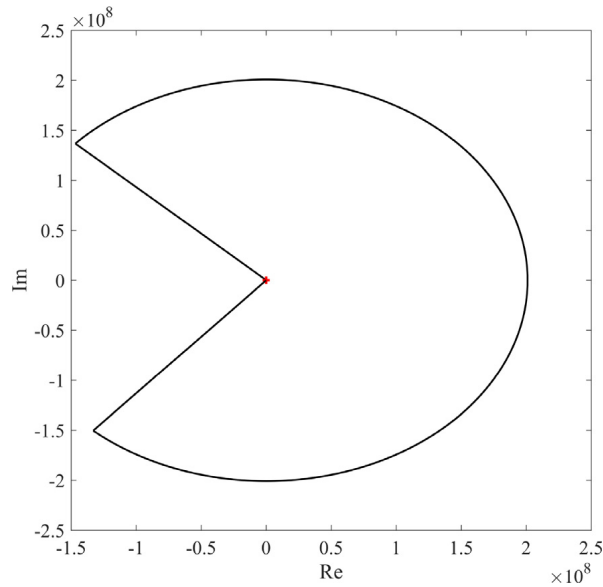


Fig. 4. The path given by $\Delta_0(s)$ for s on the Jordan curve.

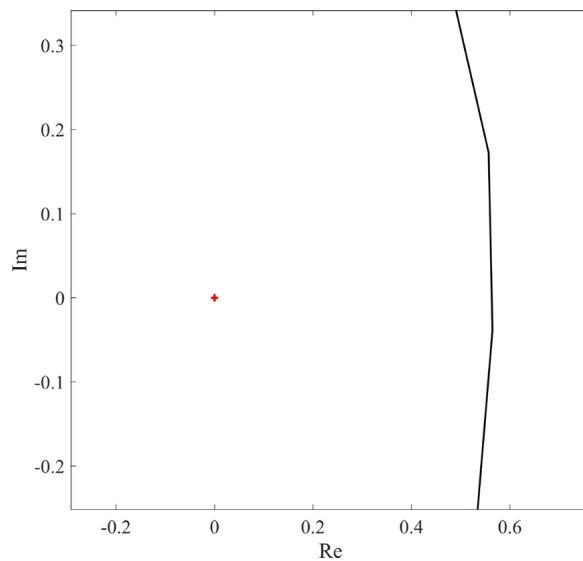


Fig. 5. Zoomed in around the origin of Fig. 4.

$\{s = S_{\min} e^{j\theta} | \theta \in [-\frac{\pi}{2}, \frac{\pi}{2}]\} \cup \{s = S_{\max} e^{j\theta} | \theta \in [-\frac{\pi}{2}, \frac{\pi}{2}]\}$. The path given by $\Delta_0(s)$ when s traverses the Jordan curve is determined as Figs. 4 and 5. The number of encirclements of the origin by the path equals zero, as seen in these figures. By the Principle of Argument, $\Delta_0(s)$ is stable. In addition, the curve of $\Xi(\omega)$ is plotted in Figs. 6 and 7. Robust stability of the considered system can be simply inferred from Corollary 1, Figs. 6 and 7.

According to the methods proposed in Moornani and Haeri [17,18], Mohsenipour and Liu [30], by plotting randomly produced points in the uncertainty space, the approximated

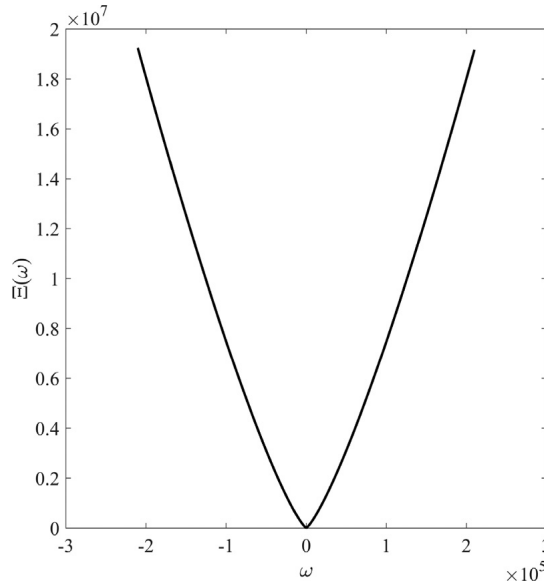


Fig. 6. $\Xi(\omega)$ within the frequency range.

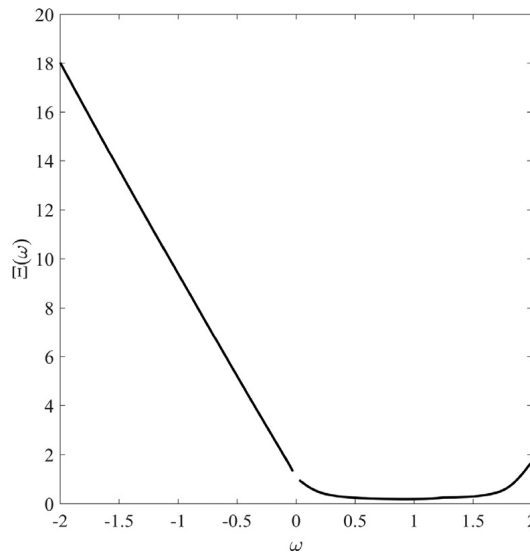


Fig. 7. A better view of Fig. 6 around $\Xi(\omega) = 0$.

shape has been determined. For example, the approximated shape of the value set is obtained by plotting one million randomly produced points at $\omega = 1$ rad/s in Fig. 8. Whereas, eight polynomial vertices have been only used to construct the function $\Xi(\omega)$. Also, the sign of $\Xi(\omega)$ can easily investigate whether or not the origin is a part of $\Delta(j\omega)$ at each frequency. This implies that the results of this paper increase the computational efficiency in comparison to the existing methods.

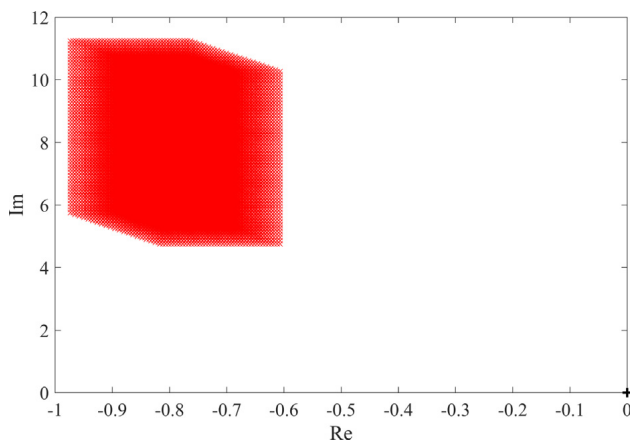


Fig. 8. The approximated shape of the value set by plotting randomly huge produced points at $\omega = 1$ rad/s.

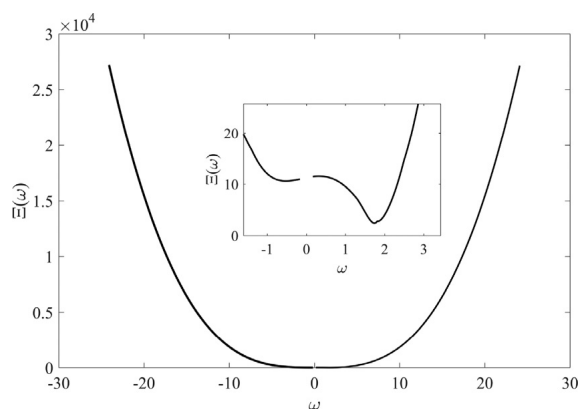


Fig. 9. $\Xi(\omega)$ within the frequency range.

Example 3. Consider the following integer-order polynomial with complex uncertain parameters:

$$\delta(s) = s^3 + (4 - j[-0.7, 0.7])s^2 + ([6.3, 7.7] - 3j)s + [5.3, 6.7] - 2j. \quad (25)$$

In [27], it was shown that $\delta(s)$ is robust stable. In the following, the robust stability of $\delta(s)$ is checked by Remark 3 presented in this paper. According to Theorem 4, one obtains $S_{\min} = 0.3345$ and $S_{\max} = 24.1$. Hence, the values of $\Xi(\omega)$ are checked for $\omega \in [-S_{\max}, -S_{\min}] \cup [S_{\min}, S_{\max}]$ rad/s. As can be seen in Fig. 9, the inequality $\Xi(\omega) > 0$ holds, indicating that the system is robustly stable. This is the same result as [27]. Hence, the proposed robust stability criteria can be also applied for integer-order systems with complex uncertain parameters.

Example 4. Consider the following FO polynomial with complex uncertain parameters:

$$\Delta(s) = s^{3.2} + ([5, 5.5] + [-0.25, 0.25]j)s^{1.9} + ([7, 7.5] + 3j)s^{0.9} + [6, 6.5] + [-2.2, -1.8]j. \quad (26)$$

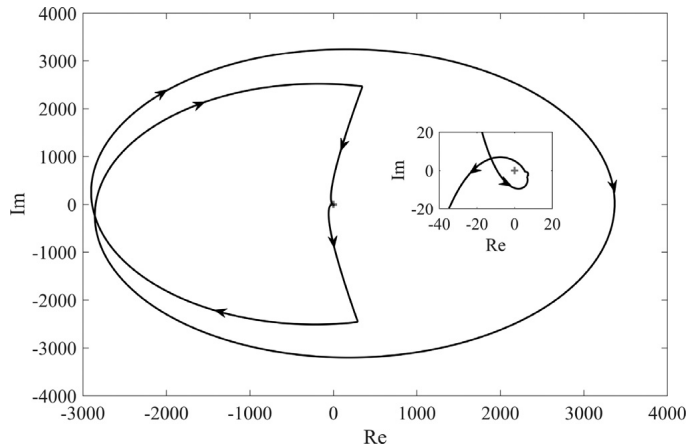


Fig. 10. The path given by $\Delta_0(s)$ in Eq. (27) for s on the Jordan curve.

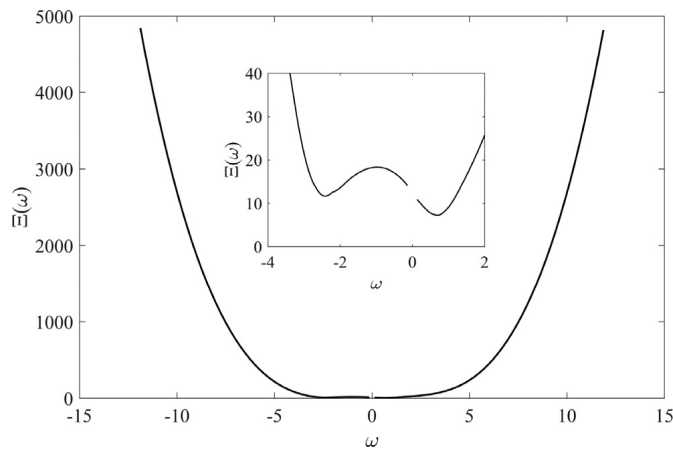


Fig. 11. $\Xi(\omega)$ in Eq. (18) within the frequency range.

Based on Theorem 4, S_{\min} and S_{\max} are respectively obtained as 0.3631 rad/s and 11.876 rad/s. Also, $\Delta_0(s)$ is considered as Eq. (27).

$$\Delta_0(s) = s^{3.2} + 5s^{1.9} + (7 + 3j)s^{0.9} + 6 - 2j. \quad (27)$$

The path of $\Delta_0(s)$ when s traverses the Jordan curve can be obtained as Fig. 10. Also, the values of $\Xi(\omega)$ in Eq. (18) are reported in Fig. 11. From Fig. 11, $\Xi(\omega) > 0$ holds over the whole interval. Therefore, the system is robustly stable.

Now, assume that the interval $[5, 5.5]$ before the term $s^{1.9}$ is enlarged to $[3, 5.5]$. $\Xi(\omega)$ in Eq. (18) is plotted in Fig. 12. $\Xi(\omega) = 0$ occurs at some frequencies in Fig. 12. Therefore, this system is not robustly stable for the enlarged interval in this example. The exposed edges $-P_E^D(s)$ and $P_E^N(s)$ are drawn at $\omega = -2.6$ rad/s in Fig. 13. By Fig. 13, these exposed edges have an overlap in the complex plane at $\omega = -2.6$ rad/s. Thus, based on Theorem 1, the system cannot also be robust stable.

Based on the procedures presented in Moornani and Haeri [17,18], Mohsenipour and Liu [30], the approximated shape of the value set has to be determined at each frequency. Now, let

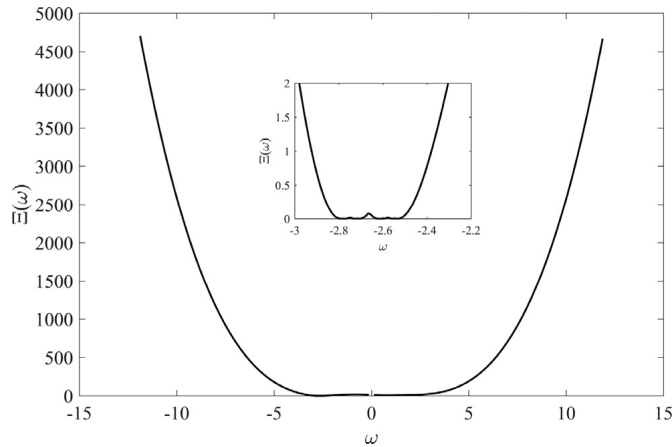


Fig. 12. $\Xi(\omega)$ in Eq. (18) within the frequency range for the enlarged coefficient before the term $s^{1.9}$.

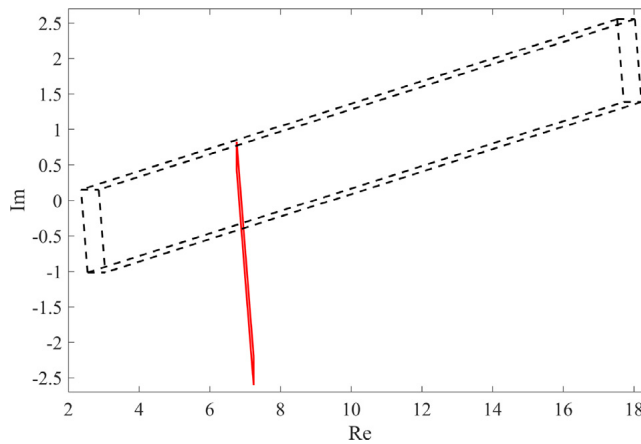


Fig. 13. The overlap between the exposed edges $-P_E^R(j\omega)$ (dotted line) and $jP_E^L(j\omega)$ (solid line) at $\omega = -2.6$ rad/s.

us obtain the approximated shape of the value set at $\omega = -2.6$ rad/s by the methods proposed in Moornani and Haeri [17,18], Mohsenipour and Liu [30]. In Fig. 14, the approximated shape of the value set is obtained by plotting two millions randomly produced points in the uncertainty space at $\omega = -2.6$ rad/s. As depicted in this figure, the origin is a part of the value set. Whereas, based on Theorem 3, 32 vertex polynomials are needed to show that whether or not the origin is a part of $\Delta(j\omega)$. It is visible that the method presented here has much less computational burden than the existing methods.

5. Conclusion

This paper investigated the robust stability of a family of interval fractional-order systems with complex coefficients. In Theorem 1, to verify the robust stability of the systems under consideration, an effective graphical approach was devised. Furthermore, Theorem 2 revealed additional interesting properties that were helpful in finding the overlap between two parpolygons. Moreover, in Theorem 3, a simple auxiliary function was proposed to assess the zero

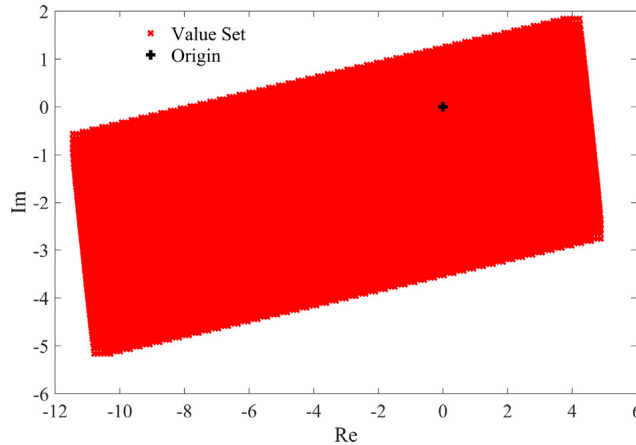


Fig. 14. The approximated shape of the value set by plotting randomly huge produced points at $\omega = -2.6$ rad/s.

exclusion principle as a robust stability testing function. In [Theorem 4](#), specific areas for the roots of the characteristic function were introduced. These areas contribute to reducing the computational burden of analyzing robust stability. Finally, the usefulness of the paper results in analyzing the derived robust stability conditions was confirmed through four examples. Future works may include analyzing the robust stability of fractional-order systems having uncertain orders and complex uncertain coefficients.

Declaration of Competing Interest

The authors declare that they have no known competing financial interests or personal relationships that could have appeared to influence the work reported in this paper.

References

- [1] I.N. Doye, K.N. Salama, T.-M. Laleg-Kirati, Robust fractional-order proportional-integral observer for synchronization of chaotic fractional-order systems, *IEEE/CAA J. Autom. Sin.* 6 (1) (2018) 268–277.
- [2] J. Huang, Y. Chen, H. Li, X. Shi, Fractional order modeling of human operator behavior with second order controlled plant and experiment research, *IEEE/CAA J. Autom. Sin.* 3 (3) (2016) 271–280.
- [3] S. Victor, R. Malti, H. Garnier, A. Oustaloup, Parameter and differentiation order estimation in fractional models, *Automatica* 49 (4) (2013) 926–935.
- [4] A. Mujumdar, B. Tamhane, S. Kurode, Observer-based sliding mode control for a class of noncommensurate fractional-order systems, *IEEE/ASME Trans. Mechatron.* 20 (5) (2015) 2504–2512.
- [5] S.T. Mohyud-Din, A. Ali, B. Bin-Mohsin, On biological population model of fractional order, *Int. J. Biomath.* 9 (05) (2016) 1650070.
- [6] G. Sun, L. Wu, Z. Kuang, Z. Ma, J. Liu, Practical tracking control of linear motor via fractional-order sliding mode, *Automatica* 94 (2018) 221–235.
- [7] G. Sun, Z. Ma, Practical tracking control of linear motor with adaptive fractional order terminal sliding mode control, *IEEE/ASME Trans. Mechatron.* 22 (6) (2017) 2643–2653.
- [8] M.S. Tavazoei, M. Tavakoli-Kakhki, Compensation by fractional-order phase-lead/lag compensators, *IET Control Theory Appl.* 8 (5) (2014) 319–329.
- [9] A. Tepljakov, E. Petlenkov, J. Belikov, S. Astapov, Tuning and digital implementation of a fractional-order pd controller for a position servo, *Int. J. Microelectron. Comput. Sci.* 4 (3) (2013) 116–123.

- [10] A. Tepljakov, E. Petlenkov, J. Belikov, FOPID controller tuning for fractional FOPDT plants subject to design specifications in the frequency domain, in: 2015 European Control Conference (ECC), 2015, pp. 3502–3507, doi:10.1109/ECC.2015.7331076.
- [11] W. Zheng, Y. Luo, Y. Chen, X. Wang, Synthesis of fractional order robust controller based on bodes ideas, *ISA Trans.* 111 (2021) 290–301.
- [12] P.P. Arya, S. Chakrabarty, A robust internal model-based fractional order controller for fractional order plus time delay processes, *IEEE Control Syst. Lett.* 4 (4) (2020) 862–867.
- [13] M. Ghorbani, M. Tavakoli-Kakhki, A. Tepljakov, E. Petlenkov, A. Farnam, G. Crevecoeur, Robust stability analysis of interval fractional-order plants with interval time delay and general form of fractional-order controllers, *IEEE Control Syst. Lett.* 6 (2021) 1268–1273.
- [14] S. Zheng, B. Liang, F. Liu, Z. Yang, Y. Xie, Robust stability of fractional order system with polynomial uncertainties based on sum-of-squares approach, *J. Frankl. Inst.* 357 (12) (2020) 8035–8058.
- [15] Q. Zhang, J. Lu, Robust stability of output feedback controlled fractional-order systems with structured uncertainties in all system coefficient matrices, *ISA Trans.* 105 (2020) 51–62.
- [16] Z.S. Aghayan, A. Alf, J.T. Machado, Robust stability of uncertain fractional order systems of neutral type with distributed delays and control input saturation, *ISA Trans.* 111 (2021) 144–155.
- [17] K.A. Moornani, M. Haeri, On robust stability of LTI fractional-order delay systems of retarded and neutral type, *Automatica* 46 (2) (2010) 362–368.
- [18] K.A. Moornani, M. Haeri, On robust stability of linear time invariant fractional-order systems with real parametric uncertainties, *ISA Trans.* 48 (4) (2009) 484–490.
- [19] K.A. Moornani, M. Haeri, Robust stability testing function and Kharitonov-like theorem for fractional order interval systems, *IET Control Theory Appl.* 4 (10) (2010) 2097–2108.
- [20] M. Ghorbani, M. Tavakoli-Kakhki, A.A. Estarami, Robust FOPID stabilization of retarded type fractional order plants with interval uncertainties and interval time delay, *J. Frankl. Inst.* 356 (16) (2019) 9302–9329.
- [21] M. Ghorbani, M. Tavakoli-Kakhki, Robust stabilizability of fractional order proportional integral controllers for fractional order plants with uncertain parameters: a new value set based approach, *J. Vib. Control* 26 (11–12) (2020) 965–975.
- [22] M. Ghorbani, Robust stability analysis of interval fractional-order plants by fractional-order controllers: an approach to reduce additional calculation, *Int. J. Gen. Syst.* 50 (1) (2021) 1–25.
- [23] M. Ghorbani, M. Tavakoli-Kakhki, Robust stability analysis of uncertain incommensurate fractional order quasi-polynomials in the presence of interval fractional orders and interval coefficients, *Trans. Inst. Meas. Control* 43 (5) (2021) 1117–1125.
- [24] J. Wei, K. Liu, G. Radice, Study on stability and rotating speed stable region of magnetically suspended rigid rotors using extended Nyquist criterion and gain-stable region theory, *ISA Trans.* 66 (2017) 154–163.
- [25] Y. Ren, J. Fang, Complex-coefficient frequency domain stability analysis method for a class of cross-coupled antisymmetrical systems and its extension in MSR systems, *Math. Probl. Eng.* (2014), doi:10.1155/2014/765858.
- [26] M.-S. Jha, G. Dauphin-Tanguy, B. Ould-Bouamama, Robust fault detection with interval valued uncertainties in bond graph framework, *Control Eng. Pract.* 71 (2018) 61–78.
- [27] H.C. S. P. Bhattacharyya, L.H. Keel, *Robust Control: The Parametric Approach*, Prentice-Hall, Upper Saddle River, NJ, 1995.
- [28] R.J. Minnichelli, J.J. Anagnost, C.A. Desoer, An elementary proof of Kharitonov's stability theorem with extensions, *IEEE Trans. Autom. Control* 34 (9) (1989) 995–998.
- [29] F.L. Janssens, J.C. van der Ha, Stability of spinning satellite under axial thrust, internal mass motion, and damping, *J. Guid., Control, Dyn.* 38 (4) (2015) 761–771.
- [30] R. Mohsenipour, X. Liu, Robust D-stability test of LTI general fractional order control systems, *IEEE/CAA J. Autom. Sin.* 7 (3) (2020) 853–864.
- [31] N. Tan, Ö. F. Özgüven, M.M. Özyetkin, Robust stability analysis of fractional order interval polynomials, *ISA Trans.* 48 (2) (2009) 166–172.
- [32] N. Tan, Computation of the frequency response of multilinear affine systems, *IEEE Trans. Autom. Control* 47 (10) (2002) 1691–1696.
- [33] X. Shao, G. Sun, W. Yao, J. Liu, L. Wu, Adaptive sliding mode control for quadrotor UAVs with input saturation, *IEEE/ASME Trans. Mechatron.* (2021), doi:10.1109/TMECH.2021.3094575.
- [34] J. Závacká, M. Bakošová, K. Vaneková, Design of robust PI controllers for control of an exothermic chemical reactor, in: *Proceedings of the 14th WSEAS International Conference on Systems*, 2010.
- [35] R. Matusu, B. Senol, L. Pekar, Robust PI control of interval plants with gain and phase margin specifications: application to a continuous stirred tank reactor, *IEEE Access* 8 (2020) 145372–145380.

- [36] Y.-W. Tu, M.-T. Ho, Robust second-order controller synthesis for model matching of interval plants and its application to servo motor control, *IEEE Trans. Control Syst. Technol.* 20 (2) (2011) 530–537.
- [37] D.D. Simfukwe, B.C. Pal, Robust and low order power oscillation damper design through polynomial control, *IEEE Trans. Power Syst.* 28 (2) (2012) 1599–1608.
- [38] M. Marden, *Geometry of Polynomials*, vol. 3, American Mathematical Soc., 1949.

Appendix 4

IV

M. Ghorbani, M. Tavakoli-Kakhki, A. Tepljakov, and E. Petlenkov. Robust stability analysis of Smith predictor based interval fractional-order control systems: a case study in level control process. *IEEE/CAA Journal of Automatica Sinica*, 10(3):762–780, 2022.

Robust Stability Analysis of Smith Predictor Based Interval Fractional-Order Control Systems: A Case Study in Level Control Process

Majid Ghorbani, Mahsan Tavakoli-Kakhki, Aleksei Tepljakov, *Senior Member, IEEE*, and Eduard Petlenkov

Abstract—The robust stability study of the classic Smith predictor-based control system for uncertain fractional-order plants with interval time delays and interval coefficients is the emphasis of this work. Interval uncertainties are a type of parametric uncertainties that cannot be avoided when modeling real-world plants. Also, in the considered Smith predictor control structure it is supposed that the controller is a fractional-order proportional integral derivative (FOPID) controller. To the best of the authors' knowledge, no method has been developed until now to analyze the robust stability of a Smith predictor based fractional-order control system in the presence of the simultaneous uncertainties in gain, time-constants, and time delay. The three primary contributions of this study are as follows: i) a set of necessary and sufficient conditions is constructed using a graphical method to examine the robust stability of a Smith predictor-based fractional-order control system—the proposed method explicitly determines whether or not the FOPID controller can robustly stabilize the Smith predictor-based fractional-order control system; ii) an auxiliary function as a robust stability testing function is presented to reduce the computational complexity of the robust stability analysis; and iii) two auxiliary functions are proposed to achieve the control requirements on the disturbance rejection and the noise reduction. Finally, four numerical examples and an experimental verification are presented in this study to demonstrate the efficacy and significance of the suggested technique.

Index Terms—Interval uncertainty, FOPID controller, fractional-order systems, robust stability analysis, smith predictor.

I. INTRODUCTION

A. Background

IN process control, the Smith predictor control structure is a well-known dead time compensator for stable processes with large time delay [1]. When the model is accurate, the

closed-loop characteristic polynomial of the Smith predictor control structure will be delay free. However, in real-world applications, due to process parameter change, the plant model cannot adequately capture the dynamic behavior of the process, necessitating a robust stability study of the Smith predictor control system [2].

In [2], at first, a set of necessary and sufficient conditions for the robust stability analysis of the Smith predictor based interval integer-order plants with PI controller has been presented. Then, an application has been developed for the robust control of a first order plant with interval time delay. Moreover, some modifications of the Smith predictor have been mentioned in order to facilitate the tuning of the controller parameters in industrial applications and to improve the robustness [3]–[5]. Also, in [6], the Kharitonov's theorem has been employed to enhance the robustness of the Smith predictor based integer-order control system. Furthermore, in [7]–[9], the stability regions of PID and PI controllers have been obtained for tuning PI and PID controllers in Smith predictor control structure.

In control theory, fractional-order calculus has been widely utilized to improve the performance of control loops [10]–[16], the robustness properties [17]–[21] and to identify more precise models of physical systems [22] [23]. Also, in [24], a procedure has been presented to analyze the robust stability of a class of interval fractional-order polynomials.

Recently, fractional-order controllers based on the Smith predictor structure have been used in a variety of engineering applications. In [25], a simple method has been presented to design internal model based fractional-order Smith predictor control systems for first order plus time delay plants. The main disadvantages of the method in [25] are that it cannot guarantee the robust performance and robust stability of the closed-loop control system in the presence of simultaneous uncertainties. In [26], another method has been proposed to tune the parameters of a filtered Smith predictor based fractional integral-fractional derivative controller. Also, the method in [26] cannot guarantee the robust performance and robust stability of the system in the presence of simultaneous uncertainties. In [27] and [28], the robustness analysis of fractional-order controllers combined with Smith predictor structure has been investigated in the case of the existence of time delay variations. Two main disadvantages of the method presented in [27] and [28] are that only sufficient conditions for robust stability analysis have been presented in these articles

Manuscript received April 4, 2022; revised May 6, 2022; accepted June 12, 2022. This work was supported by the Estonian Research Council (PRG658). Recommended by Associate Editor Qinglai Wei. (Corresponding author: Majid Ghorbani.)

Citation: M. Ghorbani, M. Tavakoli-Kakhki, A. Tepljakov, and E. Petlenkov, "Robust stability analysis of smith predictor based interval fractional-order control systems: A case study in level control process," *IEEE/CAA J. Autom. Sinica*, vol. 10, no. 3, pp. 762–780, Mar. 2023.

M. Ghorbani, A. Tepljakov, and E. Petlenkov are with the Department of Computer Systems, Tallinn University of Technology, Tallinn 12618, Estonia (e-mail: majid.ghorbani@taltech.ee; aleksei.tepljakov@taltech.ee; eduard.petlenkov@taltech.ee).

M. Tavakoli-Kakhki is with the Faculty of Electrical Engineering, K. N. Toosi University of Technology, Tehran 1631714191, Iran (e-mail: matava.koli@kntu.ac.ir).

Color versions of one or more of the figures in this paper are available online at <http://ieeexplore.ieee.org>.

Digital Object Identifier 10.1109/JAS.2022.105986

and also the simultaneous uncertainties in time delay term, model gain and time constants of the model have been not considered. Therefore, these methods cannot guarantee the robust performance and robust stability of the system having simultaneous uncertainties. Furthermore, various design methods of fractional-order controllers such as FOPI and FOPID controllers have been given in [29]–[34]. However, none of the methods in the aforementioned papers have discussed the stability of the Smith predictors having uncertain models. In [35], the flat phase property was used to design FOPI controllers for a long time-delay system in order to improve the robustness of the Smith predictor, but no discussion of robust performance was provided. In [36], by benefiting from the direct synthesis, a method has been presented to design a fractional-order controller for integer-order time-delay systems without considering an uncertain model in the Smith predictor structure. It is worth mentioning that many other methods have been proposed based on gain and phase margins to design controllers in order to improve the robustness of the Smith predictor control system (see [37]–[44]). However, as it is shown in the Section V of the present paper, satisfying gain and phase margins may not be a reliable method for uncertain systems in general.

B. Motivations, Challenges and Problem Statement

This paper does a further study on robust stability analysis of the Smith predictor based fractional-order control system. Controlling time delay processes is well-known to be a major challenge in industry. This is because the system time delay makes the closed-loop control system unstable, potentially resulting in poor performance. To address the issue of large time delay compensation, the Smith predictor structures are frequently used in engineering disciplines, especially control systems engineering [45], [46]. On the other hand, in real applications, because of the variation of the process parameters, the plant model can be considered as a transfer function whose denominator and numerator coefficients are all uncertain and lie in specified intervals. To the best of the authors' knowledge, no works consider the problem of analyzing the robust stability of Smith predictor based fractional-order control systems suffering from simultaneous uncertainties in the delay term, the model gain and coefficients. In the previous works, for simplicity, the robust stability analysis has been only addressed the uncertain time delay (see [28]) or the open-loop gain (see [1] and [25]) and clearly such procedures cannot be employed for robust stability analysis of the Smith predictor based fractional-order control systems having simultaneous independent uncertainties in the open-loop gain, the delay term and the real uncertain coefficients. The authors of [28] exclusively discuss the robust stability analysis of a Smith predictor based control structure in the presence of time delay variations. However, in practice, simultaneous uncertainties in all model parameters, including the time delay term, model gain, numerator and denominator coefficients, are more common. Example of Section IV-B in this paper provides an illustration of such a circumstance. The findings of the identification of a level control process in the aforementioned example reveal that the transfer function of the system model

contains simultaneous uncertainties in the delay term, model gain, and time-constants. As a result, the method in [28] cannot be used to analyze the robust stability of such a system. Furthermore, the approaches provided in [26]–[36] do not take into account the influence of simultaneous uncertainty in gain, time-constants, and time delay on the robust stability of Smith predictor controllers. As a result, there is a requirement to establish necessary and sufficient conditions for the robust stability analysis of a fractional-order control system in the face of simultaneous uncertainties in the delay term, the model gain, and the coefficients. The major problem is that the uncertain parameters of the characteristic function of the Smith predictor structures do not depend linearly on the polynomial terms due to the uncertain time delay. As a result, the characteristic function's value set is non-convex. As a consequence, traditional methods in robust stability analysis, such as Kharitanov's theorem [47] are no longer applicable. Therefore, the initial challenge lies in presenting necessary and sufficient conditions for robust stability analysis of Smith predictor based control systems. Also, the existing methods [37]–[39], [48]–[53] cannot analyze the robust stability of the Smith predictor with high-order systems. Hence, robust stability analysis of the Smith predictor with high-order systems is the second challenge. Moreover, because of the uncertain model, it is very difficult to determine the uncertainty bounds of the complementary sensitivity function and the sensitivity function. Hence, the next challenge in this literature is to achieve the control requirements on the disturbance rejection and the noise reduction in the presence of uncertainties. The current research investigates these three problems as the primary unsolved problems of Smith predictor-based fractional-order control systems. In summary, based on the above explanations, the following control problems can be formulated as the main challenges for the Smith predictor control structure considered in this study.

Problem 1: Despite extensive research into the problem of robust stability analysis of the Smith predictor-based fractional-order control system, **necessary and sufficient conditions** for robust stability analysis of this type of system with simultaneous independent uncertainties in the open-loop gain, the delay term, and the time-constants appear elusive.

Problem 2: Some industrial processes are modeled with high-order transfer functions [48], and the methods such as those presented in [48]–[53] are inefficient in designing robust controllers for these processes in the presence of uncertainties. Therefore, the other challenge is robust stability analysis of high-order systems compensated by Smith predictor based fractional-order controllers.

Problem 3: In addition to the robust stability analysis, it is necessary to ensure that some performance specifications are met for all processes of the uncertain system. For example, in this paper, the control requirements on the disturbance rejection and the noise reduction are considered as robust performance specifications. However, as it is well known, due to the uncertain model, it is very difficult to determine the bounds of the complementary sensitivity function and the sensitivity function in the presence of uncertainties. Hence, most of the

papers have only satisfied the constraint on the magnitude of the nominal complementary sensitivity function and the nominal sensitivity function (i.e., they assumed that the real model and the estimated model are the same, while in practice the estimated model can never fully replicate the properties real system. For some examples in this regard, see [25] and [36]). Therefore, another difficulty is to achieve robust performance for the control requirements on the disturbance rejection and the noise reduction in the presence of uncertainties.

The above mentioned issues motivate the authors of this paper to give an efficient and exact method for robust stability analysis of the Smith predictor based control systems suffering from the simultaneous uncertainties in the delay term and the plant coefficients.

C. Main Work and Contributions

Recently, the zero exclusion principle attracts many researchers to analyze the robust stability of linear time invariant (LTI) fractional-order systems with interval time delay. Based on this principle, the value set of the characteristic function of the interval fractional-order systems is plotted for all non-negative frequencies with a subsequent check whether the value set of the characteristic function includes the origin or not [54]–[57]. Three main contributions of this paper can be summarized as follows.

1) Based on a graphical method, a set of necessary and sufficient conditions is obtained to analyze the robust stability of a Smith predictor based control system. The proposed method allows to explicitly determine whether or not the FOPID controller can robustly stabilize the fractional-order Smith predictor based control system.

2) An auxiliary function as a robust stability testing function is presented to improve the computational efficiency of robust stability analysis.

3) Improving robust performance of a designed controller by two auxiliary functions.

Also, the innovations of the present paper are summarized as follows:

1) Presenting a finite frequency range for verifying the robust stability of a Smith predictor based control system (see Theorem 1).

2) Obtaining necessary and sufficient conditions for robust stability analysis of a designed Smith predictor based control system (see Theorem 2).

3) Introducing a robust stability testing function to investigate the robust stability of Smith predictor based fractional-order control system (see Theorem 3). To the best of the authors' knowledge, no robust stability testing function has been presented up to now to analyze the robust stability of the Smith predictor based control systems.

4) Presenting sufficient robust condition of a Smith predictor for high-order systems (see Remark 5).

5) Presenting two auxiliary functions to improve the control requirements on the disturbance rejection and the noise reduction (see Remark 6).

D. Organization

This paper is organized as follows: In Section II, some

required definitions are stated. The main results of the paper are presented in Section III. In Section IV, four numerical examples and an experimental verification assure the efficiency of the proposed procedure. Moreover, in Section V, some comparisons are performed about the obtained results in this paper and the existing methods. Finally, the paper is concluded in Section VI.

II. PRELIMINARIES

Notations: Assume $\sum_{i=k_1}^{k_2} f_i = 0$ for $k_2 < k_1$ and $\bigcup_{i=k_1}^{k_2} F_i = \emptyset$ for $k_2 < k_1$. Also, $A_1 \setminus A_2 \triangleq \{x \in A_1 | x \notin A_2\}$ and $A_1 \cup A_2 \triangleq \{x | x \in A_1 \text{ or } x \in A_2\}$ for any two sets A_1 and A_2 . $\partial(X)$ symbolizes the boundary of the value set X in the complex plane. $e(x_1(j\omega), x_2(j\omega)) \triangleq \eta x_1 + (1 - \eta)x_2$, $\eta \in [0, 1]$ for any two complex numbers x_1 and x_2 . $n(B)$ denotes the number of the distinct members of the set B . $\text{floor}(x)$ is the largest integer less than or equal to $x \in \mathbb{R}$. $\text{frac}(x) \triangleq x - \text{floor}(x)$ for all $x \in \mathbb{R}$.

Fractional-order calculus is the development of integer order calculus [11]. The Caputo derivative is widely used in control systems and is defined as follows:

$${}_b^C D_t^\gamma x(t) = \frac{1}{\Gamma(n - \gamma)} \int_b^t \frac{x^n(\tau)}{(t - \tau)^{\gamma - n + 1}} d\tau \quad (1)$$

where γ ($n - 1 < \gamma < n$), n is an integer number. In (1), Γ is the Euler's Gamma function. Also, b and t are respectively the lower and the upper terminals of the integral [11]. Based on [11], the Laplace transform of the Caputo's fractional-order derivative for $a = 0$ is given by

$$\mathcal{L}[_a^C D_t^\gamma x(t)] = s^\gamma \mathcal{L}[x(t)] - \sum_{i=0}^{n-1} s^{\gamma-i-1} x^{(i)}(0) \quad (2)$$

which for zero initial conditions is obtained as

$$\mathcal{L}[_a^C D_t^\gamma x(t)] = s^\gamma \mathcal{L}[x(t)]. \quad (3)$$

The structure of a standard Smith predictor based control system is shown in Fig. 1. In this figure, $C(s)$, $P(s)$, $P_0(s)$ and $\hat{\tau}$ are an FOPID controller, the process transfer function, the delay free model and the estimated value of the dead time of the process, respectively. In this paper, it is considered that the process $P(s)$ is described as (4) which is a more general form than an integer-order process.

$$P(s) = \frac{N_p(s, \mathbf{u})}{D_p(s, \mathbf{q})} = \frac{ke^{-\tau s}}{\sum_{i=0}^n q_i s^{\alpha_i}}. \quad (4)$$

In (4), $\mathbf{q} = (q_0, q_1, \dots, q_n)$ and $\mathbf{u} = (k, \tau)$ are the uncertainties and $\alpha_0 = 0 < \alpha_1 < \dots < \alpha_n$ are the fractional orders and $\alpha_i \in \mathbb{R}^{\geq 0}$. The process uncertainties belong to the uncertainty bounding sets defined as (5).

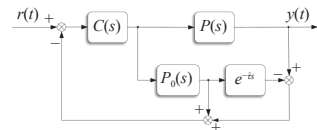


Fig. 1. The Smith predictor controller [1], [2].

$$\begin{aligned} \mathbf{q} \in \mathbf{Q} &= \left\{ \mathbf{q} = (q_0, q_1, \dots, q_n) \in \mathbb{R}^{n+1} \mid q_i \in [\underline{q}_i, \bar{q}_i], \right. \\ &\quad \left. i \in \mathbb{Z}_{\geq 0}^n, q_n \neq 0, n \geq 1 \right\} \\ \mathbf{u} \in \mathbf{U} &= \left\{ \mathbf{u} = (\tau, k) \in \mathbb{R}^2 \mid \tau \in [\underline{\tau}, \bar{\tau}], k \in [\underline{k}, \bar{k}], \right. \\ &\quad \left. \bar{\tau} > \underline{\tau} > 0, \bar{k} > \underline{k} > 0 \right\} \end{aligned} \quad (5)$$

where $[\underline{q}_i, \bar{q}_i]$ ($i = 0, 1, \dots, n$) are the specified intervals and $0 \notin [\underline{q}_n, \bar{q}_n]$. Also, $[\underline{q}_i, \bar{q}_i]$ ($i = 0, 1, \dots, n$), k and τ are the independent real uncertain parameters.

In Fig. 1, $\hat{\tau} = \frac{\bar{\tau} + \underline{\tau}}{2}$. Also, $P_0(s)$ is the delay free nominal model of the process which is defined as follows:

$$P_0(s) = \frac{\hat{k}}{\hat{D}(s)} = \frac{\hat{k}}{\sum_{i=0}^n \hat{q}_i s^{\alpha_i}} \quad (6)$$

where $\hat{k} = \frac{\bar{k} + \underline{k}}{2}$ and $\hat{q}_i = \frac{\bar{q}_i + \underline{q}_i}{2}$, $i \in \mathbb{Z}_{\geq 0}^n$. In Fig. 1, the controller $C(s)$ is an FOPID controller defined in (7).

$$C(s) = \frac{N(s)}{s^\lambda} = \frac{k_p s^\lambda + k_i + k_d s^{\mu+\lambda}}{s^\lambda} \quad (7)$$

where $\lambda, \mu \in (0, 2)$, $k_p, k_d \in \mathbb{R}$, $k_i \in \mathbb{R} \setminus \{0\}$ and $\mu < \alpha_n$. Accordingly, the results of this paper are also valid for FOPI and the fractional-order integral controllers.

The corresponding characteristic function for $P(s)$ in (4), $P_0(s)$ in (6) and $C(s)$ in (7) is given by

$$\begin{aligned} \Delta(s, \mathbf{q}, \mathbf{u}) &= \Delta_p(s, \mathbf{q}) + \Delta_a(s, \mathbf{u}) \\ &= \left(\sum_{i=0}^n q_i s^{\alpha_i} \right) \left(\sum_{i=0}^n \hat{q}_i s^{\alpha_i+\lambda} + \hat{k}(k_p s^\lambda + k_i + k_d s^{\mu+\lambda}) \right) \\ &\quad (1 - e^{-\hat{\tau}s}) + k \left(\sum_{i=0}^n \hat{q}_i s^{\alpha_i} \right) (k_p s^\lambda + k_i + k_d s^{\mu+\lambda}) e^{-\tau s} \\ \left\{ \begin{aligned} \Delta_p(s, \mathbf{q}) &\triangleq D_p(s, \mathbf{q}) \hat{N}(s) \\ \Delta_a(s, \mathbf{u}) &\triangleq N_p(s, \mathbf{u}) N(s) \hat{D}(s) \\ \hat{N}(s) &\triangleq \sum_{i=0}^n \hat{q}_i s^{\alpha_i+\lambda} + \hat{k} N(s) (1 - e^{-\hat{\tau}s}) \\ N(s) &= k_p s^\lambda + k_i + k_d s^{\mu+\lambda} \\ D_p(s, \mathbf{q}) &= \sum_{i=0}^n q_i s^{\alpha_i} \\ N_p(s, \mathbf{u}) &= k e^{-\tau s} \\ \hat{D}(s) &= \sum_{i=0}^n \hat{q}_i s^{\alpha_i} \end{aligned} \right. \quad (8) \end{aligned}$$

Remark 1: The transfer function $P(s)$ in (4) can be used for modeling wide real world phenomena. Some examples of physical systems identified as the transfer function $P(s)$ in (4) are level control process (see Section IV-B of the present paper), Pressure tanks [25], Cryogenic carbon isotopes separation process [26], Furnace preheating zone [27], Irrigation

canal pool [28], Interacting tank process [30], Air heating process [32], DC motor position servo system [58], Titanium billet heating process [59], Electric air heater [60] and Bagasse fired boiler [61]. Therefore, the problem of designing robust controller for such Smith predictor based control systems is of great importance.

Assumption 1: Because of the internal instability, it is assumed that the actual process $P(s)$ is stable and the nominal process $P_0(s)$ does not have any unstable pole.

Assumption 2: Based on the zero exclusion principle, the Smith predictor based control system in Fig. 1 is robust stable, if and only if $\Delta(s, \mathbf{q}, \mathbf{u})$ has one Hurwitz-stable member and the origin is not included in the value set of $\Delta(j\omega, \mathbf{q}, \mathbf{u})$ in (8) for $\omega \geq 0$. Therefore, it is assumed that the nominal closed-loop system for $k = \hat{k}$, $\tau = \hat{\tau}$ and $q_i = \hat{q}_i$ ($i = 1, 2, \dots, n$) can be stabilized by using FOPID controller in (7). Hence, the nominal characteristic function is considered as $\Delta^*(s)$ in (9).

$$\Delta^*(s) = \sum_{i=0}^n \hat{q}_i s^{\alpha_i+\lambda} + \hat{k}(k_p s^\lambda + k_i + k_d s^{\mu+\lambda}). \quad (9)$$

Definition 1: The principal branch of $\Delta(s, \mathbf{q}, \mathbf{u})$ in (8) is defined such as Definition 1 in [54], i.e., $\text{Arg}(s) \in (-\pi, \pi]$, where $\text{Arg}(s) \in (-\pi, \pi]$ denotes the principal value of the argument of s assuming $s \neq 0$ [54]. Also based on [47], the value set of $D_p(s, \mathbf{q}) = \sum_{i=0}^n q_i s^{\alpha_i}$, $s = j\omega$, $\omega > 0$ is a parpolygon shape in the complex plane. In this study, the vertices $v_i(j\omega)$ ($i = 1, 2, \dots, 2m$) of this parpolygon are determined by benefiting from the Procedure 1 presented in the following.

Procedure 1 [47]: Let D be a family of interval fractional-order functions as (10).

$$\begin{aligned} D &\triangleq \{D(s, q) : q \in Q\}, D_p(s, q) = \sum_{i_2=0}^n q_{i_2} s^{\alpha_{i_2}} + q_0 \\ Q &\triangleq \{[q_0, \dots, q_n]^T : q_{i_2} \in [\underline{q}_{i_2}, \bar{q}_{i_2}], i_2 = 0, 1, \dots, n\}. \end{aligned} \quad (10)$$

Define $M_0 \triangleq \{i_2 \in \mathbb{Z}_{\geq 0}^n : q_{i_2} < \bar{q}_{i_2}\}$. The value set $D(j\omega, q)$ is determined for $\omega \in \mathbb{R}_{\geq 0}$ as follows:

1) For $M_0 = \emptyset$ and $\omega \geq 0$, $D(j\omega, q) = D_0(j\omega, q)$ where

$$D_0(j\omega, q) \triangleq \sum_{i_2=0}^n \underline{q}_{i_2} s^{\alpha_{i_2}}. \quad (11)$$

2) For $M_0 \neq \emptyset$,

i) If $\omega = 0$, then $D(j\omega, q) = D(j0, q) = [q_0, \bar{q}_0]$.

ii) If $\omega > 0$, then define $T_0 \triangleq \{\text{frac}(0.5\alpha_{i_2}) : i_2 \in M_0\}$ and $m \triangleq n(T_0)$. Consider $\gamma_1, \dots, \gamma_{m-1}, \gamma_m$ as all the distinct members of T_0 sorted as $0 \leq \gamma_1 < \dots < \gamma_{m-1} < \gamma_m < 1$. Then, define the following sets:

$$M'_r \triangleq \{i_2 \in M_0 : \text{floor}(0.5\alpha_{i_2}) \text{ is an odd number and}$$

$$\text{frac}(0.5\alpha_{i_2}) = \gamma_r\}$$

$$M_r \triangleq \{i_2 \in M_0 : \text{floor}(0.5\alpha_{i_2}) \text{ is an even number and}$$

$$\text{frac}(0.5\alpha_{i_2}) = \gamma_r\}, \quad r = 1, 2, \dots, m. \quad (12)$$

Also, the vectors q^1, q^2, \dots, q^{2m} are defined as follows:

$$\begin{aligned} q^k &\triangleq [q_0^k \ q_1^k \ \dots \ q_n^k]^T, q^{m+k} \triangleq [q_0^{m+k} \ q_1^{m+k} \ \dots \ q_n^{m+k}]^T \\ &= \bar{q} + q - q^k, \quad k = 1, \dots, m \\ \underline{q} &\triangleq [q_0 \ q_1 \ \dots \ q_n]^T, \bar{q} \triangleq [\bar{q}_0 \ \bar{q}_1 \ \dots \ \bar{q}_n]^T \end{aligned} \quad (13)$$

$$q_{i_2}^k \triangleq \begin{cases} \bar{q}_{i_2}, & \text{for } i_2 \in (\bigcup_{i=1}^{k-1} M_i) \cup (\bigcup_{i=k}^m M'_i) \\ q_{-i_2}, & \text{for otherwise} \end{cases} \quad (14)$$

$$q_{i_2}^{m+k} \triangleq \bar{q}_{i_2} + q_{i_2} - q_{i_2}^k \quad (15)$$

where $i_2 = 0, 1, \dots, n$ and $k = 1, \dots, m$. Hence, for $\omega > 0$ the consecutive vertices $v_i(j\omega)$ ($i = 1, \dots, 2m$) are calculated by

$$\begin{aligned} v_k(j\omega) &\triangleq D(j\omega, q^k) \\ v_{m+k}(j\omega) &\triangleq D(j\omega, q^{m+k}) \quad (k = 1, 2, \dots, m). \end{aligned} \quad (16)$$

III. MAIN RESULT

In this section, three useful theorems are proved in order to analyze the robust stability of the Smith predictor based fractional-order control system. In Theorem 1, it is proved that the origin is not included in the value set of $\Delta(j\omega, \mathbf{q}, \mathbf{u})$ in (8) for $\omega > \omega_{\max}$, where ω_{\max} is as (17).

$$\begin{aligned} \omega_{\max} &\triangleq \max\{1, \sigma^{\frac{1}{\alpha_n - \epsilon}}\} \\ \sigma &\triangleq \left(\left(\sum_{i=0}^{n-1} |\hat{q}_i| + 2|\hat{k}|(|k_p| + |k_i| + |k_d|) \right) \right. \\ &\quad \left(\sum_{i=0}^{n-1} \max\{|\underline{q}_i|, |\bar{q}_i|\} \right) + |\hat{q}_n| \left(\sum_{i=0}^{n-1} \max\{|\underline{q}_i|, |\bar{q}_i|\} \right) \\ &\quad + \max\{|\underline{q}_n|, |\bar{q}_n|\} \left(\sum_{i=0}^{n-1} |\hat{q}_i| + 2|\hat{k}|(|k_p| + |k_i| + |k_d|) \right) \\ &\quad \left. + |\bar{k}|(|k_p| + |k_i| + |k_d|) \left(\sum_{i=0}^n |\hat{q}_i| \right) \right) / (|\hat{q}_n| \min\{|\underline{q}_n|, |\bar{q}_n|\}) \\ \epsilon &\triangleq \max\{\alpha_{n-1}, \mu\}. \end{aligned} \quad (17)$$

Also, new necessary and sufficient conditions for the robust stability analysis of the closed-loop system are provided in Theorem 2. Eventually, a robust stability testing function is presented in Theorem 3 whose sign check helps to analyze the robust stability of the closed-loop control system. Moreover, an evaluation on the disturbance rejection and the noise reduction of the Smith predictor based control system in the presence of uncertainties is further studied in Remark 6.

Theorem 1: Assume that ω_{\max} is defined as (17). Then, the characteristic function $\Delta(j\omega, \mathbf{q}, \mathbf{u})$ presented in (8) would not be equal to zero for $\omega > \omega_{\max}$.

Proof: If we show that in the frequency range $\omega \in (\omega_{\max}, \infty)$, the term $\min\{|\underline{q}_n|, |\bar{q}_n|\} \omega^{2\alpha_n + \lambda}$ cancels out the rest of terms, then the inequality $|\Delta(j\omega, \mathbf{q}, \mathbf{u})| > 0$ is met at the frequency range. On the other hand, satisfying the inequality $|\Delta(j\omega, \mathbf{q}, \mathbf{u})| > 0$ for $\omega > \omega_{\max}$ implies that $0 \notin \Delta(j\omega, \mathbf{q}, \mathbf{u})$. Based on the triangle inequality $|A + B + C| \geq |A| - |B + C| \geq$

$|A| - |B| - |C|$ and by considering $\omega > 1$, the following inequalities can be inferred for $\Delta(j\omega, \mathbf{q}, \mathbf{u})$ in (8):

$$\begin{aligned} |\Delta(j\omega, \mathbf{q}, \mathbf{u})| &\geq |\hat{q}_n| \min\{|\underline{q}_n|, |\bar{q}_n|\} \omega^{2\alpha_n + \lambda} \\ &\quad - \left(\left(\sum_{i=0}^{n-1} \max\{|\underline{q}_i|, |\bar{q}_i|\} \omega^{\alpha_i} \right) \left(\sum_{i=0}^{n-1} |\hat{q}_i| \omega^{\alpha_i + \lambda} \right) \right. \\ &\quad \left. + (1 + |e^{\hat{\tau}s}|) |\hat{k}| (|k_p| \omega^\lambda + |k_i| + |k_d| \omega^{\lambda + \mu}) \right. \\ &\quad \left. + |\hat{q}_n| \omega^{\alpha_n + \lambda} \left(\sum_{i=0}^{n-1} \max\{|\underline{q}_i|, |\bar{q}_i|\} \omega^{\alpha_i} \right) \right. \\ &\quad \left. + \max\{|\underline{q}_n|, |\bar{q}_n|\} \omega^{\alpha_n} \left(\sum_{i=0}^{n-1} |\hat{q}_i| \omega^{\alpha_i + \lambda} \right) \right. \\ &\quad \left. + (1 + |e^{\hat{\tau}s}|) |\hat{k}| (|k_p| \omega^\lambda + |k_i| + |k_d| \omega^{\lambda + \mu}) \right. \\ &\quad \left. + |\bar{k}| (|k_p| \omega^\lambda + |k_i| + |k_d| \omega^{\lambda + \mu}) \left(\sum_{i=0}^n |\hat{q}_i| \omega^{\alpha_i} \right) \right). \end{aligned} \quad (18)$$

Also, for $\omega > 1$, (19) are satisfied.

$$|\omega|^{2\alpha_n + \lambda} > |\omega|^{\alpha_n + \max\{\mu, \alpha_{n-1}\} + \lambda} > \dots > |\omega|^{\alpha_0}. \quad (19)$$

According to (18) and (19), it can be concluded that

$$\begin{aligned} |\Delta(j\omega, \mathbf{q}, \mathbf{u})| &\geq |\hat{q}_n| \min\{|\underline{q}_n|, |\bar{q}_n|\} \omega^{2\alpha_n + \lambda} \\ &\quad - \left(\left(\sum_{i=0}^{n-1} \max\{|\underline{q}_i|, |\bar{q}_i|\} \omega^{\alpha_i} \right) \left(\sum_{i=0}^{n-1} |\hat{q}_i| \omega^{\alpha_i + \lambda} \right) \right. \\ &\quad \left. + (1 + |e^{\hat{\tau}s}|) |\hat{k}| (|k_p| \omega^\lambda + |k_i| + |k_d| \omega^{\lambda + \mu}) \right. \\ &\quad \left. + |\hat{q}_n| \omega^{\alpha_n + \lambda} \left(\sum_{i=0}^{n-1} \max\{|\underline{q}_i|, |\bar{q}_i|\} \omega^{\alpha_i} \right) \right. \\ &\quad \left. + \max\{|\underline{q}_n|, |\bar{q}_n|\} \omega^{\alpha_n} \left(\sum_{i=0}^{n-1} |\hat{q}_i| \omega^{\alpha_i + \lambda} \right) \right. \\ &\quad \left. + (1 + |e^{\hat{\tau}s}|) |\hat{k}| (|k_p| \omega^\lambda + |k_i| + |k_d| \omega^{\lambda + \mu}) \right. \\ &\quad \left. + |\bar{k}| (|k_p| \omega^\lambda + |k_i| + |k_d| \omega^{\lambda + \mu}) \left(\sum_{i=0}^n |\hat{q}_i| \omega^{\alpha_i} \right) \right) \\ &\geq |\hat{q}_n| \min\{|\underline{q}_n|, |\bar{q}_n|\} \omega^{2\alpha_n + \lambda} \\ &\quad - \left(\left(\sum_{i=0}^{n-1} \max\{|\underline{q}_i|, |\bar{q}_i|\} \right) \left(\sum_{i=0}^{n-1} |\hat{q}_i| + 2|\hat{k}|(|k_p| + |k_i| + |k_d|) \right) \right. \\ &\quad \left. + |\hat{q}_n| \left(\sum_{i=0}^{n-1} \max\{|\underline{q}_i|, |\bar{q}_i|\} \right) \right. \\ &\quad \left. + \max\{|\underline{q}_n|, |\bar{q}_n|\} \left(\sum_{i=0}^{n-1} |\hat{q}_i| + 2|\hat{k}|(|k_p| + |k_i| + |k_d|) \right) \right. \\ &\quad \left. + |\bar{k}| (|k_p| + |k_i| + |k_d|) \left(\sum_{i=0}^n |\hat{q}_i| \right) \right) \omega^{\alpha_n + \max\{\mu, \alpha_{n-1}\} + \lambda}. \end{aligned} \quad (20)$$

Inequality (20) can be rewritten as (21),

$$|\Delta(j\omega, \mathbf{q}, \mathbf{u})| \geq |\hat{q}_n| \min\{|\underline{q}_n|, |\bar{q}_n|\} |\omega|^{\alpha_n + \max\{\mu, \alpha_{n-1}\} + \lambda} (|\omega|^{\alpha_n - \max\{\mu, \alpha_{n-1}\}} - \sigma). \quad (21)$$

From (21) and the inequality $|\omega|^{\alpha_n + \max\{\mu, \alpha_{n-1}\} + \lambda} |\hat{q}_n| \min\{|\underline{q}_n|, |\bar{q}_n|\} > 0$, the inequality $|\Delta(j\omega, \mathbf{q}, \mathbf{u})| > 0$ holds for $\omega > \sigma^{\frac{1}{\alpha_n - \epsilon}}$. ■

To tackle the first Problem mentioned in Section I-B, in the following theorem, by using the value set concept a set of necessary and sufficient conditions is presented for the robust stability analysis of a Smith predictor based fractional-order control system.

Theorem 2: Assume that two sets $\chi_1(j\omega)$ and $\chi_2(j\omega)$ are defined as (22) and (23), respectively.

$$\begin{aligned} \chi_1(j\omega) \triangleq & \{e(-\hat{N}(j\omega)v_1(j\omega), -\hat{N}(j\omega)v_2(j\omega)), \\ & e(-\hat{N}(j\omega)v_2(j\omega), -\hat{N}(j\omega)v_3(j\omega)), \dots, \\ & e(-\hat{N}(j\omega)v_{2m}(j\omega), -\hat{N}(j\omega)v_1(j\omega))\} \end{aligned} \quad (22)$$

$$\begin{aligned} \chi_2(j\omega) \triangleq & \{e(kN(j\omega)\hat{D}(j\omega)e^{-\tau j\omega}, \bar{k}N(j\omega)\hat{D}(j\omega)e^{-\tau j\omega}), \\ & e(kN(j\omega)\hat{D}(j\omega)e^{-\bar{\tau} j\omega}, \bar{k}N(j\omega)\hat{D}(j\omega)e^{-\bar{\tau} j\omega}), \\ & kN(j\omega)\hat{D}(j\omega)e^{-e(\underline{\tau}, \bar{\tau})j\omega}, \bar{k}N(j\omega)\hat{D}(j\omega)e^{-e(\underline{\tau}, \bar{\tau})j\omega}\}. \end{aligned} \quad (23)$$

Case I: Suppose that the inequality $\omega_{\max} \geq \frac{2\pi}{\bar{\tau} - \underline{\tau}}$ holds, then the Smith predictor control system depicted in Fig. 1 for $P(s)$ in (4), $P_0(s)$ in (6) and $C(s)$ in (7) is robust stable if and only if

- 1) $\Delta(j\omega, \mathbf{q}, \mathbf{u}) \neq 0$ for $\omega = 0$.
- 2) Two sets $\chi_1(j\omega)$ in (22) and $\chi_2(j\omega)$ in (23) do not have any overlap for $\omega \in (0, \frac{2\pi}{\bar{\tau} - \underline{\tau}})$ in the complex plane.
- 3) Inequality $\kappa(\omega) > 0$ is met for $\omega \in [\frac{2\pi}{\bar{\tau} - \underline{\tau}}, \omega_{\max}]$, where $\kappa(\omega)$ is defined in (24).

$$\begin{aligned} \kappa(\omega) &\triangleq \min_{e_i \in P_E} |e_i| - |\bar{k}N(j\omega)\hat{D}(j\omega)| \\ P_E &\triangleq \{e_1, e_2, \dots, e_{2m}\} \\ \begin{cases} e_1 &\triangleq e(\hat{N}(j\omega)v_1(j\omega), \hat{N}(j\omega)v_2(j\omega)) \\ e_2 &\triangleq e(\hat{N}(j\omega)v_2(j\omega), \hat{N}(j\omega)v_3(j\omega)) \\ \dots & \\ e_{2m-1} &\triangleq e(\hat{N}(j\omega)v_{2m-1}(j\omega), \hat{N}(j\omega)v_{2m}(j\omega)) \\ e_{2m} &\triangleq e(\hat{N}(j\omega)v_{2m}(j\omega), \hat{N}(j\omega)v_1(j\omega)). \end{cases} \end{aligned} \quad (24)$$

Case II: Suppose that the inequality $0 < \omega_{\max} < \frac{2\pi}{\bar{\tau} - \underline{\tau}}$ holds, then the Smith predictor control system depicted in Fig. 1 for $P(s)$ in (4), $P_0(s)$ in (6) and $C(s)$ in (7) is robust stable if and only if

- 1) $\Delta(j\omega, \mathbf{q}, \mathbf{u}) \neq 0$ for $\omega = 0$.
- 2) Two sets $\chi_1(j\omega)$ in (22) and $\chi_2(j\omega)$ in (23) do not have any overlap for $\omega \in (0, \frac{2\pi}{\bar{\tau} - \underline{\tau}})$ in the complex plane.

Proof: Based on the zero exclusion principle and Theorem 1, the value set $\Delta(j\omega, \mathbf{q}, \mathbf{u})$ needs to be checked for $\omega \in [0, \omega_{\max}]$. Due to $\Delta(j\omega, \mathbf{q}, \mathbf{u}) = 0$, the following equality is resulted from (8):

$$-\Delta_p(j\omega, \mathbf{q}) = \Delta_a(j\omega, \mathbf{u}). \quad (25)$$

According to the Procedure 1, the value set $D_p(s, \mathbf{q})$ is par-polygon. On the other hand, there is no uncertainty in $-\hat{N}(j\omega)$. Therefore, the vertices of $\partial(-\Delta_p(j\omega, \mathbf{q}))$ are $-\hat{N}(j\omega) v_i(j\omega)$ ($i = 1, 2, \dots, 2m$) [62], [63], where $v_i(j\omega)$ ($i = 1, 2, \dots, 2m$) are the vertices of $D(j\omega, \mathbf{q})$ and they are defined based on Procedure 1.

Proof of Case I: Suppose that $\omega_{\max} \geq \frac{2\pi}{\bar{\tau} - \underline{\tau}}$.

Sufficiency: In this case, the frequency range $(0, \omega_{\max}]$ can be divided into $\omega \in (0, \frac{2\pi}{\bar{\tau} - \underline{\tau}})$ and $\omega \in [\frac{2\pi}{\bar{\tau} - \underline{\tau}}, \omega_{\max}]$. $\chi_2(j\omega)$ in (23) is the boundary $\partial(\Delta_a(j\omega, \mathbf{u}))$ depicted in Fig. 2 for $\omega \in (0, \frac{2\pi}{\bar{\tau} - \underline{\tau}})$. Also, the boundary $\partial(\Delta_a(j\omega, \mathbf{u}))$ is shown in Fig. 3 for $\omega \in [\frac{2\pi}{\bar{\tau} - \underline{\tau}}, \omega_{\max}]$. Furthermore, in Fig. 3, $\underline{R}(\omega)$ and $\bar{R}(\omega)$ are

$$\begin{cases} \underline{R}(\omega) \triangleq |kN(j\omega)\hat{D}(j\omega)| \\ \bar{R}(\omega) \triangleq |\bar{k}N(j\omega)\hat{D}(j\omega)|. \end{cases} \quad (26)$$

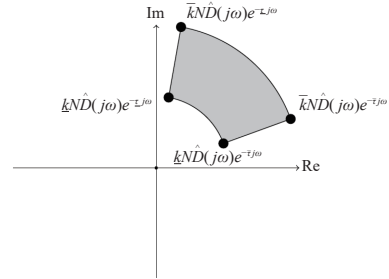


Fig. 2. Schematic of the value set $\Delta_a(j\omega)$ and its boundary $\partial(\Delta_a(j\omega))$ for $(0, \frac{2\pi}{\bar{\tau} - \underline{\tau}})$.

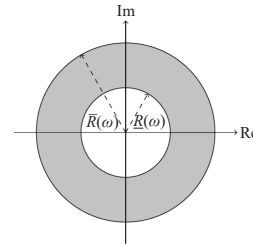


Fig. 3. Schematic of the value set $\Delta_a(j\omega)$ and its boundary $\partial(\Delta_a(j\omega))$ for $[\frac{2\pi}{\bar{\tau} - \underline{\tau}}, \omega_{\max}]$ (solid line) and two radiuses $\underline{R}(\omega)$ and $\bar{R}(\omega)$ (dashed line).

Assume that Z_0 represents an arbitrary complex number in the complex plane and $Z_0 \in \Delta_a(j\omega, \mathbf{u})$ for $\omega = \omega_0$. If $0 \in \Delta(j\omega_0, \mathbf{q}, \mathbf{u})$, then from (25) it can be inferred that $-Z_0 \in \Delta_p(j\omega_0, \mathbf{q})$. On the other hand, if $-Z_0 \in \Delta_p(j\omega_0, \mathbf{q})$ then $Z_0 \in -\Delta_p(j\omega_0, \mathbf{q})$ and this implies that the value sets of $\Delta_a(j\omega, \mathbf{u})$ and $-\Delta_p(j\omega, \mathbf{q})$ have an overlap in the complex

plane. Accordingly, If two sets $\chi_1(j\omega)$ in (22) and $\chi_2(j\omega)$ in (23) do not have any overlap for $\omega \in (0, \frac{2\pi}{\tau-\tau})$, then $0 \notin \Delta(j\omega, \mathbf{q}, \mathbf{u})$. Likewise, for $\omega \in [\frac{2\pi}{\tau-\tau}, \omega_{\max}]$, if the value sets $-\Delta_p(j\omega, \mathbf{q})$ and $\Delta_a(j\omega, \mathbf{u})$ do not have any overlap, then $0 \notin \Delta(j\omega, \mathbf{q}, \mathbf{u})$. On the other hand, based on Theorem 2 in [64], assume that $0 \notin \Delta_p(j\omega, \mathbf{q})$ then the smallest absolute magnitude of $\Delta_p(j\omega, \mathbf{q})$ is $\min_{e_l \in P_E} |e_l|$ where e_l and P_E are defined in (24). Also, it is obviously concluded that the largest absolute magnitude of $\Delta_a(j\omega, \mathbf{u})$ is $|\bar{k}N_i(j\omega)\hat{D}(j\omega)|$. Also for $\omega \in [\frac{2\pi}{\tau-\tau}, \omega_{\max}]$, i.e., when $\partial(\Delta_a(j\omega))$ is as depicted in Fig. 3, $\Delta(j\omega, \mathbf{q}, \mathbf{u})$ does not include the origin if the inequality $\kappa(\omega) > 0$ holds. It is because that for $\omega = \infty$ the inequality $\lim_{\omega \rightarrow \infty} \min_{e_l \in P_E} |e_l| > \lim_{\omega \rightarrow \infty} |\bar{k}N_i(j\omega)\hat{D}(j\omega)|$ holds. Therefore, satisfying the inequality $\kappa(\omega) > 0$ assures that the value sets $-\Delta_p(j\omega, \mathbf{q})$ and $\Delta_a(j\omega, \mathbf{u})$ would not have any overlap for $\omega \in [\frac{2\pi}{\tau-\tau}, \omega_{\max}]$ in the complex plane and this means that $0 \notin \Delta(j\omega, \mathbf{q}, \mathbf{u})$.

Necessity: Since $\Delta(j\omega, \mathbf{q}, \mathbf{u})$ is robust stable, based on the zero exclusion principle and Theorem 1, the origin is not included in the value set $\Delta(j\omega, \mathbf{q}, \mathbf{u})$ for $\omega \in (\omega_{\max}, \infty)$. Therefore, $\Delta(0, \mathbf{q}, \mathbf{u}) \neq 0$ and two sets $\chi_1(j\omega)$ in (22) and $\chi_2(j\omega)$ in (23) do not have any overlap for $\omega \in (0, \frac{2\pi}{\tau-\tau})$. For $\omega \in [\frac{2\pi}{\tau-\tau}, \omega_{\max}]$, as a contradiction argument it is supposed that the inequality $\kappa(\omega) > 0$ is not satisfied. Because of $\lim_{\omega \rightarrow \infty} \min_{e_l \in P_E} |e_l| > \lim_{\omega \rightarrow \infty} |\bar{k}N_i(j\omega)\hat{D}(j\omega)|$ and Theorem 1, the inequality $\kappa(\omega) > 0$ holds for $\omega \in (\omega_{\max}, \infty)$. Since, $\kappa(\omega)$ is a continuous function and $\kappa(\omega) \leq 0$, there must exist at least one $\omega_0 \in [\frac{2\pi}{\tau-\tau}, \omega_{\max}]$ for which $\kappa(\omega) = 0$. This indicates that at $\omega = \omega_0 \in [\frac{2\pi}{\tau-\tau}, \omega_{\max}]$, $\Delta_a(j\omega, \mathbf{u})$ and $-\Delta_p(j\omega, \mathbf{q})$ have an overlap in the complex plane. Therefore, at the given frequency $\omega = \omega_0 \in [\frac{2\pi}{\tau-\tau}, \omega_{\max}]$, there are complex members of $\Delta_p(j\omega, \mathbf{q})$ as $\hat{\Delta}_p(j\omega, \mathbf{q})$ and $\Delta_a(j\omega, \mathbf{u})$ as $\hat{\Delta}_a(j\omega, \mathbf{u})$ which are equal to $-Z_0$ and Z_0 , respectively. Hence, at $\omega = \omega_0$, there is a member of $\Delta(j\omega_0, \mathbf{q}, \mathbf{u})$ as $\hat{\Delta}(j\omega_0, \mathbf{q}, \mathbf{u}) = \hat{\Delta}_a(j\omega, \mathbf{u}) + \hat{\Delta}_p(j\omega, \mathbf{q})$ which is equal to $Z_0 - Z_0 = 0$ and it contradicts the condition $0 \notin \Delta(j\omega, \mathbf{q}, \mathbf{u})$. This completes the proof.

Proof of Case II: Suppose that $0 < \omega_{\max} < \frac{2\pi}{\tau-\tau}$. The proof of the sufficiency and necessary conditions mentioned in this case can be done similarly to the proof of Case I based on the zero exclusion principle, Assumption 1 and Theorem 1. ■

Remark 2: Although, [26]–[46] are unable to analyze the robust stability of Smith predictor based control structures shown in Fig. 1, Theorem 2 presents necessary and sufficient conditions for robust stability analysis of a Smith predictor based control structure suffering from simultaneous uncertainties in the delay term and the plant coefficients.

Based on Theorem 2, to analyze the robust stability of the Smith predictor based fractional-order control system, the overlap between $\chi_1(j\omega)$ in (22) and $\chi_2(j\omega)$ in (23) should be checked for $\omega \in (0, \frac{2\pi}{\tau-\tau})$ and this may yield difficulty. In the following theorem for facilitating the robust stability analysis of the considered Smith predictor control structure, by using the geometry properties, the new set of the exposed edges is offered which helps to introduce a useful robust stability test-

ing function.

Theorem 3: The characteristic function $\Delta(j\omega, \mathbf{q}, \mathbf{u})$ in (8) is robust stable if $\Delta(j\omega, \mathbf{q}, \mathbf{u}) \neq 0$ for $\omega = 0$ and the inequality $\Lambda(\omega) > 0$ is met for $\omega \in (0, \omega_{\max}]$, where $\Lambda(\omega)$ is defined as

$$\Lambda(\omega) \triangleq \begin{cases} \Lambda_1(\omega) \quad \Lambda_2(\omega), & \text{if } \omega \in (0, \frac{2\pi}{\tau-\tau}) \\ \kappa(\omega), & \text{if } \omega \in [\frac{2\pi}{\tau-\tau}, \omega_{\max}] \end{cases} \quad (27)$$

$\kappa(\omega)$ is defined as (24) and the two functions $\Lambda_1(j\omega)$ and $\Lambda_2(j\omega)$ are defined as follows:

$$\begin{aligned} \Lambda_1(\omega) &\triangleq \min\{\bar{\kappa}_{h,g}(j\omega) | h \in \{1, \dots, 2m\}, g \in \{1, \dots, 4N_\theta + 2\}\} \\ \bar{\kappa}_{h,g}(j\omega) &\triangleq \left| \hat{N}(j\omega)v_h(j\omega) + \bar{P}_g(j\omega) \right| + \left| \hat{N}(j\omega)v_{h+1}(j\omega) + \bar{P}_g(j\omega) \right| \\ &\quad - \left| \hat{N}(j\omega)(v_h(j\omega) - v_{h+1}(j\omega)) \right| \\ \Lambda_2(\omega) &\triangleq \min\{\kappa_{h,g}(j\omega) | h \in \{1, \dots, 2m\}, g \in \{1, \dots, 4N_\theta + 2\}\} \\ \kappa_{h,g}(j\omega) &\triangleq \left| \hat{N}(j\omega)v_h(j\omega) + \bar{P}_g(j\omega) \right| + \left| \hat{N}(j\omega)v_{h+1}(j\omega) + \bar{P}_{g+1}(j\omega) \right| \\ &\quad - \left| \bar{P}_g(j\omega) - \bar{P}_{g+1}(j\omega) \right| \end{aligned} \quad (28)$$

where N_θ is an arbitrary number and $N_\theta \in \mathbb{N}^{\geq 3}$, $v_{2m+1}(j\omega) = v_1(j\omega)$ and $\bar{P}_{4N_\theta+3}(j\omega) = \bar{P}_1(j\omega)$. In (28), $\bar{P}_g(j\omega)$ is defined as follows:

$$\bar{P}_g(j\omega) \triangleq \begin{cases} P_{l(g-1)}(j\omega), & \text{for } 1 \leq g \leq 2N_\theta + 1 \\ P_{s(2N_\theta)}(j\omega), & \text{for } g = 2N_\theta + 2 \\ P_{s(2N_\theta-1)}(j\omega), & \text{for } g = 2N_\theta + 3 \\ \dots & \\ P_{s0}(j\omega), & \text{for } g = 4N_\theta + 2 \end{cases} \quad (29)$$

$$\begin{aligned} P_{li}(j\omega) &\triangleq \begin{cases} \bar{k}\hat{D}(j\omega)N(j\omega)e^{-j\omega(\tau+i\frac{\tau-\tau}{2N_\theta})}, & \text{for } i = 0, 2, \dots, 2N_\theta \\ \frac{\bar{k}\hat{D}(j\omega)N(j\omega)e^{-j\omega(\tau+i\frac{\tau-\tau}{2N_\theta})}}{\cos(\omega\frac{\tau-\tau}{2N_\theta})}, & \text{for } i = 1, 3, \dots, 2N_\theta - 1 \end{cases} \\ P_{si}(j\omega) &\triangleq \begin{cases} \bar{k}\hat{D}(j\omega)N(j\omega)e^{-j\omega(\tau+i\frac{\tau-\tau}{2N_\theta})}, & \text{for } i = 0, 2, \dots, 2N_\theta \\ \bar{k}\hat{D}(j\omega)N(j\omega)(2 - \frac{1}{\cos(\omega\frac{\tau-\tau}{2N_\theta})})e^{-j\omega(\tau+i\frac{\tau-\tau}{2N_\theta})}, & \text{for } i = 1, \dots, 2N_\theta - 1. \end{cases} \end{aligned}$$

Proof: The proof is given in Appendix. ■

Remark 3: Based on Theorem 3 for $0 < \omega_{\max} < \frac{2\pi}{\tau-T}$, the robust stability testing function $\Lambda(\omega)$ is modified as $\Lambda(\omega) = \Lambda_1(\omega) \Lambda_2(\omega)$, where two functions $\Lambda_1(\omega)$ and $\Lambda_2(\omega)$ are defined in Theorem 3.

Remark 4: In Theorem 2, a graphical method is presented to analyze the robust stability of a Smith predictor based fractional-order control system. According to this theorem, it is needed to depict two-dimensional graphs of the value sets in the complex plane at each positive frequency and it may be too difficult to investigate the overlap between the value sets. Accordingly, in Theorem 3 instead of depicting two-dimensional graphs of the value sets, we employ the idea of robust stability testing function based on the geometric aspects and explicit descriptions of the value sets. Therefore, the computational complexity of the robust stability conditions in Theorem 2 can be decreased significantly by the auxiliary function $\Lambda(\omega)$ presented in Theorem 3. Therefore, the robust stability analysis should be performed based on the robust stability testing function $\Lambda(\omega)$. By Theorem 2, Theorem 3 and Remark 2, the following useful algorithm is proposed to analyze the robust stability of a Smith predictor based fractional-order control system suffering from simultaneous uncertainties in gain, time-constants, and time delay.

Algorithm 1 Robust Stability Analysis

Step 1: Check the stability of the nominal characteristic function $\Delta^*(s)$ in (9). This step is because that based on Theorems 2 and 3, the stability of $\Delta^*(s)$ in (9) has to be checked. In this paper the method presented in [65] is proposed to check the stability. Based on this method, the polar plot of $\psi(j\omega)$ in (30) is plotted in the complex plane for $-\infty < \omega < \infty$. $\Delta^*(s)$ in (9) is stable if and only if $\psi(j\omega)$ in (30) does not encircle the origin in the complex plane.

$$\psi(s) = \frac{\Delta^*(s)}{\hat{q}_n(s+1)^{a_n+1}}, s = j\omega. \quad (30)$$

Moreover, one can use the design method proposed in [66]. Based on this method, the boundaries of the stabilizing region $\Delta^*(s)$ in (9) are specified by infinite root boundary (IRB), real root boundary (RRB) and complex root boundary (CRB) which can be determined by using the algorithm in [66]. In summary, the mentioned boundaries are stated based on the procedure proposed in [66] as follows.

- **RRB:** $\Delta^*(0) = k_i \hat{k}$. If $\hat{k} \neq 0$, then $k_i = 0$. Otherwise, the boundary does not exist.

- **IRB:** $\Delta^*(\infty) = 0$.

$$\begin{cases} k_d = 0 & \text{for } \mu > \alpha_n \\ k_d = \frac{-\hat{q}_0}{\hat{k}} & \text{for } \mu = \alpha_n \\ \text{none} & \text{for } \mu < \alpha_n. \end{cases} \quad (31)$$

- **CRB:** By solving $\Delta^*(j\omega) = 0$ the k_p and k_i parameters in terms of k_d , λ and μ are obtained as

$$\begin{aligned} k_p &= (A_2(\omega)B_1(\omega) - A_1(\omega)B_2(\omega) + k_d(B_1(\omega)B_6(\omega) \\ &\quad - B_2(\omega)B_5(\omega)))/(B_2(\omega)B_3(\omega) - B_1(\omega)B_4(\omega)) \\ k_i &= (A_1(\omega)B_4(\omega) - A_2(\omega)B_3(\omega) + k_d(B_4(\omega)B_5(\omega) \\ &\quad - B_3(\omega)B_6(\omega)))/(B_2(\omega)B_3(\omega) - B_1(\omega)B_4(\omega)) \end{aligned} \quad (32)$$

in which

$$\begin{cases} A_1(\omega) = \sum_{i_2=0}^n \hat{q}_{i_2} \omega^{\lambda+\alpha_{i_2}} \cos\left(\frac{\pi(\alpha_{i_2} + \lambda)}{2}\right) \\ A_2(\omega) = \sum_{i_2=0}^n \hat{q}_{i_2} \omega^{\lambda+\alpha_{i_2}} \sin\left(\frac{\pi(\alpha_{i_2} + \lambda)}{2}\right) \\ B_1(\omega) = \hat{k} \\ B_2(\omega) = 0 \\ B_3(\omega) = \hat{k} \omega^\lambda \cos\left(\frac{\pi(\lambda)}{2}\right) \\ B_4(\omega) = \hat{k} \omega^\lambda \sin\left(\frac{\pi(\lambda)}{2}\right) \\ B_5(\omega) = \hat{k} \omega^{\lambda+\mu} \cos\left(\frac{\pi(\lambda+\mu)}{2}\right) \\ B_6(\omega) = \hat{k} \omega^{\lambda+\mu} \sin\left(\frac{\pi(\lambda+\mu)}{2}\right). \end{cases} \quad (33)$$

Accordingly, the stabilizing region can be determined by checking one arbitrary test point inside each region (for details, see [66]).

Step 2: Obtain all the vertices $v_i(s)$, $i = 1, \dots, 2m$ by using *Procedure I* and calculate ω_{\max} via (17).

Step 3: By calculating ω_{\max} in (17) and the value of $\frac{2\pi}{\tau-T}$, the following two conditions may occur:

- 1) If $\omega_{\max} \geq \frac{2\pi}{\tau-T}$, then the robust stability is checked by the first case of Theorems 2 or 3 as follows:

- a) When employing *Theorem 2*, if all the conditions presented in the first case of *Theorem 2* hold for $\omega \in [0, \omega_{\max}]$, then the Smith predictor based control system is robust stable. Otherwise, it would not be robust stable.

- b) When employing *Theorem 3*, if there exists $N \in \mathbb{N}^{\geq 3}$ by which the inequality $\Lambda(\omega) > 0$ in (27) is met for $\omega \in [0, \omega_{\max}]$, then the Smith predictor based control system is robust stable. If the inequality $\Lambda(\omega) > 0$ does not hold for $\omega \in [\frac{2\pi}{\tau-T}, \omega_{\max}]$, the control system is not robust stable (see the second statement of *Theorem 2*).

- 2) If $\omega_{\max} < \frac{2\pi}{\tau-T}$, then the robust stability is checked by Remark 2 or the second case of Theorem 2 as follows:

- a) When using *Theorem 2*, if all the conditions presented in the Case II of *Theorem 2* hold for $\omega \in [0, \omega_{\max}]$, then the Smith predictor based control system is robust stable. Otherwise, it would not be robust stable.

- b) When using *Theorem 3*, if there exists $N \in \mathbb{N}^{\geq 3}$ by which the inequality $\Lambda(\omega) = \Lambda_1(\omega) \Lambda_2(\omega) > 0$ in (27) is met for $\omega \in [0, \omega_{\max}]$, then the control system is robust stable.

Remark 5: In order to find a solution for Problem 2 stated in Section I-B, assume that the process transfer function $P(s)$ is a high-order process as $P(s) = N_p(s, \mathbf{u})/D_p(s, \mathbf{q})$, where $D_p(s, \mathbf{q}) = (\tilde{q}s + 1)^n$, $\tilde{q} \in [\underline{\tilde{q}}, \bar{\tilde{q}}]$, $\tilde{q} \neq 0$ and $n \in \mathbb{N}^{\geq 2}$. The denominator of $P(s)$ can be written as $D_p(s, \mathbf{q}) = \tilde{q}_n s^n + \tilde{q}_{n-1} s^{n-1} + \dots + \tilde{q}_2 s^2 + \tilde{q}_1 s + 1$ where $\tilde{q}_i \in [\underline{\tilde{q}_i}, \bar{\tilde{q}_i}]$, $i = 1, \dots, n$. On the other hand, according to Procedure 1 and the Kharitonov's theorem [67], the value set of $D_p(s, \mathbf{q}) = 1 + \sum_{i=1}^n \tilde{q}_i s^i$ for $s = j\omega$ has a rectangle shape in the complex plane for independent uncertainties. Also, as proven in [68], $\partial((\tilde{q}s + 1)^n) \subset \partial(1 + \sum_{i=1}^n \tilde{q}_i s^i)$. Therefore, the results presented in Theorems 2 and 3 can be used for robust stability analysis of high-order systems as a sufficient condition.

Remark 6: In this remark, by paying attention to the roles of

the sensitivity functions in the system response, two auxiliary functions are presented to improve the control requirements on the disturbance rejection and the noise reduction as a solution for Problem 3 stated in Section I-B. As we know, the sensitivity function characterizes the important properties of a feedback system such as the reference tracking and the disturbance rejection. The smallness of the sensitivity function at low frequency range helps to achieve desired performance of the closed-loop system in these two aspects. Accordingly, the robust fractional-order controller $C(s)$ is designed such that the inequality constraint (34) holds.

$$|S(j\omega)| = \left| \frac{1 + C(j\omega)P_0(j\omega)(1 - e^{-j\omega\bar{\tau}})}{1 + C(j\omega)P_0(j\omega)(1 - e^{-j\omega\bar{\tau}}) + C(j\omega)P(j\omega)} \right| < |M_s(j\omega)| \quad (34)$$

where $M_s(j\omega) = N_s(j\omega)/D_s(j\omega)$ denotes the weighting function, which describes the frequency characteristic of the performance specifications and the frequency bandwidth of the disturbance [69]. Assume the inequality $\Lambda(\omega) > 0$ in (27) holds. Hence, based on Assumption 1 and Theorem 3, the closed-loop system is robust stable. According to (34), the maximum modulus theorem [70] and Theorem 3, the designed control system should satisfy the inequality $\Xi_S(\omega) < 0$ to improve the performance specifications, where $\Xi_S(\omega)$ is obtained as follows:

$$\Xi_S(\omega) \triangleq \begin{cases} \max\{\Xi_{S_i}(\omega) | i = 1, 2\}, & \text{for } \omega \in [0, \frac{2\pi}{\bar{\tau} - \underline{\tau}}) \\ \frac{1}{|\frac{\bar{D}(j\omega)N(j\omega)\bar{k}}{\min_{e_l \in P_E} |e_l|} - 1|} - |M_s(j\omega)|, & \text{for } \omega \in [\frac{2\pi}{\bar{\tau} - \underline{\tau}}, \infty) \end{cases} \quad (35)$$

where Ξ_{S_i} ($i = 1, 2$) are obtained as (36) and (37).

$$\begin{aligned} \Xi_{S_1}(\omega) &\triangleq \max_{r=1, \dots, 4N_\theta+2} \tilde{\Xi}_{S_1r}(\omega) - |M_s(j\omega)| < 0 \\ \tilde{\Xi}_{S_1r}(\omega) &\triangleq \max_{e_{S_1r_1} \in P_{S_1}} |e_{S_1r_1}|, r_1 = 1, \dots, 2m \\ P_{S_1} &\triangleq \{e_{S_11}, \dots, e_{S_12m}\} \\ e_{S_1r_1} &\triangleq \frac{\hat{N}(j\omega)}{\hat{N}(j\omega) + \frac{\bar{P}_r(j\omega)}{e(v_{r_1}(j\omega), v_{r_1+1}(j\omega))}} \\ \Xi_{S_2}(\omega) &\triangleq \max_{r=1, \dots, 2m} \frac{|\hat{N}(j\omega)v_r(j\omega)|}{\tilde{\Xi}_{S_2r}(\omega)} - |M_s(j\omega)| < 0 \\ \tilde{\Xi}_{S_2r}(\omega) &\triangleq \min_{e_{S_2r_2} \in P_{S_2}} |e_{S_2r_2}|, r_2 = 1, \dots, 4N_\theta + 2 \\ P_{S_2} &\triangleq \{e_{S_21}, \dots, e_{S_24N_\theta+2}\} \\ e_{S_2r_2} &\triangleq \hat{N}(j\omega)v_r(j\omega) + e(\bar{P}_{r_2}(j\omega), \bar{P}_{r_2+1}(j\omega)). \end{aligned} \quad (36)$$

Also, for reducing the high frequency noise, the following constraint on the complementary sensitivity function needs to

hold:

$$|T(j\omega)| = \left| \frac{C(j\omega)P(j\omega)}{1 + C(j\omega)P_0(j\omega)(1 - e^{-j\omega\bar{\tau}}) + C(j\omega)P(j\omega)} \right| < |M_T(j\omega)| \quad (38)$$

where the weighting function $M_T(j\omega)$ depends on the frequency characteristics of the noise signal. Likewise, the following inequality $\Xi_T(\omega) < 0$ is inferred from (38) and Theorem 3:

$$\Xi_T(\omega) \triangleq \begin{cases} \max\{\Xi_{T_i} | i = 1, 2\} & \text{for } \omega \in [0, \frac{2\pi}{\bar{\tau} - \underline{\tau}}) \\ \frac{1}{|\frac{\min_{e_l \in P_E} |e_l|}{|\bar{D}(j\omega)N(j\omega)\bar{k}|} - 1|} - |M_T(j\omega)|, & \text{for } \omega \in [\frac{2\pi}{\bar{\tau} - \underline{\tau}}, \infty) \end{cases} \quad (39)$$

where Ξ_{T_i} ($i = 1, 2$) are obtained as (40) and (41).

$$\begin{aligned} \Xi_{T_1}(\omega) &\triangleq \max_{r=1, \dots, 4N_\theta+2} \frac{|\bar{P}_r(j\omega)|}{\tilde{\Xi}_{T_1r}(\omega)} - |M_T(j\omega)| < 0 \\ \tilde{\Xi}_{T_1r}(\omega) &\triangleq \min_{e_{T_1r_1} \in P_{T_1}} |e_{T_1r_1}|, r_1 = 1, \dots, 2m \\ P_{T_1} &\triangleq \{e_{T_11}, \dots, e_{T_12m}\} \\ e_{T_1r_1} &\triangleq \hat{N}(j\omega)e(v_{r_1}(j\omega), v_{r_1+1}(j\omega)) + \bar{P}_r(j\omega) \\ \Xi_{T_2}(\omega) &\triangleq \max_{r=1, \dots, 2m} \tilde{\Xi}_{T_2r}(\omega) - |M_T(j\omega)| < 0 \\ \tilde{\Xi}_{T_2r}(\omega) &\triangleq \max_{e_{T_2r_2} \in P_{T_2}} |e_{T_2r_2}|, r_2 = 1, \dots, 4N_\theta + 2 \\ P_{T_2} &\triangleq \{e_{T_21}, \dots, e_{T_24N_\theta+2}\} \\ e_{T_2r_2} &\triangleq \frac{e(\bar{P}_{r_2}(j\omega), \bar{P}_{r_2+1}(j\omega))}{\hat{N}(j\omega)v_r(j\omega) + e(\bar{P}_{r_2}(j\omega), \bar{P}_{r_2+1}(j\omega))}. \end{aligned} \quad (40)$$

Hence, checking the inequality constraints $\Xi_T(\omega) < 0$ in (35) and $\Xi_S(\omega) < 0$ in (39) helps the designer to evaluate the output disturbance rejection and the noise reduction of the control systems.

Remark 7: Note that, the approximating transfer function for the simulation of s^α is given by

$$s^\alpha \approx \delta \prod_{n=1}^N \frac{1 + \frac{s}{\omega_{z,n}}}{1 + \frac{s}{\omega_{p,n}}}, \quad \alpha > 0 \quad (42)$$

where N , $\omega_{z,n}$, $\omega_{p,n}$ and δ are the unknown parameters to be determined. To select the mentioned parameters, one can use the method presented in [71].

IV. NUMERICAL AND EXPERIMENTAL EXAMPLES

In this section, four illustrative examples (Section IV-A) and an experimental verification (Section IV-B) are given to demonstrate the application of the proposed approach in this study to analyze the robust stability of a Smith predictor based fractional-order control system. Also, *Algorithm 1* is employed to analyze the robust stability of the Smith predictor structure having uncertain integer-order process, uncertain fractional-order process and high-order process.

A. Numerical Examples

Example 1: In [2], a nominal model is described by

$$P_0(s)e^{-\tau s} = \frac{0.8}{s+1}e^{-5s}. \quad (43)$$

The parametric uncertainties are $k \in [0.7, 0.9]$, $\tau \in [4, 6]$, $q_1 \in [0.8, 1.2]$ and $q_0 = 1$. In [2], a robust PI controller has been proposed as

$$C(s) = 0.28 + \frac{0.28}{s}. \quad (44)$$

Therefore, the characteristic function $\Delta(s, \mathbf{q}, \mathbf{u})$ in (8) is given by

$$\begin{aligned} \Delta(s, \mathbf{q}, \mathbf{u}) &= \Delta_p(s, \mathbf{q}) + \Delta_a(s, \mathbf{u}) \\ &= ([0.8, 1.2]s + 1)(s^2 + s + 0.8(0.28s + 0.28)(1 - e^{-5s})) \\ &\quad + [0.7, 0.9](s + 1)(0.28s + 0.28)e^{-[4, 6]s} \\ \left\{ \begin{aligned} \Delta_p(s, \mathbf{q}) &\triangleq D_p(s, \mathbf{q}) \hat{N}(s) \\ \Delta_a(s, \mathbf{u}) &\triangleq N_p(s, \mathbf{u}) N(s) \hat{D}(s) \\ \hat{N}(s) &\triangleq s^2 + s + 0.8(0.28s + 0.28)(1 - e^{-5s}) \\ N(s) &= 0.28s + 0.28 \\ D_p(s, \mathbf{q}) &= [0.8, 1.2]s + 1 \\ N_p(s, \mathbf{u}) &= [0.7, 0.9]e^{-[4, 6]s} \\ \hat{D}(s) &= s + 1. \end{aligned} \right. \end{aligned} \quad (45)$$

Also, based on Assumption 1 the nominal characteristic function $\Delta^*(s)$ is presented as (46).

$$\Delta^*(s) = s^2 + s + 0.8(0.28s + 0.28). \quad (46)$$

To check the stability of the nominal closed-loop system, the presented procedure in [65] is used. The polar plot of $\psi_1(j\omega)$ in (47) has been shown in Fig. 4. As Fig. 4 depicts, the nominal closed-loop system is stable. It is because that the polar plot of $\psi_1(j\omega)$ in (47) does not encircle the origin in the complex plane (see the first step of *Algorithm 1*).

$$\psi_1(s) = \frac{\Delta^*(s)}{(s+1)^2} = \frac{s^2 + s + 0.8(0.28s + 0.28)}{(s+1)^2}, s = j\omega. \quad (47)$$

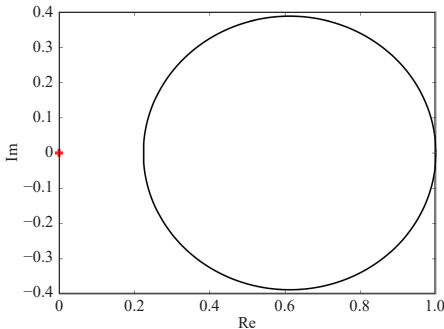


Fig. 4. The polar plot of $\psi_1(j\omega)$ in (47) for $\omega \in [-10^4, 10^4]$ rad/sec.

From (17), ω_{\max} is obtained as 7.724 rad/sec. Therefore, based on Theorems 2 and 3, it is sufficient that the robust stability of the Smith predictor based control system is checked for $\omega \in [0, 7.724]$. To analyze the robust stability, the auxiliary function $\Lambda(\omega)$ in (27) is used for $N_\theta = 3$. Based on $v_h(j\omega)$ ($h = 1, 2$) in (48), P_{li} and P_{si} in (29) and (45), the robust stability testing function $\Lambda(\omega)$ in (27) can be plotted.

$$\begin{cases} v_1(j\omega) = 0.8(j\omega) + 1 \\ v_2(j\omega) = 1.2(j\omega) + 1. \end{cases} \quad (48)$$

From Figs. 5(a) and 5(b), it is obviously concluded that the inequality $\Lambda(\omega) > 0$ holds for $\omega \in (0, 7.724]$. Therefore, based on Theorem 3, the Smith predictor based control system is robust stable.

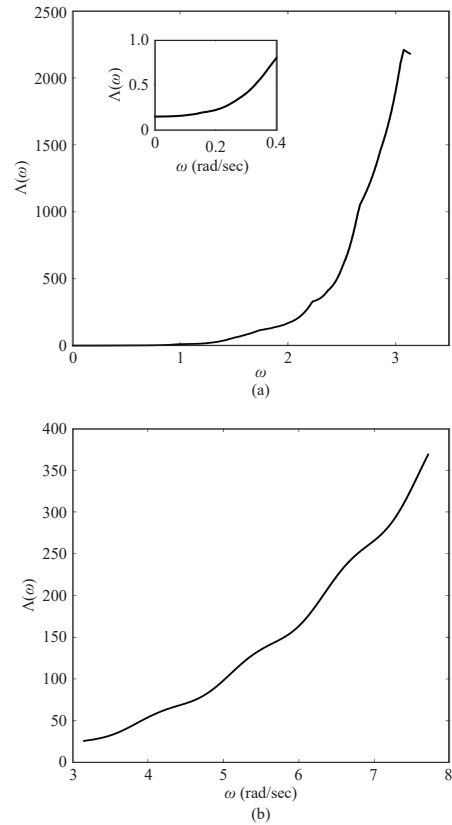


Fig. 5. (a) The values of $\Lambda(\omega)$ in (27) for $\omega \in (0, \pi)$ rad/sec; (b) The values of $\Lambda(\omega)$ in (27) for $\omega \in [\pi, 7.724]$ rad/sec.

Example 2: Consider a fractional-order plant with interval coefficients and interval time delay as

$$P(s) = \frac{k}{q_2 s^{1.7} + q_1 s^{0.8} + q_0} e^{-\tau s} \quad (49)$$

where $k \in [0.4, 0.6]$, $q_0 \in [1.8, 2]$, $q_1 \in [1.4, 1.5]$, $q_2 \in [1.2, 1.4]$ and $\tau \in [1, 8]$. For the nominal plant $P_0(s)$ in (50), the FOPID controller $C(s)$ in (51) is proposed.

$$P_0(s) = \frac{0.5}{1.3s^{1.7} + 1.45s^{0.8} + 1.9} \quad (50)$$

$$C(s) = \frac{0.5s^{0.45} + 0.4 + 0.1s^{0.95}}{s^{0.45}}. \quad (51)$$

Hence, the characteristic function $\Delta(s, \mathbf{q}, \mathbf{u})$ in (8) is given by

$$\begin{aligned} \Delta(s, \mathbf{q}, \mathbf{u}) &= \Delta_p(s, \mathbf{q}) + \Delta_a(s, \mathbf{u}) \\ &= ([1.2, 1.4]s^{1.7} + [1.4, 1.5]s^{0.8} + [1.8, 2]) \\ &\quad (s^{0.45} (1.3s^{1.7} + 1.45s^{0.8} + 1.9) \\ &\quad + 0.5 (0.5s^{0.45} + 0.4 + 0.1s^{0.95}) (1 - e^{-4.5s})) \\ &\quad + [0.4, 0.6] (1.3s^{1.7} + 1.45s^{0.8} + 1.9) \\ &\quad (0.5s^{0.45} + 0.4 + 0.1s^{0.95}) e^{-[1.8]s} \end{aligned} \quad (52)$$

$$\begin{cases} \Delta_p(s, \mathbf{q}) \triangleq D_p(s, \mathbf{q}) \hat{N}(s) \\ \Delta_a(s, \mathbf{u}) \triangleq N_p(s, \mathbf{u}) N(s) \hat{D}(s) \\ \hat{N}(s) \triangleq s^{0.45} (1.3s^{1.7} + 1.45s^{0.8} + 1.9) \\ \quad + 0.5 (0.5s^{0.45} + 0.4 + 0.1s^{0.95}) (1 - e^{-4.5s}) \\ N(s) = 0.5s^{0.45} + 0.4 + 0.1s^{0.95} \\ D_p(s, \mathbf{q}) = [1.2, 1.4]s^{1.7} + [1.4, 1.5]s^{0.8} + [1.8, 2] \\ N_p(s, \mathbf{u}) = [0.4, 0.6]e^{-[1.8]s} \\ \hat{D}(s) = (1.3s^{1.7} + 1.45s^{0.8} + 1.9). \end{cases}$$

Based on Assumption 1, the nominal characteristic function $\Delta^*(s)$ is presented as (53).

$$\begin{aligned} \Delta^*(s) &= s^{0.45} (1.9 + 1.45s^{0.8} + 1.3s^{1.7}) \\ &\quad + 0.5 (0.5s^{0.45} + 0.4 + 0.1s^{0.95}). \end{aligned} \quad (53)$$

To check the stability of the nominal closed-loop system, the method proposed in the first step of *Algorithm 1* is used. As Fig. 6 depicts, the nominal closed-loop system is stable.

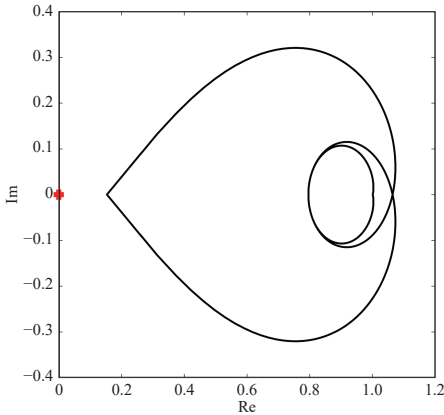


Fig. 6. The values of the transfer function $\psi(j\omega)$ in (54) for $\omega \in [-10^4, 10^4]$ rad/sec.

$$\begin{aligned} \psi(s) &= (s^{0.45} (1.9 + 1.45s^{0.8} + 1.3s^{1.7}) + 0.5 (0.5s^{0.45} \\ &\quad + 0.4 + 0.1s^{0.95})) / (1.3(s+1)^{1.7+0.45}), s = j\omega. \end{aligned} \quad (54)$$

Based on Theorem 1, the frequency ω_{\max} is obtained as 41.6017 rad/sec. The robust stability testing function $\Lambda(\omega)$ in (27) is checked to investigate the robust stability of Smith predictor control system for $N_\theta = 3$. Based on $v_h(j\omega)$ ($h = 1, \dots, 6$) in (55), P_{li} and P_{si} in (29) and (52), the robust stability testing function $\Lambda(\omega)$ in (27) can be plotted as Figs. 7(a) and 7(b).

$$\begin{cases} v_1(s) = 1.8 + 1.4s^{0.8} + 1.2s^{1.7} \\ v_2(s) = 2 + 1.4s^{0.8} + 1.2s^{1.7} \\ v_3(s) = 2 + 1.5s^{0.8} + 1.2s^{1.7} \\ v_4(s) = 2 + 1.5s^{0.8} + 1.4s^{1.7} \\ v_5(s) = 1.8 + 1.5s^{0.8} + 1.4s^{1.7} \\ v_6(s) = 1.8 + 1.4s^{0.8} + 1.4s^{1.7} \end{cases} \quad (55)$$

where $s = j\omega$. Figs. 7(a) and 7(b) depict the curve of $\Lambda(\omega)$ in (27) within $\omega \in (0, 41.6017]$ rad/sec. According to these figures, the values of $\Lambda(\omega)$ are positive within $\omega \in (0, 41.6017]$ rad/sec. Thus, the considered Smith predictor based control system is robust stable. It is worth mentioning that none of the methods proposed in [26]–[46] can be used to verify the

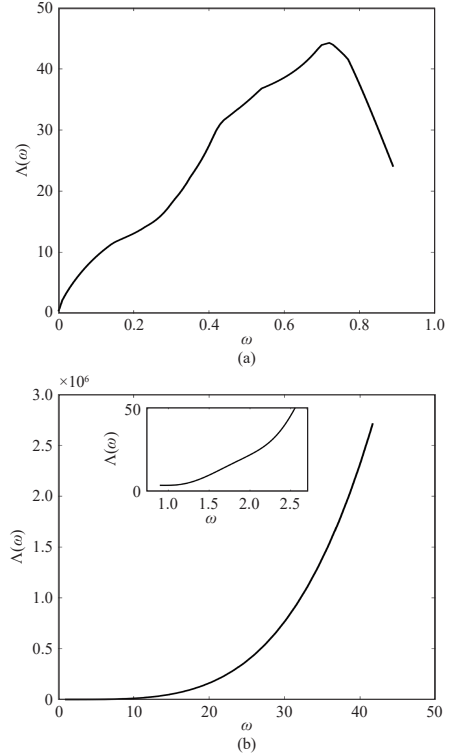


Fig. 7. (a) The values of $\Lambda(\omega)$ in (27) for $\omega \in (0, 0.8976)$ rad/sec; (b) The values of $\Lambda(\omega)$ in (27) for $\omega \in [0.8976, 41.6017]$ rad/sec.

robust stability of the Smith predictor control system in this example. It is because that the mentioned papers have failed to analyze the robust stability of the closed-loop control system in the presence of simultaneous uncertainties in the delay term and the plant gain and coefficients. While based on Theorems 2 and 3 of this paper, the robust stability of the closed-loop system is concluded simply.

Example 3: Consider the following process transfer function:

$$P(s) = \frac{k}{(qs+1)^3} e^{-\tau s} \quad (56)$$

where $k \in [0.4, 0.6]$, $\tau \in [4, 5]$ and $q \in [1.5, 2]$. The process transfer function (56) can be considered as (57).

$$\begin{aligned} P(s) &= \frac{k}{(qs+1)^3} e^{-[4,5]s} \\ &= \frac{[0.4, 0.6]}{1 + [4.5, 6]s + [6.75, 12]s^2 + [3.375, 8]s^3} e^{-[4,5]s} \end{aligned} \quad (57)$$

In the following, it is shown that the FOPID controller (58) can robustly stabilize the closed-loop system:

$$C(s) = 0.5 + \frac{0.2}{s^{0.45}} + 0.1s^{0.5}. \quad (58)$$

Fig. 8 shows the values of $\psi(s)$ in (59). Hence, the nominal closed-loop system is stable.

$$\begin{aligned} \psi(s) &= (s^{0.45}(1 + 5.25s + 9.375s^2 + 5.6875s^3) + 0.5(0.5s^{0.45} \\ &\quad + 0.2 + 0.1s^{0.95}))/((5.6875(s+1)^{3+0.45}), s = j\omega. \end{aligned} \quad (59)$$

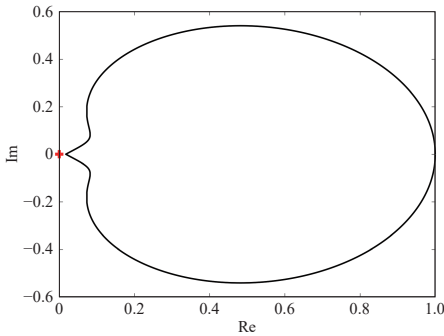


Fig. 8. The values of the transfer function $\psi(j\omega)$ in (54) for $\omega \in [-10^4, 10^4]$ rad/sec.

Also, based on Theorem 1, ω_{\max} is obtained as 20.5919 rad/sec. The values of the robust stability testing function $\Lambda(\omega)$ have been reported in Figs. 9(a) and 9(b). From Figs. 9(a) and 9(b), it can be seen that the inequality $\Lambda(\omega) > 0$ holds for $0 < \omega \leq 20.5919$ rad/sec. Accordingly, Theorem 3 ensures the robust stability of the closed-loop system. Whereas the references [48]–[53] cannot ensure the robust stability of the closed-loop control system.

Example 4: In [28], the robust fractional-order controller $C(s)$ in (60) has been designed for the plant $P(s)$ in (61).

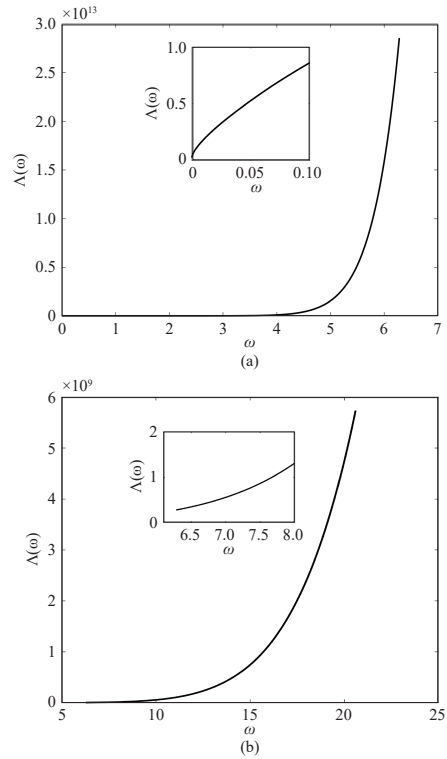


Fig. 9. (a) The values of $\Lambda(\omega)$ in (27) for $\omega \in (0, 2\pi)$ rad/sec; (b) The values of $\Lambda(\omega)$ in (27) for $\omega \in [2\pi, 20.5919]$ rad/sec.

$$C(s) = \frac{6.4}{s^{0.46}} \quad (60)$$

$$P(s) = \frac{0.053}{(1500s+1)(20s+1)} e^{-[180,720]s}. \quad (61)$$

Let us consider the plant $P(s)$ in (61) as an interval plant with simultaneous uncertainties (62).

$$\begin{aligned} P(s) &= \frac{[0.043, 0.063]}{([1450, 1550]s+1)([19, 21]s+1)} e^{-[180,720]s} \\ &= \frac{[0.043, 0.063]e^{-[180,720]s}}{[1450 \times 19, 1550 \times 21]s^2 + [1450 + 19, 1550 + 21]s + 1}. \end{aligned} \quad (62)$$

In the following, it is shown that the robust fractional-order controller $C(s)$ in (60) can robustly stabilize the interval plant (62). From (17), ω_{\max} is obtained as 1 rad/sec. Therefore, based on Theorems 2 and 3, it is sufficient that the robust stability of the Smith predictor based control system is checked for $\omega \in [0, 1]$. The values of the auxiliary function $\Lambda(\omega)$ in (27) have been plotted for $N_\theta = 3$ in Figs. 10(a) and 10(b). From these figures, it can be seen that the inequality $\Lambda(\omega) > 0$ holds for $0 < \omega \leq 1$ rad/sec. Accordingly, Theorem 3 ensures the robust stability of the closed-loop system.

It is worth mentioning that the method presented in [28] cannot be used for the robust stability analysis of the Smith

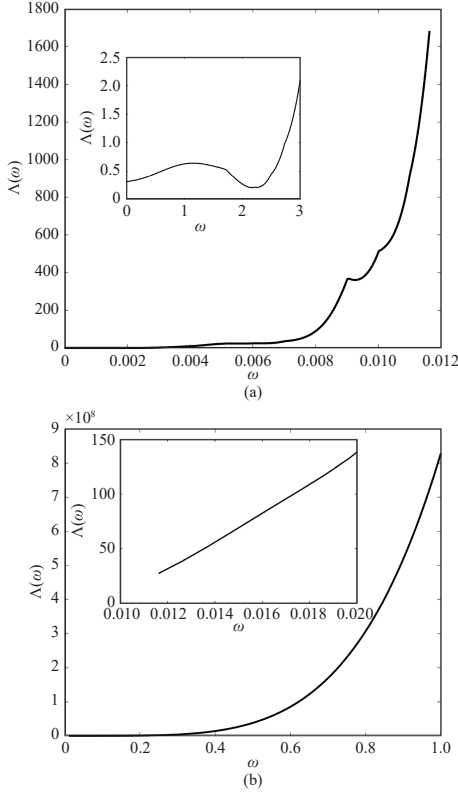


Fig. 10. (a) The values of $\Lambda(\omega)$ in (27) for $\omega \in (0, \frac{2\pi}{340})$ rad/sec; (b) The values of $\Lambda(\omega)$ in (27) for $\omega \in [\frac{2\pi}{340}, 1]$ rad/sec.

predictor based control system for the interval plant with simultaneous uncertainties in gain, time delay and time constants as (62). But, as it is seen from this example the procedure presented in this paper can analyze robust stability of the Smith predictor based control system for the interval plant $P(s)$ in (62).

B. Application to A Level Control Process

To show the applicability of the results of the paper results in a practical setting, in this example a robust FOPI controller is designed for the level control process GUNT- RT512 (see Fig. 11). Then, the robust stability of the designed Smith predictor based control system is analyzed according to the proposed procedure in this paper and the results of the practical implementation of the designed controller are provided.

The results of the identification of the level control process GUNT-RT512 for 13 iterations are provided in Table I. According to Table I, the identified model can be represented as follows:

$$P(s) = \frac{k}{q_1 s + q_0} e^{-\tau s} \quad (63)$$

where $k \in [2.94, 4.59]$, $\tau \in [4.8, 14.4]$, $q_0 = 1$ and $q_1 \in [26.4, 35.6]$. For the nominal closed-loop system, the FOPI con-



Fig. 11. Level control process (GUNT-RT512) [72].

TABLE I
IDENTIFIED PARAMETERS OF THE PLANT

Iteration number	k	q_1	τ
1	3.0033	26.4	6
2	3.2663	28.8	4.8
3	3.9648	30.4	5.2
4	3.9951	29.6	8.4
5	4.2831	35.6	9.2
6	4.5397	31.2	6
7	4.2646	33.2	12.4
8	4.5924	29.2	11.6
9	4.4571	30.4	14.4
10	2.9471	29.2	12.8
11	4.096	30	13.6
12	3.4036	30.8	12.8
13	3.9676	27.6	12.8

troller $C(s)$ in (64) is designed according to the procedure proposed in [66].

$$C(s) = 0.5 + \frac{0.01}{s^{0.92}}. \quad (64)$$

The FOPI controller (64) is implemented by leveraging the approximation method presented in Remark 3. To this end, the order and the frequency range of the approximation filter are taken as $N = 3$ and $\omega \in [0.01, 100]$ rad/sec, respectively. Also, the applied disturbance is considered as an additive step disturbance at the time instant $t = 2200$ sec.

Based on Theorem 1, ω_{\max} is obtained as 1 rad/sec. The curve of $\Lambda(\omega)$ in (27) is depicted within $\omega \in (0, 1]$ rad/sec for $N_\theta = 3$ in Figs. 12 (a) and 12 (b). According to Theorem 3, Figs. 12(a), and 12 (b), the corresponding Smith predictor based control system is robust stable. Also, the values of the auxiliary functions $\Xi_T(\omega)$ in (35) and $\Xi_S(\omega)$ in (39) have been plotted in Figs. 13(a) and 13(b) for $M_s(j\omega) = 0.004 + \frac{2.2s+0.015}{s+0.05}$.

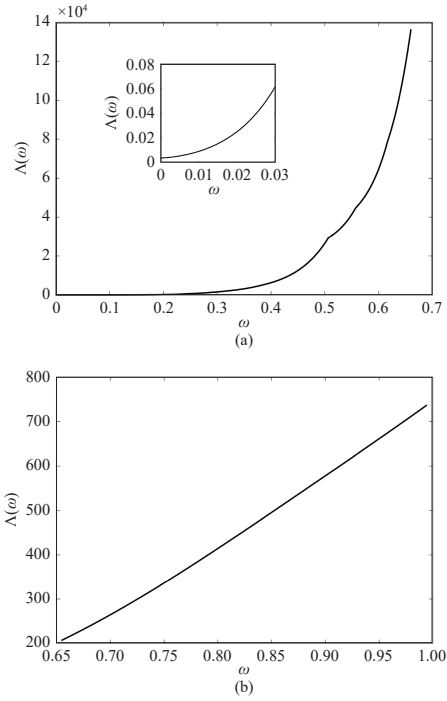


Fig. 12. (a) The values of $\Lambda(\omega)$ in (27) for $\omega \in (0, 0.6545)$ rad/sec; (b) The values of $\Lambda(\omega)$ in (27) for $\omega \in [0.6545, 1]$ rad/sec.

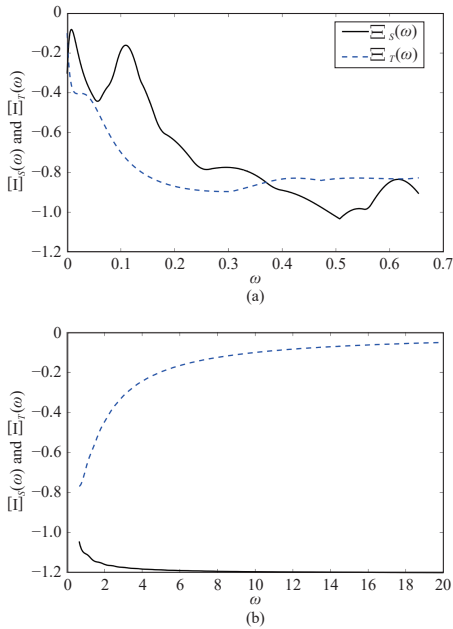


Fig. 13. (a) The values of the auxiliary functions $\Xi_T(\omega)$ in (35) and $\Xi_S(\omega)$ in (39) for $\omega \in (0, 0.6545)$ rad/sec; (b) The values of the auxiliary functions $\Xi_T(\omega)$ in (35) and $\Xi_S(\omega)$ in (39) for $\omega \in [0.6545, 20]$ rad/sec.

and $M_T(j\omega) = \frac{1}{s+1}$. As this figure depicts the inequalities $\Xi_T(\omega) < 0$ and $\Xi_S(\omega) < 0$ hold. Hence, the designed robust controller can satisfy the control requirements on the disturbance rejection and the noise reduction. The obtained experimental results by applying the FOPI controller (64) in the Smith predictor control structure in Fig. 1 are presented in Figs. 14(a) and 14(b). As this figure shows, the controller (64) exhibits good performance in the presence of the disturbance and noise.

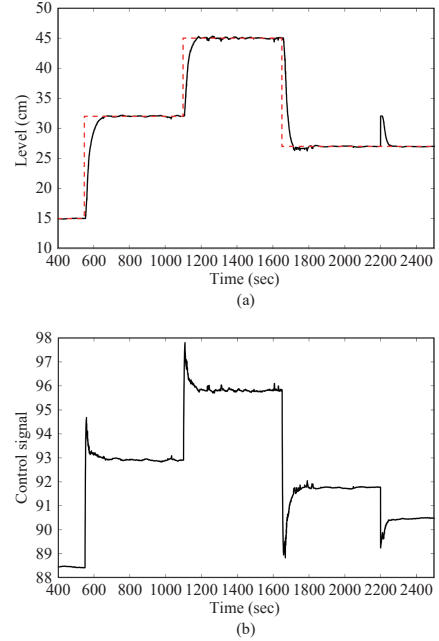


Fig. 14. (a) The level output by applying the robust FOPI controller (64) in the Smith predictor control structure; (b) The control signal by applying the robust FOPI controller (64).

V. DISCUSSION

Let us compare our results with the existing works [26]–[46] and [48]–[53]. In the present paper, we have proposed two different methods, i.e., Theorems 2 and 3 to check the robust stability of the Smith predictor based fractional-order control systems. Theorem 2 presents necessary and sufficient conditions for robust stability analysis of the Smith predictor based fractional-order control systems having simultaneous uncertainties in gain, time constants and time delay. In Theorem 3, an auxiliary function as a robust stability testing function is presented to facilitate the robust stability analysis of the Smith predictor based fractional-order control systems suffering from simultaneous uncertainties. According to the uncertainty structure, the robust stability analysis of the Smith predictor based control systems can be classified into eight categories shown in Table II. References [25] and [39] guarantee the robust stability of the Smith predictor based fractional-order control systems having only uncertain gain and [25]–

TABLE II
REVIEW OF THE SMITH PREDICTOR BASED INTEGER-ORDER CONTROL SYSTEMS (SPIOCS) AND THE SMITH PREDICTOR BASED FRACTIONAL-ORDER CONTROL SYSTEMS (SPFOCS)

Uncertainties	SPIOCS	SPFOCS
Uncertain gain	[1], [2], [49]	[25], [39]
Uncertain time constant	[1], [2], [49]	[25]
Uncertain time delay	[1], [2], [49]	[25]–[28]
Simultaneous uncertainties	[2]	The proposed results

[28] can also ensure the robust stability of the Smith predictor based fractional-order control systems having only uncertain time delay. This implies that none of [25]–[28] and [39] can analyze the robust stability of the Smith predictor based fractional-order control systems having simultaneous uncertainties in gain, time constants and time delays (such as Examples 2–4). On the other hand, in [29]–[36], [38], [41], [42], some design methods have been proposed based on gain and phase margins to improve the robustness of the Smith predictor based control system. However, gain and phase margins may lead to unreliable results. For example, in [35], the FOPID controller $C(s) = 5.1709 + 7.6428/s^{0.4587}$ has been designed for the system $P_0(s) = e^{-9s}/(12s + 1)$. Assume that the actual plant contains simultaneous uncertainties as

$$P(s) = \frac{[0.8, 1.2]}{[11, 13]s + 1} e^{-[8, 10]s}. \quad (65)$$

Now, Theorem 2 can be employed to investigate the robust stability of the system. As shown in Fig. 15, the value sets of $\chi_1(j\omega)$ (solid line) and $\chi_2(j\omega)$ (dotted line) in (22) have an overlap at $\omega = 1.143$ rad/sec in the complex plane. Therefore, this system would not be robust stable based on Theorem 2. This implies that there is at least one unstable member in the uncertain space. Let us check the stability of the characteristic function in (66) which is a member of $\Delta(s, \mathbf{q}, \mathbf{u})$.

$$\begin{aligned} \hat{\Delta}(s) = & (11.1s + 1)(s^{0.4587}(12s + 1) + (7.6428 \\ & + 5.1709s^{0.4587})(1 - e^{-9s})) \\ & + 1.19(12s + 1)(7.6428 + 5.1709s^{0.4587})e^{-8s}. \end{aligned} \quad (66)$$

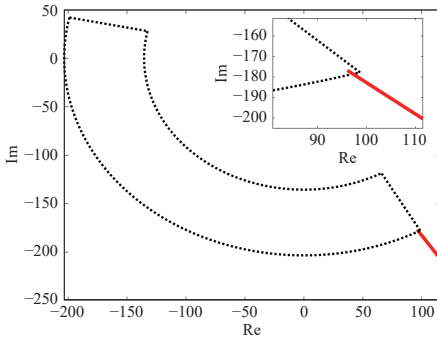


Fig. 15. The overlap between the value sets of $\chi_1(j\omega)$ (solid line) and $\chi_2(j\omega)$ (dotted line) at $\omega = 1.143$ rad/sec.

To check the stability of $\hat{\Delta}(s)$ in (66), the method proposed in [65] can be used as stated in **Algorithm 1**. Based on this method, the polar plot of $\psi(j\omega)$ in (67) is plotted in the complex plane for $-\infty < \omega < \infty$.

$$\psi(j\omega) = \frac{\hat{\Delta}(j\omega)}{12 \times 11.1 \times (j\omega + 1)^{2.4587}}. \quad (67)$$

The polar plot of $\psi(j\omega)$ in (67) is shown in Figs. 16(a) and 16(b). From these figures, it is visible that the chosen member $\hat{\Delta}(s)$ in (66) is unstable. Because the origin is encircled twice and consequently $\hat{\Delta}(s)$ has two unstable zeros. Hence, the system is not robustly stable. This demonstrates the sophistication of the method proposed in Theorem 2.

Moreover, none of [26]–[46] can be used to design a robust controller in Example 2. Also, as shown in Examples 3 and 4, a robust FOPID controller can be designed for high-order systems in the presence of uncertainties. Whereas, [48]–[53] have failed to design a robust controller for uncertain processes.

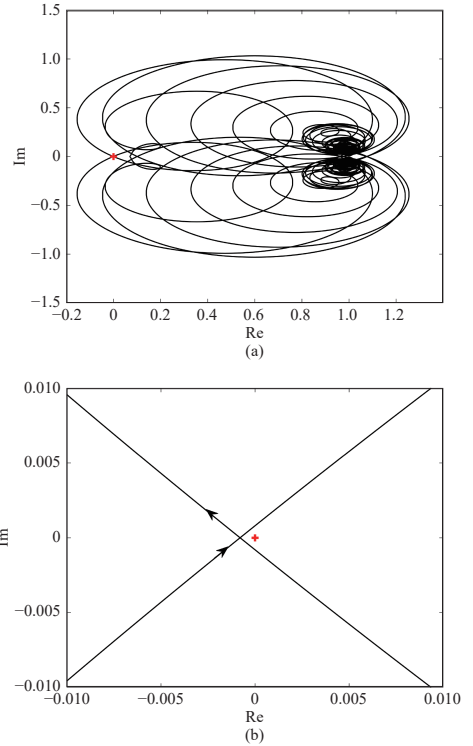


Fig. 16. (a) The polar plot of $\psi(j\omega)$ in (67); (b) A better view around the origin.

VI. CONCLUSION

In this paper, the robust stability analysis of the Smith predictor based control system with an FOPID controller for an interval delayed fractional-order plant was investigated. Necessary and sufficient conditions were proposed to analyze the robust stability of the closed-loop system. Also, a robust sta-

bility testing function was offered to facilitate the procedure of the robust stability analysis. The robust stability analysis method proposed in this paper can be used for the both integer-order and fractional-order Smith predictor based control systems. Moreover, two auxiliary functions were provided to achieve the control requirements related to the desired properties of the disturbance rejection and the noise reduction. Four numerical examples were offered to demonstrate the method's applicability and efficiency. Finally, the method was applied to a real-life plant—a level control process. Following that, a model with interval uncertainty was identified using process data. The proposed method was also effectively applied to this model, demonstrating the technology's potential for real-world applications.

APPENDIX PROOF OF THEOREM 3

Fig. 17 depicts the boundary $\partial(\Delta_a(j\omega, \mathbf{u}))$, the arrangement of the vertices $P_{li}(j\omega)$ ($i = 0, 1, \dots, 2N_\theta$) and $P_{si}(j\omega)$ ($i = 0, 1, \dots, 2N_\theta$) for $0 < \omega < \frac{2\pi}{\bar{\tau} - \underline{\tau}}$. The edge of the three consecutive vertices $P_{li}(j\omega)$, $P_{li+1}(j\omega)$ and $P_{li+2}(j\omega)$ for $i = 0, 1, \dots, 2N_\theta - 2$ are depicted in Fig. 18. Also, in this figure the angle θ equals $\omega(\bar{\tau} - \underline{\tau})$. According to Fig. 18, the three consecutive vertices for $i = 0$ are obtained as (68)–(70).

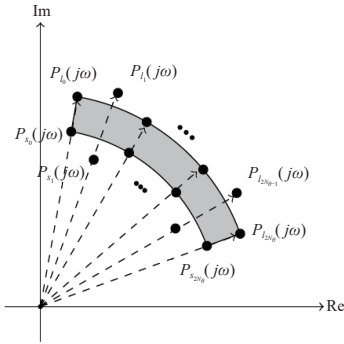


Fig. 17. Schematic of the value set $\Delta_a(j\omega)$, the vertices $P_{li}(j\omega)$ ($i = 0, 1, \dots, 2N_\theta$) and $P_{si}(j\omega)$ ($i = 0, 1, \dots, 2N_\theta$) for $0 < \omega < \frac{2\pi}{\bar{\tau} - \underline{\tau}}$.

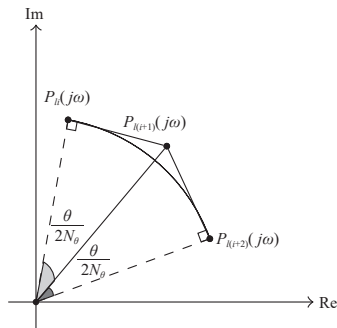


Fig. 18. The edge of the three consecutive vertices $P_{li}(j\omega)$, $P_{li+1}(j\omega)$ and $P_{li+2}(j\omega)$ for $i = 0, 2, \dots, 2N_\theta - 2$.

$$P_{l0}(j\omega) = \bar{k}\hat{D}(j\omega)N(j\omega)e^{-\underline{\tau}j\omega} \quad (68)$$

$$P_{l1}(j\omega) = \frac{\bar{k}\hat{D}(j\omega)N(j\omega)e^{-j\omega\left(\underline{\tau} + \frac{\bar{\tau} - \underline{\tau}}{2N_\theta}\right)}}{\cos\left(\omega\frac{\bar{\tau} - \underline{\tau}}{2N_\theta}\right)} \quad (69)$$

$$P_{l2}(j\omega) = \bar{k}\hat{D}(j\omega)N(j\omega)e^{-j\omega\left(\underline{\tau} + 2\frac{\bar{\tau} - \underline{\tau}}{2N_\theta}\right)}. \quad (70)$$

Also, the three consecutive vertices $P_{si}(j\omega)$, $P_{s(i+1)}(j\omega)$ and $P_{s(i+2)}(j\omega)$ for $i = 0, 1, \dots, 2N_\theta - 2$ are depicted in Fig. 19. According to Fig. 19, the three consecutive vertices for $i = 0$ are obtained as

$$P_{s0}(j\omega) = \underline{k}\hat{D}(j\omega)N(j\omega)e^{-\underline{\tau}j\omega} \quad (71)$$

$$P_{s1}(j\omega) = \frac{\underline{k}\hat{D}(j\omega)N(j\omega)e^{-j\omega\left(\underline{\tau} + \frac{\bar{\tau} - \underline{\tau}}{2N_\theta}\right)}}{\cos\left(\omega\frac{\bar{\tau} - \underline{\tau}}{2N_\theta}\right)} - \delta(j\omega) \quad (72)$$

$$P_{s2}(j\omega) = \underline{k}\hat{D}(j\omega)N(j\omega)e^{-j\omega\left(\underline{\tau} + 2\frac{\bar{\tau} - \underline{\tau}}{2N_\theta}\right)}. \quad (73)$$

From Fig. 20, $\delta(j\omega)$ in (72) can be written as

$$\delta(j\omega) = 2\left(\frac{\underline{k}\hat{D}(j\omega)N(j\omega)e^{-j\omega\left(\underline{\tau} + \frac{\bar{\tau} - \underline{\tau}}{2N_\theta}\right)}}{\cos\left(\omega\frac{\bar{\tau} - \underline{\tau}}{2N_\theta}\right)} - \underline{k}\hat{D}(j\omega)N(j\omega)e^{-j\omega\left(\underline{\tau} + \frac{\bar{\tau} - \underline{\tau}}{2N_\theta}\right)}\right). \quad (74)$$

Now by substituting (74) into (72), $P_{s1}(j\omega)$ can be obtained as (75).

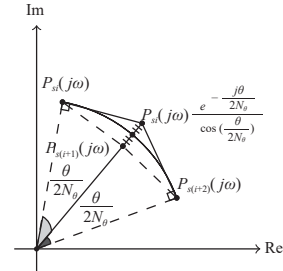


Fig. 19. The edge of the three consecutive vertices $P_{si}(j\omega)$, $P_{s(i+1)}(j\omega)$ and $P_{s(i+2)}(j\omega)$ for $i = 0, 2, \dots, 2N_\theta - 2$.

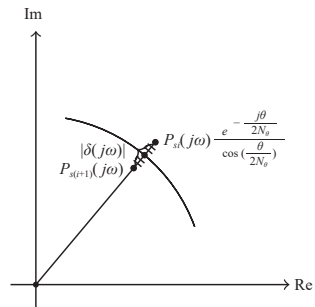


Fig. 20. A view of $\delta(j\omega)$ in (72).

$$P_{s1}(j\omega) = \underline{k}\hat{D}(j\omega)N(j\omega)e^{-j\omega\left(\frac{\bar{\tau}-\tau}{2N_\theta}\right)}\left(2 - \frac{1}{\cos\left(\omega\frac{\bar{\tau}-\tau}{2N_\theta}\right)}\right). \quad (75)$$

According to the above explanations and Fig. 17, the boundary $\partial(\Delta_a(j\omega, \mathbf{u}))$ for $0 < \omega < \frac{2\pi}{\bar{\tau}-\tau}$ is located inside the value set $P_E(j\omega)$ defined as

$$P_E(j\omega) \triangleq \{e(P_{l0}(j\omega), P_{l1}(j\omega)), e(P_{l1}(j\omega), P_{l2}(j\omega)), \dots, e(P_{l(2N_\theta-1)}(j\omega), P_{l(2N_\theta)}(j\omega)), e(P_{s0}(j\omega), P_{s1}(j\omega)), e(P_{s1}(j\omega), P_{s2}(j\omega)), \dots, e(P_{s(2N_\theta-1)}(j\omega), P_{s(2N_\theta)}(j\omega)), e(P_{l0}(j\omega), P_{s0}(j\omega)), e(P_{l(2N_\theta)}(j\omega), P_{s(2N_\theta)}(j\omega))\}. \quad (76)$$

According to Fig. 19, (77) holds.

$$|kN(j\omega)\hat{D}(j\omega)| > \frac{|\delta(j\omega)|}{2}. \quad (77)$$

By substituting (74) into (77), the following inequality is resulted:

$$1 > \left| \frac{1}{\cos\left(\omega\frac{\bar{\tau}-\tau}{2N_\theta}\right)} - 1 \right|. \quad (78)$$

On the other hand, $\omega\frac{\bar{\tau}-\tau}{2N_\theta} \in (0, \frac{\pi}{N_\theta})$. Inequality (78) can be satisfied if $\frac{\pi}{2} \notin (0, \frac{\pi}{N_\theta})$ and $\cos(\omega\frac{\bar{\tau}-\tau}{2N_\theta}) > \frac{1}{2}$. Therefore, (78) is valid for $N_\theta \geq 3$. Accordingly, from (76) and (78), one can obtain that $\partial(\Delta_a(j\omega, \mathbf{u})) \subseteq P_E(j\omega)$ for $\omega \in (0, \frac{2\pi}{\bar{\tau}-\tau})$ and $N_\theta \geq 3$. If it is proved that there exists no overlap between the two value sets $P_E(j\omega)$ in (76) and $\chi_1(j\omega)$ in (22) then Theorem 2 assures the robust stability of the Smith predictor control system depicted in Fig. 1. Therefore in the following, the overlap between the exposed edges $P_E(j\omega)$ in (76) and $\chi_1(j\omega)$ in (22) is discussed.

According to Theorem 2 if two sets $\chi_1(j\omega)$ in (22) and $\chi_2(j\omega)$ in (23) do not have any overlap for $\omega \in (0, \frac{2\pi}{\bar{\tau}-\tau})$, then $0 \notin \Delta(j\omega, \mathbf{q}, \mathbf{u})$. Based on Fig. 21 and the triangle inequality, at a given frequency $\omega = \omega_0$, we have:

1) If the inequality $|\bar{P}_g(j\omega) + \hat{N}(j\omega)v_h(j\omega)| + |\bar{P}_g(j\omega) + \hat{N}(j\omega)v_{h+1}(j\omega)| - |\hat{N}(j\omega)(v_h(j\omega) - v_{h+1}(j\omega))| > 0$ is met then $\bar{P}_g(j\omega) \notin e(-\hat{N}(j\omega)v_h(j\omega), -\hat{N}(j\omega)v_{h+1}(j\omega))$ or the vertex $\bar{P}_g(j\omega)$ does not intersect the edge $e(-\hat{N}(j\omega)v_h(j\omega), -\hat{N}(j\omega)v_{h+1}(j\omega))$.

2) If the equality $|\bar{P}_g(j\omega) + \hat{N}(j\omega)v_h(j\omega)| + |\bar{P}_g(j\omega) + \hat{N}(j\omega)v_{h+1}(j\omega)| - |\hat{N}(j\omega)(v_h(j\omega) - v_{h+1}(j\omega))| = 0$ is met then $\bar{P}_g(j\omega) \in e(-\hat{N}(j\omega)v_h(j\omega), -\hat{N}(j\omega)v_{h+1}(j\omega))$ or the vertex $\bar{P}_g(j\omega)$ intersect the edge $e(-\hat{N}(j\omega)v_h(j\omega), -\hat{N}(j\omega)v_{h+1}(j\omega))$.

Accordingly, satisfying the triangle inequality for any vertex of the value set $\chi_1(j\omega)$ in (22) and any two consecutive vertices of $P_E(j\omega)$ in (76) implies that no vertex of the value sets $\chi_1(j\omega)$ intersects $\partial(\Delta_a(j\omega, \mathbf{u}))$. Meanwhile, satisfying the triangle inequality for any vertex of the value set $P_E(j\omega)$ and any two consecutive vertices of $\chi_1(j\omega)$ implies that no vertex of the value sets of $P_E(j\omega)$ intersects $\chi_1(j\omega)$. This implies that two sets $\chi_1(j\omega)$ in (22) and $\chi_2(j\omega)$ in (23) do not have any overlap for $\omega \in (0, \frac{2\pi}{\bar{\tau}-\tau})$. Hence, according to Theorems 1 and 2, Assumptions 1 and 2, and the zero exclusion principle, one

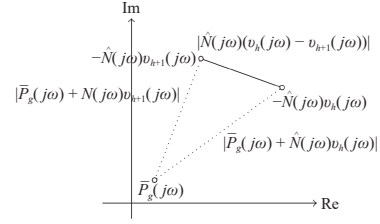


Fig. 21. A view of the triangle inequality between the vertex $\bar{P}_g(j\omega)$ and the edge $e(-\hat{N}(j\omega)v_h(j\omega), -\hat{N}(j\omega)v_{h+1}(j\omega))$.

can prove the theorem easily. ■

REFERENCES

- [1] J. E. Normey-Rico and E. F. Camacho, "Dead-time compensators: A survey," *Control Engineering Practice*, vol. 16, no. 4, pp. 407–428, 2008.
- [2] T. H. Lee, Q. G. Wang, and K. K. Tan, "Robust Smith-predictor controller for uncertain delay systems," *AIChE Journal*, vol. 42, no. 4, pp. 1033–1040, 1996.
- [3] I. Kaya, "Autotuning of a new PI-PD Smith predictor based on time domain specifications," *ISA Transactions*, vol. 42, no. 4, pp. 559–575, 2003.
- [4] M. Sarkar, B. Subudhi, and S. Ghosh, "Unified Smith predictor based H_∞ wide-area damping controller to improve the control resiliency to communication failure," *IEEE/CAA J. Autom. Sinica*, vol. 7, no. 2, pp. 584–596, 2020.
- [5] J. J. Huang and D. B. DeBra, "Automatic Smith-predictor tuning using optimal parameter mismatch," *IEEE Trans. Control Systems Technology*, vol. 10, no. 3, pp. 447–459, 2002.
- [6] I. Kaya, "PI-PD controllers for controlling stable processes with inverse response and dead time," *Electrical Engineering*, vol. 98, no. 1, pp. 55–65, 2016.
- [7] F. N. Deniz, N. Tan, S. E. Hamamci, and I. Kaya, "Stability region analysis in Smith predictor configurations using a PI controller," *Transactions of the Institute of Measurement and Control*, vol. 37, no. 5, pp. 606–614, 2015.
- [8] F. N. Deniz and N. Tan, "A model identification method for tuning of PID controller in a Smith predictor structure," *IFAC-PapersOnLine*, vol. 49, no. 10, pp. 13–18, 2016.
- [9] S.R. Veeramachaneni and J. M. Watkins, "Robust performance design of PID controllers for time-delay systems with a Smith predictor," in *Proc. American Control Conf.*, pp. 2462–2467, 2014.
- [10] I. Polubny, "Fractional-order systems and $P^I D^\mu$ controller," *IEEE Trans. Automatic Control*, vol. 44, pp. 208–214, 1999.
- [11] C. A. Monje, Y. Q. Chen, B. M. Vinagre, D. Xue, and V. Feliu-Batlle, "Fractional-order systems and controls: Fundamentals and applications," *Springer Science & Business Media*, 2010.
- [12] M. Tavakoli-Kakhki and M. Haeri, "Temperature control of a cutting process using fractional-order proportional-integral-derivative controller," *Journal of Dynamic Systems, Measurement, and Control*, vol. 133, no. 5, 2011.
- [13] A. S. Chopade, S. W. Khubalkar, A. S. Junghare, M. V. Aware, and S. Das, "Design and implementation of digital fractional order PID controller using optimal pole-zero approximation method for magnetic levitation system," *IEEE/CAA J. Autom. Sinica*, vol. 5, no. 5, pp. 977–989, 2018.
- [14] C. I. Muresan, A. Dutta, E. H. Dulf, Z. Pinar, A. Maxim, and C. M. Ionescu, "Tuning algorithms for fractional order internal model controllers for time delay processes," *Int. Journal of Control*, vol. 89, no. 3, pp. 579–593, 2016.
- [15] M. Borah and B. K. Roy, "Systematic construction of high dimensional fractional-order hyperchaotic systems," *Chaos, Solitons & Fractals*,

- vol. 131, no. 3, p. 109539, 2020.
- [16] M. Borah, P. Roy, and B. K. Roy "Synchronisation control of a novel fractional-order chaotic system with hidden attractor", in *Proc. IEEE Students' Technology Symp.*, pp. 163–168, 2016.
 - [17] V. Badri and M. S. Tavazoei, "On time-constant robust tuning of fractional order proportional derivative controllers," *IEEE/CAA J. Autom. Sinica*, vol. 6, no. 5, pp. 1179–1186, 2019.
 - [18] R. Azarmi, M. Tavakoli-Kakhki, A. Fatehi, and A. K. Sedigh, "Robustness analysis and design of fractional order I^D controllers using the small gain theorem," *Int. Journal of Control*, vol. 93, no. 3, pp. 449–461, 2020.
 - [19] Y. H. Lim, K. K. Oh, Kwang-Kyo, and H. S. Ahn, "Stability and stabilization of fractional-order linear systems subject to input saturation," *IEEE Trans. Automatic Control*, vol. 58, no. 4, pp. 1062–1067, 2012.
 - [20] E. S. A. Shahri, A. Alfi, and J. A. T. Machado, "Lyapunov method for the stability analysis of uncertain fractional-order systems under input saturation," *Applied Mathematical Modelling*, vol. 81, pp. 663–672, 2020.
 - [21] C. A. Monje, B. M. Vinagre, V. Feliu, and Y. Q. Chen, "Tuning and auto-tuning of fractional order controllers for industry applications," *Control Engineering Practice*, vol. 16, no. 7, pp. 798–812, 2008.
 - [22] L. Majhi, M. Borah, and P. Roy, "Fractional order system identification of Maglev model from real-time data", in *Proc. IEEE Int. Conf. Advanced Communications*, pp. 210–213, 2014.
 - [23] T. T. Hartley and C. F. Lorenzo, "Fractional-order system identification based on continuous order-distributions," *Signal Processing*, vol. 83, no. 11, pp. 2287–2300, 2003.
 - [24] I. Petráš, Y. Q. Chen, and B. M. Vinagre, "A robust stability test procedure for a class of uncertain LTI fractional order systems", in *Proc. ICCS*, pp. 27–30, 2002.
 - [25] R. Azarmi, M. Tavakoli-Kakhki, R. Vilanova, A. Fatehi, and A. K. Sedigh, "Robustness improvement using the filtered Smith predictor based fractional integral-fractional derivative controllers: Application to a pressure plant", in *Proc. Int. Conf. Systems and Control*, 2018.
 - [26] C. I. Pop, C. Ionescu, R. De Keyser, and E. H. Dulf, "Robustness evaluation of fractional order control for varying time delay processes," *Signal, Image and Video Processing*, vol. 6, no. 3, pp. 453–461, 2012.
 - [27] V. Feliu-Battle and R. Rivas-Perez, "Smith predictor based fractional-order integral controller for robust temperature control in a steel slab reheating furnace," *Transactions of the Institute of Measurement and Control*, vol. 41, no. 16, pp. 4521–4534, 2019.
 - [28] V. Feliu-Battle, R. R. Pérez, F. J. C. García, and L. S. Rodríguez, "Smith predictor based robust fractional order control: Application to water distribution in a main irrigation canal pool," *Journal of Process Control*, vol. 19, no. 3, pp. 506–519, 2009.
 - [29] M. Bettayeb, R. Mansouri, U. Al-Saggaf, and I. M. Mehedi, "Smith predictor based fractional-order-filter PID controllers design for long time delay systems," *Asian Journal of Control*, vol. 19, no. 2, pp. 587–598, 2017.
 - [30] P. R. Hemavathy, Y. M. Shuaib, and S. K. Lakshmanaprabu, "Design of Smith predictor based fractional controller for higher order time delay process," *CMES-Computer Modeling in Engineering & Sciences*, vol. 119, no. 3, pp. 481–498, 2019.
 - [31] M. Bolignari, G. Rizzello, L. Zaccarian, and M. Fontana, "Smith-predictor-based torque control of a rolling diaphragm hydrostatic transmission," *IEEE Robotics and Automation Letters*, vol. 6, no. 2, pp. 2970–2977, 2021.
 - [32] N. S. Özbek and İ. Eker, "An experimental comparative study of modified Smith predictor based fractional order controller design strategies for a time delay process", in *Proc. Int. Conf. Electrical and Electronic Engineering*, pp. 199–203, 2017.
 - [33] P. K. Bhamre and C. B. Kadu, "Design of a Smith predictor based fractional order PID controller for a coupled tank system", in *Proc. Int. Conf. Automatic Control and Dynamic Optimization Techniques*, pp. 705–708, 2016.
 - [34] R. Azarmi, A. K. Sedigh, M. Tavakoli-Kakhki, and A. Fatehi, "Design and implementation of Smith predictor based fractional order PID controller on MIMO flow-level plant", in *Proc. 23rd Iranian Conf. Electrical Engineering*, pp. 858–863, 2015.
 - [35] R. Xin, C. Wang, M. Li, H. Shi, and Z. Liu, "The design of FOPI and FO[PI] controllers for large time-delay system based on Smith predictor", in *Proc. IEEE Chinese Guidance, Navigation and Control Conf.*, pp. 1249–1252, 2016.
 - [36] M. Safaei and S. Tavakoli, "Smith predictor based fractional-order control design for time-delay integer-order systems," *Int. Journal of Dynamics and Control*, vol. 6, no. 1, pp. 179–187, 2018.
 - [37] V. Feliu-Battle and R. Rivas-Perez, "Control of the temperature in a petroleum refinery heating furnace based on a robust modified Smith predictor," *ISA Transactions*, vol. 112, pp. 251–270, 2021.
 - [38] I. O. B. Gonzalez, R. Rivas-Perez, V. Feliu-Battle, and F. Castillo-Garcia, "Temperature control based on a modified Smith predictor for injectable drug formulations," *IEEE Latin America Transactions*, vol. 13, no. 4, pp. 1041–1047, 2015.
 - [39] V. Feliu-Battle, R. Rivas-Perez, V. F. Battle, and F. Castillo-Garcia, "Design of a PI^μ controller for the robust control of the steam pressure in the steam drum of a bagasse-fired boiler," *IEEE Access*, vol. 9, pp. 95123–95134, 2021.
 - [40] W. Ren, Y. Luo, Q.-N. He, X. Zhou, C. Deng, Y. Mao, and G. Ren, "Stabilization control of electro-optical tracking system with fiber-optic gyroscope based on modified Smith predictor control scheme," *IEEE Sensors Journal*, vol. 18, no. 19, pp. 8172–8178, 2018.
 - [41] S. H. Nagarsheth and S. N. Sharma, "Smith predictor embedded analytical fractional-order controller design: A delayed Bode's ideal transfer function approach," *IFAC-PapersOnLine*, vol. 53, no. 2, pp. 3749–3754, 2020.
 - [42] P. A. M. Devan, F. A. B. Hussin, R. Ibrahim, K. Bingi, and H. Q. A. Abdulrab, "Fractional-order predictive PI controller for dead-time processes with set-point and noise filtering," *IEEE Access*, vol. 8, no. 2, pp. 183759–183773, 2020.
 - [43] N. S. Özbek and İ. Eker, "Experimental evaluation of various modified Smith predictor-based fractional order control design strategies in control of a thermal process with time delay," *Int. Journal of Embedded Systems*, vol. 11, no. 1, pp. 68–77, 2019.
 - [44] M. Yadav and H. K. G. Patel, "Sensitivity analysis of IMC-PID controller with smith predictor using different filters", in *Proc. IEEE 17th India Council Int. Conf.*, vol. 11, no. 1, pp. 68–77, 2019.
 - [45] M. Pătrașcu, "Smith predictor approximation for industrial control applications with genetic algorithms", in *Proc. Int. Conf. Applied Artificial Intelligence*, 2021.
 - [46] V. L. Korupu and M. Muthukumarasamy, "A comparative study of various Smith predictor configurations for industrial delay processes", *Chemical Product and Process Modeling*, vol. 17, no. 6, pp. 701–732, 2022.
 - [47] K. A. Moornani and M. Haeri, "Robust stability testing function and Kharitonov-like theorem for fractional order interval systems," *IET Control Theory Applications*, vol. 4, no. 10, pp. 2097–2108, 2010.
 - [48] D. Boudjehem, M. Sedraoui, and B. Boudjehem, "A fractional model for robust fractional order Smith predictor," *Nonlinear Dynamics*, vol. 73, no. 3, pp. 1557–1563, 2013.
 - [49] T. Liu, Z. Hu, R. Yin, and X. Xu, "New analytical design of the Smith predictor controller for high-order systems," *Proc. the Institution of Mechanical Engineers, Part I: Journal of Systems and Control Engineering*, vol. 219, no. 4, pp. 271–281, 2005.
 - [50] F. N. Deniz, "An effective Smith predictor based fractional-order PID controller design methodology for preservation of design optimality and robust control performance in practice," *International Journal of Systems Science*, pp. 1–19, 2022.
 - [51] K. V. L. Narayana, W. B. Bedada, and K. L. Nefabas, "Enhanced modified Smith predictor for higher order stable processes", in *Proc. IEEE AFRICON*, pp. 424–429, 2017.
 - [52] P. R. Hemavathy, Y. M. Shuaib, and S. K. Lakshmanaprabu, "Design of Smith predictor based fractional controller for higher order time delay process," *Computer Modeling in Engineering & Sciences*, vol. 119,

- no.3, pp.481–498, 2019.
- [53] Z. Wu, J. Yuan, D. Li, Y. Xue, and Y. Q. Chen, “The proportional-integral controller design based on a Smith-like predictor for a class of high order systems,” *Transactions of the Institute of Measurement and Control*, vol.43, no.4, pp.875–890, 2021.
- [54] K. A. Moornani and M. Haeri, “On robust stability of LTI fractional-order delay systems of retarded and neutral type,” *Automatica*, vol.46, no.2, pp.362–368, 2010.
- [55] K.A. Moornani and M. Haeri, “On robust stability of linear time invariant fractional-order systems with real parametric uncertainties,” *ISA Transactions*, vol.48, no.4, pp.484–490, 2009.
- [56] M. Ghorbani, M. Tavakoli-Kakhki, and A. A. Estarami, “Robust FOPID stabilization of retarded type fractional order plants with interval uncertainties and interval time delay,” *Journal of the Franklin Institute*, vol.356, no.16, pp.9302–9329, 2019.
- [57] M. Ghorbani, M. Tavakoli-Kakhki, A. Tepljakov, E. Petlenkov, A. Farnam, and G. Crevecoeur, “Robust stability analysis of interval fractional-order plants with interval time delay and general form of fractional-order controllers,” *IEEE Control Systems Letters*, vol.6, pp.1268–1273, 2021.
- [58] Y. Jin, Y. Q. Chen, and D. Xue, “Time-constant robust analysis of a fractional order [proportional derivative] controller,” *IET Control Theory & Applications*, vol.5, no.1, pp.164–172, 2011.
- [59] Y. Jin, Y. Q. Chen, and D. Xue, “Identification and PID control for a class of delay fractional-order systems,” *IEEE/CAA J. Autom. Sinica*, vol.3, no.4, pp.463–476, 2016.
- [60] A. Álvarez de Miguel, J. G. Mollocana Lara, C. E. García Cena, M. Romero, J. M. García de María, and J. González-Aguilar, “Identification model and PI and PID controller design for a novel electric air heater,” *Automatika*, vol.58, no.1, pp.55–68, 2017.
- [61] R. Rivas-Perez, F. Castillo-García, J. Sotomayor-Moriano, and V. Feliu-Batlle, “Design of a fractional order PI controller for steam pressure in the steam drum of a bagasse fired boiler,” *IFAC Proceedings Volumes*, vol.47, no.3, pp.1337–1342, 2014.
- [62] M. Ghorbani and M. Tavakoli-Kakhki, “Robust stabilizability of fractional order proportional integral controllers for fractional order plants with uncertain parameters: A new value set based approach,” *Journal of Vibration and Control*, vol.26, no.11–12, pp.965–975, 2020.
- [63] M. Ghorbani and M. Tavakoli-Kakhki, “Robust stability analysis of a general class of interval delayed fractional order plants by a general form of fractional order controllers,” *Mathematical Methods in the Applied Sciences*, vol.44, no.13, pp.10172–10189, 2021.
- [64] C. Yeroğlu, M. M. Özyetkin, and N. Tan, “Frequency response computation of fractional order interval transfer functions,” *Int. Journal of Control, Automation and Systems*, vol.8, no.5, pp.1009–1017, 2010.
- [65] M. Busłowicz, “Stability of linear continuous-time fractional order systems with delays of the retarded type,” *Bulletin of the Polish Academy of Sciences: Technical Sciences*, 2008.
- [66] S. E. Hamamci, “An algorithm for stabilization of fractional-order time delay systems using fractional-order PID controllers,” *IEEE Trans. Automatic Control*, vol.52, no.10, pp.1964–1969, 2007.
- [67] S.P. Bhattacharyya, H. Chapellat, and L.H. Keel, “Robust control: The parametric approach,” *Prentice Hall*, 1995.
- [68] M. Fu, S. Dasgupta, and V. Blondel, “Robust stability under a class of nonlinear parametric perturbations,” *IEEE Trans. Automatic Control*, vol.40, no.2, pp.213–223, 1995.
- [69] W. S. Levine, “The control handbook,” *CRC Press*, 1996.

- [70] J. W. Brown, R. V. Churchill, *et al.*, “Complex variables and applications,” *Boston: Birkhäuser*, 2009.
- [71] A. Oustaloup, F. Levron, B. Mathieu, and F. M. Nanot, “Frequency-band complex noninteger differentiator: Characterization and synthesis,” *IEEE Trans. Circuits and Systems I: Fundamental Theory and Applications*, vol.47, no.1, pp.25–39, 2000.
- [72] U. G. GmbH “Technical description of RT512 process trainer level”, [Online] Available: <https://www.gunt.de/en/products/mechatronics/automation-and-process-control-engineering/simple-process-engineering-control-systems/level-control-trainer/080.51200/rt512/gclt-1:pa-148:ca-83:pr-1178,2003>.



Active controllers, robust nonlinear control design, estimation and learning based controllers.

Majid Ghorbani received the B.Sc. in control engineering from Sahand University of Technology, Iran, in 2013. Then, he received the M.Sc. degree in control engineering from K. N. Toosi University of Technology, Iran, in 2016. He is currently pursuing the Ph.D. degree at Tallinn University of Technology. His research interests include fractional order control, and applications of fractional calculus in engineering, robust stability analysis of LTI systems with multiple time delays, nonlinear model predictive controllers, robust nonlinear control design, estimation and learning based controllers.



Mahsan Tavakoli-Kakhki received the B.Sc. and M.Sc. degrees from Ferdowsi University, Iran, in 2004 and 2007, respectively, and the Ph.D. degree from Sharif University of Technology, Iran, in 2011, all in electrical engineering. Currently, she is an Associate Professor with the Faculty of Electrical Engineering, K. N. Toosi University of Technology. Her research interests include robust control systems, time delayed control systems, fractional order control, and model reduction of high order systems.



Aleksei Tepljakov (Senior Member, IEEE) received the Ph.D. degree in information and communication technology from the Tallinn University of Technology, in 2015. Since November 2021, he holds a Senior Research Scientist position at the Department of Computer Systems, School of Information Technologies, Tallinn University of Technology. His main research interests include the study of cyber-physical systems: fractional-order modeling and control of complex systems and developing efficient mathematical and 3D modeling methods for virtual and augmented reality for educational and industrial applications. He is a Senior Member of the IEEE with more than 10 years of service. He has been a Member of the IEEE Control Systems Society, since 2012, and the Education Society, since 2018.



Eduard Petlenkov is currently a Tenured Full Professor in the Department of Computer Systems, Tallinn University of Technology and the Head of the Centre for Intelligent Systems. He received the B.Sc. (2001), M.Sc.(2003), and Ph.D.(2007) degrees in computer and systems engineering from the Tallinn University of Technology. His main research interests include the domain of intelligent control, system analysis and computational intelligence.

Appendix 5

V

M. Ghorbani, A. Tepljakov, and E. Petlenkov. Robust FOPID stabilization for Smith predictor structures. In *Proc. 2022 IEEE 61st Conference on Decision and Control (CDC)*, pages 1696–1701, 2022.

Robust FOPID Stabilization for Smith Predictor Structures

Majid Ghorbani, Aleksei Tepljakov (*Senior Member, IEEE*), Eduard Petlenkov

Abstract—In this letter, an effective graphical tuning method of Fractional-Order Proportional Integral Derivative (FOPID) controllers is proposed for the Smith Predictor (SP) control structure. At first, necessary and sufficient conditions are achieved for the robust stability of the SP structure based on the zero exclusion principle. Then, by benefiting from the D-decomposition technique and the value set concept, the problem of robustly stabilizing the SP scheme is solved using FOPID controllers. Moreover, an auxiliary function is provided to enhance the performance of the SP structure by the sensitivity function. Simulation results successfully confirm the validity and effectiveness of the proposed method, which is provided in illustrative examples.

I. INTRODUCTION

The presence of considerable time delays are a common phenomena in industrial processes [1], [2]. The time delay term causes some difficulties and may lead to instability and poor performance of the systems [3].

In [4], a novel dead time compensator has been proposed, more commonly, known now as the Smith predictor (SP) controllers. The SP control structures have been applied to many engineering fields, mostly in the process industry [5].

In real applications, the identified model may not be an exact representation of the process, perhaps because parameters of the actual process may change in operating conditions or a result of inaccurate modeling [6]. Hence, in practical applications it is more likely to have uncertainties in all the model parameters. In the face of the inevitable mismatch between the identified model and the actual process, the robust stability analysis is essential for the SP based control systems. Hence, numerous extensions have been proposed to improve performance and robustness of the SP based control systems in the face of plant uncertainties. For instance, in [7], an approach has been presented to design a robust PI controller for a SP control structure having a first order plant with a time delay. In addition, in [8], by using convex optimization techniques, a method has been proposed to enhance the performance of the SP based control system. Moreover, in [9], a method was proposed to tune the proportional-derivative (PD) control which is developed based on a SP control scheme. In addition, in [10], [11], various methods have been proposed to improve the performance and robustness of the SP based control systems.

Fractional calculus is recently ubiquitous in various engineering disciplines, especially control systems engineering

[12]. It has been shown that fractional-order operators may result in more accurate models [13] and enhancing the performance of the closed-loop control systems [14], [15].

The Fractional-Order Proportional Integral Derivative (FOPID) controller has been extensively employed in process control industry because of improving robustness to the modeling error and its simple structure [16], [17]. It has five tuning parameters which have to be designed. Therefore, this would provide the designer with more degrees of freedom [18]. Accordingly, fractional-order controllers have been applied to many engineering applications.

In this letter, we are particularly concerned with robustly stabilizing the SP control systems having uncertainties using FOPID controllers. As mentioned before, uncertainties naturally appear in actual processes. Hence, robust stability as a requirement has to be investigated in the literature. Therefore, different strategies have been proposed to treat the requirement. In [19], an optimization technique has been used to design a FOPID controller for the SP control structures. The works [20], [21] have been proposed some frequency-domain control methodologies to design fractional-order controllers in order to enhance the robustness of the SP control structures based on gain and phase margins. Moreover, in [22], a design method was presented to tune Fractional-Order Proportional Integral (FOPI) controllers embedded in the SP on the basis of Bode's ideal transfer function.

Recently, many investigators have employed the D-decomposition method to characterise the stability boundaries of controller parameters (For some samples, see [23], [24]). By the D-decomposition method, one can determine the stability region of controllers. In [25], [26], the stability region of PI and PID controllers has been computed for the SP control structures. However, the aforementioned papers have failed to design a robust controller in the presence of uncertainties. This issue motivates the authors to find a solution to design a robust controller for the SP control structures having uncertainties. To employ the D-decomposition method, the boundary of the value set of the characteristic function of the SP control structures has to be determined. Hence, in Theorem 1 of this letter, this boundary is obtained. Then, the necessary and sufficient conditions are presented in Lemma 4 for robust stability analysis of the SP. Moreover, an algorithm is provided to obtain the robust stability region of FOPID controllers embedded in the SP control structures. Also, an auxiliary function is offered to improve the performance of the SP.

This paper is organized as follows. Section II reviews the SP control structure and FOPID controllers. Section III provides the main results. In Section IV, numerical examples

This work was supported by the Estonian Research Council grant PRG658.

The Authors are with Department of Computer Systems, Tallinn University of Technology, Estonia (e-mail: majid.ghorbani@taltech.ee ; aleksei.tepljakov@taltech.ee ; eduard.petlenkov@taltech.ee).

are employed to evaluate the obtained results. Finally, a conclusion is given in Section V.

II. PRELIMINARIES

The conventional SP structure has been shown in Fig. 1 where $G_c(s)$, $G_n(s)$ and $G(s)$ are respectively the transfer functions of the FOPID controller, the nominal process model and the actual process. In the current research letter, the transfer function of the actual process is represented as the following form,

$$G(s) = \frac{K}{Ts + 1} e^{-Ls}, \quad (1)$$

in which the real positive parameters K, L and T can be interval uncertain parameters as follows:

$$K \in [K^-, K^+], L \in [L^-, L^+], T \in [T^-, T^+]. \quad (2)$$

Also, the nominal process model $G_n(s)$ is defined in (3).

$$G_n(s) = \frac{K_n}{T_n s + 1}, \quad (3)$$

where $K_n = \frac{K^+ + K^-}{2}$ and $T_n = \frac{T^+ + T^-}{2}$. In Fig. 1, the estimated value of the dead time of the process L_n is considered as $L_n = \frac{L^+ + L^-}{2}$. Moreover, let $G_c(s)$ be a FOPID controller with a transfer function defined in (4).

$$G_c(s) = K_p + \frac{K_i}{s^\lambda} + K_d s^\mu, \quad K_i \neq 0, \lambda \in (0, 2), \mu \in (0, 1), \quad (4)$$

where K_p, K_i and K_d are the controller coefficients, μ and λ are real derivative and integral orders of the controller. Based

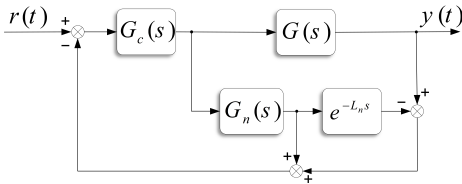


Fig. 1: The Smith predictor structure.

on Fig. 1, the transfer function of the SP structure can be obtained as

$$T(s) = \frac{G_c(s)G(s)}{1 + G_c(s)(G_n(s) + G(s) - G_n(s)e^{-L_n s})}. \quad (5)$$

From (5), it is visible that if the nominal process model $G_n(s)$ and the estimated value of the dead time of the process L_n perfectly match the transfer function of the actual process $G(s)$ i.e., $G_n(s)e^{-L_n s} = G(s)$, then the nominal transfer function of the SP control structure can be obtained as follows.

$$T_n(s) = \frac{G_c(s)G_n(s)e^{-L_n s}}{1 + G_c(s)G_n(s)}. \quad (6)$$

As mentioned before, due to the uncertainties which may exist in real systems, the FOPID controller $G_c(s)$ has to

robustly stabilize the SP control structure with the characteristic function $\Delta(s)$ in (7).

$$\Delta(s) = D_G(s)\hat{D}_G(s) + K\hat{N}_c(s)e^{-Ls}, \quad (7)$$

in which $D_G(s) = Ts + 1$, $\hat{D}_G(s) = s^\lambda D_{G_n}(s) + N_c(s)K_n(1 - e^{-L_n s})$, $D_{G_n}(s) = T_n s + 1$ and $N_c(s) = K_p s^\lambda + K_i + K_d s^{\mu+\lambda}$ and $\hat{N}_c(s) = N_c(s)D_{G_n}(s)$. Also, we need the following lemmas in the rest of the current research letter.

Lemma 1: [27] For two bounded and closed value sets Q_1 and Q_2 , $\partial(Q_1 + Q_2) \subseteq \partial(Q_1) + \partial(Q_2)$ where ∂ denotes the boundary.

Lemma 2: [2] Assume that $[x, y]$ denotes a line segment connecting pairs of x and y . Then, at a given frequency $\omega = \omega_0 \in (0, \frac{2\pi}{L^+ - L^-})$, the value set of $K e^{-Ls}$ is located inside $P_E(j\omega)$ in (8).

$$P_E(j\omega) \triangleq \{[H_1(j\omega), H_2(j\omega)], [H_2(j\omega), H_3(j\omega)], \dots, [H_{4N+1}(j\omega), H_{4N+2}(j\omega)], [H_{4N+2}(j\omega), H_1(j\omega)]\}, \quad (8)$$

$$H_r(j\omega) \triangleq \begin{cases} \overline{E}_{(r-1)}(j\omega), & \text{for } 1 \leq r \leq 2N+1, \\ \underline{E}_{(2N)}(j\omega), & \text{for } r = 2N+2, \\ \underline{E}_{(2N-1)}(j\omega), & \text{for } r = 2N+3, \\ \vdots & \\ \underline{E}_0(j\omega), & \text{for } r = 4N+2, \end{cases}$$

$$\overline{E}_r(j\omega) \triangleq$$

$$\begin{cases} K^+ e^{-j\omega \left(L^- + r \frac{L^+ - L^-}{2N} \right)}, & \text{for } r = 0, 2, \dots, 2N, \\ \frac{K^+ e^{-j\omega \left(L^- + r \frac{L^+ - L^-}{2N} \right)}}{\cos \left(\omega \frac{L^+ - L^-}{2N} \right)}, & \text{for } r = 1, 3, \dots, 2N-1, \end{cases}$$

$$\underline{E}_r(j\omega) \triangleq K^- e^{-j\omega \left(L^- + r \frac{L^+ - L^-}{2N} \right)}, \quad r = 0, 1, 2, \dots, 2N.$$

in which $N \in \mathbb{N}^{\geq 3}$. In fact N is an arbitrary member satisfying $N \in \mathbb{N}^{\geq 3}$.

Lemma 3: [30] The fractional characteristic quasi-polynomial $\delta(s)$ (of commensurate or non-commensurate degree) is stable if and only if

$$\Delta \arg \psi(j\omega) = \frac{\delta(j\omega)}{\omega_r(j\omega)} = 0, -\infty < \omega < \infty \quad (9)$$

where $\omega_r(s) = a_{0n}(s+c)^{\alpha_n}$, $c > 0$. Also, α_n is the highest order of $\delta(j\omega)$ and a_{0n} is the coefficient of the highest term s^{α_n} and c is an arbitrary positive number. In other words, the fractional characteristic quasi-polynomial $\delta(s)$ is stable if and only if the polar plot of $\psi(j\omega)$ does not encircle the origin of the complex plane as ω traverses from $-\infty$ to $+\infty$.

III. MAIN RESULTS

A. Computing method of value set

In order to compute the robust stability region of FOPID controllers for the SP structure depicted in Fig 1, at first, $\partial(\Delta(s))$ has to be determined at each frequency for $s = j\omega$. To do this, the following definition is presented.

Definition 1: For $D_G(j\omega)$, K and L , define:

$$\begin{aligned} \mathbf{V}^{D_G} &= \{D_1(j\omega) = T^- j\omega + 1, D_2(j\omega) = T^+ j\omega + 1\}, \\ \mathbf{I}^{D_G} &= \{\mathbf{I}_1^{D_G}, \mathbf{I}_2^{D_G} = [D_1(j\omega), D_2(j\omega)]\}, \\ \mathbf{V}^K &= \{K^-, K^+\}, \mathbf{I}^K = [K^-, K^+], \\ \mathbf{V}^L &= \{L^-, L^+\}, \mathbf{I}^L = [L^-, L^+]. \end{aligned} \quad (10)$$

For a given frequency ω , the shape of the interval polynomial $D_G(j\omega) = Tj\omega + 1$ is a line segment whose two vertices are $D_i(j\omega)$, $i = 1, 2$. Additionally, for a given frequency ω , it is clear that $\partial(K e^{-Lj\omega}) \subseteq \mathbf{V}^K e^{-\mathbf{I}^L s} \cup \mathbf{I}^K e^{-\mathbf{V}^L s}$. Now, in the following theorem, a set of exposed edges is presented to contain $\partial(\Delta(j\omega))$ at a given frequency.

Theorem 1: For a given frequency $\omega = \omega^*$, $\partial(\Delta(j\omega)) \subseteq \Delta^G(j\omega)$ where

$$\begin{aligned} \Delta^G(s = j\omega) &= \Delta^{G1}(s) \cup \Delta^{G2}(s), \\ \Delta^{G1}(s) &= \hat{D}_G(s) \mathbf{V}^{D_G} + \hat{N}_c(s) \mathbf{I}^K e^{-\mathbf{V}^L s}, \\ \Delta^{G2}(s) &= \\ \left\{ \begin{array}{ll} \hat{D}_G(s) \mathbf{I}^{D_G} + \hat{N}_c(s) \mathbf{V}^K e^{-\mathbf{I}^L s}, & \text{for } 0 \leq \omega^* < \frac{2\pi}{L^+ - L^-}, \\ \hat{D}_G(s) \mathbf{I}^{D_G} + \hat{N}_c(s) \mathbf{V}^K e^{-[0, 2\pi]j}, & \text{for } \omega^* \geq \frac{2\pi}{L^+ - L^-}. \end{array} \right. \end{aligned} \quad (11)$$

Proof: Assume that $0 \leq \omega^* < \frac{2\pi}{L^+ - L^-}$. Based on the property mentioned in Lemma 1, we have:

$$\partial(\Delta(j\omega)) \subseteq \left(\hat{D}_G(j\omega) \mathbf{I}^{D_G} + \hat{N}_c(j\omega) \mathbf{I}^K e^{-\mathbf{I}^L s} \right). \quad (12)$$

Additionally, we know that $\partial(K e^{-Lj\omega}) \subseteq \mathbf{V}^K e^{-\mathbf{I}^L j\omega} \cup \mathbf{I}^K e^{-\mathbf{V}^L j\omega}$. Therefore, the result concluded in (12) can be rewritten as

$$\begin{aligned} \partial(\Delta(j\omega)) &\subseteq \hat{D}_G(j\omega) \mathbf{I}^{D_G} + \hat{N}_c(j\omega) \mathbf{I}^K e^{-\mathbf{I}^L s} \\ &\subseteq \left(\hat{D}_G(j\omega) \mathbf{I}^{D_G} + \hat{N}_c(j\omega) \mathbf{V}^K e^{-\mathbf{I}^L s} \right) \cup \\ &\quad \left(\hat{D}_G(j\omega) \mathbf{I}^{D_G} + \hat{N}_c(j\omega) \mathbf{I}^K e^{-\mathbf{V}^L s} \right). \end{aligned} \quad (13)$$

Also, from Definition 1, we have:

$$\begin{aligned} \{ \hat{D}_G(j\omega) \mathbf{I}^{D_G} + \hat{N}_c(j\omega) \mathbf{I}^K e^{-\mathbf{V}^L s} = \\ \hat{D}_G(j\omega) \{ \mathbf{I}_1^{D_G} \} + \hat{N}_c(j\omega) \mathbf{I}^K e^{-\mathbf{V}^L s} \}. \end{aligned} \quad (14)$$

Now, consider $\hat{D}_G(j\omega) \mathbf{I}_1^{D_G} + \hat{N}_c(j\omega) \mathbf{I}^K e^{-\mathbf{V}^L s}$ constructed by line segment plus line segment. The shape of the sum of two independent lines would like to be a convex polygon with 4 vertices in the complex plane. Accordingly, we have:

$$\begin{aligned} \hat{D}_G(j\omega) \mathbf{I}_1^{D_G} + \hat{N}_c(j\omega) \mathbf{I}^K e^{-\mathbf{V}^L s} &\subseteq \left(\hat{D}_G(j\omega) \mathbf{I}_1^{D_G} + \hat{N}_c(j\omega) \right. \\ &\quad \left. \mathbf{V}^K e^{-\mathbf{V}^L s} \right) \cup \left(\hat{D}_G(j\omega) \{D_1(j\omega), D_2(j\omega)\} + \right. \\ &\quad \left. \hat{N}_c(j\omega) \mathbf{I}^K e^{-\mathbf{V}^L s} \right). \end{aligned} \quad (15)$$

Therefore, from (14) and (15), (16) is concluded.

$$\begin{aligned} \hat{D}_G(j\omega) \mathbf{I}^{D_G} + \hat{N}_c(j\omega) \mathbf{I}^K e^{-\mathbf{V}^L s} &\subseteq \left(\hat{D}_G(j\omega) \mathbf{I}^{D_G} + \hat{N}_c(j\omega) \right. \\ &\quad \left. \mathbf{V}^K e^{-\mathbf{V}^L s} \right) \cup \left(\hat{D}_G(j\omega) \mathbf{V}^{D_G} + \hat{N}_c(j\omega) \mathbf{I}^K e^{-\mathbf{V}^L s} \right). \end{aligned} \quad (16)$$

Now, from (12) and (16), one can infer that

$$\begin{aligned} \partial(\Delta(j\omega)) &\subseteq \hat{D}_G(j\omega) \mathbf{I}^{D_G} + \hat{N}_c(j\omega) \mathbf{I}^K e^{-\mathbf{I}^L s} \\ &\subseteq \left(\left(\hat{D}_G(j\omega) \mathbf{I}^{D_G} + \hat{N}_c(j\omega) \mathbf{V}^K e^{-\mathbf{I}^L s} \right) \cup \right. \\ &\quad \left. \left(\hat{D}_G(j\omega) \mathbf{I}^{D_G} + \hat{N}_c(j\omega) \mathbf{I}^K e^{-\mathbf{V}^L s} \right) \right) \subseteq \\ &\quad \left(\left(\hat{D}_G(j\omega) \mathbf{I}^{D_G} + \hat{N}_c(j\omega) \mathbf{V}^K e^{-\mathbf{I}^L s} \right) \cup \right. \\ &\quad \left. \left(\hat{D}_G(j\omega) \mathbf{I}^{D_G} + \hat{N}_c(j\omega) \mathbf{V}^K e^{-\mathbf{V}^L s} \right) \cup \right. \\ &\quad \left. \left(\hat{D}_G(j\omega) \mathbf{V}^{D_G} + \hat{N}_c(j\omega) \mathbf{I}^K e^{-\mathbf{V}^L s} \right) \right). \end{aligned} \quad (17)$$

Also, we know that $\hat{N}_c(j\omega) \mathbf{V}^K e^{-\mathbf{V}^L s} \subseteq \hat{N}_c(j\omega) \mathbf{V}^K e^{-\mathbf{I}^L s}$ at $\omega = \omega^*$. Therefore, the proof can be completed for $0 \leq \omega^* < \frac{2\pi}{L^+ - L^-}$. Also, the proof is completed for $\omega^* \geq \frac{2\pi}{L^+ - L^-}$ by (17) and the fact $\partial(K \hat{N}_c(j\omega) e^{-Lj\omega}) \subseteq \mathbf{V}^K \hat{N}_c(j\omega) e^{-[0, 2\pi]j}$ in a straightforward way. ■

In Theorem 1, $\partial(\Delta(j\omega))$ is determined at a given frequency. According to the results obtained in Theorem 1, the necessary and sufficient conditions are presented in the next lemma for robust stability analysis of the SP control scheme depicted in Fig 1.

Lemma 4: The SP control structure depicted in Fig. 1 can be robustly stabilized by FOPID controllers if and only if:

- $\Delta(s)$ has at least one stable member,
- $0 \notin \Delta^G(j\omega)$ for $\omega \geq 0$.

Proof: The proof can be obtained from the Zero Exclusion principle. Based on this principle, the SP with the characteristic function $\Delta(s)$ is robust stable if and only if $\Delta(s)$ has at least one stable member and $0 \notin \Delta(j\omega)$ for $\omega \geq 0$ [27], [28], [29]. Additionally, in Theorem 1, it has been proven that $\partial(\Delta(j\omega)) \subseteq \Delta^G(j\omega)$ at a given frequency. Therefore, $0 \notin \Delta(j\omega)$ if and only if $0 \notin \Delta^G(j\omega)$ for $\omega \geq 0$. ■

B. D-decomposition method

Assume that $\hat{\Delta}(s)$ is an arbitrary member of $\Delta(s)$ as follows:

$$\begin{aligned} \hat{\Delta}(s) &= s^\lambda \tilde{D}_G(s) D_{G_n}(s) + N_c(s) \left[K_n \tilde{D}_G(s) (1 - e^{-L_n s}) \right. \\ &\quad \left. + \tilde{K} D_{G_n}(s) e^{-\tilde{L} s} \right], \end{aligned} \quad (18)$$

where $\tilde{D}_G(s)$, \tilde{K} and \tilde{L} are respectively the arbitrary members of $D_G(s)$, K and L . The boundaries of the stability region of FOPID controllers for the SP control structure are described by Real Root Boundary (RRB), Infinite Root Boundary (IRB) and Complex Root Boundary (CRB) determined by the D-decomposition method [23].

RRB. $\hat{\Delta}(0) = K_i \tilde{K}_0 D_{G_n}(0)$. Due to $K_i \tilde{K}_0 D_{G_n}(0) = 0$, it yields $K_i = 0$.

IRB. $\hat{\Delta}(\infty) \neq 0$. Therefore, the boundary does not exist.

CRB. In general, the CRB boundary can be constructed by substituting $s = j\omega$ into $\hat{\Delta}(s) = 0$ in (18). Therefore, by partitioning $\hat{\Delta}(j\omega)$ into its real and imaginary parts and equating them to zero, one can obtain

$$\begin{cases} A_{11}K_p + A_{12}K_i = B_1, \\ A_{21}K_p + A_{22}K_i = B_2, \end{cases} \quad (19)$$

in which

$$\begin{aligned} A_{11} &= \text{Re}(s^\lambda [K_n \tilde{D}_G(s)(1 - e^{-L_n s}) + \tilde{K} D_{G_n}(s) e^{-\tilde{L} s}]), \\ A_{12} &= \text{Re}(K_n \tilde{D}_G(s)(1 - e^{-L_n s}) + \tilde{K} D_{G_n}(s) e^{-\tilde{L} s}), \\ A_{21} &= \text{Im}(s^\lambda [K_n \tilde{D}_G(s)(1 - e^{-L_n s}) + \tilde{K} D_{G_n}(s) e^{-\tilde{L} s}]), \\ A_{22} &= \text{Im}(K_n \tilde{D}_G(s)(1 - e^{-L_n s}) + \tilde{K} D_{G_n}(s) e^{-\tilde{L} s}), \\ B_1 &= -\text{Re}(s^\lambda \tilde{D}_G(s) D_{G_n}(s) + K_d s^{\lambda+\mu} [K_n \tilde{D}_G(s) \\ &\quad (1 - e^{-L_n s}) + \tilde{K} D_{G_n}(s) e^{-\tilde{L} s}]), \\ B_2 &= -\text{Im}(s^\lambda \tilde{D}_G(s) D_{G_n}(s) + K_d s^{\lambda+\mu} [K_n \tilde{D}_G(s) \\ &\quad (1 - e^{-L_n s}) + \tilde{K} D_{G_n}(s) e^{-\tilde{L} s}]), \end{aligned} \quad (20)$$

where $\text{Re}(\cdot)$ and $\text{Im}(\cdot)$ respectively denote the real and imaginary parts of a complex number. Finally, by solving the equations in (19), the K_p and K_i parameters in terms of λ, μ and k_d are given as follows.

$$\begin{cases} K_p = \frac{B_1 A_{22} - A_{11} B_2}{A_{11} A_{22} - A_{12} A_{21}}, \\ K_i = \frac{B_2 A_{11} - A_{21} B_1}{A_{11} A_{22} - A_{12} A_{21}}. \end{cases} \quad (21)$$

The parameter space (K_p, K_i) are divided into stable and unstable regions by the boundaries RRB, IRB and CRB. The stability region can be found by checking one arbitrary test point inside each region. To do this, one can use Lemma 3.

C. Computation of the robust stability region of FOPID Controllers

In this subsection, an stabilization algorithm (Algorithm 1) is presented to compute the robust stability region of FOPID controllers for the SP control structure shown in Fig. 1.

Algorithm 1.

Step 1. Obtain the set \mathbf{V}^{D_G} by Definition 1.

Step 2. For a fixed λ, μ and K_d , use the D-decomposition method explained in the Subsection III-B to compute the robust stability region in (K_p, K_i) plane for $\Delta^{G1}(s)$ and $\Delta^{G2}(s)$.

Step 3. The final robust stability region of FOPID controllers is the intersection of all the computed stable regions in *Step 2*.

D. Performance improvement of the SP control structure

To achieve the good reference tracking and the output disturbance rejection, a constraint on the sensitivity function

should be defined as follows:

$$|S(j\omega)| = \left| \frac{1 + G_c(j\omega)G_n(j\omega)(1 - e^{-j\omega L_n})}{1 + G_c(j\omega)G_n(j\omega)(1 - e^{-j\omega L_n}) + G_c(j\omega)G(j\omega)} \right| < |M(j\omega)|, \quad (22)$$

in which $M(j\omega)$ denotes the weighting function describing the frequency characteristic of the performance specifications [31]. Based on the inequality (22), the maximum modulus theorem [32] and Lemma 2, a robust FOPID designed by the Subsection III-C should satisfy the inequality $F_S(\omega) < 0$ to improve the performance specifications, where $F_S(\omega)$ is obtained as follows.

$$F_S(\omega) \triangleq \begin{cases} \max\{F_{Si}(\omega) | i = 1, 2\}, & \text{for } \omega \in [0, \frac{2\pi}{L^+ - L^-}), \\ F_{S3}(\omega), & \text{for } \omega \in [\frac{2\pi}{L^+ - L^-}, \infty), \end{cases} \quad (23)$$

in which F_{Si} ($i = 1, 2, 3$) can be given by (24), (25) and (26).

$$\begin{aligned} F_{S1}(\omega) &\triangleq \max_{r=1, \dots, 4N+2} \tilde{F}_{S1r}(\omega) - |M(j\omega)|, \\ \tilde{F}_{S1r}(\omega) &\triangleq \max_{e_{S11} \in P_{S1}} |e_{S11}|, \\ P_{S1} &\triangleq \{e_{S11}\}, \end{aligned} \quad (24)$$

$$e_{S11} \triangleq \frac{\hat{D}_G(j\omega)}{\hat{D}_G(j\omega) + \frac{D_{G_n}(j\omega)N_c(j\omega)H_r(j\omega)}{[D_1(j\omega), D_2(j\omega)]}}.$$

$$\begin{aligned} F_{S2}(\omega) &\triangleq \max_{r=1, 2} \frac{|\hat{D}_G(j\omega)D_r(j\omega)|}{\tilde{F}_{S2r}(\omega)} - |M(j\omega)|, \\ \tilde{F}_{S2r}(\omega) &\triangleq \min_{e_{S2r2} \in P_{S2}} |e_{S2r2}|, r_2 = 1, \dots, 4N+2, \\ P_{S2} &\triangleq \{e_{S21}, \dots, e_{S24N+2}\}, \\ e_{S2r2} &\triangleq \hat{D}_G(j\omega)D_r(j\omega) + [D_{G_n}(j\omega)N_c(j\omega)H_{r2}(j\omega), \\ &\quad D_{G_n}(j\omega)N_c(j\omega)H_{r2+1}(j\omega)], \text{ and } H_{4N+3} = H_1. \end{aligned} \quad (25)$$

$$\begin{aligned} F_{S3}(\omega) &\triangleq \frac{1}{|\frac{[D_{G_n}(j\omega)N_c(j\omega)K^+]}{\min_{d_1 \in P_D} |d_1|} - 1|} - |M(j\omega)|, \\ P_D &= \{d_1 = [V_1^D(j\omega), V_2^D(j\omega)]\}, \end{aligned} \quad (26)$$

$$V_{r1}^D(j\omega) = \hat{D}_G(j\omega)D_{r1}(j\omega), r_1 = 1, 2.$$

IV. ILLUSTRATIVE EXAMPLES

Example 1. Consider the following interval plant [25]:

$$G(s) = \frac{[0.9, 1.1]}{[3.9, 4.1]s + 1} e^{-[19, 21]s}, \quad (27)$$

Now let us find the robust stability region of PI controllers for the SP control structure. Therefore, $\lambda = 1$ and $K_d = 0$. By using the steps presented in the Algorithm 1, one can compute the robust stability region of PI controllers as depicted in Fig. 2. As a verification, Lemma 3 is employed to check the stability of some random members of the characteristic function $\Delta(s)$. From Fig. 2, it is visible that the pair $(K_p, K_i) = (3, 1)$ has been located in the robust stable

region. In Fig. 3, the stability of two hundreds members of $\Delta(s)$ has been analyzed by Lemma 3. As seen from this figure, the chosen members are stable.

The works [25], [26] have failed to present an approach for the robust PI stabilization of the SP structures. Whereas, based on the results presented in this letter, a robust PI stabilization can be designed for the SP structures depicted in Fig. 1. Moreover, in order to evaluate the performance, the weighting function $M(s) = 1.2(1.9s + 0.03)/(s + 0.05)$ is taken. Consider two controllers $C_1(s) = 1.2 + 0.2/s$ and $C_2(s) = 1.96 + 0.64/s$. The function $F_S(\omega)$ has been plotted in Fig. 4. As seen from this figure, the inequality $F_S(\omega) < 0$ is only held for $C_1(s)$. Hence, the designer should select the controller $C_1(s)$. The step responses of the controllers $C_1(s)$ and $C_2(s)$ have been plotted in Fig. 5. From Fig. 5, It is visible that the controller $C_1(s)$ has better performance.

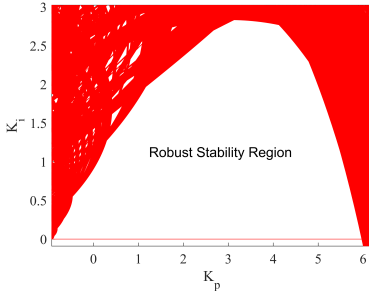


Fig. 2: The robust stability region of PI controllers.

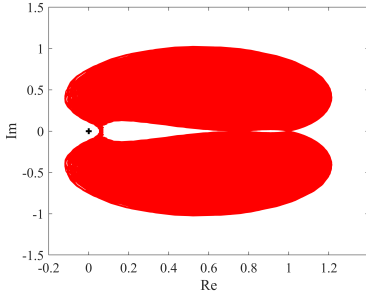


Fig. 3: The stability analysis of two hundreds members of $\Delta(s)$.

Example 2. Let us find the robust stability region of FOPID controllers for the SP structure with the plant in (27). We take $\lambda = 0.5, \mu = 0.6$ and $k_d = 0.1$. By performing the steps presented in Algorithm 1, the robust stability region of FOPID controllers can be obtained as Fig. 6. From this figure, it is clear that the pair $(K_p, K_i) = (2, 2)$ has been located in the robust stable region. The stability of two hundreds members of the system is checked by lemma 3 as shown in Fig. 7. From Fig. 7, it is clear that all random members of the SP scheme are stable.

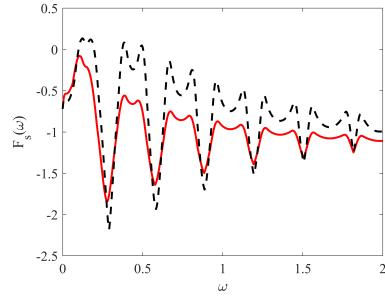


Fig. 4: $F_S(\omega)$ for $C_1(s)$ (solid line) and $C_2(s)$ (dashed line).

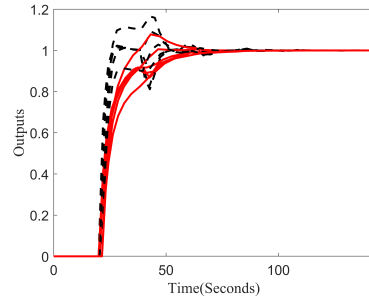


Fig. 5: The step responses corresponding to $C_1(s)$ (solid line) and $C_2(s)$ (dashed line).

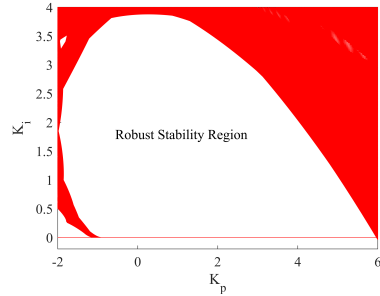


Fig. 6: The robust stability region of FOPID controllers.

V. CONCLUSION

This letter concentrates on computing the robust stability region of FOPID controllers for the Smith predictor structures. At first, the boundary of the value set of the characteristic function was determined in Theorem 1. Then, necessary and sufficient criteria were provided in Lemma 4. Moreover, by D-decomposition technique and the results presented in Lemma 4, an algorithm was proposed to design the robust stability region of FOPID controllers. Also, an auxiliary function was offered to evaluate the performance of the system. Moreover, two numerical examples were provided to evaluate the obtained results.

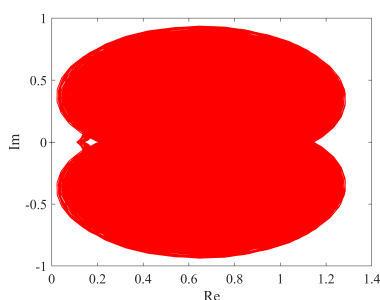


Fig. 7: The stability analysis of two hundreds members of the SP structure.

REFERENCES

- [1] Tan, KK and Lee, TH and Leu, FM, Predictive PI versus Smith control for dead-time compensation, *ISA Transactions*, vol.4, no.1, pp. 17–29, 2001.
- [2] Ghorbani, M and Tavakoli-Kakhki, M and Tepljakov, A and Petlenkov, E and Farnam, A and Crevecoeur, G, Robust Stability Analysis of Interval Fractional-Order Plants With Interval Time Delay and General Form of Fractional-Order Controllers, *IEEE Control Systems Letters*, vol.6, pp. 1268–1273, 2021.
- [3] Normey-Rico, JE and Camacho, EF, Control of dead-time processes, *Springer-Verlag*, vol. 462, 2007.
- [4] Tan, KK and Lee, TH and Leu, FM, Smith, Otto JM, *ISA Journal*, vol.6, pp. 28–33, 1959.
- [5] Normey-Rico, JE and Camacho, EF, Dead-time compensators: A survey, *Control engineering practice*, vol.16, no.4, pp. 407–428, 2008.
- [6] O'Dwyer, A, A reference guide to Smith predictor based methods for the compensation of dead-time processes, *IEE Irish Signals and Systems Conference 2005*, pp. 231–238, 2005.
- [7] Lee, TH and Wang, QG and Tan, KK, Robust Smith-predictor controller for uncertain delay systems, *AIChE Journal*, vol.42, no.4, pp. 1033–1040, 1996.
- [8] De Oliveira, V and Karimi, A, Robust Smith predictor design for time-delay systems with H_∞ performance, *IFAC Proceedings Volumes*, vol. 46, no.3, pp. 102–107, 2013.
- [9] Karan, S and Dey, C, Modified Smith predictor-based all-proportional-derivative control for second-order delay-dominated integrating processes, *Asia-Pacific Journal of Chemical Engineering*, vol. 16, no.2, pp. e2591, 2021.
- [10] Nakamura, Y and Goto, S and Wakui, S, Tuning methods of a Smith predictor for pneumatic active anti-vibration apparatuses, *Journal of Advanced Mechanical Design, Systems, and Manufacturing*, vol. 7, no.4, pp. 666–676, 2013.
- [11] Iampita, IM and Hisham, SB, Smith Predictor-based Controllers for Temperature Process with Time Delay, *2019 IEEE Student Conference on Research and Development (SCoReD)*, pp. 269–274, 2019.
- [12] Efe, M, Fractional order systems in industrial automation—A survey, *IEEE Transactions on Industrial Informatics*, vol. 7, no.4, pp. 582–591, 2011.
- [13] Ates, A and Alagoz, BB and Tepljakov, A and Petlenkov, E and Yeroglu, C and Kuznetsov, A and Sobolev, I, Fractional Order Model Identification of Receptor-Ligand Complexes Formation by Equivalent Electrical Circuit Modeling, *2019 International Artificial Intelligence and Data Processing Symposium (IDAP)*, pp. 1–4, 2019.
- [14] Ardjal, A and Mansouri, R and Bettayeb, M, Fractional sliding mode control of wind turbine for maximum power point tracking, *Transactions of the Institute of Measurement and Control*, vol. 41, no.2, pp. 447–457, 2019.
- [15] Abdelhamid, D and Bouden, T and Boulkroune, A, Design of fractional-order sliding mode controller (FSMC) for a class of fractional-order non-linear commensurate systems using a particle swarm optimization (PSO) algorithm, *Journal of control engineering and applied informatics*, vol. 16, no.3, pp. 46–55, 2014.
- [16] Monje, C A and Chen, YQ and Vinagre, BM and Xue, D and Feliu-Batlle, V, Fractional-order systems and controls: fundamentals and applications, *Springer Science & Business Media*, pp. 1033–1040, 2010.
- [17] Tepljakov, A and Alagoz, BB and Yeroglu, C and Gonzalez, EA and Hosseinnia, SH and Petlenkov, E and Ates, A and Cech, M, Towards industrialization of FOPID controllers: A survey on milestones of fractional-order control and pathways for future developments, *IEEE Access*, vol. 9, pp. 21016–21042, 2021.
- [18] Podlubny, I, Fractional-order systems and $PI^\lambda D^\mu$ -controllers, *Springer Science & Business Media*, vol. 44, no.1, pp. 208–214, 1999.
- [19] Bhamre, PK and Kadu, CB, Design of a smith predictor based fractional order PID controller for a coupled tank system, *2016 International Conference on Automatic Control and Dynamic Optimization Techniques (ICACDOT)*, pp. 705–708, 2016.
- [20] Azarmi, R and Sedigh, AK and Tavakoli-Kakhki, M and Fatehi, A, Design and implementation of Smith predictor based fractional order PID controller on MIMO flow-level plant, *2015 23rd Iranian Conference on Electrical Engineering*, pp. 858–863, 2015.
- [21] Özbek, NS and E, İlyas, An experimental comparative study of modified Smith Predictor based fractional order controller design strategies for a time delay process, *2017 4th International Conference on Electrical and Electronic Engineering (ICEEE)*, pp. 199–203, 2017.
- [22] Vu, TNL and Lee, M, Smith predictor based fractional-order PI control for time-delay processes, *Korean Journal of Chemical Engineering*, vol. 31, no.8, pp. 1321–1329, 2014.
- [23] Hamamci, SE, An algorithm for stabilization of fractional-order time delay systems using fractional-order PID controllers, *IEEE Transactions on Automatic Control*, vol. 52, no. 10, pp.1964–1969, 2007.
- [24] Chen, P and Luo, Y and Peng, Y and Chen, YQ, Optimal robust fractional order $PI^\lambda D^\mu$ controller synthesis for first order plus time delay systems, *ISA transactions*, vol. 114, pp. 136–149, 2021.
- [25] Deniz, FN and Tan, N and Hamamci, SE and Kaya, I, Stability region analysis in Smith predictor configurations using a PI controller, *Transactions of the Institute of Measurement and Control*, vol. 37, no. 5, pp. 606–614, 2015.
- [26] Deniz, FN and Tan, N, A model identification method for tuning of PID controller in a smith predictor structure, *IFAC-PapersOnLine*, vol. 49, no. 10, pp. 13–18, 2016.
- [27] Fu, M and Dasgupta, S and Blondel, V, Robust stability under a class of nonlinear parametric perturbations, *IEEE transactions on automatic control*, vol. 40, no. 2, pp. 213–223, 1995.
- [28] Moornani, KA and Haeri, M, On robust stability of LTI fractional-order delay systems of retarded and neutral type, *Automatica*, vol. 46, no. 2, pp. 362–368, 2010.
- [29] Moornani, KA and Haeri, M, On robust stability of linear time invariant fractional-order systems with real parametric uncertainties, *ISA transactions*, vol. 48, no. 4, pp. 484–490, 2009.
- [30] Busłowicz, M, Stability of linear continuous-time fractional order systems with delays of the retarded type, *Bulletin of the Polish Academy of Sciences: Technical Sciences*, vol. 56, no. 4, pp. 319–3243, 2008.
- [31] Levine, WS, The Control Handbook, *CRC press*, 2018.
- [32] Brown, JW and Churchill, RV, Complex variables and applications, *McGraw-Hill*, 2009.

Appendix 6

VI

M. Ghorbani, A. Tepljakov, and E. Petlenkov. Stabilizing region of fractional-order proportional integral derivative controllers for interval fractional-order plants. *Transactions of the Institute of Measurement and Control*, 45(3):546–556, 2023.

Stabilizing region of fractional-order proportional integral derivative controllers for interval fractional-order plants

Transactions of the Institute of
Measurement and Control
2023, Vol. 45(3) 546–556
© The Author(s) 2022
Article reuse guidelines:
sagepub.com/journals-permissions
DOI: 10.1177/01423312221117866
journals.sagepub.com/home/tim


Majid Ghorbani¹, Aleksei Tepljakov and Eduard Petlenkov

Abstract

This paper focuses on computing the stabilizing region of fractional-order proportional integral derivative (FOPID) controllers for interval fractional-order plants. In this study, first, a theorem is presented to investigate the robust stability of the given closed-loop system. Then, an algorithm is proposed to solve the problem of robustly stabilizing the interval fractional-order plant using FOPID controllers. Also, two auxiliary functions are proposed to achieve the control requirements on the disturbance rejection and the noise reduction. Finally, four numerical examples are presented to confirm the obtained results.

Keywords

Fractional-order controllers, interval fractional-order plants, stabilizing region, graphical tuning method, interval uncertainties

Introduction

Background

Nowadays, fractional-order proportional integral derivative (FOPID) controllers have attracted much attention from both an academic and industrial point of view (Idir et al., 2018; Monje et al., 2008; Zheng et al., 2021a) and (Tepljakov et al., 2021). Hence, many researchers have focused on the design of FOPID controllers. For example, in Tavakoli-Kakhki and Haeri (2011), a simple analytical method was proposed to design FOPID controllers. Moreover, a useful tuning method of FOPID controllers has been presented based on gain margin and phase margin in Tepljakov et al. (2015) and Dwivedi and Pandey (2021). Also, in Rezaei Estakhrouiyeh et al. (2018), an iterative feedback tuning algorithm has been employed to design an optimal FOPID controller. In Gad et al. (2017), a multi-objective genetic algorithm has been used for tuning the FOPID controllers. Furthermore, in Gao (2018), an analytical method has been proposed to determine whether or not a designed FOPID controller can robustly stabilize a closed-loop control system having one fractional-order term and interval uncertainties. In Ebrahimi and Asgari (2021), a method has been proposed to design robust FOPID controllers using Kharitonov's theorem and an auxiliary function.

Stability is one of the requirements for the closed-loop control systems. In this regard, some results on stability analysis of fractional-order systems can be found in Bonnet and Partington (2002), Busłowicz (2008), and Ghorbani and Tavakoli-Kakhki (2021a). However, the model parameters of

physical systems cannot be identified precisely and may contain uncertainties because of the tolerance values of elements, nonlinear effects, or environmental conditions in practice (Feliu-Batlle et al., 2021; Yeroglu and Tan, 2011). Therefore, the parametric uncertainties are unavoidable in the real systems (Ghorbani et al., 2019). Accordingly, robust stability analysis is another requirement of the control systems (Gao, 2019).

Robust stability of fractional-order systems can be checked based on the zero exclusion principle (Moornani and Haeri, 2010a). Regarding this principle, it is important to determine the exact shape of the value set of a characteristic function in the complex plane (Ghorbani et al., 2021; Moornani and Haeri, 2009). In Tan et al. (2009) and Moornani and Haeri (2010b), it has been shown that the value set of an interval fractional-order polynomial is a convex polygon in the complex plane. This feature of the value set of interval fractional-order polynomials helps to facilitate its robust stability analysis. By benefiting from the results presented in Tan et al. (2009) and Moornani and Haeri (2010b) and fractional-order controllers, the robust stability of an interval fractional-order plant subjected to the parameter uncertainties has been addressed in Gao (2015). Then, inspired by the results of the

Department of Computer Systems, Tallinn University of Technology, Estonia

Corresponding author:

Majid Ghorbani, Department of Computer Systems, Tallinn University of Technology, Tallinn 12618, Estonia.
Email: majid.ghorbani@taltech.ee

aforementioned works, in Ghorbani and Tavakoli-Kakhki (2021b), robust stability of interval-delayed fractional-order plants by a general form of linear fractional-order controllers has been investigated.

In this paper, we are particularly concerned with stabilizing the fractional-order closed-loop systems consisting of interval fractional-order plants and FOPID controllers. This problem has been treated by different strategies so far. For example, in Dulf (2019), George and Kamath (2020), the flat-phase specification has been employed to improve the robustness of the closed-loop control system. Also, in Gao et al. (2017), the σ -stability was used to enhance the robustness of fractional-order systems by FOPI controllers. Moreover, in Zheng et al. (2021), gain margin and phase margin have been used to design fractional-order controllers and to improve the robustness.

Calculation of the stabilizing region of fractional-order controllers has attracted much attention, recently. In Luo and Chen (2011), Lee and Watkins (2012), Luo and Chen (2012), and Chen et al. (2021), some graphical tuning methods have been proposed to calculate the stabilizing region of FOPID and FOPI controllers. In Hamamci (2007) and (2008), an algorithm has been presented for the stabilization of fractional-order systems by FOPID controllers. Also, computation of the stabilizing region of FOPID controllers has some advantages. For instance, a set of stabilizing FOPID controllers, instead of just one, is proposed for the control system and this provides a more flexible choice of controller parameters (Hamamci, 2007, 2008; Zheng et al., 2014).

Motivations and contributions

In Liang et al. (2013), a theorem and an algorithm have been presented to calculate the stabilizing region of an interval fractional-order plant. As shown in Example 1 of this study, the results of Liang et al. (2013) turn out to be wrong in general. However, in Zheng et al. (2014), a graphical method has been presented to calculate the stabilizing region of OPID controllers. However, the vertices and the exposed edges used in Zheng et al. (2014) are based on the method presented in Tan et al. (2009). As shown in Moornani and Haeri (2010b), the vertices proposed for the value set of an interval fractional-order polynomial in Tan et al. (2009) are not the consecutive vertices of the polygon which leads to additional computational cost. This implies that the procedure proposed in Zheng et al. (2014) leads to the redundant computational cost. However, the aforementioned work is also limited to the systems of commensurate orders. In summary, based on the above explanations, the following control problems are formulated as the main challenges for stabilization of interval fractional-order systems by FOPID controllers.

Problem 1: Calculation of the stabilizing region of FOPID controllers for interval fractional-order systems of commensurate and incommensurate orders.

Problem 2: In addition to design a robust FOPID stabilization, it is necessary to improve the performance specifications for all plants of the uncertain system. In other words, the control requirements on the noise reduction

and the disturbance rejection should be achieved for interval fractional-order systems by FOPID controllers. However, due to the uncertain plant, it is difficult to obtain the uncertainty bounds of the complementary sensitivity function and the sensitivity function in the presence of uncertainties.

Hence, the above-mentioned problems motivate the authors of this paper to give a reliable method for improving the computational efficiency of calculating the stabilizing region of FOPID controllers.

The main contributions and innovations of this study are summarized as follows:

- An algorithm is proposed to solve the problem of robustly stabilizing interval fractional-order plants using FOPID controllers.
- Unlike the existing procedures, the results of this paper reduce the computational cost.
- Two auxiliary functions are proposed to achieve the control requirements on the disturbance rejection and the noise reduction. It is notable that the sensitivity function and the complementary sensitivity function characterize the important properties of a feedback system, such as reference tracking and disturbance rejection and noise reduction (Levine, 2018). Hence, by paying attention to the roles of the sensitivity functions and the complementary sensitivity function in the system response, two auxiliary functions are proposed to evaluate the control requirements on the disturbance rejection and the noise reduction.

Organization

The rest of this paper is organized as follows. In the next section, a preliminary review is presented. In section “Main results,” two theorems and an algorithm are presented to calculate the stabilizing region of FOPID controllers. In section “Illustrative examples,” numerical examples are provided to evaluate the theoretically obtained results. Finally, section “Conclusion” gives some concluding remarks.

Preliminaries. In this section, the mathematical notation used in this paper is declared, and the related background is revisited.

Notations. Define sets $\mathbb{R}^{\geq 0} \triangleq \{x \in \mathbb{R} | x \geq 0\}$, $\mathbb{N}^{\leq n} \triangleq \{x \in \mathbb{N} | x \leq n\}$, $\mathbb{Z}_{\geq m}^{\leq n} \triangleq \{x \in \mathbb{Z} | m \leq x \leq n\}$, and $\mathbb{R}^n \triangleq \{(x_1, \dots, x_n) | x_1, \dots, x_n \in \mathbb{R}\}$. Also, consider $\text{floor}(x)$ the largest integer less than or equal to $x \in \mathbb{R}$ and $\text{frac}(x) \triangleq x - \text{floor}(x)$. Define the edge $e(x_1(j\omega), x_2(j\omega)) \triangleq \eta x_1(j\omega) + (1 - \eta)x_2(j\omega)$, $\eta \in [0, 1]$. Also, $A \cup B \triangleq \{x | x \in A \text{ or } x \in B\}$ for any two sets A, B and $n(B)$ shows the number of distinct members of the set B .

Consider the transfer function of an interval fractional-order plant given as the following expression

$$P(s, \mathbf{b}, \mathbf{a}) = \frac{N(s, \mathbf{b})}{D(s, \mathbf{a})} = \frac{\sum_{i_1=0}^m b_{i_1} s^{\beta_{i_1}}}{\sum_{i_2=0}^n a_{i_2} s^{\alpha_{i_2}}} \quad (1)$$

where s is the Laplace operator, $m \in \mathbb{Z}^{\geq 0}$, $n \in \mathbb{Z}^{\geq 1}$, $\beta_m > \beta_{m-1} > \dots > \beta_1 > \beta_0 = 0$, and $\alpha_n > \alpha_{n-1} > \dots > \alpha_1 > \alpha_0 = 0$ are arbitrary real numbers. Also, $\mathbf{b} = [b_0, b_1, \dots, b_m]^T$ and $\mathbf{a} = [a_0, a_1, \dots, a_n]^T$ are the coefficients vectors and they belong to the uncertainty bounding sets

$$\begin{aligned} \mathbf{b} \in \mathbf{B} &= \{\mathbf{b} \in \mathbb{R}^{m+1} | b_{i_1} \in [b_{i_1}^-, b_{i_1}^+], b_m, b_0 \neq 0, i_1 \in \mathbb{Z}_{\geq 0}^m\} \\ \mathbf{a} \in \mathbf{A} &= \{\mathbf{a} \in \mathbb{R}^{n+1} | a_{i_2} \in [a_{i_2}^-, a_{i_2}^+], a_n \neq 0, i_2 \in \mathbb{Z}_{\geq 1}^n\} \end{aligned} \quad (2)$$

where $[b_{i_1}^-, b_{i_1}^+]$ and $[a_{i_2}^-, a_{i_2}^+]$ are specified intervals. In this work, we consider the parallel form of the FOPID controller expressed by the transfer function

$$C(s) = \frac{k_p s^\lambda + k_i + k_d s^{\mu+\lambda}}{s^\lambda}, 0 < \lambda, \mu < 2, \alpha_n > \mu + \beta_m \quad (3)$$

Furthermore, in this study, it is considered that the fractional-order polynomial (equation (4)) represents the characteristic function of the negative unity feedback control system

$$\Delta(s) = s^\lambda D(s, \mathbf{a}) + (k_p s^\lambda + k_i + k_d s^{\mu+\lambda}) N(s, \mathbf{b}) \quad (4)$$

Remark 1. Some examples of physical systems identified as transfer function $P(s)$ in equation (1) are a continuous stirred-tank reactor (Matusu et al., 2020; Závacká and Bakošová, 2011), servo-motor (Tu and Ho, 2011), and single-machine infinite bus (Simfukwe and Pal, 2012).

Remark 2. Moornani and Haeri (2010b) shows that the value sets of $D(s, \mathbf{a})$ and $N(s, \mathbf{b})$ are two parpolygons in the complex plane for $s = j\omega$, $\omega > 0$. The vertex polynomials corresponding to $D(j\omega, \mathbf{a})$ are determined for $\omega \geq 0$ using **Procedure 1** (for more details, see Moornani and Haeri (2010b)).

Procedure 1 (Moornani and Haeri, 2010b):

Define $H_0 \triangleq \{i_2 \in \mathbb{Z}_{\geq 0}^n | a_{i_2}^- < a_{i_2}^+\}$. The value set $D(j\omega, \mathbf{a})$ is determined for $\omega \in \mathbb{R}_{\geq 0}$ as follows

1. For $H_0 = \emptyset$ and $\omega \geq 0$, one has $D(j\omega, \mathbf{a}) = D_0(j\omega)$, where

$$D_0(\omega) \triangleq \sum_{i_2=0}^n a_{i_2}^- s^{\alpha_{i_2}} \quad (5)$$

2. For $H_0 \neq \emptyset$,
3. If $\omega = 0$, then $D(j\omega, \mathbf{a}) = D(j0, \mathbf{a}) = [a_0^-, a_0^+]$.
4. If $\omega > 0$, then define $B_0 \triangleq \{\text{frac}(0.5\alpha_{i_2}) | i_2 \in H_0\}$ and $m_D \triangleq n(B_0)$. Consider also $\gamma_1, \dots, \gamma_{m_D-1}, \gamma_{m_D}$ as all the distinct members of B_0 sorted as $0 \leq \gamma_1 < \dots < \gamma_{m_D-1} < \gamma_{m_D} < 1$. Then, define the following sets

$$\begin{aligned} H_r' &\triangleq \{i_2 \in H_0 | \text{floor}(0.5\alpha_{i_2}) \text{ is an odd number and } \text{frac}(0.5\alpha_{i_2}) = \gamma_r\} \\ H_r &\triangleq \{i_2 \in H_0 | \text{floor}(0.5\alpha_{i_2}) \text{ is an even number and } \text{frac}(0.5\alpha_{i_2}) = \gamma_r\} \\ r &= 1, 2, \dots, m_D \end{aligned} \quad (6)$$

Let $a^- \triangleq [a_0^-, a_1^-, \dots, a_n^-]^T$ and $a^+ \triangleq [a_0^+, a_1^+, \dots, a_n^+]^T$. The vectors $q^1, q^2, \dots, q^{2m_D}$ are defined as follows

$$\begin{aligned} a^k &\triangleq [a_0^k, a_1^k, \dots, a_n^k]^T, a^{m_D+k} \triangleq [a_0^{m_D+k}, a_1^{m_D+k}, \dots, a_n^{m_D+k}]^T \\ &= a^+ + a^- - a^k, \quad k = 1, \dots, m_D \end{aligned} \quad (7)$$

where for $i_2 = 0, 1, \dots, n$ and $k = 1, \dots, m_D$, it can be written that

$$a_{i_2}^k \triangleq \begin{cases} a_{i_2}^+, & \text{for } i_2 \in \left(\bigcup_{i=1}^{k-1} H_i\right) \cup \left(\bigcup_{i=k}^{m_D} H_i'\right), \\ a_{i_2}^-, & \text{otherwise.} \end{cases} \quad (8)$$

and

$$a_{i_2}^{m_D+k} \triangleq a_{i_2}^+ + a_{i_2}^- - a_{i_2}^k \quad (9)$$

Hence, the consecutive vertices $V_{r_2}^-(j\omega)$ ($r_2 = 1, 2, \dots, 2m_D$) are calculated using

$$\begin{aligned} V_k^-(j\omega) &\triangleq D(j\omega, a^k) \\ V_{m_D+k}^-(j\omega) &\triangleq D(j\omega, a^{m_D+k}) = D(j\omega, a^+ + a^-) - V_k^-(j\omega), \\ k &= 1, 2, \dots, m_D \end{aligned} \quad (10)$$

Accordingly, the vertex polynomials corresponding to $N(j\omega, \mathbf{b})$ and $D(j\omega, \mathbf{a})$ are, respectively, considered as $V_{r_1}^+(\omega)$ ($r_1 = 1, 2, \dots, 2m_N$) and $V_{r_2}^-(\omega)$ ($r_2 = 1, 2, \dots, 2m_D$) and they can be calculated by **Procedure 1**.

Remark 3. Consider a certain polynomial of $\Delta(s)$ in equation (4) as $\hat{\Delta}(s)$ in equation (11)

$$\hat{\Delta}(s) = s^\lambda \sum_{i_2=0}^n \hat{a}_{i_2} s^{\alpha_{i_2}} + (k_p s^\lambda + k_i + k_d s^{\mu+\lambda}) \sum_{i_1=0}^m \hat{b}_{i_1} s^{\beta_{i_1}} \quad (11)$$

Then, the boundaries of the stabilizing region $\hat{\Delta}(s)$ in equation (11) are specified by Infinite Root Boundary (IRB), Real Root Boundary (RRB), and Complex Root Boundary (CRB) which can be determined using the algorithm in Hamamci (2007, 2008). In summary, the mentioned boundaries are stated based on the procedure proposed in Hamamci (2008) as follows

- **RRB:** $\hat{\Delta}(0) = k_i \hat{b}_0$. If $k_i \hat{b}_0 \neq 0$, then $k_i = 0$. Otherwise, the boundary does not exist.
- **IRB:** $\hat{\Delta}(\infty) = 0$

$$\begin{cases} k_d = 0 & \text{for } \alpha_n = \beta_m \text{ or } (\alpha_n > \beta_m \text{ and } \mu > \alpha_n - \beta_\mu), \\ k_d = \frac{-a_0}{b_0} & \text{for } (\alpha_n > \beta_m \text{ and } \mu = \alpha_n - \beta_\mu), \\ \text{none} & \text{for } (\alpha_n > \beta_m \text{ and } \mu < \alpha_n - \beta_\mu) \end{cases} \quad (12)$$

- **CRB:** By partitioning $\hat{\Delta}(j\omega) = 0$ into its real and imaginary parts and equating them to zero, we obtain

$$\begin{cases} \text{Real}(\hat{\Delta}(j\omega)) = 0 \Rightarrow B_1 k_p + B_3 k_i = -(A_1 + k_d B_5), \\ \text{Imag}(\hat{\Delta}(j\omega)) = 0 \Rightarrow B_2 k_p + B_4 k_i = -(A_2 + k_d B_6) \end{cases} \quad (13)$$

Finally, by solving the equation (13), the k_p and k_i parameters in terms of k_d , λ , and μ are obtained as follows

$$\begin{aligned} k_p &= (A_2(\omega)B_1(\omega) - A_1(\omega)B_2(\omega) + k_d(B_1(\omega)B_6(\omega) - B_2(\omega)B_5(\omega))) / \\ &\quad (B_2(\omega)B_3(\omega) - B_1(\omega)B_4(\omega)) \\ k_i &= (A_1(\omega)B_4(\omega) - A_2(\omega)B_3(\omega) + k_d(B_4(\omega)B_5(\omega) - B_3(\omega)B_6(\omega))) / \\ &\quad (B_2(\omega)B_3(\omega) - B_1(\omega)B_4(\omega)) \end{aligned} \quad (14)$$

in which

$$\begin{cases} A_1(\omega) = \sum_{i_2=0}^n \hat{a}_{i_2} \omega^{\lambda + \alpha_{i_2}} \cos\left(\frac{\pi(\alpha_{i_2} + \lambda)}{2}\right), \\ A_2(\omega) = \sum_{i_2=0}^n \hat{a}_{i_2} \omega^{\lambda + \alpha_{i_2}} \sin\left(\frac{\pi(\alpha_{i_2} + \lambda)}{2}\right), \\ B_1(\omega) = \sum_{i_1=0}^m \hat{b}_{i_1} \omega^{\beta_{i_1}} \cos\left(\frac{\pi\beta_{i_1}}{2}\right), \\ B_2(\omega) = \sum_{i_1=0}^m \hat{b}_{i_1} \omega^{\beta_{i_1}} \sin\left(\frac{\pi\beta_{i_1}}{2}\right), \\ B_3(\omega) = \sum_{i_1=0}^m \hat{b}_{i_1} \omega^{\beta_{i_1} + \lambda} \cos\left(\frac{\pi(\beta_{i_1} + \lambda)}{2}\right), \\ B_4(\omega) = \sum_{i_1=0}^m \hat{b}_{i_1} \omega^{\beta_{i_1} + \lambda} \sin\left(\frac{\pi(\beta_{i_1} + \lambda)}{2}\right), \\ B_5(\omega) = \sum_{i_1=0}^m \hat{b}_{i_1} \omega^{\beta_{i_1} + \lambda + \mu} \cos\left(\frac{\pi(\beta_{i_1} + \lambda + \mu)}{2}\right), \\ B_6(\omega) = \sum_{i_1=0}^m \hat{b}_{i_1} \omega^{\beta_{i_1} + \lambda + \mu} \sin\left(\frac{\pi(\beta_{i_1} + \lambda + \mu)}{2}\right) \end{cases} \quad (15)$$

Accordingly, the stabilizing region can be determined by checking one arbitrary test point inside each region (Hamamci, 2008).

Regarding the above analysis, the problem is to compute a set of FOPID controllers stabilizing the interval fractional-order plant of $P(s, \mathbf{b}, \mathbf{a})$ in equation (1).

Main results

This section is divided into three subsections. In subsection ‘‘Stabilizing region of FOPID controllers,’’ a theorem is presented to analyze the robust stability of the characteristic function (equation (4)). Then, an algorithm is proposed to calculate the stabilizing region of FOPID controllers for the interval fractional-order plant (equation (1)). Also, subsections ‘‘Good output disturbance rejection’’ and ‘‘High-frequency noise rejection’’ are devoted to the evaluation of the control requirements of disturbance rejection and noise reduction characteristics of the control system.

Stabilizing region of FOPID controllers

Theorem 1. *The characteristic function (equation (4)) is robust stable if and only if, the characteristic functions $\Delta_{r_1}^D(s)$ ($r_1 = 1, 2, \dots, 2m_N$) in equation (16) and $\Delta_{r_2}^N(s)$ ($r_2 = 1, 2, \dots, 2m_D$) in equation (17) are also robust stable*

$$\Delta_{r_1}^D(s) = s^\lambda D(s, \mathbf{a}) + (k_p s^\lambda + k_i + k_d s^{\mu + \lambda}) V_{r_1}^+(\omega), \quad (16)$$

$(r_1 = 1, \dots, 2m_N)$

$$\Delta_{r_2}^N(s) = s^\lambda V_{r_2}^-(\omega) + (k_p s^\lambda + k_i + k_d s^{\mu + \lambda}) N(s, \mathbf{b}), \quad (17)$$

$(r_2 = 1, \dots, 2m_D)$

Proof. Proof of the sufficiency: According to **Procedure 1**, the value sets of $s^\lambda D(s, \mathbf{a})$ and $(k_p s^\lambda + k_i + k_d s^{\mu + \lambda}) N(s, \mathbf{b})$ are two parpolygons in the complex plane for $s = j\omega$. If the characteristic functions $\Delta_{r_1}^D(s)$ ($r_1 = 1, 2, \dots, 2m_N$) in equation (16) are robust stable, then one can simply deduce that

$$-(k_p s^\lambda + k_i + k_d s^{\mu + \lambda}) V_{r_1}^+(\omega) \notin s^\lambda D(s, \mathbf{a}), \quad (18)$$

$(r_1 = 1, 2, \dots, 2m_N) \text{ and } s = j\omega$

Likewise, from equation (17), one can infer that

$$-s^\lambda V_{r_2}^-(\omega) \notin (k_p s^\lambda + k_i + k_d s^{\mu + \lambda}) N(s, \mathbf{b}), \quad (19)$$

$(r_2 = 1, 2, \dots, 2m_D) \text{ and } s = j\omega$

From equations (18) and (19), it is apparent that two parpolygons $s^\lambda D(j\omega, \mathbf{a})$ and $(k_p(j\omega)^\lambda + k_i + k_d(j\omega)^{\mu + \lambda}) N(j\omega, \mathbf{b})$ do not have any overlap in the complex plane and this implies that $0 \notin \Delta(j\omega)$.

Proof of the Necessity: Since the characteristic function (equation (4)) is robust stable, based on the zero exclusion principle $0 \notin \Delta(j\omega)$. Using the zero exclusion principle, the origin is located outside the value set of $\Delta(j\omega)$. Therefore, from equations (18) and (19), the robust stability of $\Delta_{r_1}^D(s)$ ($r_1 = 1, 2, \dots, 2m_N$) in equation (16) and $\Delta_{r_2}^N(s)$ ($r_2 = 1, 2, \dots, 2m_D$) in equation (17) is concluded.

Remark 4. *Theorem 1* reveals that the robust stability analysis of the characteristic function $\Delta(s)$ in equation (4) is equivalent to the robust stability analysis of the characteristic functions $\Delta_{r_1}^D(s)$ ($r_1 = 1, 2, \dots, 2m_N$) in equation (16) and $\Delta_{r_2}^N(s)$ ($r_2 = 1, 2, \dots, 2m_D$) in equation (17). Hence, the only issue lies in the determination of the boundaries (i.e. RRB, IRB, and CRB) of the characteristic functions $\Delta_{r_1}^D(s)$ ($r_1 = 1, 2, \dots, 2m_N$) in equation (16) and $\Delta_{r_2}^N(s)$ ($r_2 = 1, 2, \dots, 2m_D$) in equation (17). To do this, the calculation of the stabilizing region is presented in **Algorithm 1**.

Algorithm 1:

Step 1: Obtain the vertices $V_{r_1}^+(\omega)$ ($r_1 = 1, 2, \dots, 2m_N$) and $V_{r_2}^-(\omega)$ ($r_2 = 1, 2, \dots, 2m_D$) using **Procedure 1**.

Step 2: Obtain RRB, IRB, and CRB and the stability regions by sweeping over $\eta \in [0, 1]$ for $\Delta_{r_1}^D(s)$ in equation (20)

$$\begin{aligned} \Delta_{r_1}^D(s) &= s^\lambda (e(V_{r_2}^-(\omega), V_{r_2+1}^-(\omega))) + V_{r_1}^+(\omega) \\ &\quad (k_p s^\lambda + k_i + k_d s^{\mu + \lambda}), r_1 = 1, 2, \dots, 2m_N, \\ r_2 &= 1, 2, \dots, 2m_D, V_{2m_D+1}^-(\omega) = V_1^-(\omega) \end{aligned} \quad (20)$$

Step 3: Obtain RRB, IRB, and CRB and the stability regions by sweeping over $\eta \in [0, 1]$ for $\Delta_{r_2}^N(s)$ in equation (21):

$$\begin{aligned} \Delta_{r_2}^N(s) &= s^\lambda V_{r_2}^-(\omega) + (k_p s^\lambda + k_i + k_d s^{\mu + \lambda}) \\ &\quad (e(V_{r_1}^+(\omega), V_{r_1+1}^+(\omega))), r_1 = 1, 2, \dots, 2m_N, \\ r_2 &= 1, 2, \dots, 2m_D, V_{2m_N+1}^+(\omega) = V_1^+(\omega) \end{aligned} \quad (21)$$

Step 4: The final stabilizing region for the interval fractional-order plant is the intersection of all the computed stable regions in Step 2 and Step 3.

Now, in the next theorem, an auxiliary function is presented to determine whether or not a designed controller can robustly stabilize the closed-loop system.

Theorem 2. Assume that a certain characteristic function of $\Delta(s)$ in equation (4) as $\Delta_0(s)$ is stable. Then, the closed-loop system is robust stable if and only if the inequality $\Lambda(\omega) < 0$ holds for $\omega \geq 0$, where

$$\Lambda(\omega) \triangleq \max\{\Lambda_1(\omega), \Lambda_2(\omega)\} \quad (22)$$

in which

$$\begin{aligned} \Lambda_1(\omega) &\triangleq \max\{\Lambda_{r_1, r_2}^D(\omega) | r_1 \in \{1, \dots, 2m_N\}, r_2 \in \{1, \dots, 2m_D\}\} \\ \Lambda_{r_1, r_2}^D(\omega) &\triangleq |(j\omega)^\lambda (V_{r_2}^-(\omega) - V_{r_2+1}^-(\omega)) - \\ &|(j\omega)^\lambda V_{r_2}^-(\omega) + (k_p(j\omega)^\lambda + k_i + k_d(j\omega)^{\mu+\lambda}) V_{r_1}^+(\omega) - \\ &|(j\omega)^\lambda V_{r_2+1}^-(\omega) + (k_p(j\omega)^\lambda + k_i + k_d(j\omega)^{\mu+\lambda}) V_{r_1}^+(\omega)| \end{aligned} \quad (23)$$

$$\begin{aligned} \Lambda_2(\omega) &\triangleq \max\{\Lambda_{r_1, r_2}^N(\omega) | r_1 \in \{1, \dots, 2m_N\}, r_2 \in \{1, \dots, 2m_D\}\} \\ \Lambda_{r_1, r_2}^N(\omega) &\triangleq |(k_p(j\omega)^\lambda + k_i + k_d(j\omega)^{\mu+\lambda}) (V_{r_1}^+(\omega) - V_{r_1+1}^+(\omega)) - \\ &|(j\omega)^\lambda V_{r_2}^-(\omega) + (k_p(j\omega)^\lambda + k_i + k_d(j\omega)^{\mu+\lambda}) V_{r_1}^+(\omega) - \\ &|(j\omega)^\lambda V_{r_2}^-(\omega) + (k_p(j\omega)^\lambda + k_i + k_d(j\omega)^{\mu+\lambda}) V_{r_1+1}^+(\omega)| \end{aligned} \quad (24)$$

Proof. Based on **Procedure 1**, it is apparent that the value set of $\Delta_{r_1}^D(s)$ in equation (16) and $\Delta_{r_2}^N(s)$ in equation (17) are two parpolygons in the complex plane. Also, if the triangle inequality is satisfied for each two consecutive vertices of $\Delta_{r_1}^D(s)$ in equation (16), then one can conclude that $0 \notin \Delta_{r_1}^D(j\omega)$ and this implies that the inequality $\Lambda_1(\omega) < 0$ is satisfied. Likewise, satisfying the inequality $\Lambda_2(\omega) < 0$ leads to $0 \notin \Delta_{r_2}^N(j\omega)$ in equation (17). Hence, if the inequality $\Lambda(\omega) < 0$ in equation (22) is satisfied, then based on **Theorem 1** and the zero exclusion principle, the proof is completed.

Good output disturbance rejection

To improve the output disturbance rejection, the following constraint on the sensitivity function $S(j\omega)$ should be satisfied (Levine, 2018)

$$|S(j\omega)| = \left| \frac{1}{1 + C(j\omega)P(j\omega)} \right| < |M_s(j\omega)| \quad (25)$$

where $M_s(j\omega) = N_s(j\omega)/D_s(j\omega)$ denotes the weighting function, which describes the frequency characteristic of the performance specifications.

Based on **Theorem 1** and equation (25), a robust FOPID controller should satisfy the following inequalities

$$\left| \frac{1}{1 + \frac{(k_p s^\lambda + k_i + k_d s^{\mu+\lambda}) V_{r_1}^+(\omega)}{s^\lambda D(s, \mathbf{a})}} \right| < |M_s(s)|, \quad (r_1 = 1, 2, \dots, 2m_N), \quad s = j\omega \quad (26)$$

$$\left| \frac{1}{1 + \frac{(k_p s^\lambda + k_i + k_d s^{\mu+\lambda}) N(s, \mathbf{b})}{s^\lambda V_{r_2}^-(\omega)}} \right| < |M_s(s)|, \quad (r_2 = 1, 2, \dots, 2m_D), s = j\omega \quad (27)$$

From equations (26) and (27), and the maximum modulus theorem (Brown and Churchill, 2009), the following inequality should be satisfied

$$\Lambda_S(\omega) \triangleq \max_{r=1,2} \Lambda_r^S(\omega) < 0 \quad (28)$$

where

$$\begin{cases} \Lambda_1^S(\omega) \triangleq \max_{i=1, \dots, 2m_N} \Lambda_i^D(\omega), \\ \Lambda_i^D(\omega) \triangleq \max_{e_i^D \in P_E^D} |e_i^D| - |M_s(j\omega)|, \\ l^D = 1, 2, \dots, 2m_D, \\ P_E^D \triangleq \{e_1^D, e_2^D, \dots, e_{2m_D}^D\}, \\ e_1^D \triangleq \frac{1}{1 + \frac{(k_p s^\lambda + k_i + k_d s^{\mu+\lambda}) V_{r_1}^+(\omega)}{s^\lambda (\alpha(V_{r_1}^-(\omega), V_{r_2}^-(\omega)))}}, \\ e_2^D \triangleq \frac{1}{1 + \frac{(k_p s^\lambda + k_i + k_d s^{\mu+\lambda}) V_{r_1}^+(\omega)}{s^\lambda (\alpha(V_{r_2}^-(\omega), V_{r_3}^-(\omega)))}}, \\ \vdots \\ e_{2m_D}^D \triangleq \frac{1}{1 + \frac{(k_p s^\lambda + k_i + k_d s^{\mu+\lambda}) V_{r_1}^+(\omega)}{s^\lambda (\alpha(V_{2m_D}^-(\omega), V_{r_1}^-(\omega)))}}, \\ s = j\omega \end{cases} \quad (29)$$

$$\begin{cases} \Lambda_2^S(\omega) \triangleq \max_{i=1, \dots, 2m_D} \Lambda_i^N(\omega), \\ \Lambda_i^N(\omega) \triangleq \max_{e_i^N \in P_E^N} |e_i^N| - |M_s(j\omega)|, \\ l^N = 1, 2, \dots, 2m_N, \\ P_E^N \triangleq \{e_1^N, e_2^N, \dots, e_{2m_N}^N\}, \\ e_1^N \triangleq \frac{1}{1 + \frac{(k_p s^\lambda + k_i + k_d s^{\mu+\lambda}) \alpha(V_{r_1}^-(\omega), V_{r_2}^-(\omega))}{s^\lambda V_{r_1}^-(\omega)}}, \\ e_2^N \triangleq \frac{1}{1 + \frac{(k_p s^\lambda + k_i + k_d s^{\mu+\lambda}) \alpha(V_{r_2}^-(\omega), V_{r_3}^-(\omega))}{s^\lambda V_{r_1}^-(\omega)}}, \\ \vdots \\ e_{2m_N}^N \triangleq \frac{1}{1 + \frac{(k_p s^\lambda + k_i + k_d s^{\mu+\lambda}) \alpha(V_{r_1}^-(\omega), V_{r_1}^-(\omega))}{s^\lambda V_{r_1}^-(\omega)}}, \\ s = j\omega \end{cases} \quad (30)$$

Remark 5. Assume that a robust FOPID controller is designed by **Algorithm 1**. Then, the designed controller should satisfy the inequality $\Lambda_S(\omega) < 0$ in equation (28) to improve the output disturbance rejection. Note that some useful guidelines can be given by Skogestad and Postlethwaite (2007); Levine (2018) for the selection of the weighting function $M_s(j\omega)$.

High-frequency noise rejection

To satisfy high-frequency noise rejection, the following constraint on the complementary sensitivity function $T(j\omega)$ should be fulfilled

$$|T(j\omega)| = \left| \frac{C(j\omega)P(j\omega)}{1 + C(j\omega)P(j\omega)} \right| < |M_T(j\omega)| \quad (31)$$

where $M_T(j\omega) = N_T(j\omega)/D_T(j\omega)$ denotes the frequency characteristics of the noise signal (Levine, 2018).

Using **Theorem 1** and equation (31), a robust FOPID controller should also satisfy the inequality $\Lambda_T(\omega) < 0$ in equation (32)

$$\Lambda_T(\omega) \triangleq \max_{r=1,2} \Lambda_r^T(\omega) < 0 \quad (32)$$

where

$$\begin{cases} \Lambda_1^T(\omega) \triangleq \max_{i=1, \dots, 2m_N} \hat{\Lambda}_i^D(\omega), \\ \hat{\Lambda}_i^D(\omega) \triangleq \max_{\hat{e}_{iD}^D \in \hat{P}_E^D} |\hat{e}_{iD}^D| - |M_T(j\omega)|, \\ l^D = 1, 2, \dots, 2m_D, \\ \hat{P}_E^D \triangleq \{\hat{e}_1^D, \hat{e}_2^D, \dots, \hat{e}_{2m_D}^D\}, \\ \hat{e}_1^D \triangleq \frac{(k_p s^\lambda + k_i + k_d s^{\mu+\lambda}) V_1^+(\omega)}{s^\lambda (e(V_1^-(\omega), V_2^-(\omega))) + (k_p s^\lambda + k_i + k_d s^{\mu+\lambda}) V_1^+(\omega)}, \\ \hat{e}_2^D \triangleq \frac{(k_p s^\lambda + k_i + k_d s^{\mu+\lambda}) V_1^+(\omega)}{s^\lambda (e(V_2^-(\omega), V_3^-(\omega))) + (k_p s^\lambda + k_i + k_d s^{\mu+\lambda}) V_1^+(\omega)}, \\ \vdots \\ \hat{e}_{2m_D}^D \triangleq \frac{(k_p s^\lambda + k_i + k_d s^{\mu+\lambda}) V_1^+(\omega)}{s^\lambda (e(V_1^-(\omega), V_{2m_D}^-(\omega))) + (k_p s^\lambda + k_i + k_d s^{\mu+\lambda}) V_1^+(\omega)}, \\ s = j\omega \end{cases} \quad (33)$$

$$\begin{cases} \Lambda_2^T(\omega) \triangleq \max_{i=1, \dots, 2m_N} \hat{\Lambda}_i^N(\omega), \\ \hat{\Lambda}_i^N(\omega) \triangleq \max_{\hat{e}_{iN}^N \in \hat{P}_E^N} |\hat{e}_{iN}^N| - |M_T(j\omega)|, \\ l^N = 1, 2, \dots, 2m_N, \\ \hat{P}_E^N \triangleq \{\hat{e}_1^N, \hat{e}_2^N, \dots, \hat{e}_{2m_N}^N\}, \\ \hat{e}_1^N \triangleq \frac{(k_p s^\lambda + k_i + k_d s^{\mu+\lambda}) e(V_1^+(\omega), V_2^+(\omega))}{s^\lambda V_1^-(\omega) + (k_p s^\lambda + k_i + k_d s^{\mu+\lambda}) e(V_1^+(\omega), V_2^+(\omega))}, \\ \hat{e}_2^N \triangleq \frac{(k_p s^\lambda + k_i + k_d s^{\mu+\lambda}) e(V_2^+(\omega), V_3^+(\omega))}{s^\lambda V_1^-(\omega) + (k_p s^\lambda + k_i + k_d s^{\mu+\lambda}) e(V_2^+(\omega), V_3^+(\omega))}, \\ \vdots \\ \hat{e}_{2m_N}^N \triangleq \frac{(k_p s^\lambda + k_i + k_d s^{\mu+\lambda}) e(V_{2m_N}^+(\omega), V_1^+(\omega))}{s^\lambda V_1^-(\omega) + (k_p s^\lambda + k_i + k_d s^{\mu+\lambda}) e(V_{2m_N}^+(\omega), V_1^+(\omega))}, \\ s = j\omega \end{cases} \quad (34)$$

Remark 6. The designer can design a robust fractional-order controller using **Algorithm 1**. Besides, the designed controller should satisfy the inequalities $\Lambda_S(\omega) < 0$ in equation (28) and $\Lambda_T(\omega) < 0$ in equation (32) to improve the control requirements on the disturbance rejection and the noise reduction.

Remark 7. It is apparent that **Theorem 1**, **Algorithm 1**, the inequalities $\Lambda_S(\omega) < 0$ in equation (28) and $\Lambda_T(\omega) < 0$ in equation (32) can be employed for FOPID controllers (see **Example 1**).

Illustrative examples

In this section, three numerical examples are given to verify the obtained results. The first one is to calculate the stabilizing region of FOPI controllers. As shown in Example 1, the results in Liang et al. (2013) are unreliable. Moreover, in Example 2, the stabilizing region of FOPI controllers is calculated for incommensurate fractional-order systems as a comparison with Zheng et al. (2014). Also, in Example 3 and

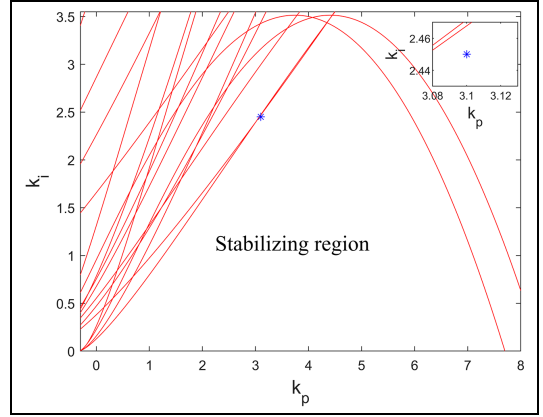


Figure 1. The stabilizing region of FOPI controllers.

Example 4, at first, **Algorithm 1** is employed to compute the stabilizing region. Then, the control requirements on the disturbance rejection and the noise reduction are evaluated by the auxiliary functions $\Lambda_S(\omega)$ in equation (28) and $\Lambda_T(\omega)$ in equation (32).

Example 1. Consider an interval fractional-order plant as equation (35)

$$P(s) = \frac{[0.5, 1.5]}{[0.5, 1.5] + [3, 5]s^{0.9} + [2, 4]s^{1.8} + s^{2.7}} \quad (35)$$

At first, the algorithm proposed in Liang et al. (2013) is employed to obtain the stabilizing region of FOPI controllers with $\lambda = 1.2$ as depicted in Figure 1. From this figure, it is visible that the FOPI controller $C(s) = 3.1 + 2.45/s^{1.2}$ is located in the stabilizing region. Now **Algorithm 1** proposed in this paper is used to determine the stabilizing region of the FOPI controller with $\lambda = 1.2$. Based on **Procedure 1**, the vertex polynomials $V_{r_1}^+(\omega)$ ($r_1 = 1, 2$) and $V_{r_2}^-(\omega)$ ($r_2 = 1, 2, \dots, 6$) are obtained as equation (43)

$$\begin{cases} V_1^+(\omega) = 0.5, \\ V_2^+(\omega) = 1.5, \\ V_1^-(\omega) = 0.5 + 3s^{0.9} + 2s^{1.8} + s^{2.7}, \\ V_2^-(\omega) = 1.5 + 3s^{0.9} + 2s^{1.8} + s^{2.7}, \\ V_3^-(\omega) = 1.5 + 5s^{0.9} + 2s^{1.8} + s^{2.7}, \\ V_4^-(\omega) = 1.5 + 5s^{0.9} + 4s^{1.8} + s^{2.7}, \\ V_5^-(\omega) = 0.5 + 5s^{0.9} + 4s^{1.8} + s^{2.7}, \\ V_6^-(\omega) = 0.5 + 3s^{0.9} + 4s^{1.8} + s^{2.7}. \end{cases} \quad (36)$$

By employing **Algorithm 1**, one can compute the final stabilizing region as shown in Figure 2. From Figure 2, it is apparent that the FOPI controller $C(s) = 3.1 + 2.45/s^{1.2}$ is not located in the stabilizing region calculated by **Algorithm 1**. We can use **Theorem 2** to check the robust stability of the closed-loop

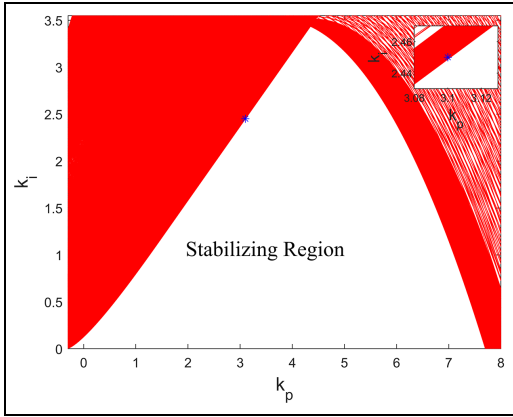


Figure 2. The stabilizing region of FOPI controllers.

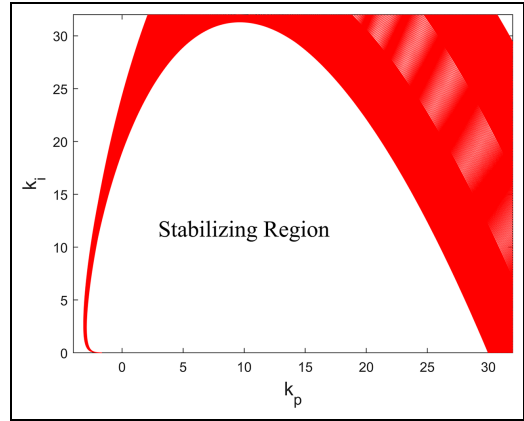


Figure 4. Stabilizing region of FOPID controllers.

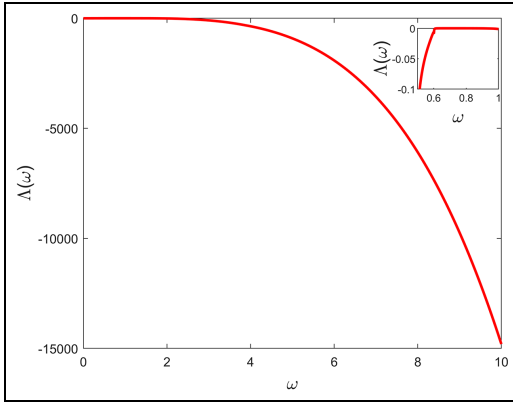


Figure 3. Curve of $\Lambda(\omega)$ in equation (37).

control system by applying the FOPI controller $C(s) = 3.1 + 2.45/s^{1.2}$. To do this, the stability of $\Delta_0(s)$ in equation (37) can be verified by Busłowicz (2008). Moreover, the curve of the function $\Lambda(\omega)$ in equation (22) has been plotted in Figure 3. As seen from this figure, there are frequencies at which $\Lambda(\omega)$ is equal to zero and consequently, the FOPI controller $C(s) = 3.1 + 2.45/s^{1.2}$ cannot robustly stabilize the closed-loop control system. Because, the inequality $\Lambda(\omega) < 0$ is not held. This example shows that the results obtained in Liang et al. (2013) are not reliable in general

$$\Delta_0(s) = s^{1.2}(0.5 + 3s^{0.9} + 2s^{1.8} + s^{2.7}) + 0.5(3.1s^{1.2} + 2.45) \quad (37)$$

Example 2. Consider the following fractional-order plant

$$P(s) = \frac{1}{[3, 3.2]s^{\frac{\sqrt{2}}{10}} + [4.5, 5.5]s + [1.8, 2.2]s^1 + \frac{\sqrt{2}}{10} + s^{2.5}} \quad (38)$$

Based on **Procedure 1**, the vertex polynomials $V_{r_2}^-(\omega)$ ($r_2 = 1, 2, \dots, 6$) are obtained as equation (39)

$$\begin{cases} V_1^-(\omega) = 3s^{\frac{\sqrt{2}}{10}} + 4.5s + 1.8s^1 + \frac{\sqrt{2}}{10} + s^{2.5}, \\ V_2^-(\omega) = 3.2s^{\frac{\sqrt{2}}{10}} + 4.5s + 1.8s^1 + \frac{\sqrt{2}}{10} + s^{2.5}, \\ V_3^-(\omega) = 3.2s^{\frac{\sqrt{2}}{10}} + 5.5s + 1.8s^1 + \frac{\sqrt{2}}{10} + s^{2.5}, \\ V_4^-(\omega) = 3.2s^{\frac{\sqrt{2}}{10}} + 5.5s + 2.2s^1 + \frac{\sqrt{2}}{10} + s^{2.5}, \\ V_5^-(\omega) = 3s^{\frac{\sqrt{2}}{10}} + 5.5s + 2.2s^1 + \frac{\sqrt{2}}{10} + s^{2.5}, \\ V_6^-(\omega) = 3s^{\frac{\sqrt{2}}{10}} + 4.5s + 2.2s^1 + \frac{\sqrt{2}}{10} + s^{2.5}. \end{cases} \quad (39)$$

The controller is a FOPID controller with $\lambda = 1, \mu = 0.4$ and $k_d = 1$. By employing **Algorithm 1**, the final stabilizing region can be obtained as Figure 4. It is notable that none of the works. Zheng et al. (2014) and Gao (2019), can be used to determine the stabilizing region of FOPID controllers. It is because that the aforementioned works are limited to the systems of commensurate orders.

Example 3. Consider the following interval plant

$$P(s) = \frac{[1, 2]s + [1, 2]}{s^2 + [1, 1.5]s + [0.5, 1.5]} \quad (40)$$

The objective is to design a robust FOPID stabilization for the closed-loop control system. Based on **Procedure 1**, the vertex polynomials $V_{r_1}^+(\omega)$ ($r_1 = 1, 2, 3, 4$) and $V_{r_2}^-(\omega)$ ($r_2 = 1, 2, 3, 4$) are obtained as (41)

$$\begin{cases} V_1^+(\omega) = s + 1, \\ V_2^+(\omega) = s + 2, \\ V_3^+(\omega) = 2s + 2, \\ V_4^+(\omega) = 2s + 1, \\ V_1^-(\omega) = s^2 + s + 0.5, \\ V_2^-(\omega) = s^2 + s + 1.5, \\ V_3^-(\omega) = s^2 + 1.5s + 1.5, \\ V_4^-(\omega) = s^2 + 1.5s + 1.5, \\ V_5^-(\omega) = s^2 + 1.5s + 0.5, \\ V_6^-(\omega) = s^2 + s + 0.5. \end{cases} \quad (41)$$

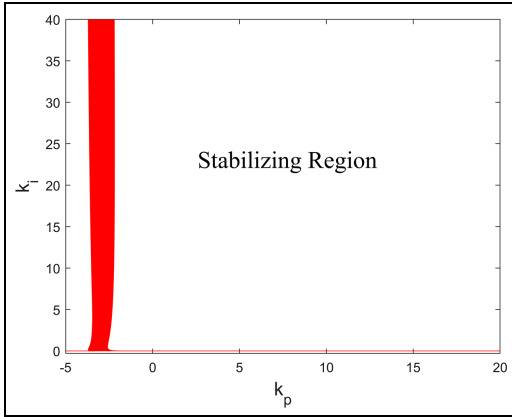


Figure 5. The stabilizing region of FOPID controllers.

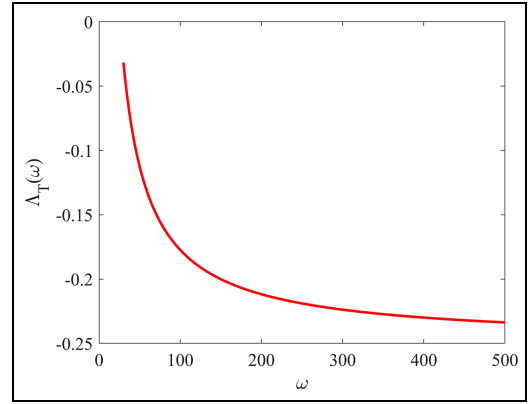


Figure 7. Curve of $\Lambda_T(\omega)$ for the FOPID controller.

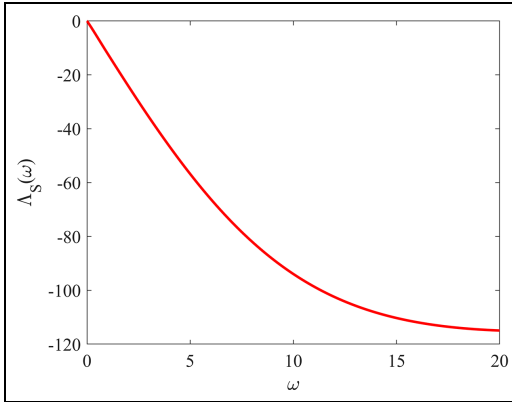


Figure 6. Curve of $\Lambda_S(\omega)$ in equation (28) for the FOPID controller.

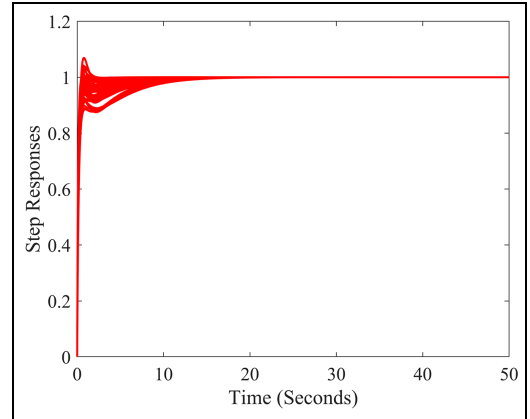


Figure 8. The closed-loop step responses corresponding to the FOPID controller.

We take $\lambda = 1$, $\mu = 0.1$ and $k_d = 2.6$ for obtaining the stabilizing region of FOPID controllers in the (k_p, k_i) plane. The final stabilizing region can be obtained as Figure 5 by performing **Algorithm 1**. From Figure 5, it is visible that the FOPID controller $C(s) = 2 + \frac{1.8}{s} + 2.6s^{0.1}$ is located in the stabilizing region. In the following, the inequalities $\Lambda_S(\omega) < 0$ in equation (28) and $\Lambda_T(\omega) < 0$ in equation (32) are checked for the weighting functions in equation (42)

$$\begin{aligned} M_S(s) &= 0.1 \frac{(s + 1000)(s + 30.67)(s + .001)}{s^2 + 30.67s + 247.3}, s = j\omega \\ M_T(j\omega) &= 0.25, \omega > 30 \end{aligned} \quad (42)$$

As depicted in Figures 6 and 7, the inequalities $\Lambda_S(\omega) < 0$ in equation (28) and $\Lambda_T(\omega) < 0$ in equation (32) are satisfied by the FOPID controller $C(s) = 2 + \frac{1.8}{s} + 2.6s^{0.1}$. Also, the step

responses of the closed-loop control system corresponding to the FOPID have been plotted in Figure 8. From this figure, it is clear that the robust FOPID stabilization has robust performance.

Example 4. Consider an interval plant having the following form

$$P(s) = \frac{[8, 12]}{[30, 50]s^{1.2} + 1} \quad (43)$$

We take $k_d = 0.05$, $\lambda = 1$, and $\mu = 0.2$ for the FOPID controller. As mentioned in the first step of Algorithm 1, the vertex polynomials $V_{r_1}^+(\omega)$ ($r_1 = 1, 2$) and $V_{r_2}^-(\omega)$ ($r_2 = 1, 2$) are obtained as

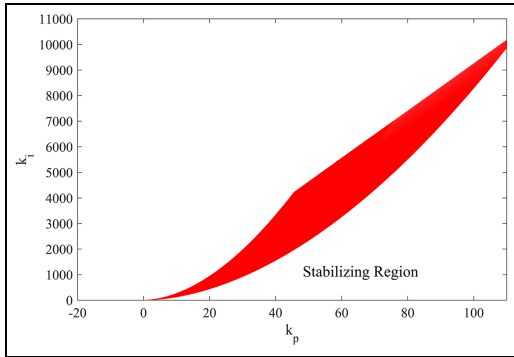


Figure 9. The stabilizing region of FOPID controllers.

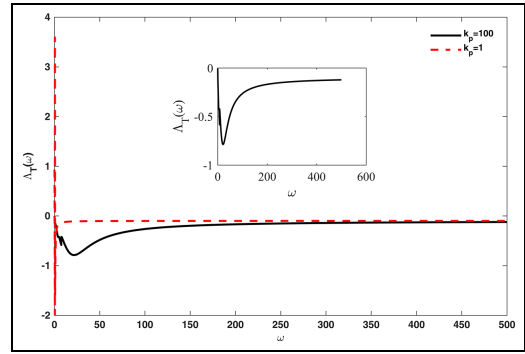


Figure 11. Curve of $\Lambda_T(\omega)$ in equation (31) for the controllers $C_1(s)$ (dashed line) and $C_2(s)$ (solid line).

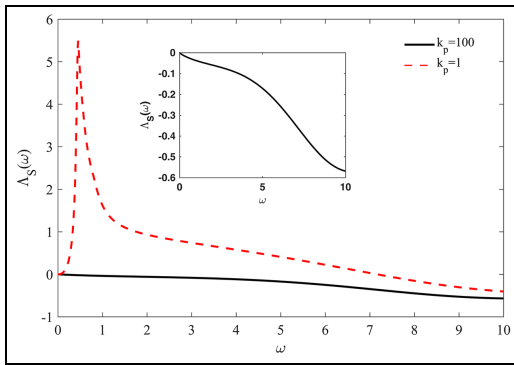


Figure 10. Curve of $\Lambda_S(\omega)$ in equation (28) for the controllers $C_1(s)$ (dashed line) and $C_2(s)$ (solid line).

$$\begin{cases} V_1^+(\omega) = 8, \\ V_2^+(\omega) = 12, \\ V_1^-(\omega) = 30s^{1.2} + 1, \\ V_2^-(\omega) = 50s^{1.2} + 1, \end{cases} \quad (44)$$

By performing the Steps 2–4 in Algorithm 1, the final stabilizing region in the (k_p, k_i) plane can be obtained as Figure 9.

Two controllers $C_1(s)$ and $C_2(s)$ lie in the stabilizing region.

$$\begin{aligned} C_1(s) &= 1 + \frac{1}{s} + 0.05s^{0.2} \\ C_2(s) &= 100 + \frac{1}{s} + 0.05s^{0.2} \end{aligned} \quad (45)$$

In the following, it is shown that which controller can satisfy the inequalities $\Lambda_S(\omega) < 0$ in equation (28) and $\Lambda_T(\omega) < 0$ in equation (32) for

$$\begin{aligned} M_S(s) &= \frac{(s + .01)(s + 10)(.001s + 1)}{s^2 + 10s + 100}, s = j\omega \\ M_T(j\omega) &= 0.1, \omega > 0.1 \end{aligned} \quad (46)$$

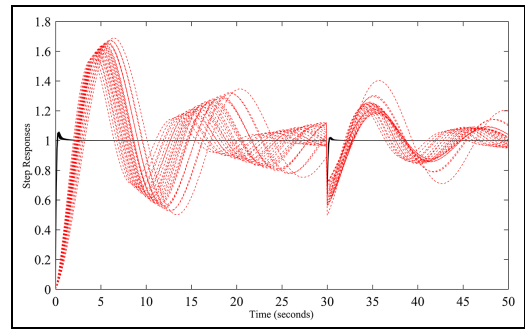


Figure 12. The closed-loop step responses corresponding to the controllers $C_1(s)$ (dashed line) and $C_2(s)$ (solid line).

As Figures 10 and 11 show, the controller $C_2(s)$ can satisfy the inequalities $\Lambda_S(\omega) < 0$ in equation (28) and $\Lambda_T(\omega) < 0$ in equation (32). This implies that the robust stability and robust performance of the closed-loop control system can be achieved by the FOPID controller $C_1(s)$. Hence, the designer should choose $C_2(s)$.

To implement the controllers $C_1(s)$ and $C_2(s)$, the approximation method proposed in Oustaloup et al. (2000) is used. Also, a disturbance is considered as an additive step disturbance at $t = 30$ seconds. Figure 12 shows the step responses of the closed-loop system corresponding to the controllers $C_1(s)$ and $C_2(s)$. From Figure 12, it is apparent that by applying the controller $C_2(s)$, the closed-loop performance is better than what is achieved by applying the controller $C_1(s)$. Also, in Figure 13, the control signals corresponding to the controllers $C_1(s)$ and $C_2(s)$ have been reported. Moreover, Figure 14 shows the values of the function $\Lambda(\omega)$ in equation (22) corresponding to the controller $C_2(s)$. As this figure shows, the inequality $\Lambda(\omega) < 0$ is satisfied. Hence, based on **Theorem 2**, the controller $C_2(s)$ can robustly stabilize the closed-loop system. Therefore, **Theorem 2** also confirms the results of **Algorithm 1**.

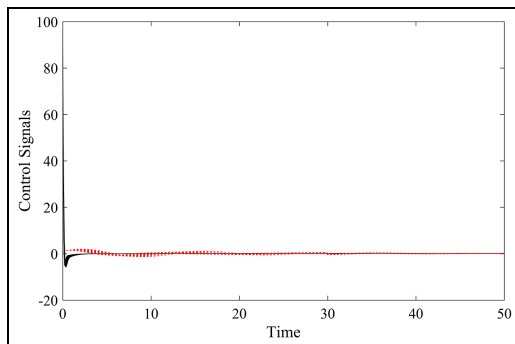


Figure 13. The control signals corresponding to the controllers $C_1(s)$ (dashed line) and $C_2(s)$ (solid line).

Conclusion

In this paper, a new method was proposed to obtain the stabilizing region of FOPID controllers for interval fractional-order plants. At first, a useful theorem was presented to analyze the robust stability of a closed-loop system consisting of a FOPID controller and an interval fractional-order plant. Inspired by **Theorem 1**, a useful algorithm was proposed to calculate the stabilizing region of FOPID controllers. Then, two auxiliary functions were presented to improve the control requirements on the disturbance rejection and the noise reduction. Finally, the usefulness of the paper results was confirmed by four examples. Future works may include determining the stabilizing region of FOPID controllers for interval fractional-order plants having uncertain orders and uncertain coefficients. Another good research line as a future work may be to calculate the stabilizing region of FOPID controllers for interval-delayed fractional-order plants.


Declaration of conflicting interests

The author(s) declared no potential conflicts of interest with respect to the research, authorship, and/or publication of this article.

Funding

The author(s) disclosed receipt of the following financial support for the research, authorship, and/or publication of this article: This work was supported by the Estonian Research Council grant PRG658.

ORCID iD

Majid Ghorbani  <https://orcid.org/0000-0001-8908-6573>

References

- Bonnet C and Partington JR (2002) Analysis of fractional delay systems of retarded and neutral type. *Automatica* 38(7): 1133–1138.
- Brown JW and Churchill RV (2009) *Complex Variables and Applications Eighth Edition*. New York, NY: McGraw-Hill Book Company.

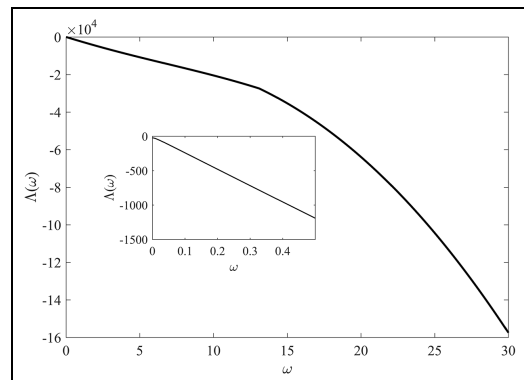


Figure 14. Curve of $\Lambda(\omega)$ in equation (22) corresponding to the FOPID controller $C_2(s)$.

- Bustowicz M (2008) Stability of linear continuous-time fractional order systems with delays of the retarded type. *Bulletin of the Polish Academy of Sciences: Technical Sciences* 56(4): 158–163.
- Chen P, Luo Y, Peng Y, et al. (2021) Optimal robust fractional order $PI^{\lambda}D$ controller synthesis for first order plus time delay systems. *ISA Transactions* 114: 136–149.
- Dulf EH (2019) Simplified fractional order controller design algorithm. *Mathematics* 7(12): 1166.
- Dwivedi P and Pandey S (2021) Tuning rules: Graphical analysis and experimental validation of a simplified fractional order controller for a class of open-loop unstable systems. *Asian Journal of Control* 23(5): 2293–2310.
- Ebrahimi M and Asgari M (2021) Robust fractional-order fixed-structure controller design for uncertain non-commensurate fractional plants using fractional Kharitonov theorem. *Proceedings of the Institution of Mechanical Engineers, Part I: Journal of Systems and Control Engineering* 235(8): 1375–1387.
- Feliu-Batlle V, Rivas-Perez R and Castillo-García F (2021) Design of a PI controller for the robust control of the steam pressure in the steam drum of a Bagasse-fired boiler. *IEEE Access* 9: 95123–95134.
- Gao S, Metered H, Bassuiny A, et al. (2017) Multi-objective genetic algorithm fractional-order PID controller for semi-active magnetorheologically damped seat suspension. *Journal of Vibration and Control* 23(8): 1248–1266.
- Gao Z (2018) An analytical method on the stabilization of fractional-order plants with one fractional-order term and interval uncertainties using fractional-order $PI^{\lambda}D^{\mu}$ controllers. *Transactions of the Institute of Measurement and Control* 40(15): 4133–4142.
- Gao Z (2015) Robust stabilization criterion of fractional-order controllers for interval fractional-order plants. *Automatica* 61: 9–17.
- Gao Z (2019) Analytical method on stabilisation of fractional-order plants with interval uncertainties using fractional-order $PI^{\lambda}D^{\mu}$ controllers. *International Journal of Systems Science* 50(5): 935–953.
- Gao Z, Zhai L-R and Yan-Dong L (2017) Robust stabilizing regions of fractional-order PI^{λ} controllers for fractional-order systems with time-delays. *International Journal of Automation and Computing* 14(3): 340–349.
- George MA and Kamath DV (2020) Design and tuning of fractional order $PI^{\lambda}D$ (FOPID) controller for speed control of electric vehicle on concrete roads. In: *2020 IEEE international conference on power electronics, smart grid and renewable energy (PESGRE)*, Cochin, India, 2–4 January 2020, pp. 1–6. New York: IEEE.

- Ghorbani M and Tavakoli-Kakhki M (2021a) Robust stability analysis of uncertain incommensurate fractional order quasi-polynomials in the presence of interval fractional orders and interval coefficients. *Transactions of the Institute of Measurement and Control* 43: 1117–1125.
- Ghorbani M and Tavakoli-Kakhki M (2021b) Robust stability analysis of a general class of interval delayed fractional order plants by a general form of fractional order controllers. *Mathematical Methods in the Applied Sciences* 44: 10172–10189.
- Ghorbani M, Tavakoli-Kakhki M and Estarami AA (2019) Robust FOPID stabilization of retarded type fractional order plants with interval uncertainties and interval time delay. *Journal of the Franklin Institute* 356(16): 9302–9329.
- Ghorbani M, Tavakoli-Kakhki M, Tepljakov A, et al. (2021) Robust stability analysis of interval fractional-order plants with interval time delay and general form of fractional-order controllers. *IEEE Control Systems Letters* 6: 1268–1273.
- Hamamci SE (2007) An algorithm for stabilization of fractional-order time delay systems using fractional-order PID controllers. *IEEE Transactions on Automatic Control* 52(10): 1964–1969.
- Hamamci SE (2008) Stabilization using fractional-order PI and PID controllers. *Nonlinear Dynamics* 51(1): 329–343.
- Idir A, Kidouche M, Bensafia Y, et al. (2018) Speed control of DC motor using PID and FOPID controllers based on differential evolution and PSO. *Evolutionary Computation* 20: 21.
- Lee YK and Watkins JM (2012) Determination of all stabilizing fractional-order PID controllers that satisfy a weighted sensitivity constraint. In: *2012 IEEE 51st IEEE conference on decision and control (CDC)*, Maui, HI, 10–13 December, pp. 254–259. New York: IEEE.
- Levine WS (2018) *The Control Systems Handbook: Control System Advanced Methods*. Boca Raton, FL: CRC Press.
- Liang T, Chen J and Zhao H (2013) Robust stability region of fractional order PI^λ controller for fractional order interval plant. *International Journal of Systems Science* 44(9): 1762–1773.
- Luo Y and Chen YQ (2011) Stabilizing and robust FOPI controller synthesis for first order plus time delay systems. In: *2011 50th IEEE conference on decision and control and European control conference*, Orlando, FL, 12–15 December, pp. 2040–2045. New York: IEEE.
- Luo Y and Chen YQ (2012) Stabilizing and robust fractional order PI controller synthesis for first order plus time delay systems. *Automatica* 48(9): 2159–2167.
- Matusu R, Şenol B and Pekař L (2020) Robust PI control of interval plants with gain and phase margin specifications: Application to a continuous stirred tank reactor. *IEEE Access* 8: 145372–145380.
- Monje CA, Vinagre BM, Feliu V, et al. (2008) Tuning and auto-tuning of fractional order controllers for industry applications. *Control Engineering Practice* 16(7): 798–812.
- Moornani KA and Haeri M (2009) On robust stability of linear time invariant fractional-order systems with real parametric uncertainties. *ISA Transactions* 48(4): 484–490.
- Moornani KA and Haeri M (2010a) On robust stability of LTI fractional-order delay systems of retarded and neutral type. *Automatica* 46(2): 362–368.
- Moornani KA and Haeri M (2010b) Robust stability testing function and Kharitonov-like theorem for fractional order interval systems. *IET Control Theory & Applications* 4(10): 2097–2108.
- Oustaloup A, Levron F, Mathieu B, et al. (2000) Frequency-band complex noninteger differentiator: Characterization and synthesis. *IEEE Transactions on Circuits and Systems I: Fundamental Theory and Applications* 47(1): 25–39.
- Rezaei Estakhrouiyeh M, Gharaveisi A and Vali M (2018) Fractional order proportional-integral-derivative controller parameter selection based on iterative feedback tuning. Case study: Ball Levitation system. *Transactions of the Institute of Measurement and Control* 40(6): 1776–1787.
- Simfukwe DD and Pal BC (2012) Multivariable feedback control: Analysis and design. *IEEE Transactions on Power Systems* 28(2): 1599–1608.
- Skogestad S and Postlethwaite I (2007) Multivariable feedback control: analysis and design. Citeseer. Available at: <https://citeseer-x.ist.psu.edu/viewdoc/summary?doi=10.1.1.466.1146>
- Tan N, Ozguven OF and Ozyetkin MM (2009) Robust stability analysis of fractional order interval polynomials. *ISA Transactions* 48(2): 166–172.
- Tavakoli-Kakhki M and Haeri M (2011) Fractional order model reduction approach based on retention of the dominant dynamics: Application in IMC based tuning of FOPI and FOPID controllers. *ISA Transactions* 50(3): 432–442.
- Tepljakov A, Alagoz BB, Yeroğlu C, et al. (2021) Towards Industrialization of FOPID controllers: A survey on milestones of fractional-order control and pathways for future developments. *IEEE Access* 9: 21016–21042.
- Tepljakov A, Petlenkov E and Belikov J (2015) Robust FOPI and FOPID controller design for FFOPDT plants in embedded control applications using frequency-domain analysis. In: *2015 American control conference (ACC)*, Chicago, IL, 1–3 July, pp. 3868–3873. New York: IEEE.
- Tu YW and Ho MT (2011) Robust second-order controller synthesis for model matching of interval plants and its application to servo motor control. *IEEE Transactions on Control Systems Technology* 20(2): 530–537.
- Yeroğlu C and Tan N (2011) Note on fractional-order proportional–integral–differential controller design. *IET Control Theory & Applications* 5(17): 1978–1989.
- Závacká J and Bakošová M (2011) Robust controller design for a laboratory process with uncertainties. In: *Proceedings of the 18th international conference on process control*, Tatranska Lomnica, Slovakia, 14–17 June 2011, pp. 72–76.
- Zheng S, Tang X and Song B (2014) A graphical tuning method of fractional order proportional integral derivative controllers for interval fractional order plant. *Journal of Process Control* 24(11): 1691–1709.
- Zheng W, Luo Y, Chen YQ, et al. (2021a) A simplified fractional order PID controller's optimal tuning: A case study on a PMSM speed servo. *Entropy* 23(2): 130.
- Zheng W, Luo Y, Chen YQ, et al. (2021b) Synthesis of fractional order robust controller based on Bode's ideas. *ISA Transactions* 111: 290–301.

Appendix 7

VII

M. Ghorbani, A. Tepljakov, and E. Petlenkov. Stabilizing region of fractional-order proportional integral derivative controllers for interval delayed fractional-order plants. *Asian Journal of Control*, 25(2):1145–1155, 2023.

RESEARCH ARTICLE

WILEY

Stabilizing region of fractional-order proportional integral derivative controllers for interval delayed fractional-order plants

Majid Ghorbani¹ | Aleksei Tepljakov | Eduard Petlenkov

Department of Computer Systems, Tallinn University of Technology, Tallinn, Estonia

Correspondence

Majid Ghorbani, Tallinn University of Technology, Department of Computer Systems, Tallinn, Estonia.
Email: majid.ghorbani@taltech.ee

Funding information

This work was supported by the Estonian Research Council grant PRG658.

Abstract

This paper concentrates on computing the stabilizing region of fractional-order proportional integral derivative (FOPID) controllers for interval delayed fractional-order plants. An interval delayed fractional-order plant is defined as a fractional-order transfer function with a time delay whose denominator and numerator coefficients are all uncertain and lie in specified intervals. In the present study, first, a theorem is proven to analyze the robust stability of the given closed-loop. Then, a method is proposed to solve the problem of robustly stabilizing interval delayed fractional-order plants by using FOPID controllers. Moreover, two auxiliary functions are presented to fulfill the additional specifications of design, ensuring better performance of the controlled system with respect to the disturbance and noise. Finally, two examples are provided to illustrate the design procedure.

KEYWORDS

fractional-order controllers, interval delayed fractional-order plants, stabilizing region

1 | INTRODUCTION

Over the past decades, many studies have been reported on fractional-order differential equations for modeling real world phenomena. It is because that real world physical systems can be better described by fractional models [1–3]. Meanwhile, it has been also shown that fractional-order controllers can achieve better robustness and performance than the integer-order counterparts [4, 5]. Hence, many innovative design methods of fractional-order controllers have been proposed in this literature [6–12].

Analyzing the robust stability is fundamental to any control system. Accordingly, various design methods for robust stability analysis of fractional-order systems have been presented in [13] and [14]. In [15, 16], the robust stability of a closed-loop system has been derived by using the value set concept. In order to reduce the computational

cost for robust stability analysis of interval fractional-order systems, four polynomials of Kharitonov's theorem have been employed in [17]. In [18], the results of [13] have been employed to analyze the robust stability of an interval fractional-order system. Moreover, in Procedure 1 of [18], it has been proven that the value set of an interval fractional-order polynomial is parpolygon shape in the complex plane. Then, the robust stability analysis has been presented by some simple methods. Using the results presented in [18] and fractional-order controllers, the robust stability of an interval fractional-order plant subjected to the parameters uncertainties has been addressed in [19].

The study of fractional-order systems with delays has been the subject of great interest during the last decades. Necessary and sufficient conditions for robust stability analysis of interval fractional-order plants with one

time-delay by using general form of fractional-order controllers have been presented in [20, 21].

Literature review shows that different tuning strategies have been employed in order to design the fractional-order proportional integral derivative (FOPID) controllers. For instance in [22, 23], the FOPID controllers have been tuned for systems having time delay by the particle swarm optimization. Moreover, the works [24–26] have proposed some numerical nonlinear optimization methods to design FOPID controllers. Also, [27–31] have proposed various methods to tune FOPID controllers for systems having time delay based on gain and phase margins. In addition, the stabilizing region of FOPI and FOPID controllers which can satisfy the H_∞ constraint of the sensitivity function has been studied in [32, 33]. In [34, 35], the stabilizing regions of fractional-order controllers for time-delay fractional-order systems (without uncertainties) have been calculated. Computation of the stabilizing region of FOPID controllers has some advantages. First, a family of stabilizing FOPID controllers, instead of just one, is proposed for the control system and this provides a more flexible choice of controller parameters. Second, the stabilizing region can facilitate to select the optimal design of other additional design criteria.

It is notable that all the above works have assumed that the transfer function of the plant has no uncertainties. But, in real world system, it is well known that the parameters of practical plants are influenced by uncertainties. In this sense, the robust stabilizing region for time-delay fractional-order systems with parametric uncertainties should be considered in this literature. In summary, based on the above explanations, the following control problems can be formulated as the main challenges for time-delay fractional-order systems by FOPID controllers.

Problem 1. The calculation of the stabilizing region of FOPID controllers for time-delay fractional-order systems in the presence of uncertainties.

Problem 2. In addition to design a robust FOPID stabilization, it is necessary to ensure that some performance specifications are met for all plants of the uncertain system. In other words, the control requirements on the disturbance rejection and the noise reduction should be achieved for time-delay fractional-order systems with parametric uncertainties. But, because of the uncertain plant, it is very difficult to determine the uncertainty bounds of the complementary sensitivity function and the sensitivity function in the presence of uncertainties.

Due to the above important meanings, in this paper, the procedure presented in [35] is developed to calculate the stabilizing region of the FOPID controllers for interval

delayed fractional-order plants as a solution for Problem 1. Also, two auxiliary functions are also offered to evaluate the control requirements on the disturbance rejection and the noise reduction as a solution for Problem 2. The main contributions of this paper lie in the following three aspects:

- Analyzing the robust stability of a closed-loop system including a FOPID controller and an interval delayed fractional-order plant.
- Presenting a method to compute the stabilizing region of FOPID controllers for interval delayed fractional-order plants.
- Presenting two auxiliary functions to assess the control requirements on the disturbance rejection and the noise reduction.

The paper is organized as follows: some preliminaries are provided in Section 2. In Section 3, the main results are presented. In Section 4, simulation results are given. Finally, Section 5 offers some conclusion remarks.

2 | BACKGROUND AND PRELIMINARIES

In this section, notations held by the paper are declared, and the related background is recalled.

Notations. Define sets $\mathbb{R}^{\geq 0} \triangleq \{x \in \mathbb{R} : x \geq 0\}$, $\mathbb{N}^{\leq n} \triangleq \{x \in \mathbb{N} : x \leq n\}$ and $\mathbb{Z}_{\geq m}^{\leq n} \triangleq \{x \in \mathbb{Z} : m \leq x \leq n\}$. $\text{floor}(x)$ is the largest integer less than or equal to $x \in \mathbb{R}$. $n(B)$ shows the number of distinct members of set B . $\text{frac}(x) \triangleq x - \text{floor}(x)$ for all $x \in \mathbb{R}$. $e(x_1(j\omega), x_2(j\omega)) \triangleq \eta x_1(j\omega) + (1 - \eta)x_2(j\omega)$, $\eta \in [0, 1]$. Also, $A \cup B \triangleq \{x : x \in A \text{ or } x \in B\}$ for any two sets A and B .

Consider an interval delayed fractional-order plant as

$$P(s, \mathbf{b}, \mathbf{a}) = \frac{N(s, \mathbf{b})}{D(s, \mathbf{a})} e^{-ls} = \frac{\sum_{i_1=0}^m b_{i_1} s^{b_{i_1}}}{\sum_{i_2=0}^n a_{i_2} s^{a_{i_2}}} e^{-ls}, \quad (1)$$

where s is the Laplace operator, $m \in \mathbb{Z}^{\geq 0}$, $n \in \mathbb{Z}^{\geq 1}$, $\beta_m > \beta_{m-1} > \dots > \beta_1 > \beta_0 = 0$ and $\alpha_n > \alpha_{n-1} > \dots > \alpha_1 > \alpha_0 = 0$ are arbitrary real numbers. Also, l is the positive time delay, and $\mathbf{b} = [b_0, b_1, \dots, b_m]^T$ and $\mathbf{a} = [a_0, a_1, \dots, a_n]^T$ are the coefficients vectors and they belong to the uncertainty bounding sets:

$$\begin{aligned} \mathbf{b} \in \mathbf{B} &= \{\mathbf{b} \in \mathbb{R}^{m+1} | b_{i_1} \in [b_{i_1}^-, b_{i_1}^+], b_m, b_0 \neq 0, i_1 \in \mathbb{Z}_{\geq 0}^{\leq m}\}, \\ \mathbf{a} \in \mathbf{A} &= \{\mathbf{a} \in \mathbb{R}^{n+1} | a_{i_2} \in [a_{i_2}^-, a_{i_2}^+], a_n \neq 0, i_2 \in \mathbb{Z}_{\geq 0}^{\leq n}\}, \end{aligned} \quad (2)$$

where $[b_{i_1}^-, b_{i_1}^+]$ and $[a_{i_2}^-, a_{i_2}^+]$ are specified intervals. Also, the FOPID controller is given as (3).

$$C(s) = \frac{k_p s^\lambda + k_i + k_d s^{\mu+\lambda}}{s^\lambda}, \quad 0 < \lambda, \mu < 2, \alpha_n > \mu + \beta_m. \quad (3)$$

In this study, it is considered that the fractional-order polynomial (4) represents the characteristic function of the negative unity feedback control system.

$$\Delta(s) = s^\lambda D(s, \mathbf{a}) + (k_p s^\lambda + k_i + k_d s^{\mu+\lambda}) N(s, \mathbf{b}) e^{-ls}. \quad (4)$$

Remark 1. The principal branch of $\Delta(s)$ in (4) is defined such as **Definition 1** in [13], that is, $\text{Arg}(s) \in (-\pi, \pi]$.

Remark 2. Based on [18], the value sets of $D(s, \mathbf{a})$ and $N(s, \mathbf{b})$ are two parpolygons in the complex plane for $s = j\omega$ & $\omega > 0$. The vertex polynomials corresponding to $D(j\omega, \mathbf{a})$ are determined for $\omega \geq 0$ by using **Procedure 1**.

Procedure 1 ([18]). Define $H_0 \triangleq \{i_2 \in \mathbb{Z}_{\geq 0}^n : a_{i_2}^- < a_{i_2}^+\}$. The value set $D(j\omega, \mathbf{a})$ is determined for $\omega \in \mathbb{R}_{\geq 0}$ as follows:

1. For $H_0 = \emptyset$ and $\omega \geq 0$, $D(j\omega, \mathbf{a}) = D_0(j\omega)$ where

$$D_0(\omega) \triangleq \sum_{i_2=0}^n a_{i_2}^- s^{\alpha_{i_2}}, \quad (5)$$

2. For $H_0 \neq \emptyset$,

- If $\omega = 0$, then $D(j\omega, \mathbf{a}) = D(j0, \mathbf{a}) = [a_0^-, a_0^+]$.
- If $\omega > 0$, then define $B_0 \triangleq \{\text{frac}(0.5\alpha_{i_2}) : i_2 \in H_0\}$ and $m_D \triangleq n(B_0)$. Consider $\gamma_1, \dots, \gamma_{m_D-1}, \gamma_{m_D}$ as all the distinct members of B_0 sorted as $0 \leq \gamma_1 < \dots < \gamma_{m_D-1} < \gamma_{m_D} < 1$. Then, define the following sets:

$$\begin{aligned} H_r' &\triangleq \{i_2 \in H_0 : \text{floor}(0.5\alpha_{i_2}) \text{ is an odd number and } \text{frac}(0.5\alpha_{i_2}) = \gamma_r\}, \\ H_r &\triangleq \{i_2 \in H_0 : \text{floor}(0.5\alpha_{i_2}) \text{ is an even number and } \text{frac}(0.5\alpha_{i_2}) = \gamma_r\}, \quad r = 1, 2, \dots, m_D. \end{aligned} \quad (6)$$

Let $a^- \triangleq [a_0^- a_1^- \dots a_n^-]^T$ and $a^+ \triangleq [a_0^+ a_1^+ \dots a_n^+]^T$. The vectors $q^1, q^2, \dots, q^{2m_D}$ are defined as follows:

$$\begin{aligned} a^k &\triangleq [a_0^k a_1^k \dots a_n^k]^T, \\ a^{m_D+k} &\triangleq [a_0^{m_D+k} a_1^{m_D+k} \dots a_n^{m_D+k}]^T \\ &= a^+ + a^- - a^k, \quad k = 1, \dots, m_D, \end{aligned} \quad (7)$$

where for $i_2 = 0, 1, \dots, n$ and $k = 1, \dots, m_D$, it can be written that

$$a_{i_2}^k \triangleq \begin{cases} a_{i_2}^+, & \text{for } i_2 \in \left(\bigcup_{l=1}^{k-1} H_l\right) \cup \left(\bigcup_{l=k}^{m_D} H_l'\right), \\ a_{i_2}^-, & \text{for otherwise.} \end{cases} \quad (8)$$

and

$$a_{i_2}^{m_D+k} \triangleq a_{i_2}^+ + a_{i_2}^- - a_{i_2}^k. \quad (9)$$

Hence, the consecutive vertices $V_{r_2}^-(j\omega)$ ($r_2 = 1, 2, \dots, 2m_D$) are calculated by

$$\begin{aligned} V_k^-(j\omega) &\triangleq D(j\omega, a^k), \\ V_{m_D+k}^-(j\omega) &\triangleq D(j\omega, a^{m_D+k}) \\ &= D(j\omega, a^+ + a^-) - V_k^-(j\omega), \\ k &= 1, 2, \dots, m_D. \end{aligned} \quad (10)$$

Accordingly, the vertex polynomials corresponding to $D(j\omega, \mathbf{b})$ and $N(j\omega, \mathbf{a})$ are respectively considered as $V_{r_1}^+(\omega)$ ($r_1 = 1, 2, \dots, m_N$) and $V_{r_2}^-(\omega)$ ($r_2 = 1, 2, \dots, m_D$) and they can be calculated by **Procedure 1**.

Remark 3. Consider a certain polynomial of $\Delta(s)$ in (4) as $\hat{\Delta}(s)$ in (11).

$$\begin{aligned} \hat{\Delta}(s) &= s^\lambda \sum_{i_2=0}^n \hat{a}_{i_2} s^{\alpha_{i_2}} \\ &+ (k_p s^\lambda + k_i + k_d s^{\mu+\lambda}) \left(\sum_{i_1=0}^m \hat{b}_{i_1} s^{\beta_{i_1}} \right) e^{-ls}. \end{aligned} \quad (11)$$

Then, the boundaries of the stabilizing region $\hat{\Delta}(s)$ in (11) are specified by infinite root boundary (IRB), real root boundary (RRB), and complex root boundary (CRB) which can be determined by [35]. In summary, the mentioned boundaries are stated based on the procedure proposed in [35] as follows.

- **RRB:** $\hat{\Delta}(0) = k_i \hat{b}_0$. If $k_i \hat{b}_0 \neq 0$, then $k_i = 0$. Otherwise, the boundary does not exist.
- **IRB:** $\hat{\Delta}(\infty) = 0$.

$$\begin{cases} k_d = 0, & \text{for } \alpha_n = \beta_m \text{ or } (\alpha_n > \beta_m \text{ and } \mu > \alpha_n - \beta_\mu), \\ k_d = \frac{-\hat{a}_0}{\hat{b}_0}, & \text{for } (\alpha_n > \beta_m \text{ and } \mu = \alpha_n - \beta_\mu), \\ \text{none}, & \text{for } (\alpha_n > \beta_m \text{ and } \mu < \alpha_n - \beta_\mu). \end{cases} \quad (12)$$

- **CRB:** By solving $\hat{\Delta}(j\omega) = 0$ the k_p and k_i parameters in terms of k_d, λ and μ are obtained as

$$\begin{aligned} k_p &= (A_2(\omega)B_1(\omega) - A_1(\omega)B_2(\omega) + k_d(B_1(\omega)B_6(\omega) \\ &\quad - B_2(\omega)B_5(\omega))) / (B_2(\omega)B_3(\omega) - B_1(\omega)B_4(\omega)), \\ k_i &= (A_1(\omega)B_4(\omega) - A_2(\omega)B_3(\omega) + k_d(B_4(\omega)B_5(\omega) \\ &\quad - B_3(\omega)B_6(\omega))) / (B_2(\omega)B_3(\omega) - B_1(\omega)B_4(\omega)), \end{aligned} \quad (13)$$

where

$$\begin{cases} A_1(\omega) = \sum_{i_2=0}^n \hat{a}_{i_2} \omega^{\lambda+a_{i_2}} \cos\left(\frac{\pi(a_{i_2}+\lambda)}{2} + l\omega\right), \\ A_2(\omega) = \sum_{i_2=0}^n \hat{a}_{i_2} \omega^{\lambda+a_{i_2}} \sin\left(\frac{\pi(a_{i_2}+\lambda)}{2} + l\omega\right), \\ B_1(\omega) = \sum_{i_1=0}^m \hat{b}_{i_1} \omega^{\beta_{i_1}} \cos\left(\frac{\pi\beta_{i_1}}{2}\right), \\ B_2(\omega) = \sum_{i_1=0}^m \hat{b}_{i_1} \omega^{\beta_{i_1}} \sin\left(\frac{\pi\beta_{i_1}}{2}\right), \\ B_3(\omega) = \sum_{i_1=0}^m \hat{b}_{i_1} \omega^{\beta_{i_1}+\lambda} \cos\left(\frac{\pi(\beta_{i_1}+\lambda)}{2}\right), \\ B_4(\omega) = \sum_{i_1=0}^m \hat{b}_{i_1} \omega^{\beta_{i_1}+\lambda} \sin\left(\frac{\pi(\beta_{i_1}+\lambda)}{2}\right), \\ B_5(\omega) = \sum_{i_1=0}^m \hat{b}_{i_1} \omega^{\beta_{i_1}+\lambda+\mu} \cos\left(\frac{\pi(\beta_{i_1}+\lambda+\mu)}{2}\right), \\ B_6(\omega) = \sum_{i_1=0}^m \hat{b}_{i_1} \omega^{\beta_{i_1}+\lambda+\mu} \sin\left(\frac{\pi(\beta_{i_1}+\lambda+\mu)}{2}\right). \end{cases} \quad (14)$$

Accordingly, the stabilizing region can be determined by checking one arbitrary test point inside each region [35].

Regarding the above analysis, the followings are mainly the purposes of this paper:

- Extending the procedure proposed in [35] to compute the stabilizing region of FOPID controllers for the interval delayed fractional-order plant (1).
- Presenting two auxiliary functions to evaluate the control requirements on the disturbance rejection and the noise reduction.

3 | MAIN RESULTS

This section is divided into three subsections. In Section 3.1, three theorems are presented to analyze the robust stability of the characteristic function (4). Then, an algorithm is proposed to calculate the stabilizing region of FOPID controllers for the interval delayed fractional-order plant (1). Finally, Sections 3.2 and 3.3 are devoted to evaluate the control requirements on the disturbance rejection and the noise reduction.

3.1 | Algorithm of FOPID stabilization

Based on the zero exclusion principle, the relationship between the origin and the value set of the characteristic function $\Delta(j\omega)$ has to be checked for $\omega \geq 0$. Hence, the following theorem is presented to check whether or not the origin is included in the value set of $\Delta(j\omega)$ for $\omega \geq 0$.

Theorem 1. Assume the value set of the characteristic function $\Delta(j\omega)$ is defined as $\Delta^{vs}(j\omega)$. Then, at a fixed frequency $\omega = \omega_0$, $0 \in \Delta^{vs}(j\omega)$, if and only if the value sets of $\Delta_1^{vs}(s = j\omega_0) = -s^\lambda D(s, \mathbf{a})$ and $\Delta_2^{vs}(s = j\omega_0) = (k_p s^\lambda + k_i + k_d s^{\mu+\lambda}) N(s, \mathbf{b}) e^{-ls}$ have an overlap in the complex plane.

Proof. Proof of the sufficiency: Since $\Delta_1^{vs}(j\omega_0)$ and $\Delta_2^{vs}(j\omega_0)$ have an overlap in the complex plane, then there is an arbitrary complex number as $z_0 \in \mathbb{C}$ such that $z_0 \in \Delta_1^{vs}(j\omega_0)$ and $z_0 \in \Delta_2^{vs}(j\omega_0)$. This implies that there is a member of the family $\Delta_1^{vs}(j\omega_0)$ as $\tilde{\Delta}_1(j\omega_0)$ which is equal to z_0 , that is,

$$z_0 = \tilde{\Delta}_1(j\omega_0). \quad (15)$$

Likewise, one can show that $z_0 = \tilde{\Delta}_2(j\omega_0)$. Consider $\{\tilde{\Delta}(j\omega) = -\tilde{\Delta}_1(j\omega) + \tilde{\Delta}_2(j\omega)\} \in \Delta(j\omega)$. Hence, at the fixed frequency $\omega = \omega_0$, it is apparent that $0 \in \Delta^{vs}(j\omega)$.

Proof of the necessity: $0 \in \Delta^{vs}(j\omega_0)$ can be written as $\{z_0 - z_0\} \in \Delta^{vs}(j\omega_0)$. Hence, one can simply deduce that $z_0 \in \Delta_1^{vs}(j\omega_0)$ and $z_0 \in \Delta_2^{vs}(j\omega_0)$. This implies that the value sets of $\Delta_1^{vs}(j\omega_0)$ and $\Delta_2^{vs}(j\omega_0)$ have an overlap in the complex plane. \square

Regarding **Theorem 1**, we present the following result which can be used to investigate the robust stability of the closed-loop system.

Theorem 2. The characteristic function (4) is robust stable if and only if, the characteristic functions $\Delta_{r_1}^D(s)(r_1 = 1, 2, \dots, m_N)$ in (16) and $\Delta_{r_2}^N(s)(r_2 = 1, 2, \dots, m_D)$ in (17) are also robust stable.

$$\begin{aligned} \Delta_{r_1}^D(s) &= s^\lambda D(s, \mathbf{a}) + (k_p s^\lambda + k_i + k_d s^{\mu+\lambda}) V_{r_1}^+(\omega) e^{-ls}, \\ (r_1 &= 1, 2, \dots, m_N). \end{aligned} \quad (16)$$

$$\begin{aligned} \Delta_{r_2}^N(s) &= s^\lambda V_{r_2}^-(\omega) + (k_p s^\lambda + k_i + k_d s^{\mu+\lambda}) N(s, \mathbf{b}) e^{-ls}, \\ (r_2 &= 1, 2, \dots, m_D). \end{aligned} \quad (17)$$

Proof. Proof of the sufficiency: According to **Procedure 1**, the value sets of $s^\lambda D(s, \mathbf{a})$ and $e^{-ls}(k_p s^\lambda + k_i + k_d s^{\mu+\lambda}) N(s, \mathbf{b})$ would be two parpolygons in the complex plane for $s = j\omega$. If the characteristic functions $\Delta_{r_1}^D(s)(r_1 = 1, 2, \dots, m_N)$ in (16) are robust stable, then based on Theorem 1, one can simply deduce that

$$-(k_p s^\lambda + k_i + k_d s^{\mu+\lambda}) V_{r_1}^+(\omega) e^{-ls} \notin s^\lambda \quad (18)$$

$$D(s, \mathbf{a}), (r_1 = 1, 2, \dots, m_N) \text{ and } s = j\omega.$$

Likewise, from (17) and Theorem 1, one can infer that

$$-s^\lambda V_{r_2}^-(\omega) \notin (k_p s^\lambda + k_i + k_d s^{\mu+\lambda}) N(s, \mathbf{b}) e^{-ls}, \quad (19)$$

$$(r_2 = 1, 2, \dots, m_D) \text{ and } s = j\omega.$$

From (18) and (19) and Theorem 1, it is apparent that two parpolygons $s^\lambda D(j\omega, \mathbf{a})$ and $(k_p(j\omega)^\lambda + k_i + k_d(j\omega)^{\mu+\lambda})N(j\omega, \mathbf{b})$ do not have any overlap in the complex plane and this implies that $0 \notin \Delta(j\omega)$.

Proof of the Necessity: Since the characteristic function (4) is robust stable, based on the zero exclusion principle $0 \notin \Delta(j\omega)$. By using the zero exclusion principle, the origin is located outside the value set of $\Delta(j\omega)$. On the other hand, it is apparent that for a value set as $H(j\omega)$ the following holds.

$$-z_0 \in H(j\omega_0) \iff 0 \in z_0 + H(j\omega_0), z_0 \in \mathbb{C}. \quad (20)$$

Therefore, from (18)-(20) and Theorem 1, the robust stability of $\Delta_{r_1}^D(s)$ ($r_1 = 1, 2, \dots, m_N$) in (16) and $\Delta_{r_1}^N(s)$ ($r_2 = 1, 2, \dots, m_D$) in (17) are concluded. \square

Remark 4. Theorem 2 reveals that the robust stability analysis of the characteristic function $\Delta(s)$ in (4) is equivalent to the robust stability analysis of the characteristic functions $\Delta_{r_1}^D(s)$ ($r_1 = 1, 2, \dots, m_N$) in (16) and $\Delta_{r_1}^N(s)$ ($r_2 = 1, 2, \dots, m_D$) in (17). Hence, the difficulties only lie on the fact that how to determine the boundaries (i.e., RRB, IRB, and CRB) of the characteristic functions $\Delta_{r_1}^D(s)$ ($r_1 = 1, 2, \dots, m_N$) in (16) and $\Delta_{r_1}^N(s)$ ($r_2 = 1, 2, \dots, m_D$) in (17). To do this, the calculation of the stabilizing region is presented in Algorithm 1 for the fixed values of λ , μ , and k_d .

Algorithm 1.

Step 1: Obtain the vertices $V_{r_1}^+(\omega)$ ($r_1 = 1, 2, \dots, m_N$) and $V_{r_2}^-(\omega)$ ($r_2 = 1, 2, \dots, m_D$) by Procedure 1.

Step 2: Obtain RRB, IRB and CRB and the stability regions by sweeping over $\eta \in [0, 1]$ for $\Delta_{r_1}^D(s)$ in (21) as stated in Remark 3.

$$\begin{aligned} \Delta_{r_1}^D(s) &= s^\lambda (e(V_{r_2}^-(\omega), V_{r_2+1}^-(\omega))) \\ &\quad + V_{r_1}^+(\omega)(k_p s^\lambda + k_i + k_d s^{\mu+\lambda}) e^{-ls}, \\ r_1 &= 1, 2, \dots, m_N, r_2 = 1, 2, \dots, \\ m_D, V_{m_D+1}^-(\omega) &= V_1^-(\omega). \end{aligned} \quad (21)$$

Step 3: Obtain RRB, IRB, and CRB and the stability regions by sweeping over $\eta \in [0, 1]$ for $\Delta_{r_2}^N(s)$ in (22) as stated in Remark 3.

$$\begin{aligned} \Delta_{r_2}^N(s) &= s^\lambda V_{r_2}^-(\omega) + (k_p s^\lambda + k_i + k_d s^{\mu+\lambda}) \\ &\quad e^{-ls} (e(V_{r_1}^-(\omega), V_{r_1+1}^-(\omega))), \\ r_1 &= 1, 2, \dots, m_N, r_2 = 1, 2, \dots, \\ m_D, V_{m_N+1}^+(\omega) &= V_1^+(\omega). \end{aligned} \quad (22)$$

Step 4: The final stabilizing region for the interval delayed fractional-order plant is the intersection of all the computed stable regions in Step 2 and Step 3.

tion of all the computed stable regions in Step 2 and Step 3.

It may be questionable how to determine robust stability of the closed-loop system by a designed controller. In the following theorem, an auxiliary function is presented to determine whether or not a designed controller can robustly stabilize the closed-loop system.

Theorem 3. Assume that a certain characteristic function of $\Delta(s)$ in (4) as $\Delta_0(s)$ is stable. Then, the closed-loop system is robust stable if and only if the inequality $\Lambda(\omega) < 0$ holds for $\omega \geq 0$, where

$$\Lambda(\omega) \triangleq \max\{\Lambda_1(\omega), \Lambda_2(\omega)\}, \quad (23)$$

in which

$$\begin{aligned} \Lambda_1(\omega) &\triangleq \max\{\Lambda_{r_1, r_2}^D(\omega) | r_1 \in \{1, \dots, m_N\}, \\ &\quad r_2 \in \{1, \dots, m_D\}\}, \\ \Lambda_{r_1, r_2}^D(\omega) &\triangleq \left| (j\omega)^\lambda (V_{r_2}^-(\omega) - V_{r_2+1}^-(\omega)) \right| \\ &\quad - \left| (j\omega)^\lambda V_{r_2}^-(\omega) + (k_p(j\omega)^\lambda + k_i \right. \\ &\quad \left. + k_d(j\omega)^{\mu+\lambda}) V_{r_1}^+(\omega) e^{-ls} \right| \\ &\quad - \left| (j\omega)^\lambda V_{r_2+1}^-(\omega) + (k_p(j\omega)^\lambda + k_i \right. \\ &\quad \left. + k_d(j\omega)^{\mu+\lambda}) V_{r_1}^+(\omega) e^{-ls} \right|. \end{aligned} \quad (24)$$

$$\begin{aligned} \Lambda_2(\omega) &\triangleq \max\{\Lambda_{r_1, r_2}^N(\omega) | r_1 \in \{1, \dots, m_N\}, \\ &\quad r_2 \in \{1, \dots, m_D\}\}, \\ \Lambda_{r_1, r_2}^N(\omega) &\triangleq \left| (k_p(j\omega)^\lambda + k_i + k_d(j\omega)^{\mu+\lambda}) \right. \\ &\quad \left. (V_{r_1}^+(\omega) - V_{r_1+1}^+(\omega)) \right| \\ &\quad - \left| (j\omega)^\lambda V_{r_2}^-(\omega) + (k_p(j\omega)^\lambda + k_i \right. \\ &\quad \left. + k_d(j\omega)^{\mu+\lambda}) V_{r_1}^+(\omega) e^{-ls} \right| \\ &\quad - \left| (j\omega)^\lambda V_{r_2}^-(\omega) + (k_p(j\omega)^\lambda + k_i \right. \\ &\quad \left. + k_d(j\omega)^{\mu+\lambda}) V_{r_1+1}^+(\omega) e^{-ls} \right|. \end{aligned} \quad (25)$$

Proof. Based on Procedure 1, it is apparent that the value set of $\Delta_{r_1}^D(s)$ in (16) and $\Delta_{r_2}^N(s)$ in (17) are two parpolygons in the complex plane. Also, if the triangle inequality is satisfied for each two consecutive vertices of $\Delta_{r_1}^D(s)$ in (16), then one can conclude that $0 \notin \Delta_{r_1}^D(j\omega)$ and this implies that the inequality $\Lambda_1(\omega) < 0$ is met. Likewise, satisfying the inequality $\Lambda_2(\omega) < 0$ leads to $0 \notin \Delta_{r_2}^N(j\omega)$ in (17). Hence, if the inequality $\Lambda(\omega) < 0$ in (23) is satisfied, then based on Theorem 1, Theorem 2 and the zero exclusion principle, the proof is completed. \square

3.2 | Good output disturbance rejection

In this subsection, an auxiliary function is proposed to improve the output disturbance rejection. Therefore, the following constraint should be satisfied [36].

$$|S(j\omega)| = \left| \frac{1}{1 + C(j\omega)P(j\omega)} \right| < |M_s(j\omega)|, \quad (26)$$

where, $M_s(j\omega) = N_s(j\omega)/D_s(j\omega)$ denotes the weighting function, which describes the frequency characteristic of the performance specifications.

Based on **Theorem 2** and (26), a robust FOPID controller should satisfy the following inequalities:

$$\left| \frac{1}{1 + \frac{(k_p s^d + k_i + k_d s^{d+\lambda}) V_1^+(s, \mathbf{a})}{s^d D(s, \mathbf{a})} e^{-ls}} \right| < |M_s(s)|, \quad (27)$$

$(r_1 = 1, 2, \dots, m_N), s = j\omega.$

$$\left| \frac{1}{1 + \frac{(k_p s^d + k_i + k_d s^{d+\lambda}) N(s, \mathbf{b}) e^{-ls}}{s^d V_2^-(s, \mathbf{a})}} \right| < |M_s(s)|, \quad (28)$$

$(r_2 = 1, 2, \dots, m_D), s = j\omega.$

From (27), (28) and the maximum modulus theorem [37], the following inequality should be satisfied.

$$\Lambda_s(\omega) \triangleq \max_{r=1,2} \Lambda_r^S(\omega) < 0, \quad (29)$$

where

$$\left\{ \begin{array}{l} \Lambda_1^S(\omega) \triangleq \max_{i=1, \dots, m_N} \Lambda_i^D(\omega), \\ \Lambda_i^D(\omega) \triangleq \max_{e_{iD}^D \in P_E^D} \left| \hat{e}_{iD}^D \right| - |M_s(j\omega)|, \\ l^D = 1, 2, \dots, m_D, \\ P_E^D \triangleq \{e_1^D, e_2^D, \dots, e_{m_D}^D\}, \\ e_1^D \triangleq \frac{1}{1 + \frac{(k_p s^d + k_i + k_d s^{d+\lambda}) V_1^+(s, \mathbf{a}) e^{-ls}}{s^d (e(V_1^-(s, \mathbf{a}), V_2^-(s, \mathbf{a})))}}}, \\ e_2^D \triangleq \frac{1}{1 + \frac{(k_p s^d + k_i + k_d s^{d+\lambda}) V_1^+(s, \mathbf{a}) e^{-ls}}{s^d (e(V_2^-(s, \mathbf{a}), V_3^-(s, \mathbf{a})))}}}, \\ \dots \\ e_{m_D}^D \triangleq \frac{1}{1 + \frac{(k_p s^d + k_i + k_d s^{d+\lambda}) V_1^+(s, \mathbf{a}) e^{-ls}}{s^d (e(V_{m_D}^-(s, \mathbf{a}), V_1^-(s, \mathbf{a})))}}}, \end{array} \right. \quad (30)$$

$s = j\omega.$

$$\left\{ \begin{array}{l} \Lambda_2^S(\omega) \triangleq \max_{i=1, \dots, m_D} \Lambda_i^N(\omega), \\ \Lambda_i^N(\omega) \triangleq \max_{e_{iN}^N \in P_E^N} \left| \hat{e}_{iN}^N \right| - |M_s(j\omega)|, \\ l^N = 1, 2, \dots, m_N, \\ P_E^N \triangleq \{e_1^N, e_2^N, \dots, e_{m_N}^N\}, \\ e_1^N \triangleq \frac{1}{1 + \frac{(k_p s^d + k_i + k_d s^{d+\lambda}) e(V_1^+(s, \mathbf{a}), V_2^+(s, \mathbf{a})) e^{-ls}}{s^d V_1^-(s, \mathbf{a})}}}, \\ e_2^N \triangleq \frac{1}{1 + \frac{(k_p s^d + k_i + k_d s^{d+\lambda}) e(V_2^+(s, \mathbf{a}), V_3^+(s, \mathbf{a})) e^{-ls}}{s^d V_1^-(s, \mathbf{a})}}}, \\ \dots \\ e_{m_N}^N \triangleq \frac{1}{1 + \frac{(k_p s^d + k_i + k_d s^{d+\lambda}) e(V_1^+(s, \mathbf{a}), V_{m_N}^+(s, \mathbf{a})) e^{-ls}}{s^d V_1^-(s, \mathbf{a})}}}, \end{array} \right. \quad (31)$$

$s = j\omega.$

Remark 5. Assume that a robust FOPID controller is designed by **Algorithm 1**. Then, the designed controller should satisfy the inequality $\Lambda_s(\omega) < 0$ in (29) to improve the output disturbance rejection. Note that some useful guidelines can be given by [36] for the selection of the weighting function $M_s(j\omega)$.

3.3 | High-frequency noise rejection

To satisfy high-frequency noise rejection, the following condition should be fulfilled.

$$|T(j\omega)| = \left| \frac{C(j\omega)P(j\omega)}{1 + C(j\omega)P(j\omega)} \right| < |M_T(j\omega)|, \quad (32)$$

where $M_T(j\omega) = N_T(j\omega)/D_T(j\omega)$ denotes the frequency characteristics of the noise signal [36].

By using **Theorem 2** and (32), a robust FOPID controller should also satisfy the inequality $\Lambda_T(\omega) < 0$ in (33).

$$\Lambda_T(\omega) \triangleq \max_{r=1,2} \Lambda_r^T(\omega) < 0, \quad (33)$$

where

$$\left\{ \begin{array}{l} \Lambda_1^T(\omega) \triangleq \max_{i=1, \dots, m_N} \hat{\Lambda}_i^D(\omega), \\ \hat{\Lambda}_i^D(\omega) \triangleq \max_{\hat{e}_{iD}^D \in \hat{P}_E^D} \left| \hat{\hat{e}}_{iD}^D \right| - |M_T(j\omega)|, \\ l^D = 1, 2, \dots, m_D, \\ \hat{P}_E^D \triangleq \{\hat{e}_1^D, \hat{e}_2^D, \dots, \hat{e}_{m_D}^D\}, \\ \hat{e}_1^D \triangleq \frac{(k_p s^d + k_i + k_d s^{d+\lambda}) V_i^+(s, \mathbf{a}) e^{-ls}}{s^d (e(V_1^-(s, \mathbf{a}), V_2^-(s, \mathbf{a}))) + (k_p s^d + k_i + k_d s^{d+\lambda}) V_i^+(s, \mathbf{a}) e^{-ls}}, \\ \hat{e}_2^D \triangleq \frac{(k_p s^d + k_i + k_d s^{d+\lambda}) V_i^+(s, \mathbf{a}) e^{-ls}}{s^d (e(V_2^-(s, \mathbf{a}), V_3^-(s, \mathbf{a}))) + (k_p s^d + k_i + k_d s^{d+\lambda}) V_i^+(s, \mathbf{a}) e^{-ls}}, \\ \dots \\ \hat{e}_{m_D}^D \triangleq \frac{(k_p s^d + k_i + k_d s^{d+\lambda}) V_i^+(s, \mathbf{a}) e^{-ls}}{s^d (e(V_1^-(s, \mathbf{a}), V_{m_D}^-(s, \mathbf{a}))) + (k_p s^d + k_i + k_d s^{d+\lambda}) V_i^+(s, \mathbf{a}) e^{-ls}}, \end{array} \right. \quad (34)$$

$s = j\omega.$

$$\begin{cases}
\Lambda_2^T(\omega) \triangleq \max_{i=1, \dots, m_D} \hat{\Lambda}_i^N(\omega), \\
\hat{\Lambda}_i^N(\omega) \triangleq \max_{\hat{c}_i^N \in \hat{P}_E^N} |\hat{c}_i^N| - |M_T(j\omega)|, \\
l^N = 1, 2, \dots, m_N, \\
\hat{P}_E^N \triangleq \{\hat{c}_1^N, \hat{c}_2^N, \dots, \hat{c}_{m_N}^N\}, \\
\hat{c}_1^N \triangleq \frac{(k_p s^2 + k_i + k_d s^{\mu+\lambda}) e(V_1^+(\omega), V_2^+(\omega)) e^{-ls}}{s^2 V_1^-(\omega) + (k_p s^2 + k_i + k_d s^{\mu+\lambda}) e(V_1^+(\omega), V_2^+(\omega)) e^{-ls}}, \\
\hat{c}_1^N \triangleq \frac{(k_p s^2 + k_i + k_d s^{\mu+\lambda}) e(V_2^+(\omega), V_3^+(\omega)) e^{-ls}}{s^2 V_1^-(\omega) + (k_p s^2 + k_i + k_d s^{\mu+\lambda}) e(V_2^+(\omega), V_3^+(\omega)) e^{-ls}}, \\
\vdots \\
\hat{c}_{m_N}^N \triangleq \frac{(k_p s^2 + k_i + k_d s^{\mu+\lambda}) e(V_{m_N}^+(\omega), V_1^+(\omega)) e^{-ls}}{s^2 V_1^-(\omega) + (k_p s^2 + k_i + k_d s^{\mu+\lambda}) e(V_{m_N}^+(\omega), V_1^+(\omega)) e^{-ls}}, \\
s = j\omega.
\end{cases} \quad (35)$$

Remark 6. The designer can tune a robust fractional-order controller by using **Algorithm 1**. Besides, the designed controller should satisfy the inequalities $\Lambda_S(\omega) < 0$ in (29) and $\Lambda_T(\omega) < 0$ in (33) to improve the control requirements on the disturbance rejection and the noise reduction.

Remark 7. It is apparent that **Theorem 2**, **Algorithm 1** and the inequalities $\Lambda_S(\omega) < 0$ in (29) and $\Lambda_T(\omega) < 0$ in (33) can be also employed for FOPI controllers (see **Example 1**).

4 | ILLUSTRATIVE EXAMPLES

Example 1. In [34], the stabilizing region of the fractional-order controller PI^λ , $\lambda = 0.4$ has been investigated for the following delayed fractional-order plant.

$$P(s) = \frac{5}{10s^{0.5} + 1} e^{-0.4s}. \quad (36)$$

Let us consider $P(s)$ in (36) as the following interval delayed fractional-order plant.

$$P(s) = \frac{[4, 6]}{[9, 11]s^{0.5} + 1} e^{-0.4s}. \quad (37)$$

Algorithm 1 is used to determine the stabilizing region of the FOPI controller with $\lambda = 0.4$. As mentioned in the first step of **Algorithm 1**, the vertex polynomials $V_{r_1}^+(\omega)$ ($r_1 = 1, 2$) and $V_{r_2}^-(\omega)$ ($r_2 = 1, 2$) can be obtained as (38) by Procedure 1.

$$\begin{cases}
V_1^+(\omega) = 4, \\
V_2^+(\omega) = 6, \\
V_1^-(\omega) = 9s^{0.5} + 1, \\
V_2^-(\omega) = 11s^{0.5} + 1.
\end{cases} \quad (38)$$

Based on the steps 2–4 in **Algorithm 1**, we need to obtain the boundaries RRB, IRB, and CRB for all members

of $\Delta_{r_1}^D(s)$ and $\Delta_{r_2}^N(s)$ as explained in Remark 3. Accordingly, one can compute the final stabilizing region of FOPI controllers as shown in Figure 1. It is notable that one can use the method presented in [38] in order to determine the stabilizing region inside each region.

At it is seen from Figure 1, the parameters $(k_p, k_i) = (2, 2)$ lie in the stabilizing region of FOPI controllers with $\lambda = 0.4$. The curve of the auxiliary function $\Lambda(\omega)$ has been plotted in Figure 2. As depicts this figure, the inequality $\Lambda(\omega) < 0$ is held. Therefore, based on **Theorem 3**, the closed-loop system is robust stable. Hence, **Theorem 3** also confirms the results of **Algorithm 1**.

Moreover, Figure 3 shows the stabilizing region of FOPI controllers for $\lambda = 1$. From Figure 3, it is apparent that two controllers $C_1(s) = 1.5 + 3/s$ and $C_2(s) = 3 + 0.1/s$ are located in the stabilizing region. In the following, the inequalities $\Lambda_S(\omega) < 0$ in (29) and $\Lambda_T(\omega) < 0$ in (33) for $M_S(s)$ and $M_T(s)$ in (39) are checked for both controllers

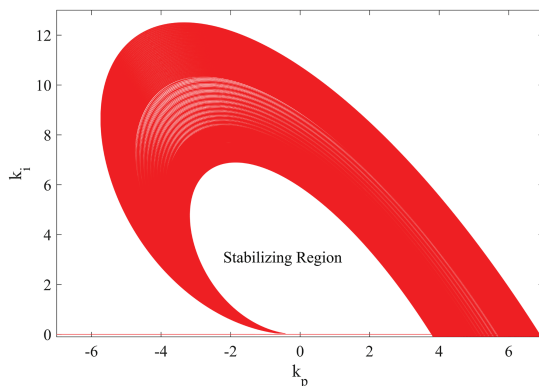


FIGURE 1 The stabilizing region of fractional-order proportional integral (FOPI) controllers with $\lambda = 0.4$

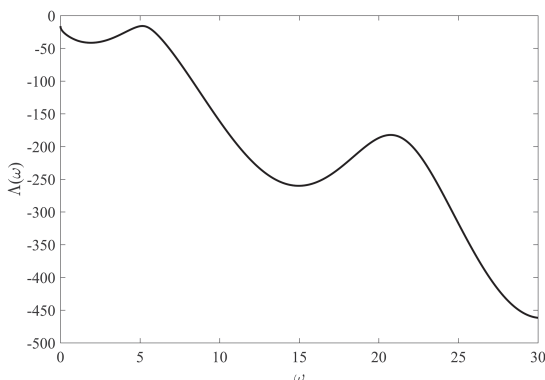


FIGURE 2 Curve of $\Lambda(\omega)$ in (23)

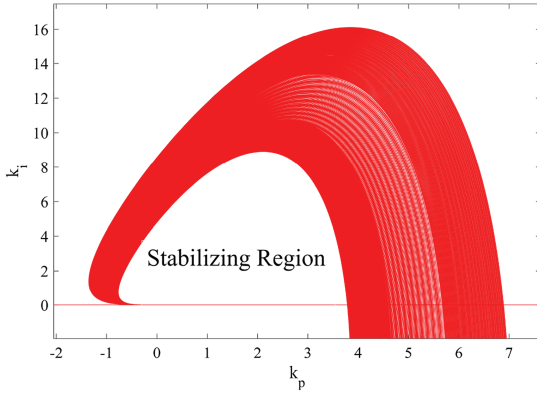


FIGURE 3 The stabilizing region of fractional-order proportional integral (FOPI) controllers with $\lambda = 1$

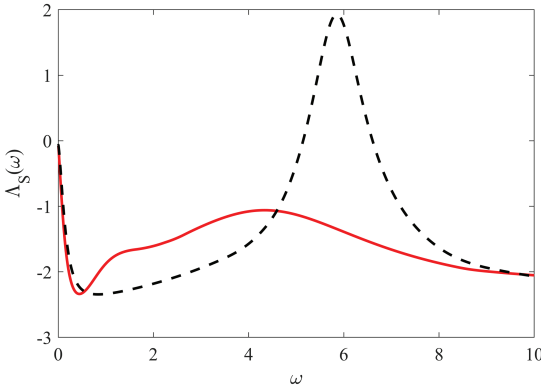


FIGURE 4 Curve of $\Lambda_S(\omega)$ in (29) for $C_1(s)$ (solid line) and $C_2(s)$ (dashed line)

$C_1(s)$ and $C_2(s)$.

$$\begin{cases} M_S(s) = 3 \frac{s+0.005}{s+0.224}, s = j\omega \\ M_T(j\omega) = 0.1, \omega > 10. \end{cases} \quad (39)$$

As Figures 4 and 5 show, the controller $C_1(s)$ can only satisfy the inequalities $\Lambda_S(\omega) < 0$ in (29) and $\Lambda_T(\omega) < 0$ in (33). Hence, this controller satisfy the desired performance and the designer should select the controller $C_1(s)$. To implement the function s^α , the approximation method proposed in [39] is used. To this end, the order and the frequency range of the approximation filter are considered as $N = 5$ and $[\omega_l, \omega_h] = [0.001, 100]$ rad/s. Also, a disturbance is considered as an additive step disturbance at $t = 50$ s. Figure 6 shows the step responses of the closed-loop system corresponding to the controllers $C_1(s)$ and $C_2(s)$. It is

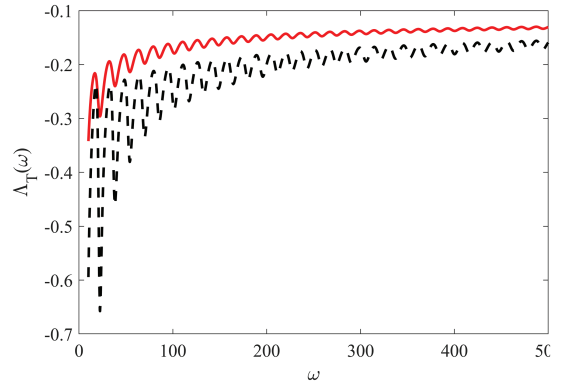


FIGURE 5 Curve of $\Lambda_T(\omega)$ in (32) for $C_1(s)$ (solid line) and $C_2(s)$ (dashed line)

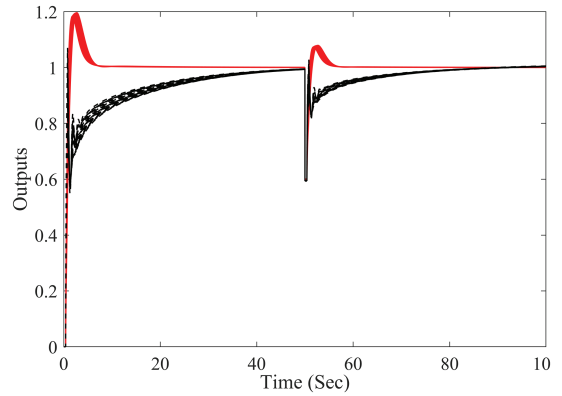


FIGURE 6 The step responses of the closed-loop control system corresponding to $C_1(s)$ (solid line) and $C_2(s)$ (dotted line)

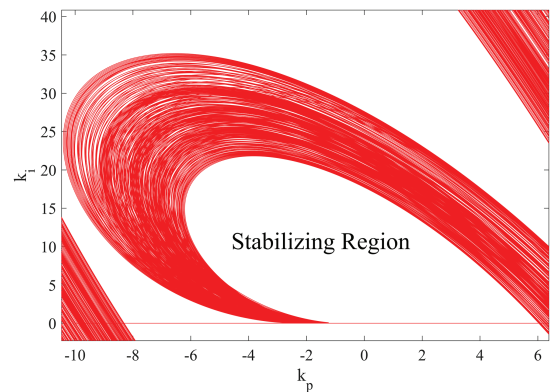


FIGURE 7 The stabilizing region of FOPID controllers for $\lambda = 0.4$, $\mu = 0.1$, and $k_d = 0.001$

visible that the controller $C_1(s)$ outperforms $C_2(s)$ in the sense of smaller oscillations and faster responses.

Example 2. Consider the following interval delayed fractional-order plant.

$$P(s) = \frac{[0.9, 1.1]s^{0.5} + [1.5, 2.5]}{s + [4.5, 5.5]s^{0.5} + [2.5, 3.5]}e^{-0.1s}, \quad (40)$$

We take $\lambda = 0.4$, $\mu = 0.1$ and $k_d = 0.001$ for the FOPID controller. Based on **Procedure 1**, the vertex polynomials $V_{r_1}^+(\omega)$ ($r_1 = 1, 2, 3, 4$) and $V_{r_2}^-(\omega)$ ($r_2 = 1, 2, 3, 4$) are obtained as (41).

$$\begin{cases} V_1^+(\omega) = 0.9s + 1.5, \\ V_2^+(\omega) = 1.1s + 1.5, \\ V_3^+(\omega) = 1.1s + 2.5, \\ V_4^+(\omega) = 0.9s + 2.5, \\ V_1^-(\omega) = s + 4.5s^{0.5} + 2.5, \\ V_2^-(\omega) = s + 4.5s^{0.5} + 3.5, \\ V_3^-(\omega) = s + 5.5s^{0.5} + 3.5, \\ V_4^-(\omega) = s + 5.5s^{0.5} + 2.5. \end{cases} \quad (41)$$

Based on the steps 2–4 in **Algorithm 1**, the boundaries RRB, IRB, and CRB explained in Remark 3 are calculated for all members of $\Delta_{r_1}^D(s)$ and $\Delta_{r_2}^N(s)$ as depicted in Figure 7.

5 | CONCLUSION

In this paper, a new method was proposed to obtain the stabilizing region of FOPID controllers for interval delayed fractional-order plants. At first, two useful theorems were presented to analyze the robust stability of a closed-loop system consisting of a FOPID controller and an interval delayed fractional-order plant. Inspired by these theorems, a useful algorithm was proposed to calculate the stabilizing region of FOPID controllers. Then, two auxiliary functions were presented to improve the control requirements on the disturbance rejection and the noise reduction. At the end, an assessment of the results was offered by some numerical examples. Future works may include further improving the computational efficiency of Algorithm 1 in order to compute the stabilizing region of FOPID controllers for fractional-order systems having an interval time delay.

CONFLICT OF INTEREST

The authors declare no potential conflict of interests.

AUTHOR CONTRIBUTIONS

Majid Ghorbani: Conceptualization, data curation, formal analysis, investigation, methodology, resources, validation. **Aleksei Tepljakov:** Supervision. **Eduard Petlenkov:** Project Administration.

ORCID

Majid Ghorbani  <https://orcid.org/0000-0001-8908-6573>

REFERENCES

1. S. Victor, R. Malti, H. Garnier, and A. Oustaloup, *Parameter and differentiation order estimation in fractional models*, *Automatica* **49** (2013), no. 4, 926–935.
2. R. Agarwal, S. Hristova, and D. O'Regan, *Noninstantaneous impulses in Caputo fractional differential equations and practical stability via Lyapunov functions*, *J. Franklin Inst.* **354** (2017), no. 7, 3097–3119.
3. M. Boudana, S. Ladaci, and J.-J. Loiseau, *Fractional order $PI^\lambda d^\mu$ control design for a class of cyber-physical systems with fractional order time-delay models: fractional $PI^\lambda d^\mu$ design for CPS with time-delay models*, *Int. J. Cyber-Phys. Syst. (IJCPS)* **1** (2019), no. 2, 1–18.
4. I. Podlubny, *Fractional-order systems and $PI^\lambda d^\mu$ -controllers*, *IEEE Trans. Autom. Control* **44** (1999a), no. 1, 208–214.
5. I. Podlubny, *Fractional differential equations: an introduction to fractional derivatives, fractional differential equations, to methods of their solution and some of their applications*, Academic Press, San Diego California, 1999b.
6. M. Tavakoli-Kakhki and M. Haeri, *Temperature control of a cutting process using fractional order proportional-integral-derivative controller*, *J. Dyn. Syst. Measure. Control* **133** (2011), no. 5, 51014.
7. I. Kheirizad, A. A. Jalali, and K. Khandani, *Stabilisation of unstable FOPDT processes with a single zero by fractional-order controllers*, *Int. J. Syst. Sci.* **44** (2013), no. 8, 1533–1545.
8. N. Fergani and A. Charef, *Process step response based fractional $PI^\lambda d^\mu$ controller parameters tuning for desired closed loop response*, *Int. J. Syst. Sci.* **47** (2016), no. 3, 521–532.
9. D. F. Novella-Rodríguez, B. D. M. Cuéllar, J. F. Márquez-Rubio, M. Á. Hernández-Pérez, and M. Velasco-Villa, *PD–PID controller for delayed systems with two unstable poles: a frequency domain approach*, *Int. J. Control* **92** (2019), no. 5, 1196–1208.
10. I. Kheirizad, K. Khandani, and A. A. Jalali, *Stabilisability analysis of high-order unstable processes by fractional-order controllers*, *Int. J. Control* **86** (2013b), no. 2, 244–252.
11. M. Bettayeb, R. Mansouri, U. Al-Saggaf, and I. M. Mehedi, *Smith predictor based fractional-order-filter PID controllers design for long time delay systems*, *Asian J. Control* **19** (2017), no. 2, 587–598.
12. P. Gholamin and A. H. Refahi Sheikhan, *Stabilization of a new commensurate/incommensurate fractional order chaotic system*, *Asian J. Control* **23** (2021), no. 2, 882–893.
13. K. A. Moornani and M. Haeri, *On robust stability of LTI fractional-order delay systems of retarded and neutral type*, *Automatica* **46** (2010a), no. 2, 362–368.
14. M. Ghorbani and M. Tavakoli-Kakhki, *Robust stability analysis of uncertain incommensurate fractional order quasi-polynomials in the presence of interval fractional orders and interval coefficients*, *Trans. Inst. Measurement Control* **43** (2021), no. 5, 1117–1125. <https://doi.org/10.1177/0123456789123456>
15. K. A. Moornani and M. Haeri, *On robust stability of linear time invariant fractional-order systems with real parametric uncertainties*, *ISA Trans.* **48** (2009), no. 4, 484–490.

16. M. Ghorbani and M. Tavakoli-Kakhki, *Robust stabilizability of fractional order proportional integral controllers for fractional order plants with uncertain parameters: a new value set based approach*, J. Vibr. Control **26** (2020b), no. 11–12, 965–975.
17. S. Sondhi and Y. V. Hote, *Relative stability test for fractional-order interval systems using kharitonov's theorem*, J. Control Autom. Electrical Syst. **27** (2016), no. 1, 1–9.
18. K. A. Moornani and M. Haeri, *Robust stability testing function and Kharitonov-like theorem for fractional order interval systems*, IET Control Theory Appl. **4** (2010b), no. 10, 2097–2108.
19. M. Ghorbani, *Robust stability analysis of interval fractional order plants by fractional order controllers: an approach to reduce additional calculation*, Int. J. Gen. Syst. **50** (2021), no. 1, 1–25.
20. Z. Gao, *Robust stabilization of interval fractional-order plants with one time-delay by fractional-order controllers*, J. Franklin Inst. **354** (2017), no. 2, 767–786.
21. M. Ghorbani and M. Tavakoli-Kakhki, *Robust stability analysis of a general class of interval delayed fractional order plants by a general form of fractional order controllers*, Math. Methods Appl. Sci. **44** (2021), no. 13, 10172–10189. <https://doi.org/10.1002/mma.7397>
22. J. Chen, M. N. Omidvar, M. Azad, and X. Yao, *Knowledge-based particle swarm optimization for PID controller tuning*, 2017 IEEE Congress on Evolutionary Computation (CEC), 2017, pp. 11819–1826.
23. Z. Bingul and O. Karahan, *Comparison of PID and FOPID controllers tuned by PSO and ABC algorithms for unstable and integrating systems with time delay*, Optim. Control Appl. Methods **39** (2018), no. 4, 1431–1450.
24. C. A. Monje, B. M. Vinagre, V. Feliu, and Y. Q. Chen, *Tuning and auto-tuning of fractional order controllers for industry applications*, Control Eng. Pract. **16** (2008), no. 7, 798–812.
25. A. Tepljakov, E. Petlenkov, and J. Belikov, *FOPID controller tuning for fractional FOPDT plants subject to design specifications in the frequency domain*, 2015 European Control Conference (ECC), 2015, pp. 3502–3507.
26. S. Tufenkci, B. Senol, and B. B. Alagoz, *Stabilization of fractional order PID controllers for time-delay fractional order plants by using genetic algorithm*, 2018 International Conference on Artificial Intelligence and Data Processing (IDAP), 2018, pp. 1–6.
27. Z. Wu, J. Viola, Y. Luo, Y. Q. Chen, and D. Li, *Robust fractional-order [proportional integral derivative] controller design with specification constraints: More flat phase idea*, Int. J. Control (2021), 1–19. <https://doi.org/10.1080/00207179.2021.1992498>
28. X. Yu, F. Yang, L. Ou, Q. Wu, and W. Zhang, *General stabilization method of fractional-order $PI^\lambda D^\mu$ controllers for fractional-order systems with time delay*, ISA Trans. **28** (2018), no. 16, 4999–5018.
29. R. Trivedi and P. K. Padhy, *Fractional order automatic tuning of $PI^\lambda D$ controller for stable processes*, ISA Trans. **99** (2020), 351–360.
30. P. Chen, Y. Luo, Y. Peng, and Y. Q. Chen, *Optimal robust fractional order $PI^\lambda D$ controller synthesis for first order plus time delay systems*, ISA Trans. **114** (2021), 136–149.
31. C. I. Muresan, A. Dutta, E. H. Dulf, Z. Pinar, A. Maxim, and C. M. Ionescu, *Tuning algorithms for fractional order internal model controllers for time delay processes*, Int. J. Control **89** (2016), no. 3, 579–593.
32. D.-J. Wang and X.-L. Gao, *Stability margins and H_∞ co-Design with fractional-order PI^λ Controllers*, Asian J. Control **15** (2013), no. 3, 691–697.
33. S. Zheng, X. Tang, and B. Song, *Graphical tuning method for non-linear fractional-order PID-type controllers free of analytical model*, Trans. Inst. Measure. Control **38** (2016), no. 12, 1442–1459.
34. Z. Gao, L.-R. Zhai, and Y.-D. Li, *Robust stabilizing regions of fractional-order PI^λ controllers for fractional-order systems with time-delays*, Int. J. Autom. Comput. **14** (2017), no. 3, 340–349.
35. S. E. Hamamci, *An algorithm for stabilization of fractional-order time delay systems using fractional-order PID controllers*, IEEE Trans. Autom. Control **52** (2007), no. 10, 1964–1969.
36. W. S. Levine, *The Control Handbook*, CRC Press, 1996.
37. J. W. Brown and R. V. Churchill, *Complex variables and applications eighth*, McGraw-Hill Book Company, 2009.
38. M. Busłowicz, *Stability of linear continuous-time fractional order systems with delays of the retarded type*, Bull. Polish Acad. Sci.: Techn. Sci. **56** (2008), no. 4, 319–324.
39. A. Oustaloup, F. Levron, B. Mathieu, and F. M. Nanot, *Frequency-band complex noninteger differentiator: characterization and synthesis*, IEEE Trans. Circ. Syst. I: Fundamental Theory Appl. **47** (2000), no. 1, 25–39.

AUTHOR BIOGRAPHIES



Majid Ghorbani received his BSc in control engineering from Sahand University of Technology, Tabriz, Iran, in 2013. Then, he obtained his MSc degree in control engineering from K. N. Toosi University of Technology, Tehran, Iran, in 2016. His research interests include fractional order control, and applications of fractional calculus in engineering, robust stability analysis of LTI systems with multiple time delays, nonlinear model predictive controllers and robust nonlinear control design.



Aleksei Tepljakov received the PhD degree in information and communication technology from the Tallinn University of Technology, in 2015. Since November 2021, he holds a Senior Research Scientist position at the Department of Computer Systems, School of Information Technologies, Tallinn University of Technology. His main research interests include the study of cyber-physical systems: fractional-order modeling and control of complex systems and developing efficient mathematical and 3D modeling methods for virtual and augmented reality for educational and industrial applications. He is a

Senior Member of the IEEE with more than 10 years of service. He has been a member of the IEEE Control Systems Society, since 2012, and the Education Society, since 2018.



Eduard Petlenkov is currently a Tenured Full Professor in the Department of Computer Systems, Tallinn University of Technology and the head of the Centre for Intelligent Systems. He received the BSc (2001), MSc (2003), and PhD (2007) degrees in computer and systems engineering from the Tallinn University of Technology. His main research interests include the domain of intelligent control, system analysis and computational intelligence.

How to cite this article: M. Ghorbani, A. Tepljakov, and E. Petlenkov, *Stabilizing region of fractional-order proportional integral derivative controllers for interval delayed fractional-order plants*, *Asian J Control* **25** (2023), 1145–1155. <https://doi.org/10.1002/asjc.2894>

Appendix 8

VIII

M. Ghorbani, A. Teplyakov, and E. Petlenkov. Fractional-order interval polynomials, stability and robust stability analysis and FOMCON implementation.² In *Proc. 2023 International Conference on Fractional Differentiation and Its Applications (ICFDA)*, pages 1–6, 2023.

²This paper was selected as the **Best Student Paper** at the ICFDA Conference.

Fractional-Order Interval Polynomials, Stability and Robust stability Analysis and FOMCON Implementation

1st Majid Ghorbani
Department of Computer Systems
Tallinn University of Technology
Tallinn, Estonia
majid.ghorbani@taltech.ee

2nd Aleksei Tepljakov
Department of Computer Systems
Tallinn University of Technology
Tallinn, Estonia
aleksei.tepljakov@taltech.ee

3rd Eduard Petlenkov
Department of Computer Systems
Tallinn University of Technology
Tallinn, Estonia
eduard.petlenkov@taltech.ee

Abstract—In this paper, a newly developed module for FOMCON toolbox for MATLAB that brings initial support for studying systems with interval uncertainties is introduced for the first time. The MATLAB class that corresponds to a fractional-order polynomial with interval uncertainties is implemented and endowed with basic functionality. Also, the robust stability checking procedure is implemented based on the class formulation as one of the methods by using the value set concept for fractional-order interval polynomials. The presented methods are applicable to both fractional-order polynomials of commensurate and non-commensurate. Moreover, the necessary and sufficient conditions are derived for robust stability analysis of such fractional-order interval polynomials. Finally, an example is provided to show the presented methodology.

Index Terms—Fractional-order polynomials, interval uncertainties, robust stability analysis.

I. INTRODUCTION

Fractional equations are being used in many disciplines such as mathematical biology, control engineering, signal processing, physics and son on [1], [2]. The stability is a fundamental requirement of control systems. Some useful stability criteria have been derived in [3]–[5]. Due to operating conditions and modelling errors the real systems may suffer from uncertainties. The interval uncertainty structure is one of the most popular ways for engineers to incorporate uncertainty into system models [6]. For such a kind of uncertain fractional-order polynomials, the zero exclusion condition theorem is one of the best way to check robust stability [7]. It is because that this theorem presents necessary and sufficient conditions for robust stability analysis and it is applicable to both fractional-order polynomials of commensurate and non-commensurate [8]. Therefore, some methods have been proposed to investigate the robust stability of fractional-order interval polynomials. For instance, in [9], a graphical method was proposed for robust stability analysis of fractional-order interval uncertainties. Moreover, the work [10] proposed an auxiliary function to facilitate the process of robust stability

assessment of such interval polynomials. Furthermore, in [11]–[13], the zero exclusion condition theorem has been employed to design robust fractional-order controllers.

In this paper, the FOMCON toolbox [14], [15] is developed to check the robust stability of fractional-order interval polynomials. Therefore, in Section II, a review of fractional-order interval polynomials is presented. In Section III, novel necessary and sufficient robust conditions are derived. The developed module for FOMCON toolbox is elaborately stated in Section IV. Moreover, an example is provided in Section V to explain how to use new MATLAB tools for robust stability analysis. Finally, Section VI has some concluding remarks.

II. PRELIMINARIES AND DEFINITIONS

In this paper, we will discuss the robust stability of a fractional-order interval system whose characteristic polynomials are as follows.

$$\Delta(s, \mathbf{q}) = \mathbf{q}_0 s^{\alpha_0} + \mathbf{q}_1 s^{\alpha_1} + \cdots + \mathbf{q}_n s^{\alpha_n}. \quad (1)$$

where $\alpha_i \in \mathbb{R}^+$ (\mathbb{R} and \mathbb{R}^+ respectively denote the set of real numbers and positive real numbers.) and $\alpha_0 = 0 < \alpha_1 < \alpha_2 < \cdots < \alpha_n$. Supposing that $\mathbf{q}_i, i = 0, 1, \dots, n$ are the interval coefficients as $\mathbf{q}_i \in [\underline{q}_i, \bar{q}_i]$ and $\mathbf{q}_n \neq 0$.

Now, the following definitions are introduced for the rest of the paper.

Definition 1: The principal branch of fractional-order interval polynomials $\Delta(s)$ in (1) is defined as a single-valued function $\Delta_{pb}(s, \mathbf{q}) : \mathbb{C} \rightarrow \mathbb{C}$ such that

$$\Delta_{pb}(s, \mathbf{q}) = \begin{cases} \mathbf{q}_0 + \sum_{r=1}^n \mathbf{q}_r |s|^{\alpha_r} e^{j\alpha_r \arg(s)}, & \text{for } s \neq 0, \\ \mathbf{q}_0, & \text{for } s = 0. \end{cases} \quad (2)$$

Definition 2: $\Delta(s, \mathbf{q})$ in (1) is of commensurate order γ if and only if $\gamma \in \mathbb{R}^+$ and $\frac{\alpha_i}{\gamma} \in \mathbb{N}$ for $i = 1, 2, \dots, n$ (\mathbb{N} is set of natural numbers.). Otherwise, the fractional-order interval polynomial $\Delta(s, \mathbf{q})$ is referred as incommensurate order.

Definition 3: Based on [3], a fractional-order system is stable if and only if the principal branch of the characteristic

This work was supported by the Estonian Research Council grant PRG658.

function of the system has no zero in the closed right-half plane. Therefore, a fractional-order system with the fractional-order interval polynomials $\Delta(s, \mathbf{q})$ in (1) is robust stable if and only if all members of $\Delta(s)$ have no zero in the closed right-half plane.

Zero Exclusion Condition Theorem: [7] $\Delta(s, \mathbf{q})$ in (1) is robust stable if and only if $\Delta(s, \mathbf{q})$ contains at least one stable polynomial and $0 \notin \Delta(s, \mathbf{q})$ for $\omega \in [0, +\infty)$.

According to this theorem, stability of one member of the family $\Delta(s, \mathbf{q})$ in (1) as $\delta(s)$ must be checked. So, the following lemma should be used for stability analysis.

Lemma 1: [5] (**Mikhailov stability criterion**) The fractional-order polynomial $\delta(s) = \hat{\mathbf{q}}_0 + \hat{\mathbf{q}}_1 s^{\alpha_1} + \dots + \hat{\mathbf{q}}_n s^{\alpha_n}$ (of commensurate or non-commensurate type) is stable if and only if

$$\Delta \arg \psi(j\omega) = \frac{\delta(j\omega)}{\hat{\mathbf{q}}_n (j\omega + c)^{\alpha_n}} = 0, -\infty < \omega < \infty, c \in \mathbb{R}^+. \quad (3)$$

Lemma 1 implies that $\delta(s)$ is stable if and only if $\psi(j\omega)$ does not encircle the origin of the complex plane as ω traverses from $-\infty$ to $+\infty$.

Now, to derive the necessary and sufficient robust conditions of the fractional-order interval system, the value set of $\Delta(s, \mathbf{q})$ in (1) must be checked. Just we need to investigate the zero exclusion condition $0 \notin \Delta(j\omega, \mathbf{q})$ and $\omega \geq 0$. Fortunately, the value set of $\Delta(j\omega, \mathbf{q})$ would be a convex shape in the complex plane as shown by the following lemma.

Lemma 2: [10] Consider the set $M = M_0 + \sum_{r=1}^m q_r e^{j\pi\gamma_r}$ where M_0 can be a complex/real number, $q_r \in [q_r^-, q_r^+]$, $0 \leq \gamma_0 < \gamma_1 < \gamma_2 < \dots < \gamma_m < 1$. Then, the value set of M is a convex parpolygon in the complex plane with the following $2m$ consecutive vertices:

$$v_k = \sum_{r=1}^{k-1} q_r^+ e^{j\pi\gamma_r} + \sum_{r=k}^m q_r^- e^{j\pi\gamma_r} + M_0, \\ v_{k+m} = \sum_{r=1}^{k-1} q_r^- e^{j\pi\gamma_r} + \sum_{r=k}^m q_r^+ e^{j\pi\gamma_r} + M_0, \quad k = 1, \dots, m. \quad (4)$$

Based on Lemma 2, the following procedure can be employed to obtain the vertices. In this procedure, the following notations are held: $\text{floor}(x)$ shows the largest integer less than or equal to $x \in \mathbb{R}$ and $\text{frac}(x) = x - \text{floor}(x)$.

Procedure 1: Assume that $H_0 = \{b : q_b < \bar{q}_b\}$ and $H_0 \neq \emptyset$. For $\omega = 0$, the value set of $\Delta(j0, \mathbf{q})$ is equal to $[\underline{\mathbf{q}}_0, \bar{\mathbf{q}}_0]$. For $\omega > 0$, define $\beta_0 = \{\text{frac}(0.5\alpha_b) : b \in H_0\}$. Also, assume that the distinct numbers of the set β_0 is m and these distinct members are $\beta_r, r = 1, \dots, m$ and sorted as $0 \leq \beta_1 < \beta_2 < \dots < \beta_m$. Now, define the following sets:

$$H_i = \{b \in H_0 : \text{floor}(0.5\alpha_b) \text{ is an even number} \\ \text{and } \text{frac}(0.5\alpha_b) = \beta_i\},$$

$$H'_i = \{b \in H_0 : \text{floor}(0.5\alpha_b) \text{ is an odd number} \\ \text{and } \text{frac}(0.5\alpha_b) = \beta_i\}, i = 1, 2, 3, \dots, m.$$

and the following vectors for $k = 1, 2, \dots, m$ and $b = 0, 1, \dots, n$:

$$\mathbf{q}^k = [\mathbf{q}_0^k \mathbf{q}_1^k \dots \mathbf{q}_n^k], \bar{\mathbf{q}} = [\bar{\mathbf{q}}_0 \bar{\mathbf{q}}_1 \dots \bar{\mathbf{q}}_n], \underline{\mathbf{q}} = [\underline{\mathbf{q}}_0 \underline{\mathbf{q}}_1 \dots \underline{\mathbf{q}}_n] \\ \mathbf{q}^{m+k} = [\mathbf{q}_0^{m+k} \mathbf{q}_1^{m+k} \dots \mathbf{q}_n^{m+k}] = \bar{\mathbf{q}} + \underline{\mathbf{q}} - \mathbf{q}^k, \\ q_b^k = \begin{cases} \bar{q}_b, & \text{if } b \in \left(\bigcup_{i=1}^{k-1} H_i\right) \cup \left(\bigcup_{i=k}^m H'_i\right), \\ \underline{q}_b, & \text{otherwise.} \end{cases} \\ q_b^{m+k} = \bar{q}_b + \underline{q}_b - q_b^k.$$

Then, the consecutive vertices $V_k(j\omega), k = 1, 2, \dots, 2m$ are defined as follows:

$$V_k(j\omega) = \Delta(j\omega, \mathbf{q}^k), V_{m+k}(j\omega) = \Delta(j\omega, \mathbf{q}^{m+k}). \quad (5)$$

Now, we should also use the following lemma which is valuable for simulation purposes.

Lemma 3: [10] All zeros of $\Delta(s, \mathbf{q})$ in (1) lie in the set $\{s \in \mathbb{C} : |s| \leq S_{\max}\}$ where S_{\max} is defined as follows.

$$S_{\max} = \left(\frac{\sum_{i=0}^{n-1} \max\{|\underline{q}_i|, |\bar{q}_i|\}}{\min\{|\underline{q}_n|, |\bar{q}_n|\}} \right)^{\frac{1}{\alpha_n - \alpha_{n-1}}}.$$

So, based on this lemma, the condition $0 \in \Delta(s, \mathbf{q})$ is only checked for the frequencies lying in the interval $[0, S_{\max}]$. Moreover, the following theorem is also needed to analyze the robust stability.

Value Sets Overlap Theorem: [16] Assume that $\Delta(s, \mathbf{q})$ can be written as $\Delta(s, \mathbf{q}) = \Delta^1(s, \mathbf{q}^1) + \Delta^2(s, \mathbf{q}^2)$. Then, at a given frequency $\omega = \omega_0$, $0 \in \Delta(j\omega_0, \mathbf{q})$ if and only if the value sets of $\Delta^1(j\omega_0, \mathbf{q}^1)$ and $-\Delta^2(j\omega_0, \mathbf{q}^2)$ have an overlap.

III. ROBUST STABILITY ANALYSIS

In this section, we derive necessary and sufficient conditions for robust stability analysis of the fractional-order interval polynomial $\Delta(s, \mathbf{q})$ in (1). Due to the programming purposes, a robust stability testing function should be constructed to check the zero exclusion condition easier. Indeed, by this auxiliary function, it can be derived if the boundary of the value set of $\Delta(j\omega, \mathbf{q})$ touches the origin in the complex. The auxiliary function introduced in the next lemma, is constructed by a few members of the uncertainty space of $\Delta(s, \mathbf{q})$ i.e., vertex polynomials for the robust stability assessment of both fractional-order interval polynomials of commensurate and non-commensurate.

Lemma 4: The fractional-order polynomial $\Delta(s, \mathbf{q})$ in (1) is robust stable if and only if:

- one member of the fractional-order interval polynomial is stable.
- the inequality $\Lambda_1(\omega) > 0$ holds for $\omega \in [0, S_{\max}]$.

$$\Lambda_1(\omega) = \min\{\lambda_r(\omega) : r = 1, 2, \dots, 2m, V_{2m+1}(j\omega) = V_1(j\omega)\}, \\ \lambda_r(\omega) = |V_r(j\omega)| + |V_{r+1}(j\omega)| - |V_r(j\omega) - V_{r+1}(j\omega)|. \quad (6)$$

Proof 1: According to the zero exclusion condition theorem and Lemma 3, we show that if $\Lambda_1(\omega) > 0$ holds then the origin

does not intersect the boundary of $\Delta(s, \mathbf{q})$ for all frequencies lying in $[0, S_{\max}]$. Indeed, the sufficient conditions can be simply proved by the triangle inequality. So, the necessary condition is only discussed in the following. As a contradiction argument, it is supposed that $\Lambda_1(\omega) > 0$ does not hold at a given frequency $\omega = \omega_0$ i.e., $\Lambda_1(\omega) = 0$. This means that there are at least one $\lambda_x(\omega_0), x \in \{1, \dots, 2m\}$ such that

$$\begin{aligned} |V_x(j\omega)| + |V_{x+1}(j\omega)| - |V_x(j\omega) - V_{x+1}(j\omega)| &= 0, \implies \\ |V_x(j\omega)| |V_{x+1}(j\omega)| + \text{real}(V_x(j\omega)V_{x+1}^*(j\omega)) &= 0 \end{aligned} \quad (7)$$

$\text{real}(C)$ and C^* denote the real part and the complex conjugate of the complex number C . From (7), it is visible that $V_x(j\omega_0)V_{x+1}^*(j\omega_0) \in \mathbb{R}^{\leq 0}$. Therefore, we only need to show that $V_x(j\omega_0)V_{x+1}^*(j\omega_0) \in \mathbb{R}^{\leq 0}$ leads to $0 \in \lambda V_x(j\omega_0) + (1 - \lambda)V_{x+1}(j\omega_0)$ and consequently $0 \in \partial(\Delta(j\omega, \mathbf{q}))$ ($\partial(\cdot)$ shows the boundary of a value set.). Therefore, we have

$$\begin{aligned} \lambda V_x(j\omega_0) + (1 - \lambda)V_{x+1}(j\omega_0) &= 0 \implies \\ \lambda V_x(j\omega_0)V_{x+1}^*(j\omega_0) + (1 - \lambda)|V_{x+1}(j\omega_0)|^2 &= 0 \end{aligned} \quad (8)$$

From (8), one can simply deduce $V_x(j\omega_0)V_{x+1}^*(j\omega_0) \in \mathbb{R}^{\leq 0}$. This implies $0 \in \partial(\Delta(j\omega, \mathbf{q}))$ and consequently $0 \in \Delta(j\omega_0, \mathbf{q})$. This contradicts the zero exclusion condition and the proof is completed. \square

Now, we take another approach to derive robust stability analysis. Indeed, $\Delta(s, \mathbf{q})$ in (1) can be rewritten as $\Delta(s, \mathbf{q}) = \Delta^1(s, \mathbf{q}^1) + \Delta^2(s, \mathbf{q}^2)$. For example, $\Delta(s, \mathbf{q}) = [1, 2]s^{1+\sqrt{5}} + [-1, 1]s^{\sqrt{5}} + [2, 4]s + [0.3, 1]$ can be written as $\Delta(s, \mathbf{q}) = \Delta^1(s, \mathbf{q}^1) + \Delta^2(s, \mathbf{q}^2)$ where $\Delta^1(s, \mathbf{q}^1) = [1, 2]s^{1+\sqrt{5}} + [-1, 1]s^{\sqrt{5}}$ and $\Delta^2(s, \mathbf{q}^2) = [2, 4]s + [0.3, 1]$ or $\Delta^1(s, \mathbf{q}^1) = [1, 2]s^{1+\sqrt{5}}$ and $\Delta^2(s, \mathbf{q}^2) = [-1, 1]s^{\sqrt{5}} + [2, 4]s + [0.3, 1]$ and so on. Now, the next lemma presents necessary and sufficient conditions for robust stability assessment of $\Delta(s, \mathbf{q})$ in (1).

Lemma 5: The fractional-order polynomial $\Delta(s, \mathbf{q})$ in (1) is robust stable if and only if:

- one member of the fractional-order interval polynomial is stable.
- the value sets of $\Delta^1(s, \mathbf{q}^1)$ and $-\Delta^2(s, \mathbf{q}^2)$ do not have any overlap for $s = j\omega$ and $\omega \in [0, S_{\max}]$.

Proof 2: The proof is directly from the value sets overlap theorem and the zero exclusion condition theorem.

Lemma 5 gives us a way to present another robust stability testing function in the following lemma. \square

Lemma 6: The fractional-order polynomial $\Delta(s, \mathbf{q})$ in (1) is robust stable if and only if:

- one member of the fractional-order interval polynomial is stable.

- the inequality $\Lambda_2(\omega) > 0$ holds for $\omega \in [0, S_{\max}]$.

$$\begin{aligned} \Lambda_2(\omega) &= \min\{\lambda_r^2(\omega) : r = 1, 2\}, \\ \lambda_1^2(\omega) &= \min\{\tilde{\lambda}_{r_1, r_2}^2(\omega) : r_1 = 1, \dots, 2m_1, \\ r_2 &= 1, \dots, 2m_2\}, \\ \tilde{\lambda}_{r_1, r_2}^2(\omega) &= |V_{r_1}^1(j\omega) + V_{r_2}^2(j\omega)| + \\ |V_{r_1+1}^1(j\omega) + V_{r_2+1}^2(j\omega)| - |V_{r_1}^1(j\omega) - V_{r_1+1}^1(j\omega)|, \quad (9) \\ \lambda_2^2(\omega) &= \min\{\tilde{\lambda}_{r_1, r_2}^2(\omega) : r_1 = 1, \dots, 2m_1, \\ r_2 &= 1, \dots, 2m_2\}, \\ \tilde{\lambda}_{r_1, r_2}^2(\omega) &= |V_{r_1}^1(j\omega) + V_{r_2}^2(j\omega)| + \\ |V_{r_1}^1(j\omega) + V_{r_2+1}^2(j\omega)| - |V_{r_2}^2(j\omega) - V_{r_2+1}^2(j\omega)|, \end{aligned}$$

where $V_{i_1}^1(j\omega), i_1 = 1, \dots, 2m_1$ and $V_{i_2}^2(j\omega), i_2 = 1, \dots, 2m_2$ show the vertices of the value set of $\Delta^1(s, \mathbf{q}^1)$ and $\Delta^2(s, \mathbf{q}^2)$ calculated by Procedure 1. Moreover, $V_{2m_1+1}^1(j\omega) = V_1^1(j\omega)$ and $V_{2m_2+1}^2(j\omega) = V_1^2(j\omega)$.

Proof 3: We show that if $\Lambda_2(\omega) > 0$ holds then the statements of Lemma 5 are satisfied. According to Lemma 4, $\tilde{\lambda}_{r_1, r_2}^2(\omega) > 0$ implies that the vertices $-V_{i_2}^2(j\omega), i_2 = 1, \dots, 2m_2$ do not intersect the value set of $\Delta^1(s, \mathbf{q}^1)$. In the same way, $\tilde{\lambda}_{r_1, r_2}^2(\omega) > 0$ assures that the vertices $V_{i_1}^1(j\omega), i_1 = 1, \dots, 2m_1$ do not intersect $-\Delta^2(s, \mathbf{q}^2)$. This means that convex polygons $\Delta^1(s, \mathbf{q}^1)$ and $-\Delta^2(s, \mathbf{q}^2)$ have no overlap for $\omega \in [0, S_{\max}]$ and based on Lemma 5, the robust stability is guaranteed. \square

Remark 1: In Lemmas 4-6, various necessary and sufficient conditions have been presented to inspect the robust stability of fractional-order interval polynomials $\Delta(s, \mathbf{q})$. All the results of the aforementioned lemmas are applicable to both fractional-order interval polynomials of commensurate and non-commensurate. Moreover, in Lemma 5, a graphical method has been proposed which may be arduous. So, we should use the auxiliary functions obtained in Lemma 4 and Lemma 6. Also, one can check the stability of a chosen member of $\Delta(s, \mathbf{q})$ by Lemma 1 as a suggestion.

IV. SOFTWARE IMPLEMENTATION

In the following section, a possible software implementation of the above items is presented. The implementation is a new development for the popular FOMCON toolbox for MATLAB [14]. The toolbox is currently one of the most popular toolboxes for fractional-order modeling and control, and the present contribution serves as the foundation for further development of a framework for studying systems with interval uncertainties, including integer-order and fractional-order models.

Concerning the placement of the current contribution into the toolbox architecture, the best fit for it is a new module dedicated to implementing Robust Control with fractional-order systems. The updated structure of the toolbox is depicted in Fig. 1.

In fact, the present contribution does not yet provide the ability to create, e.g., fractional-order transfer functions with

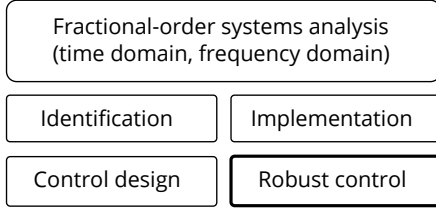


Fig. 1. The modules of FOMCON toolbox for MATLAB. The newly developed module for Robust Control is highlighted.

interval uncertainties, but what it does provide is a fundamental part of the implementation of a `ufotf` object, namely, a fractional-order polynomial with interval uncertainties.

Remark 2: The following examples should not be considered as an ultimate reference implementation. This FOMCON toolbox module is still under active development, and has not been released yet, available only for testing purposes. Consequently, some items, such as function calling sequences or class names may eventually change. However, the presented results may be useful to early adopters of these new features.

Remark 3: The original `fotf` object in FOMCON toolbox was implemented without introducing the concept of a fractional-order polynomial `fpoly` first, but with this development, in the upcoming major version of the toolbox the architecture may change to be consistent with the present development.

A. Formulation of the fractional-order polynomial with uncertainty intervals and related functionality

In the present contribution, the fundamental mathematical object is a fractional-order polynomial with uncertainties having the following form:

$$p(s) = [a_0, \bar{a}_0] s^{[\alpha_0, \bar{\alpha}_0]} + [a_1, \bar{a}_1] s^{[\alpha_1, \bar{\alpha}_1]} + \dots + [a_n, \bar{a}_n] s^{[\alpha_n, \bar{\alpha}_n]}, \quad (10)$$

where $[a_i, \bar{a}_i]$ denotes an uncertainty interval for the coefficient a_i , and $[\alpha_i, \bar{\alpha}_i]$ denotes the same for the exponent α_i . Furthermore, for generality, if in a given uncertain k th interval the limits are equal, i.e., $a_k = \bar{a}_k$, then the interval collapses to a fixed scalar value a_k . Finally, we assume that

$$a_i, \bar{a}_i, \alpha_i, \bar{\alpha}_i \in \mathbb{R}, \quad \forall i. \quad (11)$$

With these considerations, a class called `ufpoly` is designed in MATLAB, meaning “a fractional polynomial with uncertainty intervals”. The calling sequence to create the corresponding object can be

$$p = \text{ufpoly}(a, na)$$

where a is an $n \times 2$ matrix containing the lower and upper bounds for the n th coefficient, and na is a matrix having the exactly same dimensions as a and containing the lower and upper bounds for the n th exponent. Or, the polynomial can also be created in a more convenient way by passing a string:

$$p = \text{ufpoly}(\text{str})$$

In the latter case, the string may be, e.g.,

$$\text{str} = 's^{[1.5, 1.7]} + [1.2, 1.9]s^{0.2+10}';$$

which corresponds to the polynomial

$$s^{[1.5, 1.7]} + [1.2, 1.9]s^{0.2} + 10. \quad (12)$$

By default, the variable symbol is s , but it can be changed by providing the optional final argument to the call to `ufpoly`.

The following basic methods have been implemented for the class:

- `display` — the method by which the object is printed in the MATLAB Command Window.
- `eq(p1, p2)` — compare two `ufpoly` polynomials $p1$ and $p2$; they are considered equal only if corresponding matrices $a1$ and $a2$ have the same dimensions, all parameters in the matrices $a1$ and $a2$ and also in $na1$ and $na2$ are equal and `symb` is the same in both polynomials.
- `polyval(p, x)` — evaluate a sampled `ufpoly` object p (a fractional polynomial with fixed coefficients and exponents) at points specified in vector x and return a vector y . Running this on a fractional polynomial that has interval uncertainties results in an error.
- `sample(p)` — returns a *sample* (a member) of a set of fractional-order polynomials with interval uncertainties specified by p . By default, for each interval uncertainty, a value is sampled assuming a uniform distribution. Choosing other types of distributions are going to be eventually supported as well.
- `ufpoly2str(p)` — a convenience function that returns a string corresponding to the object p . This can be used, for example, to copy the string into word processing software such as \LaTeX for rendering the corresponding equation in a document.

Besides that, two additional utilities have been implemented to support the functionality related to parsing and generating strings representing the `ufpoly` object:

- `[a, na]=str2ufpoly(str)` — convert a string to two matrices a (matrix which holds the coefficient intervals), and na (matrix which holds the exponent intervals). The rules for formatting the string are described below.
- `ufpoly2str(a, na, symb, muls)` — convert a set of matrices a and na to a string. Optional arguments `symb` and `muls` represent the desired variable symbol, and the kind of multiplication sign to use (by default, the symbol is s , and the multiplication sign is omitted, i.e., `muls=''`).

The string parsers assumes the same format of the string as in (10) with the following additional conditions:

- Exponentiation signs \wedge are required.
- Multiplication signs $*$ are optional, the parser automatically detects multiplications.
- The intervals must be specified in square brackets $[]$.

- The lower and upper bounds in the uncertainty intervals may be separated by either a comma , (default and preferred method) or a semicolon ; .
- The minus sign appearing before an uncertainty interval is treated as a factor by which both lower and upper bounds are multiplied. So, for example, when the parser encounters an expression $-[2, 3]$, the expression is interpreted as $[-3, -2]$ which also emits a warning.
- Each term must have a unique exponent or a unique exponent interval. For example, using a string 's+s+[1, 2]' to create a `ufpoly` will fail.
- Only one variable is allowed, and is automatically inferred from the string.

These utilities may be used independently from the `ufpoly` object and hence may be generally useful to the user.

The current development version of the toolbox which has the above described features can be found in the `devel-ufotf` branch on the official GitHub repository [15].

B. Basic usage example

In this section, a basic usage example is provided based on the discussion above. The procedure for checking stability is described in a separate section. Suppose, that the object of study is a fractional-order polynomial with interval uncertainties defined as

$$[6, 21.5]s^{[1.5, 1.8]} + 5s^{[0.5, 0.7]} + [11, 19]. \quad (13)$$

Let us first define this fractional polynomial with uncertainty intervals in two different ways which are absolutely equivalent. The first way is to use a string:

```
pstr = ['[6,21.5]s^[1.5,1.8]' ...
        '+5s^[0.5,0.7]+[11,19]'];
p1 = ufpoly(pstr);
```

And the second way is to provide matrix definitions for the same:

```
a = [6, 21.5; 5 5; 11, 19];
na = [1.5, 1.8; 0.5, 0.7; 0 0];
p2 = ufpoly(a, na);
```

One can check whether the two objects are equivalent by simply doing

```
p1 == p2
```

which should result in a logical 1. To sample 100 members from the fractional-order polynomial with interval uncertainties one can run

```
m = {};
numSamples = 100;
for k=1:100, m{k} = sample(p1); end
```

Finally, to plot 1000 points of the magnitude response of all the sampled members in the frequency range between $[10^{-2}, 10^2]$ rad/s, one can do

```
figure; w = logspace(-2, 2, 1000);
for k=1:numSamples
    r = polyval(m{k}, sqrt(-1)*w);
    semilogx(w, 20*log10(abs(r)), 'b');
    hold on;
end
grid; xlabel('w [rad/s]');
ylabel('Magnitude [dB]');
t = sprintf('Magnitude response of %d'...
            ' members', numSamples);
title(t);
```

The resulting plot is shown in Fig. 2.

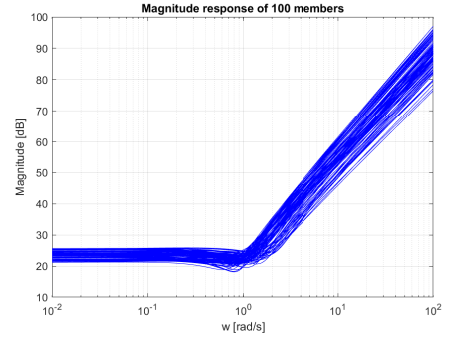


Fig. 2. The magnitude response of a randomly sampled member subset of 100 of the fractional-order polynomial with interval uncertainties in (13).

V. ROBUST STABILITY ASSESSMENT BY FOMCON TOOLBOX

In order to check the robust stability of a fractional-order interval polynomial as $\Delta(s, \mathbf{q})$ in (1) some steps should be performed. Therefore, we demonstrate these steps by an example. In [9], it has been shown that $\Delta(s, \mathbf{q}) = [6, 14] + [9, 12]s^{0.5} + [0.4, 1.6]s + [0.8, 1.2]s^{1.5} + s^2$ is robust stable (see Example 1 in [9]).

Step 1: Check the stability of one chosen member in the uncertainty space of $\Delta(s, \mathbf{q})$. We use Lemma 1 to check the stability of the following chosen member.

$$P = 6 + 9s^{0.5} + 0.4s + 0.8s^{1.5} + s^2. \quad (14)$$

Hence, at first, the polynomial P in (14) can be defined by `ufpoly` tool as follows.

```
P = ufpoly('6+9s^0.5+0.4s+0.8s^1.5 +s^2')
```

A method `mikhailovfo` has been provided to check the *Mikhailov stability criterion* (see Lemma 1). So, by typing `mikhailovfo(P)`, the Mikhailov's resulting plot is depicted as Fig. 3. Therefore, the stability of the polynomial P can be inferred from this figure and *Mikhailov stability criterion* in Lemma 1. Surely, if the chosen member P is unstable then there is no need to perform next step. Since, the interval polynomial cannot be robustly stable.

Step 2: Lemma 4 and Lemma 6 have presented two different robust stability checking functions. Hence, the user can select

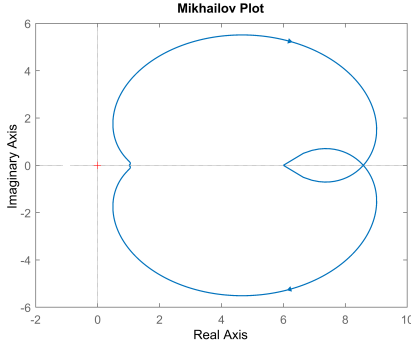


Fig. 3. Mikhailov'plot for the fractional-order polynomial P in (14).

one of the methods as stated in the following.

For those who want to check the robust stability by Lemma 4, `robstabf01` tool has been provided. As discussed earlier, the fractional-order interval polynomial $\Delta(s, \mathbf{q})$ can be made by `ufpoly` tool as follows.

```
Delta=ufpoly(' [6, 14]+[9,12]s^0.5+
[0.4,1.6]s + [0.8,1.2]s^1.5 + s^2')
s^2)+[0.8, 1.2]s^{1.5}+[0.4, 1.6]s+
[9, 12]s^{0.5}+[6, 14]
Fractional polynomial with uncertainty
intervals.
```

Now, by typing `robstabf01(Delta)` in command window we have:

```
robstabf01(Delta)
"robustly stable"
```

This shows that all members of the interval polynomial $\Delta(s, \mathbf{q})$ are robust stable.

For those who want to check the robust stability by Lemma 6, `robstabf02` tool has been provided. At first the interval polynomials $\Delta^1(s, \mathbf{q}^1)$ and $\Delta^2(s, \mathbf{q}^2)$ should be selected. For this example, we consider $\Delta^1(s, \mathbf{q}^1) = [6, 14] + [9, 12]s^{0.5}$ and $\Delta^2(s, \mathbf{q}^2) = [0.4, 1.6]s + [0.8, 1.2]s^{1.5} + s^2$. Then by `ufpoly` tool, the both interval polynomials can be defined as follows.

```
Delta1=ufpoly(' [6, 14]+[9,12]s^0.5')
[9, 12]s^{0.5}+[6, 14]
Fractional polynomial with uncertainty
intervals.
Delta2=ufpoly(' [0.4,1.6]s + [0.8,1.2]s^1.5
+ s^2')
s^2)+[0.8, 1.2]s^{1.5}+[0.4, 1.6]s
Fractional polynomial with uncertainty
intervals.
```

`robstabf02` tool can be used to check the robust stability of $\Delta(s, \mathbf{q})$ as follows.

```
robstabf02(Delta1,Delta2)
"robustly stable"
```

So, the robust stability is also verified by this method.

VI. CONCLUSIONS

Robust stability analysis of fractional-order interval polynomials was studied in the present paper. To focus on the simplicity of the criteria, two robust stability checking functions were provided. The presented solution shall also be included in FOMCON toolbox—which is a popular MATLAB/Simulink toolbox for working with fractional-order systems and controls. That way, the results presented in this work will be made available to the community of research scholars and practitioners working in the area of fractional-order systems.

REFERENCES

- [1] R. Hilfer, "Applications of fractional calculus in physics," World scientific, 2000.
- [2] C. A. Monje, Y. Q. Chen, B. M. Vinagre, D. Xue, and V. Feliu-Battle, "Fractional-order systems and controls: fundamentals and applications," 2010.
- [3] C. Bonnet, and J. R. Partington, "Coprime factorizations and stability of fractional differential systems," *Systems & Control Letters*, vol. 41, no. 3, pp. 167–174, 2000.
- [4] C. Hwang, and Y. C. Cheng, "A numerical algorithm for stability testing of fractional delay systems," *Automatica*, vol. 42, no. 5, pp. 825–831, 2006.
- [5] M. Buslowicz, "Stability of linear continuous-time fractional order systems with delays of the retarded type," *Bulletin of the Polish Academy of Sciences: Technical Sciences*, vol. 56, no. 4, pp. 319–324, 2008.
- [6] M. Ghorbani, M. Tavakoli-Kakhki, and A. Tepljakov, and E. Petlenkov, "Robust stability analysis of smith predictor based interval fractional-order control systems: A case study in level control process," *IEEE/CAA Journal of Automatica Sinica*, DOI: 10.1109/JAS.2022.105986, 2022.
- [7] K. Akbari Moornani and M. Haeri, "On robust stability of LTI fractional-order delay systems of retarded and neutral type," *Automatica*, vol. 46, no. 2, pp. 362–368, 2010.
- [8] K. Akbari Moornani and M. Haeri, "On robust stability of linear time invariant fractional-order systems with real parametric uncertainties," *ISA transactions*, vol. 48, no. 4, pp. 484–490, 2009.
- [9] N. Tan, Ö. Özgüven, and M. M. Özyetkin, "Robust stability analysis of fractional order interval polynomials," *ISA transactions*, vol. 48, no. 2, pp. 166–172, 2009.
- [10] K. Akbari Moornani, and M. Haeri, "Robust stability analysis of fractional order interval polynomials," *IET control theory & applications*, vol. 4, no. 10, pp. 2097–2108, 2010.
- [11] D. Casagrande, W. Krajewski, and U. Viaro, "On the robust stability of commensurate fractional-order systems," *Journal of the Franklin Institute*, vol. 359, no. 11, pp. 5559–5574, 2022.
- [12] M. Ghorbani, A. Tepljakov, and E. Petlenkov, "Robust FOPID Stabilization for Smith Predictor Structures," 2022 IEEE 61st Conference on Decision and Control (CDC), pp. 1696–1701, 2022.
- [13] M. Asadi, A. Farnam, H. Nazifi, S. Roozbehani, and G. Crevecoeur, "Robust Stability Analysis of Unstable Second Order Plus Time-Delay (SOPTD) Plant by Fractional-Order Proportional Integral (FOPI) Controllers," *Mathematics*, vol. 10, no. 4, pp. 567, 2022.
- [14] A. Tepljakov, FOMCON Toolbox for MATLAB on MathWorks File Exchange. [Online]. Available: <https://se.mathworks.com/matlabcentral/fileexchange/66323-fomcon-toolbox-for-matlab>. Retrieved January 25, 2023.
- [15] A. Tepljakov, FOMCON Toolbox for MATLAB: development branch for the uncertainty modeling features. [Online]. Available: <https://github.com/extall/fomcon-matlab/tree/devel-ufotf>. Retrieved January 25, 2023.
- [16] M. Ghorbani, M. Tavakoli-Kakhki, A. Tepljakov, E. Petlenkov, A. Farnam, and G. Crevecoeur, "Robust stability analysis of interval fractional-order plants with interval time delay and general form of fractional-order controllers," *IEEE Control Systems Letters*, vol. 6, pp. 1268–1273, 2021.

Appendix 9

IX

M. Ghorbani, A. Tepljakov, and E. Petlenkov. Robust d-stability analysis of fractional-order controllers. In *Proc. 2023 American Control Conference (ACC)*, pages 3871–3876, 2023.

Robust \mathcal{D} -Stability Analysis of Fractional-Order Controllers

Majid Ghorbani, Aleksei Tepljakov (*Senior Member, IEEE*), Eduard Petlenkov

Abstract—This paper focuses on analyzing the robust \mathcal{D} -stability of fractional-order systems having uncertain coefficients using fractional-order controllers. Robust \mathcal{D} -stability means that each polynomial in a family of an uncertain fractional-order system has all its roots in a prescribed region of the complex plane. By employing the concept of the value set, two distinct methodologies are introduced for scrutinizing the robust \mathcal{D} -stability of the system. Although the outcomes of both approaches are equivalent, their computational appeal may differ. The first approach entails a graphical technique for the analysis of robust \mathcal{D} -stability, while the second approach furnishes a robust \mathcal{D} -stability testing function based on the shape properties of the value set, thereby establishing necessary and sufficient conditions for verifying the robust \mathcal{D} -stability of fractional-order systems using fractional-order controllers. Finally, a numerical example is provided to validate the results presented in this paper.

I. INTRODUCTION

In contemporary engineering disciplines, fractional calculus has become pervasive, particularly in the field of control systems engineering. This is due to the fact that fractional-order operators have the potential to yield more precise models of physical systems, thereby enhancing their descriptive capacity [1], [2] and upon conducting a meticulous comparison between controllers designed using the same methods, fractional-order controllers have demonstrated superior performance in relation to their integer-order counterparts [3], [4], [5].

In the realm of practical applications, it is an inescapable reality that real-world systems frequently harbor uncertainties. To effectively accommodate these uncertainties, an interval uncertainty structure can be deemed a viable approach. Specifically, these uncertain systems are postulated to encompass a set of unknown parameters whose values exist within the confines of two discernible bounds [6], [7], [8]. Given the inevitability of discrepancies between the identified model and the actual underlying process, the robust stability analysis and performance enhancement measures become indispensable prerequisites for real-world systems [9].

The robust stability of fractional-order systems has been checked by means of Linear Matrix Inequality (LMI) in [11], [12] in the time domain. Whilst the use of LMI approaches can be advantageous in the analysis of control systems, it is crucial to note that they are prone to amplified conservatism.

This work was supported by the Estonian Research Council grant PRG658.

The Authors are with Department of Computer Systems, Tallinn University of Technology, Estonia (e-mail: majid.ghorbani@taltech.ee ; aleksei.tepljakov@taltech.ee ; eduard.petlenkov@taltech.ee).

Furthermore, their applicability is limited to systems of commensurate order, thereby constraining their utility in more intricate scenarios. [13]. Novel techniques in the frequency-domain have been presented in [14] for robust stability of uncertain fractional-order systems by the value set concept. Furthermore, it has been demonstrated that the necessary and sufficient criteria obtained in [14] are universally applicable to fractional-order systems, regardless of whether their orders are commensurate or incommensurate. As a result of its ability to facilitate the robust stability analysis of systems marked by inherent uncertainties, the value set approach has garnered considerable attention from a diverse range of researchers [15], [16], [17]. Inspired by the polynomial vertices proposed in [14], the robust stability of uncertain delayed fractional-order systems has been also developed in [18], [19], [20].

The principal objective of the current manuscript is to furnish a robust \mathcal{D} -stability method for closed-loop control systems of fractional order, which accounts for the influence of fractional-order controllers and uncertain fractional-order plants. Furthermore, it has been determined that the proposed robust \mathcal{D} -stability framework exhibits utility beyond the realm of stability analysis, and can engender improved performance in control systems. In other words, the advantages conferred by robust \mathcal{D} -stability are not restricted to the preservation of system stability, but extend to the augmentation of its overall performance [22]. The aforementioned observation is attributable to the fact that every root of the characteristic function of the system is situated within a specific region of the complex plane. This noteworthy revelation serves to underscore the vast potential of robust \mathcal{D} -stability in a variety of control system applications. Despite the enormous potential of the tool of robust \mathcal{D} -stability in the field of control systems engineering, numerous challenges continue to persist in this area of research. Among these obstacles is the determination of whether a fractional-order controller, such as Fractional-Order Proportional Integral Derivative (FOPID) controllers, FOPD, FOPI, or fractional-order lead-lag controllers, is capable of ensuring the robust \mathcal{D} -stability of the closed-loop control system.

In this paper, with the above-mentioned motivation, two different approaches are presented to check the robust \mathcal{D} -stability of fractional-order control closed-loop systems by fractional-order controllers. Therefore, he/she can utilize one of the approaches for robust \mathcal{D} -stability analysis of the system. It is notable that the only difference of the approaches is the computational point of view. Moreover, in each approach, at first, a graphical method is proposed for robust \mathcal{D} -stability analysis. Since, the graphical method may

tend to be cumbersome, a robust \mathcal{D} -stability testing function is then proposed by exploiting some certain polynomials and this obviates the use of numerous polynomials of a family of fractional-order systems. Consequently, the robust \mathcal{D} -stability can be only determined by finite polynomials of the uncertain system. Moreover, an upper frequency bound needed to plot the curve of the robust \mathcal{D} -stability testing function is provided.

The present paper is methodically structured as follows: In Section II, the problem at hand is precisely and rigorously formulated, employing advanced mathematical techniques. Foundations of robust \mathcal{D} -stability analysis are constructed in Section III. In Section IV provides the numerical evaluation of the results. Finally, conclusion remarks are given in Section V.

II. PRELIMINARIES

Notations. Suppose $\sum_{i=r_1}^{r_2} u_i = 0$ for $r_2 < r_1$ and $\bigcup_{i=r_1}^{r_2} U_i = \emptyset$ for $r_2 < r_1$. Also, $\partial(F)$ shows the boundary of the value set U in the complex plane. $e(u_1, u_2) \triangleq \eta u_1 + (1-\eta)u_2$, $\eta \in [0, 1]$ for any two complex numbers u_1 and u_2 . $n(H)$ signifies the number of the distinct members of the set H . $\text{floor}(x)$ is also the largest integer less than or equal to $x \in \mathbb{R}$. $\text{frac}(x) \triangleq x - \text{floor}(x)$ for all $x \in \mathbb{R}$. Consider a general fractional-order controller defined as follows:

$$C(s) = \frac{N_C(s)}{D_C(s)} = \frac{\sum_{i_n=0}^{n_C} b_{i_n}^C s^{\beta_{i_n}^C}}{\sum_{i_d=0}^{d_C} a_{i_d}^C s^{\alpha_{i_d}^C}}, \quad (1)$$

in which the coefficients $b_{i_n}^C$ and $a_{i_d}^C$ are real numbers and $\beta_{n_C}^C > \beta_{n_C-1}^C > \dots > \beta_1^C > \beta_0^C = 0$ and $\alpha_{d_C}^C > \alpha_{d_C-1}^C > \dots > \alpha_1^C > \alpha_0^C = 0$. Also, the transfer function of the fractional-order plant is represented by

$$P(s) = \frac{N_P(s)}{D_P(s)} = \frac{\sum_{r_n=0}^{n_P} b_{r_n}^P s^{\beta_{r_n}^P}}{\sum_{r_d=0}^{d_P} a_{r_d}^P s^{\alpha_{r_d}^P}}. \quad (2)$$

In (2), let $b_{r_n}^P$ and $a_{r_d}^P$ be unknown lying between the two known bounds $b_{r_n}^P \in [b_{r_n}^{P-}, b_{r_n}^{P+}]$ and $a_{r_d}^P \in [a_{r_d}^{P-}, a_{r_d}^{P+}]$, $a_{d_P}^P \neq 0$. Moreover, the orders satisfy $\beta_{n_P}^P > \beta_{n_P-1}^P > \dots > \beta_1^P > \beta_0^P = 0$ and $\alpha_{d_P}^P > \alpha_{d_P-1}^P > \dots > \alpha_1^P > \alpha_0^P = 0$, $\alpha_{d_P}^P > \beta_{n_P}^P$ and $\alpha_{d_P}^P + \alpha_{d_C}^C > \beta_{n_P}^P + \beta_{n_C}^C$. Assume that the characteristic function of the closed-loop control system is $H(s) = D_C(s)D_P(s) + N_C(s)N_P(s)$. This paper aims to explore the robust \mathcal{D} -stability of systems with the characteristic function $H(s)$ in the presence of uncertainties.

Definition 1: It is assumed that the set \mathcal{D} is a symmetrical set with respect to the real axis.

Lemma 1: [14] Consider the set $M = M_0 + \sum_{r=1}^m q_r e^{j\pi\gamma_r}$ where M_0 can be a complex/real number, $q_r \in [q_r^-, q_r^+]$, $0 \leq \gamma_0 < \gamma_1 < \gamma_2 < \dots < \gamma_m < 1$. Then, the value set of M is a convex parpolygon in the complex plane with the

following $2m$ consecutive vertices:

$$\begin{aligned} v_k &= \sum_{r=1}^{k-1} q_r^+ e^{j\pi\gamma_r} + \sum_{r=k}^m q_r^- e^{j\pi\gamma_r} + M_0, \\ v_{k+m} &= \sum_{r=1}^{k-1} q_r^- e^{j\pi\gamma_r} + \sum_{r=k}^m q_r^+ e^{j\pi\gamma_r} + M_0, \quad k = 1, \dots, m. \end{aligned} \quad (3)$$

III. MAIN RESULTS

Robust \mathcal{D} -stability analysis of the system on the assumption that there are parametric uncertainties in this system is discussed in this section. Our main results are based on the following lemma specifying necessary and sufficient conditions of robust \mathcal{D} -stability problem.

Lemma 2: The fractional-order polynomial family $H(s)$ is robust \mathcal{D} -stable if and only if $H(s)$ contains at least one robust \mathcal{D} -stable polynomial and $0 \notin H(s)$, $\{s \in \partial D | \text{Im}(s) \geq 0, B_{\min} \leq |s| \leq B_{\max}\}$ where B_{\min} and B_{\max} are as follows.

$$\begin{aligned} B_{\max} &= \max\left\{1, \left(\frac{B_1 + B_2 + B_3}{B_4}\right)^{\frac{1}{\alpha_{d_P}^P + \alpha_{d_C}^C - \beta_0}}\right\}, \\ B_0 &= \max\{\alpha_{d_P-1}^P + \alpha_{d_C}^C, \alpha_{d_P}^P + \alpha_{d_C-1}^C, \beta_{n_P}^P + \beta_{n_C}^C\}, \\ B_1 &= \left(\sum_{i_d=0}^{d_C} |a_{i_d}^C|\right) \left(\sum_{r_d=0}^{d_P-1} \max\{|a_{r_d}^{P-}|, |a_{r_d}^{P+}|\}\right), \\ B_2 &= \left(\sum_{i_d=0}^{d_C-1} |a_{i_d}^C|\right) (\max\{|a_{d_P}^{P-}|, |a_{d_P}^{P+}|\}), \\ B_3 &= \left(\sum_{i_n=0}^{n_C} |b_{i_n}^C|\right) \left(\sum_{r_n=0}^{n_P} \max\{|b_{r_n}^{P-}|, |b_{r_n}^{P+}|\}\right), \\ B_4 &= |a_{d_C}^C| \min\{|a_{d_P}^{P-}|, |a_{d_P}^{P+}|\}, \\ B_{\min} &= \min\left\{1, \left(\frac{A_1}{\sum_{i=2}^7 A_i}\right)^{\frac{1}{\lambda_0}}\right\}, \\ A_0 &= \min\{\alpha_1^P, \alpha_1^C, \beta_1^P, \beta_1^C\}, \\ A_1 &= \begin{cases} A_1^1, & \text{if } 0 \notin [a_0^{P-}, a_0^{P+}] \text{ and } A_1^1 > 0, \\ A_1^2, & \text{if } 0 \notin [b_0^{P-}, b_0^{P+}] \text{ and } A_1^2 > 0, \\ 0, & \text{otherwise,} \end{cases} \\ A_1^1 &= \min\{|a_0^{P-}|, |a_0^{P+}|\} |a_0^C| - \max\{|b_0^{P-}|, |b_0^{P+}|\} |b_0^C|, \\ A_1^2 &= \min\{|b_0^{P-}|, |b_0^{P+}|\} |b_0^C| - \max\{|a_0^{P-}|, |a_0^{P+}|\} |a_0^C|, \\ A_2 &= \left(\sum_{i_d=1}^{d_C} |a_{i_d}^C|\right) \left(\sum_{r_d=1}^{d_P} \max\{|a_{r_d}^{P-}|, |a_{r_d}^{P+}|\}\right), \\ A_3 &= (|a_0^C|) \left(\sum_{r_d=1}^{d_P} \max\{|a_{r_d}^{P-}|, |a_{r_d}^{P+}|\}\right), \\ A_4 &= \left(\sum_{i_d=1}^{d_C} |a_{i_d}^C|\right) (\max\{|a_0^{P-}|, |a_0^{P+}|\}), \\ A_5 &= \left(\sum_{i_n=1}^{n_C} |b_{i_n}^C|\right) \left(\sum_{r_n=1}^{n_P} \max\{|b_{r_n}^{P-}|, |b_{r_n}^{P+}|\}\right), \end{aligned} \quad (5)$$

$$A_6 = |b_0^C| \left(\sum_{r_n=1}^{n_P} \max\{|b_{r_n}^{P-}|, |b_{r_n}^{P+}|\} \right),$$

$$A_7 = \left(\sum_{i_n=1}^{n_C} |b_{i_n}^C| \right) (\max\{|b_0^{P-}|, |b_0^{P+}|\}).$$

Proof: The demonstration of this statement can be attained through the application of the Zero Exclusion Principle, as outlined in [23]. Hence, in the following, the upper bound B_{max} is only proven. By assuming $|s| > 1$, it is shown that $0 \notin H(s)$ for $|s| \leq B_{max}$. Based on the triangle inequality, we have:

$$\begin{aligned} |H(s)| &\geq B_4 |s|^{\alpha_{d_P}^P + \alpha_{d_C}^C} - \\ &\left(\left(\sum_{i_d=0}^{d_C} |a_{i_d}^C| |s|^{\alpha_{i_d}^C} \right) \left(\sum_{r_d=0}^{d_P-1} \max\{|a_{r_d}^{P-}|, |a_{r_d}^{P+}|\} |s|^{\alpha_{r_d}^P} \right) + \right. \\ &\left. \left(\sum_{i_d=0}^{d_C-1} |a_{i_d}^C| |s|^{\alpha_{i_d}^C + \alpha_{d_P}^P} \right) (\max\{|a_{d_P}^{P-}|, |a_{d_P}^{P+}|\}) + \right. \\ &\left. \left(\sum_{i_n=0}^{n_C} |b_{i_n}^C| |s|^{\beta_{i_n}^C} \right) \left(\sum_{r_n=0}^{n_P} \max\{|b_{r_n}^{P-}|, |b_{r_n}^{P+}|\} |s|^{\beta_{r_n}^P} \right) \right) \\ &\geq B_4 |s|^{\alpha_{d_P}^P + \alpha_{d_C}^C} - \\ &\left(\left(\sum_{i_d=0}^{d_C} |a_{i_d}^C| |s|^{\alpha_{i_d}^C} \right) \left(\sum_{r_d=0}^{d_P-1} \max\{|a_{r_d}^{P-}|, |a_{r_d}^{P+}|\} |s|^{\alpha_{r_d}^P - 1} \right) + \right. \\ &\left. \left(\sum_{i_d=0}^{d_C-1} |a_{i_d}^C| |s|^{\alpha_{i_d}^C - 1 + \alpha_{d_P}^P} \right) (\max\{|a_{d_P}^{P-}|, |a_{d_P}^{P+}|\}) + \right. \\ &\left. \left(\sum_{i_n=0}^{n_C} |b_{i_n}^C| |s|^{\beta_{i_n}^C} \right) \left(\sum_{r_n=0}^{n_P} \max\{|b_{r_n}^{P-}|, |b_{r_n}^{P+}|\} |s|^{\beta_{r_n}^P} \right) \right) \\ &\geq B_4 |s|^{B_0} \left(|s|^{\alpha_{d_P}^P + \alpha_{d_C}^C - B_0} - \frac{B_1 + B_2 + B_3}{B_4} \right). \end{aligned} \quad (6)$$

From (6), it is clear that for $|s| > B_{max}$ the inequality $|H(s)| > 0$ is held and consequently one can conclude that $0 \notin H(s)$. For $|s| < B_{min}$, the conclusion $0 \notin H(s)$ is derived in the same way. ■

The ensuing subsections proffer two distinct methodologies for addressing the robust \mathcal{D} -stability problem of $H(s)$, utilizing the zero exclusion principle elucidated in Lemma 2.

A. First Approach for Robust \mathcal{D} -Stability Analysis

Initially, we shall present the following definition:

Definition 2: Assume that for the polynomial $N_P(s)$, the following vertex polynomials $V_i^N(s)$, $i = 1, 2, \dots, 2^{n_P+1}$:

$$\begin{cases} V_1^N(s) = b_0^{P-} + b_1^{P-} s^{\beta_1^P} + \dots + b_{n_P}^{P-} s^{\beta_{n_P}^P}, \\ V_2^N(s) = b_0^{P+} + b_1^{P-} s^{\beta_1^P} + \dots + b_{n_P}^{P-} s^{\beta_{n_P}^P}, \\ \vdots \\ V_{2^{n_P+1}}^N(s) = b_0^{P+} + b_1^{P+} s^{\beta_1^P} + \dots + b_{n_P}^{P+} s^{\beta_{n_P}^P}. \end{cases} \quad (7)$$

Furthermore, let us define the exposed edges $P_E^N(s)$, which consist of $(n_P + 1)2^{n_P}$ edges linking the vertex polynomials that share identical structures, but vary only with respect to

the parameter b_i^P , as illustrated in (8).

$$\begin{aligned} P_E^N(s) &= \{\eta V_1^N(s) + (1 - \eta) V_2^N(s), V_1^N(s) + \\ &(1 - \eta) V_3^N(s), \dots, V_{2^{n_P+1}-1}^N(s) + (1 - \eta) V_{2^{n_P+1}}^N(s)\}. \end{aligned} \quad (8)$$

Likewise, the vertex polynomials and the edges of $D_P(s)$ are considered as $V_i^D(s)$, $i = 1, 2, \dots, 2^{d_P+1}$ and $P_E^D(s)$.

Theorem 1: The system is robust \mathcal{D} -stable, if and only if:

- $H(s)$ has at least one robust \mathcal{D} -stable polynomial,
- The value sets $-N_C(s)P_E^N(s)$ and $D_C(s)P_E^D(s)$ do not have any overlap for $\{s \in \partial D | \text{Im}(s) \geq 0, B_{min} \leq |s| \leq B_{max}\}$.

Proof: It is proven by the zero exclusion principle in Lemma 2. Based on Lemma 1, it is obvious that the value set of $N_P(s)$ and $D_P(s)$ would be convex parpolygon shapes in the complex plane. Also, from Definition 2, it can be derived that $\partial N_C(s) \subseteq P_E^N(s)$ and $\partial D_C(s) \subseteq P_E^D(s)$. Now, the proof of necessary and sufficient conditions in statement 2 of the theorem is provided as follows.

The ‘if’ portion: Assume that $-N_C(s)P_E^N(s)$ and $D_C(s)P_E^D(s)$ contains an overlap at $s = z_0$. Then, it can be concluded that $Z_0 = D_C(s)\hat{D}_P(s) = -N_C(s)\hat{N}_P(s)$ and Z_0 is an arbitrary complex number in the complex plane and $\hat{D}_P(s)$ and $\hat{N}_P(s)$ are respectively two members of the family $D_P(s)$ and $N_P(s)$. This implies that $\hat{H}(z_0) = D_C(z_0)\hat{D}_P(z_0) + N_C(z_0)\hat{N}_P(z_0)$ is equal to zero or $\hat{H}(z_0) = 0$ and it contradicts the condition $0 \notin H(s)$ (see Lemma 2).

The ‘only if’ portion: Since, the system is robust \mathcal{D} -stable, then from Lemma 2, it is deduced that $0 \notin H(s)$. Now, assume that $Z_1 \in -N_C(s)P_E^N(s)$ and $Z_2 \in D_C(s)P_E^D(s)$ at $s = z_0$. Because of $0 \notin H(z)$, $Z_2 - Z_1 \neq 0$. Therefore, Z_1 cannot be equal to Z_2 or $Z_2 \neq Z_1$. Consequently, the second statement of theorem is also met. ■

Now, based on Theorem 1 and some interesting features of convex polygons, the following theorem is presented to simply assess the robust \mathcal{D} -stability of the system.

Theorem 2: The system is robust \mathcal{D} -stable, if and only if:

- $H(s)$ contains at least one robust \mathcal{D} -stable polynomial,
- the polynomials $H_N^{r_1}(s) = D_C(s)D_P(s) + N_C(s)V_{r_1}^N(s)$ ($r_1 = 1, 2, \dots, 2^{n_P+1}$) and $H_D^{r_2}(s) = D_C(s)V_{r_2}^D(s) + N_C(s)N_P(s)$ ($r_2 = 1, 2, \dots, 2^{d_P+1}$) are also robust \mathcal{D} -stable polynomials.

Proof: It is shown that robust \mathcal{D} -stability of the polynomials $H_N^{r_1}(s)$ and $H_D^{r_2}(s)$ are equivalent to not having the overlap between the value sets $-N_C(s)P_E^N(s)$ and $D_C(s)P_E^D(s)$ for $s \in \partial D$, $\text{Im}(s) \geq 0$.

The ‘if’ portion: Since, the polynomials $H_N^{r_1}(s)$ and $H_D^{r_2}(s)$ are robust \mathcal{D} -stable, then $0 \notin H_N^{r_1}(s)$ and $0 \notin H_D^{r_2}(s)$ and this implies that

$$\begin{cases} -N_C(s)V_{r_1}^N(s) \notin D_C(s)D_P(s), \\ D_C(s)V_{r_2}^D(s) \notin -N_C(s)N_P(s). \end{cases} \quad (9)$$

From (9), it is deduced that the value sets $-N_C(s)P_E^N(s)$ and $D_C(s)P_E^D(s)$ would not have any overlap for $s = z_0$. Because, no vertices of the convex polygons $-N_C(s)P_E^N(s)$

and $D_C(s)P_E^D(s)$ are located in each other.

The ‘only if’ portion: To establish the ‘only if’ part, we assume that the value sets $-N_C(s)P_E^N(s)$ and $D_C(s)P_E^D(s)$ have an overlap for $s = z_0$. Then, there is at least one vertex polynomial such that $-N_C(s)V_{r_1}^N(s) \in D_C(s)P_E^D(s)$ or $D_C(s)V_{r_2}^D(s) \in -N_C(s)P_E^N(s)$. This means that $0 \in D_C(s)P_E^D(s) + N_C(s)V_{r_1}^N(s)$ or $0 \in D_C(s)V_{r_2}^D(s) + N_C(s)P_E^N(s)$ and it contradicts the robust \mathcal{D} -stability of the polynomials $H_N^{r_1}(s)$ and $H_D^{r_2}(s)$. ■

For a convenient use of the robust \mathcal{D} -stability conditions derived in Theorem 1 and Theorem 2, a robust \mathcal{D} -stability checking function is provided in the next theorem. This function facilitates the robust \mathcal{D} -stability analysis. Consider the following definition before presenting the function.

Definition 3: It is assumed that $E_1 = V(s)e(V_1(s), V_2(s))$ is an edge of the exposed edges of a value set. Then, define:

$$Tr^{\hat{v}}(s)(E_1) \triangleq |V(s)V_1(s) + \hat{v}(s)| + |V(s)V_2(s) + \hat{v}(s)| - |V(s)V_1(s) - V(s)V_2(s)|, \quad (10)$$

in which, $\hat{v}(s)$ is a polynomial.

Theorem 3: Let $E_1^N, E_2^N, \dots, E_{t_N}^N$ and $E_1^D, E_2^D, \dots, E_{t_D}^D$ be respectively all edges of $P_E^N(s)$ and $P_E^D(s)$. Then, the system is robust \mathcal{D} -stable, if and only if:

- 1) $H(s)$ has at least one robust \mathcal{D} -stable polynomial,
- 2) The inequality $\chi(s) > 0$ is held for $\{s \in \partial D | \text{Im}(s) \geq 0, B_{\min} \leq |s| \leq B_{\max}\}$ where $\chi(s)$ is defined in (11).

$$\chi(s) \triangleq \min \left\{ \bar{\chi}_1(s), \bar{\chi}_2(s), \dots, \bar{\chi}_{t_N}(s), \right. \\ \left. \underline{\chi}_1(s), \underline{\chi}_2(s), \dots, \underline{\chi}_{t_D}(s) \right\}, \quad (11)$$

$$\bar{\chi}_{i_1}(s) \triangleq \min_{i=1,2,\dots,2^{d_P}+1} Tr^{D_C(s)V_i^D(s)}(N_C(s)E_{i_1}^N), \\ i_1 \in \{1, 2, \dots, t_N\}, \\ \underline{\chi}_{i_2}(s) \triangleq \min_{i=1,2,\dots,2^{n_P}+1} Tr^{N_C(s)V_i^N(s)}(D_C(s)E_{i_2}^D), \\ i_2 \in \{1, 2, \dots, t_D\}.$$

Proof: Drawing upon the fundamental principles of the triangle inequality, one can readily deduce the subsequent assertions.

- If the values of the function $|N_C(s)V_1^N(s) + D_C(s)V_1^D(s)| + |N_C(s)V_2^N(s) + D_C(s)V_1^D(s)| - |N_C(s)V_1^N(s) - N_C(s)V_2^N(s)|$ are positive, then the vertex $-V_1^D(s)$ does not intersect the edge $E = e(V_1^N(s), V_2^N(s))$ in the complex plane.
- If the value of the function $|N_C(s)V_1^N(s) + D_C(s)V_1^D(s)| + |N_C(s)V_2^N(s) + D_C(s)V_1^D(s)| - |N_C(s)V_1^N(s) - N_C(s)V_2^N(s)|$, then the vertex $-V_1^D(s)$ intersects the edge $E = e(V_1^N(s), V_2^N(s))$ in the complex plane.

We also know that $\partial(N_C(s)N_P(s)) \subseteq N_C(s)P_E^N(s)$ at a fixed frequency $s = z_0$. Hence, satisfying the inequalities

$\Xi_{i_1}(s) > 0$ assures that the vertices $V_i^D(s)$ do not intersect the value set of $N_C(s)N_P(s)$. Likewise, if the inequalities $\Xi_{i_2}(s) > 0$ are satisfied then one can simply infer that the value sets $-N_C(s)P_E^N(s)$ and $D_C(s)P_E^D(s)$ have no overlap for $s \in \partial D, \text{Im}(s) \geq 0$. Therefore, based on Theorem 1 and Lemma 2, the proof is completed. ■

Remark 1: The utility of Theorems 1-3 extends to robust \mathcal{D} -stability analysis of the system. Specifically, the depiction of two-dimensional graphs of the value sets, as required by Theorems 1 and 2, may present a challenging task for some. In such cases, the employment of Theorem 3 serves as a more expedient and effective means for robust \mathcal{D} -stability analysis.

B. Second Approach for Robust \mathcal{D} -Stability Analysis

At first, an exact description of the vertices and edges of the value sets $N_P(s)$ and $D_P(s)$ are explained in the following lemma.

Lemma 3: Consider the uncertain fractional-order polynomial $N_P(s)$. Define the set $A_0 = \{h \in \mathbb{Z}_{\geq 0}^n | b_{r_n}^{P-} < b_{r_n}^{P+}\}$. Then, for each $z \in \mathbb{C}$, $\partial(N_P(z))$ can be obtained as:

- If $A_0 = \emptyset$, then $N_P(z) = b_0^{P-} + \sum_{r_n=1}^{n_P} b_{r_n}^{P-} |z|^{\beta_{r_n}^P} e^{j\beta_{r_n}^P \text{Arg}(z)}$.
 - If $z = 0$ and $A_0 \neq \emptyset$, then $N_P(z) = [b_0^{P-}, b_0^{P+}]$.
 - If $z \neq 0$ and $A_0 \neq \emptyset$, then the consecutive vertices of $N_P(z)$ are calculated by $v_i^N(z)$, ($i = 1, 2, \dots, 2l_N$) as follows.
- $$v_r^N(z) = N_P(z, \mathbf{B}^r), v_{r+l_N}^N(z) = N_P(z, \mathbf{B}^{r+l_N}), \quad (12)$$
- $$r = 1, 2, \dots, n(A_0),$$

in which

$$\mathbf{B}^r = [b_0^{P_r} \ b_1^{P_r} \ \dots \ b_{n_P}^{P_r}], \mathbf{B}^{r+l_N} = \mathbf{B}^+ + \mathbf{B}^- - \mathbf{B}^r, \\ \mathbf{B}^+ = [b_0^{P+} \ b_1^{P+} \ \dots \ b_{n_P}^{P+}], \mathbf{B}^- = [b_0^{P-} \ b_1^{P-} \ \dots \ b_{n_P}^{P-}], \\ b_{r_n}^{P_r} = \begin{cases} b_{r_n}^{P+}, & r_n \in \left(\bigcup_{i=1}^{r-1} A_i \right) \cup \left(\bigcup_{i=r}^{l_N} A_i \right), \\ b_{r_n}^{P-}, & \text{otherwise,} \end{cases} \\ A_r = \{r_n \in A_0 | \text{frac}\left(\frac{\beta_{r_n}^P}{\pi} \text{Arg}(z)\right)\pi = \gamma_r, \\ \text{floor}\left(\frac{\beta_{r_n}^P}{\pi} \text{Arg}(z)\right) \text{ is an even number} \}, \\ A'_r = \{r_n \in A_0 | \text{frac}\left(\frac{\beta_{r_n}^P}{\pi} \text{Arg}(z)\right)\pi = \gamma_r, \\ \text{floor}\left(\frac{\beta_{r_n}^P}{\pi} \text{Arg}(z)\right) \text{ is an odd number} \}, \\ F_0 = \{\text{frac}\left(\frac{\beta_{r_n}^P}{\pi} \text{Arg}(z)\right) | r_n \in A_0\}, \quad (13)$$

and also $\gamma_1, \gamma_2, \dots, \gamma_{l_N}$ are the distinct members of F_0 and are ordered as $0 \leq \gamma_1 < \gamma_2 < \dots < \gamma_{l_N} < \pi$.

Proof: It is a straightforward result based on Lemma 1 and Procedure 1 in [14] and Theorem 3 in [22]. ■

Distinct configurations of vertices and edges of $N_P(s)$ may be observed for varying values of s . The following lemma states that these vertices may be changed only at some finite intervals.

Lemma 4: The roots of the following equations

$$\begin{aligned} \text{Real}(s^{\beta_{r_1}^P}) \text{Imag}(s^{\beta_{r_2}^P}) - \text{Real}(s^{\beta_{r_2}^P}) \text{Imag}(s^{\beta_{r_1}^P}) &= 0, \\ r_1, r_2 &= 0, 1, \dots, n_P, r_1 \neq r_2. \end{aligned} \quad (14)$$

divide the curve $s \in \partial D$ into some finite intervals, where in each of the intervals, the outermost vertices of $N_P(s)$ remain fixed and unaltered. The transition points of the value set of $N_P(s)$ are defined as those critical points at which the outer edges and vertices of the set may undergo modifications or variations.

Proof: It is followed from Lemma 1. It can be deduced that the transition points may occur at the edges of the value set paralleled with each other. On the other hand if the conditions $\arg(s^{\beta_{r_1}^P}) = \arg(s^{\beta_{r_2}^P})$ or $\arg(s^{\beta_{r_1}^P}) = \arg(s^{\beta_{r_2}^P}) \pm \pi$ are satisfied then the both edges have the same direction or paralleled to each other. Therefore, from $\arg(s^{\beta_{r_1}^P}) = \arg(s^{\beta_{r_2}^P})$, it can be concluded that

$$\tan^{-1} \left(\frac{\text{Im}(s^{\beta_{r_1}^P})}{\text{Re}(s^{\beta_{r_1}^P})} \right) = \tan^{-1} \left(\frac{\text{Im}(s^{\beta_{r_2}^P})}{\text{Re}(s^{\beta_{r_2}^P})} \right). \quad (15)$$

By solving (15), one can obtain (14). ■

Remark 2: Based on Lemma 3 and lemma 4, the outer and consecutive vertices of $N_P(s)$ and $D_P(s)$ can be obtained and they are respectively considered as $v_r^N(s), r = 0, 1, \dots, 2l_N$ and $v_r^D(s), r = 0, 1, \dots, 2l_D$.

Now, the robust stability of the system is again investigated based on Remark 2, Lemma 3, lemma 4 and the results provided in Subsection III-A.

Theorem 4: The system is robust \mathcal{D} -stable, if and only if:

- 1) $H(s)$ has at least one robust \mathcal{D} -stable polynomial,
- 2) The inequality $\chi(s) > 0$ is held for $\{s \in \partial D | \text{Im}(s) \geq 0, 0 \leq |s| \leq B_{max}\}$ where $\chi(s)$ is defined in (16).

$$\begin{aligned} \chi(s) &\triangleq \min \left\{ \bar{\chi}_1(s), \bar{\chi}_2(s), \dots, \bar{\chi}_{2l_N}(s), \right. \\ &\quad \left. \underline{\chi}_1(s), \underline{\chi}_2(s), \dots, \underline{\chi}_{2l_D}(s) \right\}, \end{aligned} \quad (16)$$

$$\begin{aligned} \bar{\chi}_{i_1}(s) &\triangleq \min_{i=1,2,\dots,2l_D} T_{r^{DC}(s)v_i^D(s)}(N_C(s)e(v_{i_1}^N(s), v_{i_1+1}^N(s))), \\ i_1 &\in \{1, 2, \dots, 2l_N\}, \\ \underline{\chi}_{i_2}(s) &\triangleq \min_{i=1,2,\dots,2l_N} T_{r^{NC}(s)v_i^N(s)}(D_C(s)e(v_{i_2}^D(s), v_{i_2+1}^D(s))), \\ i_2 &\in \{1, 2, \dots, 2l_D\}, \end{aligned}$$

in which $v_{i_1}^N(s), i_1 = 1, 2, \dots, 2l_N$ and $v_{i_2}^D(s), i_2 = 1, 2, \dots, 2l_D$ are respectively the vertices of the polynomials $N_P(s)$ and $D_P(s)$ calculated by Lemma 3, and $v_{2l_N+1}^N(s) = v_1^N(s)$.

Proof: The proof can be simply completed by Theorem 3, Lemma 3 and lemma 4. ■

IV. ILLUSTRATIVE EXAMPLES

Example 1. In [24], the FOPID controller $C(s)$ in (17) has been designed for a Delta aircraft having the transfer function $P(s)$ in (18).

$$C_1(s) = -1.7518 - \frac{0.807}{s^{0.0217}} - 1.8146s^{1.0457}. \quad (17)$$

$$P(s) = \frac{-1.228s - 1.135}{0.8185s^3 + 1.799s^2 + s}. \quad (18)$$

Let us consider the transfer function $P(s)$ in (18) as (19).

$$P(s) = \frac{[-2, -1]s + [-2, -1]}{[0.5, 1.5]s^3 + [1, 2]s^2 + [0.5, 1]s}. \quad (19)$$

Assume that the goal is to investigate the robust \mathcal{D} -stability of the closed-loop control system for $\partial D = \{s \in \mathbb{C} | \text{Re}(s) < -0.41\}$. One can calculate $B_{\min} \approx 0$ rad/sec and $B_{\max} = 2.0682e + 74$ rad/sec by Lemma 2. By benefiting from the Principle of Argument, the \mathcal{D} -stability of $H_0(s)$ can be verified.

$$\begin{aligned} H_0(s) &= s^{0.0217}(0.8185s^3 + 1.799s^2 + s) + \\ &\quad (-1.228s - 1.135) \\ &\quad (-1.7518s^{0.0217} - 0.807 - 1.8146s^{1.0457+0.0217}). \end{aligned} \quad (20)$$

Also, the curve of $\chi(s)$ is plotted in Fig. 1. From this figure, $\chi(s) = 0$ occurs in low frequencies. Hence, the system is not robustly \mathcal{D} -stable. Now, consider the FOPID controller in (21). It is shown that the FOPID controller (21) can ensure the robust \mathcal{D} -stability of the closed-loop control system.

$$C_2(s) = -2.1 - \frac{1.807}{s^{0.0217}} - 2.6146s^{1.0457}. \quad (21)$$

By invoking the Principle of Argument, one can demonstrate the robust \mathcal{D} -stability of the closed-loop control system. The values of $\chi(s)$ are provided in Fig. 2, revealing that the condition $\chi(s) > 0$ is satisfied, thereby establishing the robust \mathcal{D} -stability of the closed-loop control system. Figures 3 and 4 show the step responses of the closed-loop control system corresponding to both FOPID controllers $C_1(s)$ and $C_2(s)$. It is visible that the FOPID controller $C_2(s)$ outperforms the FOPID controller $C_1(s)$ in the sense of faster responses and smaller overshoots.

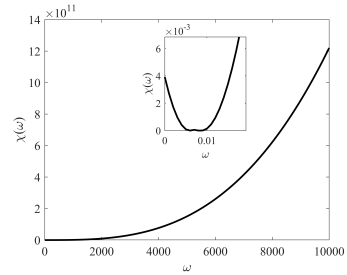


Fig. 1: Curve of $\chi(s)$ for $C_1(s)$.

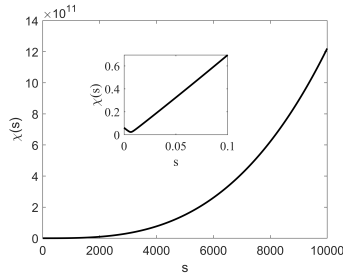


Fig. 2: Curve of $\chi(s)$ for $C_2(s)$.

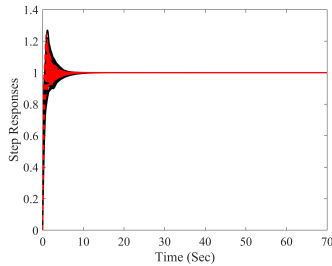


Fig. 3: Step responses corresponding to the controllers $C_1(s)$ (solid line) and $C_2(s)$ (dashed line).

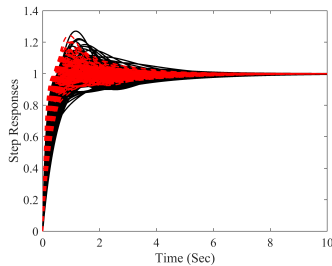


Fig. 4: A better view of Fig. 3.

V. CONCLUSION

In this paper, the robust \mathcal{D} -stability analysis of interval fractional-order plants with fractional-order controllers for was investigated. Necessary and sufficient conditions were proposed for robust \mathcal{D} -stability analysis interval fractional-order closed-loop control systems. Moreover, two different approaches were presented. Finally, a numerical example was offered to demonstrate the method's applicability and efficiency.

REFERENCES

- [1] Efe, Mehmet Önder. (2011). Fractional order systems in industrial automation—a survey. *IEEE Transactions on Industrial Informatics*, 7(4), 582-591.
- [2] Gabano, Jean-Denis, Thierry Pointot, and Houcem Kanoun. (2015). LPV continuous fractional modeling applied to ultracapacitor impedance identification. *Control Engineering Practice*, 45, 86-97.

- [3] Tepljakov, Aleksei, et al. (2013). Tuning and digital implementation of a fractional-order PD controller for a position servo. *International Journal of Microelectronics and Computer Science*, 4(3), 116–123.
- [4] Tepljakov, Aleksei, et al. (2021). Towards Industrialization of FOPID Controllers: A Survey on Milestones of Fractional-Order Control and Pathways for Future Developments. *IEEE Access*, 9, 21016-21042.
- [5] Tepljakov, Aleksei, et al. (2018). FOPID controllers and their industrial applications: a survey of recent results. *IFAC-PapersOnLine*, 51(4), 25-30.
- [6] Tan, Nusret, Ö. Faruk Özgüven, and M. Mine Özyetkin. (2009). Robust stability analysis of fractional order interval polynomials. *ISA transactions*, 48(2), 166-172.
- [7] Moornani, Kamran Akbari, and Mohammad Haeri. (2009). On robust stability of linear time invariant fractional-order systems with real parametric uncertainties. *ISA transactions*, 48(4), 484-490.
- [8] Ghorbani, Majid, Mahsan Tavakoli-Kakhki, and Ali Akbar Estarami. (2019). Robust FOPID stabilization of retarded type fractional order plants with interval uncertainties and interval time delay. *Journal of the Franklin Institute*, 356(16), 9302-9329.
- [9] Matusů, Radek, and Libor Pekář. (2017). Robust stability of thermal control systems with uncertain parameters: the graphical analysis examples. *Applied Thermal Engineering*, 125, 1157-1163.
- [10] Ghorbani, M. (2022). Robust stabilization criteria of a general form of fractional-order controllers for interval fractional-order plants with complex uncertain parameters. *ISA Transactions*, <https://doi.org/10.1016/j.isatra.2022.02.014>.
- [11] Chen, Liping, et al. (2015). Robust stability and stabilization of fractional-order linear systems with polytopic uncertainties. *Applied mathematics and computation*, 257, 274-284.
- [12] Ma, Yingdong, Junguo Lu, and Weidong Chen. (2014). Robust stability and stabilization of fractional order linear systems with positive real uncertainty. *ISA transactions*, 53(2), 199-209.
- [13] Lu, Jun-Guo, and Yang-Quan Chen. (2009). Robust Stability and Stabilization of Fractional-Order Interval Systems with the Fractional Order α : The $0 \leq \alpha \leq 1$ Case. *IEEE transactions on automatic control*, 55(1), 152-158.
- [14] Moornani, K. Akbari, and M. Haeri. (2010A). Robust stability testing function and Kharitonov-like theorem for fractional order interval systems. *IET control theory & applications*, 4(10), 2097-2108.
- [15] Moornani, K. Akbari, and M. Haeri. (2010B). Robustness in fractional proportional-integral-derivative-based closed-loop systems. *IET control theory & applications*, 4(10), 1933-1944.
- [16] Ghorbani, Majid, et al. (2021). Robust Stability Analysis of Interval Fractional-Order Plants with Interval Time delay and General Form of Fractional-Order Controllers. *IEEE Control Systems Letters*, 6, 1268–1273.
- [17] Yeroglu, Celalettin, and Bilal Senol. (2013). Investigation of robust stability of fractional order multilinear affine systems: 2q-convex parpolygon approach. *Systems & Control Letters*, 62(10), 845-855.
- [18] Akbari Moornani, Kamran, and Mohammad Haeri. (2013). Robust stability check for fractional PID-based control systems. *Transactions of the Institute of Measurement and Control*, 35(2), 236-246.
- [19] Ghorbani, Majid, and Mahsan Tavakoli-Kakhki. (2021). Robust stability analysis of a general class of interval delayed fractional order plants by a general form of fractional order controllers. *Mathematical Methods in the Applied Sciences*, 44(13), 10172–10189.
- [20] Ghorbani, Majid, and Mahsan Tavakoli-Kakhki. (2021). Stabilizing region of fractional-order proportional integral derivative controllers for interval delayed fractional-order plants. *Asian Journal of Control*, <https://doi.org/10.1002/asjc.2894>.
- [21] Bhattacharyya, Shankar P., and Lee H. Keel. (1994). Robust control: the parametric approach. *Advances in control education 1994*. Pergamon, 49-52.
- [22] Mohsenipour, Reza, and Mohsen Fathi Jegarkandi. (2019). Robust D-stability analysis of fractional order interval systems of commensurate and incommensurate orders. *IET Control Theory & Applications*, 13(8) (2019), 1039-1050.
- [23] Moornani, Kamran Akbari, and Mohammad Haeri. (2010C). On robust stability of LTI fractional-order delay systems of retarded and neutral type. *Automatica*, 46(2), 362-368.
- [24] Kumar, Parvesh and et al., (2010C). Optimal design of robust fractional order PID for the flight control system. *International Journal of Computer Applications*, 128(14), 31–35.

Appendix 10

X

M. Ghorbani, A. Tepljakov, and E. Petlenkov. On robust stability analysis of interval time delay systems using delayed controllers. In *Proc. 2023 European Control Conference (ECC)*, pages 1–6, 2023.

On robust stability analysis of interval time delay systems using delayed controllers

Majid Ghorbani, Aleksei Tepljakov (Senior Member, IEEE) and Eduard Petlenkov

Abstract—The focus of this research is to explore the robust stability of interval time delay systems that utilize delayed controllers. Specifically, the study assumes the use of a Proportional-Integral-Retarded (PIR) controller in conjunction with a first-order plus dead-time (FOPDT) model of the time delay system. The parameters of the system, including the gain, time constant, and time delay, are subject to interval uncertainties, which are a type of structured uncertainties for the plant model. To investigate the robust stability of the system, the study derives necessary and sufficient conditions, accounting for the presence of uncertainties. To facilitate the assessment of robust stability, the study also introduces a frequency range and robust stability checking function. Ultimately, the study aims to demonstrate the accuracy of its findings through the presentation of two numerical examples.

I. INTRODUCTION

The ubiquitous nature of time delay in engineering systems, including chemical processes [1], communication channels [2], power systems [3], and biological systems [4], has made the study of stability and stabilization of such systems a topic of immense interest. Indeed, various techniques have been proposed to analyze the stability of time delay systems in both frequency and time domains, as evidenced by the literature [5], [6].

Meanwhile, in the realm of industrial control systems, the Proportional-Integral-Derivative (PID) controller continues to hold its place as a reliable solution due to its ease of implementation and efficient parameter tuning for meeting control loop requirements. Therefore, numerous methodologies have been advanced to design PID controllers for time delay systems. For example, a technique was proposed in [7] for designing PID controllers for systems with two unstable poles. Similarly, in [8], [9], two distinct methodologies were proposed for the design of PID controllers tailored to time delay systems.

As discussed in [10], the derivative term in PID controllers has the potential to amplify high frequency measurement noise, yielding undesirable control efforts. As such, various studies [11], [12], [13] have proposed the Euler approximation of the derivative term

$$e'(t) \approx \frac{e(t) - e(t - \varepsilon)}{\varepsilon}, \quad (1)$$

where ε is a small positive value as a solution to this issue. This approach involves replacing the derivative term with an

This work was supported by the Estonian Research Council grant PRG658.

The Authors are with Department of Computer Systems, Tallinn University of Technology, Estonia (e-mail: majid.ghorbani@taltech.ee ; aleksei.tepljakov@taltech.ee ; eduard.petlenkov@taltech.ee).

appropriate delay, effectively rendering the system response impervious to high frequency noise.

While the presence of time delay is commonly associated with instability and oscillations of closed-loop responses, recent research has shown that under certain circumstances, the delay term may actually improve the stability of control systems [14], [15], [16]. In addition, analytical investigations into the stabilization of linear systems using Proportional-Retarded (PR) controllers have been conducted [17]. Moreover, the superior performance of Proportional-Integral-Retarded (PIR) controllers in comparison to regular PID controllers has been demonstrated in various studies, such as [18]. Furthermore, the σ -stabilizing region of PIR controllers for second-order systems has been determined in [19], [20], and a graphical tuning approach for PR controllers has been introduced in [21] for a specific class of linear systems. Notably, experimental results presented in the latter work indicate that the PR controller surpasses the performance of a PD controller in a fair comparison.

The presence of uncertainties, much like time delays in engineering systems, is a ubiquitous reality in control systems. Several studies have highlighted this fact, as demonstrated in [22], [23]. Therefore, robust stabilization of control systems has emerged as a crucial problem in the literature. Notably, none of the previously mentioned works [14]-[21] have succeeded in designing a robust PIR controller for time delay systems. Consequently, this paper aims to address this shortcoming by first considering the interval uncertainties in gain, delay, and time constant of a first-order plus dead time model, and subsequently deriving the stabilization conditions. Additionally, we provide some extensions that are particularly appealing from a computational standpoint.

The paper is structured as follows. Section II presents the preliminary material, including the PIR controller, the transfer function of the plant, and the characteristic function of the closed-loop system under investigation. In Section III, the study reviews the foundations of robust stability analysis. Section IV provides numerical evaluations of the findings. Finally, Section V presents concluding remarks.

II. PRELIMINARIES

Fig. 1 depicts a typical negative unity feedback control system. In this figure, $C(s)$ and $P(s)$ represent a PIR controller and an interval plant with an interval time delay, respectively. The transfer function of PIR controllers has the following form:

$$C(s) = k_p + \frac{k_i}{s} + k_r e^{-hs}, \quad (2)$$

where the parameters k_p, k_i , and $k_r \in \mathbb{R} \setminus 0$ denote the proportional, integral, and retarded gains, respectively, while $h > 0$ represents the time delay term. Additionally, the study considers an interval first-order plant with an interval time delay, as described in equation (3):

$$P(s) = \frac{K}{T s + 1} e^{-\tau s}, \quad (3)$$

where K, T and τ are positive values and lie in specified intervals as follows.

$$K \in [K^-, K^+], T \in [T^-, T^+], \tau \in [\tau^-, \tau^+]. \quad (4)$$

Drawing upon the information presented in Figure 1, it is possible to derive the characteristic quasi-polynomial of the system in the following manner.

$$Q(s) = T s^2 + s + K (k_p s + k_i) e^{-\tau s} + k_r K s e^{-(\tau+h)s}. \quad (5)$$

For the simplicity, $Q(s)$ is rewritten as follows.

$$\begin{aligned} Q(s) &= Q_1(s) + K Q_2(s) e^{-\tau s}, \\ Q_1(s) &= s (T s + 1), Q_2(s) = k_p s + k_i + s k_r e^{-hs}. \end{aligned} \quad (6)$$

As a result of the uncertain nature of the gain, delay, and

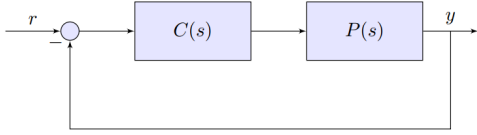


Fig. 1. A classic negative unity feedback control system involving a plant $P(s)$ and a controller $C(s)$.

time constant of $P(s)$, the task of analyzing the system's robust stability presents a primary challenge for researchers in this field. Consequently, the paper endeavors to address this challenge by proposing the following design problem:

Problem 1. Devise a highly effective and efficient approach to comprehensively investigate robust stability of the system characterized by multiple interval time delays in its characteristic function.

Assumption 1: As discussed earlier, in this paper, it is assumed that K, T and τ are positive values and $k_p, k_i, k_r \in \mathbb{R} \setminus \{0\}$.

III. MAIN RESULTS

It is imperative to make note of the following remark as it holds significance for the remainder of this paper.

Remark 1: Assume that the value sets of $\Xi_i(j\omega), i = 1, 2$ (Value set of $\Xi(j\omega)$ means the possible values of $\Xi(j\omega)$ by considering all uncertainties while keeping ω fixed.) are closed and bounded in the complex plane and $\partial(\cdot)$ shows the boundary. If $\partial(\Xi_1(j\omega))$ and $\partial(\Xi_2(j\omega))$ have no overlap at a given frequency in the complex plane, then it means that there is no common complex/real numbers in their value sets.

One can infer from Remark 1 that the crux of the matter lies in the fact that the overlap between the two value

sets, namely $\Xi_1(j\omega)$ and $\Xi_2(j\omega)$, can be readily ascertained solely by analyzing their respective boundaries. As a consequence, there is no compelling rationale for plotting all elements of their value sets, thereby resulting in a significant reduction of the computational cost. The theorem that follows sets forth the necessary and sufficient conditions for a thorough stability analysis of the control system.

Theorem 1: The robust stability of the closed-loop system under Assumption 1 can be ensured if and only if:

- the PIR controller can stabilize one member of $Q(s)$,
- the sets $F_1(s)$ and $F_2(s)$ have no overlap for $s = j\omega$ and $\omega \geq 0$ where

$$\begin{aligned} F_1(s) &= -s (e(T^-, T^+) s + 1), \\ F_2(s) &= \begin{cases} F_2^1(s), & \text{for } 0 \leq \omega < \frac{2\pi}{\tau^+ - \tau^-}, \\ F_2^2(s), & \text{for } \omega \geq \frac{2\pi}{\tau^+ - \tau^-}, \end{cases} \\ F_2^1(s) &= \left\{ e(Q_2(s)K^- e^{-\tau^- s}, Q_2(s)K^+ e^{-\tau^- s}), \right. \\ &\quad \left. e(Q_2(s)K^- e^{-\tau^+ s}, Q_2(s)K^+ e^{-\tau^+ s}), \right. \\ &\quad \left. Q_2(s)K^+ e^{-e(\tau^-, \tau^+)s}, Q_2(s)K^- e^{-e(\tau^-, \tau^+)s} \right\}, \\ F_2^2(s) &= \left\{ Q_2(s)K^- e^{-j[0, 2\pi]}, Q_2(s)K^+ e^{-j[0, 2\pi]} \right\}, \end{aligned} \quad (7)$$

where $e(h_1, h_2) = \eta h_1 + (1 - \eta) h_2$ and $\eta \in [0, 1]$.

Proof: By the zero exclusion principle, we only need to show that the zero exclusion condition $0 \notin Q(j\omega)$ holds for all $\omega \geq 0$, $K \in [K^-, K^+]$, $T \in [T^-, T^+]$ and $\tau \in [\tau^-, \tau^+]$ [24]. Also, it is clear that $-F_1(s)$ and $F_2(s)$ are respectively the boundary of the value sets of $Q_1(s)$ and $K Q_2(s) e^{-\tau s}$ as depicted in Fig. 2 and Fig. 3.

Sufficiency: Assume that z_1 and z_2 respectively represent

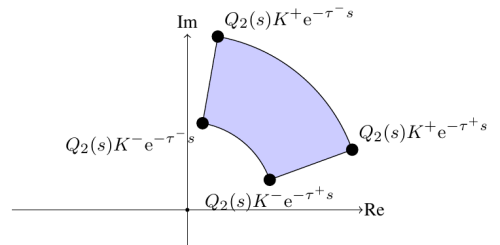


Fig. 2. Value set (shaded area) and boundary (solid line) of $K Q_2(s) e^{-\tau s}$ i.e., $F_2(s)$ for $s = j\omega$, $0 \leq \omega < \frac{2\pi}{\tau^+ - \tau^-}$.

two complex numbers in the value set of $-F_1(s)$ and $F_2(s)$. Since, the exposed edges $F_1(s)$ and $F_2(s)$ have no overlap at a given frequency, then the complex numbers z_1 and z_2 are not equal to each other and consequently $z_1 \neq z_2$. Moreover, this implies that for the complex number z_1 in the value set of $Q_1(s)$, there does not exist $-z_1$ in the value set of $K Q_2(s) e^{-\tau s}$. Therefore, the zero exclusion condition is held.

Necessity: Due to the robust stability of the system, $0 \notin$

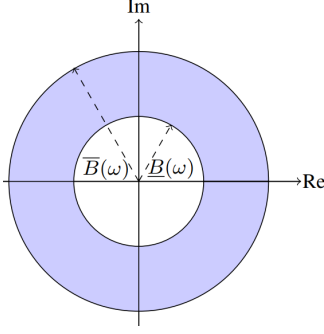


Fig. 3. Value set (shaded area) and boundary (solid line) of $K Q_2(s) e^{-\tau s}$ i.e., $F_2(s)$ for $\omega \geq \frac{2\pi}{\tau^+ - \tau^-}$ where $\bar{B}(\omega) = K^+ Q_2(j\omega)$ and $\underline{B}(\omega) = K^- Q_2(j\omega)$

$Q(s)$ is met. As a contradiction argument, assume that $0 \in Q(s)$ at $s = j\omega_0$. Then, one can simply deduce that there is a complex number z_0 located in the value sets of $-Q_1(s)$ and $K Q_2(s) e^{-\tau s}$. This means that $F_1(s)$ and $F_2(s)$ have an overlap and this contradicts the second statement in this theorem. ■

Now, in Proposition 1, a simple conclusion of Theorem 1 is presented.

Proposition 1: The robust stability of the closed-loop system under Assumption 1 can be ensured if and only if:

- the PIR controller can stabilize one member of $Q(s)$,
- the sets $F_1(s)$ and $F_2^1(s)$ have no overlap for $s = j\omega$ and $\omega \in [0, \frac{2\pi}{\tau^+ - \tau^-})$,
- $\bar{\Lambda}(\omega) > 0$ for $\omega \in [\frac{2\pi}{\tau^+ - \tau^-}, \infty)$ where

$$\bar{\Lambda}(\omega) = \min_{e_1 \in P_E} |e_1| - K^+ |Q_2(j\omega)|, \quad (8)$$

$$P_E(s = j\omega) = \{s (e(T^-, T^+)s + 1)\}.$$

Proof: Due to $\bar{\Lambda}(\omega) > 0$, the sufficient condition is evident. Hence, in the following, the necessary condition is stated.

Assume that $\bar{\Lambda}(\omega) > 0$ is not satisfied. Due to $\lim_{\omega \rightarrow \infty} \min_{e_1 \in P_E} |e_1| > \lim_{\omega \rightarrow \infty} |K^+ Q_2(j\omega)|$, $\bar{\Lambda}(\omega) > 0$ is met for high frequencies. Also, because of $\bar{\Lambda}(\omega) \leq 0$ at some frequencies, there may exist a frequency as ω^* at which $\bar{\Lambda}(\omega^*) = 0$. This implies that $F_1(s)$ and $F_2^1(s)$ have an overlap and this contradicts the robust stability of the system based on Theorem 1. ■

For simplicity of the stability assessment, the following theorem proposes a frequency range $[0, \omega_U]$ to check the zero exclusion condition.

Theorem 2: The zero exclusion condition $0 \notin Q(j\omega)$ holds for $\omega > \omega_U$ where

$$\omega_U = \max \left\{ 1, \frac{1 + K^+ (|k_p| + |k_i| + |k_r|)}{T^-} \right\}. \quad (9)$$

Proof: The triangle inequality is employed to prove the results. Based on the triangle inequality we can write for $\omega > 1$

$$|Q(j\omega)| \geq T^- \omega^2 - \left(\omega + K^+ (|k_p| + |k_i| + \omega |k_r|) \right) \geq T^- \omega^2 - \left(1 + K^+ (|k_p| + |k_i| + |k_r|) \right) \omega. \quad (10)$$

From (10), it is visible that $|Q(j\omega)| > 0$ for $\omega > \omega_U$. ■ Now, based on Proposition 1 and Theorem 2, the following propositions can be simply proven.

Proposition 2: Assume that $\omega_U \geq \frac{2\pi}{\tau^+ - \tau^-}$. The robust stability of the closed-loop system under Assumption 1 can be ensured if and only if:

- the PIR controller can stabilize one member of $Q(s)$,
- the sets $F_1(s)$ and $F_2^1(s)$ have no overlap for $s = j\omega$ and $\omega \in [0, \frac{2\pi}{\tau^+ - \tau^-})$,
- $\bar{\Lambda}(\omega) > 0$ for $\omega \in [\frac{2\pi}{\tau^+ - \tau^-}, \omega_U]$.

Proposition 3: Assume that $\omega_U < \frac{2\pi}{\tau^+ - \tau^-}$. Then, the robust stability of the closed-loop system under Assumption 1 can be ensured if and only if:

- the PIR controller can stabilize one member of $Q(s)$,
- the sets $F_1(s)$ and $F_2^1(s)$ have no overlap for $s = j\omega$ and $\omega \in [0, \omega_U]$.

Indeed, the endeavor of ascertaining the potential intersection of value sets could prove to be an exceedingly arduous task, particularly in scenarios where non-negative frequencies are involved. As a result, the ensuing discussion shall strive to streamline the analysis of robust stability. In light of this, the ensuing lemma puts forth a comprehensive set of exposed edges that can facilitate the examination of the control system's robust stability via an auxiliary function.

Lemma 1: At a given frequency $\omega = \omega_0 \in (0, \frac{2\pi}{\tau^+ - \tau^-})$, the value set of $K Q_2(j\omega) e^{-\tau j\omega}$ is located inside the exposed edges $P_{Q_2}(j\omega)$ in (11).

$$P_{Q_2}(j\omega) \triangleq \{e(\chi_1(j\omega), \chi_2(j\omega)), e(\chi_2(j\omega), \chi_3(j\omega)), \dots, e(\chi_{4N+1}(j\omega), \chi_{4N+2}(j\omega)), e(\chi_{4N+2}(j\omega), \chi_1(j\omega))\}, \quad (11)$$

$$\chi_i(j\omega) \triangleq \begin{cases} \bar{\chi}_{(i-1)}(j\omega), & \text{for } 1 \leq i \leq 2N+1, \\ \underline{\chi}_{(2N)}(j\omega), & \text{for } i = 2N+2, \\ \underline{\chi}_{(2N-1)}(j\omega), & \text{for } i = 2N+3, \\ \vdots & \\ \underline{\chi}_0(j\omega), & \text{for } i = 4N+2, \end{cases}$$

$$\bar{\chi}_i(j\omega) \triangleq$$

$$\begin{cases} K^+ Q_2(j\omega) e^{-j\omega \left(\tau^- + i \frac{\tau^+ - \tau^-}{2N} \right)}, & \text{for } i = 0, 2, \dots, 2N, \\ \frac{K^+ Q_2(j\omega) e^{-j\omega \left(\tau^- + i \frac{\tau^+ - \tau^-}{2N} \right)}}{\cos \left(\omega \frac{\tau^+ - \tau^-}{2N} \right)}, & \text{for } i = 1, 3, \dots, 2N-1, \end{cases}$$

$$\underline{\chi}_i(j\omega) \triangleq K^- Q_2(j\omega) e^{-j\omega \left(\tau^- + i \frac{\tau^+ - \tau^-}{2N} \right)}, \quad i = 0, 1, 2, \dots, 2N,$$

where $N \in \mathbb{N}^{\geq 3}$.

Proof: The value set of $K Q_2(j\omega) e^{-\tau j\omega}$ and the vertices $\chi_i(j\omega)$ (shown by χ_i) at a given frequency $\omega = \omega^*$ have been depicted in Fig. 4. From this figure, it is visible that $\partial(K Q_2(j\omega) e^{-\tau j\omega})$ is composed by two line segments and two arc segments. Moreover, it is observed from this figure that two line segments $e(\bar{\chi}_0(j\omega), \chi_0(j\omega))$ and $e(\bar{\chi}_{2N}(j\omega), \chi_{2N}(j\omega))$ are in $\partial(K Q_2(j\omega) e^{-\tau j\omega})$. Also, from this figure, it is apparent that the smallest arc of $\partial(K Q_2(j\omega) e^{-\tau j\omega})$ is enclosed by the line segments composed by the vertices $\chi_i(j\omega)$. Therefore, in the following, it is shown that the biggest arc of $\partial(K Q_2(j\omega) e^{-\tau j\omega})$ is enclosed by the exposed edges $P_{Q_2}(j\omega)$.

Without loss of generality, we only discuss on the sector $\frac{\theta}{2N} = \frac{(\tau^+ - \tau^-)\omega}{2N}$ of the biggest arc which can be enclosed by the edges $e(\bar{\chi}_0(j\omega), \bar{\chi}_1(j\omega))$, $e(\bar{\chi}_1(j\omega), \bar{\chi}_2(j\omega))$ as shown in Fig. 5. By the features of the right triangles, one can simply write

$$\cos\left(\frac{\theta}{2N}\right) = \frac{|\bar{\chi}_0(j\omega)|}{|\bar{\chi}_1(j\omega)|}. \quad (12)$$

Therefore, from Fig. 5 and equation (12), (13) can be concluded.

$$\begin{aligned} \bar{\chi}_1(j\omega) &= \frac{\bar{\chi}_0(j\omega)}{\cos\left(\frac{\theta}{2N}\right)} e^{-j\omega \frac{\tau^+ - \tau^-}{2N}} = \\ &= \frac{K^+ Q_2(j\omega)}{\cos\left(\omega \frac{\tau^+ - \tau^-}{2N}\right)} e^{-j\omega \left(\tau^+ + \frac{\tau^+ - \tau^-}{2N}\right)}. \end{aligned} \quad (13)$$

Therefore, the sector $\frac{\theta}{2N} = \frac{(\tau^+ - \tau^-)\omega}{2N}$ of the biggest arc can be enclosed by the edges $e(\bar{\chi}_0(j\omega), \bar{\chi}_1(j\omega))$, $e(\bar{\chi}_1(j\omega), \bar{\chi}_2(j\omega))$.

Based on the above explanations, the value set of

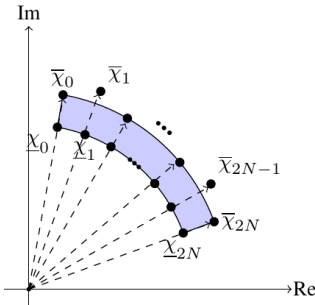


Fig. 4. A depiction of the value set of $K Q_2(j\omega) e^{-\tau j\omega}$ and the vertices $\chi_i(j\omega)$ (shown by χ_i).

$K Q_2(j\omega) e^{-\tau j\omega}$ can be included in the exposed edges $P_{Q_2}(j\omega)$ at a given frequency. ■

Now, by the exposed edges provided in Lemma 1, an auxiliary function is offered in the next theorem.

Theorem 3: Assume that $\omega_U \geq \frac{2\pi}{\tau^+ - \tau^-}$. The robust stability of the system under Assumption 1 can be ensured if:

- the PIR controller can stabilize one member of $\mathcal{Q}(s)$,

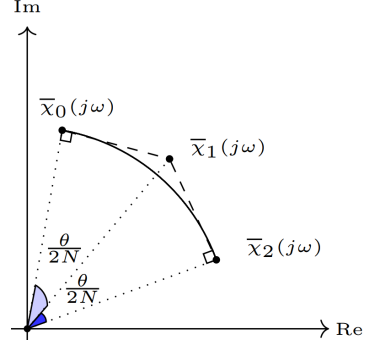


Fig. 5. Sector $\frac{\theta}{2N} = \frac{(\tau^+ - \tau^-)\omega}{2N}$ of the biggest arc (solid line) and the edges $e(\bar{\chi}_0(j\omega), \bar{\chi}_1(j\omega))$, $e(\bar{\chi}_1(j\omega), \bar{\chi}_2(j\omega))$ (dashed lines).

- $\Lambda(\omega) > 0$ holds for $\omega \in [0, \omega_U]$ where

$$\Lambda(\omega) = \begin{cases} \min\{\underline{\Delta}_i(\omega) | i = 1, 2\}, & \text{if } \omega \in [0, \frac{2\pi}{\tau^+ - \tau^-}), \\ \bar{\Lambda}(\omega), & \text{if } \omega \in [\frac{2\pi}{\tau^+ - \tau^-}, \omega_U], \end{cases} \quad (14)$$

where

$$\begin{aligned} \underline{\Delta}_1(\omega) &= \min\{\hat{\Delta}_{h,r}(\omega) | h \in \{1\}, r \in \{1, \dots, 4N+2\}\}, \\ \hat{\Delta}_{h,r}(\omega) &= |q_h(j\omega) + \chi_r(j\omega)| + |q_{h+1}(j\omega) + \chi_r(j\omega)| \\ &\quad - |q_h(j\omega) - q_{h+1}(j\omega)|, \end{aligned} \quad (15)$$

$$\begin{aligned} \underline{\Delta}_2(\omega) &= \min\{\bar{\Delta}_{h,r}(\omega) | h \in \{1, 2\}, r \in \{1, \dots, 4N+2\}\}, \\ \bar{\Delta}_{h,r}(\omega) &= |q_h(j\omega) + \chi_r(j\omega)| + |q_h(j\omega) + \chi_{r+1}(j\omega)| \\ &\quad - |\chi_r(j\omega) - \chi_{r+1}(j\omega)|, \end{aligned} \quad (16)$$

and $q_1(s) = s(T^-s + 1)$, $q_2(s) = s(T^+s + 1)$ and $\chi_{4N+3}(s) = \chi_1(s)$. Moreover, $\bar{\Lambda}(\omega)$ has been already defined in (8).

Proof: In the following, we show that at a given frequency $s = j\omega_0$ and $\omega_0 \in [0, \omega_U]$ if $\Lambda(\omega) > 0$ holds then the sets $F_1(s)$ and $P_{Q_2}(s)$ do not overlap in any way and consequently, based on the Lemma 1 and Theorem 1, the system would be robustly stable.

If the inequality $\underline{\Delta}_1(\omega) > 0$ holds then by the triangle inequality it can be understood that the points $\chi_r(s)$ do not lie on the line segment $F_1(s)$. Moreover, if $\underline{\Delta}_2(\omega) > 0$ holds then the vertices $q_i(s)$ do not intersect $P_{Q_2}(s)$ and this implies that the sets $F_1(s)$ and $P_{Q_2}(s)$ have not overlapped in the interval $\omega \in [0, \omega_U]$. ■

The following proposition can be simply proven by Theorem 3 and proposition 3.

Proposition 4: Assume that $\omega_U < \frac{2\pi}{\tau^+ - \tau^-}$ and the PIR controller can stabilize one member of $\mathcal{Q}(s)$. Then, the closed-loop system is robustly stable if $\Lambda(\omega) = \min\{\underline{\Delta}_i(\omega) | i = 1, 2\} > 0$ holds for $\omega \in [0, \omega_U]$.

IV. SIMULATION

Example 1: In [18], a plant model for the QNET-HVACT thermal platform has been identified as follows:

$$P(s) = \frac{0.9}{36s+1} e^{-s}. \quad (17)$$

Moreover, in the aforementioned paper, the following PIR controller has been designed:

$$C(s) = 0.8635 + \frac{0.62}{s} + 5.6166 e^{-1.6757s}. \quad (18)$$

Now, assume that the plant $P(s)$ in (17) has interval uncertainties as (19).

$$P(s) = \frac{[0.8, 1]}{[34, 38]s+1} e^{-[0.8, 1.2]s}. \quad (19)$$

The outcomes acquired in this paper demonstrate that the control system exhibits robust stability. Specifically, utilizing equation (9) renders ω_U equal to 1 rad/sec. Moreover, previous research in [18] had already established that the PIR controller (18) is capable of stabilizing the system in the absence of uncertainties, with the plant $P(s)$ in (17) remaining unaffected. Consequently, the sign of $\Lambda(\omega)$ must be solely evaluated within the range of $\omega \in [0, 1]$ rad/sec. Fig. 6 depicts $\Lambda(\omega)$, revealing its validity in the range of $\omega \in [0, 1]$ rad/sec. Consequently, from Proposition 4, it can be concluded that the PIR controller (18) robustly stabilizes the control system. It is worth noting that the previous works [14]-[21] lacked the capability to assess the robust stability of such systems. Conversely, the findings from the present study allow for a straightforward evaluation of the robust stability of multiple time delay systems in the presence of uncertainties.

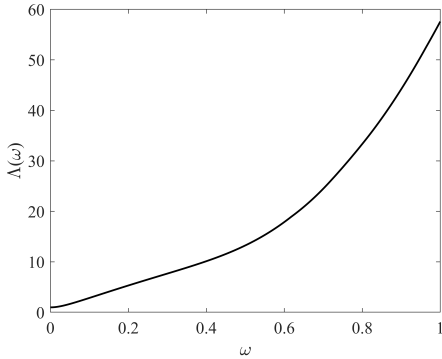


Fig. 6. $\Lambda(\omega)$ for $\omega \in [0, 1]$ rad/sec.

Example 2: Let us consider an interval plant described by equation (19) along with a PIR controller characterized by equation (21).

$$P(s) = \frac{[0.9, 1.1]}{[0.9, 1.1]s+1} e^{-[0.9, 1.1]s}. \quad (20)$$

$$C(s) = 0.1 + \frac{0.2}{s} + 0.1 e^{-s}. \quad (21)$$

Subsequently, we shall delve into the investigation of the robust stability of the system in question. By virtue of Theorem 2, ω_U can be calculated to be 1.4889 rad/sec. We shall proceed to evaluate the stability of a member of the characteristic function, namely $Q_0(s)$ in (22), by employing the argument of principle.

$$Q_0(s) = s(s+1) + (0.1s+0.2+0.1s e^{-s})e^{-s}. \quad (22)$$

The values of the function $\frac{Q_0(s)}{(s+1)^2}$ have been plotted in Fig. 8. As seen from this figure, the origin is not encircled and according to the argument of principle, so $Q_0(s)$ is stable. Therefore, from Proposition 4, the PIR controller (21) robustly stabilizes the control system.

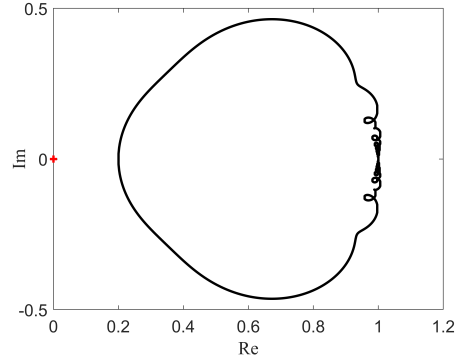


Fig. 7. $\frac{Q_0(s)}{(s+1)^2}$ for $s = j\omega$ and $-1000 \leq \omega \leq 1000$.

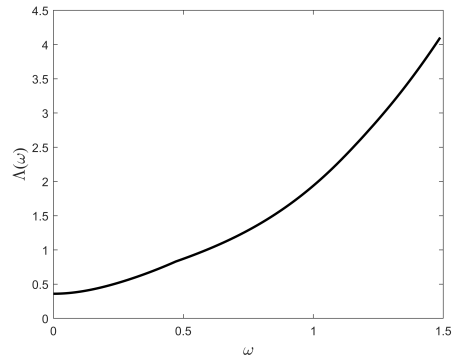


Fig. 8. $\Lambda(\omega)$ for $\omega \in [0, 1.4889]$ rad/sec.

V. CONCLUSIONS

Within the confines of this scholarly article, a comprehensive study was conducted to scrutinize the robust stability of interval time delay systems through the employment of

Proportional-Integral-Retarded (PIR) controllers. The analyzed system was assumed to have interval uncertainties with regards to its gain, delay, and time constant. The results obtained from this study encompass the necessary and sufficient conditions that lead to robust stability within the given control system. Furthermore, an upper bound and auxiliary function were introduced to expedite the analysis of the robust stability. In conclusion, two exemplars were presented to demonstrate the validity and accuracy of the aforementioned results.

REFERENCES

- [1] S. Uma, and A. S. Rao, "Enhanced modified Smith predictor for second-order non-minimum phase unstable processes," *International Journal of Systems Science*, vol. 47, no. 4, pp. 966–981, 2016.
- [2] R. A. Berry, and R. G. Gallager, "Communication over fading channels with delay constraints," *IEEE Transactions on Information theory*, vol. 48, no. 5, pp. 1135–1149, 2002.
- [3] S. Sönmez, and S. Ayasun, "Stability region in the parameter space of PI controller for a single-area load frequency control system with time delay," *IEEE Transactions on Power Systems*, vol. 31, no. 1, pp. 829–830, 2015.
- [4] J. G. Milton, "Time delays and the control of biological systems: An overview," *IFAC-PapersOnLine*, vol. 48, no. 12, pp. 87–92, 2015.
- [5] S. P. Bhattacharyya, H. Chapellat and L. H. Keel, "Robust control: the parametric approach," *Prentice Hall*, 1995.
- [6] G. R. Duan, and H. H. Yu, "LMIs in control systems: analysis, design and applications," *CRC press*, 2013.
- [7] H. Özbay, and A. N. Gündes, "PID and low-order controller design for guaranteed delay margin and pole placement," *International Journal of Robust and Nonlinear Control, International Journal of Robust and Nonlinear Control*, vol. 32, no. 18, pp. 9438–9451, 2021.
- [8] X. G. Li, S. I. Niculescu, J. X. Chen, and T. Chai, "Characterizing PID controllers for linear time-delay systems: a parameter-space approach," *IEEE Transactions on Automatic Control*, vol. 66, no. 10, pp. 4499–4513, 2020.
- [9] D. Ma, I. Boussaada, J. Chen, C. Bonnet, S. I. Niculescu, J. Chen, "PID control design for first-order delay systems via MID pole placement: Performance vs. robustness," *Automatica*, vol. 137, pp. 110102, 2022.
- [10] W. Altmann, "Practical process control for engineers and technicians," *Oxford: Newnes*, 2005.
- [11] I. Suh and Z. Bien, "Proportional minus delay controller," *IEEE Transactions on Automatic Control*, vol. 24, no. 2, pp. 370–372, 1979.
- [12] H. Suh and Z. Bien, "Use of time-delay actions in the controller design," *IEEE Transactions on Automatic Control*, vol. 25, no. 3, pp. 600–603, 1980.
- [13] S. I. Niculescu, and W. Michiels, "Stabilizing a chain of integrators using multiple delays," *IEEE Transactions on Automatic Control*, vol. 49, no. 5, pp. 802–807, 2004.
- [14] C. Abdallah, P. Dorato, J. Benites-Read, and R. Byrne, "Delayed positive feedback can stabilize oscillatory systems," *1993 American Control Conference*, pp. 3106–3107, 1993.
- [15] G. Ochoa-Ortega, R. Villafuerte-Segura, M. Ramirez-Neria, and L. Vite-Hernández, " σ -stabilization of a flexible joint robotic arm via delayed controllers," *Complexity*, <https://doi.org/10.1155/2019/7289689>.
- [16] N. S. Özbek, and I. Eker, "A novel delay-based control algorithm: Experimental application to an electromechanical system," *2017 10th International Conference on Electrical and Electronics Engineering (ELECO)*, pp. 842–846, 2017.
- [17] N. S. Özbek, and I. Eker, "Proportional-delayed controllers design for LTI-systems: a geometric approach," *International Journal of Control*, vol. 91, no. 4, pp. 907–925, 2018.
- [18] R. Villafuerte-Segura, "Controller with time-delay to stabilize first-order processes with dead-time," *Journal of Control Engineering and Applied Informatics*, vol. 20, no. 2, pp. 42–50, 2018.
- [19] R. Villafuerte-Segura, F. Medina-Dorantes, and L. Vite-Hernández, and B. Aguirre-Hernández, "Tuning of a time-delayed controller for a general class of second-order linear time invariant systems with dead-time," *IET Control Theory & Applications*, vol. 13, no. 3, pp. 451–457, 2019.
- [20] A. Ramirez, S. Mondie, R. Garrido, and R. Sipahi, "Design of proportional-integral-retarded (PIR) controllers for second-order LTI systems," *IEEE Transactions on Automatic Control*, vol. 61, no. 6, pp. 1688–1693, 2015.
- [21] R. Villafuerte, S. Mondie, and R. Garrido, "Tuning of proportional retarded controllers: theory and experiments," *IEEE Transactions on Control Systems Technology*, vol. 21, no. 3, pp. 983–990, 2012.
- [22] M. Ghorbani and M. Tavakoli-Kakhki, and A. A. Estarami, "Robust FOPID stabilization of retarded type fractional order plants with interval uncertainties and interval time delay," *Journal of the Franklin Institute*, vol. 356, no. 16, pp. 9302–9329, 2019.
- [23] M. Ghorbani, M. Tavakoli-Kakhki, A. Tepjakov, and E. Petlenkov, "Robust stability analysis of smith predictor based interval fractional-order control systems: A case study in level control process," *IEEE/CAA Journal of Automatica Sinica*, vol. 10, no. 3, pp. 762–780, 2022.
- [24] M. Fu, S. Dasgupta, and V. Blondel, "Robust stability under a class of nonlinear parametric perturbations," *IEEE Transactions on Automatic Control*, vol. 40, no. 2, pp. 213–223, 1995.


Appendix 11

XI

M. Ghorbani, A. Tepljakov, and E. Petlenkov. Robust stabilization of interval fractional-order plants with an interval time delay by fractional-order proportional integral derivative controllers. *IET Control Theory & Applications*, 18(5):614–625, 2024.

ORIGINAL RESEARCH

Robust stabilization of interval fractional-order plants with an interval time delay by fractional-order proportional integral derivative controllers

Majid Ghorbani  | Aleksei Tepljakov | Eduard Petlenkov

Department of Computer Systems, Tallinn
University of Technology, Tallinn, Estonia

Correspondence

Majid Ghorbani, Tallinn University of Technology,
Department of Computer Systems.
Email: majid.ghorbani@taltech.ee

Funding information

Estonian Research Council, Grant/Award Number:
PRG658

Abstract

This paper concentrates on presenting a reliable procedure to compute the stabilizing region of fractional-order proportional integral derivative (FOPID) controllers for interval fractional-order plants having an interval time delay. An interval fractional-order plant is defined as a fractional-order transfer function whose denominator and numerator coefficients are all uncertain and lie in specified intervals. Also, an interval time delay points to a delay term whose value varies in a specific interval. The D-decomposition technique and the value set concept are employed to determine the stabilizing region of FOPID controllers. In this study, first, a theorem is presented to compute the boundary of the value sets of systems having interval time delay. Then, a lemma is provided for robust stability analysis of the given closed-loop control system. For a convenient use of the paper results, an algorithm is proposed to solve the problem of robustly stabilizing interval fractional-order plants with an interval time delay using FOPID controllers. Finally, four examples are provided to illustrate the proposed procedure.

1 | INTRODUCTION

1.1 | Background

Recently, FOPID controllers have attracted much attention. Because, it provides more flexibility for controller design in comparison to the integer-order counterparts [1]. Meanwhile, it has been also shown that fractional-order controllers can achieve better robustness and performance than the integer-order counterparts [2]. Hence, many interesting procedures have been proposed to design FOPID controllers in [3–7]. Therefore, fractional calculus is becoming one of the powerful modern tools in engineering disciplines, especially, control systems engineering.

Time delay and uncertainties are also omnipresent in control systems. Not surprisingly, considerable attention has been paid to study the fractional-order time-delay systems having uncertainties. For some of the samples in this regard, see [8, 9].

Robust stability analysis is fundamental to any control system. Accordingly, various design methods for robust stability analysis of fractional-order systems have been presented in

[10, 11] by benefiting from the value set concept. The value set method is mainly based on the zero exclusion principle. In [12], necessary and sufficient conditions for robust stability analysis of fractional-order systems have been presented using the zero exclusion principle. Determining the precise shape of the value set of the characteristic function of the closed-loop system is essential based on this principle. Hence, in Procedure 1 of [13], it has been proven that the value set of an interval fractional-order polynomial is a parpolygon shape in the complex plane. Then, the robust stability analysis of such systems has been presented by an auxiliary function. Later, the results provided in [13] have been developed to analyze the robust stability of fractional-order controllers for systems having fractional-order characteristic functions in [14–16].

Lately, some procedures have been proposed to calculate the stabilizing region of fractional-order controllers for fractional-order plants with time delay in [17–19]. They can compute a set of all stabilizing fractional-order controllers for a given fractional-order plant without uncertainty. Therefore, the topic of calculating the stabilizing region of fractional-order controllers has been appealing among scientists.

This is an open access article under the terms of the [Creative Commons Attribution-NonCommercial](https://creativecommons.org/licenses/by-nc/4.0/) License, which permits use, distribution and reproduction in any medium, provided the original work is properly cited and is not used for commercial purposes.

© 2023 The Authors. *IET Control Theory & Applications* published by John Wiley & Sons Ltd on behalf of The Institution of Engineering and Technology.

Recently, a procedure in [20] has been incorrectly presented to calculate the stabilizing region of fractional-order proportional integral derivative (FOPID) controllers for interval fractional-order plants with an interval time delay. More precisely, in [20], by the value set concept and the D-decomposition procedure, an algorithm was presented in order to compute the robust stability region of FOPID controllers for interval plants with an interval time delay. Without any exact proof, the study [20] has shown that the stabilizing region of FOPID controllers can be calculated by some vertex polynomials. As discussed in Example 1 of the present paper, such methods cannot be correct in general and it is shown that the extensions in [20] are unreliable for robust stability analysis of a closed-loop system consisting an interval plant and a FOPID controller. Because, the boundary of the value set cannot be obtained by the method presented in [20] (see Example 1). In fact, the value set of systems having interval delay is nonconvex shape and it cannot be simply described by some certain vertices.

Despite the extensive study concerning the problem of robustly calculating the stabilizing region of FOPID controllers for fractional-order systems having time delay [21–26], a valid mathematical proof of calculating the value set for these systems seems to be elusive. It should be noted that, for the interval fractional-order plants with an interval time delay, the study of the stabilizing region of FOPID controllers has not been well elaborated and it is a renewed research area. Therefore, the boundary of the value set of such interval time delay systems are exactly investigated in Theorem 1 of the paper and necessary and sufficient robust conditions are then provided in Lemma 1. Also, for a convenient use, an algorithm is provided to calculate the stabilizing region of FOPID controllers for systems having interval time delay based on the methodology presented in this paper. This useful algorithm facilitates to obtain the stabilizing region of FOPID controllers. The computation of the stabilizing region of FOPID controllers provides the following benefits [27]:

- Instead of simply one stabilizing FOPID controller, a set is offered for the control system and this means allowing for a more flexible selection of controller parameters.
- The stabilizing region can facilitate the optimal design of other additional design criteria.

1.2 | Problem statement and main contributions

According to the discussions in the previous subsection, the following problems can be formulated as follows.

Problem 1. The value set of a characteristic function with an interval time delay is a nonconvex shape in the complex plane. On the other hand, in [20], some exposed edges have been obtained to construct the boundary of the value set. However, as it will be shown in Example 1, this method is incorrect for the general case of nonconvex shaped value sets. As a result, the first problem is how to define the boundary of the value set of

ALGORITHM 1 The calculation of the stabilizing region of FOPID controllers can be mainly performed by the following steps:

Step 1: Obtain the set of vertex polynomials V^D by **Procedure 1**.

Step 2: For fixed values of λ , μ , and k_d , determine the stabilizing region of a certain quasi-polynomial as $\hat{\Delta}(s)$ by the D-decomposition in Remark 4.

Step 3: For the same fixed values of λ , μ and k_d , determine the stabilizing region of all quasi-polynomials belonging to $\Delta_E(s)$ presented in Equation (21).

a characteristic function possessing an interval time delay which is a nonconvex shape.

Problem 2. Presenting necessary and sufficient conditions for robust stability analysis of fractional-order systems having interval time delay.

Problem 3. Finding a reliable method to determine the stabilizing region of FOPID controllers for systems having interval time delay.

Motivated by the above problems, we will focus on computing the stabilizing region for fractional-order systems having an interval time delay. The main novelties and contributions of the paper in comparison to the existing procedures can be summarized as follows:

- Presenting a procedure to exactly determine the boundary of the value set of interval fractional-order characteristic functions having an interval time delay (see Theorem 1).
- Presenting necessary and sufficient conditions for the considered types of systems having interval time delay (see Lemma 3).
- Presenting a reliable method to compute the stabilizing region of FOPID controllers (see Algorithm 1).
- Presenting some sufficient conditions in designing robust FOPID stabilization for high-order transfer functions in the presence of uncertainties (see Theorems 2 and 3).

1.3 | Organization of the manuscript

The paper is organized as follows: some preliminaries are provided in Section 2. In Section 3, the main results of the paper on robust FOPID stabilization are presented. Some special cases are investigated in Section 4. In Section 5, the paper results are evaluated in some examples. In Section 6, a comparison between our results and the existing methods will be presented. Finally, Section 7 offers some conclusion remarks.

2 | PRELIMINARIES

In this section, notations held by the paper are declared, and the related background is recalled.

Notation. Define sets $\mathbb{R}^{\geq 0} \triangleq \{x \in \mathbb{R} : x \geq 0\}$, $\mathbb{N}^{\leq n} \triangleq \{x \in \mathbb{N} : x \leq n\}$ and $\mathbb{Z}_{\geq m}^{\leq n} \triangleq \{x \in \mathbb{Z} : m \leq x \leq n\}$. $\text{floor}(x)$ is the

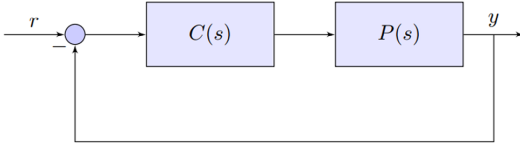


FIGURE 1 Closed-loop control system.

largest integer less than or equal to $x \in \mathbb{R}$. $n(B)$ shows the number of distinct members of set B . $\text{frac}(x) \triangleq x - \text{floor}(x)$ for all $x \in \mathbb{R}$. Also, $A \cup B \triangleq \{x : x \in A \text{ or } x \in B\}$ for any two sets A and B . Also, $\partial(\Delta)$ shows the boundary of Δ in the complex plane.

Consider the closed-loop control system as shown in Figure 1, $P(s)$ represents an interval fractional-order plant with an interval time delay as

$$P(s) = \frac{K}{D(s, \mathbf{a})} e^{-ls} = \frac{K}{\sum_{i_2=0}^n a_{i_2} s^{\alpha_{i_2}}} e^{-ls}, \quad (1)$$

where s is the Laplace operator, $n \in \mathbb{Z}^+$ and $\alpha_n > \alpha_{n-1} > \dots > \alpha_1 > \alpha_0 = 0$ are arbitrary real numbers. Also, l is the positive time delay $l \in [l^-, l^+]$ and the positive gain lies in $K \in [\underline{K}, \bar{K}]$, and $\mathbf{a} = [a_0, a_1, \dots, a_n]^T$ are the coefficients vector belonging to the following set:

$$\mathbf{a} \in \mathbf{A} = \left\{ \mathbf{a} \in \mathbb{R}^{n+1} \mid a_{i_2} \in [a_{i_2}^-, a_{i_2}^+], a_n \neq 0, i_2 \in \mathbb{Z}_{\geq 0}^n \right\}, \quad (2)$$

where, $[a_{i_2}^-, a_{i_2}^+]$ are specified intervals. Also, $C(s)$ is the FOPID controller and is given as Equation (3).

$$C(s) = \frac{N_c(s)}{s^\lambda} = \frac{k_p s^\lambda + k_i + k_d s^{\mu+\lambda}}{s^\lambda}, \quad (3)$$

$$0 < \lambda, \mu < 2, \alpha_n > \mu.$$

Remark 1. Some examples of identified physical systems as Equation (1) are a coupled-tanks apparatus [28], a heat flow equipment [29], DC- servo systems [30] and laboratory temperature control setups [31].

The characteristic function of this system can be obtained as follows.

$$\Delta(s) = s^\lambda D(s, \mathbf{a}) + (k_p s^\lambda + k_i + k_d s^{\mu+\lambda}) K e^{-ls}. \quad (4)$$

Remark 2. The principal branch of $\Delta(s)$ in Equation (4) is defined such as Definition 1 in [12] i.e. $\text{Arg}(s) \in (-\pi, \pi]$.

Definition 1. According to [32, 33], the closed-loop control system depicted in Figure 1 is stable if and only if the characteristic function $\Delta(s)$ in Equation (4) has no zero in Closed right half plane (CRHP). If all members of $\Delta(s)$ in Equation (4) have no zero in CRHP, then the robust stability of closed-loop control system is achieved. Hence, a robust FOPID controller is

able to robustly stabilize the closed-loop control system such that any arbitrary members of $\Delta(s)$ in Equation (4) has no zero in CRHP.

Remark 3. Based on [13], the value set of $D(s, \mathbf{a})$ is a parpolygon in the complex plane for $s = j\omega \wedge \omega > 0$. The vertex polynomials corresponding to $D(j\omega, \mathbf{a})$ are determined for $\omega \geq 0$ by using Procedure 1.

Procedure 1 [13]. Define $H_0 \triangleq \{i_2 \in \mathbb{Z}_{\geq 0}^n : a_{i_2}^- < a_{i_2}^+\}$. The value set $D(j\omega, \mathbf{a})$ is determined for $\omega \in \mathbb{R}_{\geq 0}^n$ as follows:

1. For $H_0 = \emptyset$ and $\omega \geq 0$, $D(j\omega, \mathbf{a}) = D_0(j\omega)$ where

$$D_0(\omega) \triangleq \sum_{i_2=0}^n a_{i_2}^- s^{\alpha_{i_2}}, \quad (5)$$

2. For $H_0 \neq \emptyset$,

- If $\omega = 0$, then $D(j\omega, \mathbf{a}) = D(j0, \mathbf{a}) = [a_0^-, a_0^+]$.
- If $\omega > 0$, then define $B_0 \triangleq \{\text{frac}(0.5\alpha_{i_2}) : i_2 \in H_0\}$ and $m_D \triangleq n(B_0)$. Consider $\gamma_1, \dots, \gamma_{m_D-1}, \gamma_{m_D}$ as all the distinct members of B_0 sorted as $0 \leq \gamma_1 < \dots < \gamma_{m_D-1} < \gamma_{m_D} < 1$. Then, define the following sets:

$$H_r' \triangleq \left\{ i_2 \in H_0 : \text{floor}(0.5\alpha_{i_2}) \text{ is an odd number and } \text{frac}(0.5\alpha_{i_2}) = \gamma_r \right\},$$

$$H_r \triangleq \left\{ i_2 \in H_0 : \text{floor}(0.5\alpha_{i_2}) \text{ is an even number and } \text{frac}(0.5\alpha_{i_2}) = \gamma_r \right\}, \quad r = 1, 2, \dots, m_D. \quad (6)$$

Let $a^- \triangleq [a_0^-, a_1^- \dots a_n^-]^T$ and $a^+ \triangleq [a_0^+, a_1^+ \dots a_n^+]^T$. The vectors q^1, q^2, \dots, q^{m_D} are defined as follows:

$$a^k \triangleq [a_0^k, a_1^k \dots a_n^k]^T, a^{m_D+k} \triangleq [a_0^{m_D+k}, a_1^{m_D+k} \dots a_n^{m_D+k}]^T$$

$$= a^+ + a^- - a^k, \quad k = 1, \dots, m_D, \quad (7)$$

where for $i_2 = 0, 1, \dots, n$ and $k = 1, \dots, m_D$, it can be written that

$$a_{i_2}^k \triangleq \begin{cases} a_{i_2}^+, & \text{for } i_2 \in \left(\bigcup_{i=1}^{k-1} H_i \right) \cup \left(\bigcup_{i=k}^{m_D} H_i' \right), \\ a_{i_2}^-, & \text{for otherwise.} \end{cases} \quad (8)$$

and

$$a_{i_2}^{m_D+k} \triangleq a_{i_2}^+ + a_{i_2}^- - a_{i_2}^k. \quad (9)$$

Hence, the consecutive vertices $V_{r_2}^-(j\omega)$ ($r_2 = 1, 2, \dots, 2m_D$) are calculated by

$$V_k^-(j\omega) \triangleq D(j\omega, a^k), V_{m_D+k}^-(j\omega) \triangleq D(j\omega, a^{m_D+k})$$

$$= D(j\omega, a^+ + a^- - a^k), \quad k = 1, 2, \dots, m_D. \quad (10)$$

Remark 4. Consider a certain polynomial of $\Delta(s)$ in Equation (4) as $\hat{\Delta}(s)$ in Equation (11).

$$\hat{\Delta}(s) = s^\lambda \sum_{i_2=0}^n \hat{a}_{i_2} s^{\alpha_{i_2}} + N_c(s) \left(\sum_{i_1=0}^m \hat{b}_{i_1} s^{\beta_{i_1}} \right) e^{-\lambda s}. \quad (11)$$

Then, the boundaries of the stabilizing region $\hat{\Delta}(s)$ in Equation (11) are specified by infinite root boundary (IRB), real root boundary (RRB) and complex root boundary (CRB) which can be determined by [17]. In summary, the mentioned boundaries are stated based on the procedure proposed in [17] as follows.

- **RRB:** $\hat{\Delta}(0) = \kappa_i \hat{b}_0$. If $\kappa_i \hat{b}_0 \neq 0$, then $\kappa_i = 0$. Otherwise, the boundary does not exist.
- **IRB:** $\hat{\Delta}(\infty) = 0$.

$$\begin{cases} \kappa_d = 0, & \text{for } \alpha_n = \beta_m \text{ or} \\ & (\alpha_n > \beta_m \text{ and } \mu > \alpha_n - \beta_\mu), \\ \kappa_d = -\frac{\hat{a}_0}{\hat{b}_0}, & \text{for } (\alpha_n > \beta_m \text{ and } \mu = \alpha_n - \beta_\mu), \\ \text{none,} & \text{for } (\alpha_n > \beta_m \text{ and } \mu < \alpha_n - \beta_\mu). \end{cases} \quad (12)$$

- **CRB:** By solving $\hat{\Delta}(j\omega) = 0$, the κ_p and κ_i parameters in terms of κ_d , λ and μ are obtained as

$$\begin{aligned} \kappa_p &= (\mathcal{A}_2(\omega)B_1(\omega) - \mathcal{A}_1(\omega)B_2(\omega) + \kappa_d (B_1(\omega)B_6(\omega) \\ &\quad - B_2(\omega)B_5(\omega))) / (B_2(\omega)B_3(\omega) - B_1(\omega)B_4(\omega)), \\ \kappa_i &= (\mathcal{A}_1(\omega)B_4(\omega) - \mathcal{A}_2(\omega)B_3(\omega) + \kappa_d (B_4(\omega)B_5(\omega) \\ &\quad - B_3(\omega)B_6(\omega))) / (B_2(\omega)B_3(\omega) - B_1(\omega)B_4(\omega)), \end{aligned} \quad (13)$$

where

$$\begin{cases} \mathcal{A}_1(\omega) = \sum_{i_2=0}^n \hat{a}_{i_2} \omega^{\lambda+\alpha_{i_2}} \cos\left(\frac{\pi(\alpha_{i_2}+\lambda)}{2} + \lambda\omega\right), \\ \mathcal{A}_2(\omega) = \sum_{i_2=0}^n \hat{a}_{i_2} \omega^{\lambda+\alpha_{i_2}} \sin\left(\frac{\pi(\alpha_{i_2}+\lambda)}{2} + \lambda\omega\right), \\ B_1(\omega) = \sum_{i_1=0}^m \hat{b}_{i_1} \omega^{\beta_{i_1}} \cos\left(\frac{\pi\beta_{i_1}}{2}\right), \\ B_2(\omega) = \sum_{i_1=0}^m \hat{b}_{i_1} \omega^{\beta_{i_1}} \sin\left(\frac{\pi\beta_{i_1}}{2}\right), \\ B_3(\omega) = \sum_{i_1=0}^m \hat{b}_{i_1} \omega^{\beta_{i_1}+\lambda} \cos\left(\frac{\pi(\beta_{i_1}+\lambda)}{2}\right), \\ B_4(\omega) = \sum_{i_1=0}^m \hat{b}_{i_1} \omega^{\beta_{i_1}+\lambda} \sin\left(\frac{\pi(\beta_{i_1}+\lambda)}{2}\right), \\ B_5(\omega) = \sum_{i_1=0}^m \hat{b}_{i_1} \omega^{\beta_{i_1}+\lambda+\mu} \cos\left(\frac{\pi(\beta_{i_1}+\lambda+\mu)}{2}\right), \\ B_6(\omega) = \sum_{i_1=0}^m \hat{b}_{i_1} \omega^{\beta_{i_1}+\lambda+\mu} \sin\left(\frac{\pi(\beta_{i_1}+\lambda+\mu)}{2}\right). \end{cases} \quad (14)$$

Accordingly, the stabilizing region can be determined by checking one arbitrary test point inside each region [17].

According to the above analysis, the followings are mainly the purposes of this paper:

- Extending the procedure proposed in [17] to compute the stabilizing region of FOPID controllers for the interval delayed fractional-order plant (1).
- Presenting a reliable method for calculating the stabilizing region of FOPID controllers.

In this study, the zero exclusion principle is employed for robust stability analysis of the system which is as follows.

Zero exclusion principle: The closed-loop system shown in Figure 1 is robust stable if and only if $\Delta(s)$ has at least one stable member and $0 \notin \Delta(j\omega)$ for $\omega \geq 0$.

To obtain the boundary of a value set, the following property is needed in the rest of this paper.

Lemma 1 [34]. For two bounded and closed value sets \mathcal{Q}_1 and \mathcal{Q}_2 , $\partial(\mathcal{Q}_1 + \mathcal{Q}_2) \subseteq \partial(\mathcal{Q}_1) + \partial(\mathcal{Q}_2)$.

3 | MAIN RESULTS

In this section, at first, the boundary of $\Delta(j\omega)$ is discussed. Then, an algorithm is presented to explain how to calculate the stabilizing region of FOPID controllers for systems having interval time delay.

To this end, at first consider the following definition.

Definition 2. For terms K , $e^{-\lambda s}$ and $D(s, a)$, define:

$$\begin{aligned} \mathbf{V}^K &= \{K^-, K^+\}, \mathbf{I}^K = [K^-, K^+], \mathbf{V}^l = \{l^-, l^+\}, \mathbf{I}^l = [l^-, l^+], \\ \mathbf{V}^D &= \{V_1^-(\omega), V_2^-(\omega), \dots, V_{2m_D}^-(\omega)\}, \\ \mathbf{I}^D &= \{\mathbf{I}_1^D, \mathbf{I}_2^D, \dots, \mathbf{I}_{2m_D}^D\} = \{\underbrace{[V_1^-(\omega), V_2^-(\omega)]}_{\mathbf{I}_1^D}, \dots, \\ &\quad \underbrace{[V_{2m_D}^-(\omega), V_1^-(\omega)]}_{\mathbf{I}_{2m_D}^D}\}, \end{aligned} \quad (15)$$

where $[V_x, V_y]$ is a line segment joining pairs of polynomials V_x and V_y .

Note that let $s = j\omega$ in $K e^{-\lambda s}$, then it can be simply concluded that $\partial(K e^{-\lambda s}) \subseteq \mathbf{V}^K e^{-\mathbf{I}^l s} \cup \mathbf{I}^K e^{-\mathbf{V}^l s}$. Accordingly, $\partial(K e^{-\lambda s})$ is constructed by two line segments and two arc segments.

In the next lemma, sum of a line segment and a convex polygon in the complex plane is investigated. Surely, this property shall be used to obtain $\partial(\Delta(j\omega))$ at a given frequency.

Lemma 2. Given a frequency $\omega_0 \geq 0$, for $s = j\omega_0$, the following property holds:

$$\begin{aligned} \partial(s^\lambda D(s, \mathbf{a}) + N_c(s) \mathbf{I}^K e^{-\mathbf{V}^l s}) &\subseteq (s^\lambda \mathbf{I}^D + N_c(s) \mathbf{V}^K e^{-\mathbf{V}^l s}) \cup \\ &\quad (s^\lambda \mathbf{V}^D + N_c(s) \mathbf{I}^K e^{-\mathbf{V}^l s}). \end{aligned} \quad (16)$$

Proof. We commence the proof by recalling the property obtained in Lemma 1:

$$\partial(s^\lambda D(s, \mathbf{a}) + N_c(s) \mathbf{I}^K e^{-\mathbf{V}^l s}) \subseteq s^\lambda \mathbf{I}^D + N_c(s) \mathbf{I}^K e^{-\mathbf{V}^l s}. \quad (17)$$

Also, from Definition 2 we have:

$$\begin{aligned} \{ (s^\lambda \mathbf{I}^D + N_c(s) \mathbf{I}^K e^{-\mathbf{V}^l s}) = (s^\lambda \{\mathbf{I}_1^D, \mathbf{I}_2^D, \dots, \mathbf{I}_{2m_D}^D\} + \\ N_c(s) \mathbf{I}^K e^{-\mathbf{V}^l s}) \}. \end{aligned} \quad (18)$$

Now, consider two independent line segments $[s^\lambda V_1^-(\omega), s^\lambda V_2^-(\omega)]$ and $[N_c(s) e^{-\mathbf{V}^l s} K^-, N_c(s) e^{-\mathbf{V}^l s} K^+]$, then based on Procedure 1, we have

$$\begin{aligned} [s^\lambda V_1^-(\omega), s^\lambda V_2^-(\omega)] + [N_c(s) e^{-\mathbf{V}^l s} K^-, N_c(s) e^{-\mathbf{V}^l s} K^+] \subseteq \\ ([s^\lambda V_1^-(\omega), s^\lambda V_2^-(\omega)] + N_c(s) e^{-\mathbf{V}^l s} \mathbf{V}^K) \cup \\ (s^\lambda \{V_1^-(\omega), V_2^-(\omega)\} + [N_c(s) e^{-\mathbf{V}^l s} K^-, N_c(s) e^{-\mathbf{V}^l s} K^+])). \end{aligned} \quad (19)$$

Now, we can extend the Equation (19) to all edges \mathbf{I}^D as shown in Equation (20).

$$\begin{aligned} [s^\lambda V_i^-(\omega), s^\lambda V_{i+1}^-(\omega)] + [N_c(s) e^{-\mathbf{V}^l s} K^-, N_c(s) e^{-\mathbf{V}^l s} K^+] \subseteq \\ ([s^\lambda V_i^-(\omega), s^\lambda V_{i+1}^-(\omega)] + N_c(s) e^{-\mathbf{V}^l s} \mathbf{V}^K) \cup \\ (s^\lambda \{V_i^-(\omega), V_{i+1}^-(\omega)\} + [N_c(s) e^{-\mathbf{V}^l s} K^-, N_c(s) e^{-\mathbf{V}^l s} K^+])). \end{aligned} \quad (20)$$

Thus from Equations (17)–(20), Equation (16) can be deduced. \square

Now, the following theorem is presented to obtain $\partial(\Delta(j\omega))$ at a given frequency.

Theorem 1. For $s = j\omega_0$, we have:

$$\begin{aligned} \partial(\Delta(s)) \subseteq \Delta_E(s) = \\ \begin{cases} (s^\lambda \mathbf{I}^D + N_c(s) \mathbf{V}^K e^{-\mathbf{I}^l s}) \cup \\ (s^\lambda \mathbf{V}^D + N_c(s) \mathbf{I}^K e^{-\mathbf{V}^l s}), & \text{for } 0 \leq \omega_0 < \frac{2\pi}{l^+ - l^-}, \\ (s^\lambda \mathbf{I}^D + N_c(s) \mathbf{V}^K e^{-[0, 2\pi]j}), & \text{for } \omega_0 \geq \frac{2\pi}{l^+ - l^-}. \end{cases} \end{aligned} \quad (21)$$

Proof. Based on Lemmas 1 and 2 and assuming $0 \leq \omega_0 < \frac{2\pi}{l^+ - l^-}$, one can write:

$$\begin{aligned} \partial(\Delta(s)) \subseteq \\ (s^\lambda \mathbf{I}^D + N_c(s) \mathbf{V}^K e^{-\mathbf{I}^l s}) \cup (s^\lambda \mathbf{I}^D + N_c(s) \mathbf{I}^K e^{-\mathbf{V}^l s}) \subseteq \\ (s^\lambda \mathbf{I}^D + N_c(s) \mathbf{V}^K e^{-\mathbf{I}^l s}) \cup (s^\lambda \mathbf{I}^D + N_c(s) \mathbf{V}^K e^{-\mathbf{V}^l s}) \cup \\ (s^\lambda \mathbf{V}^D + N_c(s) \mathbf{I}^K e^{-\mathbf{V}^l s}). \end{aligned} \quad (22)$$

On the other hand, we know that $\mathbf{V}^K e^{-\mathbf{V}^l s} \subseteq \mathbf{V}^K e^{-\mathbf{I}^l s}$. Therefore, the proof is completed for $0 \leq \omega_0 < \frac{2\pi}{l^+ - l^-}$. Also, the

proof for $\omega_0 \geq \frac{2\pi}{l^+ - l^-}$ can be obtained by using Equation (22) and the fact $\partial(K e^{-\mathbf{I}^l s}) \subseteq \mathbf{V}^K e^{-[0, 2\pi]j}$ in a straightforward way. \square

In Theorem 1, the boundary of the value set of $\Delta(j\omega)$ is determined. This theorem plays a fundamental role in deriving the necessary and sufficient robust criteria of the closed-loop control system.

Lemma 3. The closed-loop control system is robust stable, if and only if:

- $\Delta(s)$ contains at least one stable member as $\hat{\Delta}(j\omega)$.
- $0 \notin \Delta_E(s)$ for $s = j\omega$ and $\omega \geq 0$.

Proof. The proof can be given by the zero exclusion principle in [12]. According to this principle, it can be directly concluded that $\Delta(s)$ is robust stable if and only if $\Delta(s)$ contains at least one stable member as $\hat{\Delta}(j\omega)$ and $0 \notin \Delta(s)$, $s = j\omega$ and $\omega \geq 0$. Moreover, as shown in Theorem 2, $\partial(\Delta(s)) \subseteq \Delta_E(s)$ and consequently $0 \notin \Delta(s)$, if and only if $0 \notin \Delta_E(s)$. \square

Now, by benefiting from the following algorithm, the stabilizing region of FOPID controllers can be calculated for systems having an interval time delay.

Proof. Based on the zero exclusion principle, it can be inferred that the closed-loop control system is robust stable if and only if $\Delta(s)$ contains at least one stable member and $0 \notin \partial(\Delta(j\omega))$. On the other hand, stabilization of all quasi-polynomials $\Delta_E(s)$ in Equation (21) calculated by the D-decomposition method in Remark 4 can assure the robust stability of $\Delta(j\omega)$ based on Theorem 1 and Lemma 3 because of $\partial(\Delta(j\omega)) \subseteq \Delta_E(j\omega)$. This means that $0 \notin \partial(\Delta(j\omega))$ and also there is at least one stable member in $\Delta(s)$. Therefore, the zero exclusion principle completes the proof. \square

Remark 5. Because of the interval time delay term, the value set of $\Delta(j\omega)$ is nonconvex shape. However, Theorem 1 determines the boundary of $\Delta(j\omega)$ in Equation (4). Also, Lemma 3 presents necessary and sufficient conditions for robust stability analysis of fractional-order systems having interval time delay as $\Delta(s)$ in Equation (4). Note that based on Theorem 3.1 in [20], the robust stability of $\Delta(s)$ in Equation (4) can be achieved by analyzing the stability of the vertices $s^\lambda \mathbf{V}^D + N_c(s) \mathbf{V}^K e^{-\mathbf{V}^l s}$. Whereas, Lemma 3 shows that it is not enough to investigate the stability of the closed-loop system only by the vertices $s^\lambda \mathbf{V}^D + N_c(s) \mathbf{V}^K e^{-\mathbf{V}^l s}$ (see Example 1).

Remark 6. Surely, one can use the Algorithm 1 in the (k_p, k_d) plane and the (k_i, k_d) plane. To do this, the k_p and k_d parameters in terms of λ, μ and k_i can be obtained as:

$$\begin{aligned} k_p = \\ \frac{A_2(\omega)B_5(\omega) - A_1(\omega)B_6(\omega) + k_i(B_2(\omega)B_5(\omega) - B_1(\omega)B_6(\omega))}{B_3(\omega)B_6(\omega) - B_4(\omega)B_5(\omega)}, \end{aligned}$$

$$k_d = \frac{A_1(\omega)B_4(\omega) - A_2(\omega)B_3(\omega) + k_i(B_1(\omega)B_4(\omega) - B_2(\omega)B_3(\omega))}{B_3(\omega)B_6(\omega) - B_4(\omega)B_5(\omega)}. \quad (23)$$

Likewise, the k_i and k_d parameters in terms of λ , μ , and k_p are obtained as:

$$k_i = \frac{A_2(\omega)B_5(\omega) - A_1(\omega)B_6(\omega) + k_p(B_4(\omega)B_5(\omega) - B_3(\omega)B_6(\omega))}{B_1(\omega)B_6(\omega) - B_2(\omega)B_5(\omega)},$$

$$k_d = \frac{A_1(\omega)B_2(\omega) - A_2(\omega)B_1(\omega) + k_p(B_2(\omega)B_3(\omega) - B_1(\omega)B_4(\omega))}{B_1(\omega)B_6(\omega) - B_2(\omega)B_5(\omega)}. \quad (24)$$

4 | SOME SPECIAL CASES

In this section, we will discuss on calculating the stabilizing region of FOPID controllers for some special fractional-order plants having interval time delay.

4.1 | Case of $D(s) = D_1(s) = (\tau s + 1)^n, n \in \mathbb{N}$:

For the case $D(s) = D_1(s) = (\tau s + 1)^n, \tau > 0$ and $\tau \in [\tau^-, \tau^+]$, the characteristic function of the system can be rewrite as

$$\Delta_1(s) = s^\lambda (\tau s + 1)^n + (k_p s^\lambda + k_i + k_d s^{\mu+\lambda}) K e^{-ls}. \quad (25)$$

For robust stability analysis of $\Delta_1(s)$ in Equation (25), we first give the following definition:

Definition 3. Assume that

$$D_1(s) = (\tau s + 1)^n = q_n s^n + q_{n-1} s^{n-1} + \dots + q_2 s^2 + q_1 s + 1, q_i \in [\underline{q}_i, \bar{q}_i], i = 1, \dots, n. \quad (26)$$

Then, define:

$$\begin{aligned} \tilde{\mathbf{V}}^{D_1} &= \{\tilde{V}_1^{D_1}(\omega), \tilde{V}_2^{D_1}(\omega), \tilde{V}_3^{D_1}(\omega), \tilde{V}_4^{D_1}(\omega)\}, \\ \tilde{\mathbf{I}}^{D_1} &= \{\tilde{\mathbf{I}}_1^{D_1}, \tilde{\mathbf{I}}_2^{D_1}, \tilde{\mathbf{I}}_3^{D_1}, \tilde{\mathbf{I}}_4^{D_1}\} \\ &= \{[\tilde{V}_1^{D_1}(\omega), \tilde{V}_2^{D_1}(\omega)], [\tilde{V}_2^{D_1}(\omega), \tilde{V}_3^{D_1}(\omega)], \\ &\quad [\tilde{V}_3^{D_1}(\omega), \tilde{V}_4^{D_1}(\omega)], [\tilde{V}_4^{D_1}(\omega), \tilde{V}_1^{D_1}(\omega)]\}, \end{aligned} \quad (27)$$

where

$$\begin{cases} \tilde{V}_1^{D_1} = 1 + \underline{q}_1 s + \bar{q}_2 s^2 + \bar{q}_3 s^3 + \dots, \\ \tilde{V}_2^{D_1} = 1 + \underline{q}_1 s + \underline{q}_2 s^2 + \bar{q}_3 s^3 + \dots, \\ \tilde{V}_3^{D_1} = 1 + \bar{q}_1 s + \underline{q}_2 s^2 + \underline{q}_3 s^3 + \dots, \\ \tilde{V}_4^{D_1} = 1 + \bar{q}_1 s + \bar{q}_2 s^2 + \underline{q}_3 s^3 + \dots, \end{cases} \quad (28)$$

These vertices can be also calculated by Procedure 1. According to the above definition, the robust stability of $\Delta_1(s)$ in Equation (25) can be investigated by the following theorem.

Theorem 2. The closed-loop control system with the characteristic function $\Delta_1(s)$ in Equation (25) is robust stable, if:

- $\Delta_1(s)$ contains at least one stable member as $\tilde{\Delta}_1(j\omega)$.
- $0 \notin \tilde{\Delta}_E(s)$ for $s = j\omega$ and $\omega \geq 0$, where

$$\tilde{\Delta}_E^1(s) = \begin{cases} (s^\lambda \tilde{\mathbf{I}}^{D_1} + N_c(s) \mathbf{V}^K e^{-l^s}) \cup \\ (s^\lambda \tilde{\mathbf{V}}^{D_1} + N_c(s) \mathbf{I}^K e^{-\mathbf{V}^l s}), & \text{for } 0 \leq \omega < \frac{2\pi}{l^+ - l^-}, \\ (s^\lambda \tilde{\mathbf{I}}^{D_1} + N_c(s) \mathbf{V}^K e^{-[0, 2\pi]j}), & \text{for } \omega \geq \frac{2\pi}{l^+ - l^-}. \end{cases} \quad (29)$$

Proof. By substituting $s = j\omega$ in $D_1(s)$, we have:

$$D_1(j\omega) = \underbrace{1 - q_2(\omega)^2 + q_4(\omega)^4 + \dots + j(q_1\omega - q_3\omega^3 + \dots)}_{D_1^R(\omega)} + \underbrace{j(q_1\omega - q_3\omega^3 + \dots)}_{D_1^I(\omega)}. \quad (30)$$

At a fixed frequency $\omega = \omega^* > 0$, the real and imaginary parts of $D_1(j\omega)$ may respectively change in the intervals $1 - \bar{q}_2\omega^2 + \underline{q}_4\omega^4 + \dots \leq D_1^R(\omega) \leq 1 - \underline{q}_2\omega^2 + \bar{q}_4\omega^4 + \dots$ and $\underline{q}_1\omega - \bar{q}_3\omega^3 + \dots \leq D_1^I(\omega) \leq \bar{q}_1\omega - \underline{q}_3\omega^3 + \dots$. This means that the value set of $D_1(j\omega)$ can be located in a rectangle with the vertices $\tilde{\mathbf{V}}^{D_1}$ and the exposed edges $\tilde{\mathbf{I}}^{D_1}$. Therefore, the value set of $\Delta_1(j\omega)$ is located in the value set $\tilde{\Delta}_E^1(s)$ in Equation (29) based on the proofs of Lemma 2 and Theorem 1. Accordingly, by the zero exclusion principle, the robust stability can be simply deduced. \square

Remark 7. By benefiting from Theorem 2, Algorithm 1 and remark 6, one can obtain the stabilizing region of FOPID controllers for $\Delta_1(s)$ in the (k_p, k_i) plane, the (k_p, k_d) plane and the (k_i, k_d) plane.

4.2 | Case of $D(s) = D_2(s) = \prod_{i=1}^n (\tau_i s + 1), n \in \mathbb{N}$:

For the case $D(s) = D_2(s) = \prod_{i=1}^n (\tau_i s + 1), \tau_i > 0$, and $\tau_i \in [\tau_i^-, \tau_i^+], n \in \mathbb{N}$, the characteristic function of the closed-loop control system can be obtained as

$$\Delta_2(s) = s^\lambda \prod_{i=1}^n (\tau_i s + 1) + (k_p s^\lambda + k_i + k_d s^{\mu+\lambda}) K e^{-ls}. \quad (31)$$

We will present a useful definition (Definition 4) used in analyzing the robust stability of the system.

Definition 4. Assume that

$$D_2(s) = \prod_{i=1}^n (\tau_i s + 1) = \tilde{q}_n s^n + \tilde{q}_{n-1} s^{n-1} + \dots + \tilde{q}_2 s^2 + \tilde{q}_1 s + 1, \tilde{q}_i \in [\underline{\tilde{q}}_i, \bar{\tilde{q}}_i], i = 1, \dots, n. \quad (32)$$

Then, define:

$$\begin{aligned} \tilde{\mathbf{V}}^{D_2} &= \{\tilde{V}_1^{D_2}(\omega), \tilde{V}_2^{D_2}(\omega), \tilde{V}_3^{D_2}(\omega), \tilde{V}_4^{D_2}(\omega)\}, \\ \tilde{\mathbf{I}}^{D_2} &= \{\tilde{\mathbf{I}}_1^{D_2}, \tilde{\mathbf{I}}_2^{D_2}, \tilde{\mathbf{I}}_3^{D_2}, \tilde{\mathbf{I}}_4^{D_2}\} = \underbrace{\{[\tilde{V}_1^{D_2}(\omega), \tilde{V}_2^{D_2}(\omega)]\}}_{\tilde{\mathbf{I}}_1^{D_2}}, \\ &\quad \underbrace{[\tilde{V}_2^{D_2}(\omega), \tilde{V}_3^{D_2}(\omega)]}_{\tilde{\mathbf{I}}_2^{D_2}}, \underbrace{[\tilde{V}_3^{D_2}(\omega), \tilde{V}_4^{D_2}(\omega)]}_{\tilde{\mathbf{I}}_3^{D_2}}, \underbrace{[\tilde{V}_4^{D_2}(\omega), \tilde{V}_1^{D_2}(\omega)]}_{\tilde{\mathbf{I}}_4^{D_2}}, \end{aligned} \quad (33)$$

in which

$$\begin{cases} \tilde{V}_1^{D_2} = 1 + \tilde{q}_1 s + \tilde{q}_2 s^2 + \tilde{q}_3 s^3 + \dots, \\ \tilde{V}_2^{D_2} = 1 + \tilde{q}_1 s + \tilde{q}_2 s^2 + \tilde{q}_3 s^3 + \dots, \\ \tilde{V}_3^{D_2} = 1 + \tilde{q}_1 s + \tilde{q}_2 s^2 + \tilde{q}_3 s^3 + \dots, \\ \tilde{V}_4^{D_2} = 1 + \tilde{q}_1 s + \tilde{q}_2 s^2 + \tilde{q}_3 s^3 + \dots. \end{cases} \quad (34)$$

These vertices can be calculated by Procedure 1. Now, it is also possible to assess the robust stability of system $\Delta_2(s)$ by using Theorems 1 and 2 and Definition 4, which would result in the following theorem.

Theorem 3. The closed-loop control system with the characteristic function $\Delta_2(s)$ in Equation (31) is robust stable, if:

- $\Delta_2(s)$ contains at least one stable member as $\tilde{\Delta}_2(j\omega)$.
- $0 \notin \tilde{\Delta}_E^2(s)$ for $s = j\omega$ and $\omega \geq 0$, where

$$\tilde{\Delta}_E^2(s) = \begin{cases} (s^\lambda \tilde{\mathbf{I}}^{D_2} + N_c(s) \mathbf{V}^K e^{-I^+ s}) \cup (s^\lambda \tilde{\mathbf{V}}^{D_2} + N_c(s) \mathbf{I}^K e^{-V^+ s}), & \text{for } 0 \leq \omega < \frac{2\pi}{I^+ - I^-}, \\ (s^\lambda \tilde{\mathbf{I}}^{D_2} + N_c(s) \mathbf{V}^K e^{-[0, 2\pi]j}), & \text{for } \omega \geq \frac{2\pi}{I^+ - I^-}. \end{cases} \quad (35)$$

Proof. It is followed from Theorem 2 that the $\partial(\Delta_2(j\omega))$ is located in the exposed edges $\tilde{\mathbf{I}}^{D_2}$ in Equation (33) for a given frequency. On the other hand, the rectangle shape $\tilde{\mathbf{I}}^{D_2}$ in Equation (33) is a special case of a convex polygon. Therefore, based on Theorem 2, $\partial(\Delta_2(s))$ is located in $\tilde{\Delta}_E^2(s)$ for $\omega = \omega_0$ in the complex plane. Accordingly, the zero exclusion principle completes the proof. \square

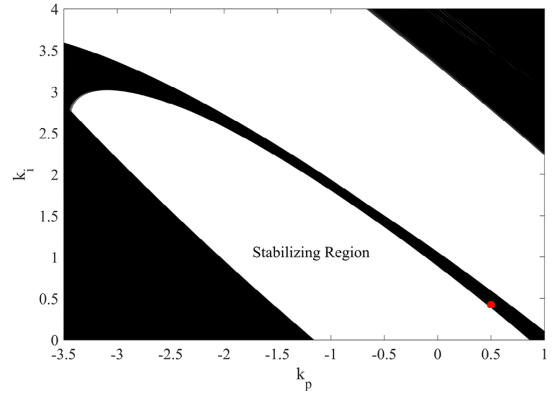


FIGURE 2 The stabilizing region of FOPID controllers based on the present paper.

Remark 8. According to Theorem 3, the robust stability of the closed-loop control system with the characteristic function $\Delta_2(s)$ in Equation (31) is investigated. In order calculate the stabilizing region of FOPID controllers, one should use **Algorithm 1** and remark 6 for $\Delta_2(s)$ in the (k_p, k_i) plane and the (k_i, k_d) plane. It is notable that all results can be also employed for FOPI controllers.

5 | ILLUSTRATIVE EXAMPLES

In this section, four illustrative examples are given to demonstrate the application of the proposed approach to calculate the stabilizing region of FOPID controllers for systems having interval time delay.

Example 1. Let us consider an interval fractional-order plant with an interval time delay as $P(s)$ in Equation (36).

$$P(s) = \frac{[0.66, 0.68]}{[0.5, 0.6]s^{1.6} + 1} e^{-[1, 2.5]s}. \quad (36)$$

In the following, **Algorithm 1** of the present paper and the algorithm proposed in [20] are employed to calculate the stabilizing region of FOPID controllers. It is shown that the algorithm proposed in [20] is unreliable.

Algorithm 1 is used to determine the stabilizing region of the FOPID controller with $\lambda = \mu = 0.2$ and $k_d = 0.001$. Based on **Procedure 1**, the vertex polynomials $V_{r_1}^+(\omega)$ ($r_1 = 1, 2$) and $V_{r_2}^-(\omega)$ ($r_2 = 1, 2$) are obtained as (37).

$$\begin{cases} V_1^+(\omega) = 0.66, \\ V_2^+(\omega) = 0.68. \end{cases} \quad \begin{cases} V_1^-(\omega) = 0.5s^{1.6} + 1, \\ V_2^-(\omega) = 0.6s^{1.6} + 1. \end{cases} \quad (37)$$

By employing **Algorithm 1**, one can compute the final stabilizing region of FOPID controllers as shown in Figure 2. In Figure 2, the parameters $(k_p, k_i) = (0.5, 0.42)$ have been

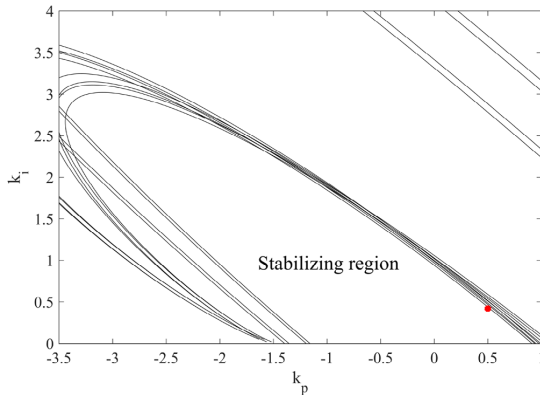


FIGURE 3 The stabilizing region of FOPID controllers based on the algorithm presented in [20].

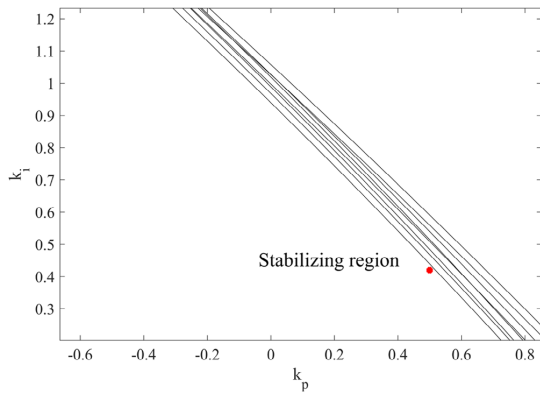


FIGURE 4 A better view around the parameters $(k_p, k_i) = (0.5, 0.42)$ in Figure 3.

also shown. As seen from Figure 2, the parameters $(k_p, k_i) = (0.5, 0.42)$ do not lie in the stabilizing region FOPID controllers and this implies that the FOPID controller with $\mu = \lambda = 0.2$, $k_p = 0.5$, $k_i = 0.42$, and $k_d = 0.001$ cannot robustly stabilize the closed-loop system based on the present paper.

Now, the stabilizing region of FOPID controllers based on [20] has been depicted in Figure 3. From Figures 3 and 4, it is apparent that the parameters $(k_p, k_i) = (0.5, 0.42)$ lie in the stabilizing region proposed in [20]. It means that the FOPID controller with $\mu = \lambda = 0.2$, $k_p = 0.5$, $k_i = 0.42$ and $k_d = 0.001$ can robustly stabilize the closed-loop system based on [20]. As a counterexample, the stabilizing region of the certain characteristic function $\hat{\Delta}(s)$ in Equation (38) has been shown in Figure 5. As depicted in Figures 5 and 6, the FOPID controller with $\mu = \lambda = 0.2$, $k_p = 0.5$, $k_i = 0.42$, and $k_d = 0.001$ cannot robustly stabilize the closed-loop system.

$$\hat{\Delta}(s) = s^{0.2}(0.5s^{1.6} + 1) + 0.67(k_p s^{0.2} + k_i + 0.001s^{0.4})e^{-1.8s} \quad (38)$$

This example shows that the value set of characteristic functions having an interval time delay is a nonconvex shape and

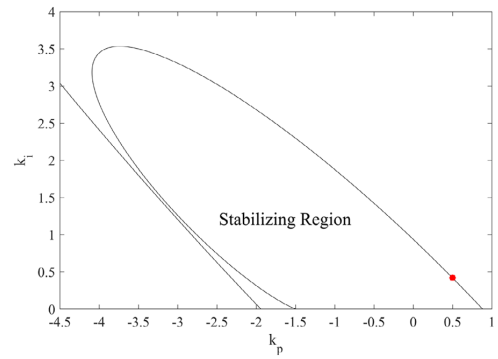


FIGURE 5 The stabilizing region of FOPID controllers for $\hat{\Delta}(s)$ in Equation (38).

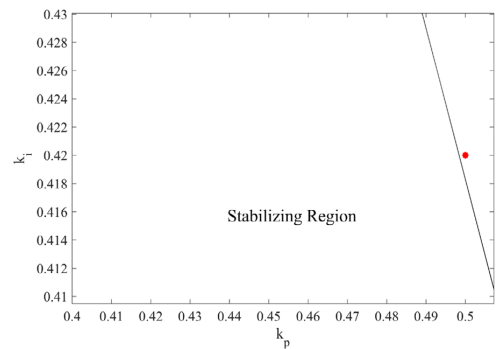


FIGURE 6 A better view around the parameters $(k_p, k_i) = (0.5, 0.42)$ in Figure 5.

the robust stability of such systems cannot be guaranteed by Theorem 3.1 in [20]. Since, the exposed edges proposed in [20] cannot contain the boundary of the value set of $\Delta(j\omega)$ or $\partial(\Delta(j\omega))$. Therefore, based on the zero exclusion principle, the robust stability is not guaranteed. Whereas, in Theorem 1, at each frequency, the boundary of the value set of $\Delta(j\omega)$ ($\partial(\Delta(j\omega))$) can be exactly determined. Hence, in this paper, a reliable method has been proposed to robustly stabilize systems having an interval time delay. Furthermore, the value set of the characteristic function at $\omega = 1.2$ rad/s has been illustrated in Figure 7. As observed from the graph, the origin is encompassed within the value set of the characteristic function. This observation suggests that the FOPID controller with parameter values $\mu = \lambda = 0.2$, $k_p = 0.5$, $k_i = 0.42$, and $k_d = 0.001$ may not be capable of robustly stabilizing the closed-loop control system. This observation aligns with the findings presented in this paper.

Example 2. Consider an interval plant as Equation (39).

$$P(s) = [1, 2] e^{-[1, 1.1]s} / ([1, 2]s + 1) \quad (39)$$

$$([1, 2]s + 1)([1, 2]s + 1).$$

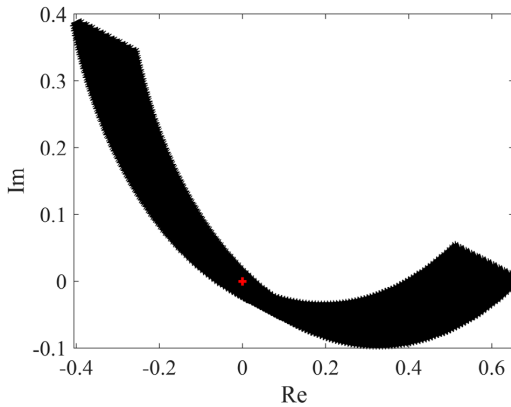


FIGURE 7 The value set of the characteristic function at $\omega = 1.2$ rad/s.

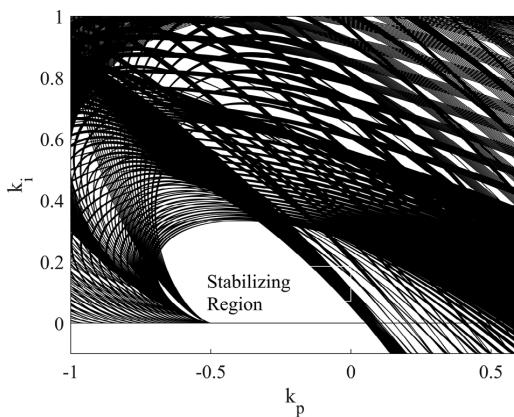


FIGURE 8 The stabilizing region of FOPI controllers.

Figure 8 shows the stabilizing region of FOPI controllers with $\lambda = 0.4$ for $P(s)$ in Equation (39). From this figure it is observed that the FOPI controller $C(s) = -0.3 + 0.2/s^{0.4}$ is located in the stabilizing region. Step responses corresponding to the FOPI controller $C(s) = -0.3 + 0.2/s^{0.4}$ for randomly generated samples of the interval plant $P(s)$ in Equation (39) have been shown in Figure 9.

Although, the methods proposed in [17–19, 21–26] and [35] are inefficient in designing a robust FOPID stabilization of the closed-loop system in the presence of uncertainty in the time delay term. The method proposed in this paper can investigate such characteristic functions having interval plant with an interval time delay.

Example 3. In [31], the following fractional-order plant has been identified for an laboratory temperature control setup.

$$P(s) = \frac{0.63705}{72.995 s^{0.81166} + 1} e^{-15.513s}. \quad (40)$$

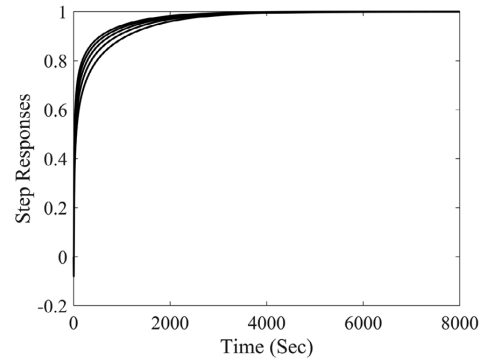


FIGURE 9 Step responses corresponding to the FOPI controller $C(s) = -0.3 + 0.2/s^{0.4}$ for randomly generated samples of the interval plant $P(s)$ in (39).

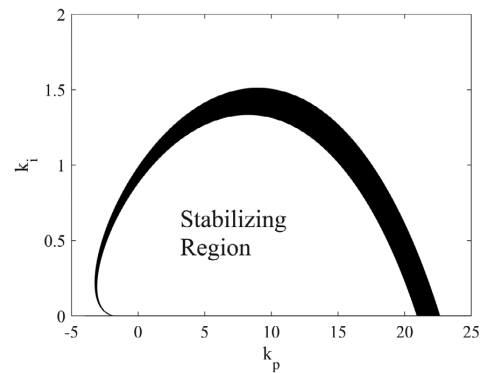


FIGURE 10 The stabilizing region of FOPI controllers.

Let us consider the plant $p(s)$ in Equation (40) as an interval fractional-order plant in the following form:

$$P(s) = \frac{[0.63, 0.64]}{[72.5, 73.5] s^{0.81166} + 1} e^{-[15, 16]s}. \quad (41)$$

Figure 10 shows the stabilizing region of FOPI controllers with $\lambda = 0.8$. It is notable that the method proposed in [31] cannot be employed for fractional-order plants having uncertainties as Equation (41). However, one can simply design a robust fractional-order controller by the method presented in this paper. This shows the sophistication of the method presented in this paper. Moreover, the step responses of the FOPI controller $C(s) = 4 + \frac{0.1}{s^{0.8}}$ have been plotted in Figure 11 for fifty randomly samples of the interval plant $P(s)$ in Equation (41).

Example 4. In paper [36], the steam pressure in the steam drum of a bagasse boiler has been identified as follows:

$$P(s) = \frac{[0.18, 1.11]}{(80.4 s + 1) (63.8 s + 1) (35.2 s + 1)} e^{-50s}. \quad (42)$$

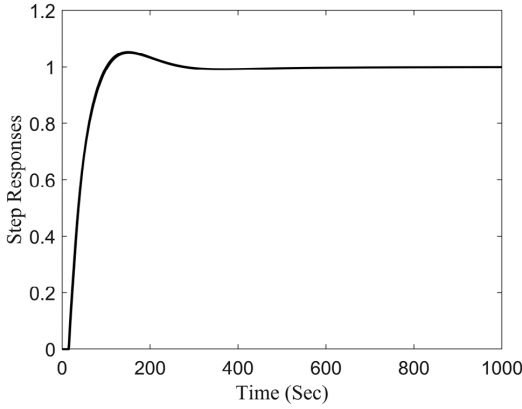


FIGURE 11 Step responses corresponding to the FOPI controller $C(s) = 4 + 0.1/s^{0.8}$ for fifty randomly generated samples of the interval plant $P(s)$ in (41).

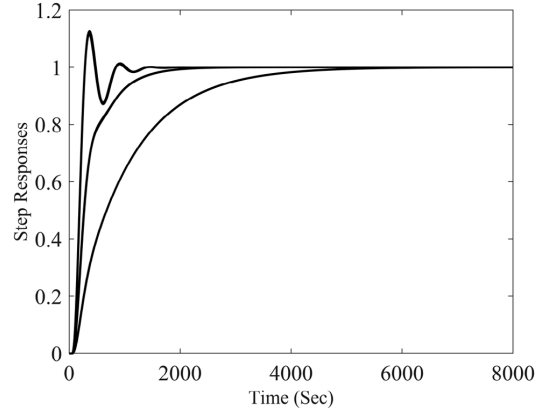


FIGURE 13 Step responses corresponding to the PID controller (44).

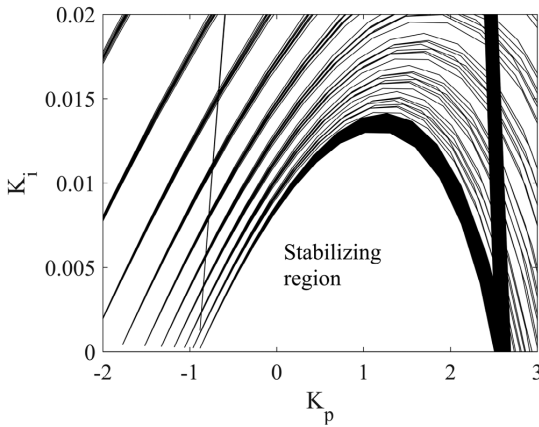


FIGURE 12 Stabilizing region of PID controllers with $K_d = 0.1$.

We consider that there are interval uncertainties associated with all time constants and the time delay term as follows:

$$P(s) = \frac{[0.18, 1.11]}{([80, 81]s + 1)([63, 64]s + 1)([35, 36]s + 1)} e^{-[49, 51]s}. \quad (43)$$

Our objective now is to determine the stabilizing region of PID controllers. We have set the value of K_d as 0.1 for the PID controller. Utilizing Algorithm 1, we have obtained the stabilizing region of PID controllers, as depicted in Figure 12. Based on the information presented in the figure, it is evident that the PID controller (44) resides within the stabilizing region.

$$C(s) = 1 + \frac{0.005}{s} + 0.1s. \quad (44)$$

In order to assess the stability of the PID controller, we have plotted the corresponding step responses in Figure 13. It is

worth noting that the method proposed in [36] does not possess robust stability for stabilizing the closed-loop control system with the interval plant (43). Conversely, the approach introduced in this paper proposes a set of robust PID controllers that address this limitation.

6 | DISCUSSION AND COMPARISONS

Let us proceed to compare our results with similar existing works. In studies conducted by [17, 18], the focus was on calculating the stabilizing region for fractional-order systems without uncertainties. Furthermore, as mentioned previously, the method proposed in [20] cannot be considered reliable in general. Moreover, the previous works [19, 21–26] and [35] do not sufficiently tackle the issue of designing robust FOPID controllers. Furthermore, the method proposed in [37] is limited to the range of $0 < \alpha < 1$, and only a sufficient condition has been derived for robust stability analysis. In contrast, the method introduced in this paper can effectively handle fractional-order interval systems with an interval time delay, and it provides both necessary and sufficient conditions for robust stability analysis. In addition, rather than computing just one stabilizing controller for the control system, a family of stabilizing controllers is computed, which provides a more flexible range of options for selecting controller parameters.

7 | CONCLUSION

In this paper, a new method was proposed to obtain the stabilizing region of FOPID controllers for interval fractional-order plants with an interval time delay. At first, a useful theorem was presented to analyze the robust stability of a closed-loop system consisting of a FOIPD controller and an interval fractional-order plant and an interval time delay. Then, a useful algorithm was proposed to calculate the stabilizing region of FOPID controllers. At the end, an assessment of the results was offered by

some numerical examples. Because of the existence of uncertain orders, it may be so difficult to calculate the stabilizing region of FOPID controllers. Hence, the study on stabilization of fractional-order plants with uncertain orders is left for the future research. Furthermore, improving computational efficiency may be a promising research area for the next future work.

AUTHOR CONTRIBUTIONS

Majid Ghorbani: Investigation; writing - original draft. **Aleksei Tepljakov:** Supervision. **Eduard Petlenkov:** Project administration.

ACKNOWLEDGEMENTS

This work was supported by the Estonian Research Council grant PRG658.

CONFLICT OF INTEREST STATEMENT

The authors declare no conflicts of interest.

DATA AVAILABILITY STATEMENT

Data available on request from the authors.

ORCID

Majid Ghorbani  <https://orcid.org/0000-0001-8908-6573>

REFERENCES

- Podlubny, I.: Fractional order systems and $P^{\lambda}D^{\mu}$. *IEEE Trans. Autom. Control.* 7(4), 582–591 (1999)
- Bettou, K., Charef, A.: Control quality enhancement using fractional $P^{\lambda}D^{\mu}$ controller. *Int. J. Syst. Sci.* 40(8), 875–888 (2009)
- Ghorbani, M.: Robust stabilization criteria of a general form of fractional-order controllers for interval fractional-order plants with complex uncertain parameters. *ISA Trans.* 129(B), 140–151 (2022). doi:<https://doi.org/10.1016/j.isatra.2022.02.014>
- Valério, D., Da Costa, J.S.: Tuning of fractional PID controllers with Ziegler Nichols-type rules. *Signal Process.* 86(10), 2771–2784 (2006)
- Ghorbani, M., Tavakoli-Kakhki, M., Estarami, A.A.: Robust FOPID stabilization of retarded type fractional order plants with interval uncertainties and interval time delay. *J. Franklin Inst.* 356(16), 9302–9329 (2019)
- Ghorbani, M., Tavakoli-Kakhki, M., Tepljakov, A., Petlenkov, E., Farnam, A., Crevecoeur, G.: Robust stability analysis of interval fractional-order plants with interval time delay and general form of fractional-order controllers. *IEEE Control Syst. Lett.* 6, 1268–1273 (2021)
- Tepljakov, A., Petlenkov, E., Belikov, J.: FOPID controller tuning for fractional FOPDT plants subject to design specifications in the frequency domain. In: 2015 European Control Conference (ECC), pp. 3502–3507. IEEE, Piscataway, NJ (2015)
- Rhouma, A., Hafsi, S., Laabidi, K.: Fractional PI stabilization of delay systems: application to a thermal system. *J. Appl. Nonlinear Dyn.* 8(3), 509–518 (2019)
- Monje, C.A., Vinagre, B.M., Feliu, V., Chen, Y.Q.: Tuning and auto-tuning of fractional order controllers for industry applications. *Control Eng. Pract.* 16(7), 798–812 (2008)
- Ghorbani, M., Tavakoli-Kakhki, M.: Robust stability analysis of a general class of interval delayed fractional order plants by a general form of fractional order controllers. *Math. Methods. Appl. Sci.* 44(13), 10172–10189 (2021)
- Ghorbani, M., Tavakoli-Kakhki, M.: Robust stability analysis of uncertain incommensurate fractional order quasi-polynomials in the presence of interval fractional orders and interval coefficients. *Trans. Inst. Meas. Control.* 43(5), 1117–1125 (2021)
- Moornani, K.A., Haeri, M.: On robust stability of LTI fractional-order delay systems of retarded and neutral type. *Automatica* 46(2), 362–368 (2010)
- Moornani, K.A., Haeri, M.: Robust stability testing function and Kharitonov-like theorem for fractional order interval systems. *IET Control Theory Appl.* 4(10), 2097–2108 (2010)
- Gao, Z.: Robust stabilization criterion of fractional-order controllers for interval fractional-order plants. *Automatica* 61, 9–17 (2010)
- Ghorbani, M., Tavakoli-Kakhki, M.: Robust stabilizability of fractional order proportional integral controllers for fractional order plants with uncertain parameters: a new value set based approach. *J. Vib. Control* 26(11–12), 965–975 (2020)
- Ghorbani, M.: Robust stability analysis of interval fractional-order plants by fractional-order controllers: an approach to reduce additional calculation. *Int. J. Gen. Syst.* 50(1), 1–25 (2021)
- Hamamci, S.E.: An algorithm for stabilization of fractional-order time delay systems using fractional-order PID controllers. *IEEE Trans. Autom. Control.* 52(10), 1964–1969 (2007)
- Farkh, R., Laabidi, K., Ksouri, M.: Computation of all stabilizing PID gain for second-order delay system. *Math. Prob. Eng.* 2009, 212053 (2009). doi:<https://doi.org/10.1155/2009/212053>
- Gao, Z., Yan, M., Wei, J.: Robust stabilizing regions of fractional-order PD^{μ} controllers of time-delay fractional-order systems. *J. Process Control* 24(1), 37–47 (2014)
- Liang, T., Chen, J., Lei, C.: Algorithm of robust stability region for interval plant with time delay using fractional order $P^{\lambda}D^{\mu}$ controller. *Commun. Nonlinear Sci. Numer. Simul.* 17(2), 979–991 (2012)
- Luo, Y., Chen, Y.Q.: Fractional order [proportional derivative] controller for a class of fractional order systems. *Automatica* 45(10), 2446–2450 (2009)
- Zhang, S., Liu, L., Chen, Y.Q., Xue, D.: Synthesised fractional-order PD controller design for fractional-order time-delay systems based on improved robust stability surface analysis. *IET Control Theory Appl.* 14(20), 3723–3730 (2020)
- Chen, P., Luo, Y., Peng, Y., Chen, Y.Q.: Optimal robust fractional order $P^{\lambda}D$ controller synthesis for first order plus time delay systems. *ISA Trans.* 114, 136–149 (2021)
- Gnaneshwar, K., Padhy, P.K.: Robust design of tilted integral derivative controller for non-integer order processes with time delay. *IETE J. Res.* 69(9), 6198–6209 (2021). doi:<https://doi.org/10.1080/03772063.2021.2004462>
- Wu, Z., Viola, J., Luo, Y., Chen, Y.Q., Li, D.: Robust fractional-order [proportional integral derivative] controller design with specification constraints: more flat phase idea. *Int. J. Control* (2021). doi:<https://doi.org/10.1080/00207179.2021.1992498>
- Liu, L., Zhang, L., Zhang, S.: Robust P^{λ} controller design for AUV motion control with guaranteed frequency and time domain behaviour. *IET Control Theory Appl.* 15(5), 784–792 (2021)
- Zheng, S., Tang, X., Song, B.: A graphical tuning method of fractional order proportional integral derivative controllers for interval fractional order plant. *J. Process Control* 24(11), 1691–1709 (2014)
- Lee, T.H., Wang, Q.G., Tan, K.K.: Robust Smith-predictor controller for uncertain delay systems. *AIChE J.* 42(4), 1033–1040 (1996)
- Malek, H., Luo, Y., Chen, Y.Q.: Identification and tuning fractional order proportional integral controllers for time delayed systems with a fractional pole. *Mechatronics* 23(7), 746–754 (2013)
- Arya, P.P., Chakrabarty, S.: A robust internal model-based fractional order controller for fractional order plus time delay processes. *IEEE Control Syst. Lett.* 4(4), 862–867 (2020)
- Gnaneshwar, K., Padhy, P.K.: Robust Design of Tilted Integral Derivative Controller for Non-integer Order Processes with Time Delay. *IETE J. Res.* 69(9), 6198–6209 (2021). doi:<https://doi.org/10.1080/03772063.2021.2004462>
- Bonnet, C., Partington, J.R.: Coprime factorizations and stability of fractional differential systems. *Syst. Control Lett.* 41(3), 167–174 (2000)
- Bonnet, C., Partington, J.R.: Analysis of fractional delay systems of retarded and neutral type. *Automatica* 38(7), 1133–1138 (2002)

34. Fu, M., Dasgupta, S., Blondel, V.: Robust stability under a class of nonlinear parametric perturbations. *IEEE Trans. Autom. Control.* 40(2), 213–223 (1995)
35. Demiroğlu, U., Şenol, B.: Frequency frame approach on tuning FOPI controller for TOPTD thermal processes. *ISA Trans.* 108, 96–105 (2021)
36. Rivas-Perez, R., Castillo-Garcia, F., Sotomayor-Moriano, J., Feliu-Batlle, V.: Design of a fractional order PI controller for steam pressure in the steam drum of a bagasse fired boiler. *IFAC Proc. Vol.* 47(3), 1337–1342 (2014)
37. Badri, P., Sojoodi, M.: LMI-based robust stability and stabilization analysis of fractional-order interval systems with time-varying delay. *Int. J. Gen. Syst.* 51(1), 1–26 (2022)

How to cite this article: Ghorbani, M., Tepljakov, A., Petlenkov, E.: Robust stabilization of interval fractional-order plants with an interval time delay by fractional-order proportional integral derivative controllers. *IET Control Theory Appl.* 18, 614–625 (2024). <https://doi.org/10.1049/cth2.12594>

Appendix 12

XII

M. Ghorbani, K. Nosrati, A. Tepljakov, J. Belikov, and E. Petlenkov. Robust stability region of PI controllers for an interval time delayed load frequency control. In *Proc. 2024 IEEE PES Innovative Smart Grid Technologies Europe (ISGT Europe)*, pages 1–5, 2024.

Robust Stability Region of PI Controllers for an Interval Time Delayed Load Frequency Control

1st Majid Ghorbani

*the Department of Computer Systems
Tallinn University of Technology
Tallinn, Estonia*

2nd Komeil Nosrati

*the Department of Computer Systems
Tallinn University of Technology
Tallinn, Estonia*

3rd Aleksei Tepljakov

*the Department of Computer Systems
Tallinn University of Technology
Tallinn, Estonia*

4th Juri Belikov

*Department of Software Science
Tallinn University of Technology
Tallinn, Estonia*

5th Eduard Petlenkov

*the Department of Computer Systems
Tallinn University of Technology
Tallinn, Estonia*

Abstract—Transmission delays, load fluctuations, and intermittent output power of renewable energy sources will all have a substantial impact on frequency stability in microgrids (MGs). In response, various types of advanced control techniques were employed to improve the performance of the load frequency control (LFC) systems. Notwithstanding this, the fragility of the current techniques makes LFC systems vulnerable to parametric (interval) uncertainties associated with communication time delay. Inspired by recent breakthroughs in robust control, in this study, we devise a novel graphical tuning method of the PI controller for tackling this issue. First, we determine the shape of the value set for the characteristic function of uncertain LFC system. Then, the exposed edges are constructed to the boundary of this set under interval uncertainties. To accomplish this step and thanks to the D-decomposition method, the robust stability region in the parameter space of the controllers are determined. Our devised methodology contributes a family of robust stabilizing controllers, instead of just one, where it enables a more flexible choice for the controller parameters. The efficacy of the proposed methodology is indicated on a given single-area MG.

Index Terms—Load frequency control, Robust PI controller, Interval uncertainty, Time delay.

I. INTRODUCTION

Load frequency control (LFC) is an ancillary service to regulate net scheduled power exchange and frequency fluctuations to meet the load demand [1]. In the power systems, the generated power and the total load demand have to be in balance [2], otherwise, it will experience technical issues. Uncertainties of power generations, sudden changes in the total load, and faults in the system may cause some fluctuations in system frequency. For this reason, the LFC system is considered for the power systems to achieve the desired performance [3]. The LFC system stabilizes the frequency and power profile which can be achieved by properly tuning the controller to manage the generation unit [4]. Modern power systems are getting more complicated due to the existence of time delays of the

data transmission from the power generations to the central controller [5]–[7]. To ensure good performance despite time delays, this problem has been treated using various approaches found in the existing literature. For instance, in [8], a unified tuning based Proportional-Integral-Derivative (PID) controller has been used to improve the performance and robustness of the system. Also, based on a maximum peak resonance specification in [9], an approach has been proposed to tune the PID controllers for LFC systems.

In real applications and due to the parameters variations, coefficients of the plant transfer function are all uncertain and lie in specified intervals [10]. Accordingly, these variations and uncertainties of the parameters significantly influence the system frequency in the modern power systems [11], [12]. Hence, various robust controllers have been presented for LFC systems in [13]–[17] to deal with the uncertainties and enhance the control performances. Recently, the D-decomposition method, a graphically tuning strategy to determine the complete set of controllers achieving stability of the control systems [18], has attracted many researchers providing with a more flexible choice of the parameters of controllers. An application of the D-decomposition method has been applied to the LFC systems in order to determine the stability region of the PI controllers [19]. To enhance the robustness of the system, this technique was employed to tune the parameters of different (non-)integer PID-type controllers satisfying the gain and phase margins under communication delays [20]–[22]. Notwithstanding the aforementioned efforts, the plant's parameters in the all studies were assumed to be fixed without any uncertainties [23]. In the light of this gap and based on the zero exclusion theorem and depiction of the value sets, we propose here a novel graphical tuning method of the PI controller robustly stabilizing LFC systems by taking the following objectives into account:

- Derive a robust stability region for LFC systems subject to parametric uncertainties.
- Determine the shape of the value set for the characteristic

The work was supported by Estonian Research Council grants PRG658 and PRG1463.

979-8-3503-9042-1/24/\$31.00 ©2024 IEEE

function of LFC systems in the complex plane for each positive frequency.

- Give a theorem for constructing the exposed edges to determine the boundary of the value set.
- Derive an algorithm to compute the robust stability region in the parameter space of PI controllers (i.e., the pair of the coefficients for the proportional and integral terms as (K_P, K_I)) by benefiting from the D-decomposition method and the results obtained in the theorem.

Compared with the existing robust methods, our computationally simple method proposes a graphical tuning method of PI controllers for the interval LFC system with an interval time delay. Our devised methodology contributes a family of robust stabilizing controllers enabling a more flexible choice for the controller parameters.

The organization for the rest of the paper is as follows: Section II reviews a single-area LFC system with a communication time delay in the presence of interval uncertainties. Section III provides the robust stability analysis of the single-area LFC system and the determination of the robust stability region of PI controllers by the D-decomposition method and the value set concept. The stability region results of the proposed method are resented in Section IV. Finally, the conclusion of this study is presented in Section V.

II. PRELIMINARIES

For the modern single-area LFC schemes, the traditional models are changed to include the time delay into the control loop as depicted in Fig. 1. The addressed schematic also includes a thermal power plant (TPP), photovoltaic (PV) panels, wind turbine generators (WTGs), and load associated with power electronic interfaces. Any changes in active power demand causes a change in the frequency affecting its stability and even degrading power quality. Therefore, the purpose of the LFC systems is to secure the desired frequency against these issues. Fig. 2 depicts the block diagram of the LFC system with delay, primary and secondary control loops. In this model, ΔP_m and ΔP_v are the changes of the turbine and governor outputs, respectively, T_g and T_{ch} are the time constants of the governor and turbine. Also, β and R are the frequency bias factor and droop constant, respectively. In addition, due to the variable and non-measurable nature of input powers of PV, WTG, and load, they can be considered as input disturbance signal as ΔP_d . Furthermore, Δf is the system frequency deviations, M is the moment of inertia, and D is the damping coefficient. For robust stability analysis, the characteristic equation of the LFC system with the communication time delay needs to be obtained. From Fig. 2, one can simply derive this equation by forming the closed loop transfer function as $T(s) = \frac{\Delta f}{\Delta P_d}$, and excluding the denominator of this function as the characteristic equation or $\delta(s)$ which can be given as

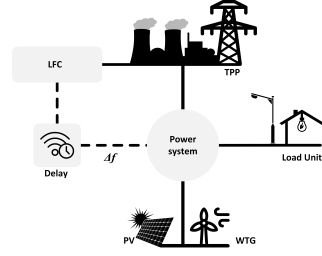


Fig. 1. Schematic of the power system with communication time delay.

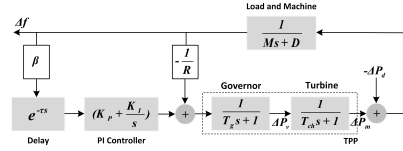


Fig. 2. Scheme of the single-area time delayed LFC system.

$$\begin{aligned}
 \delta(s) &= p(s) + q(s)e^{-\tau s}, \\
 p(s) &= a_4 s^4 + a_3 s^3 + a_2 s^2 + a_1 s, \\
 q(s) &= b_1 (K_P s + K_I), \\
 a_4 &= R T_g T_{ch} M, \\
 a_3 &= M R T_{ch} + R D T_g T_{ch} + R T_g M, \\
 a_2 &= M R + R D T_{ch} + R T_g D, \\
 a_1 &= R D + 1, \\
 b_1 &= \beta R.
 \end{aligned} \tag{1}$$

Now, assume that there are interval uncertainties in the parameters of the block diagram of the single-area time delayed LFC system, i.e., $\tau \in [\underline{\tau}, \bar{\tau}]$ and

$$\begin{aligned}
 T_g &\in [\underline{T}_g, \bar{T}_g], T_{ch} \in [\underline{T}_{ch}, \bar{T}_{ch}], M \in [\underline{M}, \bar{M}], \\
 D &\in [\underline{D}, \bar{D}], R \in [\underline{R}, \bar{R}], \beta \in [\underline{\beta}, \bar{\beta}],
 \end{aligned} \tag{2}$$

where \underline{X} and \bar{X} show the lower and upper bound of the parameter X . Therefore, the characteristic function of the interval LFC system associated with the interval time delay can be represented as

$$\begin{aligned}
 \Delta(s) &= P(s) + Q(s) e^{-[\underline{\tau}, \bar{\tau}]s}, \\
 P(s) &= a_4 s^4 + a_3 s^3 + a_2 s^2 + a_1 s, \\
 Q(s) &= b_1 (K_P s + K_I), \\
 a_i &\in [\underline{a}_i, \bar{a}_i], b_1 \in [\underline{b}_1, \bar{b}_1], \quad i = 1, 2, 3, 4, \quad a_4 \neq 0.
 \end{aligned} \tag{3}$$

The main purpose of this paper is to design robust PI controllers for the interval time delayed LFC system which has the characteristic equation $\Delta(s)$ in (3). In fact, in the present work, the robust stability region in the parameter space of PI controllers are determined for the interval LFC system with an interval communication time delay depicted in Fig. 2. To

cope with this idea, we will use the following lemma to step forward towards our analysis.

Lemma 1 ([23]): For two bounded and closed value sets Q_1 and Q_2 , $\partial(Q_1 + Q_2)$ is a subset of $(\partial(Q_1) + \partial(Q_2))$, or equivalently, $\partial(Q_1 + Q_2) \subseteq \partial(Q_1) + \partial(Q_2)$, where ∂ denotes the boundary.

III. MAIN RESULTS

In what follows, the boundary of the value set of $\Delta(j\omega)$ in (3) is primarily checked. Then, robust stability analysis of the interval LFC system is discussed. Finally, the D-decomposition method is employed to compute the robust stability region of PI controllers. We illustrate these steps in three following subsections:

A. Determination of $\partial(\Delta(j\omega))$

At first, let us discuss on the value set of $Q(j\omega)$. According to the Kharitonov's theorem [10], the value set of $Q(j\omega)$ is located in a convex shape in the complex plane i.e., $\partial(Q(j\omega)) \subset P_{EQ}(j\omega)$, where $P_{EQ}(j\omega)$ is defined as follows.

$$P_{EQ}(j\omega) = \{[\mathbf{V}_q^1, \mathbf{V}_q^2], [\mathbf{V}_q^1, \mathbf{V}_q^3], [\mathbf{V}_q^2, \mathbf{V}_q^4], [\mathbf{V}_q^3, \mathbf{V}_q^4]\},$$

$$\begin{cases} \mathbf{V}_q^1 = s(\underline{a}_1 + \underline{a}_2 s + \underline{a}_3 s^2 + \underline{a}_4 s^3), \\ \mathbf{V}_q^2 = s(\underline{a}_1 + \underline{a}_2 s + \underline{a}_3 s^2 + \underline{a}_4 s^3), \\ \mathbf{V}_q^3 = s(\bar{a}_1 + \underline{a}_2 s + \underline{a}_3 s^2 + \bar{a}_4 s^3), \\ \mathbf{V}_q^4 = s(\bar{a}_1 + \bar{a}_2 s + \underline{a}_3 s^2 + \underline{a}_4 s^3), \end{cases} \quad (4)$$

in which $[x, y]$ is a line segment joining the pairs of polynomials x and y . Also, one can simply infer that $\partial(Q(j\omega)e^{-\tau j\omega})$ is constructed by two line segments and two arc segments. As a result,

$$\partial(Q(j\omega)e^{-\tau j\omega}) \subseteq \{\mathbf{V}^{b_1}(K_P j\omega + K_I)e^{-\mathbf{I}^\tau j\omega} \cup \{\mathbf{I}^{b_1}(K_P j\omega + K_I)e^{-\mathbf{V}^\tau j\omega}\}, \quad (5)$$

where $\mathbf{V}^{b_1} = \{\underline{b}_1, \bar{b}_1\}$, $\mathbf{I}^{b_1} = [\underline{b}_1, \bar{b}_1]$, $e^{-\mathbf{I}^\tau j\omega} = \{e^{-[\underline{\tau}, \bar{\tau}]j\omega}\}$, and $e^{-\mathbf{V}^\tau j\omega} = \{e^{-\underline{\tau}j\omega}, e^{-\bar{\tau}j\omega}\}$. Now, in the following theorem, a set of exposed edges is presented to determine $\partial(\Delta(j\omega))$ at a given frequency.

Theorem 1: For a given frequency $\omega = \omega^*$, the following statement holds:

$$\begin{aligned} \partial(\Delta(j\omega)) &\subseteq \Delta_E(s = j\omega), \\ \Delta_E(s = j\omega) &= \Delta_E^1(s) \cup \Delta_E^2(s), \\ \Delta_E^1(s) &= \mathbf{V}_q + (K_P s + K_I) \mathbf{I}^{b_1} e^{-\mathbf{V}^\tau s}, \\ \Delta_E^2(s) &= \begin{cases} P_{EQ}(s) + (K_P s + K_I) \mathbf{V}^{b_1} e^{-\mathbf{I}^\tau s}, & \omega^* \in [0, \eta), \\ P_{EQ}(s) + (K_P s + K_I) \mathbf{V}^{b_1} e^{-[0, 2\pi]j}, & \omega^* \in [\eta, \infty), \end{cases} \end{aligned} \quad (6)$$

with $\mathbf{V}_q = \{\mathbf{V}_q^1, \mathbf{V}_q^2, \mathbf{V}_q^3, \mathbf{V}_q^4\}$ and $\eta = \frac{2\pi}{\bar{\tau} - \underline{\tau}}$.

Proof. Assume that $\omega^* \in [0, \eta)$. According to the given property in Lemma 1, for $\omega = \omega^*$, one can conclude that

$$\partial(\Delta(j\omega)) \subseteq P_{EQ}(s) + (K_P s + K_I) \mathbf{I}^{b_1} e^{-\mathbf{I}^\tau s}. \quad (7)$$

Also, it was already mentioned that

$$\partial(Q(j\omega)e^{-\tau j\omega}) \subseteq \{\mathbf{V}^{b_1}(K_P j\omega + K_I)e^{-\mathbf{I}^\tau j\omega} \cup \{\mathbf{I}^{b_1}(K_P j\omega + K_I)e^{-\mathbf{V}^\tau j\omega}\}. \quad (8)$$

Therefore, (7) can be rewritten as

$$\begin{aligned} \partial(\Delta(j\omega)) &\subseteq P_{EQ}(s) + (K_P s + K_I) \mathbf{I}^{b_1} e^{-\mathbf{I}^\tau s} \\ &\subseteq (\Phi(s) \cup \Psi(s)), \end{aligned} \quad (9)$$

where

$$\begin{aligned} \Phi(s) &= (P_{EQ}(s) + (K_P s + K_I) \mathbf{I}^{b_1} e^{-\mathbf{V}^\tau s}), \\ \Psi(s) &= (P_{EQ}(s) + (K_P s + K_I) \mathbf{V}^{b_1} e^{-\mathbf{I}^\tau s}). \end{aligned}$$

At first, the value set of $\Phi(s)$ should be discussed. From (4), it can be inferred that

$$\begin{aligned} \Phi(s) &= \left\{ [\mathbf{V}_q^1, \mathbf{V}_q^2] + (K_P s + K_I) \mathbf{I}^{b_1} e^{-\mathbf{V}^\tau s}, \right. \\ &\quad [\mathbf{V}_q^1, \mathbf{V}_q^3] + (K_P s + K_I) \mathbf{I}^{b_1} e^{-\mathbf{V}^\tau s}, \\ &\quad [\mathbf{V}_q^2, \mathbf{V}_q^4] + (K_P s + K_I) \mathbf{I}^{b_1} e^{-\mathbf{V}^\tau s}, \\ &\quad \left. [\mathbf{V}_q^3, \mathbf{V}_q^4] + (K_P s + K_I) \mathbf{I}^{b_1} e^{-\mathbf{V}^\tau s} \right\}. \end{aligned} \quad (10)$$

The expression $[\mathbf{V}_q^1, \mathbf{V}_q^2] + (K_P s + K_I) \mathbf{I}^{b_1} e^{-\mathbf{V}^\tau s}$ can be considered as the sum of two line segments. The shape of two added independent lines would like to be a convex polygon with four vertices in the complex plane. Accordingly, we have

$$\begin{aligned} &[\mathbf{V}_q^1, \mathbf{V}_q^2] + (K_P s + K_I) \mathbf{I}^{b_1} e^{-\mathbf{V}^\tau s} \subseteq \\ &([\mathbf{V}_q^1, \mathbf{V}_q^2] + (K_P s + K_I) \mathbf{V}^{b_1} e^{-\mathbf{V}^\tau s}) \cup \\ &(\{\mathbf{V}_q^1, \mathbf{V}_q^2\} + (K_P s + K_I) \mathbf{I}^{b_1} e^{-\mathbf{V}^\tau s}). \end{aligned} \quad (11)$$

Therefore, from (11), (9) can be rewritten as follows.

$$\begin{aligned} \partial(\Delta(j\omega)) &\subseteq P_{EQ}(s) + (K_P s + K_I) \mathbf{I}^{b_1} e^{-\mathbf{I}^\tau s} \\ &\subseteq \left((P_{EQ}(s) + (K_P s + K_I) \mathbf{I}^{b_1} e^{-\mathbf{V}^\tau s}) \right. \\ &\quad \left. \cup (P_{EQ}(s) + (K_P s + K_I) \mathbf{V}^{b_1} e^{-\mathbf{I}^\tau s}) \right) \\ &\subseteq \left((P_{EQ}(s) + (K_P s + K_I) \mathbf{V}^{b_1} e^{-\mathbf{V}^\tau s}) \right. \\ &\quad \left. \cup \left((\mathbf{V}_q + (K_P s + K_I) \mathbf{I}^{b_1} e^{-\mathbf{V}^\tau s}) \right. \right. \\ &\quad \left. \left. \cup (P_{EQ}(s) + (K_P s + K_I) \mathbf{V}^{b_1} e^{-\mathbf{I}^\tau s}) \right) \right) \\ &\subseteq \left((\mathbf{V}_q + (K_P s + K_I) \mathbf{I}^{b_1} e^{-\mathbf{V}^\tau s}) \right. \\ &\quad \left. \cup (P_{EQ}(s) + (K_P s + K_I) \mathbf{V}^{b_1} e^{-\mathbf{I}^\tau s}) \right). \end{aligned} \quad (12)$$

This completes the proof for $\omega^* \in [0, \eta)$. The proof is completed for $\omega^* \in [\eta, \infty)$ in a straightforward way using (12) and $\partial(Q(j\omega)e^{-\tau j\omega}) \subseteq (K_P j\omega + K_I) \mathbf{V}^{b_1} e^{-[0, 2\pi]j}$. \square

B. Robust stability analysis of the interval LFC system

In this subsection, we present a stability theorem to analyze the robust stability of the interval LFC system depicted in Fig. 2.

Theorem 2: The interval LFC system depicted in Fig.2 with the characteristic equation $\Delta(s)$ in (3) is robust stable if the following two statements hold:

- $\Delta(s)$ has at least one stable member,
- $0 \notin \Delta_E(j\omega)$ for $\omega \geq 0$.

Proof. Based on the the Zero Exclusion Principle, the control system with the characteristic equation $\Delta(s)$ is robust stable if $\Delta(s)$ has at least one stable member and $0 \notin \Delta(j\omega)$ for $\omega \geq 0$. Also, according to Theorem 1, we have $\partial(\Delta(j\omega)) \subseteq \Delta_E(j\omega)$ at a given frequency. Therefore, $0 \notin \Delta(j\omega)$ if $0 \notin \Delta_E(j\omega)$ for $\omega \geq 0$. \square

C. Robust stability region derivation of PI controllers

At first, assume that there is no uncertainties in the parameters of the block diagram of the LFC system in Fig (2). Therefore, the characteristic equation of the control system can be simply obtained as $\delta(s)$ given in (1). Here, the purpose is to compute the stability region of PI controllers for the time delayed single-area LFC system without uncertainties. In other words, a set of PI controllers are determined for the control system. It is obvious that the poles of the closed-loop control system can be obtained by calculating the roots of the characteristic equation $\delta(s) = 0$, or equivalently,

$$a_4 s^4 + a_3 s^3 + a_2 s^2 + a_1 s + b_1(K_P s + K_I)e^{-\tau s} = 0. \quad (13)$$

Now, to determine the stability region of the control system in the parameter space of PI controllers, three boundaries i.e., real root boundary (RRB), infinite root boundary (IRB) and complex root boundary (CRB) have to be calculated using the D-decomposition method. In summary, these three mentioned boundaries are stated as follows:

RRB: This boundary can be determined by substituting $s = 0$ in the characteristic equation $\delta(s) = 0$ i.e., $\delta(s = 0) = 0$ resulting in $K_I = 0$.

IRB: This boundary can be also calculated by substituting $s \rightarrow \infty$ in the characteristic function $\delta(s) = 0$. Therefore, the coefficient of the highest order can only equal to zero. In other words, $\delta(s = \infty) = 0$ leads to $a_4 = 0$. Therefore, the boundary does not exist.

CRB: This boundary can be determined by substituting $s = j\omega$ in the characteristic function $\delta(s) = 0$, i.e., $\delta(s = j\omega) = 0, \omega > 0$. To construct the CRB boundary, one can write $\delta(s = j\omega) = 0$, or equivalently,

$$a_4(\omega)^4 - a_2(\omega)^2 + b_1 K_I \cos(\tau\omega) + b_1 K_P \omega \sin(\tau\omega) + j(-a_3(\omega)^3 + a_1(j\omega) + b_1 K_P \omega \cos(\tau\omega) - b_1 K_I \sin(\tau\omega)) = 0. \quad (14)$$

Now, by equating the real and imaginary parts of (14) to zero, one has

$$\begin{cases} A_{11}K_P + A_{12}K_I = B_1, \\ A_{21}K_P + A_{22}K_I = B_2, \\ A_{11} = b_1 \omega \sin(\tau\omega), \\ A_{12} = b_1 \cos(\tau\omega), \\ B_1 = -a_4(\omega)^4 + a_2(\omega)^2, \\ A_{21} = b_1 \omega \cos(\tau\omega), \\ A_{22} = -b_1 \sin(\tau\omega), \\ B_2 = a_3(\omega)^3 - a_1(j\omega). \end{cases} \quad (15)$$

Finally, by solving equations (15), the parameters K_P and K_I are derived as

$$\begin{cases} K_P = \frac{B_1 B_{22} - A_{12} B_2}{A_{11} A_{22} - A_{12} A_{21}}, \\ K_I = \frac{B_2 A_{11} - A_{21} B_1}{A_{11} A_{22} - A_{12} A_{21}}, \end{cases} \quad (16)$$

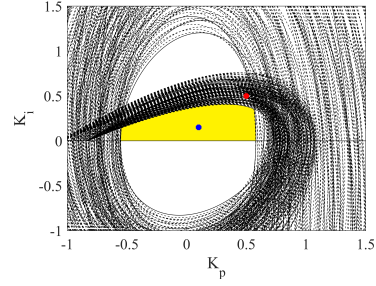


Fig. 3. Robust stability region of PI controllers (yellow region).

The stability region is determined by RRB, IRB and CRB, which divide the parameter space (K_P, K_I) into stable and unstable regions. To check the stability of the characteristic equation $\delta(s)$, [10] should be employed. Now, the next purpose is to use the D-decomposition method to determine the robust stability region of PI controllers for the interval LFC system. To do this the following algorithm is presented.

Algorithm 1: Derivation of robust stability regions.

Step 1. Obtain the set $\Delta_E(j\omega)$ in (6).

Step 2. Perform the D-decomposition method.

Step 3. Compute the robust stability region in (K_P, K_I) plane.

Step 4. Obtain the intersection of all stable regions to derive the robust stability region of PI controllers.

IV. SIMULATION RESULTS

The parametric uncertainties of the load frequency control system used in this example are as follows.

$$\tau \in [2, 3], R = [0.05, 0.06], T_g = [0.1, 0.15], T_{ch} = [0.25, 0.3], D = [0.8, 1], \beta = [20, 21], M = [9, 10]. \quad (17)$$

Therefore, the characteristic function of the interval load frequency control system with an interval time delay can be obtained as follows.

$$\Delta(s) = [0.0113, 0.027]s^4 + [0.1585, 0.2727]s^3 + [0.464, 0.627]s^2 + [1.04, 1.06]s + [1, 1.26](K_P s + K_I)e^{-[2,3]s}. \quad (18)$$

Now, by benefiting from **Algorithm 1**, the robust stability region of PI controllers for the interval load frequency control system has been obtained as Fig. 3 (the yellow region). The work [19] has failed to present an approach for the robust PI stabilization of the load frequency control systems. Whereas, based on the results presented in this letter, a robust PI stabilization can be designed for the load frequency control system structure depicted in Fig. 2. Also, from Fig. 3, it is apparent that the pair $(K_P, K_I) = (0.5, 0.5)$ (the red point) do not lie in the robust stability region. This implies that the load frequency control system is not robustly stabilized by the PI controller $(K_P, K_I) = (0.5, 0.5)$. In Fig. 4, the stability of one member of $\Delta(s) = 0.0113s^4 + 0.1585s^3 + 0.464s^2 + 1.04s + 1.1(0.5s + 0.5)e^{-3s}$ has been checked

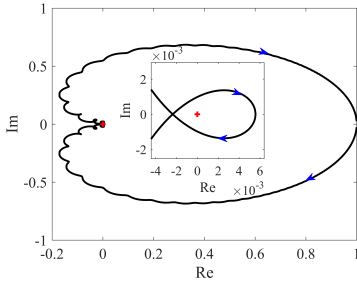


Fig. 4. The stability analysis of $\Delta(s)$.

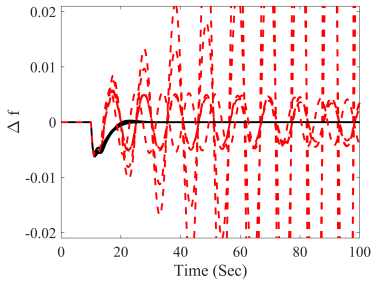


Fig. 5. Time-domain simulations corresponding to the PI controllers $(K_P, K_I) = (0.5, 0.5)$ (dashed lines) and $(K_P, K_I) = (0.1, 0.15)$ (dotted lines).

by applying the PI controller $(K_P, K_I) = (0.5, 0.5)$. As seen from this figure, the chosen member is not stable and this verifies the results. Time-domain simulations for a 0.1 pu step increase in the load ΔP_d at $t = 10$ sec are plotted in Fig. 5 by applying the PI controllers $(K_P, K_I) = (0.5, 0.5)$ and $(K_P, K_I) = (0.1, 0.15)$ for the chosen members randomly generated in the characteristic function of the interval load frequency control system. This figure also indicates that the PI controller $(K_P, K_I) = (0.5, 0.5)$ cannot robustly stabilize the interval load frequency control system.

V. CONCLUSION

This paper proposed a novel graphical tuning method of PI controllers for the interval load frequency control system with an interval time delay. It was assumed that all parameters of the load frequency control system had interval uncertainties. Then, by the D-decomposition method and the value set concept, **Algorithm 1** was presented to determine PI controllers which can robustly stabilize the interval load frequency control system. Finally, a numerical example was provided to verify the effectiveness of the proposed results.

REFERENCES

- [1] S. Hanwate, Y.V. Hote, and S. Saxena, "Adaptive policy for load frequency control," *IEEE Transactions on Power Systems*, vol. 33, no. 1, pp. 1142–1144, 2017.
- [2] H. Saadat, "Power system analysis," McGraw-hill, 1999.
- [3] M. Saka, M. Demirci, I. Eke, H. Gozde, M. Dursun, and M.C. Taplamacioglu, "Analysis of Fuel Cell Based Time Delayed Load Frequency Control Having Energy Storage Systems," *2022 9th International Conference on Electrical and Electronics Engineering (ICEEE)*, pp. 270–274, 2022.
- [4] M. Ranjan and R. Shankar, "A literature survey on load frequency control considering renewable energy integration in power system: Recent trends and future prospects," *Journal of Energy Storage*, vol. 45, pp. 103717, 2022.
- [5] B. Naduvathuparambil, M. C. Valenti, and A. Feliachi, "Communication delays in wide area measurement systems," *Proceedings of the thirty-fourth southeastern symposium on system theory*, pp. 118–122, 2002.
- [6] S. Saxena, Y. V. Hote, "PI controller based load frequency control approach for single-area power system having communication delay," *IFAC-PapersOnLine*, vol. 51, no. 4, pp. 622–626, 2018.
- [7] J. Sharma, Y. V. Hote, and R. Prasad, "PID controller design for interval load frequency control system with communication time delay," *Control Engineering Practice*, vol. 89, pp. 154–168, 2019.
- [8] T. Wen, "Unified tuning of PID load frequency controller for power systems via IMC," *IEEE Transactions on power systems*, vol. 25, no. 1, pp. 341–350, 2009.
- [9] A. Khodabakhshian and M. Edrisi, "A new robust PID load frequency controller," *Control Engineering Practice*, vol. 16, no. 9, pp. 1069–1080, 2008.
- [10] S. P. Bhattacharyya, and L. H. Keel, "Robust control: the parametric approach," *rentice-Hall*, 1995.
- [11] H. Bevrani, M. R. Feizi, and S. Atae, "Robust frequency control in an islanded microgrid: H_∞ and μ -synthesis approaches," *IEEE Transactions on Smart Grid*, vol. 7, no. 2, pp. 706–717, 2015.
- [12] A. Al-Muhanna, A. Al-Nujaimi, S. Al-Baiyat, "Robust H_∞ and μ -Synthesis frequency control for two-bus islanded microgrid," *2017 Saudi Arabia Smart Grid (SASG)*, pp. 1–9, 2017.
- [13] N. Chuang, "Robust H_∞ load-frequency control ininterconnected power systems," *IET control theory & Applications*, vol. 10, no. 1, pp. 67–75, 2016.
- [14] P. Ojaghi, M. Rahmani, "LMI-based robust predictive load frequency control for power systems with communication delays," *IEEE Transactions on Power Systems*, vol. 32, no. 5, pp. 4091–4100, 2017.
- [15] X. Lv, Y. Sun, W. Hu, V. Dinavahi, "Robust load frequency control for networked power system with renewable energy via fractional-order global sliding mode control," *IET renewable power generation*, vol. 15, no. 5, pp. 1046–1057, 2021.
- [16] M. Kumar, Y. V. Hote, "Robust PID2 controller design for perturbed load frequency control of an interconnected time-delayed power systems," *IEEE Transactions on Control Systems Technology*, vol. 29, no. 6, pp. 2662–2669, 2020.
- [17] Z. Wu, P. Z. Li, Y. Liu, D. Li, and Y. Q. Chen, "Optimized cascaded PI controller for the load frequency regulation of multi-area power systems with communication delays," *Energy Reports*, vol. 8, pp. 469–477, 2022.
- [18] M. Ghorbani, A. Tepljakov, and E. Petlenkov, "Stabilizing region of fractional-order proportional integral derivative controllers for interval fractional-order plants," *Transactions of the Institute of Measurement and Control*, <https://doi.org/10.1177/01423312221117866>.
- [19] S. Sönmez, S. Ayasun, "Stability region in the parameter space of PI controller for a single-area load frequency control system with time delay," *IEEE Transactions on Power Systems*, vol. 31, no. 1, pp. 829–830, 2015.
- [20] S. Sönmez, S. Ayasun, "Gain and phase margins based stability region analysis of time-delayed shipboard microgrid with sea wave energy," *IET Electric Power Applications*, vol. 14, no. 8, pp. 1347–1359, 2020.
- [21] A. Kumar, and S. Pan, "Design of fractional order PID controller for load frequency control system with communication delay," *ISA transactions*, <https://doi.org/10.1016/j.isatra.2021.12.033>.
- [22] S. Saxena, and Y. V. Hote, "PI controller based load frequency control approach for single-area power system having communication delay," *IFAC-PapersOnLine*, vol. 51, no. 4, pp. 622–626, 2018.
- [23] M. Fu, S. Dasgupta, V. Blondel, "PI controller based load frequency control approach for single-area power system having communication delay," *IEEE Transactions on Automatic Control*, vol. 40, no. 2, pp. 213–223, 1995.

Appendix 13

XIII

M. Ghorbani, B. Mehdizadeh Gavgani, A. Farnam, A. Tepljakov, E. Petlenkov, and G. Crevecoeur. Computing stabilising regions: FOPID controller methodology for interval fractional-order plants with time delay. *International Journal of Systems Science*, 56(8):1884–1896, 2025.



Computing stabilising regions: FOPID controller methodology for interval fractional-order plants with time delay

Majid Ghorbani, Babak Mehdizadeh Gavani, Arash Farnam, Aleksei Tepljakov, Eduard Petlenkov & Guillaume Crevecoeur

To cite this article: Majid Ghorbani, Babak Mehdizadeh Gavani, Arash Farnam, Aleksei Tepljakov, Eduard Petlenkov & Guillaume Crevecoeur (2025) Computing stabilising regions: FOPID controller methodology for interval fractional-order plants with time delay, International Journal of Systems Science, 56:8, 1884-1896, DOI: [10.1080/00207721.2024.2435569](https://doi.org/10.1080/00207721.2024.2435569)

To link to this article: <https://doi.org/10.1080/00207721.2024.2435569>



Published online: 08 Dec 2024.



Submit your article to this journal [↗](#)



Article views: 108



View related articles [↗](#)



View Crossmark data [↗](#)



Computing stabilising regions: FOPID controller methodology for interval fractional-order plants with time delay

Majid Ghorbani^a, Babak Mehdizadeh Gavgani^{b,c}, Arash Farnam^{b,c}, Aleksei Tepljakov^a, Eduard Petlenkov^a and Guillaume Crevecoeur^{b,c}

^aDepartment of Computer Systems, Tallinn University of Technology, Tallinn, Estonia; ^bDepartment of Electromechanical, Systems and Metal Engineering, Ghent University, Ghent, Belgium; ^cFlandersMake@UGent - Corelab MIRO, Ghent, Belgium

ABSTRACT

Recently, certain methods have inaccurately presented the computation of the robust stability region of Fractional-Order Proportional Integral Derivative (FOPID) controllers for interval fractional-order plants with an interval time delay. Motivated by the necessity for accuracy and reliability as well as the growing importance and widespread application of fractional-order controllers in control systems, which offer increased flexibility in controller design, this paper focuses on introducing a dependable procedure for determining the stabilising region of FOPID controllers applicable to interval fractional-order plants with an interval time delay. An interval fractional-order plant is characterised by a fractional-order transfer function wherein the coefficients are uncertain and confined within specified intervals in both the numerator and denominator. Moreover, an interval time delay pertains to a delay term whose value varies within a specified interval. To comprehensively analyze the robust stability of the resulting system, we introduce two theorems and two lemmas in this study. Following this, we propose a method to address the challenge of achieving robust stabilisation for interval plants with an interval time delay using FOPID controllers. Moreover, an additional function is introduced to improve the performance of the systems. To illustrate the proposed procedure, we provide numerical examples and an experimental verification.

ARTICLE HISTORY

Received 29 February 2024
Accepted 22 November 2024

KEYWORDS

FOPID controllers;
fractional-order plants;
interval time delay;
stabilising region

1. Introduction

Fractional-order controllers have recently attracted considerable interest owing to their enhanced flexibility in controller design, as opposed to their integer-order counterparts (Podlubny, 1999). Fractional-Order Proportional Integral Derivative (FOPID) control offers greater flexibility and improved performance over traditional PID controllers. FOPID controllers allow for more tuning parameters, which can result in better adaptability to complex system dynamics, including time delays and uncertainties. This is particularly beneficial in addressing the limitations of classical PID control in managing systems with non-integer dynamics, leading to improved control accuracy, stability, and robustness in various industrial applications. The fractional-order derivative and integral components provide finer control adjustments, allowing for more effective compensation of disturbances and system uncertainties (Mohamed & Khashan, 2014;

Tepljakov et al., 2021). As a result, a vast array of approaches has been suggested in earlier studies for formulating designs of fractional-order controllers (Bettou & Charef, 2009; Dastjerdi et al., 2018; Valério & Da Costa, 2006).

Due to the inherent uncertainties in real-life systems, the examination of robust stability is as a foundational aspect in the study of any control system. As a result, diverse approaches for evaluating the robust stability of interval fractional-order systems have been presented in Zheng (2017) and Ghorbani and Tavakoli-Kakhki (2021), employing the notion of value sets. The value set method primarily relies on the zero exclusion principle. In Moornani and Haeri (2010a) and Moornani and Haeri (2009), necessary and sufficient conditions for analyzing the robust stability of interval fractional-order systems were introduced, making use of the zero exclusion principle. According to the zero exclusion principle, it

is essential to ascertain the exact configuration of the value set of interval fractional-order systems. In this context, Procedure 1 in Moornani and Haeri (2010b) affirmed that the value set of an interval fractional-order system takes on a polygon form. Moreover, the improvement of robust stability analysis for such systems was achieved by introducing an auxiliary function. Furthermore, in Ghorbani et al. (2023b), a function for assessing the robust stability of interval fractional-order systems was initially introduced. The paper subsequently offered insights into the procedure for examining the robust stability of such systems and provided instructions of using the well-known FOMCON toolbox (Tepljakov et al., 2019). To improve the performance of interval fractional-order systems, Ghorbani et al. (2023c) also incorporated the concept of D-robust stability.

The computation of the stability region for fractional-order controllers offers several advantages. For instance, it proposes a family of stabilising controllers, providing a more flexible range of controller parameters compared to just a single option for the control system. The D-decomposition method has been extensively utilised to manually determine the stability region of controllers. In this approach, a point must be selected within each region. Therefore, several approaches have been suggested for determining the stability region of FOPID controllers for interval fractional-order systems in Zheng et al. (2014) and Ghorbani et al. (2023d).

Time delays are a common occurrence in industrial systems, posing numerous challenges in control engineering. Consequently, stabilising time-delayed systems stands as a fundamental concern within the control field. In Hamamci (2007), an algorithm was presented for calculating the stability region of FOPID controllers tailored to delayed fractional-order plants (without uncertainty). Moreover, the stability region for FOPID controllers has been derived for specific instances of systems with interval time delays as discussed in Ghorbani et al. (2024) and Zheng and Li (2018). Furthermore, in Wu et al. (2024), a graphical tuning approach was introduced to calculate the robust stability region of FOPID controllers for interval systems. In Liang et al. (2012), the robust stability region of FOPID controllers has been established for interval plants with interval uncertainties in their numerator, denominator, and time delay terms. Nevertheless, as demonstrated in Zheng et al. (2014), the methodologies proposed in Liang et al. (2012)

and Hamidian and Beheshti (2018) are not universally accurate. Hence, this concern has motivated the authors to seek a dependable solution for computing the stability region of FOPID controllers applied to interval plants with interval time delays. The aforementioned papers assumed that the value set of an interval time delay system is convex. However, as indicated in Remark 3.1, due to the interval time delay, the value set is non-convex.

The primary contribution of this investigation lies in expanding upon the methodology outlined in Hamamci (2007) to determine the stability region of FOPID controllers applicable to interval fractional-order systems, including an interval time delay. Moreover, in this paper, the results outlined in Liang et al. (2012) and Hamidian and Beheshti (2018) have undergone revisions to incorporate modifications and ensure the application of reliable methods.

The paper is structured as follows: Section 2 furnishes some preliminary information. In Section 3, the primary findings are outlined. Section 4 showcases and analyzes several illustrative examples. Lastly, Section 5 provides concluding remarks.

2. Background and preliminaries

In this section, the paper introduces the notations used and revisits the relevant background information.

Notations. Define sets $\mathbb{R}^{\geq 0} \triangleq \{x \in \mathbb{R} : x \geq 0\}$, $\mathbb{N}^{\leq n} \triangleq \{x \in \mathbb{N} : x \leq n\}$ and $\mathbb{Z}_{\leq m}^{\leq n} \triangleq \{x \in \mathbb{Z} : m \leq x \leq n\}$. Furthermore,

- $\text{floor}(x)$ is the largest integer less than or equal to $x \in \mathbb{R}$,
- $n(C)$ denotes the count of distinct members of C ,
- $\text{frac}(x) \triangleq x - \text{floor}(x)$,
- $e(x_1(j\omega), x_2(j\omega)) \triangleq \eta x_1(j\omega) + (1 - \eta)x_2(j\omega)$, $\eta \in [0, 1]$.
- $\partial(X)$ represents the boundary of X .

The Caputo derivative is commonly utilised in control systems and is defined as follows:

$${}_b^C D_t^\gamma x(t) = \frac{1}{\Gamma(n - \gamma)} \int_b^t \frac{x^n(\tau)}{(t - \tau)^{\gamma - n + 1}} d\tau, \quad (1)$$

where γ ($n - 1 < \gamma < n$), n is an integer number. In (1), Γ is the Gamma function. Also, b and t are respectively the lower and the upper terminals of the integral (Monje et al., 2010). Based on Monje et al. (2010), the Laplace transform of the Caputo's

fractional-order derivative is given by

$$\mathcal{L}[{}_a^C D_t^\gamma x(t)] = s^\gamma \mathcal{L}[x(t)] - \sum_{i=0}^{n-1} s^{\gamma-i-1} x^{(i)}(0), \quad (2)$$

which for zero initial conditions is obtained as

$$\mathcal{L}[{}_a^C D_t^\gamma x(t)] = s^\gamma \mathcal{L}[x(t)]. \quad (3)$$

Next, consider

- β_{i_1} and α_{i_2} are the fractional orders of the system which satisfy $\beta_m > \beta_{m-1} > \dots > \beta_1 > \beta_0 = 0$ and $\alpha_n > \alpha_{n-1} > \dots > \alpha_1 > \alpha_0 = 0$,
- l is the positive time delay $l \in [l^-, l^+]$,
- $N(s, \mathbf{b})$ and $D(s, \mathbf{a})$ are the numerator and denominator of the actual system and $\mathbf{a} = [a_0, a_1, \dots, a_n]^T$ and $\mathbf{b} = [b_0, b_1, \dots, b_m]^T$ belong to the following sets:

$$\begin{aligned} \mathbf{a} \in \mathbf{A} &= \{\mathbf{a} \in \mathbb{R}^{n+1} | a_{i_2} \in [a_{i_2}^-, a_{i_2}^+], \\ &\quad a_n \neq 0, i_2 \in \mathbb{Z}_{\geq 1}^n\}, \\ \mathbf{b} \in \mathbf{B} &= \{\mathbf{b} \in \mathbb{R}^{m+1} | b_{i_1} \in [b_{i_1}^-, b_{i_1}^+], b_m, b_0 \neq 0, \\ &\quad i_1 \in \mathbb{Z}_{\geq 0}^m\}. \end{aligned} \quad (4)$$

The fractional-order plant with uncertainties is then represented as follows:

$$P(s, \mathbf{b}, \mathbf{a}, \mathbf{l}) = \frac{N(s, \mathbf{b})}{D(s, \mathbf{a})} e^{-ls} = \frac{\sum_{i_1=0}^m b_{i_1} s^{\beta_{i_1}}}{\sum_{i_2=0}^n a_{i_2} s^{\alpha_{i_2}}} e^{-ls}. \quad (5)$$

The transfer function of the parallel form of a FOPID controller is given as (6).

$$\begin{aligned} C(s) &= \frac{N_c(s)}{s^\lambda} = \frac{K_p s^\lambda + K_i + K_d s^{\mu+\lambda}}{s^\lambda}, \\ 0 &< \lambda, \mu < 2, \alpha_n > \beta_m + \mu. \end{aligned} \quad (6)$$

In this investigation, $\Delta(s)$ in (7) is assumed to represent the characteristic function of the negative unity control system.

$$\Delta(s) = s^\lambda D(s, \mathbf{a}) + N_c(s) N(s, \mathbf{b}) e^{-ls}. \quad (7)$$

Remark 2.1: Referring to Moornani and Haeri (2010b), the value sets of $D(s, \mathbf{a})$ and $N(s, \mathbf{b})$ form two parpolygons for $s = j\omega$ and $\omega > 0$. The vertex polynomials corresponding to $D(j\omega, \mathbf{a})$ are derived for $\omega \geq 0$ using **Procedure 1**.

Procedure 1 (Moornani & Haeri, 2010b): Assume $H_0 \triangleq \{i_2 \in \mathbb{Z}_{\geq 0}^n : a_{i_2}^- < a_{i_2}^+\}$.

- (1) If $H_0 = \emptyset$ and $\omega \geq 0$, $D(j\omega, \mathbf{a}) = D_0(j\omega)$ where

$$D_0(\omega) \triangleq \sum_{i_2=0}^n a_{i_2}^- s^{\alpha_{i_2}}. \quad (8)$$

- (2) If $H_0 \neq \emptyset$,

- For $\omega = 0$, $D(j\omega, \mathbf{a}) = D(j0, \mathbf{a}) = [a_0^-, a_0^+]$.
- For $\omega > 0$, define $B_0 \triangleq \{\text{frac}(0.5\alpha_{i_2}) : i_2 \in H_0\}$ and $m_D \triangleq n(B_0)$. Consider $\gamma_1, \dots, \gamma_{m_D-1}, \gamma_{m_D}$ as all the distinct members of B_0 sorted as $0 \leq \gamma_1 < \dots < \gamma_{m_D-1} < \gamma_{m_D} < 1$. Subsequently, the following sets are established for $r = 1, 2, \dots, m_D$:

$$\begin{aligned} H_r' &\triangleq \{i_2 \in H_0 : \text{floor}(0.5\alpha_{i_2}) \text{ is an odd} \\ &\quad \text{number and } \text{frac}(0.5\alpha_{i_2}) = \beta_r\}, \\ H_r &\triangleq \{i_2 \in H_0 : \text{floor}(0.5\alpha_{i_2}) \text{ is an even} \\ &\quad \text{number and } \text{frac}(0.5\alpha_{i_2}) = \beta_r\}. \end{aligned} \quad (9)$$

Assume $a^- \triangleq [a_0^- a_1^- \dots a_n^-]^T$ and $a^+ \triangleq [a_0^+ a_1^+ \dots a_n^+]^T$. The vectors $a^1, a^2, \dots, a^{2m_D}$ are specified for $k = 1, \dots, m_D$ as follows:

$$\begin{aligned} a^k &\triangleq [a_0^k a_1^k \dots a_n^k]^T, \\ a^{m_D+k} &\triangleq [a_0^{m_D+k} a_1^{m_D+k} \dots a_n^{m_D+k}]^T \\ &= a^+ + a^- - a^k. \end{aligned} \quad (10)$$

For $i_2 = 0, 1, \dots, n$, it can be written that

$$a_{i_2}^k \triangleq \begin{cases} a_{i_2}^+, & \text{for } i_2 \in \left(\bigcup_{i=1}^{k-1} H_i\right) \cup \left(\bigcup_{i=k}^m H_i\right), \\ a_{i_2}^-, & \text{otherwise.} \end{cases} \quad (11)$$

and

$$a_{i_2}^{m_D+k} \triangleq a_{i_2}^+ + a_{i_2}^- - a_{i_2}^k. \quad (12)$$

Therefore, the successive vertices $V_{r_2}^-(j\omega)$ ($r_2 = 1, 2, \dots, 2m_D$) are computed using

$$\begin{aligned} V_k^-(j\omega) &\triangleq D(j\omega, a^k), \\ V_{m_D+k}^-(j\omega) &\triangleq D(j\omega, a^{m_D+k}) \\ &= D(j\omega, a^+ + a^-) - V_k^-(j\omega), \\ k &= 1, 2, \dots, m_D. \end{aligned} \quad (13)$$

Thus, the vertex polynomials corresponding to $N(j\omega, \mathbf{b})$ and $D(j\omega, \mathbf{a})$ are denoted as $V_{r_1}^+(\omega)$ ($r_1 = 1, 2, \dots, 2m_N$) and $V_{r_2}^-(\omega)$ ($r_2 = 1, 2, \dots, 2m_D$), respectively, and can be computed using Procedure 1.

Remark 2.2: Let us regard a specific quasi-polynomial $\Delta(s)$ in (7) as $\hat{\Delta}(s)$ in (14).

$$\hat{\Delta}(s) = s^\lambda \sum_{i_2=0}^n \hat{a}_{i_2} s^{\alpha_{i_2}} + N_c(s) \left(\sum_{i_1=0}^m \hat{b}_{i_1} s^{\beta_{i_1}} \right) e^{-ls}. \quad (14)$$

Subsequently, the boundaries of the stability region defined by $\hat{\Delta}(s)$ in (14) are delineated by the Infinite Root Boundary (IRB), Complex Root Boundary (CRB), and Real Root Boundary (RRB), which can be ascertained through the procedure outlined in Hamamci (2007). To summarise, these boundaries are established based on the method proposed in Hamamci (2007) as follows. RRB and IRB can be simply obtained by substituting $\omega = 0$ and $\omega = \infty$ in $\hat{\Delta}(j\omega)$. The CRB can be determined by solving $\hat{\Delta}(j\omega) = 0$, yielding the parameters K_p and K_i as follows:

$$\begin{aligned} K_p &= (E_2(\omega)F_1(\omega) - E_1(\omega)F_2(\omega) + K_d(F_1(\omega)F_6(\omega) \\ &\quad - F_2(\omega)F_5(\omega))) / \\ &\quad (F_2(\omega)F_3(\omega) - F_1(\omega)F_4(\omega)), \\ K_i &= (E_1(\omega)F_4(\omega) - E_2(\omega)F_3(\omega) + K_d(F_4(\omega)F_5(\omega) \\ &\quad - F_3(\omega)F_6(\omega))) / \\ &\quad (F_2(\omega)F_3(\omega) - F_1(\omega)F_4(\omega)), \end{aligned} \quad (15)$$

where

$$\left\{ \begin{aligned} E_1(\omega) &= \sum_{i_2=0}^n \hat{a}_{i_2} \omega^{\lambda+\alpha_{i_2}} \cos\left(\frac{\pi(\alpha_{i_2} + \lambda)}{2} + l\omega\right), \\ E_2(\omega) &= \sum_{i_2=0}^n \hat{a}_{i_2} \omega^{\lambda+\alpha_{i_2}} \sin\left(\frac{\pi(\alpha_{i_2} + \lambda)}{2} + l\omega\right), \\ F_1(\omega) &= \sum_{i_1=0}^m \hat{b}_{i_1} \omega^{\beta_{i_1}} \cos\left(\frac{\pi\beta_{i_1}}{2}\right), \\ F_2(\omega) &= \sum_{i_1=0}^m \hat{b}_{i_1} \omega^{\beta_{i_1}} \sin\left(\frac{\pi\beta_{i_1}}{2}\right), \\ F_3(\omega) &= \sum_{i_1=0}^m \hat{b}_{i_1} \omega^{\beta_{i_1}+\lambda} \cos\left(\frac{\pi(\beta_{i_1} + \lambda)}{2}\right), \\ F_4(\omega) &= \sum_{i_1=0}^m \hat{b}_{i_1} \omega^{\beta_{i_1}+\lambda} \sin\left(\frac{\pi(\beta_{i_1} + \lambda)}{2}\right), \\ F_5(\omega) &= \sum_{i_1=0}^m \hat{b}_{i_1} \omega^{\beta_{i_1}+\lambda+\mu} \cos\left(\frac{\pi(\beta_{i_1} + \lambda + \mu)}{2}\right), \\ F_6(\omega) &= \sum_{i_1=0}^m \hat{b}_{i_1} \omega^{\beta_{i_1}+\lambda+\mu} \sin\left(\frac{\pi(\beta_{i_1} + \lambda + \mu)}{2}\right). \end{aligned} \right. \quad (16)$$

Hence, the stabilising region can be established by examining one arbitrary test point within each region (Hamamci, 2007).

Lemma 2.1 (Ghorbani et al., 2023a): Denote by $e(x, y)$ a line segment connecting the points x and y . Also, M is a member of the set of natural numbers greater than or equal to 3. At a particular frequency $\omega \in (0, \frac{2\pi}{l+\frac{1}{2}})$, the set of values of $b_1 e^{-ls}$ is situated within $G_E(j\omega)$ as expressed in (17).

$$\begin{aligned} G_E(j\omega) &\triangleq \{e(G_1(j\omega), G_2(j\omega), e(G_2(j\omega), G_3(j\omega)), \dots, \\ &\quad e(G_{4N+1}(j\omega), G_{4N+2}(j\omega)), \\ &\quad \times e(G_{4N+2}(j\omega), G_1(j\omega))\}, \end{aligned} \quad (17)$$

$$G_k(j\omega) \triangleq \begin{cases} \bar{G}_{(k-1)}(j\omega), & \text{if } 1 \leq k \leq 2M+1, \\ \underline{G}_{(2M)}(j\omega), & \text{if } k = 2M+2, \\ \underline{G}_{(2M-1)}(j\omega), & \text{if } k = 2M+3, \\ \vdots & \\ \underline{G}_0(j\omega), & \text{if } k = 4M+2. \end{cases}$$

$$\bar{G}_k(j\omega) \triangleq \begin{cases} b_1 e^{-j\omega\left(l+k\frac{l+\frac{1}{2}}{2M}\right)}, & \text{if } k = 0, 2, \dots, 2M, \\ b_1 e^{-j\omega\left(l+k\frac{l+\frac{1}{2}}{2M}\right)} & \text{if } k = 1, 3, \\ \cos\left(\omega\frac{l+\frac{1}{2}}{2M}\right), & \dots, 2M-1. \end{cases}$$

$$\underline{G}_k(j\omega) \triangleq b_1 e^{-j\omega\left(l+k\frac{l+\frac{1}{2}}{2M}\right)}, \quad k = 0, 1, 2, \dots, 2M.$$

Lemma 2.2 (Buslowicz, 2008): The fractional-order system with $\delta(s)$ is stable if and only if for $-\infty < \omega < \infty$

$$\begin{aligned} \Delta \arg \psi(j\omega) &= \frac{\delta(j\omega)}{\omega_r(j\omega)} = 0, \quad \omega_r(s) = a_{0n}(s+f)^{\alpha_n}, \\ c &> 0. \end{aligned} \quad (18)$$

α_n represents the highest order of $\delta(j\omega)$, while a_{0n} stands for the coefficient of the highest term s^{α_n} , and f is an arbitrary positive number.

Remark 2.3: Assume that the value sets of $X_1(j\omega)$ and $X_2(j\omega)$ are both bounded and closed in the complex plane. If at a particular frequency, the boundaries $\partial(X_1(j\omega))$ and $\partial(X_2(j\omega))$ have no overlap in the complex plane, it implies that no common real or complex number exists in their respective value sets.

3. Main results

3.1. Characterizing robust stability regions

In accordance with the zero exclusion principle, It is imperative to scrutinise how the complex plane origin is encompassed within the value set of the characteristic function $\Delta(j\omega)$ for $\omega \geq 0$. In this section, we present Theorem 3.1, Lemmas 3.1, and 3.2 to determine whether the condition $0 \in \Delta(j\omega)$ for $\omega \geq 0$. Additionally, Theorem 3.2 is introduced to analyze the robust stability of $\Delta(s)$ in (7). Finally, an algorithm is proposed for calculating the robust stability region of FOPID controllers.

Theorem 3.1: Let $\Delta^{vs}(j\omega)$ denote the value set of the characteristic function $\Delta(j\omega)$. Consider $\Delta(j\omega) = \Delta_1(j\omega) + \Delta_2(j\omega)$. Then, at a specific frequency $\omega = \omega_0$, $0 \in \Delta^{vs}(j\omega)$ if and only if $-\Delta_1^{vs}(s = j\omega_0)$ and $\Delta_2^{vs}(s = j\omega_0)$ overlap in the complex plane.

Proof: Sufficiency: Given that $-\Delta_1^{vs}(j\omega_0)$ and $\Delta_2^{vs}(j\omega_0)$ overlap in the complex plane, there exists $z_0 \in \mathbb{C}$ such that $z_0 \in -\Delta_1^{vs}(j\omega_0)$ and $z_0 \in \Delta_2^{vs}(j\omega_0)$. Consequently, there exists a member $\tilde{\Delta}_1(j\omega_0)$ of the family $-\Delta_1^{vs}(j\omega_0)$ that equals z_0 i.e. $z_0 = -\tilde{\Delta}_1(j\omega_0)$. Likewise, one can show that $z_0 = \tilde{\Delta}_2(j\omega_0)$. Consider $\{\tilde{\Delta}(j\omega) = \tilde{\Delta}_1(j\omega) + \tilde{\Delta}_2(j\omega)\} \in \Delta(j\omega)$. Hence, at the specific frequency $\omega = \omega_0$, it is obvious that $0 \in \Delta^{vs}(j\omega)$.

Necessity: The condition $0 \in \Delta^{vs}(j\omega_0)$ can be denoted as $z_0 - z_0 \in \Delta^{vs}(j\omega_0)$. Consequently, it follows that z_0 lies in both $-\Delta_1^{vs}(j\omega_0)$ and $\Delta_2^{vs}(j\omega_0)$. This suggests an overlap between the value sets of $-\Delta_1^{vs}(j\omega_0)$ and $\Delta_2^{vs}(j\omega_0)$ in the complex plane. ■

Based on Theorem 3.1, we introduce the following result, which can be used to examine whether the origin is included in the value set of $\Delta(j\omega)$.

Lemma 3.1: Assume $s^\lambda D(s, \mathbf{a}) \neq 0$ for $s = j\omega_0$. Then, $0 \notin \Delta^{vs}(j\omega_0)$ if and only if, $\Theta_1(j\omega_0)$ in (19) and $\Theta_2(j\omega_0)$ in (20) do not have any overlap.

$$\Theta_1(j\omega) = -e^{lj\omega}. \quad (19)$$

$$\Theta_2(j\omega) = \left(\frac{N_v^{r_1}}{D_v^{r_2}} \right) \cup \left(\frac{N_E^{r_1}}{D_v^{r_2}} \right), \quad (20)$$

in which

$$\begin{cases} N_v^{r_1} = N_c(j\omega) V_{r_1}^+(\omega), & r_1 = 1, 2, \dots, 2m_N, \\ D_v^{r_2} = s^\lambda V_{r_2}^-(j\omega), & r_2 = 1, 2, \dots, 2m_D, \\ N_E^{r_1} = e(N_c(j\omega) V_{r_1}^+(\omega), N_c(j\omega) V_{r_1+1}^+(\omega)), \\ D_E^{r_2} = e((j\omega)^\lambda V_{r_2}^-(j\omega), (j\omega)^\lambda V_{r_2+1}^-(j\omega)), \\ V_1^+(\omega) = V_{2m_N+1}^+(\omega), & V_1^-(j\omega) = V_{2m_D+1}^-(j\omega). \end{cases} \quad (21)$$

Proof: According to Procedure 1, $s^\lambda D(s, \mathbf{a})$ and $N_c(s) N(s, \mathbf{b}) e^{-ls}$ would be two polygons for $s = j\omega$. Additionally, (22) holds for $s = j\omega_0$.

$$0 \in \Delta(s) \iff 0 \in e^{ls} + \frac{(K_p s^\lambda + K_i + K_d s^{\mu+\lambda}) N(j\omega_0, \mathbf{b})}{s^\lambda D(s, \mathbf{a})}. \quad (22)$$

Furthermore, as stated in Tan (2002), it can be deduced that

$$\partial \left(\frac{(K_p s^\lambda + K_i + K_d s^{\mu+\lambda}) N(s, \mathbf{b})}{s^\lambda D(s, \mathbf{a})} \right) \subset \Theta_2(s), \quad s = j\omega_0. \quad (23)$$

Based on (22), (23), and Theorem 3.1, and assuming $\Delta_1(s) = e^{ls}$ and $\Delta_2(s) = \frac{(K_p s^\lambda + K_i + K_d s^{\mu+\lambda}) N(j\omega_0, \mathbf{b})}{s^\lambda D(s, \mathbf{a})}$, the proof follows straightforwardly. ■

Lemma 3.2: Assume $N_c(s) N(s, \mathbf{b}) \neq 0$ for $s = j\omega_0$. Then, $0 \notin \Delta^{vs}(j\omega_0)$ if and only if, $(\Theta_1(\omega_0))^{-1}$ and $(\Theta_2(\omega_0))^{-1}$ do not have any overlap in the complex plane.

Proof: The proof is completely similar to Lemma 2.1. ■

Now, considering Theorem 3.1, Lemmas 2.1 and 2.2, and the zero exclusion principle, the following theorem presents the analysis of robust stability for $\Delta(j\omega)$.

Theorem 3.2: Assume that a certain quasi-polynomial of $\Delta(s)$ in (7) as $\hat{\Delta}(s)$ in (14) is stable. Then, $\Delta(s)$ is robust stable if and only if, the characteristic functions $\Delta_{h_1}^D(s) (h_1 = 1, \dots, 2m_N)$ in (24) and $\Delta_{h_2}^N(s) (h_2 = 1, \dots, 2m_D)$ in (25) are also robustly stable.

$$\Delta_{h_1}^D(s) = s^\lambda D(s, \mathbf{a}) + N_c(s) e^{-ls} V_{h_1}^+(\omega), \quad (h_1 = 1, \dots, 2m_N). \quad (24)$$

$$\Delta_{h_2}^N(s) = s^\lambda V_{h_2}^-(\omega) + N_c(s) e^{-ls} N(s, \mathbf{b}), \quad (h_2 = 1, \dots, 2m_D). \quad (25)$$

Proof: *Sufficiency:* If the characteristic functions $\Delta_{h_1}^D(s)$ (for $h_1 = 1, \dots, 2m_N$) in (24) exhibit robust stability, then according to the zero exclusion principle and Theorem 3.1, it follows that

$$-N_c(s) V_{h_1}^+(\omega) e^{-ls} \notin s^\lambda D(s, \mathbf{a}), \quad (h_1 = 1, 2, \dots, 2m_N) \text{ and } s = j\omega. \quad (26)$$

Likewise, from (25) and Theorem 3.1, one can infer that

$$-s^\lambda V_{h_2}^-(\omega) \notin N_c(s) N(s, \mathbf{b}) e^{-ls}, \quad (h_2 = 1, 2, \dots, m_D) \text{ and } s = j\omega. \quad (27)$$

From (26) and (27) and Theorem 3.1, it is apparent that $\Theta_1(\omega_0)$ in (19) and $\Theta_2(\omega_0)$ in (20) do not have any overlap in the complex plane for $s^\lambda D(s, \mathbf{a}) \neq 0$ and $s = j\omega_0$. Likewise, $(\Theta_1(\omega_0))^{-1}$ and $(\Theta_2(\omega_0))^{-1}$ do not have any overlap for $(K_p s^\lambda + K_i + K_d s^{\mu+\lambda}) N(j\omega_0, \mathbf{b}) \neq 0$ and $s = j\omega_0$. This implies that $0 \notin \Delta(j\omega)$.

Necessity: Given that the characteristic function (7) is robustly stable, as per the zero exclusion principle, the origin is not included in $\Delta(j\omega)$. This implies that the origin lies outside the value set of $\Delta(j\omega)$. Suppose $s^\lambda D(s, \mathbf{a}) \neq 0$ for $s = j\omega_0$. Then, from Lemma 2.1, it can be inferred that $\Theta_1(\omega_0)$ in (19) and $\Theta_2(\omega_0)$ in (20) do not overlap in the complex plane for $s^\lambda D(s, \mathbf{a}) \neq 0$ and $s = j\omega_0$. Consequently, the robust stability of $\Delta_{h_1}^D(s)$ (for $h_1 = 1, 2, \dots, 2m_N$) in (19) and $\Delta_{h_2}^N(s)$ (for $h_2 = 1, 2, \dots, 2m_D$) in (20) is inferred based on the zero exclusion principle. ■

Remark 3.1: According to Theorem 3.2, Theorem 3.1 in Liang et al. (2012) and the method proposed in Hamidian and Beheshti (2018) are not universally valid. This discrepancy is due to the non-convex shape of the value sets of $\Delta_{r_1}^D(s)$ for $r_1 = 1, 2, \dots, 2m_N$ in (24) and $\Delta_{r_2}^N(s)$ for $r_2 = 1, 2, \dots, 2m_D$ in (25) with respect to e^{-ls} .

Remark 3.2: Theorem 3.2 illustrates that examining the robust stability properties of the characteristic function $\Delta(s)$ in (7) is tantamount to evaluating the robust stability of $\Delta_{h_1}^D(s)$ (for $h_1 = 1, \dots, 2m_N$)

in (24) and $\Delta_{h_2}^N(s)$ (for $h_2 = 1, \dots, 2m_D$) in (25). As a result, the primary hurdles involve delineating RRB, IRB, and CRB of $\Delta_{h_1}^D(s)$ (for $h_1 = 1, \dots, 2m_N$) in (24) and $\Delta_{h_2}^N(s)$ (for $h_2 = 1, \dots, 2m_D$) in (25). To accomplish this task, Algorithm 1 outlines the procedure for computing the stability region while maintaining fixed values of λ , μ , and k_d .

Algorithm 1: *Step 1:* Derive the vertices $V_{h_1}^+(\omega)$ (for $h_1 = 1, \dots, 2m_N$) and $V_{h_2}^-(\omega)$ (for $h_2 = 1, \dots, 2m_D$) using Procedure 1.

Step 2: Determine RRB, IRB and CRB by sweeping over $\eta \in [0, 1]$ for

$$\Delta_{r_1}^D(j\omega) = \begin{cases} \Delta_{r_1}^{D_1}(j\omega), & 0 < \omega < \frac{2\pi}{l^+ - l^-}, \\ \Delta_{r_1}^{D_2}(j\omega), & \omega \geq \frac{2\pi}{l^+ - l^-}, \end{cases} \quad (28)$$

in which,

$$\begin{cases} \Delta_{h_1}^{D_1}(j\omega) = s^\lambda e(V_{h_2}^-(\omega), \\ V_{h_2+1}^-(\omega) + V_{h_1}^+(\omega) N_c(s) e^{-ls}), \\ \Delta_{h_1}^{D_2}(j\omega) = s^\lambda e(V_{h_2}^-(\omega), \\ V_{h_2+1}^-(\omega) + V_{h_1}^+(\omega) N_c(s) e^{j[0, 2\pi]}), \\ h_1 = 1, 2, \dots, 2m_N, \quad h_2 = 1, 2, \dots, 2m_D. \end{cases} \quad (29)$$

Step 3: Obtain RRB, IRB and CRB by sweeping over $\eta \in [0, 1]$ for

$$\Delta_{h_2}^N(s) = \begin{cases} \Delta_{h_2}^{N_1}(j\omega), & 0 < \omega < \frac{2\pi}{l^+ - l^-}, \\ \Delta_{h_2}^{N_2}(j\omega), & \omega \geq \frac{2\pi}{l^+ - l^-}, \end{cases} \quad (30)$$

where

$$\begin{cases} \Delta_{h_2}^{N_1}(s) = s^\lambda V_{h_2}^-(\omega) \\ + N_c(s) e^{-ls} e(V_{h_1}^-(\omega), V_{h_1+1}^-(\omega)), \\ \Delta_{h_2}^{N_2}(s) = s^\lambda V_{h_2}^-(\omega) \\ + N_c(s) e^{j[0, 2\pi]} e(V_{h_1}^-(\omega), V_{h_1+1}^-(\omega)), \\ h_1 = 1, \dots, 2m_N, \quad h_2 = 1, \dots, 2m_D. \end{cases} \quad (31)$$

Step 4: The final robust stability region for $\Delta(s)$ is the intersection of all the computed stable regions in Step 2 and Step 3.

Proof: Based on the zero exclusion principle, it can be inferred that the closed-loop control system is robustly stable if and only if $\Delta(s)$ in (7) contains at least one stable member and $0 \notin \partial(\Delta(j\omega))$. Furthermore, stabilisation of all quasi-polynomials $\Delta_{h_1}^D(s) (h_1 = 1, \dots, 2m_N)$ in (24) and $\Delta_{h_2}^N(s) (h_2 = 1, \dots, 2m_D)$ in (25), calculated using the D-decomposition method, ensures the robust stability of $\Delta(j\omega)$ based on Theorem 3.2, because $\partial(\Delta(j\omega)) \subseteq \Delta_{h_1}^D(s) \cup \Delta_{h_2}^N(s)$. This implies that $0 \notin \partial(\Delta(j\omega))$ and that there is at least one stable member in $\Delta(s)$. Therefore, the zero exclusion principle completes the proof. ■

3.2. High-performance output disturbance rejection

As noted by Levine (2018), the sensitivity function encompasses crucial aspects of a feedback system, including its capability to track references and reject disturbances. A low sensitivity function at lower frequencies plays a pivotal role in attaining the desired performance of the closed-loop system. Hence, we formulate a robust fractional-order controller to fulfill the inequality constraint (32). In (32), $M_s(s)$ represents the weighting function, elucidating the frequency characteristics of performance specifications and the frequency bandwidth of disturbances.

$$|S(j\omega)| = \left| \frac{1}{1 + C(j\omega)P(j\omega, \mathbf{b}, \mathbf{a}, \mathbf{l})} \right| < |M_s(j\omega)|$$

$$\rightarrow \left| \frac{1}{1 + \frac{N_c(s)N(s, \mathbf{b})}{s^\lambda D(s, \mathbf{a})} e^{-ls}} \right| < |M_s(s)|,$$

$$M_s(s) = \frac{N_m(s)}{D_m(s)}, \quad s = j\omega. \quad (32)$$

As per (32), the maximum modulus theorem (Brown & Churchill, 2009), Lemma 2.1 and Theorem 3.2, the robustly designed FOPID controller should adhere to the inequality $\chi_S(\omega) < 0$.

$$\chi_S(\omega) \triangleq \begin{cases} \max\{\chi_S^i | i = 1, 2, 3, 4\}, & \text{for } \omega \in \left[0, \frac{2\pi}{T^+ - T^-}\right), \\ \frac{\max\{V_1^+(j\omega), \dots, V_{2m_N}^+(j\omega)\}}{\min_{P \in P_E^2} |e^P| = e^{(j\omega)^2 V_{r_2}^-(\omega)}, -|M_s(j\omega)|, (j\omega)^\lambda V_{r_2+1}^-(\omega)}} - 1 & \text{for } \omega \in \left[\frac{2\pi}{T^+ - T^-}, \infty\right), \end{cases} \quad (33)$$

where

$$\chi_S^1(\omega) \triangleq \max_{r=1, \dots, 4N+1} |\tilde{\chi}_{S_1}^r(\omega) - |M_s(j\omega)||,$$

$$\tilde{\chi}_{S_1}^r(\omega) \triangleq \max_{e_{S_1 r_1, r_2} \in P_{S_1}} |e_{S_1 r_1, r_2}|,$$

$$r_1 \in \{1, \dots, 2m_N\}, r_2 \in \{1, \dots, 2m_D\},$$

$$P_{S_1} \triangleq \{e_{S_1 1, 1}, \dots, e_{S_1 r_1, r_2}, \dots, e_{S_1 2m_N, 2m_D}\},$$

$$e_{S_1 r_1, r_2} \triangleq \frac{1}{1 + \frac{N_c(s)V_{r_1}^+(\omega)G_r(s)}{s^\lambda e^{(V_{r_2}^-(\omega), V_{r_2+1}^-(\omega))}}}. \quad (34)$$

$$\chi_S^2(\omega) \triangleq \max_{r_1=1, \dots, 2m_D} |\tilde{\chi}_{S_2}^{r_1}(\omega) - |M_s(j\omega)||,$$

$$\tilde{\chi}_{S_2}^{r_1}(\omega) \triangleq \max_{e_{S_2 r, r_2} \in P_{S_2}} |e_{S_2 r, r_2}|,$$

$$r \in \{1, \dots, 4N+1\}, r_2 \in \{1, \dots, 2m_N\},$$

$$P_{S_2} \triangleq \{e_{S_2 1, 1}, \dots, e_{S_2 r, r_2}, \dots, e_{S_2 4N+1, 2m_D}\},$$

$$e_{S_2 r, r_2} \triangleq \frac{1}{1 + \frac{N_c(s)V_{r_2}^+(\omega)e^{(G_r(s), G_{r+1}(s))}}{s^\lambda V_{r_1}^-(\omega)}}. \quad (35)$$

$$\chi_S^3(\omega) \triangleq \max_{r=1, \dots, 4N+1} |\tilde{\chi}_{S_3}^r(\omega) - |M_s(j\omega)||,$$

$$\tilde{\chi}_{S_3}^r(\omega) \triangleq \max_{e_{S_3 r_1, r_2} \in P_{S_3}} |e_{S_3 r_1, r_2}|,$$

$$r_1 \in \{1, \dots, 2m_N\}, r_2 \in \{1, \dots, 2m_D\},$$

$$P_{S_3} \triangleq \{e_{S_3 1, 1}, \dots, e_{S_3 r_1, r_2}, \dots, e_{S_3 2m_N, 2m_D}\},$$

$$e_{S_3 r_1, r_2} \triangleq \frac{s^\lambda V_{r_2}^-(\omega)}{s^\lambda V_{r_2}^-(\omega)G_r'(s) + N_c(s)e^{(V_{r_1}^+(\omega), V_{r_1+1}^+(\omega))}}. \quad (36)$$

$$\chi_S^4(\omega) \triangleq \max_{r_2=1, \dots, 2m_N} |\tilde{\chi}_{S_4}^{r_2}(\omega) - |M_s(j\omega)||,$$

$$\tilde{\chi}_{S_4}^{r_2}(\omega) \triangleq \max_{e_{S_4 r_1, r} \in P_{S_4}} |e_{S_4 r_1, r}|,$$

$$r_1 \in \{1, \dots, 2m_D\}, r \in \{1, \dots, 4N+1\},$$

$$P_{S_4} \triangleq \{e_{S_4 1, 1}, \dots, e_{S_4 r_1, r}, \dots, e_{S_4 2m_N, 4N+1}\},$$

$$e_{S_4 r_1, r_2} \triangleq \frac{s^\lambda V_{r_2}^-(\omega)}{s^\lambda V_{r_1}^-(\omega)e^{(G_r'(s), G_{r+1}'(s))} + N_c(s)V_{r_2}^+(\omega)}. \quad (37)$$

In (37), $G_r'(j\omega)$ is given by

$$G_i'(j\omega) \triangleq \begin{cases} \overline{G}_{(i-1)}'(j\omega), & \text{if } 1 \leq i \leq 2M+1, \\ \underline{G}_{(2M)}'(j\omega), & \text{if } i = 2M+2, \\ \overline{G}_{(2M-1)}'(j\omega), & \text{if } i = 2M+3, \\ \vdots & \\ \underline{G}_0'(j\omega), & \text{if } i = 4M+2, \end{cases}$$

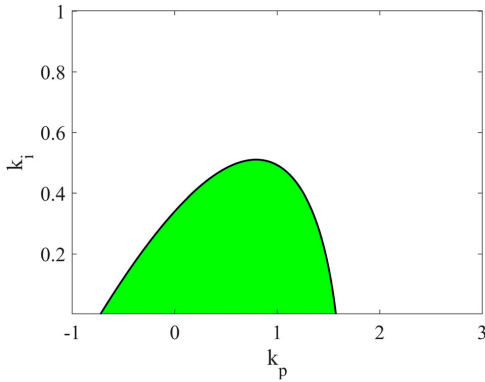


Figure 1. Robust stability region of PI controllers.

$$\bar{G}_i(j\omega) \triangleq \begin{cases} e^{j\omega(l^- + i\frac{l^+ - l^-}{2M})}, & \text{if } i = 0, 2, \dots, 2M, \\ \frac{e^{j\omega(l^- + i\frac{l^+ - l^-}{2M})}}{\cos(\omega\frac{l^+ - l^-}{2M})}, & \text{if } i = 1, 3, \dots, 2M - 1, \end{cases}$$

$$\bar{G}_i(j\omega) \triangleq e^{j\omega(l^- + i\frac{l^+ - l^-}{2N})}, \quad i = 0, 1, 2, \dots, 2M.$$

The bound on the sensitivity function (32) typically represents the potential benefits of feedback such as disturbance rejection and robust performance (Levine, 2018). If the inequality $\chi_S(\omega) < 0$ holds, then the condition $\|M_s^{-1}(j\omega)S(j\omega)\|_\infty < 1$ might be satisfied, which may ensure robust performance. Therefore, the designer only needs to check the sign of the function $\chi_S(\omega)$ to assess robust performance.

Remark 3.3: Using the graphical tuning method proposed in Algorithm 1, a robust FOPID controller for the interval system can be designed. To enhance the system's performance, the designed robust controller should satisfy $\chi_S(\omega) \leq 0$ in (33). The subsequent section will complement the results presented in this paper with illustrative examples demonstrating the application of the contributed methods.

4. Numerical and experimental examples

In this section, we present two examples that demonstrate the sophistication of the proposed methodologies. In Example 4.1, we compute the robust stability region for three controllers: PI, FOPI and FOPID. Additionally, to validate the identified region, we

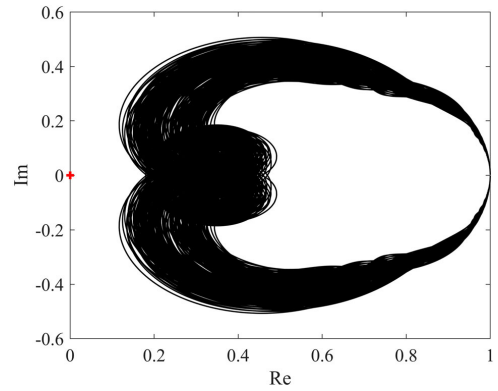


Figure 2. Verification of the robust PI stabilisation $C(s) = 1 + \frac{0.2}{s}$ using Lemma 2.2.

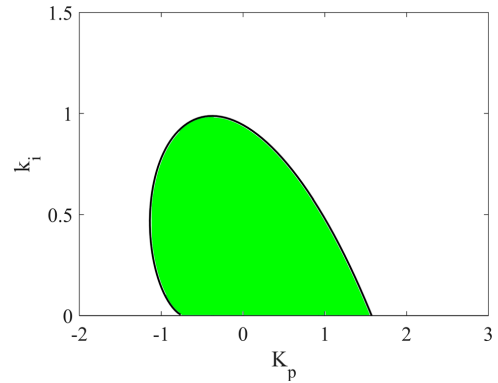


Figure 3. Robust stability region of FOPI controllers with $\lambda = 0.5$.

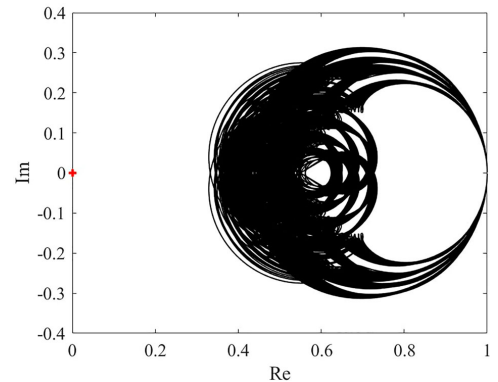


Figure 4. Verification of the robust FOPI stabilisation $C(s) = \frac{0.5}{s^{0.5}}$ using Lemma 2.2.

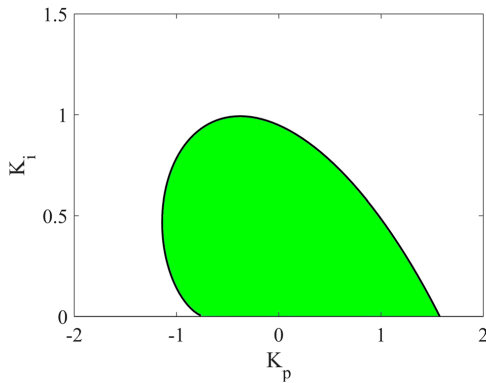


Figure 5. Robust stability region of FOPID controllers with $\lambda = 0.5$, $\mu = 1$ and $K_d = 0.01$.

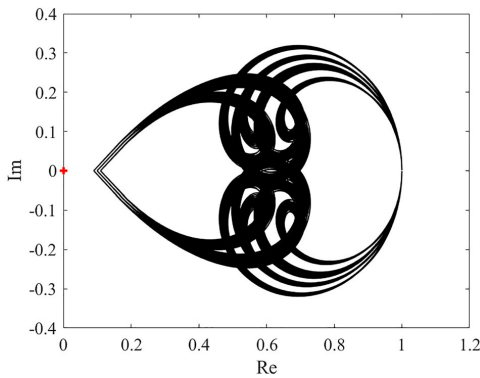


Figure 6. Verification of the robust FOPID stabilisation $C(s) = 0.1 + \frac{0.1}{s^{0.5}} + 0.01s$ using Lemma 2.2.

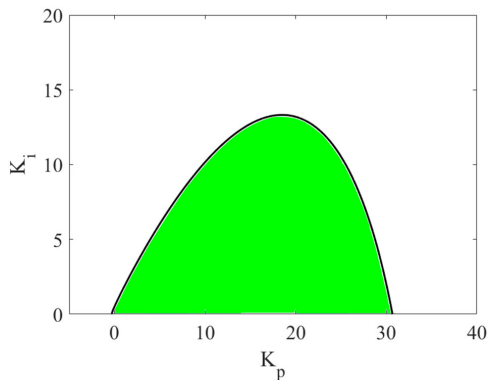


Figure 7. Robust stability region of FOPID controllers with $\mu = 0.65$, $\lambda = 1$ and $k_d = 1$.

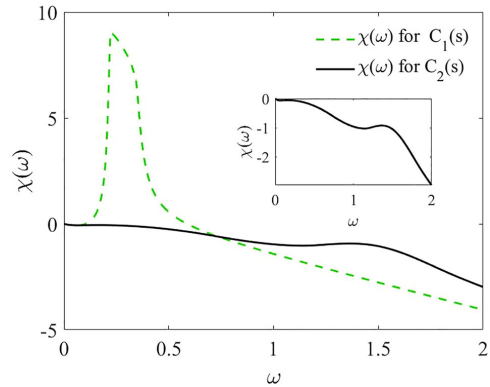


Figure 8. Curves of $\chi(\omega)$ corresponding to the controllers $C_1(s)$ (dashed line) and $C_2(s)$ (solid line).

ensure the stability of the characteristic function by testing it with randomly generated values within the uncertainty space, employing Lemma 2.2. Furthermore, in Example 4.2, we initially determined the robust stability region for FOPI controllers. Subsequently, within this stability region, we selected a FOPI controller that meets the inequality $\chi_s(\omega) < 0$ to enhance the system's performance. Moreover, in Example 4.3, experimental verification is provided to demonstrate the application of the proposed approach in designing robust fractional-order controllers.

Example 4.1: Consider a plant with interval uncertainties as follows:

$$\begin{aligned} \mathbf{P}(s) &= \frac{\mathbf{N}_P(s)}{\mathbf{D}_P(s)} e^{-[0.5, 0.9]s}, \\ \mathbf{N}_P(s) &= [-0.6, -0.3]s + [0.9, 1.1], \\ \mathbf{D}_P(s) &= s^3 + [1.8, 2.2]s^2 + [2.8, 3.2]s + [0.8, 1]. \end{aligned} \quad (38)$$

Suppose our initial objective is to determine the stability region of the proportional-integral (PI) controller by setting $k_d = 0$ and $\lambda = 1$ in the FOPID controller introduced in (6). In this scenario, we utilise Algorithm 1 to identify the robust stability region of PI controllers, as illustrated in Figure 1 (green region). From this figure, it becomes apparent that the PI controller $C(s) = 1 + \frac{0.2}{s}$ is located in the green region and using Lemma 2.2, the stability of the characteristic function has been checked for some randomly generated values in the uncertainty space. From Figure 2,

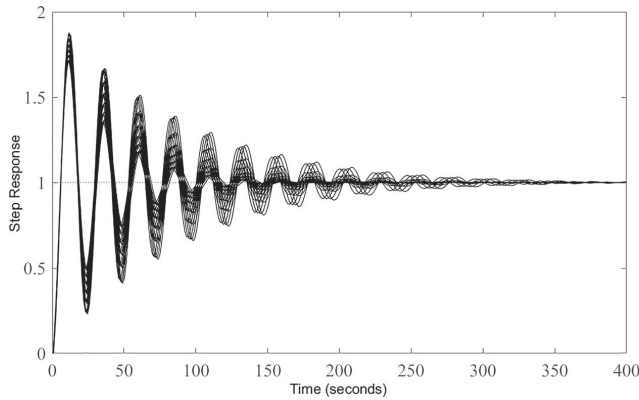


Figure 9. Step responses corresponding to $C_1(s)$.

all chosen characteristic functions are stable. From the given figure, it is evident that the PI controller, denoted as $C(s) = 1 + \frac{0.2}{s}$, is positioned within the green region. By applying Lemma 2.2, the stability of the characteristic function has been verified using randomly generated values within the uncertainty space. As illustrated in Figure 2, all selected characteristic functions are observed to be stable.

The robust stability region (depicted in green) of FOPI controllers has been illustrated in Figure 3 for $\lambda = 0.5$. To validate this region, the robust stability of the closed-loop system has been examined in Figure 4 using one of the controllers situated within the green region, such as the controller $C(s) = \frac{0.5}{s^{0.5}}$, as demonstrated in Lemma 2.2.

Similarly, the robust stability region (also in green) of FOPID controllers has been delineated in Figure 5 for $\lambda = 0.5$, $\mu = 1$, and $K_d = 0.01$. To confirm the obtained region, Figure 6 verifies the robust stability of the system using a controller located within the green region, for instance, the controller $C(s) = 0.1 + \frac{0.1}{s^{0.5}} + 0.01s$, as per Lemma 2.2.

It is important to note that the methods proposed in the existing literature, as referenced in Zheng et al. (2014), Ghorbani et al. (2023d), Hamidian and Beheshti (2018), Hamamci (2007), Ghorbani et al. (2024), Zheng and Li (2018), Liang et al. (2012), Ghorbani et al. (2023a) and Wu et al. (2024), are insufficient for establishing the robust stability region of the plant described in (38). This highlights the sophistication and novelty of the method introduced in this paper.

Example 4.2: Consider a plant with interval uncertainties as follows:

$$P(s) = \frac{[2, 4]}{[70, 80]s + 1} e^{-[0.5, 1]s}. \quad (39)$$

Our objective is to ascertain the robust stability region of FOPID controllers with $\mu = 0.65$, $\lambda = 1$, and $k_d = 1$. Utilizing Algorithm 1, we have delineated the robust stability region of the controller in the green area, as depicted in Figure 7. According to this figure, the controllers identified fall within the confines of the green region.

$$C_1(s) = 2 + \frac{2}{s} + s^{0.65}. \quad (40)$$

$$C_2(s) = 18 + \frac{1.3}{s} + s^{0.65}. \quad (41)$$

Additionally, the plot of $\chi(\omega)$ is presented in Figure 8 for $M_s(s) = 0.021 \frac{(s+1000)(s+30.67)(s+0.001)}{s^2+30.67s+247.3}$ corresponding to both controllers $C_1(s)$ and $C_2(s)$. Observing this figure, it is evident that controller $C_2(s)$ satisfies the inequality $\chi(\omega) < 0$. Consequently, the designer should opt for controller $C_2(s)$. Figures 9 and 10 depict the step responses of the closed-loop system. Notably, these figures highlight that controller $C_2(s)$ exhibits superior performance, characterised by fewer oscillations.

Example 4.3: In this example, the primary objective is to control the pitch of the TRAS, as illustrated in Figure 11. The open-loop system has been identified

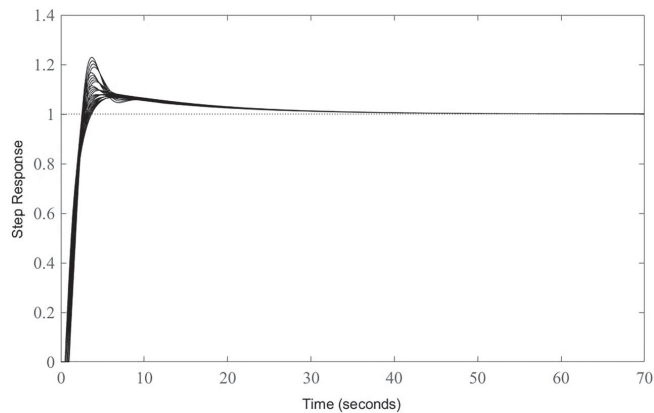


Figure 10. Step responses corresponding to $C_2(s)$.

as (42).

$$P(s) = \frac{[6, 8]s + [2.5, 3.7]}{[13, 15]s^3 + [10, 11]s^2 + [4.5, 6]s - 1} \times e^{-[0.1, 0.15]s}. \quad (42)$$

Our aim is to identify the stability region for FOPID controllers with parameters $\mu = 1.3$, $\lambda = 1$, and $k_d = 0.9$. By applying Algorithm 1, we have mapped the robust stability area of the controller, highlighted in green in Figure 12. Moreover, the fractional-order controller $C(s)$ is designed to ensure that the inequality $\chi_s(\omega) < 0$ in (43), is satisfied. This condition holds for $M_s(s) = 0.021 \frac{(s+1000)(s+30.67)(s+0.001)}{s^2+30.67s+247.3}$ over the frequency range $\omega \in [0, 0.4]$ rad/sec, as illustrated in Figure 13.

$$C(s) = 1.9 + \frac{0.65}{s} + 0.9s^{1.3}. \quad (43)$$

Figures 14 and 15 present the pitch angle response and the control signal of the TRMS system, respectively. This example demonstrates the applicability of the proposed method for real-world systems.

5. Conclusion

In this paper, a new method was proposed to obtain the stabilising region of FOPID controllers for interval delayed fractional-order plants. At first, two useful theorems were presented to analyze the robust stability of a closed-loop system consisting of a FOIPD controller and an interval delayed fractional-order plant. Inspired by these theorems, a useful algorithm was



Figure 11. TRMS system.

proposed to calculate the stabilising region of FOPID controllers. Then, an auxiliary function was presented to improve the control requirement on the disturbance rejection. At the end, an assessment of the

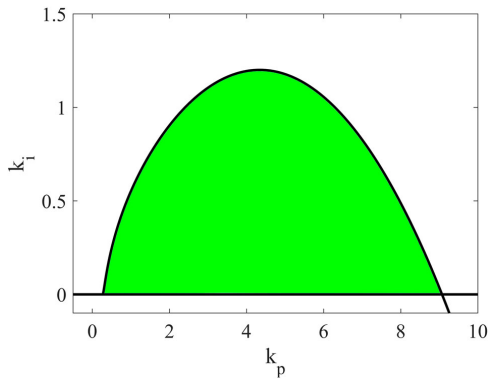


Figure 12. Robust stability region of FOPID controllers with $\mu = 1.3$, $\lambda = 1$ and $k_d = 0.9$.

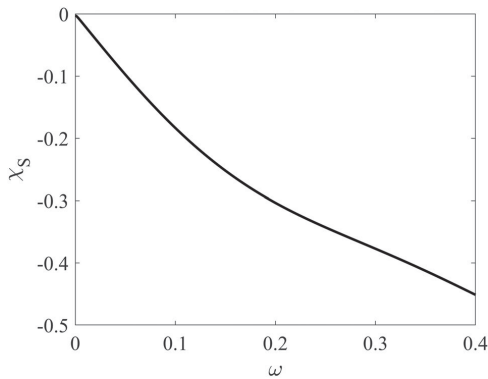


Figure 13. Curves of $\chi(\omega)$.

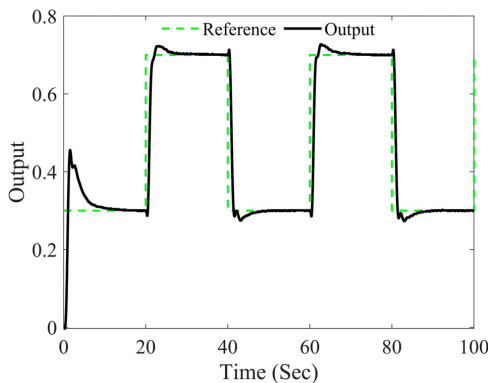


Figure 14. Output (the pitch angle).

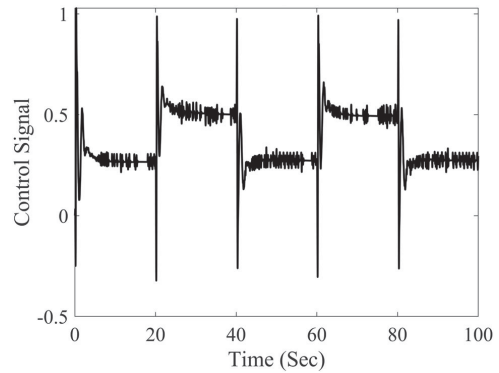


Figure 15. Control signal.

results was offered by some numerical examples and an experimental verification. Future work may involve improving computational efficiency and addressing more complex uncertainty structures.

Disclosure statement

No potential conflict of interest was reported by the author(s).

Funding

This work was supported by Eesti Teadusagentuur [PRG658].

Data availability statement

Data available on request from the authors.

References

- Bettou, K., & Charef, A. (2009). Control quality enhancement using fractional $PI^\lambda D^\mu$ controller. *International Journal of Systems Science*, 40(8), 875–888. <https://doi.org/10.1080/00207720902974546>
- Brown, J. W., & Churchill, R. V. (2009). *Complex variables and applications*. McGraw-Hill.
- Buslowicz, M. (2008). Stability of linear continuous-time fractional order systems with delays of the retarded type. *Bulletin of the Polish Academy of Sciences: Technical Sciences*, 56(4), 319–3243.
- Dastjerdi, A. A., Saikumar, N., & HosseinNia, S. H. (2018). Tuning guidelines for fractional order PID controllers: Rules of thumb. *Mechatronics*, 56, 26–36. <https://doi.org/10.1016/j.mechatronics.2018.10.004>
- Ghorbani, M., & Tavakoli-Kakhki, M. (2021). Robust stability analysis of a general class of interval delayed fractional order plants by a general form of fractional order controllers. *Mathematical Methods in the Applied Sciences*, 44(13), 10172–10189. <https://doi.org/10.1002/mma.v44.13>

- Ghorbani, M., Tepljakov, A., & Petlenkov, E. (2023a). On robust stability analysis of interval time delay systems using delayed controllers. In *2023 European Control Conference (ECC)* (pp. 1–6). IEEE.
- Ghorbani, M., Tepljakov, A., & Petlenkov, E. (2023b). Fractional-order interval polynomials, stability and robust stability analysis and FOMCON implementation. In *2023 International Conference on Fractional Differentiation and Its Applications (ICFDA)* (pp. 1–6). IEEE.
- Ghorbani, M., Tepljakov, A., & Petlenkov, E. (2023c). Robust D-stability analysis of fractional-order controllers. In *2023 American Control Conference (ACC)* (pp. 3871–3876). IEEE.
- Ghorbani, M., Tepljakov, A., & Petlenkov, E. (2023d). Stabilizing region of fractional-order proportional integral derivative controllers for interval fractional-order plants. *Transactions of the Institute of Measurement and Control*, 45(3), 546–556. <https://doi.org/10.1177/01423312221117866>
- Ghorbani, M., Tepljakov, A., & Petlenkov, E. (2024). Robust stabilization of interval fractional-order plants with an interval time delay by fractional-order proportional integral derivative controllers. *IET Control Theory & Applications*, 18(5), 614–625. <https://doi.org/10.1049/cth2.v18.5>
- Hamamci, S.E. (2007). An algorithm for stabilization of fractional-order time delay systems using fractional-order PID controllers. *IEEE Transactions on Automatic Control*, 52(10), 1964–1969. <https://doi.org/10.1109/TAC.2007.906243>
- Hamidian, H., & Beheshti, M. T. H. (2018). A robust fractional-order PID controller design based on active queue management for TCP network. *International Journal of Systems Science*, 49(1), 211–216. <https://doi.org/10.1080/00207721.2017.1397801>
- Levine, W. S. (2018). *The control handbook (three volume set)*. CRC Press.
- Liang, T., Chen, J., & Lei, C. (2012). Algorithm of robust stability region for interval plant with time delay using fractional order PI^1D^μ controller. *Communications in Nonlinear Science and Numerical Simulation*, 17(2), 979–991. <https://doi.org/10.1016/j.cnsns.2011.06.029>
- Mohamed, M. J., & Khashan, A. (2014). Comparison between PID and FOPID controllers based on particle swarm optimization. In *Proceedings of the 2nd-Engineering Conference of Control, Computers and Mechatronics Engineering*. Baghdad, Iraq (pp. 1–8).
- Monje, C. A., Chen, Y., Vinagre, B. M., Xue, D., & Feliu, V. (2010). *Vicente fractional-order systems and controls: Fundamentals and applications*. Springer Science & Business Media.
- Moornani, K. A., & Haeri, M. (2009). On robust stability of linear time invariant fractional-order systems with real parametric uncertainties. *ISA Transactions*, 48(4), 484–490. <https://doi.org/10.1016/j.isatra.2009.04.006>
- Moornani, K. A., & Haeri, M. (2010a). On robust stability of LTI fractional-order delay systems of retarded and neutral type. *Automatica*, 46(2), 362–368. <https://doi.org/10.1016/j.automatica.2009.11.006>
- Moornani, K. A., & Haeri, M. (2010b). Robust stability testing function and Kharitonov-like theorem for fractional order interval systems. *IET Control Theory & Applications*, 4(10), 2097–2108. <https://doi.org/10.1049/iet-cta.2009.0485>
- Podlubny, I. (1999). Fractional-order systems and PI^1D^μ controllers. *IEEE Transactions on Automatic Control*, 44(1), 208–214. <https://doi.org/10.1109/9.739144>
- Tan, N. (2002). Computation of the frequency response of multilinear affine systems. *IEEE Transactions on Automatic Control*, 47(10), 1691–1696. <https://doi.org/10.1109/TAC.2002.803537>
- Tepljakov, A., Alagoz, B. B., Yeroglu, C., Gonzalez, E. A., Hosseinnia, S. H., Petlenkov, E., Ates, A., & Cech, M. (2021). Towards industrialization of FOPID controllers: A survey on milestones of fractional-order control and pathways for future developments. *IEEE Access*, 9, 21016–21042. <https://doi.org/10.1109/Access.6287639>
- Tepljakov, A., Petlenkov, E., Belikov, J., & Petras, I. (2019). FOMCON toolbox for modeling, design and implementation of fractional-order control systems. *Applications in Control*, 6, 211–236.
- Valério, D., & Da Costa, J. S. (2006). Tuning of fractional PID controllers with Ziegler–Nichols-type rules. *Signal Processing*, 86(10), 2771–2784. <https://doi.org/10.1016/j.sigpro.2006.02.020>
- Wu, Z., Viola, J., Luo, Y., Chen, Y., & Li, D. (2024). Robust fractional-order [proportional integral derivative] controller design with specification constraints: More flat phase idea. *International Journal of Control*, 97(1), 111–129. <https://doi.org/10.1080/00207179.2021.1992498>
- Zheng, S. (2017). Robust stability of fractional order system with general interval uncertainties. *Systems & Control Letters*, 99, 1–8.
- Zheng, S., & Li, W. (2018). Stabilizing region of PD^μ controller for fractional order system with general interval uncertainties and an interval delay. *Journal of the Franklin Institute*, 355(3), 1107–1138. <https://doi.org/10.1016/j.jfranklin.2017.12.020>
- Zheng, S., Tang, X., & Song, B. (2014). A graphical tuning method of fractional order proportional integral derivative controllers for interval fractional order plant. *Journal of Process Control*, 24(11), 1691–1709. <https://doi.org/10.1016/j.jprocont.2014.08.011>

Appendix 14

XIV

M. Ghorbani, A. Farnam, A. Tepljakov, E. Petlenkov, G. Crevecoeur, and A. Eskandarian. Graphical tuning for robust stabilization: implementable stability regions for fractional-order proportional integral controllers in interval fractional-order systems. In *Proc. 2024 IEEE 63rd Conference on Decision and Control (CDC)*, pages 8902–8907, 2024.

Graphical Tuning for Robust Stabilization: Implementable Stability Regions for Fractional-Order Proportional Integral Controllers in Interval Fractional-Order Systems

Majid Ghorbani*, Arash Farnam, Aleksei Tepljakov, Eduard Petlenkov, Guillaume Crevecœur, and Azim Eskandarian

Abstract—As it is commonly acknowledged, implementing a fractional-order proportional integral controller involves replacing its fractional term with integer-order approximations. In this letter, we present a graphical tuning approach aimed at robustly stabilizing interval fractional-order systems by employing integer-order approximations of fractional-order proportional integral controllers. Specifically, we calculate the implementable robust stability region of an interval fractional-order proportional integral controller and delineate the robust stability region of its integer-order approximations. It is demonstrated that the robust stability region of a fractional-order proportional integral controller differs from that of its integer-order approximation. Consequently, values conducive to practical controller design reside within the implementable robust stability region. Initially, robust stability analysis of the fractional-order system is conducted using integer-order approximations of fractional-order proportional integral controllers. Subsequently, an algorithm is proposed for computing the implementable robust stability regions of fractional-order proportional integral controllers. Additionally, an auxiliary function is introduced to enhance the performance of the closed-loop control system. Finally, simulation results are offered to verify the theoretical expectations and analyses.

I. INTRODUCTION

Studies on how fractional calculus can be used in designing control systems are gaining popularity among control systems experts. Essentially, fractional-order systems, which are an extension of traditional integer-order systems, are described by differential equations that include fractional derivatives [1]. Fractional-order proportional integral controllers have drawn considerable attention from academic and industrial sectors. They have proven successful in practical applications such as electrical drive with induction motor [2], DC-DC converter [3] and coupled tank system [4]. The literature review highlights the utilization of various tuning strategies, including IMC-based methods [5] and optimization-based methods [6], [7], for the design of fractional-order proportional integral controllers. Moreover,

[8] introduced a strategy for computing the stability region for fractional-order proportional integral controllers using the D-decomposition method.

In real-world systems, the analytical model of the plant dynamics is subject to uncertainties stemming from nonlinearities, modeling errors, and other factors [9], [10]. Therefore, many tools have been proposed to investigate the robust stability of uncertain systems. For instance, the robust stability of uncertain fractional-order systems has been checked in [11], [12] using graphical tools. In [13], it was demonstrated that the value set of interval fractional-order polynomials forms a convex shape, followed by the proposal of a robust stability verification function. Moreover, in [14], [15], [16], the method proposed in [13] has been employed to design robust fractional-order controllers.

A. Motivation, challenge and contributions

Fractional-order controllers can only be realized through suitable approximation using finite differential or difference equations. Various established methods, such as those by Oustaloup [17] and Matsuda [18], offer approximations of fractional-order functions, either in the frequency domain for integer orders or in discrete-time domain. In scenarios where implementation of fractional-order controllers is necessary or simulations are conducted, fractional transfer functions are often substituted with integer transfer functions. These approximations emulate the behavior of fractional functions within specific frequency ranges or under particular conditions [19]. Therefore, in practical applications, ensuring the stability of the closed-loop control system is crucial, achieved by utilizing integer-order approximations of fractional-order controllers. In [19], a graphical method was proposed to ascertain the stability region of integer-order approximations of fractional-order proportional integral controllers for fractional-order systems without uncertainties. However, real-world systems often encounter uncertainties, as exemplified in [20], [21]. In this letter, we present a graphical approach to determine the robust stability region of integer-order approximations of fractional-order proportional integral controllers for interval fractional-order systems. We establish necessary and sufficient conditions for robust stability analysis of interval fractional-order systems in Theorems 1 and 2 using integer-order approximations of fractional-order proportional integral controllers. Additionally, we provide an algorithm to compute the robust stability domain of

This work was supported by the Estonian Research Council grant PRG658.

Majid Ghorbani, Aleksei Tepljakov and Eduard Petlenkov are with Department of Computer Systems, Tallinn University of Technology.

Arash Farnam and Guillaume Crevecœur are with Department of Electrical Energy, Metals, Mechanical Constructions and Systems, Ghent University, and FlandersMake@UGent - Corelab MIRO, Ghent, Belgium.

Azim Eskandarian is with the College of Engineering, Virginia Commonwealth University, Richmond, United States.

*Corresponding author: majid.ghorbani@taltech.ee

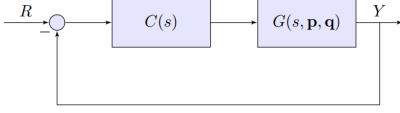


Fig. 1: Interval fractional order system.

fractional-order proportional integral controllers and propose an auxiliary function to enhance system performance.

B. Organization

The structure of the rest of this letter is as follows: In Section II, we outline the overall framework of our study and present the transfer functions for both the plant and the controller. Section III introduces two theorems aimed at verifying the robust stability of the closed-loop control system. Moreover, we propose an algorithm to determine the robust stability region of integer-order approximations of fractional-order proportional integral controllers. Furthermore, an illustrative example is provided in Section IV. Finally, we conclude our paper with Section V.

II. PRELIMINARIES AND PROBLEM FORMULATION

Notations [13]: $\text{floor}(x)$ is the largest integer less than or equal to $x \in \mathbb{R}$. $n(B)$ shows the number of distinct members of set B . $\text{frac}(x) \triangleq x - \text{floor}(x)$ for all $x \in \mathbb{R}$. $e(x_1(j\omega), x_2(j\omega)) \triangleq \eta x_1(j\omega) + (1 - \eta)x_2(j\omega)$, $\eta \in [0, 1]$.

A. Background materials

Consider the fractional-order system depicted in Fig. 1. In this diagram, $G(s, \mathbf{p}, \mathbf{q})$ represents the uncertain fractional-order plant, characterized by

$$G(s, \mathbf{p}, \mathbf{q}) = \frac{N(s, \mathbf{p})}{D(s, \mathbf{q})} = \frac{\sum_{r_1=0}^m p_{r_1} s^{\beta_{r_1}}}{\sum_{r_2=0}^m q_{r_2} s^{\alpha_{r_2}}}, \quad (1)$$

where $\beta_m > \beta_{m-1} > \dots > \beta_1 > \beta_0 = 0$ and $\alpha_n > \alpha_{n-1} > \dots > \alpha_1 > \alpha_0 = 0$ are arbitrary real numbers. Moreover, the vectors $\mathbf{p} = [p_0, p_1, \dots, p_m]^T$ and $\mathbf{q} = [q_0, q_1, \dots, q_n]^T$ belong to the following uncertainty sets:

$$\mathbf{p} \in \mathbf{P} = \{\mathbf{p} \in \mathbb{R}^{m+1} | p_{r_1} \in [p_{r_1}^-, p_{r_1}^+], b_m, b_0 \neq 0, i_1 \in \mathbb{Z}_{\geq 0}^{\leq m}\},$$

$$\mathbf{q} \in \mathbf{Q} = \{\mathbf{q} \in \mathbb{R}^{n+1} | q_{r_2} \in [q_{r_2}^-, q_{r_2}^+], a_n \neq 0, i_2 \in \mathbb{Z}_{\geq 1}^{\leq n}\}, \quad (2)$$

where, $[p_{r_1}^-, p_{r_1}^+]$ and $[q_{r_2}^-, q_{r_2}^+]$ denote specified intervals. Let us regard $C(s)$ as the fractional-order proportional integral controller (3).

$$C(s) = K_p + \frac{K_i}{s^\lambda}, \quad K_p, K_i \in \mathbb{R}, \lambda \in (0, 2). \quad (3)$$

Referring to equations (1) and (3), we can derive the characteristic function of the closed-loop control system depicted in Fig. 1 as follows:

$$\Delta(s, \mathbf{p}, \mathbf{q}) = \sum_{r_2=0}^m q_{r_2} s^{\alpha_{r_2} + \lambda} + K_p \sum_{r_1=0}^m p_{r_1} s^{\beta_{r_1} + \lambda} + K_i \sum_{r_1=0}^m p_{r_1} s^{\beta_{r_1}}. \quad (4)$$

Now, let us consider a nominal member of the interval polynomial $\Delta(s, \mathbf{p}, \mathbf{q})$ as

$$\hat{\Delta}(s) = \sum_{r_2=0}^n \hat{q}_{r_2} s^{\alpha_{r_2} + \lambda} + K_p \sum_{r_1=0}^m \hat{p}_{r_1} s^{\beta_{r_1} + \lambda} + K_i \sum_{r_1=0}^m \hat{p}_{r_1} s^{\beta_{r_1}}. \quad (5)$$

By employing the D-decomposition technique and setting $\hat{\Delta}(j\omega)$ to zero, we can compute the complex root boundaries (CRBs) as follows:

$$K_p = \frac{N_1(\omega)M_2(\omega) - N_2(\omega)M_1(\omega)}{N_3(\omega)N_2(\omega) - N_4(\omega)N_1(\omega)},$$

$$K_i = \frac{N_4(\omega)M_1(\omega) - N_3(\omega)M_2(\omega)}{N_3(\omega)N_2(\omega) - N_4(\omega)N_1(\omega)}, \quad (6)$$

where

$$\begin{cases} M_1(\omega) = \sum_{r_2=0}^n \hat{q}_{r_2} \omega^{\alpha_{r_2} + \lambda} \cos((\lambda + \alpha_{r_2})\frac{\pi}{2}), \\ M_2(\omega) = \sum_{r_2=0}^n \hat{q}_{r_2} \omega^{\alpha_{r_2} + \lambda} \sin((\lambda + \alpha_{r_2})\frac{\pi}{2}), \\ N_1(\omega) = \sum_{r_1=0}^m \hat{p}_{r_1} \omega^{\beta_{r_1}} \cos(\beta_{r_1}\frac{\pi}{2}), \\ N_2(\omega) = \sum_{r_1=0}^m \hat{p}_{r_1} \omega^{\beta_{r_1}} \sin(\beta_{r_1}\frac{\pi}{2}), \\ N_3(\omega) = \sum_{r_1=0}^m \hat{p}_{r_1} \omega^{\beta_{r_1} + \lambda} \cos((\beta_{r_1} + \lambda)\frac{\pi}{2}), \\ N_4(\omega) = \sum_{r_1=0}^m \hat{p}_{r_1} \omega^{\beta_{r_1} + \lambda} \sin((\beta_{r_1} + \lambda)\frac{\pi}{2}). \end{cases} \quad (7)$$

By substituting $\omega = 0$ and $\omega = \infty$ into equation (4), one can readily calculate the boundaries for Real Root Boundaries (RRBs) and Infinite Root Boundaries (IRBs) [8].

B. Stability region for the integer-order approximations

As discussed in [22], implementing fractional-order controllers relies on high-order integer-order approximations, which makes tuning all the parameters of the resulting high-order controller more challenging compared to tuning fractional-order controllers. Therefore, in this letter, the term $\frac{1}{s^\lambda}$ in the fractional-order proportional integral controller $C(s)$ from equation (3) is approximated by an integer-order function using any of the established approximation schemes [17], [18]. Based on the chosen order of approximation (p_o), it is possible to express:

$$\frac{1}{s^\lambda} \approx P_I(s) = \frac{\sum_{i=0}^{p_o} d_i s^i}{\sum_{i=0}^{p_o} c_i s^i}, c_{p_o} \& d_{p_o} \neq 0, 0 < \lambda < 1. \quad (8)$$

Using the approximation (8), (4) can be written as

$$\Delta_{approx}(s, \mathbf{p}, \mathbf{q}) = D_C(s)D(s, \mathbf{q}) + (K_p D_C(s) + K_i N_C(s))N(s, \mathbf{p}). \quad (9)$$

where

$$D_C(s) = \begin{cases} \sum_{i=0}^{p_o} c_i s^i, & \text{if } \lambda \in (0, 1), \\ \sum_{i=0}^{p_o} c_i s^{i+1}, & \text{if } \lambda \in (1, 2), \end{cases}$$

$$N_C(s) = \sum_{i=0}^{p_o} d_i s^i.$$

Consider a nominal member of $\Delta_{approx}(s, \mathbf{p}, \mathbf{q})$ in (9) as $\hat{\Delta}_{approx}(s)$. In this case, the CRBs can be obtained for

$\lambda \in (0, 1)$ as follows:

$$\begin{aligned} K_p &= \frac{K_1(\omega)H_2(\omega) - K_2(\omega)H_1(\omega)}{K_3(\omega)K_2(\omega) - K_4(\omega)K_1(\omega)}, \\ K_i &= \frac{K_4(\omega)H_1(\omega) - K_3(\omega)H_2(\omega)}{K_3(\omega)K_2(\omega) - K_4(\omega)K_1(\omega)}, \end{aligned} \quad (10)$$

where

$$\begin{cases} H_1(\omega) = \sum_{i=0}^{p_o} \sum_{r_2=0}^n c_i \hat{q}_{r_2} \omega^{\alpha_{r_2}+i} \cos((\alpha_{r_2}+i)\frac{\pi}{2}), \\ H_2(\omega) = \sum_{i=0}^{p_o} \sum_{r_2=0}^n c_i \hat{q}_{r_2} \omega^{\alpha_{r_2}+i} \sin((\alpha_{r_2}+i)\frac{\pi}{2}), \\ K_1(\omega) = \sum_{i=0}^{p_o} \sum_{r_1=0}^m d_i \hat{p}_{r_1} \omega^{\beta_{r_1}+i} \cos((\beta_{r_1}+i)\frac{\pi}{2}), \\ K_2(\omega) = \sum_{i=0}^{p_o} \sum_{r_1=0}^m d_i \hat{p}_{r_1} \omega^{\beta_{r_1}+i} \sin((\beta_{r_1}+i)\frac{\pi}{2}), \\ K_3(\omega) = \sum_{i=0}^{p_o} \sum_{r_1=0}^m c_i \hat{p}_{r_1} \omega^{\beta_{r_1}+i} \cos((\beta_{r_1}+i)\frac{\pi}{2}), \\ K_4(\omega) = \sum_{i=0}^{p_o} \sum_{r_1=0}^m c_i \hat{p}_{r_1} \omega^{\beta_{r_1}+i} \sin((\beta_{r_1}+i)\frac{\pi}{2}). \end{cases} \quad (11)$$

Upon inserting $\omega = 0$ and $\omega = \infty$ into $\Delta_{approx}(j\omega, \mathbf{p}, \mathbf{q})$ in (9), the boundaries for RRBs and IRBs can be easily determined, as detailed in [19].

C. Problem statement

Consider the following plant:

$$G(s) = \frac{1}{39.69s^{1.26} + 0.598}. \quad (12)$$

Consider a fractional-order PI controller with a fractional-order of $\lambda = 1.2$. The approximation of $\frac{1}{s^{1.2}}$ for the frequency range of $[0.01, 100]$ rad/sec can be calculated as follows [19]:

$$\frac{1}{s^{1.2}} \approx \frac{0.1s^4 + 6.248s^3 + 35.45s^2 + 19.7s + 1}{s^5 + 19.76s^4 + 35.45s^3 + 6.248s^2 + 0.1s}. \quad (13)$$

Fig. 2 depicts the stability regions of the fractional-order proportional integral controller (highlighted in yellow) alongside its integer-order approximation (stripe region). In this paper, the stripe region is denoted as the implementable stability region of the fractional-order controllers. As illustrated in the figure, the fractional-order controller maintains stability within the yellow region, whereas its integer-order counterpart does not. Hence, values conducive to the practical application of the designed controller are situated within the implementable stability region. Consequently, in this study, we identify these two aspects as the primary challenges:

- 1) Real-world systems often involve uncertainties, commonly addressed by using interval uncertainty structures like $G(s, \mathbf{p}, \mathbf{q})$ in Equation (1). The challenge is determining the robust stability region of integer-order approximations of fractional-order controllers C for the uncertain plant $G(s, \mathbf{p}, \mathbf{q})$.
- 2) Given the uncertain model $G(s, \mathbf{p}, \mathbf{q})$, defining the bounds of uncertainty for the sensitivity function is challenging. Thus, the main research challenge is to meet control objectives for disturbance rejection amidst these uncertainties to enhance system performance.

To tackle the aforementioned challenges, the following materials will be necessary for the rest of the paper.

Vertices of $D(j\omega, \mathbf{q})$:

Define $H_0 = \{i \in \mathbb{Z}_{\geq 0}^n : q_i^- < q_i^+\}$. Assume $H_0 \neq \emptyset$, then

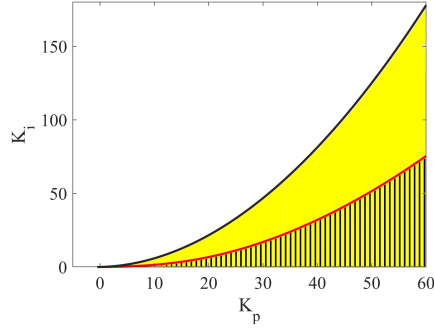


Fig. 2: Fractional-order PI controller stability regions (yellow region) compared to its integer-order approximation (stripe region).

- If $\omega = 0$, then $D(j\omega, \mathbf{a}) = [q_0^-, q_0^+]$.
- If $\omega > 0$, then define $F_0 = \{\text{frac}(0.5\alpha_i) : i \in H_0\}$ and $N = n(F_0)$. Consider f_1, \dots, f_{N-1}, f_N as all the distinct members of F_0 sorted as $0 \leq f_1 < \dots < f_{N-1} < f_N < 1$. Then, define the following sets:

$$\begin{aligned} H_r' &= \left\{ i \in H_0 : \text{floor}(0.5\alpha_i) \text{ is an odd number and} \right. \\ &\quad \left. \text{frac}(0.5\alpha_i) = f_r \right\}, \\ H_r &= \left\{ i \in H_0 : \text{floor}(0.5\alpha_i) \text{ is an even number and} \right. \\ &\quad \left. \text{frac}(0.5\alpha_i) = f_r \right\}, \quad r = 1, 2, \dots, N. \end{aligned} \quad (14)$$

The vectors q^1, q^2, \dots, q^{2N} are defined as follows:

$$\begin{aligned} q^k &= [q_0^k q_1^k \dots q_n^k]^T, q^{M+k} = q^+ + q^- - q^k, k = 1, \dots, N, \\ q^- &= [q_0^- q_1^- \dots q_n^-]^T, q^+ = [q_0^+ q_1^+ \dots q_n^+]^T, \end{aligned} \quad (15)$$

$$q_i^k = \begin{cases} q_i^+, & \text{for } i \in \left(\bigcup_{r=1}^{k-1} H_r \right) \cup \left(\bigcup_{r=k}^N H_r' \right), \\ q_i^-, & \text{for otherwise.} \end{cases} \quad (16)$$

$$q_i^{M+k} = q_i^+ + q_i^- - q_i^k. \quad (17)$$

Therefore, the consecutive vertices $V_{i_2}^D(j\omega)$ ($i_2 = 1, 2, \dots, 2N$) are computed using

$$\begin{aligned} V_k^D(j\omega) &= D(j\omega, q^k), \\ V_{M+k}^D(j\omega) &= D(j\omega, q^{M+k}), \quad k = 1, 2, \dots, N. \end{aligned} \quad (18)$$

Similarly, the consecutive vertices of $N(j\omega, \mathbf{p})$ can be derived and designated as $V_{i_1}^N(j\omega)$ ($i_1 = 1, 2, \dots, 2M$).

III. MAIN RESULT

A. Implementable Robust Stability Region of fractional-order proportional integral

To derive the implementable robust stability region of fractional-order proportional integral controllers, our initial

step involves extracting the robust stability conditions for $\Delta_{approx}(s, \mathbf{p}, \mathbf{q})$ in (9), as stated in the following theorem.

Theorem 1: The interval fractional-order system illustrated in Fig. 1, defined by $\Delta_{approx}(s, \mathbf{p}, \mathbf{q})$ as expressed in (9), is robustly stable if and only if the corresponding characteristic functions, $\Delta_D^{iN}(s, \mathbf{q})$ detailed in (19), and $\Delta_N^{iD}(s, \mathbf{p})$ elaborated in (20), exhibit robust stability as well.

$$\Delta_D^{iN}(s, \mathbf{q}) = D_C(s)D(s, \mathbf{q}) + (K_p D_C(s) + K_i N_C(s))V_{iN}^N(\omega), i_N = 1, \dots, 2M. \quad (19)$$

$$\Delta_N^{iD}(s, \mathbf{p}) = D_C(s)V_{iD}^D(\omega) + (K_p D_C(s) + K_i N_C(s))N(s, \mathbf{p}), i_D = 1, \dots, 2N. \quad (20)$$

Proof: To complete the proof, we must demonstrate that $\partial(\Delta_{approx}(j\omega, \mathbf{p}, \mathbf{q})) = \partial(\Delta_D^{iN}(j\omega, \mathbf{q})) \cup \partial(\Delta_N^{iD}(j\omega, \mathbf{p}))$ holds at a specific frequency $\omega = \omega_0$.

The ‘if’ portion: Given that $\Delta_D^{iN}(j\omega, \mathbf{q})$ and $\Delta_N^{iD}(j\omega, \mathbf{p})$ exhibit robust stability, it follows that $0 \notin \Delta_D^{iN}(j\omega, \mathbf{q})$ and $0 \notin \Delta_N^{iD}(j\omega, \mathbf{p})$. Additionally, we have:

$$0 \notin \Delta_D^{iN}(s, \mathbf{q}) \iff -(K_p D_C(s) + K_i N_C(s))V_{iN}^N(\omega) \notin D_C(s)D(s, \mathbf{q}), i_N = 1, \dots, 2M. \quad (21)$$

$$0 \notin \Delta_N^{iD}(s, \mathbf{p}) \iff -D_C(s)V_{iD}^D(\omega) \notin (K_p D_C(s) + K_i N_C(s))N(s, \mathbf{p}), i_D = 1, \dots, 2N. \quad (22)$$

As mentioned earlier (Section II), both $D(s, \mathbf{q})$ and $N(s, \mathbf{p})$ are convex polygons. Moreover, according to equations (21) and (22), the vertices of the convex polygon $D_C(s)D(s, \mathbf{p})$ are not contained within $-(K_p D_C(s) + K_i N_C(s))N(s, \mathbf{q})$. Similarly, the vertices of the convex polygon $(K_p D_C(s) + K_i N_C(s))N(s, \mathbf{p})$ do not fall within $-D_C(s)D(s, \mathbf{q})$. Consequently, these convex polygons do not overlap, implying that $0 \notin \Delta_{approx}(j\omega, \mathbf{p}, \mathbf{q})$.

The ‘if’ portion: Given the robust stability exhibited by $\Delta_{approx}(j\omega, \mathbf{p}, \mathbf{q})$, it directly follows from the exclusion principle that 0 is not a member of $\Delta_{approx}(j\omega, \mathbf{p}, \mathbf{q})$. Moreover, $\Delta_{approx}(j\omega, \mathbf{p}, \mathbf{q})$ comprises two convex polygons: $D_C(s)D(s, \mathbf{q})$ and $(K_p D_C(s) + K_i N_C(s))N(s, \mathbf{p})$. The absence of 0 in $\Delta_{approx}(j\omega, \mathbf{p}, \mathbf{q})$ requires that the convex polygons $-D_C(s)D(s, \mathbf{q})$ and $(K_p D_C(s) + K_i N_C(s))N(s, \mathbf{p})$ do not overlap within the complex plane. Consequently, it can be inferred that $0 \notin \Delta_D^{iN}(j\omega, \mathbf{p})$ and $0 \notin \Delta_N^{iD}(j\omega, \mathbf{q})$. ■

Algorithm 1 illustrates the process of identifying the implementable robust stability region of fractional-order proportional integral controllers for the interval system $\Delta_{approx}(s, \mathbf{p}, \mathbf{q})$ in (9).

Algorithm 1: Determining Implementable Robust Stability Regions for fractional-order proportional integral Controllers

Step 1. Obtain the vertices $V_i^D(\omega)$ ($i = 1, 2, \dots, 2N$) and $V_r^N(\omega)$ ($r = 1, 2, \dots, 2M$) using the method proposed in Section II.

Step 2. Determine RRB, IRB and CRB and the imple-

mentable robust stability regions for

$$\left(\sum_{r=0}^{p_o'} c_r s^r \right) e(V_i(\omega), V_{i+1}(\omega)) + \left(K_p \sum_{r=0}^{p_o'} c_r s^r + K_i \sum_{r=0}^{p_o} d_r s^r \right) V_{iN}^N(\omega), V_{2N+1}^D(\omega) = V_1^D(\omega). \quad (23)$$

Step 3. Calculate RRB, IRB and CRB and the implementable robust stability regions for

$$\left(\sum_{r=0}^{p_o'} c_r s^r \right) V_{iD}^D(\omega) + \left(K_p \sum_{r=0}^{p_o'} c_r s^r + K_i \sum_{r=0}^{p_o} d_r s^r \right) e(V_r^N(\omega), V_{r+1}^N(\omega)), V_{2M+1}^N(\omega) = V_1^N(\omega). \quad (24)$$

Step 4. The final stabilizing region is the intersection of all the computed stable regions obtained in Steps 2 and 3.

Proof of Algorithm 1: The stabilization of $\Delta_D^{iN}(s, \mathbf{q})$ as detailed in Equation (19), and $\Delta_N^{iD}(s, \mathbf{p})$, implies that 0 does not belong to $\Delta_D^{iN}(j\omega, \mathbf{q})$ and $\Delta_N^{iD}(j\omega, \mathbf{p})$. Additionally, according to Theorem 1, it has been demonstrated that $\partial(\Delta_{approx}(j\omega, \mathbf{p}, \mathbf{q})) = \partial(\Delta_D^{iN}(j\omega, \mathbf{q})) \cup \partial(\Delta_N^{iD}(j\omega, \mathbf{p}))$. This indicates that $0 \notin \Delta_{approx}(j\omega, \mathbf{p}, \mathbf{q})$ and there exists at least one stable member within $\Delta_{approx}(j\omega, \mathbf{p}, \mathbf{q})$. Thus, the zero exclusion principle concludes the proof. ■

B. Robust Stability Analysis

This subsection assesses the controller's ability to robustly stabilize the closed-loop system. For this evaluation, the following theorem is introduced.

Theorem 2: The system depicted in Fig. 1 exhibits robust stability if and only if a nominal member of $\Delta_{approx}(s, \mathbf{p}, \mathbf{q})$ remains stable, and the inequality $T(\omega) > 0$ holds true, where $T(\omega)$ is defined in (25).

$$\begin{aligned} T(\omega) &= \min\{T_1(\omega), T_2(\omega)\}, \\ T_1(\omega) &= \min\{T_{r_1, r_2}^D(\omega) | r_1 \in \{1, \dots, 2M\}, r_2 \in \{1, \dots, 2N\}\}, \\ T_2(\omega) &= \min\{T_{r_1, r_2}^N(\omega) | r_1 \in \{1, \dots, 2M\}, r_2 \in \{1, \dots, 2N\}\}, \\ T_{r_1, r_2}^D(\omega) &= |D_C(s)V_{r_2}^D(\omega) + (K_p D_C(s) + K_i N_C(s))V_{r_1}^N(\omega)| + \\ &\quad |D_C(s)V_{r_2+1}^D(\omega) + (K_p D_C(s) + K_i N_C(s))V_{r_1}^N(\omega)| - \\ &\quad |D_C(s)(V_{r_2+1}^D(\omega) - V_{r_2}^D(\omega))|, \\ T_{r_1, r_2}^N(\omega) &= |D_C(s)V_{r_2}^D(\omega) + (K_p D_C(s) + K_i N_C(s))V_{r_1}^N(\omega)| + \\ &\quad |D_C(s)V_{r_2}^D(\omega) + (K_p D_C(s) + K_i N_C(s))V_{r_1+1}^N(\omega)| - \\ &\quad |(K_p D_C(s) + K_i N_C(s))(V_{r_1+1}^N(\omega) - V_{r_1}^N(\omega))|. \end{aligned} \quad (25)$$

Proof: Our aim is to demonstrate that the value zero does not reside within $\Delta_{approx}(s, \mathbf{p}, \mathbf{q})$ for frequencies that are non-negative. As discussed in Section II, the value sets of $\Delta_D^{iN}(s, \mathbf{q})$ detailed and $\Delta_N^{iD}(s, \mathbf{p})$ exhibit a polygonal shape in the complex plane. Denoted by $T_1(\omega)$ is the triangle inequality involving any two consecutive vertices

of $\Delta_N^{h_D}(s, \mathbf{p})$, and similarly, $T_2(\omega)$ denotes the triangle inequality for any two consecutive vertices of $\Delta_N^{h_D}(s, \mathbf{p})$. Consequently, if $T_1(\omega) = 0$ at $\omega = \omega_0$, it can be deduced from the triangle inequality that $0 \in \Delta_N^{h_D}(j\omega_0, \mathbf{p})$. Therefore, if both inequalities $T_1(\omega) > 0$ and $T_2(\omega) > 0$ are satisfied, it implies that $0 \notin \Delta_N^{h_D}(s, \mathbf{p})$ and $0 \notin \Delta_D^{h_N}(s, \mathbf{q})$. Therefore, the robust stability of the system is simply derived using Theorem 1. ■

C. Enhanced Performance in Disturbance Rejection

To boost the attenuation of external disturbances, it is vital to verify that the sensitivity function $S(j\omega)$ (26) satisfies the prescribed constraint [23].

$$|S(j\omega, \mathbf{p}, \mathbf{q})| < |W_s(j\omega)| \rightarrow \left| \frac{1}{1 + \frac{(K_p D_C(s) + K_i N_C(s)) N(s, \mathbf{p})}{D_C(s) D(s, \mathbf{q})}} \right| < |W_s(j\omega)|. \quad (26)$$

Per Theorem 1 and (26), a robust controller should adhere to the subsequent inequalities:

$$\left| \frac{1}{1 + \frac{(K_p D_C(s) + K_i N_C(s)) V_{r1}^N(\omega)}{D_C(s) D(s, \mathbf{q})}} \right| < |W_s(s)|, \quad (27)$$

($r_1 = 1, \dots, 2M$).

$$\left| \frac{1}{1 + \frac{(K_p D_C(s) + K_i N_C(s)) N(s, \mathbf{p})}{D_C(s) V_{r2}^D(\omega)}} \right| < |W_s(s)|, \quad (28)$$

($r_2 = 1, 2, \dots, 2N$).

By employing equations (27) and (28), in conjunction with the maximum modulus theorem [24], the controller should guarantee the fulfillment of the following inequality.

$$T_S(\omega) = \max_{k=1,2} T_k^S(\omega) < 0, \quad (29)$$

$$\begin{cases} T_1^S(\omega) = \max_{h=1, \dots, 2M} T_h^D(\omega), \\ T_h^D(\omega) = \max_{e_k^D \in E_D} |e_k^D| - |W_s(j\omega)|, \\ E_D = \{e_1^D, e_2^D, \dots, e_{2N}^D\}, \\ e_k^D = \frac{1}{1 + \frac{(K_p D_C(s) + K_i N_C(s)) V_{k+1}^N(\omega)}{D_C(s) e(V_k^D(\omega), V_{k+1}^D(\omega))}}, \\ V_{2N+1}^D(\omega) = V_1^D(\omega), k = 1, \dots, 2N, s = j\omega. \end{cases} \quad (30)$$

$$\begin{cases} T_2^S(\omega) = \max_{h=1, \dots, 2N} T_h^N(\omega), \\ T_h^N(\omega) = \max_{e_k^N \in E_N} |e_k^N| - |W_s(j\omega)|, \\ E_N = \{e_1^N, e_2^N, \dots, e_{2M}^N\}, \\ e_k^N = \frac{1}{1 + \frac{(K_p D_C(s) + K_i N_C(s)) e(V_k^N(\omega), V_{k+1}^N(\omega))}{D_C(s) V_k^D(\omega)}}, \\ V_{2mN+1}^+(\omega) = V_1^+(\omega), k = 1, \dots, 2M, s = j\omega. \end{cases} \quad (31)$$

The bound on the sensitivity function (26) typically represents the potential benefits of feedback such as disturbance rejection and robust performance [23]. If the inequality (29) holds, then the condition $\|W_s^{-1}(j\omega)S(j\omega, \mathbf{p}, \mathbf{q})\|_\infty < 1$ is satisfied, which ensures robust performance. Therefore, the designer only needs to check the sign of the function $T_S(\omega)$ to assess robust performance.

IV. ILLUSTRATIVE EXAMPLES

Example 1. Consider the interval plant presented below:

$$P(s) = \frac{[1, 2]s + [1, 2]}{s^{1.5} + [1, 1.5]s^{0.5} + [0.5, 1.5]}. \quad (32)$$

The implementable robust stability region for fractional-order proportional integral controllers applied to the interval plant (32) has been established for $\lambda = 1.2$. The Oustaloup approximation (using the `oustafod` tool from the FOMCON toolbox [10]) is applied to replace ' $s^{0.2}$ ' over the frequency range of $[0.001, 100]$, as outlined below:

$$\frac{1}{s^{0.2}} \approx P_I(s) = \frac{s^3 + 22.02s^2 + 10.22s + 0.1}{2.512s^3 + 25.67s^2 + 5.531s + 0.02512}. \quad (33)$$

Fig. 3 illustrates the implementable robust stability region of the fractional-order proportional integral controller, highlighted in yellow. Both controllers $C_1(s)$ and $C_2(s)$ are situated within the stability region (yellow region in Fig. 3). Nevertheless, the plot of $H(\omega)$ for both controllers $C_1(s)$ and $C_2(s)$ is depicted in Fig. 4. According to Theorem 2, the robust stability of the system is ensured by employing either controller $C_1(s)$ or $C_2(s)$.

$$\begin{cases} C_1(s) = 3 + \frac{1.5}{s} P_I(s), \\ C_2(s) = 1 + \frac{0.01}{s} P_I(s). \end{cases} \quad (34)$$

The following analysis demonstrates which controller can meet the inequality $T_S(\omega) < 0$ for the specified weighting function $W_s(s) = \frac{(s+0.1)(s+10)(.001s+1)}{s^2+30.67s+247.3}$. Fig. 5 illustrates the curve of $T_S(\omega)$ corresponding to $C_1(s)$ and $C_2(s)$. As observed from this figure, only $C_1(s)$ satisfies $T_S(\omega) < 0$. Therefore, the designer should opt for controller $C_1(s)$. Fig. 5 presents the step responses of $C_1(s)$ (depicted in black) and $C_2(s)$ (depicted in red). It is evident from this figure that the step response associated with $C_1(s)$ exhibits better performance in terms of faster response.

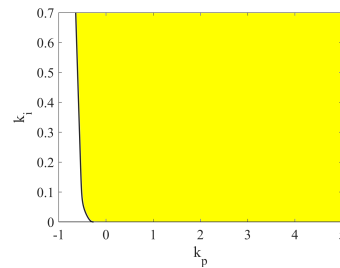


Fig. 3: Implementable robust stability region.

V. CONCLUSION

A methodology for computing the implementable robust stability regions for fractional-order proportional integral controllers within the framework of interval fractional-order plants was presented. The significance of determining the robust stability region of the controller in comparison to their integer-order approximations was demonstrated, highlighting

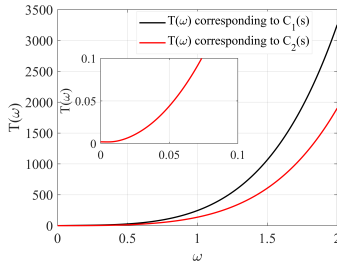


Fig. 4: Curve of $H(\omega)$ corresponding to $C_1(s)$ (black color) and $C_2(s)$ (red color).

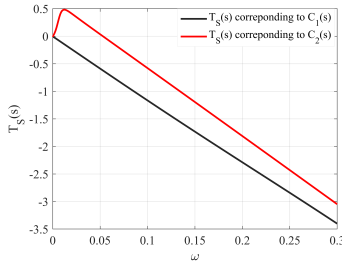


Fig. 5: Curve of $T_S(\omega)$ corresponding to $C_1(s)$ (black color) and $C_2(s)$ (red color).

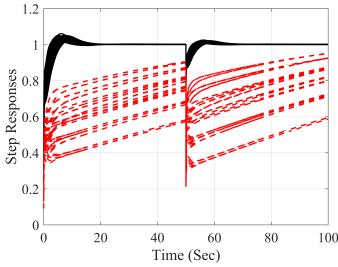


Fig. 6: Step responses corresponding to $C_1(s)$ (black color) and $C_2(s)$ (red color).

the distinctiveness of these regions. The methodology began with a comprehensive robust stability analysis of fractional-order systems utilizing integer-order approximations of the fractional-order controller. Furthermore, an auxiliary function was introduced to enhance the performance of the control system.

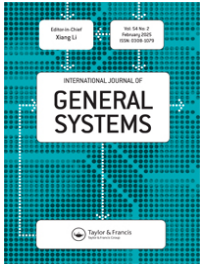
REFERENCES

- [1] I. Podlubny. "Fractional differential equations: an introduction to fractional derivatives, fractional differential equations, to methods of their solution and some of their applications," 1998.
- [2] D. M. Kumar, H. K. Mudaliar, M. Cirrincione, U. Mehta, and M. Pucci, "Design of a fractional order PI (FOPI) for the speed control of a high-performance electrical drive with an induction motor," in 2018 21st International Conference on Electrical Machines and Systems (ICEMS), IEEE, 2018, pp. 1198-1202.
- [3] C. Komathi and M.G. Umamaheswari, "Design of gray wolf optimizer algorithm-based fractional order PI controller for power factor correction in SMPS applications," IEEE Transactions on Power Electronics, vol. 35, no. 2, pp. 2100-2118, 2019.
- [4] P. Roy and B.K. Roy, "Fractional order PI control applied to level control in coupled two-tank MIMO system with experimental validation," Control Engineering Practice, vol. 48, pp. 119-135, 2016.
- [5] M. Tavakoli-Kakhki and M. Haeri, "Fractional order model reduction approach based on retention of dominant dynamics: Application in IMC-based tuning of FOPI and FOPID controllers," ISA Transactions, vol. 50, no. 3, pp. 432-442, 2011.
- [6] Y. Arya, "A new optimized fuzzy FOPI-FOPD controller for automatic generation control of electric power systems," Journal of the Franklin Institute, vol. 356, no. 11, pp. 5611-5629, 2019.
- [7] Z. Miao, T. Han, J. Dang, and M. Ju, "FOPI/PI controller parameters optimization using PSO with different performance criteria," in 2017 IEEE 2nd Information Technology, Networking, Electronic and Automation Control Conference (ITNEC), IEEE, 2017, pp. 250-255.
- [8] S.E. Hamamci, "Stabilization using fractional-order PI and PID controllers," Nonlinear Dynamics, vol. 51, pp. 329-343, 2008.
- [9] S. Zheng, X. Tang, and B. Song, "A graphical tuning method of fractional order proportional integral derivative controllers for interval fractional order plant," Journal of Process Control, vol. 24, no. 11, pp. 1691-1709, 2014.
- [10] M. Ghorbani, A. Tepljakov, and E. Petlenkov, "Fractional-Order Interval Polynomials, Stability and Robust Stability Analysis and FOM-CON Implementation," in 2023 International Conference on Fractional Differentiation and Its Applications (ICFDA), IEEE, 2023, pp. 1-6.
- [11] K.A. Moormani and M. Haeri, "On robust stability of LTI fractional-order delay systems of retarded and neutral type," Automatica, vol. 46, no. 2, pp. 362-368, 2010.
- [12] K.A. Moormani and M. Haeri, "On robust stability of linear time invariant fractional-order systems with real parametric uncertainties," ISA Transactions, vol. 48, no. 4, pp. 484-490, 2009.
- [13] K. Akbari Moormani and M. Haeri, "Robust stability testing function and Kharitonov-like theorem for fractional order interval systems," IET Control Theory & Applications, vol. 4, no. 10, pp. 2097-2108, 2010.
- [14] M. Ghorbani, M. Tavakoli-Kakhki, "Robust stability analysis of a general class of interval delayed fractional order plants by a general form of fractional order controllers," Mathematical Methods in the Applied Sciences, vol. 44, no. 13, pp. 10172-10189, 2021.
- [15] S. Zheng, X. Tang, and B. Song, "Graphical tuning method of FOPID controllers for fractional order uncertain system achieving robust stability," International Journal of Robust and Nonlinear Control, vol. 26, no. 5, pp. 1112-1142, 2016.
- [16] M. Ebrahimi and M. Asgari, "Robust fractional-order fixed-structure controller design for uncertain non-commensurate fractional plants using fractional Kharitonov theorem," Proceedings of the Institution of Mechanical Engineers, Part I: Journal of Systems and Control Engineering, vol. 235, no. 8, pp. 1375-1387, 2021.
- [17] A. Oustaloup, F. Levron, B. Mathieu, and F. M. Nanot, "Frequency-band complex noninteger differentiator: characterization and synthesis," IEEE Transactions on Circuits and Systems I: Fundamental Theory and Applications, vol. 47, no. 1, pp. 25-39, 2000.
- [18] M. Khoichi and F. Hironori, " H_∞ Optimized wave-absorbing control: Analytical and experimental results," Journal of Guidance, Control, and Dynamics, vol. 16, no. 6, pp. 1146-1153, 1993.
- [19] M.A. Rahimian and M.S. Tavazoei, "Stabilizing fractional-order PI and PD controllers: an integer-order implemented system approach," Proceedings of the Institution of Mechanical Engineers, Part I: Journal of Systems and Control Engineering, vol. 224, no. 8, pp. 893-903, 2010.
- [20] U. Demiroglu and B. Şenol, "Frequency frame approach on tuning FOPI controller for TOPTD thermal processes," ISA Transactions, vol. 108, pp. 96-105, 2021.
- [21] P.P. Arya and S. Chakrabarty, "A robust internal model-based fractional order controller for fractional order plus time delay processes," IEEE Control Systems Letters, vol. 4, no. 4, pp. 862-867, 2020.
- [22] Tepljakov, A., et al., "Towards industrialization of FOPID controllers: A survey on milestones of fractional-order control and pathways for future developments," IEEE Access, vol. 9, pp. 21016-21042, 2021.
- [23] W.S. Levine, "The Control Handbook (three volume set)," CRC Press, 2018.
- [24] J.W. Brown, R.V. Churchill, "Complex Variables and Applications," McGraw-Hill, 2009.

Appendix 15

XV

M. Ghorbani, B. B. Alagoz, A. Tepljakov, and E. Petlenkov. A graphical method to determine robust stabilizing region of FOPID controllers for stable/unstable fractional-order plants with interval uncertainties of a fractional order and model coefficients. *International Journal of General Systems*, 54(2):198–217, 2025.



A graphical method to determine robust stabilizing region of FOPID controllers for stable/unstable fractional-order plants with interval uncertainties of a fractional order and model coefficients

Majid Ghorbani, Baris Baykant Alagoz, Aleksei Tepljakov & Eduard Petlenkov

To cite this article: Majid Ghorbani, Baris Baykant Alagoz, Aleksei Tepljakov & Eduard Petlenkov (2025) A graphical method to determine robust stabilizing region of FOPID controllers for stable/unstable fractional-order plants with interval uncertainties of a fractional order and model coefficients, International Journal of General Systems, 54:2, 198-217, DOI: [10.1080/03081079.2024.2375442](https://doi.org/10.1080/03081079.2024.2375442)

To link to this article: <https://doi.org/10.1080/03081079.2024.2375442>



Published online: 09 Jul 2024.



Submit your article to this journal [↗](#)



Article views: 244



View related articles [↗](#)



View Crossmark data [↗](#)



A graphical method to determine robust stabilizing region of FOPID controllers for stable/unstable fractional-order plants with interval uncertainties of a fractional order and model coefficients

Majid Ghorbani^a, Baris Baykant Alagoz^b, Aleksei Tepljakov^a and Eduard Petlenkov^a

^aDepartment of Computer Systems, Tallinn University of Technology, Tallinn, Estonia; ^bDepartment of Computer Engineering, Inonu University, Malatya, Turkey

ABSTRACT

This paper focuses on robustly stabilizing stable and unstable fractional-order plants with one uncertain fractional-order term and interval uncertainties using fractional order $PI^\mu D^\lambda$ controllers. Two necessary and sufficient conditions are provided to check the robust stability of the closed-loop control system. Moreover, the D-decomposition technique is utilized to determine the robust stability region of the system. Subsequently, evolutionary algorithms, such as the Genetic Algorithm (GA), Particle Swarm Optimization (PSO), and Differential Evolution (DE), can be utilized to discover a fractional-order controller within the region of robust stability. This work introduces three primary contributions, outlined as follows: (1) Utilizing a graphical approach, a set of stabilizing controller is obtained. (2) Rather than employing just a single stabilizing fractional-order controller, a collection of controllers is provided for the control system. (3) Employing evolutionary algorithms to find an optimal fractional-order controller. Finally, four numerical examples are presented to validate the results.

ARTICLE HISTORY

Received 30 November 2022
Accepted 27 June 2024

KEYWORDS

Robust stability analysis;
fractional-order plant;
fractional-order PID
controller; parametric
uncertainty; value set

1. Introduction

Fractional calculus has gained widespread use in all engineering fields, particularly in control systems engineering. The reason for this is that fractional-order operators can be used to more accurately describe the behavior of real-world systems (Alagoz et al. 2017; Efe 2011; Gabano, Poinot, and Kanoun 2015) and fractional-order controllers have shown to outperform their integer-order counterparts in a fair comparison where they are designed using the same methods (Prakosa, Alias, and Astuti 2023; Tepljakov et al. 2018, 2021; Tepljakov, Petlenkov, and Belikov 2013).

Fractional-order controllers offer superior performance in control loops compared to integer-order controllers due to their additional design parameters, which enhance robustness against plant parameter variations (Kumar and Rana 2017; Monje et al. 2008;

Moornani and Haeri 2010a; Wang, San-Millan, and Aphale 2024). Due to these prominent features of fractional-order controllers, the tuning thereof has received significant attention. For some examples of proposed tuning and design methods see, e.g. Moornani and Haeri (2013), Matušů and Pekař (2017), Wu et al. (2021), Badri and Sojoodi (2022), Kang et al. (2022), Ghorbani, Tepljakov, and Petlenkov (2020a) and Yumuk, Güzelkaya, and Eksin (2023).

Looking from the practical perspective, it is inevitable that real-world systems contain uncertainties. One appropriate way to include uncertainties in a system model is to utilize the interval uncertainty structure. It is assumed that these uncertain systems have entirely unknown parameters that lie between two well-known bounds (Ghorbani et al. 2021; Moornani and Haeri 2009; Senol et al. 2014; Tan, Özgüven, and Özyetkin 2009). Therefore, when faced with the inevitable disparity between the identified model and the actual process, robust stability analysis and performance enhancement are vital for real-world systems (Moornani and Haeri 2010b; Yeroglu and Senol 2013).

Taking the foregoing into consideration, researchers have developed a number of graphical tools for analyzing the robust stability of fractional-order systems or for robustly stabilizing such systems. One of these tools is the zero exclusion principle which is a graphical method to investigate the robust stability of fractional-order systems (Moornani and Haeri 2010c). Based on this principle, the value set of the characteristic equations of the uncertain fractional-order systems must be plotted at each frequency and then the zero exclusion condition is checked (Ghorbani, Tepljakov, and Petlenkov 2023). The robust stability is guaranteed, if the value set excludes the origin and the system has at least one stable member (Fu, Dasgupta, and Blondel 1995; Zheng 2017).

The D-decomposition method is one of the simplest ways to design fractional-order controllers. Based on this method, the boundaries of the stability region can be determined by real root boundary (RRB), infinite root boundary (IRB) and complex root boundary (CRB) in the space of controller parameters (Hamamci 2007, 2008; Luo and Chen 2012). Moreover, in Liang, Chen, and Zhao (2013), Zheng, Tang, and Song (2014) and Ghorbani, Tepljakov, and Petlenkov (2020b), the D-decomposition method has been employed to robustly compute the robust stability region of fractional-order controllers for systems having uncertainties. In Liang, Chen, and Zhao (2013), a theorem was proven to analyze the robust stability of fractional-order systems having uncertain orders. In illustrative example 1, we observe that Theorem 3.2 in Liang, Chen, and Zhao (2013) may not cover whole cases associated with robust stability of interval systems. The stability of some specified vertices cannot guarantee the robust stability of fractional-order systems having uncertain orders. Indeed, in Moornani and Haeri (2010b), it was proven that the value set of a fractional-order polynomials whose coefficients lie in specified intervals has a convex shape in the complex plane and it does not mean that the value set of the fractional-order polynomials whose coefficients and orders have interval uncertainties also has a convex shape (Ghorbani and Tavakoli-Kakhki 2021; Zheng and Li 2018). In fact, due to the uncertain orders, the value set of such fractional-order polynomials is nonconvex in the complex plane. There are primarily three benefits accounting for the presence of uncertainties in fractional orders and coefficients in control engineering practice:

- (1) Real world systems require robust stable control systems in order to perform long-term reliable operations. To design robust fractional order control systems,

consideration of parametric uncertainties in fractional order system models is inevitable. First of all, an inherent source for uncertainty can arise from the selected methodologies (i.e. the determination of model presumptions (Chen, Basu, and McCabe 2016; Shah and Sekhar 2019), the selection of a model identification scheme (Alagoz et al. 2019; Nasser-Eddine 2019)], and the selection of a fractional order approximation method (Deniz et al. 2020). These options can produce differences in the identified model parameters and become a source of parametric uncertainty in model identification due to methodological discrepancies. Such parametric uncertainty in a fractional model encompasses both fractional orders and coefficients. The other source of parametric uncertainty is closely related to measurement and data collection techniques. For instance, the collected data utilized for system identification might be affected by noise or disturbance, imprecise measurements, or data dropout (Khemane et al. 2011; Liao et al. 2010; Malti et al. 2010). The length of data window considered in modeling can affect the identified fractional order model parameters (Alagoz et al. 2019). Sufficiency of collected data to represent significant system dynamics is a practical concern and it can be a source of uncertain model parameters. Temporal changes occur in system operating conditions depending on many natural factors, such as material aging, change of environmental circumstances etc. All these limitations and factors increase the need for uncertainty consideration in fractional order models. Therefore, during the parameter identification and modeling process, consideration of both the order and coefficient uncertainty is a necessity for design of robust control systems.

- (2) The magnitudes of fractional orders can be influenced by fluctuations in operational circumstances, external perturbations, and internal nonlinearity. For instance, the fractional model representing viscoelastic materials may be susceptible to variations in frequency, tension amplitude, and other factors (Tabatabaei, Talebi, and Tavakoli 2017). In real-world electrical systems that encompass a diverse range of fractional-order components, the orders themselves may have uncertainties (Schäfer and Krüger 2008; Zhang and Lu 2023).
- (3) Determination of robust stability regions can be particularly useful to limit the parameter search space of optimization algorithms while performing metaheuristic tuning of FOPID controllers. By limiting search ranges of controller coefficients, metaheuristic optimization algorithms can seek optimal FOPID coefficients within the subspace that is determined by graphical robust stabilization tools. This can confine the whole search space into a subspace of robust stable FOPID controllers. Thus, algorithms avoid wasting their search efforts and computation time inside the search space sections that do not promise the robust stability of the resulting optimal control systems. It allows more efficient use of the computation time and computational resources while seeking optimal coefficients to achieve a optimal robust stable FOPID controller, and thus contribute to performance improvement of metaheuristic based optimal tuning of robust stable FOPID controllers.

This paper presents the necessary and sufficient conditions for robust stability analysis of stable/unstable fractional-order plants with one uncertain fractional-order term and interval uncertainties using fractional-order $PI^\lambda D^\mu$ controllers. Consequently, the presented Theorem 3.2, leads to obtaining the boundary of the value set of the characteristic

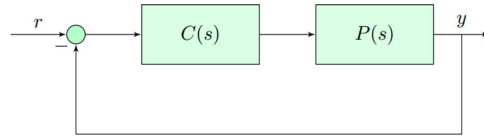


Figure 1. A classic negative unity feedback system where the plant $P(s)$ is assumed to be represented interval fractional-order system.

function. Then, Theorems 3.3 and 3.4 present the necessary and sufficient conditions for robust stability analysis of the system. Moreover, by benefiting from the D-decomposition method and the zero exclusion principle, the robust stability region of fractional-order $PI^\lambda D^\mu$ controllers is calculated.

This paper is organized as follows: Some background materials and definitions are given in Section 2. Foundations of robust-stability analysis and determination of the robust stability region of fractional-order $PI^\lambda D^\mu$ controllers are presented in Section 3. Section 4 provides the numerical evaluation of the results. Finally, concluding remarks are given in Section 6.

2. Preliminaries

Consider the interval fractional-order systems as shown in Figure 1. The transfer function of the stable fractional-order plant is represented in the following form

$$P(s) = \frac{K}{Ts^\alpha + 1}, \quad (1)$$

where the real positive parameters K , α and T are interval uncertain parameters defined as follows:

$$K \in [K^-, K^+], \quad T \in [T^-, T^+], \quad \alpha \in [\alpha^-, \alpha^+], \quad 0 \leq \alpha^+ - \alpha^- < 2. \quad (2)$$

Moreover, the transfer function of the unstable fractional-order plant is represented as follows:

$$P(s) = \frac{K}{Ts^\alpha - 1}, \quad (3)$$

where the interval uncertainties K , α and T have been defined in (2). Then, let $C(s)$ be a fractional-order $PI^\lambda D^\mu$ controller with a transfer function defined in (4).

$$C(s) = K_p + \frac{K_i}{s^\lambda} + K_d s^\mu, \quad K_i \neq 0, \quad \lambda \in (0, 2), \quad \mu \in (0, \alpha^-), \quad (4)$$

where K_p , K_i and K_d are the proportional coefficient, the integral coefficient and the derivative coefficient, respectively, and μ and λ are fractional orders of derivative and integral operators.

The characteristic function of the closed-loop control system depicted in Figure 1 for the stable plant in (1) can be written as

$$H(s) = s^\lambda (Ts^\alpha + 1) + K(K_p s^\lambda + K_i + K_d s^{\mu+\lambda}). \quad (5)$$

In a similar way, the characteristic function of the closed-loop control system for the unstable plant in (3) can be obtained as

$$H(s) = s^\lambda (Ts^\alpha - 1) + K(K_p s^\lambda + K_i + K_d s^{\mu+\lambda}). \quad (6)$$

For the sake of simplicity, the characteristic function of the system for both stable and unstable plants is considered as follows.

$$H(s) = s^\lambda (Ts^\alpha \pm 1) + K(K_p s^\lambda + K_i + K_d s^{\mu+\lambda}). \quad (7)$$

In (7), $Ts^\alpha \pm 1$ represent the denominators of both stable/unstable plants respectively defined in (1) and (3) i.e. $Ts^\alpha + 1$ and $Ts^\alpha - 1$.

Now, let us rewrite $H(s)$ in (7) as (8).

$$\begin{aligned} H(s) &= H_1(s) + H_2(s), \\ H_1(s) &= s^\lambda (Ts^\alpha \pm 1), \\ H_2(s) &= KN(s), \\ N(s) &= (K_p s^\lambda + K_i + K_d s^{\mu+\lambda}). \end{aligned} \quad (8)$$

Remark 2.1: In practice, the identification is usually done through step test application. Assume that the plant is $P(s) = \frac{K}{Ts^\alpha \pm 1}$. By considering the iteration number of identification as n , we can identify the different models $P_i(s) = \frac{K_i}{T_i s^{\alpha_i} \pm 1}$ for $i = 1, \dots, n$ by applying different step inputs. Hence, we should consider the plant as $P(s) = \frac{[\min\{K_i\}, \max\{K_i\}]}{[\min\{T_i\}, \max\{T_i\}] s^{[\min\{\alpha_i\}, \max\{\alpha_i\}] \pm 1}}$.

Lemma 2.1 (Fu, Dasgupta, and Blondel 1995): For two bounded and closed value sets Q_1 and Q_2 , $\partial(Q_1 + Q_2) \subseteq \partial(Q_1) + \partial(Q_2)$ where ∂ denotes the boundary.

Lemma 2.2 (Busłowicz 2008): The fractional-order polynomial $\delta(s)$ (of commensurate or non-commensurate degree) is stable if and only if

$$\Delta \arg \psi(j\omega) = \frac{\delta(j\omega)}{\omega_r(j\omega)} = 0, \quad -\infty < \omega < \infty \quad (9)$$

where $\omega_r(s) = a_{0n}(s + c)^{a_n}$, $c > 0$. Also, a_n is the highest order of $\delta(j\omega)$ and a_{0n} is the coefficient of the highest term s^{a_n} and c is an arbitrary positive number.

Lemma 2.3 (Moornani and Haeri 2010b): Consider the set $M = M_0 + \sum_{r=1}^m q_r e^{j\pi\gamma_r}$ where M_0 can be a complex/real number, $q_r \in [q_r^-, q_r^+]$, $0 \leq \gamma_0 < \gamma_1 < \gamma_2 < \dots < \gamma_m <$

1. Then, the value set of M is a convex parpolygon in the complex plane with the following $2m$ consecutive vertices:

$$\begin{aligned} v_k &= \sum_{r=1}^{k-1} q_r^+ e^{j\pi \gamma_r} + \sum_{r=k}^m q_r^- e^{j\pi \gamma_r} + M_0, \\ v_{k+m} &= \sum_{r=1}^{k-1} q_r^- e^{j\pi \gamma_r} + \sum_{r=k}^m q_r^+ e^{j\pi \gamma_r} + M_0, \quad k = 1, \dots, m. \end{aligned} \quad (10)$$

3. Main results

3.1. Computing method of value set

In order to compute the robust stability region of fractional-order $PI^\lambda D^\mu$ controllers for the closed-loop control system with the characteristic function $H(s)$ in (7), at first, $\partial(H(j\omega))$ (the boundary of $H(j\omega)$) must be determined at each frequency for $s = j\omega$. To achieve this, the following definition is provided.

Definition 3.1: For T, α and K define:

$$\begin{aligned} \mathbf{V}^T &= \{T^-, T^+\}, \mathbf{V}^\alpha = \{\alpha^-, \alpha^+\}, \mathbf{V}^K = \{K^-, K^+\}, \\ \mathbf{I}^T &= e(T^-, T^+), \mathbf{I}^\alpha = e(\alpha^-, \alpha^+), \mathbf{I}^K = e(K^-, K^+). \end{aligned} \quad (11)$$

where $e(x_1, x_2) = \eta x_1 + (1 - \eta)x_2$, $\eta \in [0, 1]$.

For a given frequency ω , it is apparent that the value set of $\partial(T(j\omega)^\alpha) \subseteq \mathbf{I}^T(j\omega)^{\mathbf{V}^\alpha} \cup \mathbf{V}^T(j\omega)^{\mathbf{I}^\alpha}$ as plotted in Figure 2. As seen from this figure, $\partial(T(j\omega)^\alpha)$ have two arc segments $\mathbf{V}^T(j\omega)^{\mathbf{I}^\alpha}$ (dotted line) and line segments $\mathbf{I}^T(j\omega)^{\mathbf{V}^\alpha}$ (solid line) (Zheng 2017). Therefore, based on Lemma 2.1, it is concluded that $\partial(H_1(j\omega)) \subseteq H_{E_1}(j\omega)$ in (12).

$$H_{E_1}(j\omega) = (j\omega)^\lambda (\mathbf{I}^T(j\omega)^{\mathbf{V}^\alpha} \pm 1) \cup (j\omega)^\lambda (\mathbf{V}^T(j\omega)^{\mathbf{I}^\alpha} \pm 1). \quad (12)$$

Also, it is also apparent that for a given frequency, $\partial(H_2(j\omega)) \subseteq \mathbf{I}^K N(j\omega)$. Now, in the following theorem, $\partial(H(j\omega))$ is determined for a given frequency.

Theorem 3.2: For a given frequency $\omega = \omega^*$, $\partial(H(j\omega)) \subseteq H_E(j\omega)$ where

$$\begin{aligned} H_E(j\omega) &= H_E^1(j\omega) \cup H_E^2(j\omega), \\ H_E^1(j\omega) &= (j\omega)^\lambda (\mathbf{I}^T(j\omega)^{\mathbf{V}^\alpha} \pm 1) + \mathbf{V}^K N(j\omega), \\ H_E^2(j\omega) &= (j\omega)^\lambda (\mathbf{V}^T(j\omega)^{\mathbf{I}^\alpha} \pm 1) + \mathbf{I}^K N(j\omega). \end{aligned} \quad (13)$$

Proof: According to the property mentioned in Lemma 2.1, one has

$$\partial(H(j\omega)) \subseteq ((j\omega)^\lambda (\mathbf{I}^T(j\omega)^{\mathbf{I}^\alpha} \pm 1) + \mathbf{I}^K N(j\omega)). \quad (14)$$

Based on the equation (12), the result concluded in (14) can be rewritten as

$$\partial(H(j\omega)) \subseteq ((j\omega)^\lambda (\mathbf{I}^T(j\omega)^{\mathbf{I}^\alpha} \pm 1) + \mathbf{I}^K N(j\omega))$$

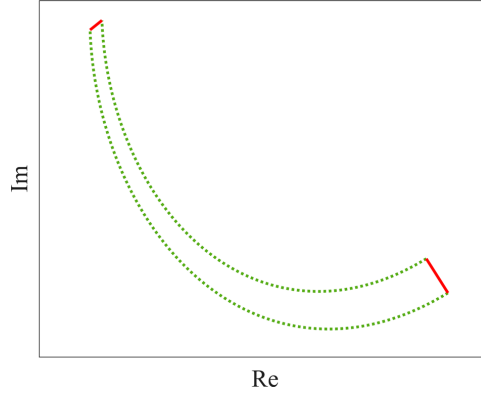


Figure 2. Depiction of two arc segments $\mathbf{V}^T(j\omega)^{\mathbf{I}^\alpha}$ (dotted line) and line segments $\mathbf{I}^T(j\omega)^{\mathbf{V}^\alpha}$ (solid line).

$$\begin{aligned} &\subseteq (((j\omega)^\lambda)(\mathbf{I}^T(j\omega)^{\mathbf{V}^\alpha} \pm 1) + \mathbf{I}^K N(j\omega)) \\ &\cup (((j\omega)^\lambda)(\mathbf{V}^T(j\omega)^{\mathbf{I}^\alpha} \pm 1) + \mathbf{I}^K N(j\omega)). \end{aligned} \quad (15)$$

Now, let us discuss on the value set of $(j\omega)^\lambda(\mathbf{I}^T(j\omega)^{\mathbf{V}^\alpha} \pm 1) + \mathbf{I}^K N(j\omega)$ constructed by line segment plus line segment. The shape of the sum of two independent lines would like to be a convex polygon with 4 vertices in the complex plane based on Lemma 2.3. Therefore, one can write

$$\begin{aligned} &(j\omega)^\lambda(\mathbf{I}^T(j\omega)^{\mathbf{V}^\alpha} \pm 1) + \mathbf{I}^K N(j\omega) \\ &\subseteq (j\omega)^\lambda(\mathbf{I}^T(j\omega)^{\mathbf{V}^\alpha} \pm 1) + \mathbf{V}^K N(j\omega) \\ &\cup (j\omega)^\lambda(\mathbf{V}^T(j\omega)^{\mathbf{I}^\alpha} \pm 1) + \mathbf{I}^K N(j\omega). \end{aligned} \quad (16)$$

From (16), the relation (15) can be rewritten as (17).

$$\begin{aligned} \partial(H(j\omega)) &\subseteq ((j\omega)^\lambda)(\mathbf{I}^T(j\omega)^{\mathbf{I}^\alpha} \pm 1) + \mathbf{I}^K N(j\omega) \\ &\subseteq (((j\omega)^\lambda)(\mathbf{I}^T(j\omega)^{\mathbf{V}^\alpha} \pm 1) + \mathbf{I}^K N(j\omega)) \\ &\cup (((j\omega)^\lambda)(\mathbf{V}^T(j\omega)^{\mathbf{I}^\alpha} \pm 1) + \mathbf{I}^K N(j\omega)) \\ &\subseteq ((j\omega)^\lambda)(\mathbf{I}^T(j\omega)^{\mathbf{V}^\alpha} \pm 1) + \mathbf{V}^K N(j\omega) \\ &\cup ((j\omega)^\lambda)(\mathbf{V}^T(j\omega)^{\mathbf{V}^\alpha} \pm 1) + \mathbf{I}^K N(j\omega) \\ &\cup (((j\omega)^\lambda)(\mathbf{V}^T(j\omega)^{\mathbf{I}^\alpha} \pm 1) + \mathbf{I}^K N(j\omega)) \\ &\subseteq H_E^1(j\omega) \cup H_E^2(j\omega). \end{aligned} \quad (17)$$

■

Now, by the results obtained in Theorem 3.2, the necessary and sufficient conditions are presented in the next theorem for robust stability analysis of the closed-loop control system.

Theorem 3.3: *The closed-loop control system can be robustly stabilized by the fractional-order $PI^\lambda D^\mu$ controllers if and only if:*

- the fractional-order $PI^\lambda D^\mu$ can stabilize the nominal closed-loop control system with the nominal characteristic function $H_0(s)$ in (18).

$$H_0(s) = s^\lambda \left(\left(\frac{T^+ + T^-}{2} \right) s^{\frac{\alpha^+ + \alpha^-}{2}} \pm 1 \right) + \frac{K^+ + K^-}{2} N(s), \quad (18)$$

- $0 \notin H_E(j\omega)$ for $\omega \in [0, \infty)$. This means that the value set of $H_E(j\omega)$ does not contain the origin for $\omega \in [0, \infty)$.

Proof: The proof is obtained from the Zero Exclusion principle. According to this principle, the closed-loop control system with the characteristic function $H(s)$ is robust stable if and only if $H(s)$ has at least one stable member and $0 \notin H(j\omega)$ for $\omega \geq 0$ (Moornani and Haeri 2010c). Also, in Theorem 3.2, it has been proven that $\partial(H(j\omega)) \subseteq H_E(j\omega)$ at a given frequency. Therefore, one can simply infer that $0 \notin H(j\omega)$ if and only if $0 \notin H_E(j\omega)$ for $\omega \geq 0$. ■

Theorem 3.4: *The closed-loop control system can be robustly stabilized by the fractional-order $PI^\lambda D^\mu$ controllers if and only if:*

- the fractional-order $PI^\lambda D^\mu$ can stabilize the nominal closed-loop control system with the nominal characteristic function $H_0(s)$ in (18).
- two sets $H_{E_1}(j\omega)$ in (12) and $H_{E_2}(j\omega) = -I^K N(j\omega)$ have no overlap for each frequency belonging to $[\omega_l, \omega_u]$, where ω_l and ω_u are defined as follows.

$$\omega_l = \min \left\{ 1, \left(\frac{K^- |K_i|}{T^+ + 1 + K^+ (|K_p| + |K_d|)} \right)^{\frac{1}{\lambda}} \right\}, \quad (19)$$

$$\omega_u = \max \left\{ 1, \left(\frac{1 + K^+ (|K_p| + |K_i| + |K_d|)}{T^-} \right)^{\frac{1}{\alpha^- - \hat{\mu}}} \right\}, \quad (20)$$

$$\hat{\mu} = \begin{cases} \mu, & \text{if } K_d \neq 0, \\ 0, & \text{if } K_d = 0. \end{cases}$$

Proof: First, we show that the zero exclusion condition is held for $\omega > \omega_u$ and $\omega < \omega_l$. Assume $|s| < 1$ or $|\omega| < 1$. Therefore, according to the triangle inequality we have

$$\begin{aligned} |H(s)| &\geq K^- |K_i| - (|s|^\lambda (T^+ |s|^\alpha + 1) + K^+ (|K_p| |s|^\lambda + |K_d| |s|^{\mu+\lambda})) \\ &\geq K^- |K_i| - (|s|^\lambda (T^+ |s|^{\alpha^-} + 1) + K^+ (|K_p| |s|^\lambda + |K_d| |s|^{\mu+\lambda})) \end{aligned}$$

$$\geq K^-|K_i|-|s|^\lambda((T^++1)+K^+ (|K_p|+|K_d|)). \quad (21)$$

From (21), it is visible that if $\omega < \omega_l$ then $|H(s)| > 0$ and consequently $0 \notin H(j\omega)$. Now assume that $|s = j\omega| > 1$, then one can write

$$\begin{aligned} |H(s)| &\geq T^-|s|^{\alpha^-+\lambda} - (|s|^\lambda + K^+ (|K_p||s|^\lambda + |K_i| + |K_d||s|^{\mu+\lambda})) \\ &\geq T^-|s|^{\alpha^-+\lambda} - |s|^{\mu+\lambda}(1 + K^+ (|K_p| + |K_i| + |K_d|)). \end{aligned} \quad (22)$$

From (22), one can simply infer $0 \notin H(j\omega)$ for if $\omega > \omega_u$. Now, we only need to prove that the overlap between two sets $H_{E_1}(j\omega)$ in (12) and H_{E_2} are equivalent to necessary and sufficient conditions for $0 \in H(j\omega)$. Assume that at a given frequency $\omega = \omega_0$, there is a complex number as z_0 and $z_0 \in H_1(j\omega_0)$. If $0 \in H(s = j\omega_0)$ then it can be simply concluded from $H(s) = H_1(s) + H_2(s)$ that $-z_0 \in H_2(j\omega_0)$ and consequently $z_0 \in -H_2(j\omega_0)$. Therefore, two value sets of $H_1(s)$ and $-H_2(s)$ have an overlap at $s = j\omega_0$. Hence, if the mentioned value sets do not have any overlap in the complex plane then $0 \notin H(j\omega)$. ■

3.2. D-decomposition method

The stability boundaries of a characteristic function can be defined within the space of controller parameters using the D-decomposition method. Assume that $\hat{H}(s)$ is an arbitrary member of $H(s)$ in (7) as follows:

$$\hat{H}(s) = s^\lambda (\hat{T}s^{\hat{\alpha}} \pm 1) + \hat{K}(K_p s^\lambda + K_i + K_d s^{\mu+\lambda}). \quad (23)$$

The boundaries of the stability region of $\hat{H}(s)$ in (23) which are described by Real Root Boundary (RRB), Infinite Root Boundary (IRB) and Complex Root Boundary (CRB) can be computed by the D-decomposition method (Hamamci 2007, 2008; Luo and Chen 2012).

RRB. $\hat{H}(0) = \hat{K}K_i$. It yields $K_i = 0$.

IRB. $\hat{H}(\infty) \neq 0$. Therefore, the boundary does not exist.

CRB. The CRB boundary can be obtained by substituting $s = j\omega$ into $\hat{H}(s) = 0$ in (23). Therefore, by partitioning $\hat{\Delta}(j\omega)$ into its real and imaginary parts and equating them to zero, one obtains

$$\begin{cases} A_{11}K_p + A_{12}K_i = B_1, \\ A_{21}K_p + A_{22}K_i = B_2, \\ A_{11} = \hat{K}\omega^\lambda \cos\left(\lambda\frac{\pi}{2}\right), \\ A_{12} = \hat{K}, \\ A_{21} = \hat{K}\omega^\lambda \sin\left(\lambda\frac{\pi}{2}\right), \\ A_{22} = 0, \\ B_1 = -\hat{T}\omega^{\hat{\alpha}+\lambda} \cos\left((\hat{\alpha}+\lambda)\frac{\pi}{2}\right) \mp \omega^\lambda \cos\left(\lambda\frac{\pi}{2}\right) \\ \quad - \hat{K}K_d\omega^{\lambda+\mu} \cos\left((\lambda+\mu)\frac{\pi}{2}\right), \\ B_2 = -\hat{T}\omega^{\hat{\alpha}+\lambda} \sin\left((\hat{\alpha}+\lambda)\frac{\pi}{2}\right) \mp \omega^\lambda \sin\left(\lambda\frac{\pi}{2}\right) \\ \quad - \hat{K}K_d\omega^{\lambda+\mu} \sin\left((\lambda+\mu)\frac{\pi}{2}\right), \end{cases} \quad (24)$$

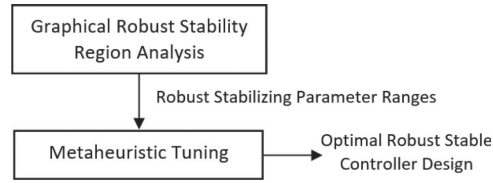


Figure 3. Application of the robust stability region in metaheuristic tuning of controllers.

The parameter space (K_p, K_i) is divided into stable and unstable regions for fixed K_d, λ and μ . One arbitrary test point can be used to find the stabilizing region.

3.3. Computation of the robust stability region of fractional-order $PI^\lambda D^\mu$ controllers

In this subsection, an stabilization algorithm (Algorithm 1) is presented to determine the robust stability region of fractional-order $PI^\lambda D^\mu$ controllers.

Algorithm 1: Step 1. Determine all polynomials of the set $H_E(j\omega)$ in (12). Step 2. For a fixed λ, μ and K_d , use the D-decomposition method stated in the Subsection 3.2 to calculate the robust stability region in (K_p, K_i) plane for all polynomials of the set $H_E(j\omega)$. Step 3. The final robust stability region of fractional-order $PI^\lambda D^\mu$ controllers is the intersection of all the computed stable regions in Step 2.

Remark 3.1: Based on Algorithm 1, a set of robust fractional-order $PI^\lambda D^\mu$ controllers is determined to robustly stabilize the closed-loop control system. Hence, the robust stability of the system is guaranteed by choosing fractional-order $PI^\lambda D^\mu$ controllers located in the robust stability region. In order to tune a controller improving the performance of the nominal closed-loop control system with the characteristic function $H_0(s)$ in (18), evolutionary algorithms such as Genetic Algorithm (GA), Particle Swarm Optimization (PSO), and Differential Evolution (DE) could be employed. Figure 3 illustrates a simple flowchart depicting the integration of graphical tuning with metaheuristic tuning methods. This showcases the application of the proposed graphical stability analysis for solving the optimal robust controller design problem.

4. Illustrative examples

Example 4.1: In Liang, Chen, and Zhao (2013), the robust stability region of the fractional-order controllers $K_p + \frac{K_i}{s^\lambda}$ has been calculated for interval fractional-order plants. Consider the following interval plants in (25).

$$P(s) = \frac{[0.5, 1.2]}{[29, 31]s^{[0.5, 1.7]} + 1}. \quad (25)$$

Let us compute the robust stability region by Algorithm 1 proposed in the present paper as shown in Figure 4 by the green color. The blue and red lines are the boundaries of

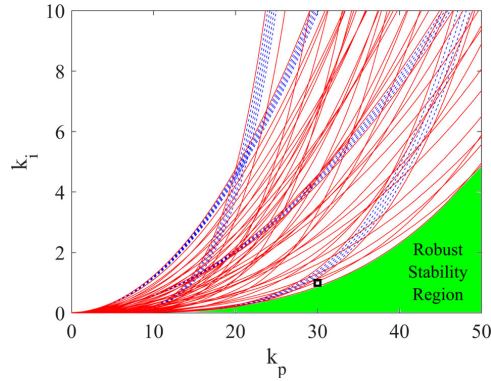


Figure 4. The robust stability region (green color) proposed by Algorithm 1 and the fractional-order controller $C(s) = 30 + \frac{1}{s^{1.8}}$ (black square) and the blue and red lines are the boundaries of the stabilizing regions corresponding to the polynomials in $H_E^1(j\omega)$ and $H_E^2(j\omega)$.

the stabilizing regions corresponding to the polynomials in $H_E^1(j\omega)$ and $H_E^2(j\omega)$. As seen from this figure, the fractional-order controller $C(s) = 30 + \frac{1}{s^{1.8}}$ shown by the black square does not lie in the green region which is the robust stability region. Therefore, the controller $C(s) = 30 + \frac{1}{s^{1.8}}$ cannot robustly stabilize the interval uncertain plant $P(s)$. In the following, it is shown that there is one unstable polynomial which has not been stabilized by the fractional-order controller $C(s) = 30 + \frac{1}{s^{1.8}}$. For instance, consider the following polynomial:

$$\hat{H}(s) = s^{1.8}(31s^{0.73} + 1) + 0.5(30s^{1.8} + 1). \quad (26)$$

Lemma 2.2 should be used to check the stability of $\hat{H}(s)$. As seen from Figure 5, $\hat{H}(s)$ is unstable because the origin is encircled twice and according to Lemma 2.2, $\hat{H}(s)$ is unstable. This example shows the correctness and the validity of the obtained results. Moreover, Theorem 3.4 can be employed to check the robust stability of the closed-loop control system controlled by the fractional-order controller $C(s) = 30 + \frac{1}{s^{1.8}}$. Figure 6 also shows the overlap between two sets $H_{E_1}(j\omega)$ (solid line) and $H_{E_2}(j\omega)$ (dotted line) in $\omega = 0.12$ rad/sec. This theorem also confirms that the fractional-order controller $C(s) = 30 + \frac{1}{s^{1.8}}$ cannot robustly stabilize the closed-loop control system. Figure 7 shows the step response of closed-loop control system and it confirms the plant $P(s) = \frac{0.5}{31s^{0.73} + 1}$ is not stabilized by the controller $C(s) = 30 + \frac{1}{s^{1.8}}$.

Example 4.2: Consider the following interval plant in (27).

$$P(s) = \frac{[0.8, 1.2]}{[1, 2]s^{[1, 1.5]} - 1}. \quad (27)$$

Utilizing Algorithm 1, an exhaustive analysis has been conducted to ascertain the robust stability boundaries of fractional-order $PI^\lambda D^\mu$ controllers, where λ and μ denote the fractional orders and K_d represents the differential gain. Figure 8 showcases the robust stability

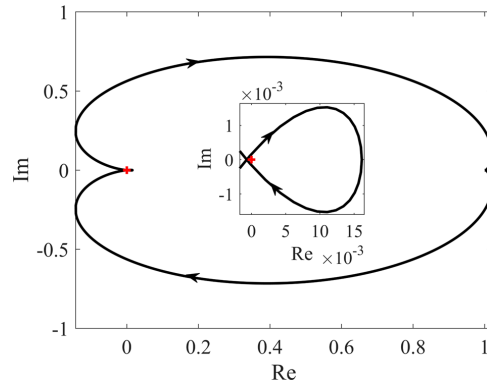


Figure 5. Investigation on the stability of $\hat{H}(s)$ by Lemma 2.2.

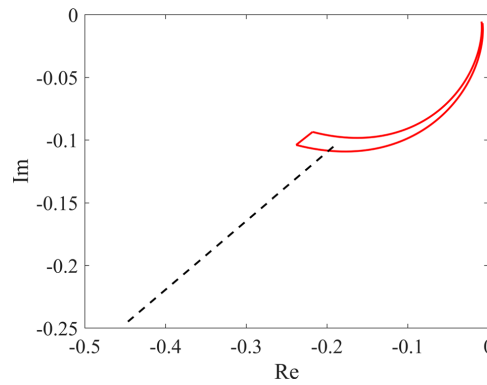


Figure 6. Overlap between two sets $H_{E_1}(j\omega)$ (solid line) and $H_{E_2}(j\omega)$ (dotted line) in $\omega = 0.12$ rad/sec.

region for $\lambda = 0.8$, $\mu = 0.1$, and $K_d = 0.1$ with the delineation highlighted in green. The blue and red lines are the boundaries of the stabilizing regions corresponding to the polynomials in $H_E^1(j\omega)$ and $H_E^2(j\omega)$. Notably, the robust stable region envelops the fractional-order $PI^\lambda D^\mu$ controller $C(s) = 20 + \frac{0.01}{s^{0.8}} + 0.1s^{0.1}$, as observed from the green-hued shading in the figure. In order to evaluate the stability of the system in the presence of a multitude of uncertainties, Lemma 2.2 has been employed to analyze the behavior of members that have been generated within the uncertainty space with $c = 1$. The results have been presented in Figure 9, clearly indicating that all the random members within the uncertain system are stable. Because, the Mikhailov's plot $\frac{\delta(j\omega)}{\omega_r(j\omega)}$ does not encircle the origin. Additionally, Figure 10 illustrates the step responses of the closed-loop control system employing the fractional-order $PI^\lambda D^\mu$ controller $C(s) = 20 + \frac{0.01}{s^{0.8}} + 0.1s^{0.1}$.

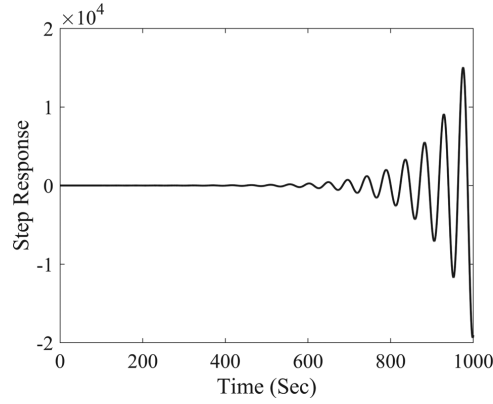


Figure 7. The step response of closed-loop control system in terms of the fractional-order controller $C(s) = 30 + \frac{1}{s^{1.8}}$ and the plant $P(s) = \frac{0.5}{31s^{0.73} + 1}$.

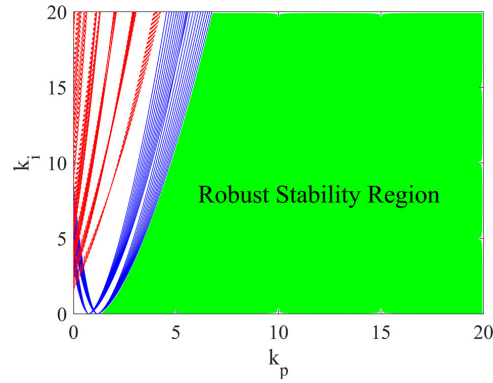


Figure 8. Robust stability region (green color) of fractional-order $PI^\lambda D^\mu$ controllers with $\lambda = 0.8$, $\mu = 0.1$ and $K_d = 0.1$.

Example 4.3: Consider the following interval plant in (28)

$$P(s) = \frac{[2, 4]}{[60, 70]s^{[0.8, 1.2]} + 1}. \quad (28)$$

By benefiting from Algorithm 1, the robust stability region of fractional-order $PI^\lambda D^\mu$ controllers with $\lambda = 0.1$, $\mu = 0.1$ and $K_d = 0.006$ has been computed in Figure 11 by the green color. The blue and red lines are the boundaries of the stabilizing regions corresponding to the polynomials in $H_E^1(j\omega)$ and $H_E^2(j\omega)$. Moreover, by using GA, the fractional-order

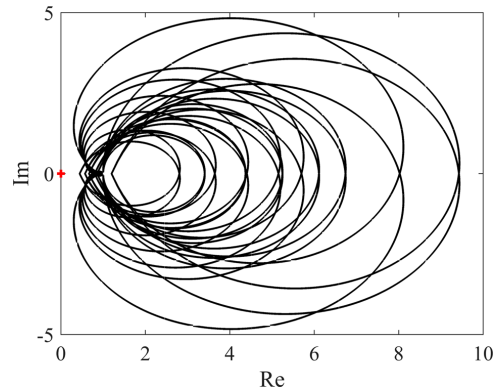


Figure 9. The stability analysis of the system controlled by $C(s) = 20 + \frac{0.01}{s^{0.8}} + 0.1s^{0.1}$ using Lemma 2.2.

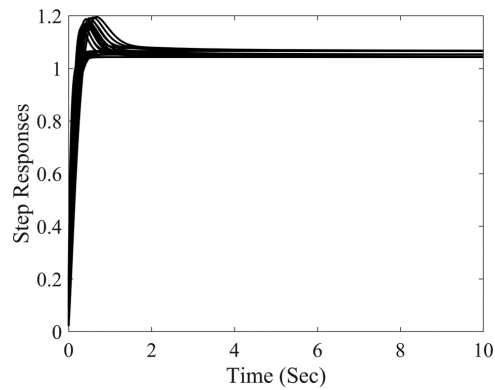


Figure 10. Step responses corresponding to $C(s) = 20 + \frac{0.01}{s^{0.8}} + 0.1s^{0.1}$.

$PI^\lambda D^\mu$ controller is tuned for the nominal closed-loop control system as follows:

$$C(s) = 100 + \frac{4.6809}{s^{0.1}} + 0.006s^{0.1}. \quad (29)$$

The step responses of the control system have been shown in Figure 12.

Example 4.4: Consider the following unstable interval plant in (30).

$$P(s) = \frac{[0.8, 1.2]}{[0.8, 1.2]s^{[0.8, 1.2]} - 1}. \quad (30)$$

The stabilizing region of PI controllers has been determined in Figure 13. Now, we employ the PSO algorithm to find a robust PI controller located in the robust stability region (green

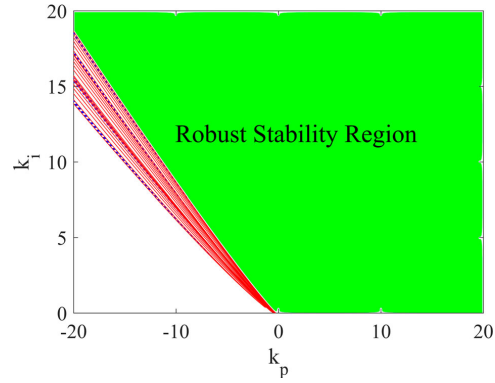


Figure 11. Robust stability region (green color) of fractional-order $PI^\lambda D^\mu$ controllers with $\lambda = 0.1$, $\mu = 0.1$ and $K_d = 0.006$ in Example 3.

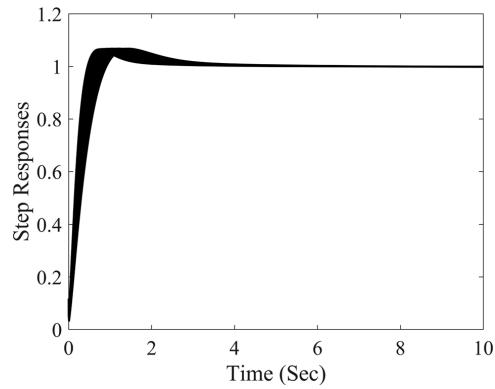


Figure 12. Step responses corresponding to the fractional-order $PI^\lambda D^\mu$ controllers in (29).

region) in Figure 13. So the resulting robust PI controller has been obtained as follows.

$$C(s) = 10 + \frac{5.8943}{s}. \quad (31)$$

Figure 14 illustrates the closed-loop performance and robustness of the system discussed in Example 4.4 under the influence of measurement noise. As evident from the figure, all selected samples within the uncertainty space exhibit stability.

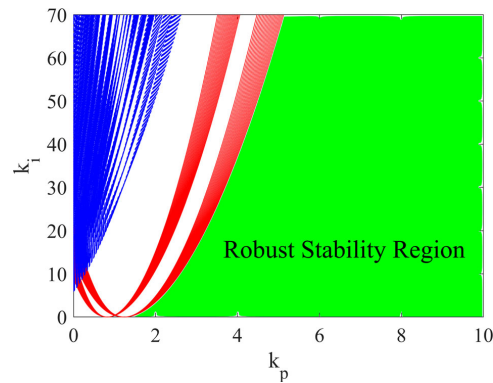


Figure 13. Robust stability region of PI controllers (green region) in Example 4.4.

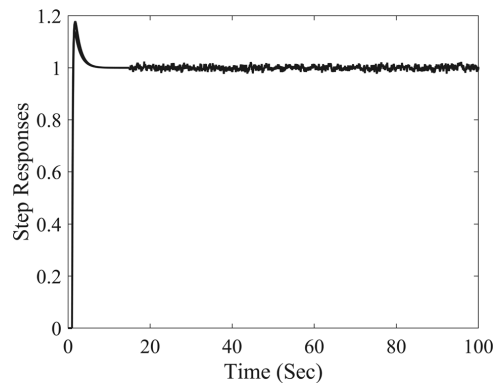


Figure 14. Step responses corresponding to the PI controller in (31) in the presence of the measurement noise.

5. Discussion

In this work, a graphical methodology is employed to introduce a set of necessary and sufficient criteria. These criteria serve to effectively tackle the intricate stabilization challenges associated with interval fractional-order systems having an uncertain order. Furthermore, rather than relying on a single stabilizing FOPID controller, this paper introduces a diverse ensemble of controllers for implementation within the control system. This innovative approach provides increased flexibility, enabling a wider range of possibilities for carefully selecting controller parameters. The study also aims to demonstrate the selection of an optimal robust stable FOPID design within the robust stability region of stability boundary locus in cooperation with metaheuristic optimization methods. Let us now progress to the comparative analysis of our findings with those of analogous extant studies.

In studies conducted by Hamamci (2007, 2008), the focus was on graphical extraction of the stabilizing region according to the stability boundary locus of fractional-order systems without dealing with parametric uncertainties of models. Similar to the proposed method, several previous works have considered graphical stabilization of interval uncertain fractional order systems in the literature: Zheng, Tang, and Song (2014) addressed the computation of the stabilizing region for fractional-order interval systems where only the coefficients exhibited uncertainties (with the fractional order assumed to be fixed). Furthermore, in Liang, Chen, and Zhao (2013), a method was proposed to compute the stabilizing region of FOPI (Fractional-Order Proportional-Integral) controllers for fractional-order systems with uncertain coefficients and orders. However, as highlighted in Zheng, Tang, and Song (2014, Remark 5.4) and demonstrated in Example 1 in Ghorbani, Tepljakov, and Petlenkov (2020b), the results presented in Liang, Chen, and Zhao (2013) cannot be generalized for all cases. This clearly illustrates the contributions of the theorems presented in our current paper.

In recent years, Tufenkci et al. (2021) have discussed optimal robust stabilization of FOPID controllers in the v -plane for interval uncertain plant models. However, their work hasn't considered the case of uncertainty in the fractional orders. They worked in a different design domain (v -domain) according to the system pole placement strategy.

Broadly speaking, the utilization of Hamamci (2007, 2008), Liang, Chen, and Zhao (2013), Zheng, Tang, and Song (2014), Tufenkci et al. (2021), Ghorbani, Tepljakov, and Petlenkov (2020b) for the purpose of designing fractional-order controllers that robustly stabilize fractional-order systems with general uncertainties in both coefficients and orders is not feasible. Nonetheless, this limitation is alleviated through the discoveries presented within the context of this study.

6. Conclusion

This study focused on demonstration of a graphical design method for the stabilization of FOPID control systems that can involve interval uncertainties for the fractional order and gain coefficients. At first, necessary and sufficient conditions were derived by the zero exclusion principle. Then, the D-decomposition method and the value set concept were employed to compute the robust stability region of fractional-order $PI^\lambda D^\mu$ controllers. Moreover, four numerical examples were provided which successfully validated the obtained results. It is important to highlight that the current discussion does not delve into the intricacies of tuning FOPID controllers for interval plants with multiple uncertain orders. Therefore, future research endeavors may involve exploring methods to determine the stabilizing region of fractional PID controllers for such complex systems. Additionally, a potential area of future work could focus on calculating the robust stabilizing region of interval plants (1) and (3) in the presence of interval time delays.

Disclosure statement

No potential conflict of interest was reported by the author(s).

Funding

This work was supported by the Estonian Research Council [grant number PRG658].

References

- Alagoz, Baris Baykant, Gulizar Alisoy, Serkan Alagoz, and Hafiz Alisoy. 2017. "A Note on Applications of Time-Domain Solution of Cole Permittivity Models." *OptiK* 139:272–282. <https://doi.org/10.1016/j.ijleo.2017.04.010>.
- Alagoz, Baris Baykant, Aleksei Tepljakov, Abdullah Ates, Eduard Petlenkov, and Celaledin Yeroglu. 2019. "Time-Domain Identification of One Noninteger Order Plus Time Delay Models From Step Response Measurements." *International Journal of Modeling, Simulation, and Scientific Computing* 10 (01): 1941011. <https://doi.org/10.1142/S1793962319410113>.
- Badri, Pouya, and Mahdi Sojoodi. 2022. "LMI-based Robust Stability and Stabilization Analysis of Fractional-Order Interval Systems with Time-Varying Delay." *International Journal of General Systems* 51 (1): 1–26. <https://doi.org/10.1080/03081079.2021.1993847>.
- Busłowicz, Mikołaj. 2008. "Stability of Linear Continuous-Time Fractional Order Systems with Delays of the Retarded Type." *Bulletin of the Polish Academy of Sciences: Technical Sciences* 56 (4): 319–3243.
- Chen, Lin, Biswajit Basu, and David McCabe. 2016. "Fractional Order Models for System Identification of Thermal Dynamics of Buildings." *Energy and Buildings* 133:381–388. <https://doi.org/10.1016/j.enbuild.2016.09.006>.
- Deniz, Furkan Nur, Baris Baykant Alagoz, Nusret Tan, and Murat Koseoglu. 2020. "Revisiting Four Approximation Methods for Fractional Order Transfer Function Implementations: Stability Preservation, Time and Frequency Response Matching Analyses." *Annual Reviews in Control* 49:239–257. <https://doi.org/10.1016/j.arcontrol.2020.03.003>.
- Efe, Mehmet Önder. 2011. "Fractional Order Systems in Industrial Automation: A Survey." *IEEE Transactions on Industrial Informatics* 7 (4): 582–591. <https://doi.org/10.1109/TII.2011.2166775>.
- Fu, Minyue, Soura Dasgupta, and Vincent Blondel. 1995. "Robust Stability Under a Class of Nonlinear Parametric Perturbations." *IEEE Transactions on Automatic Control* 40 (2): 213–223. <https://doi.org/10.1109/9.341786>.
- Gabano, Jean-Denis, Thierry Poinot, and Houcem Kanoun. 2015. "LPV Continuous Fractional Modeling Applied to Ultracapacitor Impedance Identification." *Control Engineering Practice* 45:86–97. <https://doi.org/10.1016/j.conengprac.2015.09.001>.
- Ghorbani, Majid, and Mahsan Tavakoli-Kakhki. 2021. "Robust Stability Analysis of Uncertain Incommensurate Fractional Order Quasi-Polynomials in the Presence of Interval Fractional Orders and Interval Coefficients." *Transactions of the Institute of Measurement and Control* 43 (5): 1117–1125. <https://doi.org/10.1177/0142331220968965>.
- Ghorbani, Majid, Mahsan Tavakoli-Kakhki, Aleksei Tepljakov, Eduard Petlenkov, Arash Farnam, and Guillaume Crevecoeur. 2021. "Robust Stability Analysis of Interval Fractional-Order Plants with Interval Time Delay and General Form of Fractional-Order Controllers." *IEEE Control Systems Letters* 6:1268–1273. <https://doi.org/10.1109/LCSYS.2021.3091525>.
- Ghorbani, Majid, Aleksei Tepljakov, and Eduard Petlenkov. 2020a. "Stabilizing Region of Fractional-Order Proportional Integral Derivative Controllers for Interval Delayed Fractional-Order Plants." *Asian Journal of Control* 25 (2): 1145–1155. <https://doi.org/10.1002/asjc.2894>.
- Ghorbani, Majid, Aleksei Tepljakov, and Eduard Petlenkov. 2020b. "Stabilizing Region of Fractional-Order Proportional Integral Derivative Controllers for Interval Fractional-Order Plants." *Transactions of the Institute of Measurement and Control* 45 (3): 546–556. <https://doi.org/10.1177/01423312221117866>.
- Ghorbani, Majid, Aleksei Tepljakov, and Eduard Petlenkov. 2023. "Fractional-Order Interval Polynomials, Stability and Robust stability Analysis and FOMCON Implementation." In *2023 International Conference on Fractional Differentiation and Its Applications (ICFDA)*, 1–6. Ajman, United Arab Emirates: IEEE.
- Hamamci, Serdar Ethem. 2007. "An Algorithm for Stabilization of Fractional-Order Time Delay Systems Using Fractional-Order PID Controllers." *IEEE Transactions on Automatic Control* 52 (10): 1964–1969. <https://doi.org/10.1109/TAC.2007.906243>.
- Hamamci, Serdar Ethem. 2008. "Stabilization Using Fractional-Order PI and PID Controllers." *Nonlinear Dynamics* 51 (1): 329–343.

- Kang, Chenfei, Jun-Guo Lu, Xu-Yi Qiu, and Qing-Hao Zhang. 2022. "Novel Robust Stability Conditions of Fractional-Order Systems with Structured Uncertain Parameters Based on Parameter-Dependent Functions: The $0 < \alpha < 1$ Case." *International Journal of General Systems* 52 (2): 169–190.
- Khemane, Firas, Rachid Malti, Tarek Raïssi, and Xavier Moreau. 2011. "Robust Estimation of Fractional Models in the Frequency Domain Using Set Membership Methods." *Signal Processing* 92 (7): 1591–1601. <https://doi.org/10.1016/j.sigpro.2011.12.008>.
- Kumar, Vineet, and K. P. S. Rana. 2017. "Nonlinear Adaptive Fractional Order Fuzzy PID Control of a 2-link Planar Rigid Manipulator with Payload." *Journal of the Franklin Institute* 354 (2): 993–1022. <https://doi.org/10.1016/j.jfranklin.2016.11.006>.
- Liang, Taonian, Jianjun Chen, and Huihuang Zhao. 2013. "Robust Stability Region of Fractional Order PI^λ Controller for Fractional Order Interval Plant." *International Journal of Systems Science* 44 (9): 1762–1773. <https://doi.org/10.1080/00207721.2012.670291>.
- Liao, Zeng, Cheng Peng, Wang Li, and Yong Wang. 2010. "Robust Stability Analysis for a Class of Fractional Order Systems with Uncertain Parameters." *Journal of the Franklin Institute* 348 (6): 1101–1113. <https://doi.org/10.1016/j.jfranklin.2011.04.012>.
- Luo, Ying, and YangQuan Chen. 2012. "Stabilizing and Robust Fractional Order PI Controller Synthesis for First Order Plus Time Delay Systems." *Automatica* 48 (9): 2159–2167. <https://doi.org/10.1016/j.automatica.2012.05.072>.
- Malti, Rachid, Tarek Raïssi, Magalie Thomassin, and Firas Khemane. 2010. "Set Membership Parameter Estimation of Fractional Models Based on Bounded Frequency Domain Data." *Communications in Nonlinear Science and Numerical Simulation* 15 (4): 927–938. <https://doi.org/10.1016/j.cnsns.2009.05.005>.
- Matušů, Radek, and Libor Pekař. 2017. "Robust Stability of Thermal Control Systems with Uncertain Parameters: The Graphical Analysis Examples." *Applied Thermal Engineering* 125:1157–1163. <https://doi.org/10.1016/j.applthermaleng.2017.07.089>.
- Monje, Concepción A., Blas M. Vinagre, Vicente Feliu, and YangQuan Chen. 2008. "Tuning and Auto-Tuning of Fractional Order Controllers for Industry Applications." *Control Engineering Practice* 16 (7): 798–812. <https://doi.org/10.1016/j.conengprac.2007.08.006>.
- Moornani, Kamran Akbari, and Mohammad Haeri. 2009. "On Robust Stability of Linear Time Invariant Fractional-Order Systems with Real Parametric Uncertainties." *ISA Transactions* 48 (4): 484–490. <https://doi.org/10.1016/j.isatra.2009.04.006>.
- Moornani, Kamran Akbari, and Mohammad Haeri. 2010a. "Robustness in Fractional Proportional-Integral-derivative-Based Closed-Loop Systems." *IET Control Theory & Applications* 4 (10): 1933–1944. <https://doi.org/10.1049/iet-cta.2009.0313>.
- Moornani, Kamran Akbari, and Mohammad Haeri. 2010b. "Robust Stability Testing Function and Kharitonov-Like Theorem for Fractional Order Interval Systems." *IET Control Theory & Applications* 4 (10): 2097–2108. <https://doi.org/10.1049/iet-cta.2009.0485>.
- Moornani, Kamran Akbari, and Mohammad Haeri. 2010c. "On Robust Stability of LTI Fractional-Order Delay Systems of Retarded and Neutral Type." *Automatica* 46 (2): 362–368. <https://doi.org/10.1016/j.automatica.2009.11.006>.
- Moornani, Kamran Akbari, and Mohammad Haeri. 2013. "Robust Stability Check for Fractional PID-based Control Systems." *Transactions of the Institute of Measurement and Control* 35 (2): 236–246. <https://doi.org/10.1177/0142331212440477>.
- Nasser-Eddine, Achraf. 2019. "A Two Steps Method for Electrochemical Impedance Modeling Using Fractional Order System in Time and Frequency Domains." *Control Engineering Practice* 86:96–104. <https://doi.org/10.1016/j.conengprac.2019.03.001>.
- Prakosa, Jalu A., Norma Alias, and Chifayah Astuti. 2023. "Performance Comparison of Applying Integer and Fractional Order Calculus to DC Motor Speed Control Experiments." In *2023 International Conference on Radar, Antenna, Microwave, Electronics, and Telecommunications (ICRAMET)*, 79–83. Bandung, Indonesia: IEEE.
- Schäfer, Ingo, and Klaus Krüger. 2008. "Modelling of Lossy Coils Using Fractional Derivatives." *Journal of Physics D: Applied Physics* 41 (4): 045001. <https://doi.org/10.1088/0022-3727/41/4/045001>.

- Senol, Bilal, Abdullah Ates, Baris Baykant Alagoz, and Celaledin Yeroglu. 2014. "A Numerical Investigation for Robust Stability of Fractional-Order Uncertain Systems." *ISA Transactions* 53 (2): 189–198. <https://doi.org/10.1016/j.isatra.2013.09.004>.
- Shah, Pritesh, and Ravi Sekhar. 2019. "Closed Loop System Identification of a DC Motor Using Fractional Order Model." In *2019 International Conference on Mechatronics, Robotics and Systems Engineering (MoRSE)*, 69–74. Bali, Indonesia: IEEE.
- Tabatabaei, S. Sepehr, Heidar Ali Talebi, and Mahdi Tavakoli. 2017. "A Novel Adaptive Order/parameter Identification Method for Variable Order Systems Application in Viscoelastic Soft Tissue Modeling." *Chaos, Solitons & Fractals* 102:447–455. <https://doi.org/10.1016/j.chaos.2017.04.005>.
- Tan, Nusret, Ö. Faruk Özgüven, and M. Mine Özyetkin. 2009. "Robust Stability Analysis of Fractional Order Interval Polynomials." *ISA Transactions* 48 (2): 166–172. <https://doi.org/10.1016/j.isatra.2009.01.002>.
- Tepljakov, Aleksei, Baris Baykant Alagoz, Celaledin Yeroglu, Emmanuel Gonzalez, S. Hassan HosseinNia, and Eduard Petlenkov. 2018. "FOPID Controllers and Their Industrial Applications: A Survey of Recent Results." *IFAC-PapersOnLine* 51 (4): 25–30. <https://doi.org/10.1016/j.ifacol.2018.06.014>.
- Tepljakov, Aleksei, Baris Baykant Alagoz, Celaledin Yeroglu, Emmanuel Gonzalez, Hassan Hosseinnia, Eduard Petlenkov, Abdullah Ates, and Martin Cech. 2021. "Towards Industrialization of FOPID Controllers: A Survey on Milestones of Fractional-Order Control and Pathways for Future Developments." *IEEE Access* 9:21016–21042. <https://doi.org/10.1109/Access.6287639>.
- Tepljakov, Aleksei, Eduard Petlenkov, and Juri Belikov. 2013. "Tuning and Digital Implementation of a Fractional-Order PD Controller for a Position Servo." *International Journal of Microelectronics and Computer Science* 4 (3): 116–123.
- Tufenkci, S., B. Senol, R. Matušů, and B. B. Alagoz. 2021. "Design of Robust PI Controllers for Interval Plants With Worst-Case Gain and Phase Margin Specifications in Presence of Multiple Crossover Frequencies." *Fractal and Fractional* 5 (1): 3. <https://doi.org/10.3390/fractalfract5010003>.
- Wang, Tiecheng, Andres San-Millan, and Sumeet S. Aphale. 2024. "Robustness in Fractional Proportional-Integral-derivative-Based Closed-Loop Systems." *ISA Transactions* 147:153–162. <https://doi.org/10.1016/j.isatra.2024.01.033>.
- Wu, Zhenlong, Jairo Viola, Ying Luo, YangQuan Chen, and Donghai Li. 2021. "Robust Fractional-Order [proportional Integral Derivative] Controller Design with Specification Constraints: More Flat Phase Idea." *International Journal of Control* 97 (1): 111–129. <https://doi.org/10.1080/00207179.2021.1992498>.
- Yeroglu, Celaledin, and Bilal Senol. 2013. "Investigation of Robust Stability of Fractional Order Multilinear Affine Systems: 2q-Convex Parapolygon Approach." *Systems & Control Letters* 62 (10): 845–855. <https://doi.org/10.1016/j.sysconle.2013.06.005>.
- Yumuk, Erhan, Mijde Güzelkaya, and İbrahim Eksin. 2023. "Fractional-Order PID Controller Design Via Optimal Selection Strategy of Frequency Domain Specifications." *International Journal of Systems Science* 54 (10): 2239–2252. <https://doi.org/10.1080/00207721.2023.2225497>.
- Zhang, Qing-Hao, and Jun-Guo Lu. 2023. "Robust Stability of Fractional-Order Systems with Mixed Uncertainties: The $0 < \alpha < 1$ Case." *Communications in Nonlinear Science and Numerical Simulation* 126:107511. <https://doi.org/10.1016/j.cnsns.2023.107511>.
- Zheng, Shiqi. 2017. "Robust Stability of Fractional Order System with General Interval Uncertainties." *Systems & Control Letters* 99:1–8. <https://doi.org/10.1016/j.sysconle.2016.11.001>.
- Zheng, Shiqi, and Wenjie Li. 2018. "Robust Stabilization of Fractional-Order Plant with General Interval Uncertainties Based on a Graphical Method." *International Journal of Robust and Nonlinear Control* 28 (5): 1672–1692. <https://doi.org/10.1002/rnc.v28.5>.
- Zheng, Shiqi, Xiaoqi Tang, and Bao Song. 2014. "A Graphical Tuning Method of Fractional Order Proportional Integral Derivative Controllers for Interval Fractional Order Plant." *Journal of Process Control* 24 (11): 1691–1709. <https://doi.org/10.1016/j.jprocont.2014.08.011>.

Appendix 16

XVI

M. Ghorbani, B. Mehdizadeh Gavgani, A. Farnam, A. Tepljakov, E. Petlenkov, and G. Crevecoeur. Implementable robust stability regions for fractional-order PD controllers with an application to servo system control. *Asian Journal of Control*, 2025. doi:10.1002/asjc.3881.

ARTICLE TYPE

Implementable Robust Stability Regions for Fractional-Order PD Controllers with an Application to Servo System Control

Majid Ghorbani¹ | Babak Mehdizadeh Gavgani² | Arash Farnam² | Aleksei Tepljakov¹ | Eduard Petlenkov¹ | Guillaume Crevecoeur²

¹Department of Computer Systems, Tallinn University of Technology, Estonia.

²Department of Electrical Energy, Metals, Mechanical Constructions and Systems, Ghent University, and FlandersMake@UGent - Corelab MIRO, Ghent, Belgium.

Correspondence

Majid Ghorbani, Tallinn University of Technology, Department of Computer Systems, Tallinn, Estonia.
Email: majid.ghorbani@taltech.ee

Present address

This work has been supported by the European Union's Horizon Europe research and innovation programme under the grant agreement No 101120657, project ENFIELD (European Lighthouse to Manifest Trustworthy and Green AI), by the Estonian Research Council through the grant PRG658, and by the Estonian Centre of Excellence in Energy Efficiency, ENER (grant TK230) funded by the Estonian Ministry of Education and Research.)

Abstract

This paper presents a methodology aimed at computing the implementable robust stability regions for Fractional-Order Proportional-Derivative (FOPD) controllers in the context of interval fractional-order plants. The implementable robust stability region of an FOPD controller refers to determining the robust stability region of its integer-order approximations for interval systems. It is demonstrated that the robust stability region of an FOPD controller differs from that of its integer-order approximation. Consequently, values conducive to practical controller design are situated within the implementable robust stability region. Initially, robust stability analysis of the fractional-order system is conducted using integer-order approximations of FOPD controllers. Subsequently, an algorithm is proposed for computing the implementable robust stability regions of FOPD controllers. Additionally, an auxiliary function is introduced to enhance the performance of the closed-loop control system. Finally, the proposed approach is applied to the position control of a laboratory modular servo system.

KEYWORDS

Robust control, FOPD controller, implementable robust stability region, graphical tuning, uncertainties.

1 | INTRODUCTION

1.1 | Background

Recently, there has been a growing interest among control systems experts in using fractional calculus. This is because they have found that fractional calculus techniques work well for describing and controlling many different kinds of systems¹. Additionally, numerous studies^{2,3,4,5,6} have illustrated that the utilization of fractional controllers results in superior performance compared to classical control techniques in closed-loop control systems.

When modeling real-world systems, uncertainties are often encountered^{7,8,9,10}. One of the most common approaches among engineers to incorporate uncertainty into system models is by utilizing interval uncertainty structures^{11,12}. Therefore, ensuring robust stability analysis, which is fundamental to every control system, is essential. Hence, graphical methods have been proposed in works^{13,14} to assess the robust stability of interval fractional-order systems.

Determining the stability region of fractional-order controllers is an appealing approach to design, as it introduces not just one stabilizing controller, but a set of them. In works^{15,16,17}, the stability region of Fractional-Order Proportional-Derivative (FOPD)

controllers has been calculated for fractional-order systems. A recent study¹⁸ introduced a tuning method for FOPD controllers tailored to second-order plants, achieving a flat phase response at the specified gain crossover frequency to ensure robustness against gain variations, alongside favorable dynamic performance. In study¹⁹, an FOPD controller is designed and implemented to stabilize load frequency control in an interconnected hydrothermal power system. Moreover, the study²⁰ proposed a method for computing the stability region of FOPD controllers in time-delayed systems. A recent study²¹ addressed level control in a coupled two-tank SISO system using a cascade control strategy with a Fractional-Order Proportional Integral (FOPI) and FOPD controllers, achieving reduced steady-state error and energy consumption compared to integer-order controllers.

1.2 | Motivation and contributions

Fractional-order controllers can only be implemented through appropriate approximation using finite differential or difference equations. Several established and well-known methods offer approximations of fractional-order functions in either the frequency domain for integer orders or in the discrete-time domain such that Oustaloup²², Matsuda²³.

In practical applications, implementing or simulating fractional-order controllers often requires replacing fractional transfer functions with integer-order approximations that replicate their behavior over a specific frequency range or under certain conditions²⁴. Ensuring the stability of the closed-loop control system when using these integer-order approximations is critical for real-world effectiveness. While previous work²⁵ has proposed a graphical method to determine the stability region of integer-order approximations for FOPD controllers in fractional-order systems without uncertainties, real systems frequently encounter uncertainties, as illustrated in the example in Section 4 of this paper. This gap has led us to develop an innovative graphical method to determine the robust stability region for integer-order approximations of FOPD controllers specifically for interval fractional-order systems, addressing the challenge highlighted in Section 2 (Problem Formulation).

In this paper, a graphical method is presented to determine the robust stability region of integer-order approximations of FOPD controllers for interval fractional-order systems. To achieve this, the necessary and sufficient conditions for robust stability analysis of interval fractional-order systems are derived in Theorem 1 and Theorem 2 by employing integer-order approximations of FOPD controllers. Subsequently, an algorithm is provided for calculating the robust stability region of FOPD controllers. Moreover, an auxiliary function is offered to improve the performance of the system. In summary, the main contributions and innovations of this paper are as follows:

1. Establishing necessary and sufficient conditions for robust stability analysis of interval fractional-order systems using integer-order approximations of FOPD controllers.
2. Presenting a graphical method for designing integer-order approximations of FOPD controllers.
3. Enhancing system performance through an auxiliary function.

The remainder of this paper is organized as follows. In Section 2, we introduce the general framework of this study and provide the transfer functions for both the plant and the controller. In Section 3, two theorems are presented for verifying the robust stability of the closed-loop control system. Additionally, an algorithm is proposed to determine the robust stability region of integer-order approximations of FOPD controllers. Furthermore, Section 4 applies the proposed approach to a lab-scale modular servo system. Lastly, the paper concludes with Section 5.

2 | PRELIMINARIES

2.1 | Background materials

Consider the fractional-order system illustrated in FIGURE 1. In this figure, $P(s, \mathbf{b}, \mathbf{a})$ denotes the uncertain fractional-order plant described by

$$P(s, \mathbf{b}, \mathbf{a}) = \frac{N_P(s, \mathbf{b})}{D_P(s, \mathbf{a})} = \frac{\sum_{i_1=0}^m b_{i_1} s^{\beta_{i_1}}}{\sum_{i_2=0}^n a_{i_2} s^{\alpha_{i_2}}}, \quad (1)$$

where $\beta_m > \beta_{m-1} > \dots > \beta_1 > \beta_0 = 0$ and $\alpha_n > \alpha_{n-1} > \dots > \alpha_1 > \alpha_0 = 0$ and $\alpha_n > \beta_m$ are arbitrary real numbers. Moreover, the vectors $\mathbf{b} = [b_0 \ b_1 \ \dots \ b_m]^T$ and $\mathbf{a} = [a_0 \ a_1 \ \dots \ a_n]^T$ represent the coefficient vectors, both of which are members of the

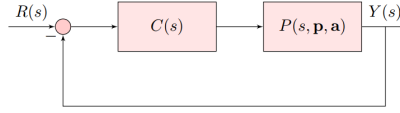


FIGURE 1 A fundamental closed-loop control system employing negative unity feedback.

following uncertainty bounding sets:

$$\begin{aligned} \mathbf{b} \in \mathbf{B} &= \{\mathbf{b} \in \mathbb{R}^{m+1} | b_{i_1} \in [b_{i_1}^-, b_{i_1}^+], b_m, b_0 \neq 0, i_1 \in \mathbb{Z}_{\geq 0}^{\leq m}\}, \\ \mathbf{a} \in \mathbf{A} &= \{\mathbf{a} \in \mathbb{R}^{n+1} | a_{i_2} \in [a_{i_2}^-, a_{i_2}^+], a_n \neq 0, i_2 \in \mathbb{Z}_{\geq 1}^{\leq n}\}, \end{aligned} \quad (2)$$

where, $[b_{i_1}^-, b_{i_1}^+]$ and $[a_{i_2}^-, a_{i_2}^+]$ are specified intervals.

Let us denote by $C(s)$ a FOPD controller defined in (3).

$$C_{FOPD}(s) = K_p + K_d s^\mu, K_p, K_d \in \mathbb{R}, \mu \in (0, \alpha_n - \beta_m). \quad (3)$$

Therefore, the characteristic function of the closed-loop control system illustrated in FIGURE 1 is obtained as follows:

$$\Delta_{FOPD}(s, \mathbf{b}, \mathbf{a}) = \sum_{i_2=0}^n a_{i_2} s^{\alpha_{i_2}} + (K_p + K_d s^\mu) \sum_{i_1=0}^m b_{i_1} s^{\beta_{i_1}}. \quad (4)$$

Consider a nominal member of the interval polynomial $\Delta_{FOPD}(s, \mathbf{b}, \mathbf{a})$ as

$$\tilde{\Delta}_{FOPD}(s) = \sum_{i_2=0}^n \tilde{a}_{i_2} s^{\alpha_{i_2}} + (K_p + K_d s^\mu) \sum_{i_1=0}^m \tilde{b}_{i_1} s^{\beta_{i_1}}. \quad (5)$$

Utilizing the D-decomposition technique and setting $\tilde{\Delta}_{FOPD}(j\omega)$ to zero, the Complex Root Boundaries (CRBs) can be computed as follows:

$$\begin{aligned} K_p &= \frac{B_1(\omega)A_2(\omega) - B_2(\omega)A_1(\omega)}{B_3(\omega)B_2(\omega) - B_4(\omega)B_1(\omega)}, \\ K_d &= \frac{B_4(\omega)A_1(\omega) - B_3(\omega)A_2(\omega)}{B_3(\omega)B_2(\omega) - B_4(\omega)B_1(\omega)}, \end{aligned} \quad (6)$$

where

$$\begin{cases} A_1(\omega) = \sum_{i_2=0}^n \tilde{a}_{i_2} \omega^{\alpha_{i_2}} \cos(\frac{\pi}{2} \alpha_{i_2}), \\ A_2(\omega) = \sum_{i_2=0}^n \tilde{a}_{i_2} \omega^{\alpha_{i_2}} \sin(\frac{\pi}{2} \alpha_{i_2}), \\ B_1(\omega) = \sum_{i_2=0}^n \tilde{b}_{i_2} \omega^{\beta_{i_2} + \mu} \cos(\frac{\pi}{2} (\beta_{i_2} + \mu)), \\ B_2(\omega) = \sum_{i_2=0}^n \tilde{b}_{i_2} \omega^{\beta_{i_2} + \mu} \sin(\frac{\pi}{2} (\beta_{i_2} + \mu)), \\ B_3(\omega) = \sum_{i_2=0}^n \tilde{b}_{i_2} \omega^{\beta_{i_2}} \cos(\frac{\pi}{2} \beta_{i_2}), \\ B_4(\omega) = \sum_{i_2=0}^n \tilde{b}_{i_2} \omega^{\beta_{i_2}} \sin(\frac{\pi}{2} \beta_{i_2}). \end{cases} \quad (7)$$

By substituting $\omega = 0$ and $\omega = \infty$ into equation (4), one can readily calculate the boundaries for Real Root Boundaries (RRBs) and Infinite Root Boundaries (IRBs) as detailed in work¹⁵. Then, the stabilizing region can be identified by examining an arbitrary test point within each region¹⁵. The term s^μ in the FOPD controller $C_{FOPD}(s)$ from (3) can be approximated by an integer-order function using any of the established approximation schemes^{22,23}. In accordance with the order of approximation (n_o), it is feasible to express:

$$s^\mu \approx P_D(s) = \frac{N_\mu(s)}{D_\mu(s)} = \frac{\sum_{r=0}^{n_o} d_r s^r}{\sum_{r=0}^{n_o} c_r s^r}, \quad d_{n_o} \wedge c_{n_o} \neq 0. \quad (8)$$

Using the approximation (8), (4) can be written as

$$\Delta_{FOPD}(s, \mathbf{b}, \mathbf{a}) = D_\mu(s) \left(\sum_{i_2=0}^n a_{i_2} s^{\alpha_{i_2}} \right) + (K_p D_\mu(s) + K_d N_\mu(s)) \left(\sum_{i_1=0}^m b_{i_1} s^{\beta_{i_1}} \right). \quad (9)$$

Consider a nominal member of $\Delta_{FOPD}(s)$ as $\hat{\Delta}_{FOPD}(s)$. In this case, the CRBs can be obtained as follows:

$$\begin{aligned} K_p &= \frac{B_1(\omega)A_2(\omega) - B_2(\omega)A_1(\omega)}{B_3(\omega)B_2(\omega) - B_4(\omega)B_1(\omega)}, \\ K_d &= \frac{B_4(\omega)A_1(\omega) - B_3(\omega)A_2(\omega)}{B_3(\omega)B_2(\omega) - B_4(\omega)B_1(\omega)}, \end{aligned} \quad (10)$$

where

$$\begin{cases} A_1(\omega) = \sum_{r=0}^{n_0} \sum_{i_2=0}^n c_r \hat{a}_{i_2} \omega^{\alpha_{i_2}+r} \cos(\frac{\pi}{2}(\alpha_{i_2} + r)), \\ A_2(\omega) = \sum_{r=0}^{n_0} \sum_{i_2=0}^n c_r \hat{a}_{i_2} \omega^{\alpha_{i_2}+r} \sin(\frac{\pi}{2}(\alpha_{i_2} + r)), \\ B_1(\omega) = \sum_{r=0}^{n_0} \sum_{i_2=0}^n d_r \hat{b}_{i_2} \omega^{\beta_{i_2}+r} \cos(\frac{\pi}{2}(\beta_{i_2} + r)), \\ B_2(\omega) = \sum_{r=0}^{n_0} \sum_{i_2=0}^n d_r \hat{b}_{i_2} \omega^{\beta_{i_2}+r} \sin(\frac{\pi}{2}(\beta_{i_2} + r)), \\ B_3(\omega) = \sum_{r=0}^{n_0} \sum_{i_2=0}^n c_r \hat{b}_{i_2} \omega^{\beta_{i_2}+r} \cos(\frac{\pi}{2}(\beta_{i_2} + r)), \\ B_4(\omega) = \sum_{r=0}^{n_0} \sum_{i_2=0}^n c_r \hat{b}_{i_2} \omega^{\beta_{i_2}+r} \sin(\frac{\pi}{2}(\beta_{i_2} + r)). \end{cases} \quad (11)$$

By substituting $\omega = 0$ and $\omega = \infty$ into equation (9), one can easily determine the boundaries for RRBs and IRBs. Furthermore, the stabilizing region can be discerned by evaluating an arbitrary test point within each respective region²⁵.

2.2 | Problem formulation

Based on the explanations provided in the preceding subsection, it can be inferred that the stability region of a fractional-order controller differs from that of its integer-order approximation. To illustrate this disparity, let us examine a particular example where the following fractional-order plant

$$G(s) = \frac{1}{s^{0.3} (30s + 1)}. \quad (12)$$

Suppose a FOPD controller is employed to regulate its output, and a sampling value of $\mu = 0.8$ is utilized for the order of the fractional term s^μ . The approximation of s^μ for the range of frequencies $[0.01, 100]$ rad/sec can be computed as follows²⁵:

$$s^{0.78} \approx \frac{36.31s^4 + 519.7s^3 + 675.5s^2 + 86.24s + 1}{s^4 + 86.24s^3 + 675.5s^2 + 519.7s + 36.31}. \quad (13)$$

FIGURE 2 illustrates the stability regions of a FOPD controller (depicted in green) alongside its integer-order approximation (stripe region). In this paper, this region (stripe region) is referred to as the *implementable stability region* of the fractional-order controllers. As evident from this figure, there is a region where the fractional-order controller exhibits stability, while its integer-order approximation remains unstable. Therefore, those values suitable for the practical application of the designed controller are located within the implementable stability region. Hence, within this literature, we address these two subjects:

1. As previously mentioned, modeling real-world systems often encounters uncertainties. One of the most common approaches among engineers to incorporate uncertainty into system models is by utilizing interval uncertainty structures like $P(s, \mathbf{b}, \mathbf{a})$ in Equation (1). Now, the question arises: how we can determine the robust stability region of integer-order approximations of fractional-order controllers $C_{FOPD}(s)$ for $P(s, \mathbf{b}, \mathbf{a})$. *In other words, the primary and foremost challenge is to ascertain the implementable robust stability region of $C_{FOPD}(s)$ for $P(s, \mathbf{b}, \mathbf{a})$.*
2. Because of the uncertain model $P(s, \mathbf{b}, \mathbf{a})$, it becomes quite challenging to ascertain the bounds of uncertainty for both the complementary sensitivity function and the sensitivity function. Consequently, the subsequent challenge in this literature lies in meeting the control requirements for disturbance rejection amidst these uncertainties.

To address the aforementioned challenges, the following materials will be required for the remainder of the paper.

As stated in work¹⁴, $N_P(s, \mathbf{b})$ and $D_P(s, \mathbf{a})$ would like to be a convex shape in the complex plane whose vertices can be obtained by the following procedure.

Procedure 1:

Define $H_0 = \{i_2 \in \mathbb{Z}_{\geq 0}^n : a_{i_2}^- < a_{i_2}^+\}$. The value set $D_P(j\omega, \mathbf{a})$ is determined for $\omega \in \mathbb{R}_{\geq 0}$ as follows:

1. For $H_0 = \emptyset$ and $\omega \geq 0$, $D_P(j\omega, \mathbf{a}) = D_0(j\omega) = \sum_{i_2=0}^n a_{i_2}^- s^{\alpha_{i_2}}$. 2. For $H_0 \neq \emptyset$,

- If $\omega = 0$, then $D_P(j\omega, \mathbf{a}) = D_P(j0, \mathbf{a}) = [a_0^-, a_0^+]$.

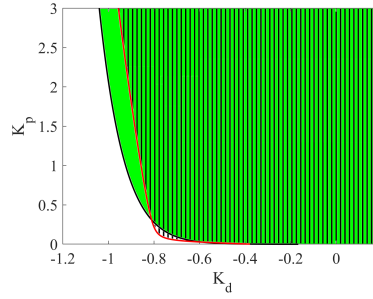


FIGURE 2 Stability regions of a FOPD controller (depicted in yellow and green) alongside its integer-order approximation (shown in yellow).

- If $\omega > 0$, then define $B_0 = \{\text{frac}(0.5\alpha_{i_2}) : i_2 \in H_0\}$ and $m_D = n(B_0)$. Consider $\gamma_1, \dots, \gamma_{m_D-1}, \gamma_{m_D}$ as all the distinct members of B_0 sorted as $0 \leq \gamma_1 < \dots < \gamma_{m_D-1} < \gamma_{m_D} < 1$. Then, define the following sets:

$$\begin{aligned} H'_r &= \left\{ i_2 \in H_0 : \text{floor}(0.5\alpha_{i_2}) \text{ is an odd number and } \text{frac}(0.5\alpha_{i_2}) = \beta_r \right\}, \\ H_r &= \left\{ i_2 \in H_0 : \text{floor}(0.5\alpha_{i_2}) \text{ is an even number and } \text{frac}(0.5\alpha_{i_2}) = \beta_r \right\}, \quad r = 1, 2, \dots, m_D. \end{aligned} \quad (14)$$

Let $a^- = [a_0^- a_1^- \dots a_n^-]^T$ and $a^+ = [a_0^+ a_1^+ \dots a_n^+]^T$. The vectors q^1, q^2, \dots, q^{2m} are defined as follows:

$$a^k = [a_0^k a_1^k \dots a_n^k]^T, a^{m_D+k} = [a_0^{m_D+k} a_1^{m_D+k} \dots a_n^{m_D+k}]^T = a^+ + a^- - a^k, \quad k = 1, \dots, m, \quad (15)$$

where for $i_2 = 0, 1, \dots, n$ and $k = 1, \dots, m_D$, it can be written that

$$a_{i_2}^k = \begin{cases} a_{i_2}^+, & \text{for } i_2 \in \left(\bigcup_{i=1}^{k-1} H_i \right) \cup \left(\bigcup_{i=k}^m H'_i \right), \\ a_{i_2}^-, & \text{otherwise,} \end{cases} \quad (16)$$

and

$$a_{i_2}^{m_D+k} = a_{i_2}^+ + a_{i_2}^- - a_{i_2}^k. \quad (17)$$

Hence, the consecutive vertices $V_{r_2}^-(j\omega)$ ($r_2 = 1, 2, \dots, 2m_D$) are calculated by

$$V_k^-(j\omega) = D(j\omega, a^k), V_{m_D+k}^-(j\omega) = D(j\omega, a^{m_D+k}) = D(j\omega, a^+ + a^- - a^k) = V_k^-(j\omega), \quad k = 1, 2, \dots, m_D. \quad (18)$$

The vertex polynomials corresponding to $N_P(j\omega, \mathbf{a})$ and $D_P(j\omega, \mathbf{b})$ are respectively denoted as $V_{r_1}^+(\omega)$ ($r_1 = 1, 2, \dots, 2m_N$) and $V_{r_2}^-(\omega)$ ($r_2 = 1, 2, \dots, 2m_D$), and they can be computed using *Procedure 1*.

Remark 1. It is important to note that **Procedure 1** defines the vertex polynomials for the characteristic function's denominator, $D_P(j\omega, a)$ and $N_P(j\omega, b)$, under uncertainty conditions. This procedure specifies how the vertices are determined by evaluating various combinations of interval coefficients over a frequency range. By identifying these vertices, **Procedure 1** helps construct the value set of the polynomial in the complex plane. This value set is essential for assessing the robust stability of the system, as it ensures that all potential variations of the plant's parameters are considered when computing the robust stability region. The vertices obtained from **Procedure 1** are used in subsequent stability analysis steps to verify that the closed-loop system remains stable across all uncertainties. Thus, **Procedure 1** plays a critical role in forming the robust stability region boundaries, confirming that the characteristic polynomial does not enclose the origin in the complex plane. As an example for **Procedure 1**, consider the interval fractional-order polynomial $D_P(j\omega, \mathbf{a}) = [0.6, 1]s^{2.2} + 3.73s^{1.15} + [0.3, 0.7]s^{0.9} + [21.3, 21.7]$. We have the

followings based on **Procedure 1**:

$$\begin{aligned} H_0 &= \{0, 1, 3\}, \quad B_0 = \{0, 0.1, 0.45\}, \quad m_D = 3, \quad \beta_1 = 0, \\ \beta_2 &= 0.1, \quad \beta_3 = 0.45, \quad H_1 = \{0\}, \quad H'_2 = \{3\}, \quad H_3 = \{1\}, \quad H'_1 = H_2 = H'_3 = \emptyset. \end{aligned}$$

Therefore, the vertices of the interval polynomial $D_P(j\omega, \mathbf{a}) = [0.6, 1]s^{2.2} + 3.73s^{1.15} + [0.3, 0.7]s^{0.9} + [21.3, 21.7]$ can be computed as follows:

$$\begin{aligned} V_1^-(j\omega) &= 1s^{2.2} + 3.73s^{1.15} + 0.3s^{0.9} + 21.3, \\ V_2^-(j\omega) &= 1s^{2.2} + 3.73s^{1.15} + 0.3s^{0.9} + 21.7, \\ V_3^-(j\omega) &= 0.6s^{2.2} + 3.73s^{1.15} + 0.3s^{0.9} + 21.7, \\ V_4^-(j\omega) &= 0.6s^{2.2} + 3.73s^{1.15} + 0.7s^{0.9} + 21.7, \\ V_5^-(j\omega) &= 0.6s^{2.2} + 3.73s^{1.15} + 0.7s^{0.9} + 21.3, \\ V_6^-(j\omega) &= 1s^{2.2} + 3.73s^{1.15} + 0.7s^{0.9} + 21.3. \end{aligned}$$

To ascertain the robust stability region of fractional-order controllers, it is imperative to verify the stability of one member of the uncertain system. Hence, this paper utilizes the Principle of Argument Theorem for stability checking, outlined as follows:

Principle of Argument Theorem²⁶: Let $f(z)$ be analytic interior to a simple closed Jordan curve Γ and continuous and different from zero on Γ . Let K be the curve described in the w -plane by the mapping $w = f(z)$ and let $\Delta_\Gamma \arg f(z)$ denote the net change in $\arg f(z)$ as the point z traverses Γ once over in the counterclockwise direction. Then the number of zeros p of $f(z)$ located in the interior of the Jordan curve Γ counted with their multiplicities, is obtained as

$$p = \frac{\Delta_\Gamma \arg f(z)}{2\pi}. \quad (19)$$

That is the net number of times that K winds about the point $w = 0$.

Zero Exclusion Principle¹³: A control system with the characteristic function $\Delta_{FOPD}(s)$ is robust stable if $\Delta_{FOPD}(s)$ has at least one stable member and $0 \notin \Delta_{FOPD}(j\omega)$ for $\omega \geq 0$.

3 | MAIN RESULTS

This section is divided into three subsections, “Characterizing Implementable Stability Regions for FOPD Controllers”, “Robust stability evaluation of interval fractional-order systems” and “Good output disturbance rejection”. In the subsection “Characterizing implementable stability regions for FOPD Controllers”, a novel graphical tuning method is proposed to determined the implementable robust stability region of FOPD controllers for the interval plant $P(s, \mathbf{b}, \mathbf{a})$. In the subsection “Robust stability evaluation of interval fractional-order systems”, an auxiliary function is provided for the robust stability analysis of interval fractional-order systems. Moreover, in the subsection “Good output disturbance rejection”, our objective is to propose an auxiliary function aimed at enhancing the performance of the system.

3.1 | Characterizing Implementable robust Stability Regions for FOPD Controllers

To compute the implementable robust stability regions for FOPD Controllers, it is imperative to derive the necessary and sufficient conditions for the robust stability of the closed-loop control system, as illustrated in FIGURE 1. Therefore, the following theorem initially establishes these conditions for the interval system with the characteristic function $\Delta_{FOPD}(s, \mathbf{b}, \mathbf{a})$ in (9).

Theorem 1. *The interval system depicted in FIGURE 1, characterized by the function $\Delta_{FOPD}(s, \mathbf{b}, \mathbf{a})$ in (9), is robustly stable if and only if the subsequent characteristic functions $\Delta_{FOPD}^{h_N}(s, \mathbf{a})$ in (20) and $\Delta_{FOPD}^{h_D}(s, \mathbf{b})$ in (21) also demonstrate robust*

stability.

$$\Delta_{FOPD_D}^{h_N}(s, \mathbf{a}) = \left(\sum_{r=0}^{n_o} c_r s^r \right) D_P(s, \mathbf{a}) + \left(K_p \sum_{r=0}^{n_o} c_r s^r + K_d \sum_{r=0}^{n_o} d_r s^r \right) V_{h_N}^+(\omega), h_N = 1, \dots, 2m_N. \quad (20)$$

$$\Delta_{FOPD_N}^{h_D}(s, \mathbf{b}) = \left(\sum_{r=0}^{n_o} c_r s^r \right) V_{h_D}^-(\omega) + \left(K_p \sum_{r=0}^{n_o} c_r s^r + K_d \sum_{r=0}^{n_o} d_r s^r \right) N_P(s, \mathbf{b}), h_D = 1, \dots, 2m_D. \quad (21)$$

Proof. **The ‘if’ portion:** Since $\Delta_{FOPD_D}^{h_N}(s, \mathbf{a})$ and $\Delta_{FOPD_N}^{h_D}(s, \mathbf{b})$ are robustly stable, it can be concluded that $0 \notin \Delta_{FOPD_D}^{h_N}(j\omega, \mathbf{a})$ and $0 \notin \Delta_{FOPD_N}^{h_D}(j\omega, \mathbf{b})$. Moreover, one has

$$0 \notin \Delta_{FOPD_D}^{h_N}(s, \mathbf{a}) \iff -\left(K_p \sum_{r=0}^{n_o} c_r s^r + K_d \sum_{r=0}^{n_o} d_r s^r \right) \times V_{h_N}^+(\omega) \notin \left(\sum_{r=0}^{n_o} c_r s^r \right) D_P(s, \mathbf{a}), h_N = 1, \dots, 2m_N. \quad (22)$$

$$0 \notin \Delta_{FOPD_N}^{h_D}(j\omega, \mathbf{b}) \iff -\left(\sum_{r=0}^{n_o} c_i s^i \right) V_{h_D}^-(\omega) \notin \left(K_p \left(\sum_{i=0}^{n_o} c_i s^i \right) + K_d \left(\sum_{i=0}^{n_o} d_i s^i \right) \right) N_P(s, \mathbf{b}), h_D = 1, \dots, 2m_D. \quad (23)$$

According to **Procedure 1**, $D_P(s, \mathbf{a})$ and $N_P(s, \mathbf{b})$ are both convex polygons. Furthermore, based on equations (22) and (23), the vertices of the convex polygon $\left(\sum_{i=0}^{n_o} c_i s^i \right) D_P(s, \mathbf{a})$ do not lie within $-\left(K_p \left(\sum_{i=0}^{n_o} c_i s^i \right) + K_d \left(\sum_{i=0}^{n_o} d_i s^i \right) \right) N_P(s, \mathbf{b})$. Similarly, the vertices of the convex polygon $\left(K_p \left(\sum_{i=0}^{n_o} c_i s^i \right) + K_d \left(\sum_{i=0}^{n_o} d_i s^i \right) \right) N_P(s, \mathbf{b})$ do not lie within $-\left(\sum_{i=0}^{n_o} c_i s^i \right) D_P(s, \mathbf{a})$. Consequently, both convex polygons do not overlap in the complex plane, indicating that $0 \notin \Delta_{FOPD}(s, \mathbf{b}, \mathbf{a})$.

The ‘if’ portion: Given that $\Delta_{FOPD}(s, \mathbf{b}, \mathbf{a})$ exhibits robust stability, it follows straightforwardly from the zero exclusion principle that 0 does not belong to $\Delta_{FOPD}(j\omega, \mathbf{b}, \mathbf{a})$. Furthermore, this transfer function $\Delta_{FOPD}(s, \mathbf{b}, \mathbf{a})$ is composed of two convex polygons, namely $\left(\sum_{i=0}^{n_o} c_i s^i \right) D_P(s, \mathbf{a})$ and $\left(K_p \left(\sum_{i=0}^{n_o} c_i s^i \right) + K_d \left(\sum_{i=0}^{n_o} d_i s^i \right) \right) N_P(s, \mathbf{b})$. The absence of 0 in $\Delta_{FOPD}(j\omega, \mathbf{b}, \mathbf{a})$ necessitates that the convex polygons $-\left(\sum_{i=0}^{n_o} c_i s^i \right) D_P(s, \mathbf{a})$ and $\left(K_p \left(\sum_{i=0}^{n_o} c_i s^i \right) + K_d \left(\sum_{i=0}^{n_o} d_i s^i \right) \right) N_P(s, \mathbf{b})$ (or $-\left(K_p \left(\sum_{i=0}^{n_o} c_i s^i \right) + K_d \left(\sum_{i=0}^{n_o} d_i s^i \right) \right) N_P(s, \mathbf{b})$ and $\left(\sum_{i=0}^{n_o} c_i s^i \right) D_P(s, \mathbf{a})$) do not overlap within the complex plane. Consequently, it can be inferred that $0 \notin \Delta_{FOPD_D}^{h_N}(j\omega, \mathbf{a})$ and $0 \notin \Delta_{FOPD_N}^{h_D}(j\omega, \mathbf{b})$. \square

Now, **Algorithm 1** demonstrates how to determine the implementable robust stability region of FOPD controllers for the interval plant $\Delta_{FOPD}(s, \mathbf{b}, \mathbf{a})$ in (9).

Algorithm 1. Characterizing implementable robust Stability Regions for FOPD Controllers

Step 1. Obtain the vertices $V_{r_1}^+(\omega)$ ($r_1 = 1, 2, \dots, 2m_N$) and $V_{r_2}^-(\omega)$ ($r_2 = 1, 2, \dots, 2m_D$) using **Procedure 1**.

Step 2. Obtain RRB, IRB and CRB and the implementable robust stability regions for $\partial(\Delta_{FOPD_D}^{h_N}(s, \mathbf{a}))$ in (20) and $\partial(\Delta_{FOPD_N}^{h_D}(s, \mathbf{b}))$ in (21).

Step 3. The final stabilizing region is the intersection of all the computed stable regions obtained in Step 2.

3.2 | Robust stability evaluation

In this subsection, our focus lies in determining whether a designed controller can robustly stabilize the closed-loop system. To achieve this, the following theorem is presented.

Theorem 2. *The interval system illustrated in FIGURE 1 is robust stable if and only if a nominal member of the function $\Delta_{FOPD}(s, \mathbf{b}, \mathbf{a})$ is stable and the inequality $H(\omega) > 0$ is satisfied, where $H(\omega)$ is defined in (24).*

$$H(\omega) = \min\{H_1(\omega), H_2(\omega)\}, \quad (24)$$

in which

$$H_1(\omega) = \min \left\{ H_{h_1, h_2}^D(\omega) \mid h_1 \in \{1, \dots, 2m_N\}, h_2 \in \{1, \dots, 2m_D\} \right\}, \quad (25)$$

$$\begin{aligned}
H_{h_1, h_2}^D(\omega) &= \left| \left(\sum_{r=0}^{n_o} c_r (j\omega)^r \right) V_{h_2}^-(\omega) + \left(K_p \left(\sum_{r=0}^{n_o} c_r (j\omega)^r \right) + K_d \left(\sum_{r=0}^{n_o} d_r (j\omega)^r \right) \right) V_{h_1}^+(\omega) \right| + \\
&\left| \left(\sum_{r=0}^{n_o} c_r (j\omega)^r \right) V_{h_2+1}^-(\omega) + \left(K_p \left(\sum_{r=0}^{n_o} c_r (j\omega)^r \right) + K_d \left(\sum_{r=0}^{n_o} d_r (j\omega)^r \right) \right) V_{h_1}^+(\omega) \right| - \left| \left(\sum_{r=0}^{n_o} c_r (j\omega)^r \right) (V_{h_2+1}^-(\omega) - V_{h_2}^-(\omega)) \right|, \\
H_2(\omega) &= \min \left\{ H_{h_1, h_2}^N(\omega) | h_1 \in \{1, \dots, 2m_N\}, h_2 \in \{1, \dots, 2m_D\} \right\}, \\
H_{h_1, h_2}^N(\omega) &= \left| \left(\sum_{r=0}^{n_o} c_r (j\omega)^r \right) V_{h_2}^-(\omega) + \left(K_p \left(\sum_{r=0}^{n_o} c_r (j\omega)^r \right) + K_d \left(\sum_{r=0}^{n_o} d_r (j\omega)^r \right) \right) V_{h_1}^+(\omega) \right| + \\
&\left| \left(\sum_{r=0}^{n_o} c_r (j\omega)^r \right) V_{h_2}^-(\omega) + \left(K_p \left(\sum_{r=0}^{n_o} c_r (j\omega)^r \right) + K_d \left(\sum_{r=0}^{n_o} d_r (j\omega)^r \right) \right) V_{h_1+1}^+(\omega) \right| - \\
&\left| \left(K_p \left(\sum_{r=0}^{n_o} c_r (j\omega)^r \right) + K_d \left(\sum_{r=0}^{n_o} d_r (j\omega)^r \right) \right) (V_{h_1+1}^+(\omega) - V_{h_1}^+(\omega)) \right|. \tag{26}
\end{aligned}$$

Proof. We aim to demonstrate that 0 does not belong to $\Delta_{FOPD_D}^{h_N}(j\omega, \mathbf{a})$ and 0 does not belong to $\Delta_{FOPD_N}^{h_D}(j\omega, \mathbf{b})$ for non-negative frequencies. As per **Procedure 1**, the value sets of $\Delta_{FOPD_D}^{h_N}(j\omega, \mathbf{a})$ and $\Delta_{FOPD_N}^{h_D}(j\omega, \mathbf{b})$ exhibit a polygonal shape in the complex plane. Denoted by $H_1(\omega)$ is the triangle inequality involving any two consecutive vertices of $\Delta_{FOPD_D}^{h_N}(j\omega, \mathbf{a})$, and similarly, $H_2(\omega)$ denotes the triangle inequality for any two consecutive vertices of $\Delta_{FOPD_N}^{h_D}(j\omega, \mathbf{b})$. Consequently, if $H_1(\omega) = 0$ at $\omega = \omega_0$, it can be deduced from the triangle inequality that 0 lies on the boundary of $\Delta_{FOPD_D}^{h_N}(j\omega_0, \mathbf{a})$ i.e., $0 \in \Delta_{FOPD_D}^{h_N}(j\omega_0, \mathbf{a})$. Therefore, if both inequalities $H_1(\omega) > 0$ and $H_2(\omega) > 0$ are satisfied, it implies that 0 does not belong to $\Delta_{FOPD_D}^{h_N}(j\omega, \mathbf{a})$ and 0 does not belong to $\Delta_{FOPD_N}^{h_D}(j\omega, \mathbf{b})$. \square

Remark 2. Referring to Theorem 2, it is necessary to verify the stability of one element within $\Delta_{FOPD}(s, \mathbf{b}, \mathbf{a})$ as $\Delta_{FOPD}^0(s)$. A straightforward approach to assess stability involves plotting the polar plot of $\psi(s) = \frac{\Delta_{FOPD}^0(s)}{a(s+b)^{\alpha_p+\eta_0}}$ for $s = j\omega$, where $-\infty < \omega < \infty$, and a and b are positive real numbers. According to the principle of argument theorem, $\Delta_{FOPD}^0(s)$ is stable if and only if $\psi(s)$ does not encircle the origin in the complex plane for $s = j\omega$ where $-\infty < \omega < \infty$.

3.3 | Good output disturbance rejection

To enhance the rejection of output disturbances, it is important to ensure that the sensitivity function $S(j\omega)$ (27) meets the following constraint²⁷.

$$|S(j\omega)| < |M_s(j\omega)| \rightarrow \left| \frac{1}{1 + \frac{(K_p \sum_{r=0}^{n_o} c_r s^r + K_d \sum_{r=0}^{n_o} d_r s^r) N_P(s, \mathbf{b})}{(\sum_{r=0}^{n_o} c_r s^r) D_P(s, \mathbf{a})}} \right| < |M_s(j\omega)|. \tag{27}$$

According to **Theorem 1** and equation (27), a robust FOPD controller should meet the following inequalities for $s = j\omega$:

$$\left| \frac{1}{1 + \frac{(K_p \sum_{r=0}^{n_o} c_r s^r + K_d \sum_{r=0}^{n_o} d_r s^r) V_{h_1}^+(\omega)}{(\sum_{r=0}^{n_o} c_r s^r) D(s, \mathbf{a})}} \right| < |M_s(s)|, (h_1 = 1, 2, \dots, 2m_N). \tag{28}$$

$$\left| \frac{1}{1 + \frac{(K_p \sum_{r=0}^{n_o} c_r s^r + K_d \sum_{r=0}^{n_o} d_r s^r) N(s, \mathbf{b})}{(\sum_{r=0}^{n_o} c_r s^r) V_{h_2}^-(\omega)}} \right| < |M_s(s)|, (h_2 = 1, 2, \dots, 2m_D). \tag{29}$$

Using equations (28) and (29), along with the maximum modulus theorem²⁸, we ensure the following inequality is satisfied.

$$H_S(\omega) = \max_{r=1,2} H_r^S(\omega) < 0, \tag{30}$$

where

$$\begin{cases} H_1^S(\omega) = \max_{i=1, \dots, 2m_N} H_i^P(\omega), \\ H_1^D(\omega) = \max_{e_p^D \in P_E^D} |e_p^D| - |M_s(j\omega)|, \\ l^D = 1, 2, \dots, 2m_D, \\ P_E^D = \{e_1^D, e_2^D, \dots, e_{2m_D}^D\}, \\ e_h^D = \frac{1}{1 + \frac{(K_p \sum_{r=0}^{n_0} c_r s^r + K_d \sum_{r=0}^{n_0} d_r s^r) V_1^D(\omega)}{(\sum_{r=0}^{n_0} c_r s^r)(V_h^-(\omega), V_{h+1}^-(\omega))}}, \\ V_{2m_D+1}^-(\omega) = V_1^-(\omega), h = 1, \dots, 2m_D, s = j\omega. \end{cases} \quad (31)$$

$$\begin{cases} H_2^S(\omega) = \max_{i=1, \dots, 2m_D} H_i^N(\omega), \\ H_2^N(\omega) = \max_{e_p^N \in P_E^N} |e_p^N| - |M_s(j\omega)|, \\ l^N = 1, 2, \dots, 2m_N, \\ P_E^N = \{e_1^N, e_2^N, \dots, e_{2m_N}^N\}, \\ e_h^N = \frac{1}{1 + \frac{(K_p \sum_{r=0}^{n_0} c_r s^r + K_d \sum_{r=0}^{n_0} d_r s^r) V_1^N(\omega), V_{h+1}^N(\omega)}{(\sum_{r=0}^{n_0} c_r s^r) V_r^-(\omega)}}, \\ V_{2m_N+1}^+(\omega) = V_1^+(\omega), h = 1, \dots, 2m_N, s = j\omega. \end{cases} \quad (32)$$

Remark 3. To design a robust FOPD stabilization, the steps outlined in **Algorithm 1** should be followed. This process results in a computed set of robust FOPD controllers. To enhance the performance of the closed-loop control system, the robust controller must be selected such that the inequality $H_S(\omega) < 0$ in (30) is fulfilled. This condition ensures compliance with the inequalities (27-29), which, in turn, guarantees that $H_S(\omega) < 0$ is satisfied. Consequently, the robust condition $\|M_s^{-1}(j\omega)S(j\omega)\|_\infty < 1$ is upheld, confirming the system's robust stability.

Remark 4. By substituting $D_\mu(s) = 1$ and $N_\mu(s) = s^\mu$ into the characteristic function $\Delta_{\text{FOPD}}(s, \mathbf{b}, \mathbf{a})$ in (9), all the results presented in Theorem 1, Theorem 2, Algorithm 1, and the subsection on Good Output Disturbance Rejection remain valid. This demonstrates that the method proposed in this paper enables the tuning of a robust FOPD controller, both with and without approximation, for commensurate and noncommensurate interval fractional-order systems.

4 | PRACTICAL APPLICATION

In this section, we utilize the theoretical results obtained in the previous section to implement position control for a modular servo system of the Centre for Intelligent Systems of TalTech University, as depicted in FIGURE 3.

The velocity transfer function is identified using the MATLAB system identification toolbox²⁹ as follows:

$$P_v(s) = \frac{[558, 565.5]s^2 + [9.2, 10.3]s + [0.02, 0.04]}{s^3 + [3, 4]s^2 + [0.06, 0.07]s + [0.0002, 0.0003]}. \quad (33)$$

and the angle transfer function is derived by incorporating an integrator

$$P(s) = \frac{[558, 565.5]s^2 + [9.2, 10.3]s + [0.02, 0.04]}{s(s^3 + [3, 4]s^2 + [0.06, 0.07]s + [0.0002, 0.0003])}. \quad (34)$$

The robust stability region and the implementable robust stability region of FOPD controllers for the interval plant (34) have been determined for $\mu = 0.8$. The Oustaloup approximation (oustafod tool in the FOMCON toolbox³⁰) has been selected to replace $s^{0.8}$ in the FOPD controller across the frequency range of [0.001, 100], as outlined below:

$$s^{0.8} \approx P_D(s) = \frac{39.81s^3 + 128.7s^2 + 8.766s + 0.01259}{s^3 + 69.63s^2 + 102.2s + 3.162}. \quad (35)$$

FIGURE 4 shows robust Stability regions of a FOPD controller (depicted in green) alongside its integer-order approximation (stripe region). To confirm the robust stability region depicted in FIGURE 4, we employ the stability analysis method outlined in Remark 2. FIGURE 5 and FIGURE 6 display the curves of $\psi(s) = \frac{\Delta_{\text{FOPD}}(s)}{(s+1)^{\alpha_p m_0}}$ for randomly generated values within the uncertainty space by applying the FOPD controller $K_p = 0.06$ and $K_d = 0.01$ and its integer-order approximation which are located in the robust stability regions. It is evident from the figures that all selected instances exhibit stability.

Two controllers $C_{FOPD}^1(s)$ and $C_{FOPD}^2(s)$ are chosen as follows:

$$\begin{aligned} C_{FOPD}^1(s) &= 0.052 + 0.018 P_D(s). \\ C_{FOPD}^2(s) &= 0.005 + 0.002 P_D(s). \end{aligned} \quad (36)$$

It is noteworthy that both controllers, $C_{FOPD}^1(s)$ and $C_{FOPD}^2(s)$, are situated within the robust stability region illustrated in FIGURE 4. However, the robust stability of the system can be ensured by utilizing the auxiliary function $H(\omega)$ as outlined in Theorem 2, as depicted in FIGURE 7. As evident from this graph, both controllers satisfy the inequality $H(\omega) > 0$, thus guaranteeing robust stability according to Theorem 2.

Assume that the design specification for the system is to satisfy $|S(j\omega)| < -20$ db for $\omega \leq 0.3$ rad/sec. As seen from FIGURE 8, the controller $C_{FOPD}^1(s)$ can satisfy the inequality $H_s(\omega) < 0$. Therefore, the designer should select $C_{FOPD}^1(s)$.

The results are compared to the PD controllers supplied by INTECO, which are configured with parameters $k_p = 0.1$ and $K_i = 0.01$. FIGURE 9 and FIGURE 10 show the responses of the control system and the control signals obtained by applying the controllers $C_{FOPD}^1(s)$ and $C_{FOPD}^2(s)$, respectively. As observed from FIGURE 9, the controller $C_{FOPD}^1(s)$ exhibits superior performance in terms of faster response. Moreover, the responses of the control system and the control signals are illustrated in Figure 11 and Figure 12, considering the presence of measurement noise and an additive step disturbance applied at $t = 15$ seconds. As observed from these figures, the controller $C_{FOPD}^1(s)$ demonstrates superior performance, characterized by a faster response and reduced oscillations.

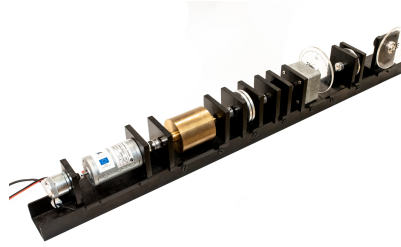


FIGURE 3 Servo system of the Centre for Intelligent Systems of TalTech University.

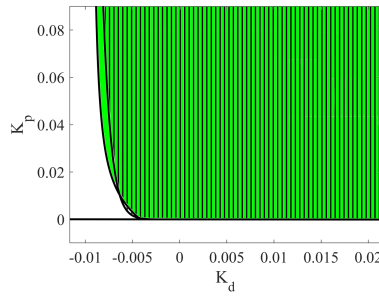


FIGURE 4 Stability regions of a FOPD controller (depicted in green) alongside its integer-order approximation (stripe region).

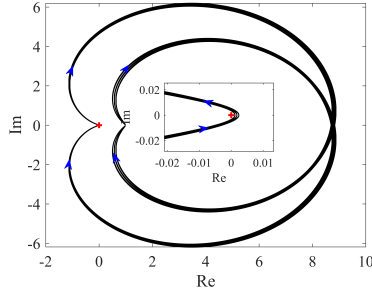


FIGURE 5 Robust stability analysis of the *FOPD* controller without approximation.

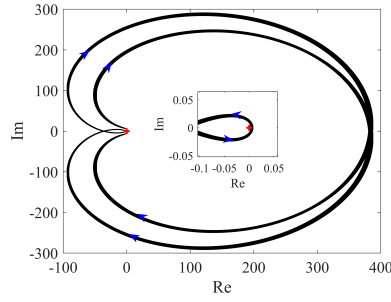


FIGURE 6 Robust stability analysis of the *FOPD* controller with integer-order approximation.

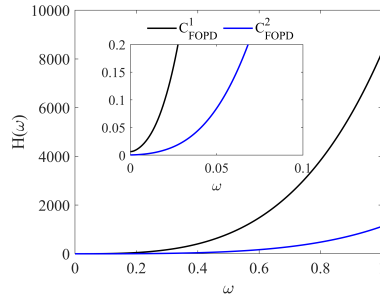


FIGURE 7 Curve of $H(\omega)$ corresponding to $C_{FOPD}^1(s)$ and $C_{FOPD}^2(s)$.

5 | CONCLUSION

In this paper, a methodology was presented aimed at computing the implementable robust stability regions for Fractional-Order Proportional-Derivative (FOPD) controllers within the framework of interval fractional-order plants. The significance of determining the robust stability region of FOPD controllers in comparison to their integer-order approximations was demonstrated, highlighting the distinctiveness of these regions. Through the analysis, it was illustrated that practical values essential for controller design were encompassed within the implementable robust stability region. The methodology began with a comprehensive robust stability analysis of fractional-order systems utilizing integer-order approximations of FOPD controllers. Subsequently, an algorithm was proposed tailored for the computation of implementable robust stability regions specific to

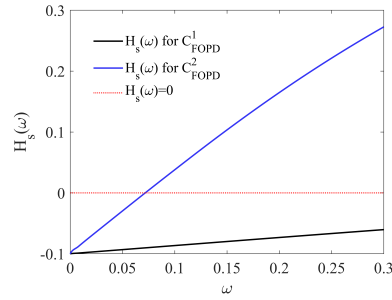


FIGURE 8 Robust stability analysis of the *FOPD* controller with integer-order approximation.

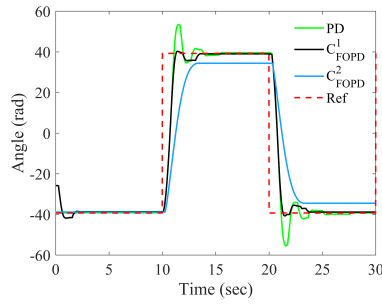


FIGURE 9 Comparison of control systems with different controllers $C_{FOPD}^1(s)$, $C_{FOPD}^2(s)$ and *PD*.

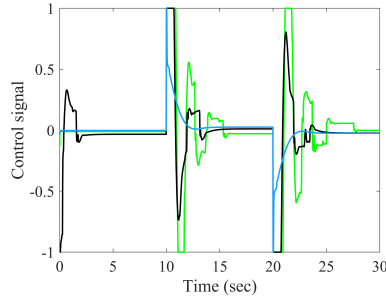


FIGURE 10 Control signals of $C_{FOPD}^1(s)$ and $C_{FOPD}^2(s)$ and *PD*.

FOPD controllers. Furthermore, an auxiliary function was introduced to enhance the performance of the closed-loop control system. Finally, the effectiveness of the proposed approach was validated through its application to the position control of a laboratory modular servo system. Through this research, not only was the understanding of robust stability regions for FOPD controllers expanded, but also a practical methodology was provided for their implementation in real-world control systems.

CONFLICT OF INTEREST

The author declares no conflicts of interest.

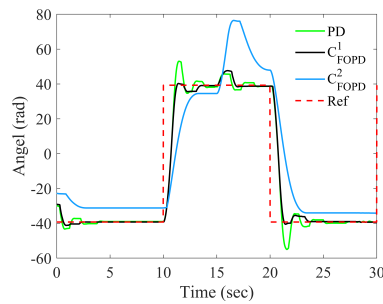


FIGURE 11 Comparison of control systems with different controllers $C_{FOPD}^1(s)$, $C_{FOPD}^2(s)$ and PD in the presence of disturbance.

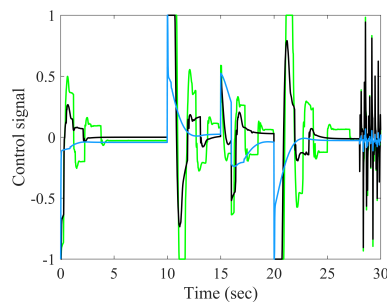


FIGURE 12 Control signals of $C_{FOPD}^1(s)$, $C_{FOPD}^2(s)$ and PD in the presence of disturbance.

REFERENCES

1. K.S. Nisar, M. Farman, M. Abdel-Aty, J. Cao, "A review on epidemic models in sight of fractional calculus", vol.75, pp. 81–113, 2023.
2. C.I. Muresan, I. Birs, R. De Keyser, "An alternative design approach for Fractional Order Internal Model Controllers for time delay systems", Journal of Advanced Research, vol. 31, pp. 177-189, 2021.
3. J. Morsali, K. Zare, M.T. Hagh, "Comparative performance evaluation of fractional order controllers in LFC of two-area diverse-unit power system with considering GDB and GRC effects", Journal of Electrical Systems and Information Technology, vol. 5, no. 3, pp. 708-722, 2018.
4. E. Çómez, İ. Kaya, "An analytical solution of fractional order PI controller design for stable/unstable/integrating processes with time delay", Turkish Journal of Electrical Engineering and Computer Sciences, vol. 31, no. 3, pp. 626-645, 2023.
5. O. Saleem, F. Abbas, J. Iqbal, "Complex fractional-order LQIR for inverted-pendulum-type robotic mechanisms: Design and experimental validation," Mathematics, vol. 11, no. 4, pp. 913, 2023.
6. D. Tiwari, N. Pachauri, A. Rani, V. Singh, "Fractional order PID (FOPID) controller based temperature control of bioreactor," 2016 International Conference on Electrical, Electronics, and Optimization Techniques (ICEEOT), pp. 2968-2973, 2016.
7. H.P. Ren, J.T. Fan, O. Kaynak, "Optimal design of a fractional-order proportional-integer-differential controller for a pneumatic position servo system," IEEE Transactions on Industrial Electronics, vol. 66, no. 8, pp. 6220-6229, 2018.
8. G. Sun, Z. Ma, J. Yu, "Discrete-time fractional order terminal sliding mode tracking control for linear motor," IEEE Transactions on Industrial Electronics, vol. 65, no. 4, pp. 3386-3394, 2017.
9. Q.-H. Zhang and J.-G. Lu, "Novel admissibility and robust stabilization conditions for fractional-order singular systems with polytopic uncertainties," Asian Journal of Control, vol. 26, no. 1, pp. 70-84, 2024.
10. S. Luo and J.-G. Lu, "Robust normalization and stabilization of descriptor fractional-order systems with polytopic uncertainties in all matrices," Asian Journal of Control, <https://doi.org/10.1002/asjc.3224>.
11. M. Ghorbani, A. Tepljakov, E. Petlenkov, "On robust stability analysis of interval time delay systems using delayed controllers", in 2023 European Control Conference (ECC), pp. 1-6, 2023.
12. M.Z. Malik, M. Asadi, H. Rezaei, "On robust stability of second order plus interval time delay plants using Fractional-Order Proportional Integral Derivative controllers", Journal of Vibration and Control, doi:10.1177/10775463231172813.
13. K.A. Moornani, M. Haeri, "On robust stability of LTI fractional-order delay systems of retarded and neutral type", Automatica, vol. 46, no. 2, pp. 362-368, 2010.
14. K. Akbari Moornani, M. Haeri, "Robust stability testing function and Kharitonov-like theorem for fractional order interval systems", IET Control Theory & Applications, vol. 4, no. 10, pp. 2097-2108, 2010.
15. S.E. Hamamci, M. Koksali, "Calculation of all stabilizing fractional-order PD controllers for integrating time delay systems", Computers & Mathematics with Applications, vol. 59, no. 5, pp. 1621-1629, 2010.

16. S. Zheng, W. Li, "Stabilizing region of PD^μ controller for fractional order system with general interval uncertainties and an interval delay", *Journal of the Franklin Institute*, vol. 355, no. 3, pp. 1107-1138, 2018.
17. J. Dong, Z. Wang, Y. Cui, D. Yao, "Calculation of Stabilizing PD^μ Controllers for a Class of Fractional Order Systems with Time Delay", in 2019 Chinese Automation Congress (CAC), pp. 1763-1767, 2019.
18. H. Li, Y. Luo, Y. Chen, "A fractional order proportional and derivative (FOPD) motion controller: tuning rule and experiments," *IEEE Transactions on Control Systems Technology*, vol. 18, no. 2, pp. 516-520, 2009.
19. M. Cui, Y. Zhao, P. Cao, Y. Tang, Y. Lu, "Load frequency control of interconnected hydrothermal power system based on FOPI+ FOPD controller," *International Journal of Dynamics and Control*, vol. 12, no. 4, pp. 1073-1085, 2024.
20. J. Dong, Z. Wang, Y. Cui, D. Yao, "Calculation of Stabilizing PD^μ Controllers for a Class of Fractional Order Systems with Time Delay," 2019 Chinese Automation Congress (CAC), pp. 1763-1767, 2019.
21. P. Roy, B. Kar, B.K. Roy, "Fractional order PI-PD control of liquid level in coupled two-tank system and its experimental validation," *Asian Journal of Control*, vol. 19, no. 5, pp. 1699-1709, 2017.
22. A. Oustaloup, F. Levron, B. Mathieu, F.M. Nanot, "Frequency-band complex noninteger differentiator: characterization and synthesis", *IEEE Transactions on Circuits and Systems I: Fundamental Theory and Applications*, vol. 47, no. 1, pp. 25-39, 2000.
23. K. Matsuda, H. Fujii, " H_∞ optimized wave-absorbing control: Analytical and experimental results", *Journal of Guidance, Control, and Dynamics*, vol. 16, no. 6, pp. 1146-1153, 1993.
24. M.A. Rahimian, M.S. Tavazoei, "Improving integral square error performance with implementable fractional-order PI controllers", *Optimal Control Applications and Methods*, vol. 35, no. 3, pp. 303-323, 2014.
25. M.A. Rahimian and M.S. Tavazoei, "Stabilizing fractional-order PI and PD controllers: an integer-order implemented system approach", *Proceedings of the Institution of Mechanical Engineers, Part I: Journal of Systems and Control Engineering*, vol. 224, no. 8, pp. 893-903, 2010.
26. M. Marden, "Geometry of Polynomials", 3rd ed., American Mathematical Society, 1949.
27. W.S. Levine, "The Control Handbook (three volume set)", CRC Press, 2018.
28. J.W. Brown, R.V. Churchill, "Complex Variables and Applications", McGraw-Hill, 2009.
29. L. Ljung, "System Identification Toolbox: User's Guide", Citeseer, 1995.
30. A. Tepljakov, E. Petlenkov, J. Belikov, "FOMCOM: A MATLAB toolbox for fractional-order system identification and control," *International Journal of Microelectronics and Computer Science*, vol. 2, no. 2, pp. 51-62, 2011.

Curriculum Vitae

1. Personal data

Name	Majid Ghorbani
Date and place of birth	19 April 1990, Mamasani, Iran

2. Contact information

Address	Department of Computer Systems, Tallinn University of Technology, Akadeemia tee 15a, 12618, Tallinn, Estonia
Phone	+372 5361 6695
E-mail	majid.ghorbani@taltech.ee

3. Education

2021–2025	Tallinn University of Technology, - Information and Communication Technology, PhD studies
2014–2016	K. N. Toosi University of Technology, Control Engineering, MSc
2010–2014	Sahand University of Technology, Control Engineering, BSc

4. Language competence

Persian	native
English	fluent

5. Professional employment

2016–2019	Iranian Academic Center for Education, Culture and Research (ACECR)-Khajeh Nasir Toosi Branch, Tehran, Iran
-----------	---

6. Computer skills

- Operating systems: Windows,
- Document preparation: Latex, Microsoft Word
- Programming languages: Matlab

7. Defended theses

- 2017, Robust Fractional Order Control of Unstable Delayed Fractional Order Systems based on Smith Predictor Structure., supervisor Prof. Mahsan Tavakoli-Kakhki, K. N. Toosi University of Technology

8. Research Fields

- Robust control
- Robust stability analysis of time-delay systems
- Data-driven control
- Model predictive control (MPC)
- Data-driven MPC
- Iterative learning control
- Model-free adaptive control

9. Honors and Awards

- The paper "M. Ghorbani, A. Tepljakov, and E. Petlenkov, "Fractional-order interval polynomials, stability and robust stability analysis and FOMCON implementation," Proc. 2023 International Conference on Fractional Differentiation and Its Applications (ICFDA), pp. 1–6, 2023" was selected as the **Best Student Paper** at the ICFDA Conference
- Recipient of Erasmus+ Mobility Grant for academic collaboration and teaching visit to Tomas Bata University in Zlín
- Recipient of a competitive mobility grant for a research visit to Ghent University, Belgium
- Recipient of a competitive mobility grant for a research visit to the University of Surrey, United Kingdom

10. Scientific work Papers

"Computing stabilising regions: FOPID controller methodology for interval fractional-order plants with time delay." **International Journal of Systems Science**, <https://doi.org/10.1080/00207721.2024.2435569>.

"A graphical tuning method of robust FOPID controllers for stable and unstable fractional-order plants with interval uncertainties of a fractional order and model coefficients." **International Journal of General Systems**, <https://doi.org/10.1080/03081079.2024.2375442>.

"Implementable Robust Stability Regions for Fractional-Order PD Controllers with an Application to Servo System Control." **Asian Journal of Control**, DOI: 10.1002/asjc.3881.

"Robust Stability of Unstable Processes with Multiple Delays: A Modified Smith Predictor Approach." **2025 Conference on Decision and Control (CDC 2025)**.

"On Robust Stability of Uncertain Control Systems with Time Delay: An Approach based on the Overlap of Value Sets." **IEEE Transactions on Automatic Control**, DOI: 10.1109/TAC.2024.3381912.

"Data-Driven Model Predictive Techniques for Unknown Linear Time Invariant Systems." **IEEE Control Systems Letters**, DOI: 10.1109/LCSYS.2024.3359068.

"Robust Stabilization of Interval Fractional-Order Plants with an Interval Time Delay By Fractional-Order Proportional Integral Derivative Controllers." **IET Control Theory & Applications**, <https://doi.org/10.1049/cth2.12594>.

"From Data to Stability: A Novel Approach for Controlling Unknown Linear Time-Invariant Systems with Performance Enhancement." **Journal of Computational Applied Mechanics**, DOI: 10.22059/JCAMECH.2024.368986.913.

"Low-cost Data-Driven Predictive Stabilization of Unknown LTI Systems: Two LMI Approaches." **The 12th International Conference on Control, Mechatronics and Automation (ICCMA 2024)**, DOI: 10.1109/ICCMA63715.2024.10843884.

"Graphical Tuning for Robust Stabilization: Implementable Stability Regions for FOPI Controllers in Interval Fractional-Order Systems." **2024 Conference on Decision and Control (CDC 2024)**, DOI: 10.1109/CDC56724.2024.10885794.

"Disturbance Propagation in Vehicle Platoons: Symmetric Bidirectional Interconnections." **2024 American Control Conference (ACC)**, DOI: 10.23919/ACC60939.2024.10644505.

"Robust Stability Region of PI Controllers for an Interval Load Frequency Control System with an Interval Communication Time Delay." **IEEE ISGT EU 2024**, DOI: 10.1109/ISGTEUROPE62998.2024.10863205.

"Stabilizing Region of Fractional-Order Proportional Integral Derivative Controllers for Interval Delayed Fractional-Order Plants." **Asian Journal of Control**, <https://doi.org/10.1002/asjc.2894>.

"Stabilizing Region of Fractional-Order Proportional Integral Derivative Controllers for Interval Fractional-Order Plants." **Transactions of the Institute of Measurement and Control**, <https://doi.org/10.1177/0142331222117866>.

"Robust D-Stability Analysis of Fractional-Order Controllers." **2023 American Control Conference**, DOI: 10.23919/ACC55779.2023.10156257.

"Fractional-Order Interval Polynomials, Stability and Robust Stability Analysis and FOMCON Implementation." **International Conference on Fractional Differentiation and its Applications (ICFDA 2023)**, DOI: 10.1109/ICFDA58234.2023.10153377.

"On robust stability analysis of interval time delay systems using delayed controllers." **European Control Conference**, DOI: 10.23919/ECC57647.2023.10178325.

"Robust Stability Analysis of Smith Predictor Based Interval Fractional-Order Control Systems: A Case Study in Level Control Process." **IEEE/CAA Journal of Automatica Sinica**, DOI: 10.1109/JAS.2022.105986.

"Robust stabilization criteria of a general form of fractional-order controllers for interval fractional-order plants with complex uncertain parameters." **ISA Transactions**, <https://doi.org/10.1016/j.isatra.2022.02.014>.

"Event-triggered resilient distributed extended Kalman filter with consensus on estimation." **International Journal of Robust and Nonlinear Control**, <https://doi.org/10.1002/rnc.5881>.

"Robust stability testing function for a complex interval family of fractional-order polynomials." **Journal of the Franklin Institute**, <https://doi.org/10.1016/j.jfranklin.2022.09.042>.

"Robust FOPID Stabilization for Smith Predictor Structures." **2022 IEEE 61st Conference on Decision and Control (CDC)**, DOI: 10.1109/CDC51059.2022.9993283.

"Robust Stability Analysis of Interval Fractional-Order Plants With Interval Time Delay and General Form of Fractional-Order Controllers." **IEEE Control Systems Letters**, DOI: 10.1109/LCSYS.2021.3091525.

"Robust Stability Analysis of a General Class of Interval Delayed Fractional Order Plants by a General Form of Fractional Order Controllers." **Mathematical Methods in Applied Sciences**, <https://doi.org/10.1002/mma.7397>.

"Robust Stability Analysis of Interval Fractional Order Plants by Fractional Order Controllers: An Approach to Reduce Additional Calculation." **International Journal of General Systems**, DOI: 10.1080/03081079.2020.1832485.

"Robust Stability Analysis of Uncertain Incommensurate Fractional Order Quasi-Polynomials in the Presence of Interval Fractional Orders and Interval Coefficients." **Transactions of the Institute of Measurement and Control**, DOI: 10.1177/0142331220968965.

"Robust stabilizability of fractional order proportional integral controllers for fractional order plants with uncertain parameters: A new value set based approach." **Journal of Vibration and Control**, <https://doi.org/10.1177/1077546319890>.

"Robust FOPID stabilization of retarded type fractional order plants with interval uncertainties and interval time delay." **Journal of the Franklin Institute**, <https://doi.org/10.1016/j.jfranklin.2019.08.035>.

Elulookirjeldus

1. Isikuandmed

Nimi	Majid Ghorbani
Sünniaeg ja -koht	19 April 1990, Mamasani, Iran

2. Kontaktandmed

Aadress	Tallinna Tehnikaülikool, Akadeemia tee 15a, 12618, Tallinn, Estonia
Telefon	+372 5361 6695
E-post	majid.ghorbani@taltech.ee

3. Haridus

2021–2025	Tallinna Tehnikaülikool, Info- ja kommunikatsioonitehnoloogia, doktoriõpe
2014–2016	K. N. Toosi University of Technology, Juhtimistehnika, MSc
2010–2014	Sahand University of Technology, Juhtimistehnika, BSc

4. Keelteoskus

pärsia keel	emakeel
inglise keel	kõrgtase

5. Teenistuskäik

2016–2019	Iraani Akadeemiline Haridus-, Kultuuri- ja Uurimiskeskus (ACECR) Khajeh Nasir Toosi haru, Teheran, Iraan
-----------	---

6. Arvuti oskused

- Operatsioonisüsteemid: Windows,
- Kontoritarkvara: Latex, Microsoft Word
- Programmeerimiskeeled: Matlab

7. Kaitstud lõputööd

- 2017, ebasabiilsete ajaviitega murdjärgu süsteemide robustne juhtimine Smithi prediktori struktuuri põhjal; juhendaja: prof. Mahsan Tavakoli-Kakhki, K. N. Toosi University of Technology

8. Teadustöö põhisuunad

- Tõhus ja tõrkekindel riistvara disain
- Robustne masinõpe ja usaldusväärne tehisintellekt

- Tõhus süvaõpe manustatud rakendustes ja asjade Internetis

9. Autasud

- 2024, Infotehnoloogia teaduskonna aasta teadusartikli autor

10. Teadustööd ja publikatsioonid "Computing stabilising regions: FOPID controller methodology for interval fractional-order plants with time delay." **International Journal of Systems Science**,
<https://doi.org/10.1080/00207721.2024.2435569>.

"A graphical tuning method of robust FOPID controllers for stable and unstable fractional-order plants with interval uncertainties of a fractional order and model coefficients." **International Journal of General Systems**, <https://doi.org/10.1080/03081079.2024.2375442>.

"Implementable Robust Stability Regions for Fractional-Order PD Controllers with an Application to Servo System Control." **Asian Journal of Control**, DOI: 10.1002/asjc.3881.

"Robust Stability of Unstable Processes with Multiple Delays: A Modified Smith Predictor Approach." **2025 Conference on Decision and Control (CDC 2025)**.

"On Robust Stability of Uncertain Control Systems with Time Delay: An Approach based on the Overlap of Value Sets." **IEEE Transactions on Automatic Control**, DOI: 10.1109/TAC.2024.3381912.

"Data-Driven Model Predictive Techniques for Unknown Linear Time Invariant Systems." **IEEE Control Systems Letters**, DOI: 10.1109/LCSYS.2024.3359068.

"Robust Stabilization of Interval Fractional-Order Plants with an Interval Time Delay By Fractional-Order Proportional Integral Derivative Controllers." **IET Control Theory & Applications**, <https://doi.org/10.1049/cth2.12594>.

"From Data to Stability: A Novel Approach for Controlling Unknown Linear Time-Invariant Systems with Performance Enhancement." **Journal of Computational Applied Mechanics**, DOI: 10.22059/JCAMECH.2024.368986.913.

"Low-cost Data-Driven Predictive Stabilization of Unknown LTI Systems: Two LMI Approaches." **The 12th International Conference on Control, Mechatronics and Automation (ICCMA 2024)**, DOI: 10.1109/ICCMA63715.2024.10843884.

"Graphical Tuning for Robust Stabilization: Implementable Stability Regions for FOPI Controllers in Interval Fractional-Order Systems." **2024 Conference on Decision and Control (CDC 2024)**, DOI: 10.1109/CDC56724.2024.10885794.

"Disturbance Propagation in Vehicle Platoons: Symmetric Bidirectional Interconnections." **2024 American Control Conference (ACC)**, DOI: 10.23919/ACC60939.2024.10644505.

"Robust Stability Region of PI Controllers for an Interval Load Frequency Control System with an Interval Communication Time Delay." **IEEE ISGT EU 2024**, DOI: 10.1109/ISGTEUROPE62998.2024.10863205.

"Stabilizing Region of Fractional-Order Proportional Integral Derivative Controllers for Interval Delayed Fractional-Order Plants." **Asian Journal of Control**, <https://doi.org/10.1002/asjc.2894>.

"Stabilizing Region of Fractional-Order Proportional Integral Derivative Controllers for Interval Fractional-Order Plants." **Transactions of the Institute of Measurement and Control**, <https://doi.org/10.1177/01423312221117866>.

"Robust D-Stability Analysis of Fractional-Order Controllers." **2023 American Control Conference**, DOI: 10.23919/ACC55779.2023.10156257.

"Fractional-Order Interval Polynomials, Stability and Robust Stability Analysis and FOM-CON Implementation." **International Conference on Fractional Differentiation and its Applications (ICFDA 2023)**, DOI: 10.1109/ICFDA58234.2023.10153377.

"On robust stability analysis of interval time delay systems using delayed controllers." **European Control Conference**, DOI: 10.23919/ECC57647.2023.10178325.

"Robust Stability Analysis of Smith Predictor Based Interval Fractional-Order Control Systems: A Case Study in Level Control Process." **IEEE/CAA Journal of Automatica Sinica**, DOI: 10.1109/JAS.2022.105986.

"Robust stabilization criteria of a general form of fractional-order controllers for interval fractional-order plants with complex uncertain parameters." **ISA Transactions**, <https://doi.org/10.1016/j.isatra.2022.02.014>.

"Event-triggered resilient distributed extended Kalman filter with consensus on estimation." **International Journal of Robust and Nonlinear Control**, <https://doi.org/10.1002/rnc.5881>.

"Robust stability testing function for a complex interval family of fractional-order polynomials." **Journal of the Franklin Institute**, <https://doi.org/10.1016/j.jfranklin.2022.09.042>.

"Robust FOPID Stabilization for Smith Predictor Structures." **2022 IEEE 61st Conference on Decision and Control (CDC)**, DOI: 10.1109/CDC51059.2022.9993283.

"Robust Stability Analysis of Interval Fractional-Order Plants With Interval Time Delay and General Form of Fractional-Order Controllers." **IEEE Control Systems Letters**, DOI: 10.1109/LCSYS.2021.3091525.

"Robust Stability Analysis of a General Class of Interval Delayed Fractional Order Plants by a General Form of Fractional Order Controllers." **Mathematical Methods in Applied Sciences**, <https://doi.org/10.1002/mma.7397>.

"Robust Stability Analysis of Interval Fractional Order Plants by Fractional Order Controllers: An Approach to Reduce Additional Calculation." **International Journal of General Systems**, DOI: 10.1080/03081079.2020.1832485.

"Robust Stability Analysis of Uncertain Incommensurate Fractional Order Quasi-Polynomials in the Presence of Interval Fractional Orders and Interval Coefficients." **Transactions of the Institute of Measurement and Control**, DOI: 10.1177/0142331220968965.

"Robust stabilizability of fractional order proportional integral controllers for fractional order plants with uncertain parameters: A new value set based approach." **Journal of Vibration and Control**, <https://doi.org/10.1177/1077546319890>.

"Robust FOPID stabilization of retarded type fractional order plants with interval uncertainties and interval time delay." **Journal of the Franklin Institute**, <https://doi.org/10.1016/j.jfranklin.2019.08.035>.

ISSN 2585-6901 (PDF)
ISBN 978-9916-80-436-0 (PDF)